IMPERIAL COLLEGE OF SCIENCE AND TECHNOLOGY

DEPARTMENT OF CIVIL ENGINEERING

Steady and Transient Seepage in Soils With Non-Linear Permeability Characteristics

EDWARD NICHOLAS BROMHEAD

Thesis submitted in partial fulfilment of the requirements for the award of the Degree of Doctor of Philosophy of the University of London.

October, 1980

ACKNOWLEDGEMENTS

I would like to thank Professor J. N. Hutchinson for his support and help in the work described in this thesis.

In addition to Professor Hutchinson, Dr. P. R. Vaughan was the source of some of the fundamental ideas and Dr. A. E. Skinner was always available for discussions on the finer points of mathematics, for which I will always be grateful.

At Kingston Polytechnic, I would like to thank Dr. A. G. Catchpole (Assistant Director) and Mr. D. H. Simm (Head of School of Civil Engineering) for their support. I am also grateful for the financial support of the Royal Borough of Kingston-upon-Thames and for the moral support of my colleagues at Kingston who rallied round so that I could have a sabbatical.

Research is not carried out in a vacuum, and the atmosphere at Imperial College has benefitted many in the past thirty years. I am indebted to Professors Skempton and Bishop for the interest they have shown in my work and to Dave Evans and his staff, Lou Spall, Fred Evans, Graham Keefe, Steve Ackerley and Eileen Gibbs in the laboratory who all helped at some stage with apparatus when I thought that continuing and enlarging Dr. Walbancke's field measurements of pore water pressure would be where I could make significant advances. In particular, I would like to thank my past and present co-workers, both for their help which in some instances was considerable, but also for reminding me of the other aspects of geotechnology which are waiting to be looked at. In particular I must mention Jane Walbancke, Richard Pugh, Mamdouh Hamza, Francisco Lopes, Franco Lupini and Martin Chandler.

I would also like to thank Leandro Costa Filho, Keith Sparrow, Keith Shepherd, Dave Williams, Steve Ackerley and Graham Keefe for their help in the field.

Lastly, but by no means least, for the support at home I thank my parents and my wife Caryl.

ABSTRACT

A finite element model for analysing seepage in soils with an effective stress dependent permeability is developed and results obtained from it compared both to a number of closed form solutions and to another, simplified, numerical method. Close agreement is found.

The rates of equilibration of pore water pressures in soils with effective stress dependent permeability and/or compressibility are explored, also with the aid of finite element techniques.

Parametric studies of seepage towards trench and counterfort drains, and in slopes, are carred out with both constant permeability and effective stress dependent permeability. Design recommendations for both cases are given.

CONTENTS

Chapter		Pag
1.	Introduction	2
	1.1. General Remarks on Seepage	2
	1.2. Various Aspects of Non-Darcian Flow	2
	1.3. General Remarks on "Consolidation"	2
	1.4. The Uncoupled Consolidation Model	2
	1.5. The Role of Parametric Studies	2
	1.6. Structure of this Thesis	2
2.	Simple Analytical Solutions for Seepage in a Soil with an Effective Stress/Permeability Relationship	2
	2.1. Introduction	2
	2.2. Variation of Permeability in Space	2
	2.3. Downwards Seepage when the Permeability is Related to Effective Stress	3
	2.4. Horizontal Seepage when the Permeability is Related to Effective Stress	3
	2.5. Spherically Symmetric Seepage when the Permeability is Related to Effective Stress	3
	2.6. Radially Symmetric Seepage when the Permeability is Related to Effective Stress	4
	2.7. An Alternative Treatment for "One-dimensional" Seepage in Soils with Generalised Effective Stress - Permeability Relationships	4
	2.8. Comparison of Analytical Results with the Simple Numerical Model	4
	2.9. Field Variation of Permeability from Piezometer Measurements (including case records)	4
	2.10. Field Variation of Permeability from Flow Rate Measurements	4
	2.11. Implications	4

2.12. The Influence of Problem Scale on the One Dimensional Studies 52a

2.13. The Engineering Significance of Effective Stress Dependent Permeability 52b

		Page
3.	Finite Element Models for Seepage	72
	3.1. Introduction	72
	3.2. Energy Basis for the Theory	72
	3.3. Finite Elements	74
	3.4. Treatment of "Known Potential" and "Known Flow" Boundaries	77
	3.5. Treatment of the "Free Surface"	79
	(a) Iterative, variable stiffness, variable geometry methods	79
	(b) Iterative, variable stiffness, variable properties method	82
	(c) Iterative, constant stiffness, methods	83
	3.6. Variation of Permeability	83
	3.7. Anisotropic and Non-homogeneous Permeability	85
	3.8. Effective Stress - Permeability Relationships	85
	3.9. Testing the Effective Stress Seepage Model	87
	3.10. Finite Elements Graphical Output	92
	3.11. De Mello's Work	94
	3.12. Morgenstern & Guther's Approach	95
	3.13. Summary	97
4.	Finite Element Models for Pore Water Pressure Dissipation	112
	4.1. Introduction	112
	4.2. Coupled and Uncoupled Solutions	113
	4.3. The Zienkiewicz and Parekh Model and Modifications	114
	4.4. Element Induced Potential Oscillations	118
	4.5. Previous Work	121
	4.6. Effective Stress - Permeability and - Compressibility Relationships	122
	4.7. Parametric Study - One Dimensional Dissipation	123
	4.8. Parametric Study - Constant Head In-situ Permeability Test	135
	4.9. Summary	141

		Page
5.	Constitutive Laws and Parameters for Effective Stress Dependency in Permeability	164
	5.1. Introduction and General Remarks	164
	5.2. Constitutive Laws	166
	5.3. Suggestions for Further Work	166
6.	Study of Seepage in Counterfort Drains	168
	6.1. Introduction	168
	6.2. Approximate Theory	169
	6.3. Fully Penetrating Trench Drain - Analytical Solution	173
	(a) Potential Distribution	174
	(b) Average Pore Pressure Ratios	178
	(c) Flow Rates	180
	6.4. Finite Element Analysis of Trench Drains - Comparison with Analytical Solution	183
	6.5. Partially Penetrating Trench Drains - Finite Element Parametric Study	185
	6.6. Analysis Where Permeability is Effective Stress Dependent	187
	6.7. Comparison of Theory with Field Measurements	188
	6.8. Pore Pressure Changes on Installation of Trench Drains	188
	6.9. Rates of Equilibration of Trench and Counterfort Drains	192
	6.10. Conclusions	192
7.	Parametric Study of Seepage in Slopes	214
	7.1. Introduction to the Parametric Study	214
	7.2. Boundary Conditions	214
	7.3. Geometric Mapping	218
	7.4. Problems Arising from a Single Slope Model	220
	7.5. Analyses with Effective Stress Dependent Permeability	221

		Page
7.6.	Sweeney's Model	221
7.7.	Results of the Parametric Study	223
7.8.	Lafleur & Lefebvre's Work	226
7.9.	Permeability Changing with Depth	228
7.10.	Comparison of the Parametric Study and Field Measurements	231
7.11.	Pore Pressure Changes Accompanying Excavation and Equilibration Rates	232
7.12.	Conclusions	234
8.	Conclusions	257
8.1.	Methods of Analysing Seepage and Consolidation	257
8.2.	Realistic Simulation of Field Boundary Conditions	258
8.3.	The Use of Non-linear Models in Seepage	259
8.4.	Trench and Counterfort Drains	261
8.5.	Seepage in Slopes	262
8.6.	General Observations	262
9.	References	264

LIST OF FIGURES

Chapter		Page
1.	Introduction	20
	- No Figures	
2.	Simple Analytical Solutions for Seepage in a Soil With an Effective Stress/Permeability Relationship	26
	2.1. Key Diagram: Gravity Seepage in a Partly Underdrained Soil Layer	53
	2.2. Pore Water Pressure-Depth Variation: Strong Underdrainage, Polynomial Permeability Distribution	54
	2.3. Pore Water Pressure-Depth Variation: Weak Underdrainage, Polynomial Permeability Distribution	55
	2.4. Pore Water Pressure-Depth Variation: Strong Underdrainage, Exponential Permeability Variation	56
	2.5. Pore Water Pressure-Depth Variation: Weak Underdrainage, Exponential Permeability Variation	57
	2.6. Pore Water Pressure-Depth Variation: Strong Underdrainage, Effective Stress Dependent Permeability	58
	2.7. Pore Water Pressure-Depth Variation: Weak Underdrainage, Effective Stress Dependent Permeability	59
	2.8. Implications of the "b" Parameter	60
	2.9. Key Diagram: Horizontal and Axisymmetric Seepage in a Constant Total Stress Field	61
	2.10. Horizontal Seepage in a Constant Total Stress Field With An Effective Stress Dependent Permeability	62
	2.11. Axisymmetric Seepage in a Constant Total Stress Field. Analytical Solutions Using the "Logarithmic" Law	63
	2.12. Key Diagram: Spherically Symmetric Seepage in a Constant Total Stress Field	64
	2.13. Spherically Symmetric Seepage in a Constant Total Stress Field. Analytical Solutions Using the "Logarithmic" Law	65
	2.14. Lag in Flow Rate Ratio in Comparison to Permeability Ratio	66
	2.15. Simple Numerical Technique for Dealing with Effective Stress Dependent Permeability in One Dimensional Seepage	67
	2.16. Predictions of the Simple Model - Downward Seepage	68
	2.17. Predictions of the Simple Model - Horizontal Seepage	69
	2.18. Predictions of the Simple Model - Axisymmetric Seepage	70
	2.19. Predictions of the Simple Model - Spherically Symmetric	71

Chapter		Page
2.20.	Influence of scale on the parametric study of vertical underdrained seepage in a soil with effective stress dependent permeability	71a
2.21.	Influence of scale and the b parameter on the pore pressure distribution: vertical underdrained seepage using effective stress dependent permeability (Log Law)	71b
2.22.	Pore pressures in the core of Tarbela Dam (after Truscott 1977)	71c
2.23.	Pore pressures in the core of Balderhead Dam (after Vaughan 1980, Vaughan et al. 1970)	71d
2.24.	Pore pressure distribution in the Till slopes at Cow Green Dam abutment (after Vaughan & Walbancke 1973)	71e
2.25.	Sketch cross section of the Herne Bay cliffs showing typical piezometer locations (after Bromhead 1972)	71f
2.26.	Typical pore water pressure conditions in the slopes at Herne Bay (after Bromhead 1972)	71g
2.27.	Field pore pressure/depth curves at the University of Kent, and at Maldon (Essex)	71h

Chapter		Page
3.	Finite Element Models for Seepage	72
3.1.	Pore Fluid Pressures Acting on an Infinitesimal Soil Element	99
3.2.	Types of Boundary Condition in Seepage Analysis	100
3.3.	Aspects of the Simulation of Free Surfaces with the Finite Element Method	101
3.4.	The Positions of "Entry Singularities" and their Importance in Free Surface Analysis	102
3.5.	Fundamental Basis of "Constant Stiffness" Method	103
3.6.	Effective Stress-Permeability Relationships	104
3.7.	Principles of the Finite Element Model	105
3.8.	Finite Elements - Test 1: Comparison of Finite Element and Analytical Results (cf Figure 2.6)	106
3.9.	Convergence of Finite Element Technique: Vertical, Underdrained Seepage	107
3.10.	Finite Elements - Test 2: Actual Potentials Close to Downstream Boundary	108
3.11.	Convergence of Finite Element Technique: Horizontal Seepage	109
3.12.	Oscillation of $\int \phi$ dvol with Increasing Element Subdivision: Horizontal Seepage (cf Figure 2.10 for Mesh and Overall Problem Detail)	110
3.13.	Facilities Available Through the Finite Element Graphics Program	111
4.	Finite Element Models for Pore Water Pressure Oscillation	112
4.1.	Illustration of "Element Induced" Potential	142
4.2.	Alternative Modelling of Initial Conditions Close to Known Potential Boundaries	143
4.3.	Comparison of Results Yielded by Different Initial Conditions Assumptions Close to the Drainage Boundary	144
4.4.	Effect of the Size of the First Time Step on Average Dissipation of $\int \phi$ dvol (Zienkiewicz & Parekh Method)	145
4.5.	Effect of Size of the First Time Step on Selected Individual Potentials (Zienkiewicz & Parekh Method)	146
4.6.	The Six Basic, Unique, Horizontal One Dimensional Dissipation Cases	147

Chapter		Page
4.7.	Basic, Unique, Vertical One Dimensional Dissipation Cases	148
4.8.	Key Diagram: Cases Considered in the Parametric Study	149
4.9.	Average Degree of Pore Water Pressure Dissipation, Constant c_v Model. Horizontal Flow	150
4.10.	Average Degree of Pore Water Pressure Dissipation, Constant m_v Model (N.B. In this case Average Pore Pressure Dissipation and "% Volume Change" Are Identical). Horizontal Flow	151
4.11.	Average "% Volume Change" in the Constant c_v Model. Horizontal Flow	152
4.12.	"Mid Plane" Pore Pressure Dissipation, Constant c_v Model, Horizontal Flow	153
4.13.	"Mid Plane" Pore Pressure Dissipation, Constant m_v Model, Horizontal Flow	154
4.14.	Dissipation Rates in the Underdrained Problem for Both Constant c_v and Constant m_v cases, N.B. Even the "Constant Properties" Solution Goes to 50% $\int \phi$ dvol	155
4.15.	Final Settlements in the Effective Stress Dependent Permeability Solutions Compared to the Constant Properties Theory. Complete Underdrainage.	156
4.16.	Average "% Settlement", Constant c_v Model. Vertical Flow with Sudden Underdrainage	157
4.17.	Average Degree of Pore Water Pressure Dissipation, Constant c_v Model. Doubly Drained Vertical Flow with a Constant Initial Excess Pore Pressure	158
4.18.	Average Degree of Pore Water Pressure Dissipation, Constant m_v Model. Doubly Drained Vertical Flow with a Constant Initial Excess Pore Pressure	159
4.19.	Average "% Settlement", Constant c_v Model. Doubly Drained Vertical Flow with a Constant Initial Excess Pore Pressure	160
4.20.	Observations of Flow Rate in Constant Head In-Situ Permeability Tests	161
4.21.	Finite Element Mesh Used in Analysis of Spherically Symmetric Consolidation with Effective Stress Dependent Properties	162
4.22.	Results of the Parametric Study of Spherically Symmetric Seepage	163
4.23.	Possible Explanation of Curved q vs $1/\sqrt{t}$ plots	163a

Chapter		Page
5.	Constitutive Laws and Parameters for Effective Stress Dependency in Permeability	164
	- No Figures	
6.	Study of Seepage in Counterfort Drains	168
6.1.	Key Diagram: Cross Section Through a Typical Trench Drain Installation (Generally After Hutchinson 1977)	194
6.2.	Schematic Diagram Showing Distribution of Boundary Potentials Used in the Analytical Solution	195
6.3.	Comparison of Fourier and Finite Element Solutions to Richardson's Problem	196
6.4.	Summary of Piezometric Levels at Drain Invert Level in the Richardson Problem	197
6.5.	Influence of Counterfort Drains at Various Depths (Closed Form Solution)	198
6.6.	Finite Element Meshes Used in Parametric Study of Trench and Counterfort Drains	199
6.7.	Typical Flow Nets Derived from Finite Element Analysis of Trench Drains (Largely after Hutchinson 1977)	200
6.8.	Trench Drains: Reduction of Pore Water Pressure at Drain Invert Level and at Base of Soil Layer (Impermeable Base)	201
6.9.	Pore Water Pressures at Drain Invert Level in Trench Drain Installations with Different Depth Factors	202
6.10.	Impermeable Base Solution: Average Pore Water Pressure Heads at Base of Soil Layer for Trench Drains of Various Penetrations	203
6.11.	Impermeable Base Solution: Average and Maximum Pore Water Pressure Heads at Base of Soil Layer for Trench Drains of Various Penetrations	204
6.12.	Effect of Trench Drains in a Partly Underdrained Soil Layer - Influence of Underdrainage Ratio D_u	205
6.13.	Effect of Trench Drains with Different Penetrations into a Partly Underdrained Soil Layer	206
6.14.	Flow where the Permeability is Dependent on Effective Stress - Piezometric Heads at Drain Invert Level	207
6.15.	Equipotentials in the Effective Stress - Permeability Analyses	208
6.16.	Comparison of Theory with Field Measurements	209
6.17.	Finite Element Model for Stress Changes on Installation of Trench Drains	210

Chapter		Page
6.18.	Typical Calculated Pore Water Pressures Immediately After Excavation of Trench Drains	211
6.19.	Initial and Final Pore Water Pressures in a Counterfort Drain Installation	212
6.20.	Field Measurements of Pore Water Pressures in Trench Drain Installations (After Hutchinson 1977)	213
7.	Parametric Study of Seepage in Slopes	214
7.1.	Key Diagram: Seepage in Slopes and Boundary Conditions	235
7.2.	Use of Non-Homogenous Permeability to Transform the Geometry of a Single Finite Element Model	236
7.3.	Basic Finite Element Mesh and Zoning Convention for Parametric Study	237
7.4.	Results of the Parametric Study (9 Separate Figures Subscripted A to I Inclusive)	238
7.5.	Results of the Subsidiary Parametric Study (2 Separate Figures Subscripted A and B)	247
7.6.	Average Pore Pressures in Slopes - A Summary of the Parametric Study	249
7.7.	Use of the Slope Model in Routine Design	250
7.8.	Hammer's Integration Rule for a Triangle (Based on Data in Zienkiewicz 1972)	251
7.9.	Influence of an Effective Stress Dependent Permeability	252
7.10.	Sweeney's (1970) Model for "Seepage in a Soil Slope"	253
7.11.	Lafleur and Lefebvre's Model	254
7.12.	Tailings Dam with Increasing Permeability with Depth - Wetted Boundary Solution	255
7.13.	Constant Permeability Solutions for Tailings Dam	256

LIST OF TABLES

Chapter		Page
1.	Introduction	20
2.	Simple Analytical Solutions for Seepage in a Soil with an Effective Stress/Permeability Relationship	26
	2.1. Relationship Between Parameter "b" and Depth or Increase in Effective Stress for an Order of Magnitude Change in Permeability	36
	2.2. Some Typical Back Analysed "b" Parameters	47
3.	Finite Element Models for Seepage	72
	- No Tables	
4.	Finite Element Models for Pore Water Pressure Dissipation	112
	4.1. Brief Outline of Parametric Study - Horizontal Flow	126
	4.2. Time Lag for 50% Mid-Plane Dissipation. Constant C_v Assumption	127
	4.3. Time lag for 50% Mid-Plane Dissipation. Constant M_v Assumption	128
	4.4. Brief Outline of Parametric Study - Vertical Flow	133
	4.5. Analyses of Spherically Symmetric Dissipation	137
5.	Constitutive Laws and Parameters for Effective Stress Dependency In Permeability	164
	- No Tables	

6. Study of Seepage in Counterfort Drains

6.1. Details of Counterfort Drain Installations (After Hutchinson 1977)

7. Parametric Study of Seepage in Slopes

7.1. Analyses in Slope Seepage Parametric Study

8. Conclusions

- No Tables

LIST OF SYMBOLS USED

Chapter 1

A	Area of flow
i	Hydraulic (potential) gradient
k	Permeability coefficient
q	Flow rate
n	Index

Chapter 2

A, B, C, D, E	Symbols to represent the parts of an involved formula
a_1 .....a_7	Coefficients in a general expression for permeability used in a computer program
a, b	Permeability parameters
c	Constant of integration
D_u	Underdrainage ratio (Defined in text)
d	Differential operator
e	Base of natural logarithms
F(y)	Function of elevation (y) defined in text
H, h, h_o	Elevation, pressure head
K_o	Coefficient of lateral earth pressure at rest
K(x), K(y)	Permeability as a function of x or y coordinates
k, k_o	Permeability coefficient
L	Length
ln	Natural logarithm
n	Index
q, q_∞	Flow rate, Flow rate in a constant head test at very large times (i.e. equilibrated)
R	Radius of a well or spherical piezometer cavity
R_I	Radius of influence of a well
r	Radius
r_k	Ratio of two permeabilities
r_Q	Ratio of two flow rates

u	Pore water pressure
x, y	Cartesian coordinate system (y is elevation)

Chapter 2 (Greek & Mathematical Symbols)

Δ	Increment of
Δh, $\Delta \phi$	Increment of total head or potential
γ	Unit weight of soil
γ_w	Unit weight of water
γ'	Submerged (bouyant) unit weight of soil
ϕ, ϕ_y	Potential, Potential at an elevation y
$\phi_1, \phi_2, \phi_0, \phi_2, \phi_L, \phi_I$	Boundary potentials
σ, σ', σ_v	Normal stress, effective stress, vertical effective stress

Chapters 3 & 4

α	Parameter controlling time step size
a, b	Permeability parameters
C_v, c_v	Coefficient of consolidation
d, dx, dy, dz	Differential operator
e	(superscript) Relating to a given element
e	Base of natural logarithms
h_w	Pressure head
g	Acceleration due to gravity
k	Permeability (may be subscripted to relate to direction
M_v, m_v	Compressibility coefficient
N, N_i, N_j	Shape function for a finite element, relating to Node i or j
NE	No. of elements
NE^I	No. of elements connected to a given node
NS	No. of surfaces or parts into which a surface is divided
NS^I	No. of the parts of a surface connected to a given node
n	Index

P_x, P_y, P_z	Pressure acting in x, y or z coordinate direction
q, q_t, q	Flow rate, flow rate at time t,or equilibrated flow rate
SR, SE	Surface of flow domain,or of single element of this.
t	Time
u	Water pressure
V, VR, VE	Volume, volume of a complete seepage domain and of an element of this
v, v_x, v_y, v_z	Velocity (subscripted indicates direction of velocity)
W, W_1, W_2	Work, work done against drag, Energy contributed external
x, y, z	Coordinate system
z	Elevation

Chapters 3 & 4 (Greek and Mathematical Symbols)

∂	Partial differential operator
$\Delta x, \Delta y, \Delta z$	Increment of x, y or z
ΔW_x	Work done in x direction against drag
ΔW_1	Work done against drag
Δh_w	Head (potential) increment
$\delta t, \Delta t, \Delta t_n, \Delta t_o$	Time intervals
γ_w	Unit weight of water
ϕ, ϕ_{xyz}	Potential, Potential at coordinates (x, y, z),
ϕ_i	Potential at node i
ϕ_1, ϕ_2, ϕ_3	Initial potentials defined at certain nodes
ρ	Density
σ, σ'	Total stress, effective stress

Chapters 3 & 4 (Matrix and Vector Terms)

[]	Matrix
{}	Column vector
T	Transposed
$\{\}^T$	Row vector

$[H]$, Hij, hij	Hij is an element of matrix $[H]$ comprising contributions hij from a series of finite elements.
	$[H]$ is a matrix dependent on the size, shape and permeability of the finite element mesh
$[G]$, Gij, gij	Largely defined as above, except that $[G]$ is a matrix reflecting compressibility rather than permeability
$\{F\}$, F_i, fi	Again as above, except that $\{F\}$ is a vector reflecting known flow rates and the size and shape of those parts of the surface of a finite element mesh subject to those flows
$[B]$, $[B']$, B'_i	Matrix of shape function derivatives defined in terms of global coordinate system, $[B]$, or local coordinate system, $[B']$
	B'_i is a sub-element of $[B']$
$[D]$, $[D']$	Matrix of permeability coefficients
$[T]$	Transformation matrix between coordinate systems
$[K]$	"Stiffness" matrix (function of $[H]$ and possibly of $[G]$ matrices)
$\{P\}$	"load" vector (function of $\{F\}$ vector and possibly of $[H]$ matrix)
t, $t-\frac{\delta t}{2}$, $t-\delta t$	Subscript terms: Imply matrix or vector evaluated at time indicated by subscript.
e	Superscript term: Implies matrix or vector relating to a given element

Chapter 6

a_n	nth Fourier coefficient
A	Sum of drain width and spacing
b	Twice drain depth, permeability/stress coefficient (- see Chapter 2)
B	Drain width
d	Differential operator, depth
D	Overall drain depth (interchangeable with H)
D_u	Underdrainage ratio (- see Chapter 2)

h_w	Pore water pressure head
h_d	Piezometric head in drains
h_o	Effective drain depth
$\bar{h}$	Average piezometric head
h_m	Maximum piezometric head
h', $\bar{h}'$, h'_m	Piezometric heads corrected for slope
H	Drain depth (interchangeable with D)
I_1, I_2	Integrals
k	Permeability
K	Constant
K_o	Coefficient of earth pressure at rest
m	Index
n	Index, depth factor
N_f/N_d	Ratio of number of flow paths to number of potential drops
R_k	Ratio of horizontal to vertical permeability coefficients
R_s	Composite spacing/depth/permeability anisotropy factor
s	Drain spacing
x, y x', y'	Coordinate directions

Chapter 6 (Greek symbols)

α, β	Henkel's pore pressure parameters (β not used)
β	Slope inclination angle
$\bar{\eta}$	Drain efficiency with respect to the intervening soil mass
η_{av}	Overall drain efficiency
ϕ	Potential
$\bar{\phi}$	Average potential
ϕ_{xy}	Potential at coordinates (x, y)
$\phi_A, \phi_B, \phi_C, \phi_D, \phi_E$	Potential due to boundary conditions types A, B, C, D, and E respectively (also ϕ_{xy_A} for potential at x, y due to A, $\bar{\phi}_A$ for average potential due to A, etc).

Chapter 7

b	Stress/permeability parameter (- see Chapter 2)
Du	Underdrainage ratio (- see Chapter 2)
K_o	Coefficient of lateral earth pressure at rest
K, Kx, Ky	Permeability (if subscripted, relating to x or y direction)
K_{1-5}	Permeability of zone 1-5 (also K_{x1} etc)
m	Slope angle (e.g. 1 in m)
n	Depth factor
$\bar{r}_u$	Average pore pressure ratio
$\bar{R}$	Average pore water pressure (non-dimensionalised)
u, ui	Pore water pressure
(x, y) (r, θ)	Coordinate systems

Chapter 7 (Greek Symbols)

γ_w	Unit weight (of water)

CHAPTER 1 - INTRODUCTION

1.1. General Remarks on Seepage

In comparison with many other areas in the general field of soil mechanics, the study of seepage is relatively neglected. Why this should be, is not at present clear, especially since the problems of strength and deformation when couched in terms of effective stress both demand accurate assessments of pore water pressure. One possible explanation may be that the comparatively simple physical laws describing seepage discovered by Darcy in the middle of the nineteenth century (Darcy, 1857) together with the theoretical work in classical hydrodynamics from which it transpired that reasonable solutions for Darcian flow could be obtained to a sufficient *engineering* degree of accuracy by simply sketching the flow net led to the mistaken view that the whole problem was trivial. However, significant departures from Darcian flow occur in many situations, for example when piping occurs or where seepage becomes turbulent (such as in flow through coarse rockfill); and even in cases where Darcy's Law still holds good, the necessary coefficients of permeability may vary in space in such a way as to defy analysis. This has had the result that both numerical and analogue models have been developed to solve these problems - analogue models mainly to solve Darcian flow in homogenous but oddly shaped domains (e.g. Herbert & Rushton, 1966; Starr et al. 1969) and numerical models to solve problems incorporating anisotropic, nonhomogenous arbitrarily shaped domains (e.g. Zienkiewicz & Cheung, 1965; Zienkiewicz 1972, Zienkiewicz, Mayer and Cheung 1966; Tomlin 1970 and many others).

A fundamental problem that still remains, however, is the determination of the appropriate parameters.

A second major problem is the selection of the appropriate boundary conditions within which the problem is to be analysed. Many problems are fortuitously *confined*, that is their boundaries are either subject

to *no flow* or *known potential* conditions (or exceptionally to *known flow rate* conditions). Solution to such problems is comparatively simple by any of the numerical techniques, with the finite element technique having considerable advantages from a practical point of view - the literature on this topic being quite extensive.

The second category of problem is that in which the *geometry* of one boundary is not defined *a priori*, such as the classic "Free surface flow" problem. While much effort has been devoted to this (Taylor & Brown, 1967; France, Parekh, Peters and Taylor, 1971; Neuman and Witherspoon, 1970; Parekh, 1969; Kealy & Busch, 1971 for example) no *direct* numerical solution technique exists and most *variable geometry** methods of dealing with such a surface fail in one or more respects if used in an arbitrarily zoned domain. Desai, 1976, who has published an iterative method not based on altering mesh geometries may also fail to satisfy certain basic criteria (Bromhead 1976). However, in many situations in fine grained soils, capillary effects may dominate this undefined boundary and it may be possible to consider the soil surface to be a *known potential* boundary with zero or negative pore water pressures (Vaughan & Walbancke, 1973) especially where seasonal variations in the boundary pore water pressures are damped out with depth. In such a case the problem may be analysed as confined. This aspect of seepage is treated in greater depth below (Section 3.5).

In many field situations the permeability may be not only anisotropic and the individually anisotropic soil layers zoned, but the permeability may vary across a layer with the values of, ratio between, or inclination of, the principal permeability coefficients in general an arbitrary function of position. This in itself poses no additional problems for the finite element method provided that the user is prepared to accept piecewise - continuous variations in his properties. That this is not usually found to give rise to serious difficulties is attested to by a number of authors, typical cases being given by Zienkiewicz 1972.

**Discussed below in Section 3.5*

1.2. *Various Aspects of Non-Darcian Flow*

Some attention has been focussed on to types of flow where the seepage quantities are related not to the hydraulic gradient but to a power function of the hydraulic gradient, (Chowdhury & King, 1972; Volker, 1969).

$$q = A k i^{n}$$

This is applicable especially to turbulent flow through coarse rockfill, and non-linear models have been used for this in, for example, the analysis of "self-spillway" dams.

A different and ostensibly more important class of problems occurs where the orthodox Darcy Law applies but in which the permeability is not definable *a priori* but in which it is itself a function of the pore water pressures in the ground i.e. is related to effective stress. Rowe is frequently credited with the discovery of these effects in laminated glaciofluvial alluvia in Northern England but his work is not unique, there being much other data to support the existence of such an effect (Truscott 1977 & Walbancke 1976 are but two of the authors from Imperial College who consider the effect explicitly). However, very little has been published on the analysis of such situations.

The first part of this thesis is devoted to the solution of these problems using the following approach:-

(a) Provide as many closed form solutions as possible (Section 2.3 to 2.6).

(b) Develop simple numerical models for the cases that cannot be handled in (a) above (Section 2.7).

(c) Produce the finite element solution scheme and test it against the results of (a) and (b) (Section 3.8 and 3.9).

(d) Use the finite element scheme, the simple numerical model and the analytical solutions to:-

(i) analyse the suspected effects (Sections 2.9 to 2.11, 3.9 and 4.6. to 4.8)

and

(ii) attempt to detect novel effects (Sections 4.7., 4.8., 6.6 and 7.5)

1.3. General Remarks on "Consolidation"

The term consolidation covers both the time dependent decay or dissipation of pore water pressures and the settlement that results from that process. Many authors, following the lead of Biot (1941), have commented that for a realistic estimate of settlement, the correct stress strain behaviour coupled with the pore water pressure dissipation must be used. Conversely, if pore water pressures alone are required from the analysis, a much more simple, uncoupled, model may be used with only slight loss of accuracy. Since the preoccupation of this thesis is with pore water pressures rather than displacements, uncoupled solutions are used exclusively herein.*

The literature on consolidation suffers the same general restrictions as that on seepage. On the whole, recent research has concentrated on coupled solutions (of which only a few are closed form) with heavy reliance on the finite element method,notably Sandhu and Wilson, 1969; Boehmer and Christian, 1969; Hwang, Morgenstern & Murray, 1972. There is virtually nothing in the literature on simple, uncoupled methods analogous with that described in Section 1.2 on the subject of seepage. Some exceptions to this rather sweeping statement are discussed in Section 4.3.

**Steady seepage may be considered to be water flow with no volume change in the soil's skeletal structure. Consolidation is water flow with these volume changes. If the water flow and strains are both one dimensional (and in the same direction) then the uncoupled and coupled solutions are identical. It is only in two or three dimensional work where significant differences arise.*

1.4. The Uncoupled Consolidation Model

Since published methods of analysing consolidation do not allow for cases in which the parameters are a function of effective stress, a simple model was produced by combining the effective stress permeability seepage model with a simple uncoupled consolidation analysis (Zienkiewicz and Parekh, 1970). The compressibility of the soil skeleton is also made effective stress dependent and the effect of this on the rate and total amount of pore pressure dissipation and consolidation settlement is explored. However, the solutions are confined to one dimensional work as some of the important effects are more clearly seen in this. It is possible, however, that Mandel-Cryer effects may be intensified by effective stress dependent parameters, but this cannot be predicted using an uncoupled model (they are only predicted by two and three dimensional solutions which use a coupled theory).

1.5. Parametric Studies

So much of the literature is devoted to the presentation of new methods and concepts that systematic parametric studies have been neglected. The opportunity has been taken here to present two of these systematic investigations which have been exhaustively explored using constant permeability steady seepage models. The result of assuming permeability - effective stress relationships is then considered. In general, it is found that effective stress dependent permeability is of lesser importance in two dimensional flow than in one dimensional cases.

The rates of development of the steady seepage regimes are discussed.

1.6. Structure of This Thesis

The most important, and original, contributions of this thesis are as follows:-

(a) In developing the analytical solutions for effective stress dependent permeability so that the major one dimensional cases are covered consistently. This is an extension and enlargement of earlier work.

(b) In developing the simple numerical model so that any law relating effective stress to permeability may be used in pseudo one dimensional cases for which closed form solutions do not exist.

(c) In establishing the relationship between flow rates in a constant head test and the applied head in a soil with an effective stress dependent permeability so that the characteristics of this dependency can be explored. This does, however, have limited application since it applies only to one of the possible effective stress - permeability relations.

(d) In developing and evaluating the effective stress dependent permeability technique in finite element analysis of two dimensional cases.

(e) In developing an uncoupled consolidation (transient seepage) model based on effective stress dependent permeability *and* compressibility and investigating the result of these effects through a parametric study.

(f) To extend the present state of knowledge regarding seepage in trench and counterfort drains through both closed form and finite element solutions.

(g) To extend knowledge of seepage in slopes by a parametric study.

(h) To investigate the importance of the relationship between effective stress and permeability in the above two important cases.

The general layout of the thesis develops the argument of the importance of the effective stress - permeability relationship, reviewing previous work and introducing new matter as appropriate.

CHAPTER 2 - SIMPLE ANALYTICAL SOLUTIONS FOR SEEPAGE IN A SOIL WITH AN EFFECTIVE STRESS/PERMEABILITY RELATIONSHIP

2.1. Introduction

In later chapters, the distributions of pore water pressures in soil slopes, both modified and unmodified by shallow trench and counterfort drains, are investigated. The simple case of one dimensional percolation under gravity with a spatially or otherwise varying permeability is of importance to this later work since:-

(a) many slope seepage problems can be treated as one dimensional (Walbancke, 1976) with comparatively little loss of accuracy, since the vertical flow is the dominant component.*

(b) it may be possible to back analyse known or measured pore water pressure/depth profiles to obtain the variation of permeability with depth.

(c) the time dependent development of pore water pressures following the excavation of a cutting or the installation of trench drains is dependent on the initial conditions - themselves a probable result of vertical percolation.

The theoretical development that follows deals first with the distribution of pore water pressures in a soil layer with a permeability varying with depth, and then the influence of effective stress dependent permeability is explored. Subsequently, these analytical models provide a useful test for a finite element solution using effective stress dependent permeability (used later on two dimensional problems); the model and the test results are reported.

**The extensive parametric study of Chapter 7 partly refutes this earlier conclusion.*

2.2. *Variation of Potential and Pore Water Pressure with Depth*

Consider the steady seepage vertically through a wholly or partially underdrained layer of soil in which the permeability varies as a function of depth (or elevation). A section of unit area of such a soil layer is shown in Figure 2.1.

Boundary Conditions: At the upper surface of this layer the boundary conditions are:-

elevation	y	=	H
pore water pressure	u	=	0
hence potential	ϕ_H	=	H

(see p73)

while at the base of the layer we have:-

elevation	y	=	h
pore water pressure	u	=	$\gamma_w h_o$
hence potential	ϕ_h	=	$h + h_o$

Seepage Conditions: Since the flow of water is steady and vertical only, the quantity of seepage q through any section is constant and is related to the hydraulic or potential gradient $\frac{d\phi}{dy}$ by Darcy's law *viz:*

$$q = K(y) \frac{d\phi}{dy}$$

in which $K(y)$ is the value of the permeability of the soil at the appropriate elevation y.

Separating this and integrating we find:-

$$q \int \frac{1}{k(y)}\, dy = \phi + c$$

Substituting in firstly the upper boundary condition it is possible to evaluate the above constant of integration:-

$$c = q \int_{y=H} \frac{1}{k(y)}\, dy - H$$

and following with the lower boundary condition,since:-

$$q \left[\int_{y=h} \frac{1}{k(y)}\, dy - \int_{y=H} \frac{1}{k(y)}\, dy \right] = h + h_o - H$$

the seepage quantity q per unit area is found to be:-

$$q = \frac{H - h - h_o}{\int_h^H \frac{1}{k(y)}\, dy}$$

In general , however, for any y between h and H,

$$\phi_y = \frac{H-h-h_o}{\int_h^H \frac{1}{k(y)}\, dy} \int_H^y \frac{1}{k(y)}\, dy + H$$

or simply:-

$$\phi_y = H - \Delta h \; F(y)$$

In which Δh is the potential drop across the soil layer and F(y) a function of position within the layer and the variation of permeability with depth (or elevation), i.e.,

$$F(y) = \int_y^H \frac{1}{k(y)}\,dy \Big/ \int_h^H \frac{1}{k(y)}\,dy$$

F(y) lies between the values 0 (at the upper surface) and 1 (at the base of the layer).

The pore water pressure head at any elevation is the difference between ϕ_y and y.

Underdrainage Ratio, D_u: It is convenient to introduce a numerical parameter to describe the state of underdrainage of the soil layer if this is intermediate between the fully underdrained case and the situation where there is no underdrainage and hence no flow.

Defining this *underdrainage ratio* D_u as the ratio of the potential drop from top to bottom of the layer to its thickness:-

$$D_u = \frac{\Delta h}{H - h}$$

we have a convenient parameter that usually lies between 0 and 1 (but may be negative - implying upward flow, or greater than one - if the upper surface is flooded or the lower surface subject to suction).

Simple Cases: If the permeability is a constant then potentials are found to vary linearly with elevation and pore water pressures increase linearly with depth between the extremes of zero pore water pressure throughout a fully underdrained layer ($D_u = 1$) and a fully hydrostatic distribution in the $D_u = 0$ case.

When the permeability variation with elevation is a linear or higher order one then we usually find a "bow" in the pore water pressure distribution and can have quite appreciable pore water pressures in all but the lower part of the soil layer.* The solution for $K(y) = ay$ in which a is an arbitrary constant includes logarithmic terms:-

i.e.

$$\phi_y = H - \Delta h \frac{\ln H/y}{\ln H/h}$$

but for higher order variations of the form $K(y) = ay^n$ we obtain:-

$$\phi_y = H - \Delta h \frac{H^{1-n} - y^{1-n}}{H^{1-n} - h^{1-n}}$$

In no case does the arbitrary constant a enter into the solution; the distribution of pore water pressure and potential being a function of the *form* of the permeability variation rather than of the *magnitudes* of permeability involved. (Note should be taken of the numerical difficulties associated with y = 0 in the above formulae). Diagrams showing the variation in pore water pressure with depth for these variations in permeability and for four separate cases of D_u are given in Figures 2.2 and 2.3. The differences between the various solutions are much less marked for the lower underdrainage ratios.

Logarithmic Variation of Permeability: The case of a logarithmic variation of permeability is intrinsically more interesting since much of the field and laboratory data (see Chapter 5) points to a broadly linear variation of the logarithm of permeability with depth.

**As a corollary to this, it should be noted that negative pore water pressures are predicted if the permeability increases with depth.*

However, care must be taken in natural deposits not to overlook the increased permeability commonly found at the base of a deposit (in the transitional or basement beds) due to the lithological variation or due to an open fissure structure (at higher levels, weathering and/or a higher moisture content in the soil may not allow such a fissure structure to remain open and continuous).

The solution for potential where the permeability is of the form:-

$$k(y) = ae^{by}$$

is

$$\phi_y = H - \Delta h \frac{e^{-by} - e^{-bH}}{e^{-bh} - e^{-bH}}$$

Once again, the arbitrary constant a appears to have no influence on the solution, but the constant b (which may be viewed as a *form* rather than as a *magnitude* parameter) does appear in the final expression. The variation of pore water pressure with depth in this case depends largely upon the value of b, especially near the surface. As the parameter b tends towards zero, the solution for the variation of pore water pressure with depth converges on the constant permeability solution, that is, a linear variation of pore water pressure with depth. With b less than about 0.01 the differences between the two solutions are slight and decrease with decreasing underdrainage ratio D_u. The effect of increasing b is to make the pore water pressure profile tend to follow the hydrostatic line to greater depths with a very rapid reduction in pore water pressure in the bottom part of the soil layer. In extreme cases the pore water pressure profile may be indistinguishable from the hydrostatic line for a great deal more than half the thickness of the stratum. The effect of varying the b parameter on the profile of pore water pressures in four separate cases with different D_u values is shown diagrammatically in Figures 2.4 and 2.5.

2.3. *Vertical Downwards Percolation in a Soil Layer in Which the Permeability is a Function of Effective Stress*

In the case where the variation of permeability with depth is not a simple function of depth (such as the case when it depends on the effective stress in the soil layer) the simple expressions developed above will not suffice. Considering the logarithm of permeability to be related to the effective stress gives rise to an expression of the form:-

$$k(y) = ae^{-b\sigma'} \qquad (\ln k(y) = \ln a - b\sigma')$$

Naturally, if percolation is vertically downwards, it is the *vertical* permeability which controls this and this in turn is governed by the *lateral* effective stress, thus:-

$$k(y) = ae^{-bk_o\sigma'}$$

It is not strictly necessary to include K_o since its effect (if constant) is merely to modify the b parameter. However, if K_o varies significantly with depth the equations become substantially more complex.

Measuring y from the base of the soil layer (which is of thickness H) we obtain:-

$$\sigma_y' = \gamma(H-y) - (\phi_y - y)\gamma_w$$

$$= \gamma H - \gamma_w \phi_y - \gamma' y$$

Hence:

$$k(y) = ae^{-b\gamma H} \cdot e^{b\gamma_w \phi_y} \cdot e^{b\gamma' y}$$

Since with Darcy's Law we have flow through any section constant and dependant on the potential gradient thus:-

$$-q = K(y)\frac{d\phi}{dy}$$

(negative sign in Darcy's law because q measured in opposite sense to coordinates y)

We have:-

$$-q = ae^{-b\gamma H} \cdot e^{b\gamma_w \phi_y} \cdot e^{b\gamma' y} \cdot \frac{d\phi}{dy}$$

which may be rearranged to give:-

$$-q\,e^{-b\gamma' y}\,dy = ae^{-b\gamma H} \cdot e^{b\gamma_w \phi_y} \cdot d\phi$$

After integrating we find that:-

$$\frac{q}{b\gamma'} \cdot e^{-b\gamma H} = \frac{a}{b\gamma_w} \cdot e^{-b\gamma H} \cdot e^{b\gamma_w \phi_y} + c$$

The constant of integration is evaluated by substituting in the upper boundary condition:-

$$y = H \qquad \phi_y = H$$

to obtain:

$$c = \left(\frac{q\gamma_w - a\gamma'}{b\gamma_w \gamma'}\right) \cdot e^{-b\gamma' H}$$

The basic equation now becomes:-

$$\frac{q}{b\gamma'}\left(e^{-b\gamma' y} - e^{-b\gamma' H}\right) = \frac{a}{b\gamma_w}\left(e^{-b(\gamma H - \gamma_w \phi_y)} - e^{-b\gamma' H}\right)$$

and the flow rate q can be obtained by insertion of the lower boundary condition:-

$$y = 0 \qquad \phi_y = h_o$$

to obtain:-

$$q = \frac{a\gamma'}{\gamma_w}\left(\frac{e^{-b(\gamma H-\gamma_w h_o)} - e^{-b\gamma' H}}{1 - e^{-b\gamma' H}}\right)$$

(As a check, if $h_o = H$ there is no flow, this equation yields 0 for q).

Thus:-

$$e^{b\gamma_w \phi_y} = e^{b\gamma H}\left\{\left(\frac{e^{-b(\gamma H-\gamma_w h_o)} - e^{-b\gamma' H}}{1 - e^{-b\gamma' H}}\right)\cdot \left(e^{-b\gamma' y} - e^{-b\gamma' H}\right) + e^{-b\gamma' H}\right\}$$

taking natural logarithms of both sides:-

$$b\gamma_w \phi_y = \ln\left\{A\left(\frac{B}{D}\right)C + E\right\}$$

(In which, A, B, C, D, E are the appropriately bracketed terms from the above).

(As a check on this equation take $h_o = H$. This implies no potential gradient, i.e. $\phi_y = H$ regardless of y .

Since:-

$$B = 0$$

we have,

$$b\gamma_w \phi_y = \ln \left(e^{b\gamma H} \cdot e^{-b\gamma' H} \right)$$

$$= \ln \left(e^{b\gamma_w H} \right)$$

$$= b\gamma_w H.$$

As a further check it can be seen that potentials of h_o and H are yielded if y is set to zero or H respectively. In the limit when the term b falls to zero this equation should yield the same solution as for the case with a constant permeability (i.e. not dependent on effective stress). This can be proved by considering the limit to which the equation tends as $b \rightarrow o$, but in the present case, is only demonstrated numerically. For $b = 10^{-3}$ the results differ from the constant permeability case by less than 2.5%; for $b = 10^{-4}$ the results are indistinguishable.

Diagrams showing the variation of pore water pressure with depth for a range of values of b and four separate case of underdrainage ratio are given in Figures 2.6 and 2.7. These show a general similarity to the pore water pressure profiles where the permeability is an exponential function of elevation with, if anything, a more marked pore water pressure gradient close to the base of the stratum. This results in the pore water pressure profile following the hydrostatic line to even greater depths than in the other cases.

It is, however, more orthodox to quote the depth or increase in effective stress corresponding to an order of magnitude permeability change rather than use a parameter such as b., since the physical meaning of this depth is more readily comprehended. In Figure 2.8 this relationship is given graphically, but in approximate terms the following table may be used:-

Table 2.1. - Relationship Between Parameter "b" and the Depth or Increase in Effective Stress for an Order of Magnitude Change in Permeability

b	Depth for 10x change in k *or* Effective stress for 10x change in k
	$\ln k = a + by$ or $\ln k = a + b.\sigma'$
1.0	2.3
0.5	4.6
0.2	11.5
0.1	23.0
0.05	46.0
0.02	115.0
0.01	230.0
0.005	460.0
0.002	1150.0
0.001	2300.0

2.4. Horizontal Seepage in a Soil Layer in Which the Permeability is a Function of Effective Stress

The solution to this problem has been presented by Walbancke (1976) and is developed here only to provide a consistent picture - the equations are used as a test for the finite element model. Taking once again the same logarithmic law relating effective stress and permeability:-

$$k(y) = ae^{-b\sigma'}$$

We have seepage through any horizontal section constant and equal to q where:-

$$q = k(y)\frac{d\phi}{dx} = ae^{-b\sigma'}\frac{d\phi}{dx}$$

since $\sigma' = \sigma - \phi_x \gamma_w$ when the datum for potentials runs through the section considered, then:-

$$q = ae^{-b\sigma + b\gamma_w \phi_x}\frac{d\phi}{dx}$$

$$\frac{q}{ae^{-b\sigma}}dx = \frac{e^{b\gamma_w \phi_x}}{b\gamma_w} + c$$

which on integration yields:-

$$\frac{qx}{ae^{-b\sigma}} = \frac{e^{b\gamma_w \phi_x}}{b\gamma_w} + c$$

Thus constant of integration c is found from the boundary condition $x = 0$, $\phi_x = \phi_0$ to be:-

$$c = \frac{-e^{b\gamma_w \phi_0}}{b\gamma_w}$$

so that when the other boundary condition $x = L$, $\phi_x = \phi_L$ is inserted we find q to be:-

$$q = \frac{ae^{-b\sigma}}{b\gamma_w}\left(e^{b\phi_L \gamma_w} - e^{b\phi_0 \gamma_w}\right)$$

Reinserting both c and q in the basic formula and re-arranging we obtain:-

$$\phi_x = \frac{1}{b\gamma_w} \ln\left[\left(e^{b\gamma_w\phi_L} - e^{b\gamma_w\phi_o}\right)\frac{x}{L} + e^{b\phi_o\gamma_w}\right]$$

Not surprisingly the value of total stress σ has disappeared - this is yet another instance of the *magnitude* parameters (a & σ) being irrelevant to the solution which is governed by the *form* parameters (b & γ_w).

This equation has been solved for a variety of b parameters for comparison with the finite element model (Test 2. Section 3.9).

The ratio of the seepage quantity q for these effective stress permeability conditions to that for constant permeability conditions is:-

$$r_\phi^* = \frac{ae^{-b\sigma}}{b\gamma_w}\left(e^{b\phi_L\gamma_w} - e^{b\phi_o\gamma_w}\right) \cdot \frac{1}{k\,(\phi_L - \phi_o)}$$

Which if the homogenous permeability k is taken to be the "upstream" permeability $ae^{-b(\sigma - \phi_o\gamma_w)}$, is found to be:-

$$r_\phi = \left(e^{b\gamma_w(\phi_L - \phi_o)} - 1\right) \cdot \frac{1}{b\gamma_w(\phi_L - \phi_o)}$$

* See p.40.

2.5. *Spherically Symmetric Seepage in a Soil with Effective Stress Dependent Permeability*

The measurement of soil permeability in constant head, in situ permeability tests depends on the seepage at large times tending towards the steady seepage value, which for a spherical piezometer of radius R in soil of constant permeability k is:-

$$q = 4\pi R k (\phi_p - \phi_o)$$

in which ϕ_o is the original (uniform) potential in the soil and ϕ_p is the potential in the piezometer cavity. A substantial body of literature on this sort of test, and the theoretical background to it, exists (e.g. Gibson, 1963 and 1966; Wilkinson, 1968; Bishop & Al Dahir, 1970) but an important effect, that of the dependence of permeability on effective stress, is relatively unexplored.

Taking the same effective stress law as previously*, and making the simplifying assumption that we are in a constant total stress field, we have from considerations of continuity:-

$$q = -4\pi r^2 a e^{-b(\sigma - \phi\gamma_w)} \frac{d\phi}{dr}$$ +

which on rearrangement and integration yields:-

$$\frac{q}{4\pi r a} = \frac{e^{-b(\sigma - \phi\gamma_w)}}{b\gamma_w} + c$$

The arbitrary constant of integration may be obtained on substitution of the extreme boundary condition $r = \infty$, $\phi = \phi_o$

and thus:-

$$q = \frac{4\pi a r}{b\gamma_w} \left(e^{-b(\sigma - \phi\gamma_w)} - e^{-b(\sigma - \phi_o\gamma_w)} \right)$$

* Log law

\+ Datum at centre of piezometer.

At the other extreme we have at the surface of the piezometer cavity r = R, $\phi = \phi_0$ hence:-

$$q = \frac{4\pi a R}{b\gamma_w} \cdot \left(e^{-b(\sigma - \phi_p \gamma_w)} - e^{-b(\sigma - \phi_0 \gamma_w)} \right)$$

Reinserting this in the basic formula and manipulating we can obtain:-

$$\phi = \frac{1}{b\gamma_w} \left\{ \ln \left[\frac{R}{r} \left(e^{b\phi_p \gamma_w} - e^{b\phi_0 \gamma_w} \right) \right] + e^{b\phi_0 \gamma_w} \right\}$$

which can be compared with the steady flow in a piezometer of constant permeability

$$\phi = \phi_0 + (\phi_p - \phi_0) \frac{R}{r}$$

Take now the ratio of flow rates given by the two solutions:-

$$r_Q = \frac{q \text{ (effective stress dep. permeability)}}{q \text{ (constant permeability)}}$$

Assuming the constant permeability to be that of the soil at its in situ effective stress before perturbation of head at the piezometer is applied, we find:-

$$r_Q = \frac{4\pi R \left(k_R - k_\infty \right)}{4\pi R \, k_\infty \, (\phi_p - \phi_0) \, b\gamma_w}$$

$$= \left(e^{b\gamma_w (\phi_p - \phi_0)} - 1 \right) \cdot \frac{1}{b\gamma_w (\phi_p - \phi_0)}.$$

This is identical to the previously defined r_Q for horizontal flow.

2.6. Radially Symmetric Seepage in a Soil with Effective Stress Dependent Permeability

Common in the solution of well problems in confined aquifers is the situation of radially symmetric seepage.

Taking again:-

$$q = -2\pi r\, a e^{-b(\sigma - \phi\gamma_w)} \frac{d\phi}{dr}$$

and rearranging, we have (following integration):-

$$\frac{q}{2\pi a} \ln r = \frac{-e^{-b(\sigma-\phi\gamma_w)}}{b\gamma_w} + c$$

We find at the well surface $\phi = \phi_w$, $r = R$ and hence:-

$$c = \frac{q}{2\pi a} \ln R + \frac{1}{b\gamma_w} e^{-b(\sigma - \phi_w\gamma_w)}$$

thus:-

$$\frac{q}{2\pi a} = \frac{1}{b\gamma_w \ln \frac{r}{R}} \left(e^{-b(\sigma-\phi_w\gamma_w)} - e^{-b(\sigma-\phi\gamma_w)} \right)$$

A sensible other boundary condition $r = \infty$, $\phi = \phi_o$ is not possible, so we have to introduce *radius of influence* R_I at which the potential is equal to the basic field potential ϕ_o - this leads to a value

for q of:-

$$q = \frac{2\pi a}{b\gamma_w \ln R_I/R} \left(e^{-b(\sigma - \phi_w \gamma_w)} - e^{-b(\sigma - \phi_o \gamma_w)} \right)$$

Comparing this to the solution for a constant potential which is:-

$$q = \frac{2\pi k (\phi_w - \phi_o)}{\ln R_I/R} \quad \text{in which we will take } k = a e^{-b(\sigma - \phi_o \gamma}$$

the ratio r_Q previously defined becomes:-

$$r_Q = \left(e^{b\gamma_w (\phi_w - \phi_o)} - 1 \right) \cdot \frac{1}{b\gamma_w (\phi_w - \phi_o)}$$

or a value identical to that applicable for spherical flow and for the case of horizontal flow.

The potential at any radius r between R and R_I is given by:-

$$\phi = \frac{1}{b\gamma_w} \ln \left\{ e^{b\phi_w \gamma_w} - \frac{\ln \frac{r}{R}}{\ln \frac{R_I}{R}} \left(e^{b\phi_w \gamma_w} - e^{b\phi_o \gamma_w} \right) \right\}$$

This solution, which while it is not of immediate direct relevance to this thesis, is included as it completes the family of simple solutions and shows that the factor r_Q which is the ratio of flow rates for the problem couched in terms of effective stress permeability to that for the problem solved with a constant permeability is the same for three different situations. This reflects a fundamental property of seepage with effective stress dependent permeability in a constant total stress field.

2.7. *An Alternative Treatment for "One Dimensional" Seepage in Soil Layers with Effective Stress Permeability*

Walbancke (1976) has suggested two possible forms for the expression relating permeability to effective stress, namely:-

$$k = ae^{-b\sigma'}$$

and

$$k = a\sigma'^{(-b)}$$

(expressed in the present author's nomenclature)

corresponding respectively to the situations where the voids ratio and effective stress are assumed to have a linear or logarithmic relationship. Using the first equation it is possible to derive solutions to all the major "one dimensional" seepage problems, but the second form of the equation poses difficulties in integration. In order to obtain solutions for comparison between the two equations, a numerical method was used. This was first tested on the spatially varying permeability and the former of the two effective stress permeability laws (in most cases with excellent results when compared to the purely analytical solutions above) before being applied as intended.

The technique is simply to divide the domain into n intervals (these need not be equal but have been taken to be so). An initial flow rate together with a simple, generally linear, initial distribution of potentials are assumed, and on the basis of which it is possible to evaluate the total stress, potential, pore water pressure, effective stress and hence permeability at the centre of each interval. Making the further assumption that this permeability is constant over the interval, Darcy's Law can be invoked, and working through the intervals sequentially from one side of the domain to the other, a distribution of potentials at the interval contacts can be found, resulting in a misclosure in the potentials at the end. The potential distribution is scaled to eliminate the misclosure, and a new flow rate obtained by sampling the corrected potentials at one

point within the domain. A number of repetitions of the process are necessary to reduce the final misclosure to acceptable limits.

When using very strongly effective stress dependent permeability laws the number of intervals must be increased to conserve accuracy and an increasing number of iterations is needed to obtain a satisfactory solution.

It is probably more "cost-effective" to divide the region into non-equal intervals, with the finest subdivision where the potentials vary most rapidly, that is, close to the boundary where the lower of the two boundary potentials is applied, but this has not been explored in the present work. In view of this, the absolute limits of application of this technique have probably not been found. Failure to converge appears to be confined to the "fiercest" effective stress permeability relationships, and to cases for which no field analogues have been discovered.

The convergence problems result mainly from the simple scaling process where misclosure in the potential at one end of the problem is eliminated.

A simple computer program capable of dealing with a generic effective stress/permeability relationship of the following form* was written:-

$$k = k_0 \left(a_1 + a_2 x + a_3 x^2 + a_4 e^{-a_5 \sigma'} + a_6 \sigma'^{-a_7}\right)$$

(in which a_i terms can be set to zero to yield a subset of this general expression). All the examples discussed below were computed with its aid.

---

*In principle any "law" could be nominated.

Since this technique is only of limited general applicability and was only developed to:-

(a) provide a limited range of solutions for the "power law" effective stress permeability case equivalent to those obtained analytically for the "logarithmic law" against which the finite element solution could be appraised

and

(b) enable the two forms of the effective stress permeability relationship to be compared for simple cases at a comparatively low cost in computer resources

it was felt that the effort involved in incorporating a more efficient or more rapidly convergent numerical scheme would not be worthwhile.

2.8 Comparison of Analytical and Numerical Results.

The results of this exercise can be seen in Figures 2.16 to 2.19 and are as follows:-

Figure 2.16 (upper half) "Logarithmic" law, comparison of analytical and simple numerical solutions for a 10 m thick fully underdrained soil layer. (Vertical flow).

Figure 2.17 (upper half) "Logarithmic" law, comparison as above but for a 10 m long flow channel with purely horizontal flow.

In both of these cases excellent agreement was obtained and this allowed a measure of reliance to be placed on the later results using the "power law".

In Figures 2.16 to 2.19 inclusive both the "logarithmic law" and the "power law" are used. These cases are respectively vertical seepage in a wholly underdrained layer, horizontal seepage, axi-symmetric seepage and spherically symmetric seepage.

2.9. *Computation of the Permeability Variation from Piezometer Data*

Given a set of pore water pressure data, or piezometer readings, and an assessment of the total stress at each piezometer, it is possible to fit one of the standard curves and thus find the parameters that describe the effective stress/permeability dependency. It is also necessary to select a model for this, either the "logarithmic" or "power law" models of this thesis, or any other; but these do seem to yield largely similar results and the choice between them is probably of personal preference. In order to achieve any degree of accuracy from this procedure, the boundary conditions or potentials must be known to a fair degree of accuracy. Furthermore, the curve fitting procedure will only yield the *relative* permeability values (or in the context of the present work, the b parameter) and an independent fix on a flow rate is necessary to pin point the *absolute* permeability values.

The field data is comparatively scanty since ideally a flat site with four or five piezometers at different depths are required. In addition, further evidence that equilibration is complete must be provided and therefore such pore pressure measurements as there are in the London area in the London Clay must be discounted.

A site that does meet the basic criteria is the University of Kent site, investigated in detail after the collapse of a disused railway tunnel beneath the site led to structural distress at the surface. Underdrainage of the London Clay at this site is due to low pore pressures in the underlying sandy Oldhaven Beds which themselves outcrop within a few kilometres of the University of Kent campus. This data has already been examined for the influence of effective stress dependent permeability by Walbancke (1976).

Following this lead by Walbancke, Truscott (1977) examined piezometer records in the inclined core of the Tarbela dam. This analysis used the steady pore pressures which developed after the reservoir was filled (on two separate occasions) but is complicated by being neither purely vertical nor horizontal flow with total stresses

varying across the core. Truscott concluded that the observed pore water pressure distribution could best be accounted for by invoking an effective stress dependent permeability.

There is also some data from underdrained soil slopes that supports the general concept, notably at Cow Green (examined for varying permeability by Sweeney, 1970, and again by Walbancke, 1976) and from the coastal cliffs at Herne Bay (Bayley, 1971, Bromhead, 1972). However, there is doubt that the Herne Bay pore pressures had equilibrated after the formation of the cliffs by coastal erosion, which was rapid until a sea wall was built, or from the regrading which was needed to stabilise the slopes behind the sea wall. As at the University of Kent, the London Clay at Herne Bay is underdrained by the Oldhaven Beds, these outcropping at sea level near by.

The landslips at Folkestone Warren in the Chalk and Gault are also underdrained by a sandy layer (the Folkestone Beds) but the evidence there (Hutchinson *et* al. 1980) is if anything the opposite with some potentials below sea level being recorded. This is attributed to lack of time for pore pressure equilibration following sliding.

Where the London Clay derived colluvium from the slopes of the Downs Hill, Maldon, Essex (Ellis-Jones, 1978) overrides an alluvial gravel of the River Blackwater several piezometers indicate a dramatic decrease in pore water pressure in the basal few metres, accountable for by the concept of an effective stress dependent permeability.

Table 2.2. Some Typical Back Analysed "b" Parameters

Case	Soil	b.
University of Kent	London Clay	ca 0.004-0.005
Herne Bay	London Clay	ca 0.004-0.010
Maldon	London Clay derived colluvium	ca 0.03
Tarbela	Rolled earthfill	ca 0.002-0.030
Cow Green	Till	ca 0.002

2.10. *Computation of the Permeability Variation from Flow Tests*

Where a soil has a degree of effective stress dependency in its permeability, constant head tests will reflect this by yielding a non-linear flow rate to head difference ratio depending on the values of head difference applied. In a constant head in situ permeability test of the type commonly performed, the *apparent* permeability will be larger for a head increment (causing swelling) than for a head decrement (causing consolidation). The term "apparent" is used for this effect since we might compute this from the (usually extrapolated) steady state flow rate q_∞ and a piezometer intake factor F as:-

$$k_{app} = q_\infty / F \Delta\phi$$

Thus for a soil with the logarithmic permeability law we might have:-

$$k_{app} = \frac{a\left(e^{-b(\sigma-\phi_p\gamma_w)} - e^{-b(\sigma-\phi_o\gamma_w)}\right)}{b\gamma_w(\phi_p-\phi_o)}$$

Whereas the "true" k at the effective stress applicable to the piezometer radius would be:-

$$k_f = a e^{-b(\sigma-\phi_p\gamma_w)}$$

Thus the ratio of k's, would be:-

$$\frac{k_{app}}{k_f} = \frac{1-e^{-b\gamma_w\Delta\phi}}{b\gamma_w\Delta\phi}$$

Now suppose two tests were carried out with head differences $\Delta\phi_1$ and $\Delta\phi_2$, then:-

$$\left(\frac{k_{app}}{k_f}\right)_1 = \frac{1-e^{-b\gamma_w\Delta\phi_1}}{b\gamma_w\Delta\phi_1} \qquad \left(\frac{k_{app}}{k_f}\right)_2 = \frac{1-e^{-b\gamma_w\Delta\phi_2}}{b\gamma_w\Delta\phi_2}$$

but $$\frac{k_{f1}}{k_{f2}} = e^{b\gamma_w(\Delta\phi_1 - \Delta\phi_2)}$$

$$\therefore \frac{k_{app1}}{k_{app2}} = \frac{\Delta\phi_2}{\Delta\phi_1}\left(\frac{1 - e^{-b\gamma_w \Delta\phi_1}}{1 - e^{-b\gamma_w \Delta\phi_2}}\right) e^{-b\gamma_w(\Delta\phi_1 - \Delta\phi_2)}$$

from which first of all a b value can be obtained, then a value for the real permeability for one of the tests and thence a value for "a", the permeability for zero-effective stress.

The foregoing is not a suggestion that the a and b parameters be extracted systematically for each test. It does, however, indicate that the apparent permeability-effective stress relationship yielded by testing at different heads is likely to be incorrect. To obtain the correct relationship demands *a priori* knowledge of the form of the relationship and a more involved analysis.

This is expressed graphically in Figure 2.14.

It also appears that none of this complexity arises if the differing effective stresses at the piezometer are the result of a changed total stress state with the hydraulic conditions kept constant.

2.11. Implications

In the foregoing sections, Walbancke's (1976) work has been extended both in the number of solutions and in their range of applicability. However, the most important aspect of this work lies in the shape of the equilibrium distribution of potential through the soil in question. This, even for the most simple case of horizontal seepage, is not the straight line predicted by elementary, *constant permeability*, theory

but is bowed. It appears similar to an isochrone which may be found at some intermediate stage during a consolidation process.* Therefore, it may not be possible, on the basis of pore water pressure measurements in piezometers placed at various positions in a soil layer and using the envelope of pore water pressures given by those piezometers to state conclusively whether or not consolidation is complete. (The term consolidation as used here includes transient swelling). Thus, some additional measurement, such as the rate of settlement, or the rate of pore water pressure dissipation at the piezometers may need to be made to be conclusive. The time and degree of precision needed for this to be done with any degree of accuracy may be very great. For example, a piezometer at Folkestone Warren (Hutchinson *et al.* 1980) observed regularly over some six years showed a rising trend of 0.15m head per year. The range of observations in any one year, even discounting probable reading errors, was of this order, but distributed about the trend line.

Furthermore, we need to revise our expectations of the efficacy of drainage layers in fills since given even a modest degree of effective stress dependent permeability in the fill, the drainage layers cannot totally dissipate all the pore water pressures. Factors of safety, and the increase of these with time, may well be less than computed by simple theory. This effect has been investigated in some detail by Walbancke, but it is as well to repeat the observation (which has enormous practical significance) here.

An additional factor not previously discussed in any depth is the influence of the shape of the final steady state equipotential distribution on both the amount of, and rate of, consolidation. It is demonstrated later on in this thesis, that a degree of effective stress dependency in the permeability (and for that matter in the compressibility) has little effect on the rate

---

*Figure 1 of Skempton & Henkel (1961) may well be a final steady state pore pressure distribution but in that paper, the pore water pressures are considered to be not fully equilibrated. The conclusions of Wilson & Grace (1942) may also need revision in the light of this.

at which the average dissipation of pore water pressures takes place. However, the rate of dissipation of pore water pressure at a given point may be radically different from that predicted by simple theory, and this may appear confusing at first sight when piezometer records are examined. It is also evident that the total amount of settlement will be less than that predicted by the simple theory, as less of the "excess" pore water pressure dissipates, and the corresponding effective stress increments are smaller than predicted by simple theory.

Provided that we are confident that all transient processes are complete, it is possible to use piezometer measurements of pore water pressure to calculate permeability/effective stress relationships. However, the behaviour of the pore water pressure/"depth" profile is dominated by the magnitude of the lower of the two boundary potentials, and this needs to be measured (or estimated) to a high degree of accuracy for the results of this procedure to be entirely valid. Furthermore, the results of this type of study will give *relative* rather than *absolute* permeability variations unless some other parameter, e.g. a flow rate, is also determined.

As an alternative, the flow rates measured under different potential differences may yield information as to the effective stress/permeability relationship, provided that a procedure similar to that in Section 2.10 is followed. For example, by taking several permeability measurements at different heads in an in situ constant head test it may be possible to deduce realistic parameters for the dependency of permeability on effective stress. It will usually be found that single tests on piezometers at different depths where the variation of effective stress from one piezometer to another results from the different total stresses applied is easier to analyse. In any case it may be impossible to fully define the permeability/effective stress relationship owing to the difficulty in ensuring that ambient ground water pressure and total stress conditions are adequately known for each piezometer at the outset.

Finally, the alternative (and simple) numerical model has shown that it can yield extremely accurate results in most cases in which it has been used. The convergence problems experienced with it have all been in ranges of effective stress dependency thought to be of academic interest only, and its use in producing solutions for effective stress/ permeability relationships for which no closed form analytical solution exists is unimpaired.

2.12. *The Influence of Problem Scale on the One Dimensional Studies*

The examples presented in this Chapter, notably Figures 2.2 to 2.7 & 2.16, all deal with a 10m column of soil. This has been done so that the various factors can be compared on a simple standard basis. However this presentation obscures the very important fact that the distribution of potential, and hence of pore pressure, is highly dependent on scale; that is, for a given relationship between permeability and effective stress, the pore pressure distribution in a physically large problem will differ from the constant uniform permeability solution by a greater relative amount than in a physically small problem.

Take for example horizontal seepage in a constant total stress field, (seepage through a dam core, for instance). The solution of Section 2.4 shows that the solution for pore pressures is independent of the total stress applied, but is highly dependent on the potential drop across the section, which gives the *change* in effective stress and hence of permeability which in turn causes the pore pressure distribution to adopt the shape it does. The horizontal seepage case can therefore be scaled on the basis of the b parameter multiplied by the head or potential drop, $\Delta\phi$.

When not only does the pore pressure change in the direction of seepage, but total stresses also increase in that direction, the effective stress increase, and hence the permeability decrease, will lead to an effect of still greater magnitude. Thus the scaling factor to be applied in the underdrained cases is the product of the parameter b, the thickness of the stratum, and the underdrainage ratio D_u (this latter parameter yielding in an indirect way the potential drop across the stratum).

It is therefore possible, in a thick underdrained stratum, to have a significant bow on the pore pressure / depth plot for values of the b parameter much smaller than those annotating Figures 2.2 to 2.16, because the increased scale of the problem means that the necessary effective stress changes can be obtained.

This scale effect is shown diagrammatically on Figures 2.20 & 2.21.

2.13. *The Engineering Significance of Effective Stress Dependent Permeability*

The fundamental significance of effective stress dependent permeability is that it causes pore water pressures to be higher, sometimes much higher, than when the permeability is uniform and constant*. A correct distribution of spatially varying, but effective stress independent permeabilities would, of course, yield the same result for the pore pressures, but whereas the analysis would be easier in this situation, one is faced with a complex problem of predicting the permeability values to use.

Furthermore, and as described above, the difference between the effective stress dependent and uniform constant permeability solutions will be greater with physically large problems than with small ones. The errors in pore pressure prediction with constant permeability solutions (e.g. flow net sketching) may give rise to errors in the prediction of both strength and stiffness, usually on the unsafe side. An additional effect may be to mislead the observer into thinking that a particular field situation is not fully equilibrated when in fact it is: this in turn may give rise to faulty predictions of future consolidation settlement &/or gain in strength. These points will be illustrated by reference to case records of three different types of field problem; *viz:*

Steady seepage through dam cores
Steady seepage in underdrained natural slopes
Steady downwards seepage in underdrained soil strata

The first example is based on the work of Truscott (1977) who considers in his thesis the behaviour of embankment dams of the Tarbela scheme. He follows piezometer records through two reservoir impounding cycles, and finds a fairly rapid equilibration of the pore pressures since the core material used had a high coefficient of swelling. This circumstance also led to the construction pore pressures being largely dissipated before impounding began, and the swelling behaviour observed was from a no flow -

---

**Footnote: Subject to the proviso that flow is taking place. No flow pore pressures are the same in both cases.*

no pore water pressure case to a through flow case (as illustrated diagrammatically in Figure 4.6a). The pore pressures thus swelled *through* the constant uniform permeability solution, and did so on at least two separate occasions, as the reservoir had to be repeatedly filled and emptied as a result of the severe spillway, stilling basin and tunnel erosion. A selection of Truscott's results (the steady seepage pore pressures at two important cross sections measured during the 1975 impounding) is given in Figure 2.22.

The second example is based on data provided by Vaughan (1980), following Vaughan *et al.*(1970). In this case the steady seepage pore pressures measured in the core of the Balderhead Dam show distributions characteristic of flow with effective stress dependent permeability. This information is summarised in Figure 2.23.

In neither of these cases is there any reason to believe that the core had intrinsically different permeabilities in its upstream and downstream sides. An effective stress dependent component in the permeability is a highly probable explanation of these observations.

Miscalculation of these pore water pressures could lead to a serious overestimate of the stability of the shoulders of the dam. In the case of the Tarbela embankment where the core slopes upstream, these pore pressures could have an important bearing on the stability of the upstream shoulder during rapid draw down (the undrained unloading decrement of pore pressure resulting from the removal of the water load only partly removing the steady seepage pore pressures).

Seepage in natural slopes with underdrainage will also be illustrated by two examples: the slopes of Till at the site of the Cow Green Dam (Sweeney 1970,Vaughan & Walbancke 1973, Walbancke 1976), and of London Clay at Herne Bay((Bayley 1971, Ove Arup & Partners 1970,1971, Bromhead 1972,1978). The first of these is underdrained by a limestone with a connection to the river level in the Tees, and the latter by the Oldhaven Beds (a weak sandstone) in which the piezometric levels are controlled by sea level.

The Cow Green slope has been extensively described in the works cited, and Figure 2.24 is therefore included without further discussion as a

well documented site where the permeability decreases with depth. Unfortunately, the piezometers are not sufficiently numerous to make detailed analysis worthwhile, and it may well be that the permeability / depth realationship owes more to the genesis of the till than to effective stress dependency. The geographical and geological settings of the slope are such as to suggest that the pore pressures are fully equilibrated.

In contrast to Cow Green, the Herne Bay case is much more adequately instrumented. Piezometers were installed in boreholes at various depths through the whole thickness of the London Clay at four positions on each of six cross sections taken at right angles to the coastline (in one section there were only three locations). The groups of piezometers were numbered from 1 to 4 inclusive from the crest of the slope to its toe, and are shown diagrammatically in Figure 2.25. It was found that groups 3 & 4 were in some cases through landslip debris, and for simplicity, only groups 1 & 2 will be considered here.

(Figure 7.9 and the analyses which support it are in turn based on a further simplification of the idealisation in Figure 2.25 with the landslip debris removed from consideration entirely).

The pore pressures from the six "location 1" sites, and from five "location 2" sites is shown in Figure 2.26. To non-dimensionalise this data (the various sites have different overall thicknesses of London Clay, and the level of the Oldhaven Beds / London Clay interface dips across the site) the potential at each piezometer has been divided by the potential drop across the London Clay. This has been plotted as the abscissa: the ordinate is the elevation of the piezometer as a percentage of the thickness of the clay.The "SW-NE" diagonal on this plot is therefore the straight line joining zero pore pressure at the surface to the measured pore pressure in th Oldhaven Beds. Both groups of data are remarkably self consistent.

It appears that the piezometers at the slope crest indicate a largely (but perhaps not wholly) equilibrated pore pressure distribution with downwards seepage through the clay, and permeability reductions with depth. Those piezometers lower down the slope show that the pore pressures

contain a significant proportion of undrained unloading effects, with a tentative explanation of this given in Figure 2.26. The entire situation can be explained by the following:

a. The permeability decreases with depth,
b. Undrained unloading pore pressure reductions due to lateral stress relief are small, or absent, or have dissipated,
c. Undrained unloading pore pressure reductions due to vertical stress relief have partly dissipated,
d. Seepage in the landslip debris is generally similar to that in the undisturbed London Clay, but with a larger apparent magnitude of permeability change across the section (there are too few piezometers there to be conclusive).

Since the transition between the London Clay and the underlying Oldhaven Beds is characterised by a large number of frequent silty partings in the clay, an increase, rather than a decrease, in the intrinsic permeability is likely, and the observed pore pressures are best accounted for by invoking effective stress dependent permeability.

A correct assessment of the stability of these natural slopescould not be made without taking these pore pressures into account, and the future changes in stability will be similarly in error - for example the constant, uniform permeability solution predicts future decreases (or at the very least, lesser increases) in pore pressure when compared to the effective stress dependent permeability solution which correctly indicates pore pressure trends (Figure 7.9).

Finally, there is the underdrained soil layer. Excellent examples of this should be provided by the soils in the London Basin, under Venice and elsewhere. Unfortunately, the requisite piezometer records are either non-existant, inadequate or otherwise not available at the present time. Two cases where data is available are presented in Figure 2.27. This figure shows the piezometric levels at the University of Kent (an identical succession to that at Herne Bay) as presented and interpreted by Walbancke 1976; and in some London Clay deived colluvium at Maldon, Essex (Ellis-Jones 1978). It seems from the evidence provided in the source

documents that it is unlikely that these pore pressures are not fully equilibrated or that the permeability decreases significantly with depth due to intrinsic factors.

Such a pore pressure distribution as has been reported above could easily be ascribed to incomplete equilibration following underdrainage. This could lead to erroneous estimates of the likely amount of future settlement: the cost implications of this, say if flood defence measures were being contemplated, could be considerable. Additionally, in an *ab initio* assessment of the use of underdrainage as an alternative to preloading to strengthen the foundation before placing a fill, the use of the wrong seepage theory may lead to errors in the prediction of the ultimate settlements (conservative), and long term gain in strength (unsafe).

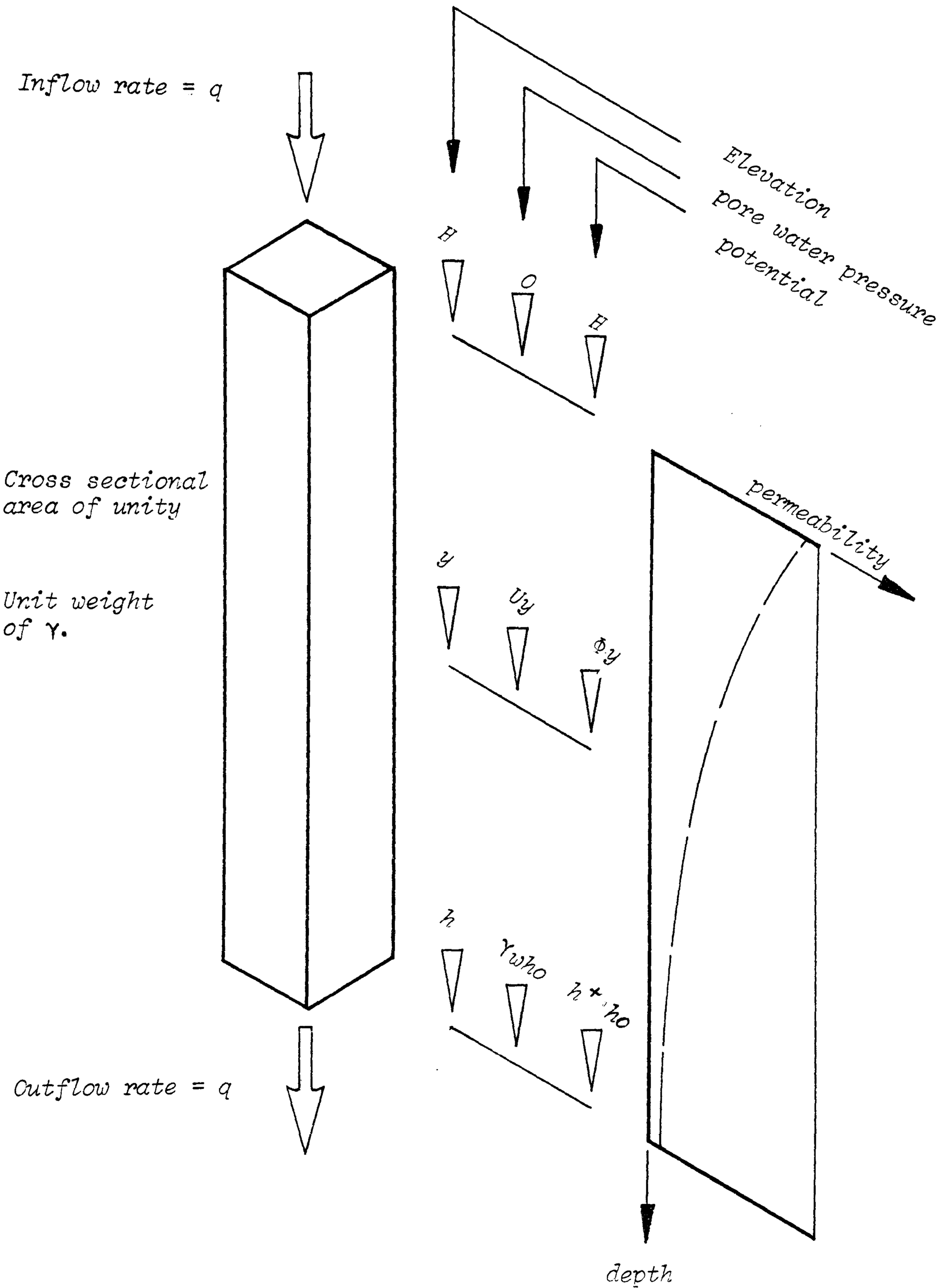


Figure 2.1. Key diagram: Gravity seepage in a partly underdrained soil layer.

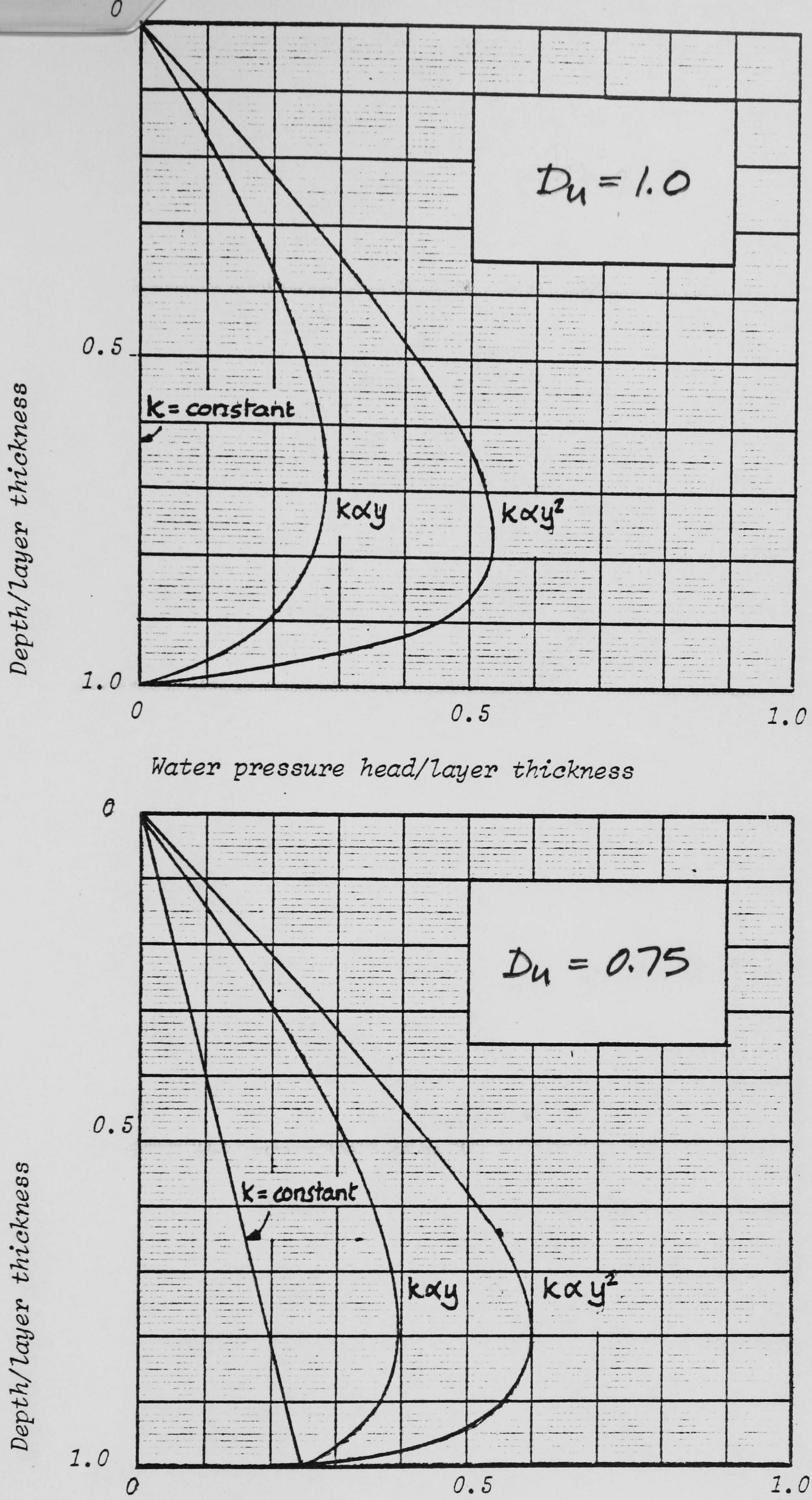


Figure 2.2. Pore water pressure-depth variation: strong underdrainage, polynomial permeability distribution.

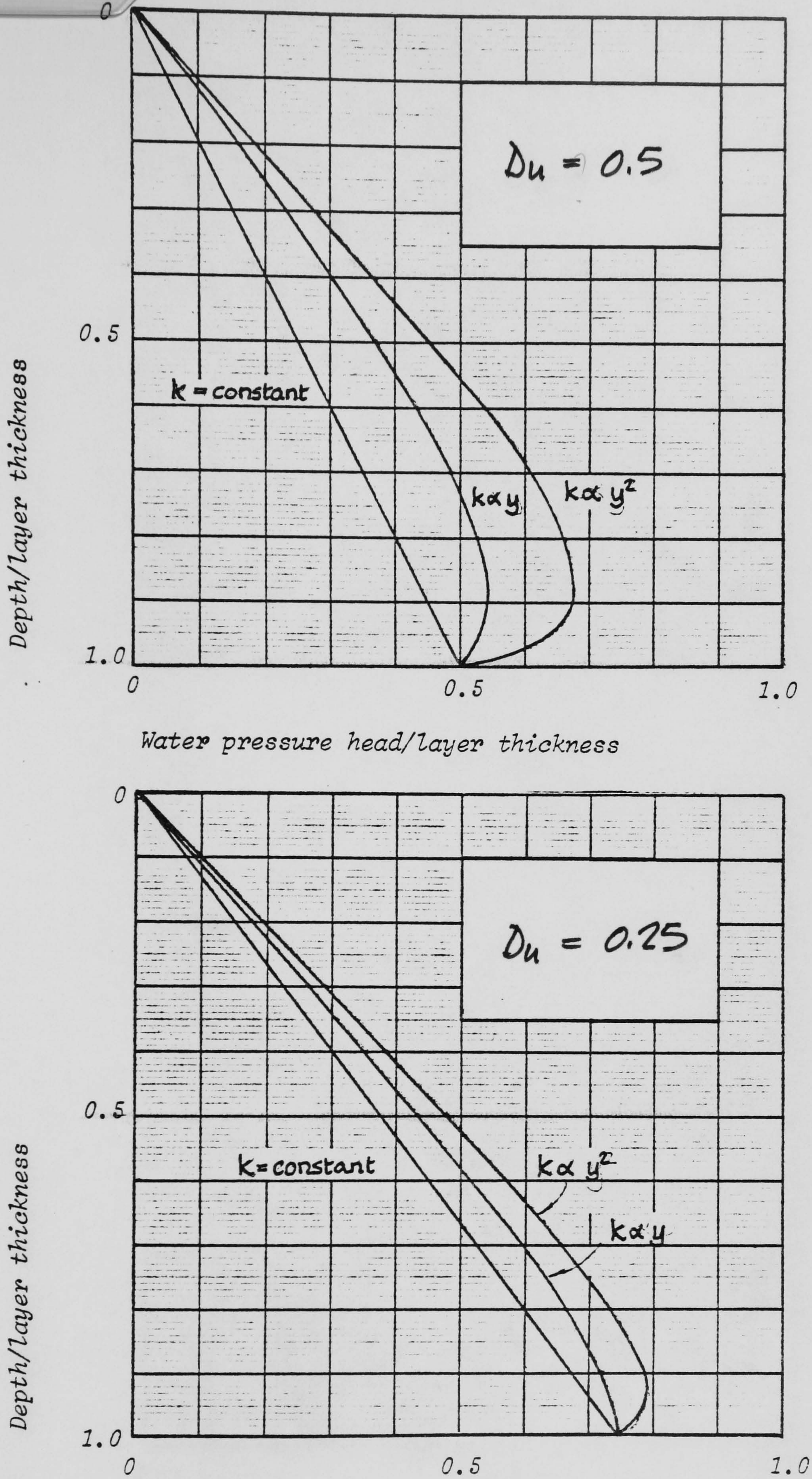


Figure 2.3. Pore water pressure-depth variation: weak underdrainage, polynomial permeability distribution.

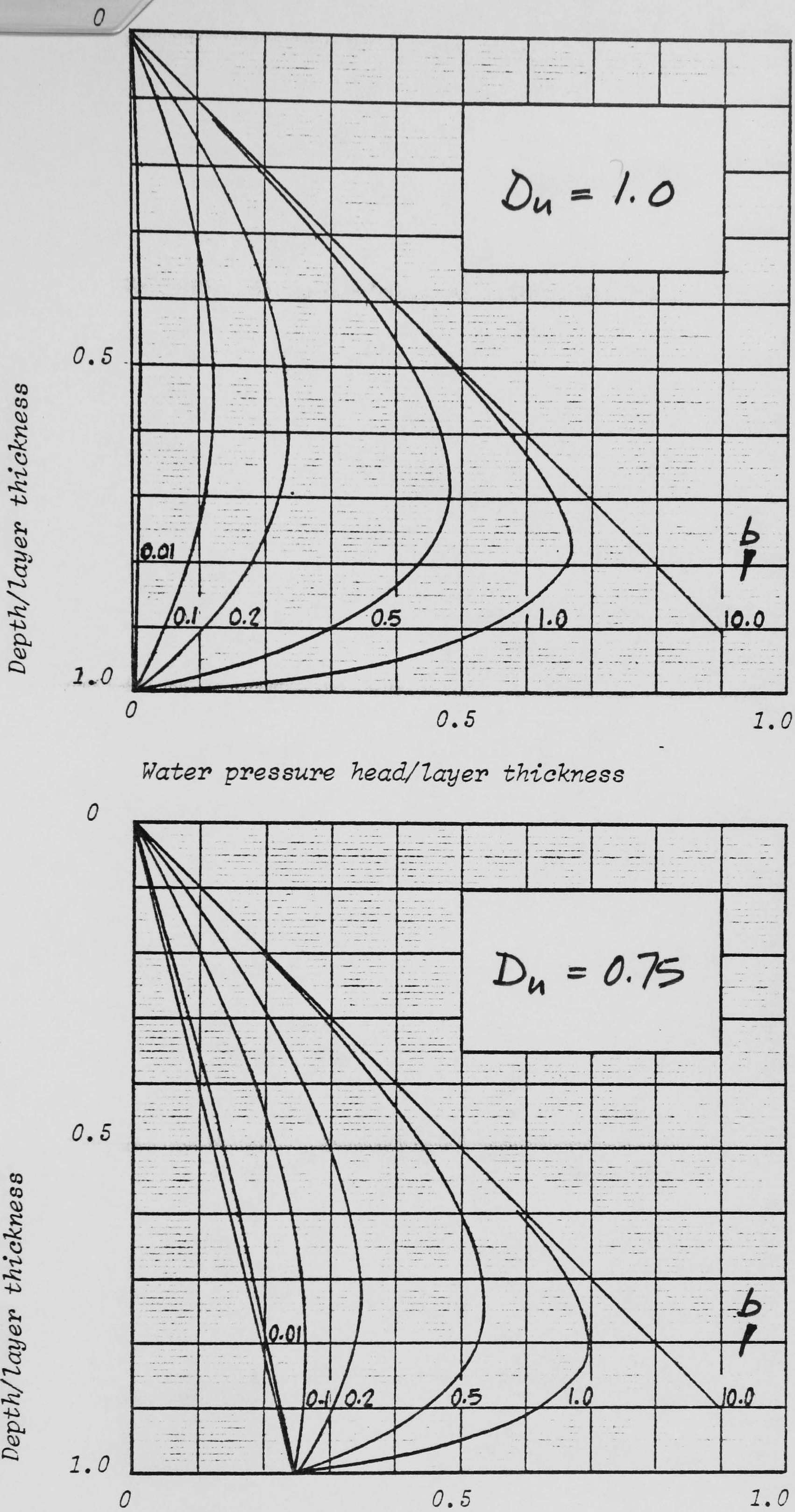
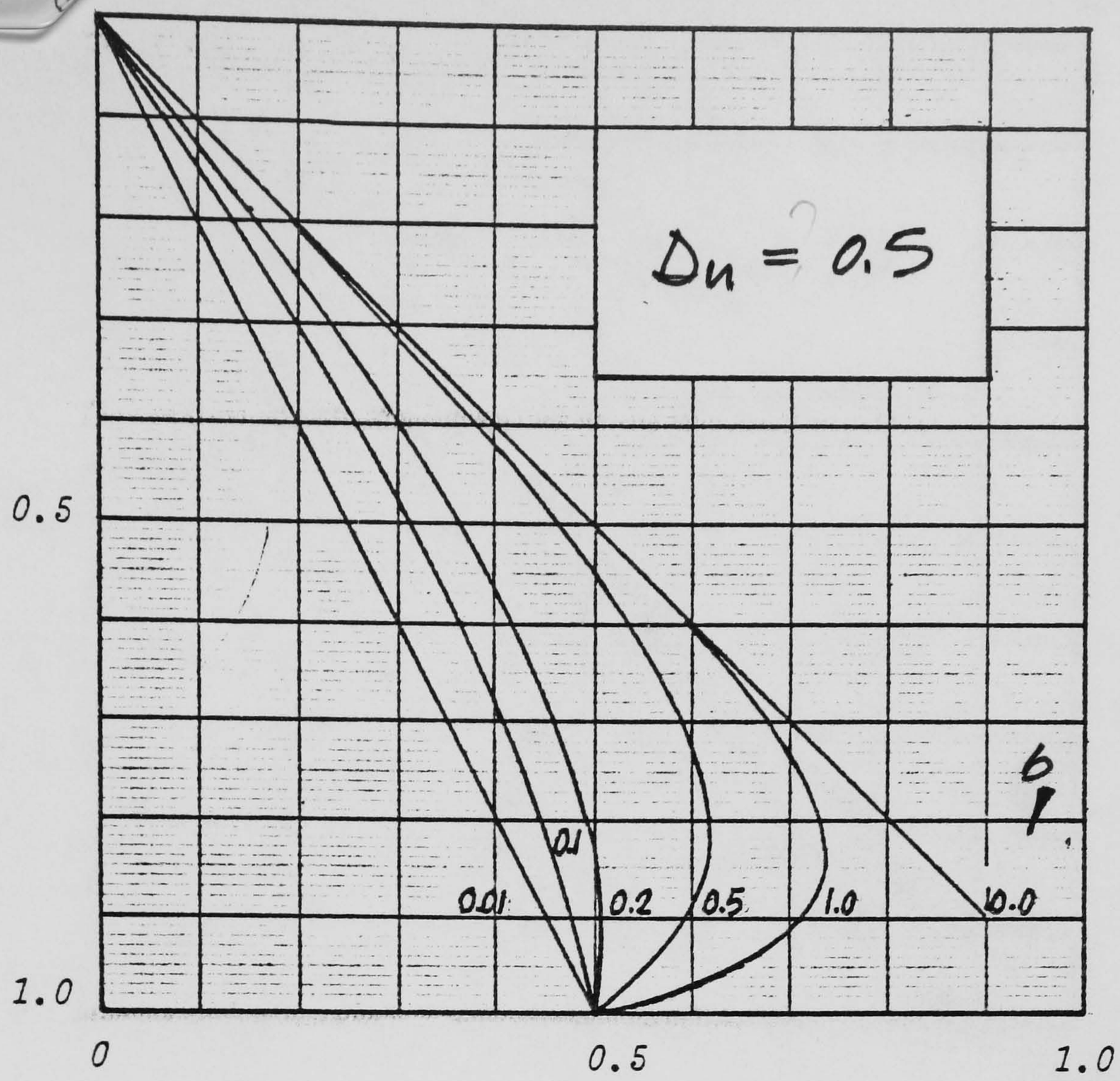


Figure 2.4. *Pore water pressure-depth variation: strong underdrainage, exponential permeability variation.*



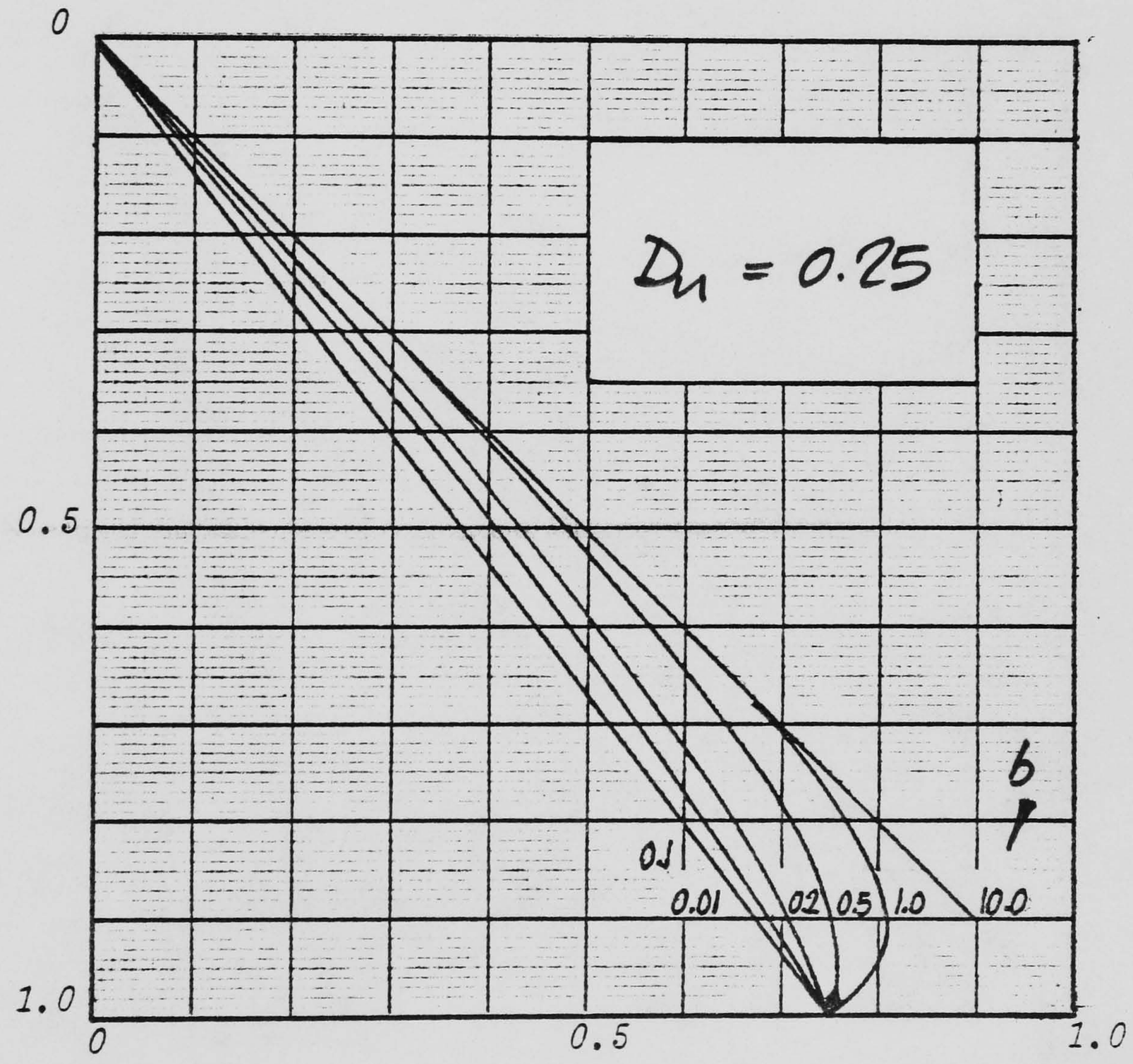


Figure 2.5. *Pore water pressure-depth variation: weak underdrainage, exponential permeability variation.*

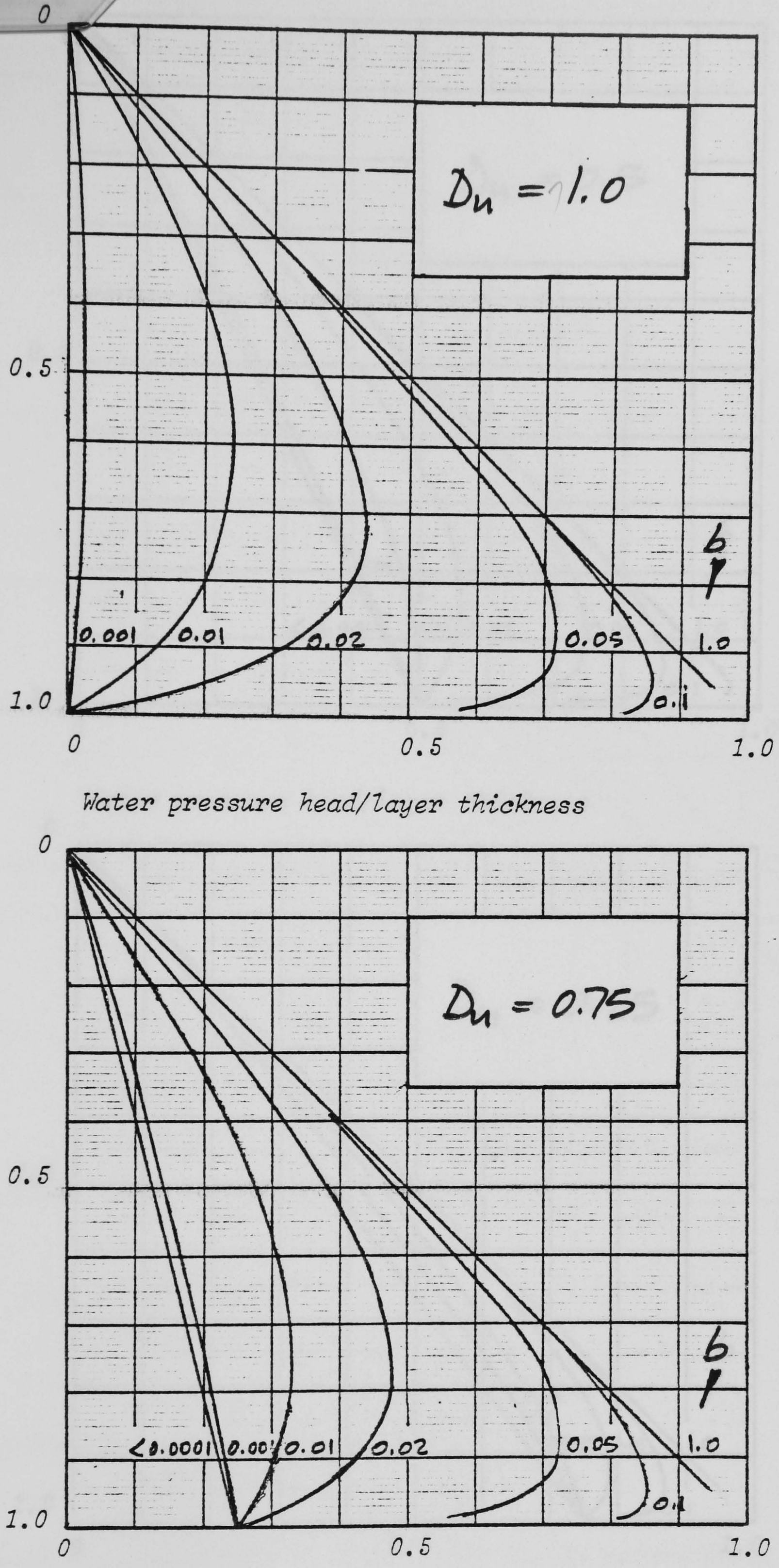


Figure 2.6. *Pore water pressure-depth variation: strong underdrainage*
Effective stress dependent permeability. (Log Law)

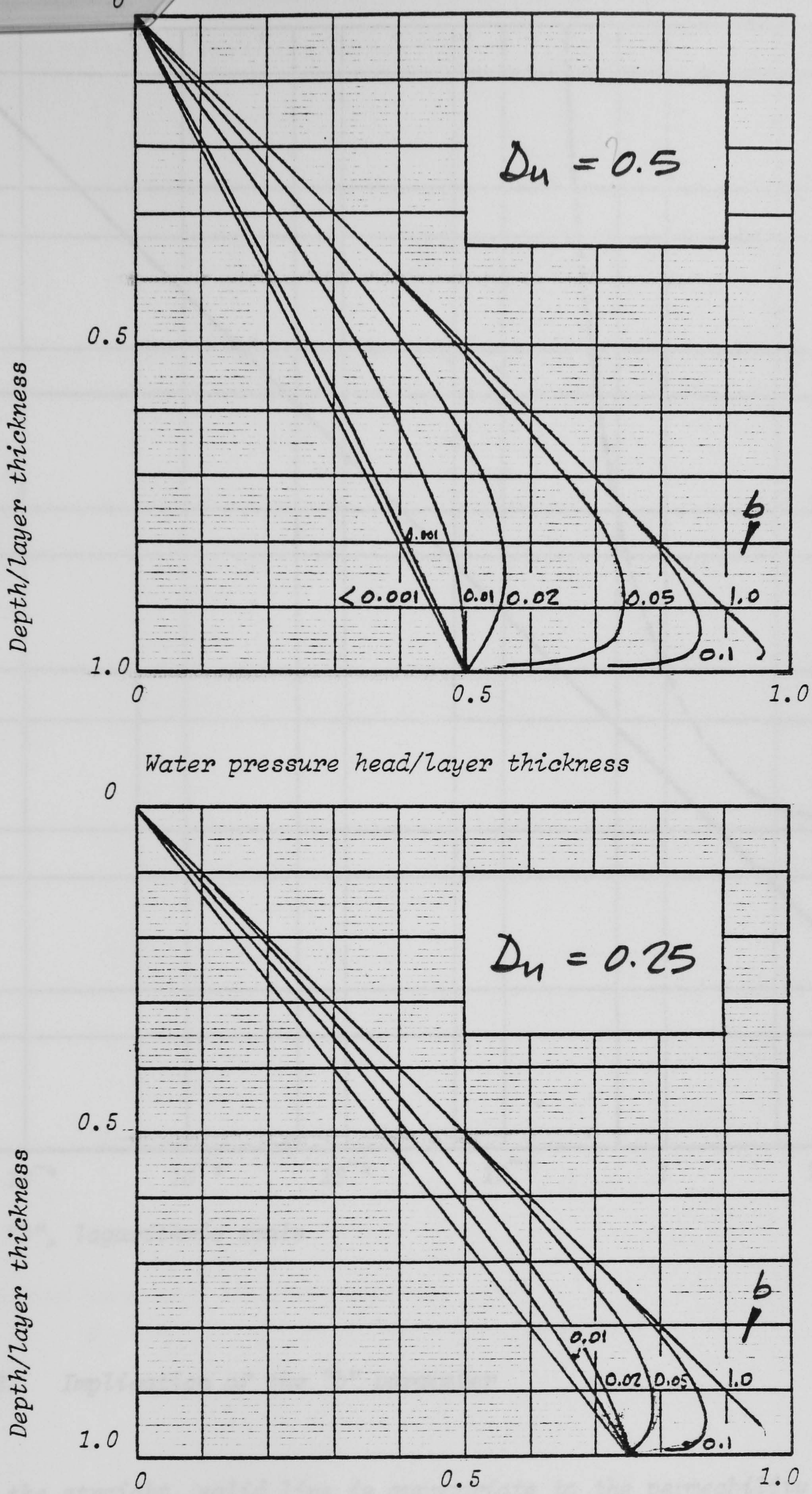


Figure 2.7. Pore water pressure-depth variation: weak underdrainage, effective stress dependent permeability. (Log Law).

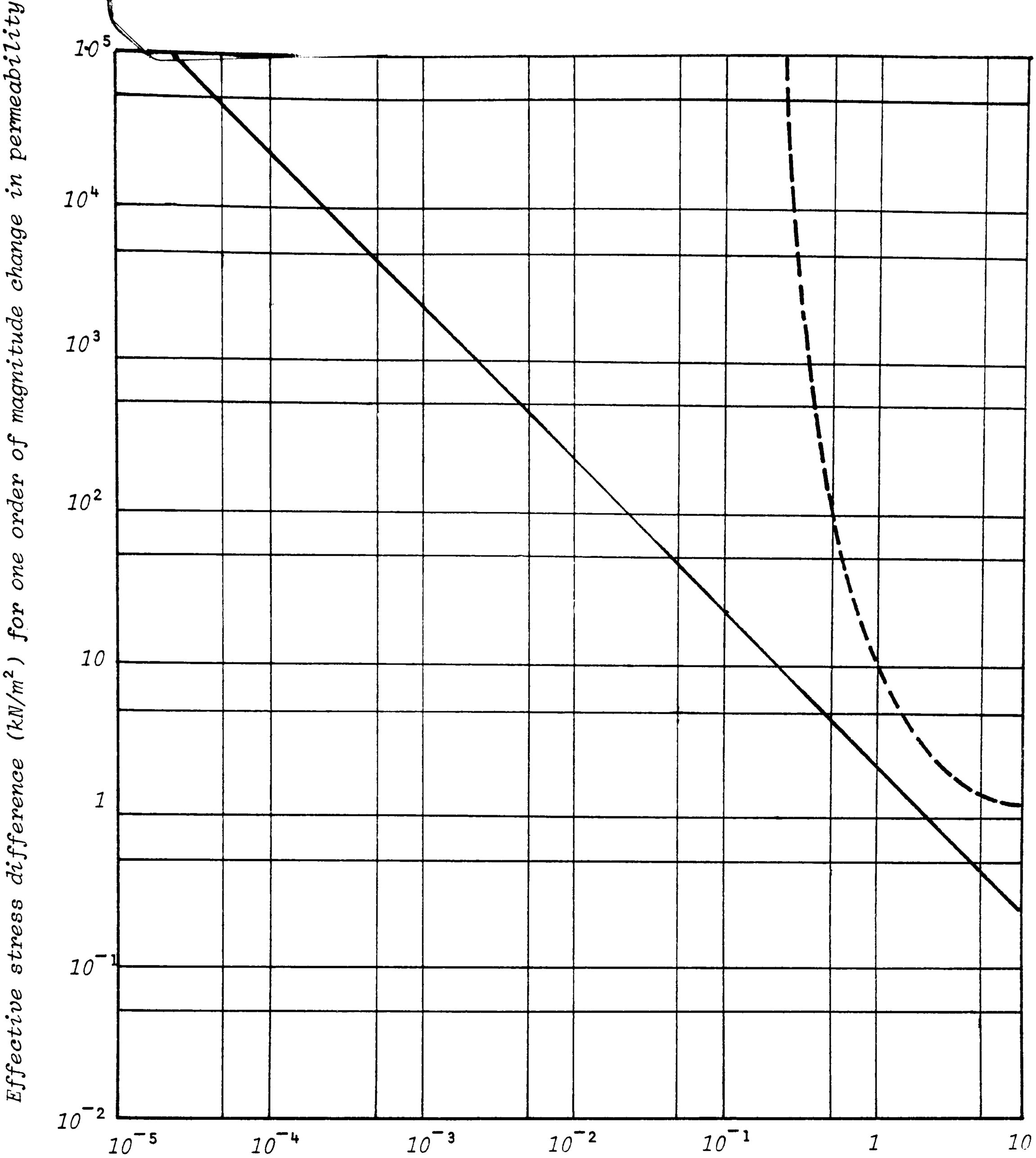
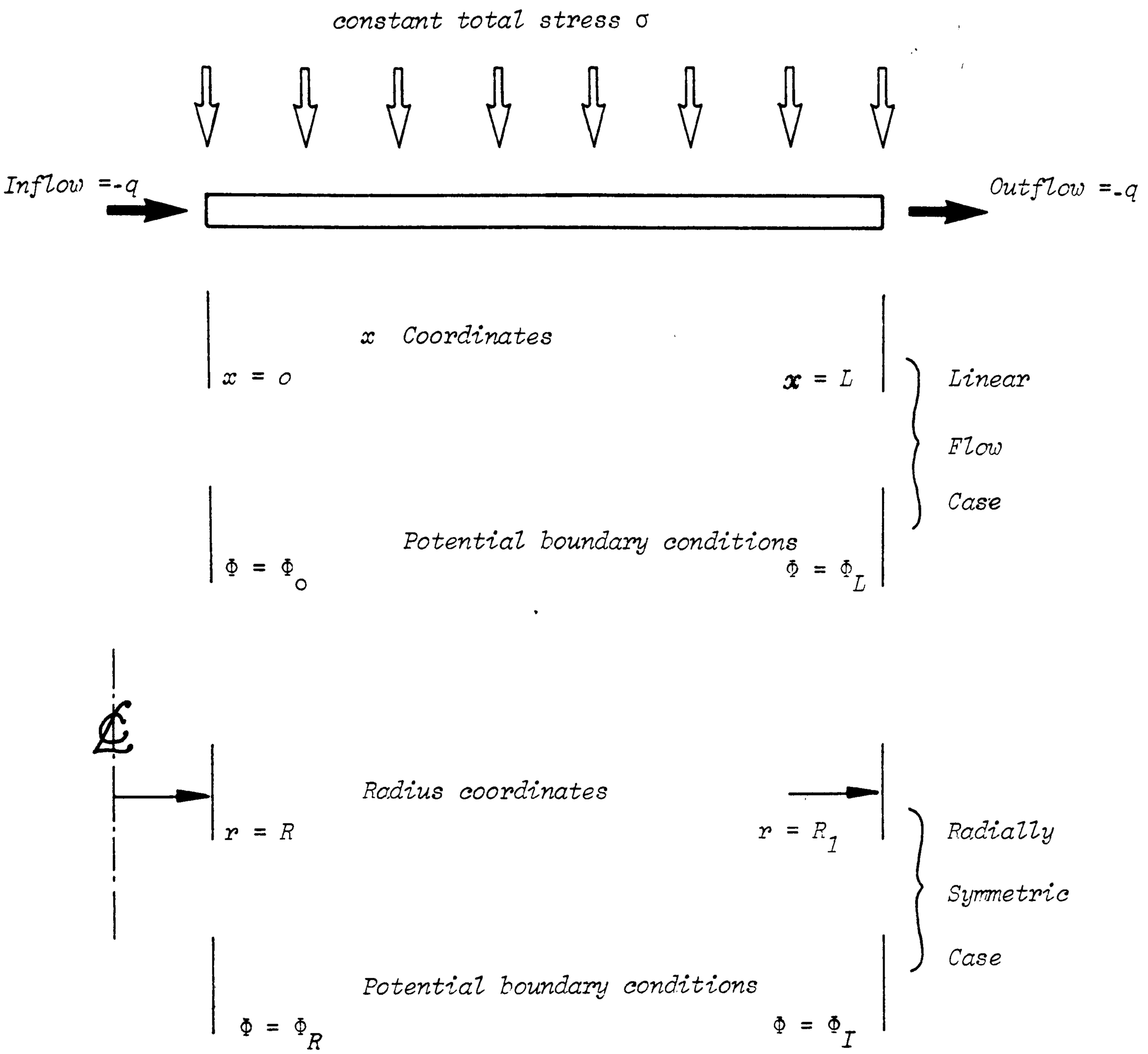


Figure 2.8. Implication of the "b" parameter

(Note that the straight, solid line is appropriate to the permeability - effective stress relationship $k = ae^{-b\sigma'}$. *For the relationship* $k = \sigma'^{(-b)}$ *the curved, broken line should be used. In this case, the label on the ordinates should be taken as reading:*

"Ratio of effective stresses for one order of magnitude change in permeability").

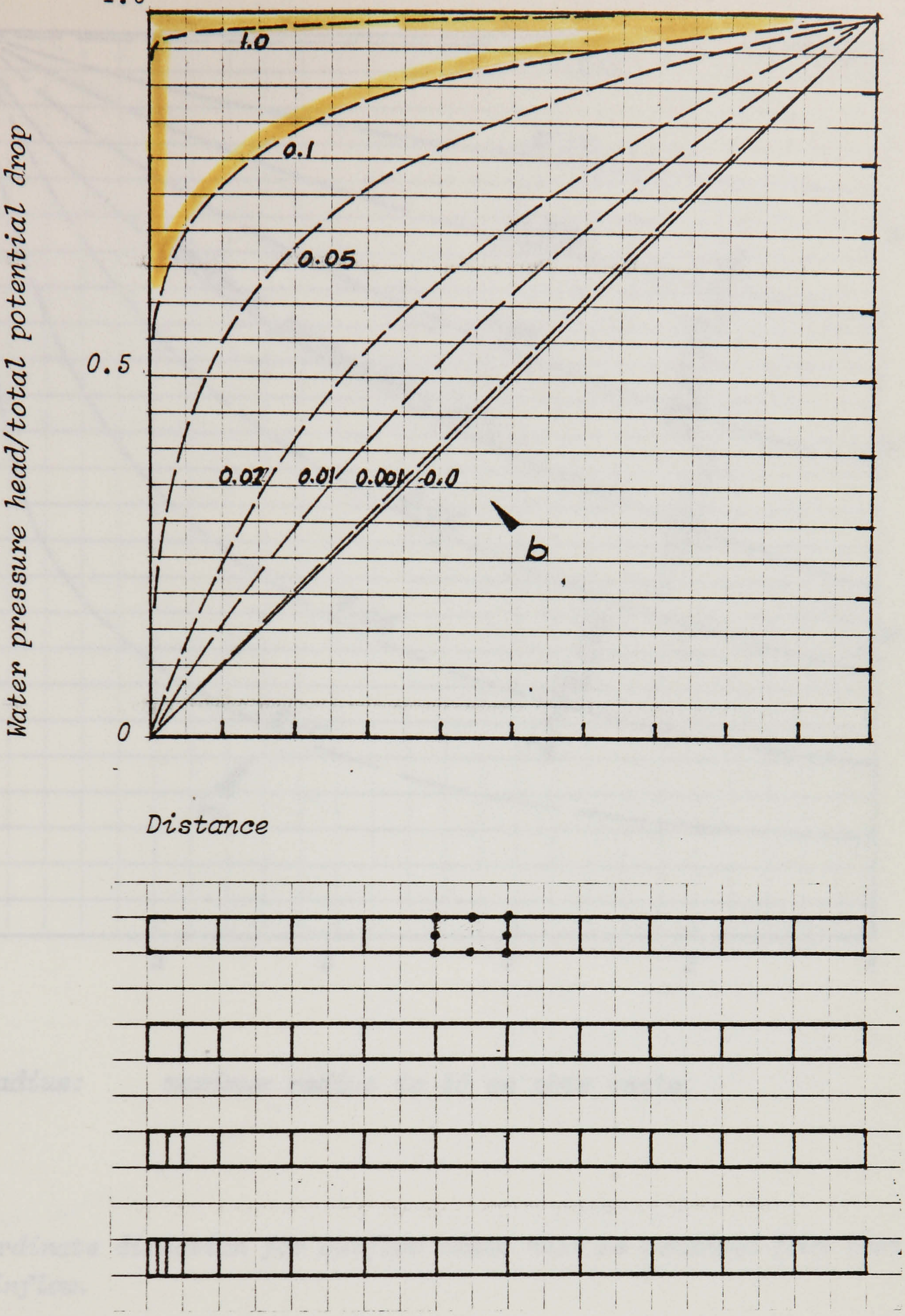


The following values were used in the parametric studies:

$L = 10$ m $\quad \Phi_o = \Phi_R = 0 \quad \Phi_L = \Phi_I = 10$ m head

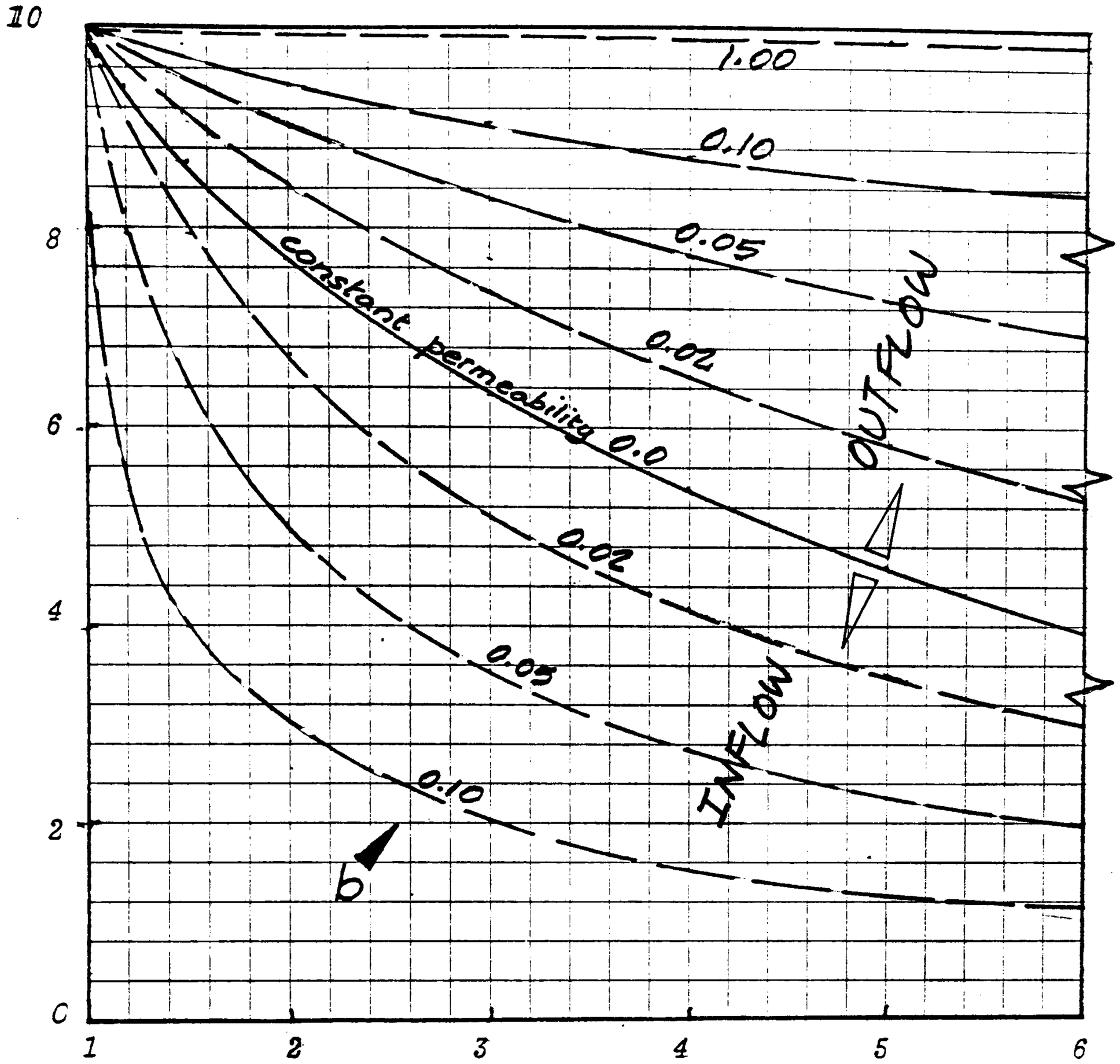
$R = 1$ m $\quad R_I = 20$ m

Figure 2.9. Key diagram: horizontal and axisymmetric seepage in a constant total stress field.



Also shown are the finite element meshes used to analyse this case (cf. Section 3.9). The region in which the finite element results are poor is shown shaded.

Figure 2.10. Horizontal seepage in a constant total stress field with an effective stress dependent permeability.



Radius: *maximum radius is 20 on this scale.*

The ordinate direction for outflow cases must be reversed from that for inflow.

Figure 2.11. Axisymmetric seepage in a constant total stress field. Analytical solutions using the "logarithmic" law.

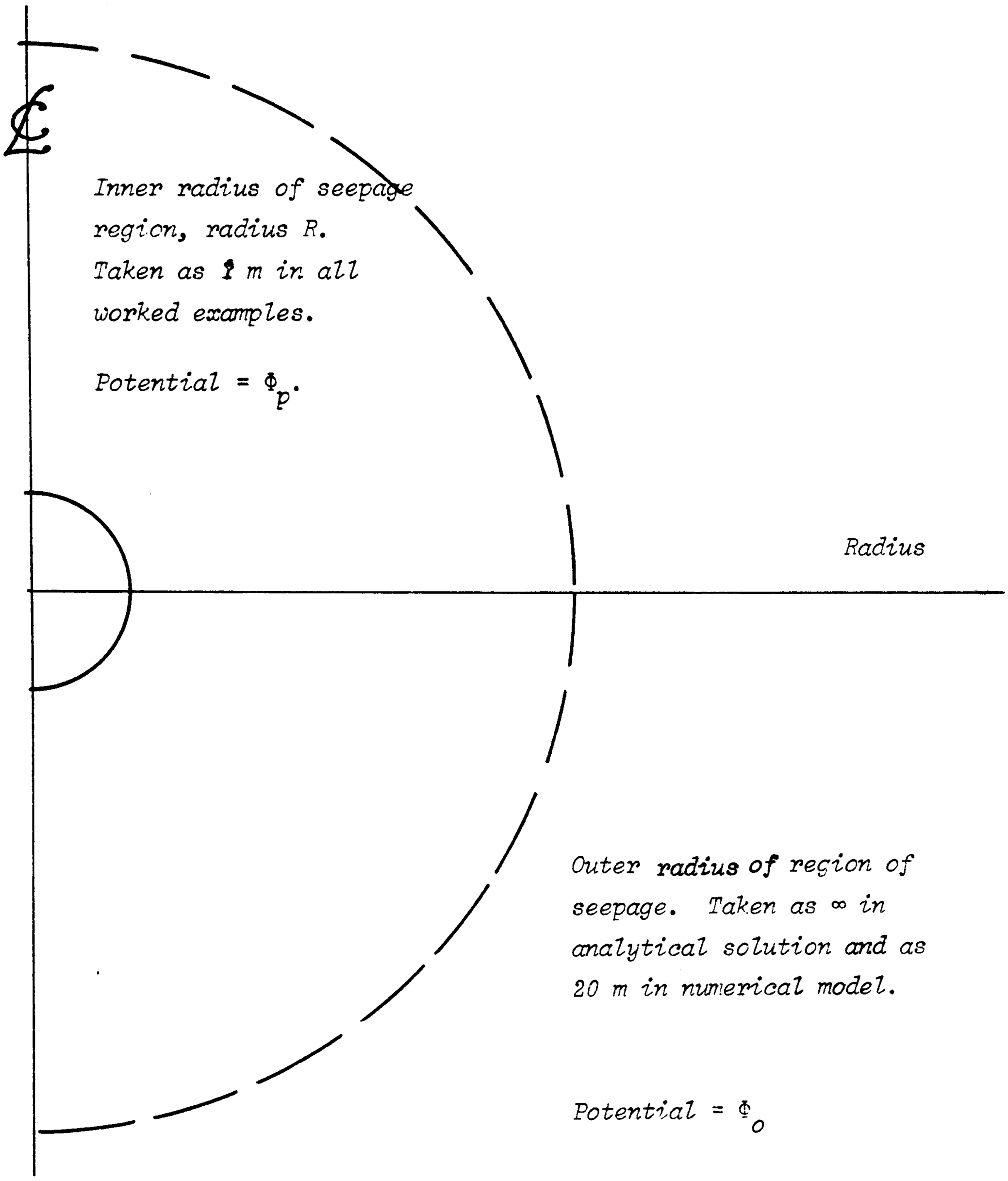
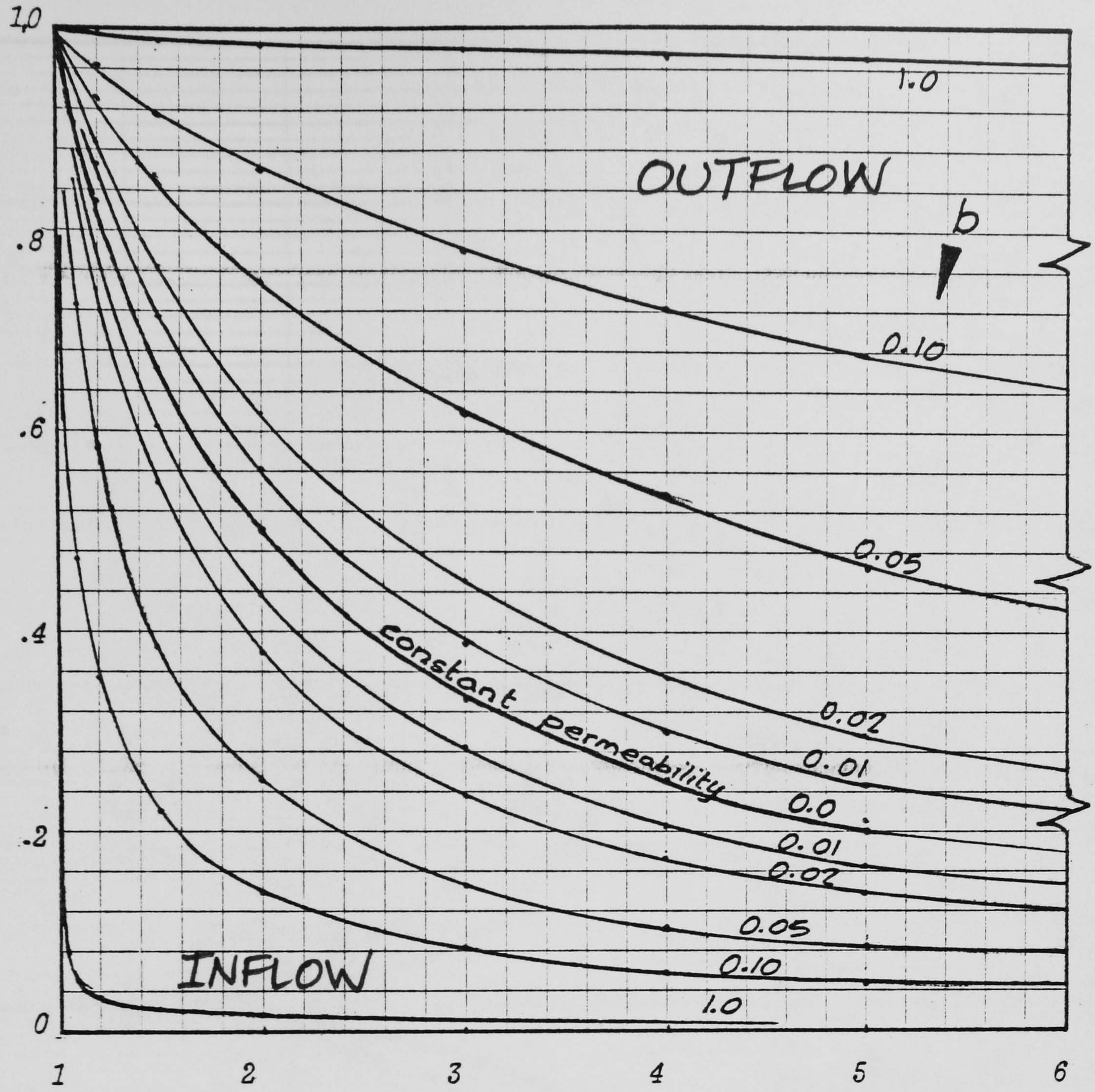


Figure 2.12. Key diagram: Spherically symmetric seepage in a constant total stress field.



Radius: maximum radius is infinity.

The ordinate direction for outflow cases must be reversed from that for inflow.

Figure 2.13. Spherically symmetric seepage in a constant total stress field. Analytical solutions using the "logarithmic" law.

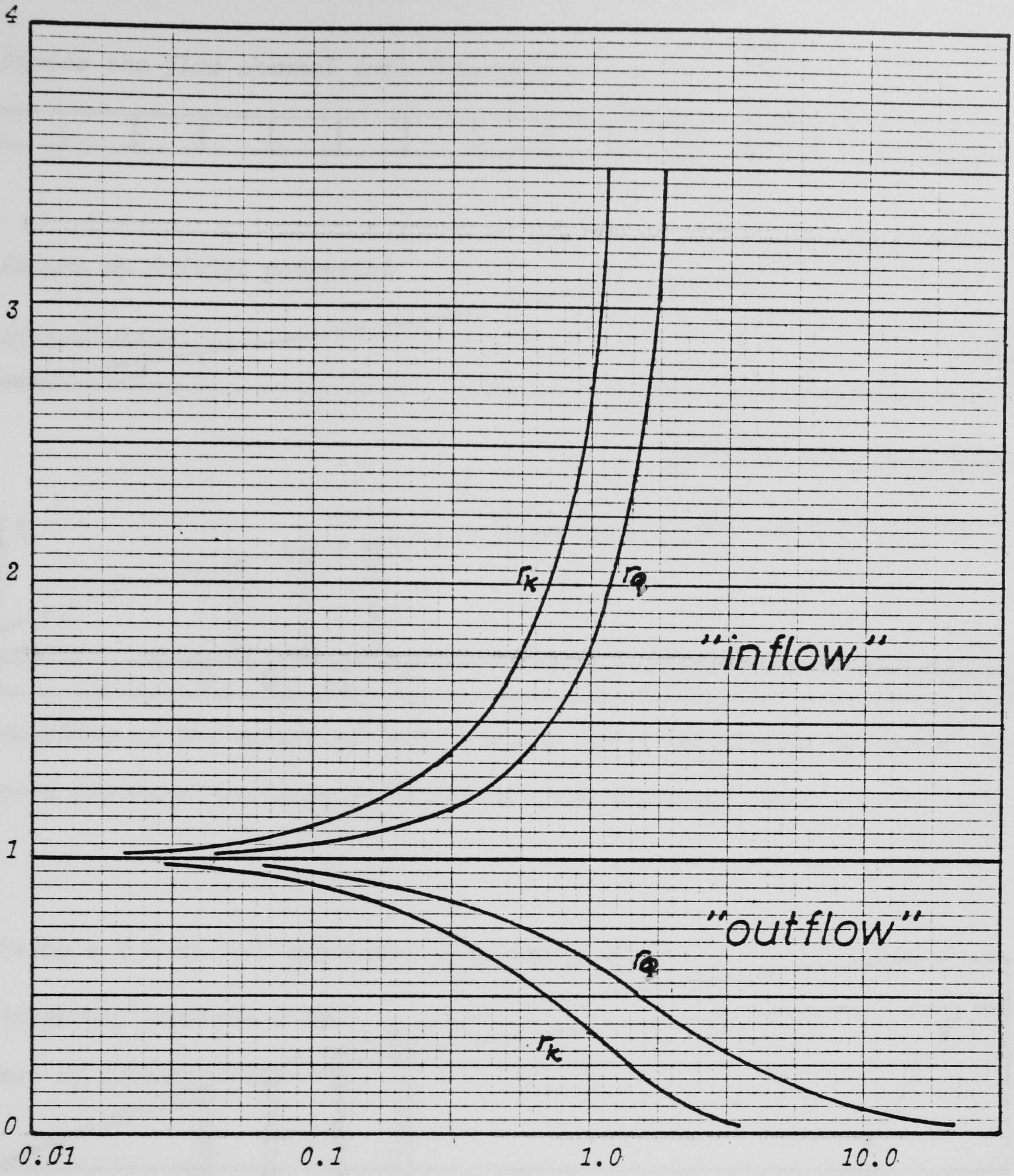
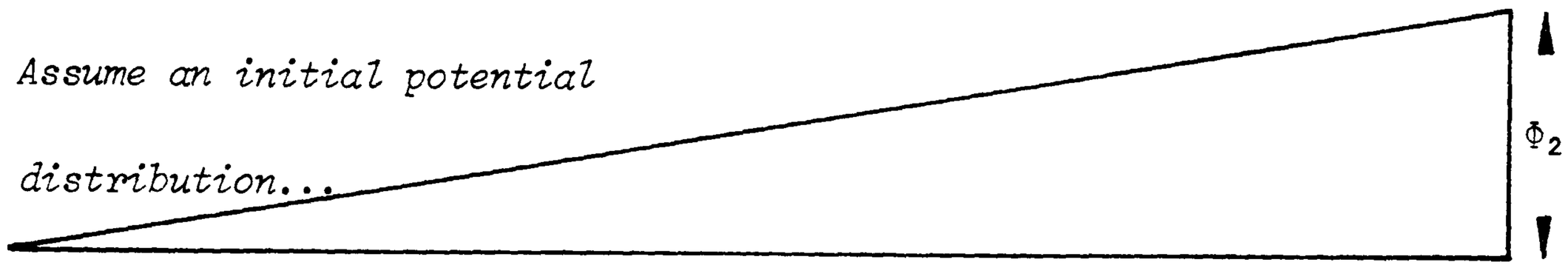


Figure 2.14. Lag in flow rate ratio in comparison to permeability ratio.

1 *Divide the flow channel into intervals*

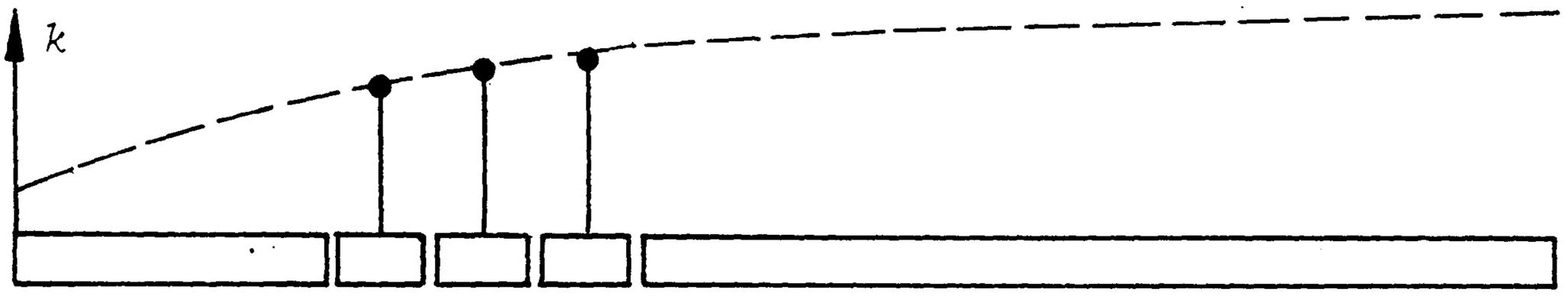


2 *Assume an initial potential distribution...*



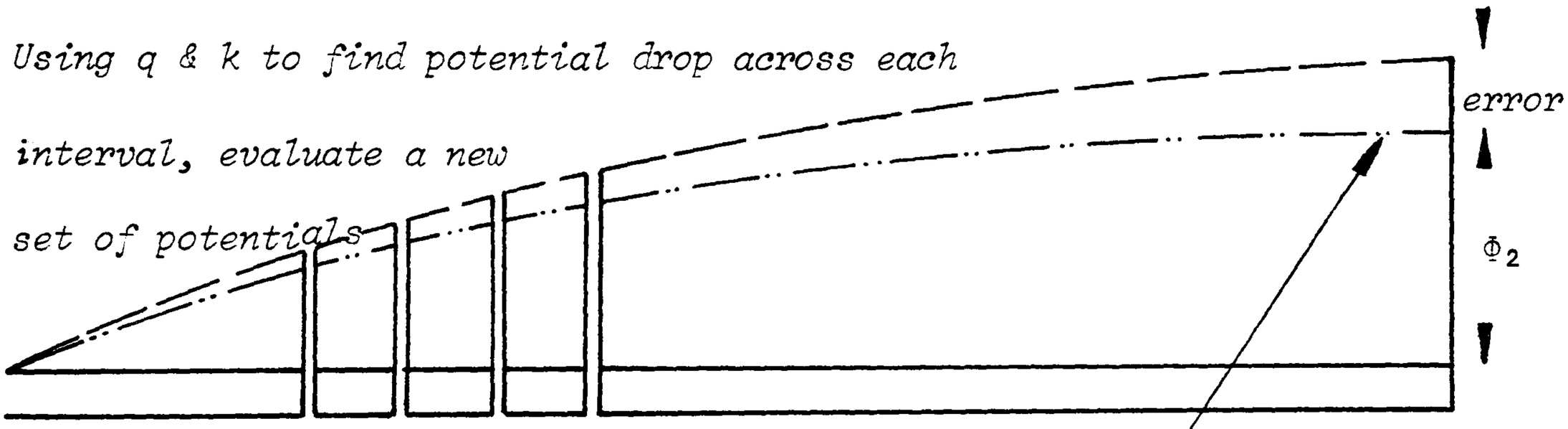
.... and flow rate, q ⇐

3



Sampling at the centre of each interval for total stress, potential (hence pore pressure) evaluate permeability from nominated law

4 *Using q & k to find potential drop across each interval, evaluate a new set of potentials*

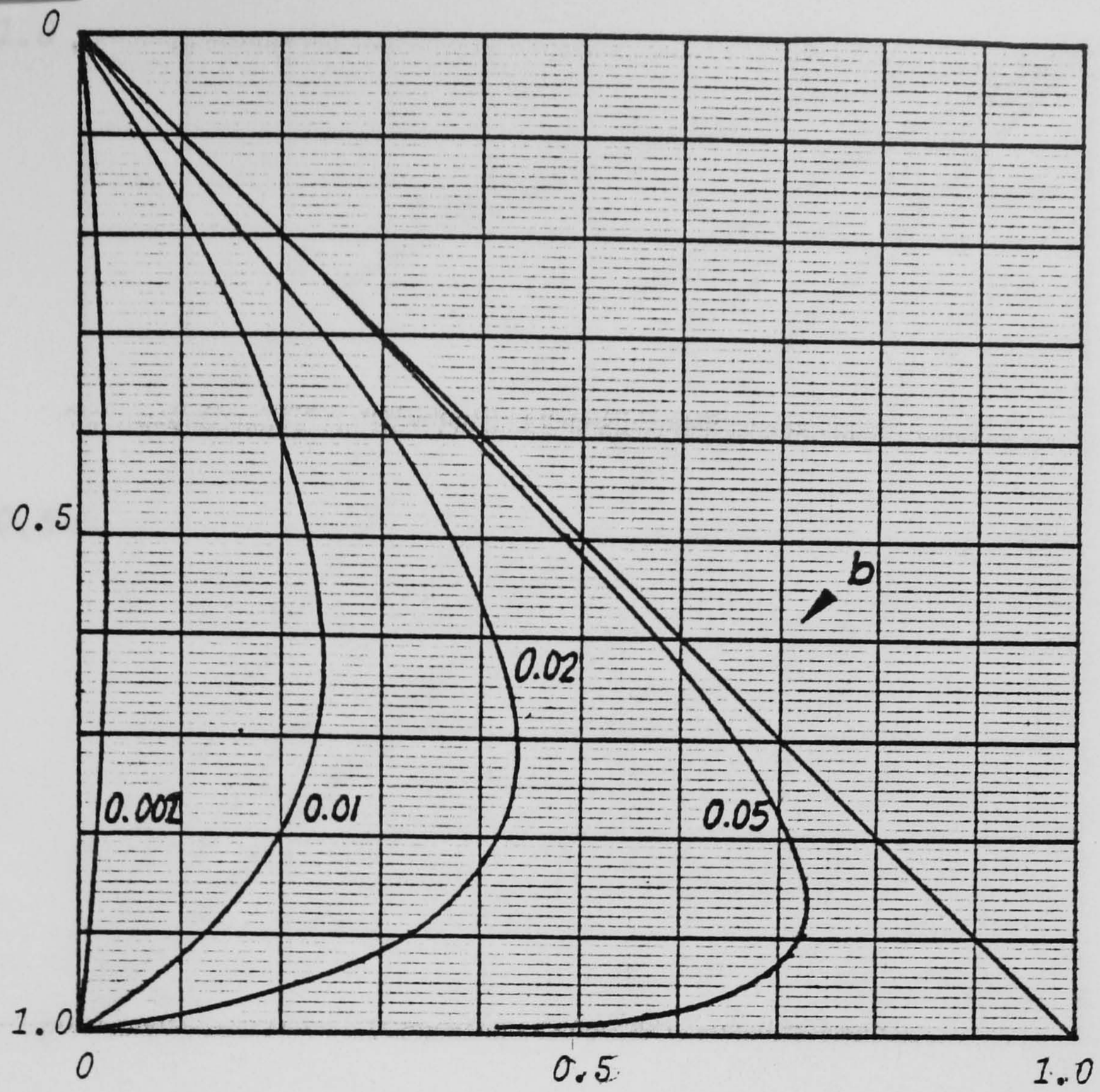


5 *"Correct" the potentials to eliminate "error" if any*

6 *Sample a point for a re-evaluation of k,* $\frac{d\Phi}{dx}$ *using corrected potentials and evaluate new q. Repeat from step 3.*

Figure 2.15. Simple numerical technique for dealing with effective stress dependent permeability in one-dimensional seepage.

"Logarithmic law"



"Power law"

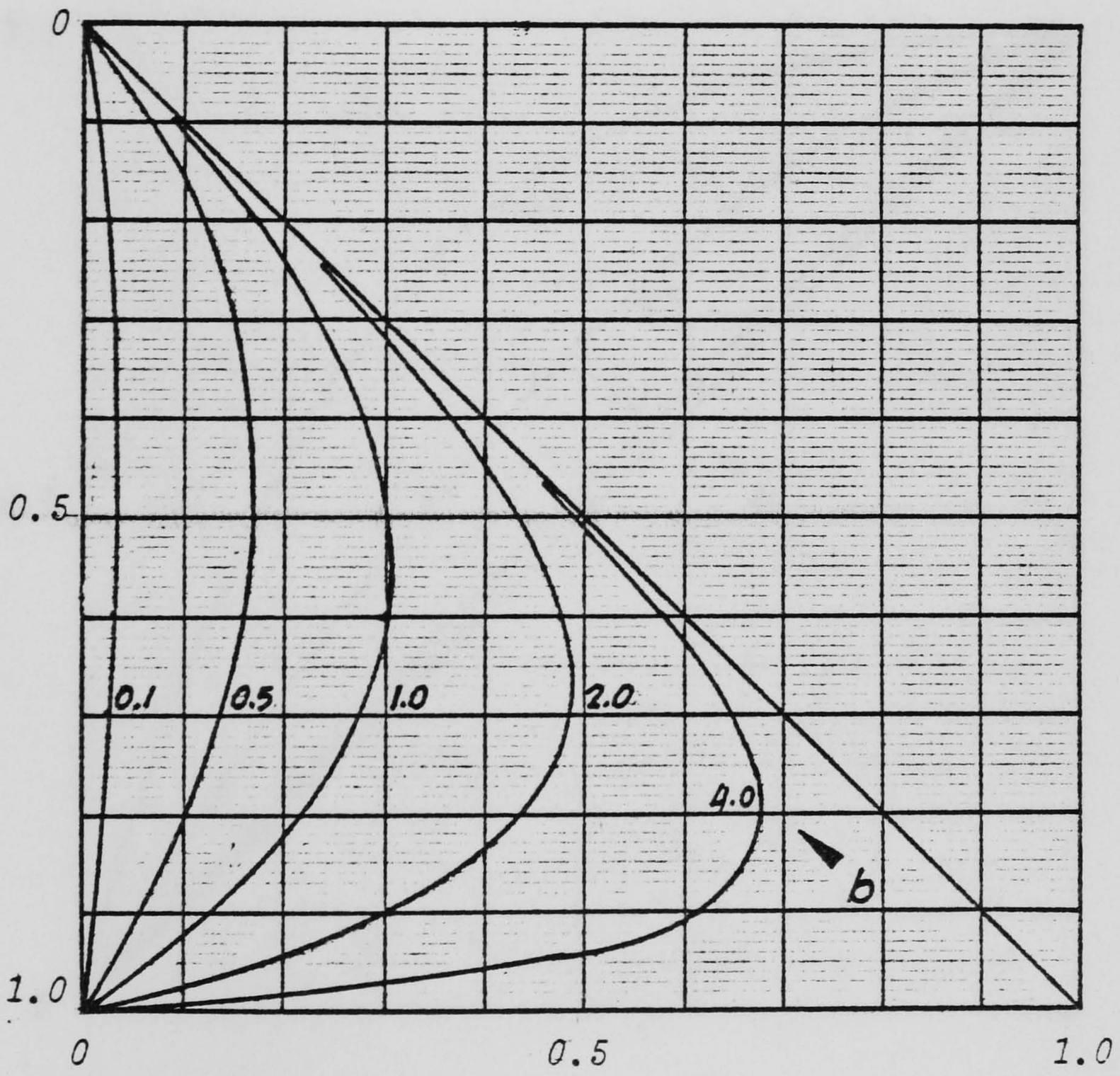
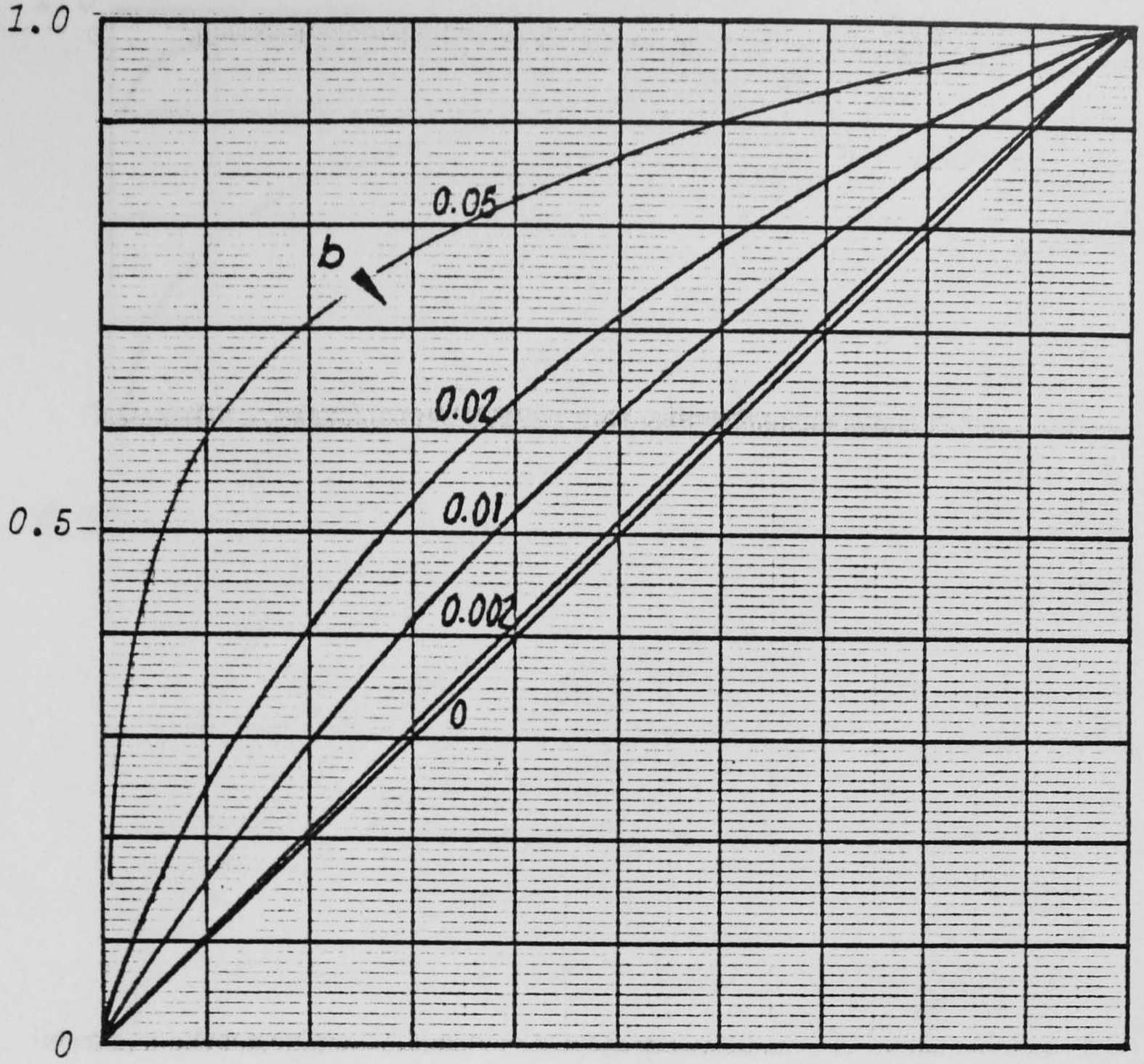


Figure 2.16. Predictions of the simple model - downward seepage

"Logarithmic law"



"Power law"

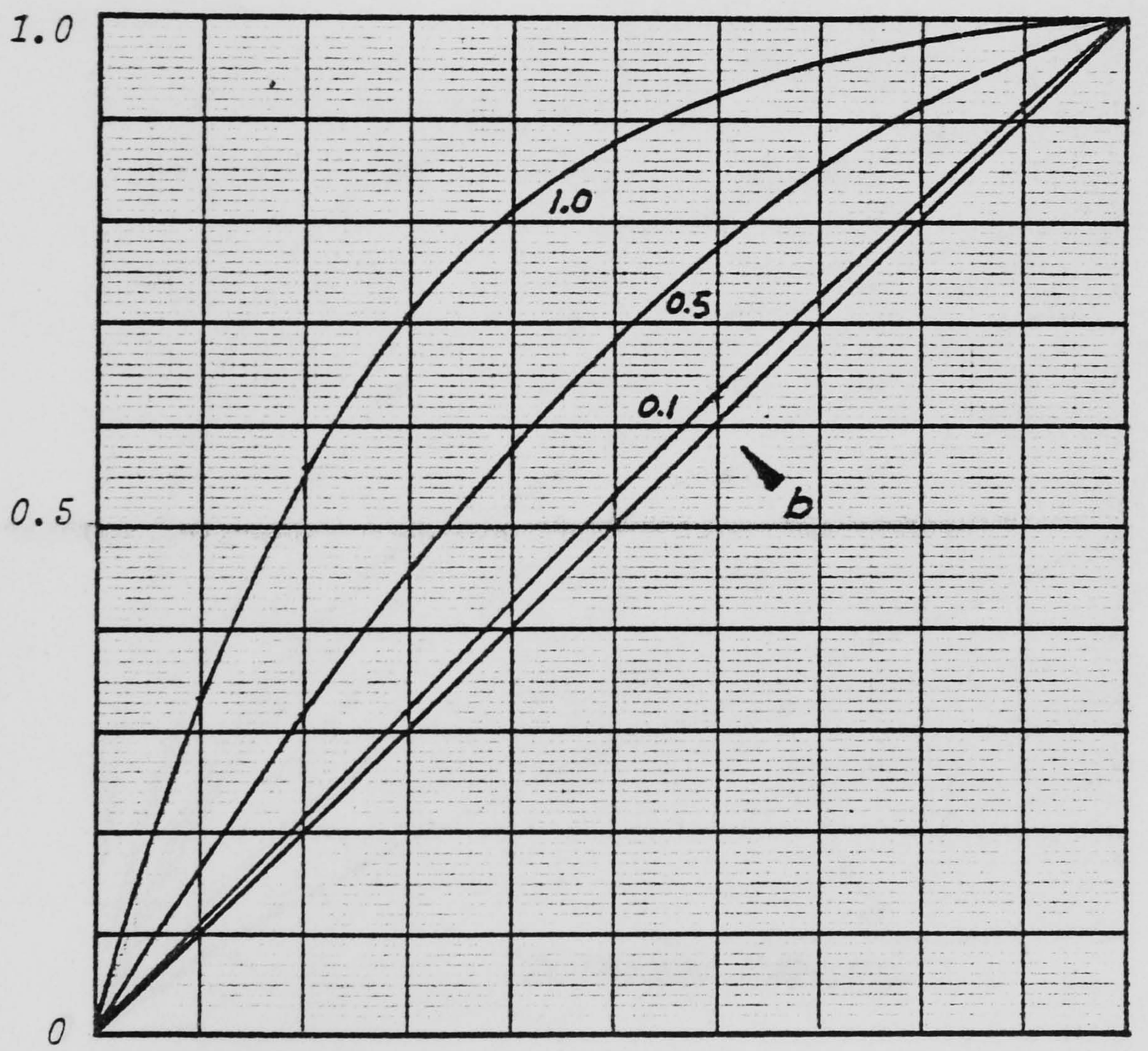
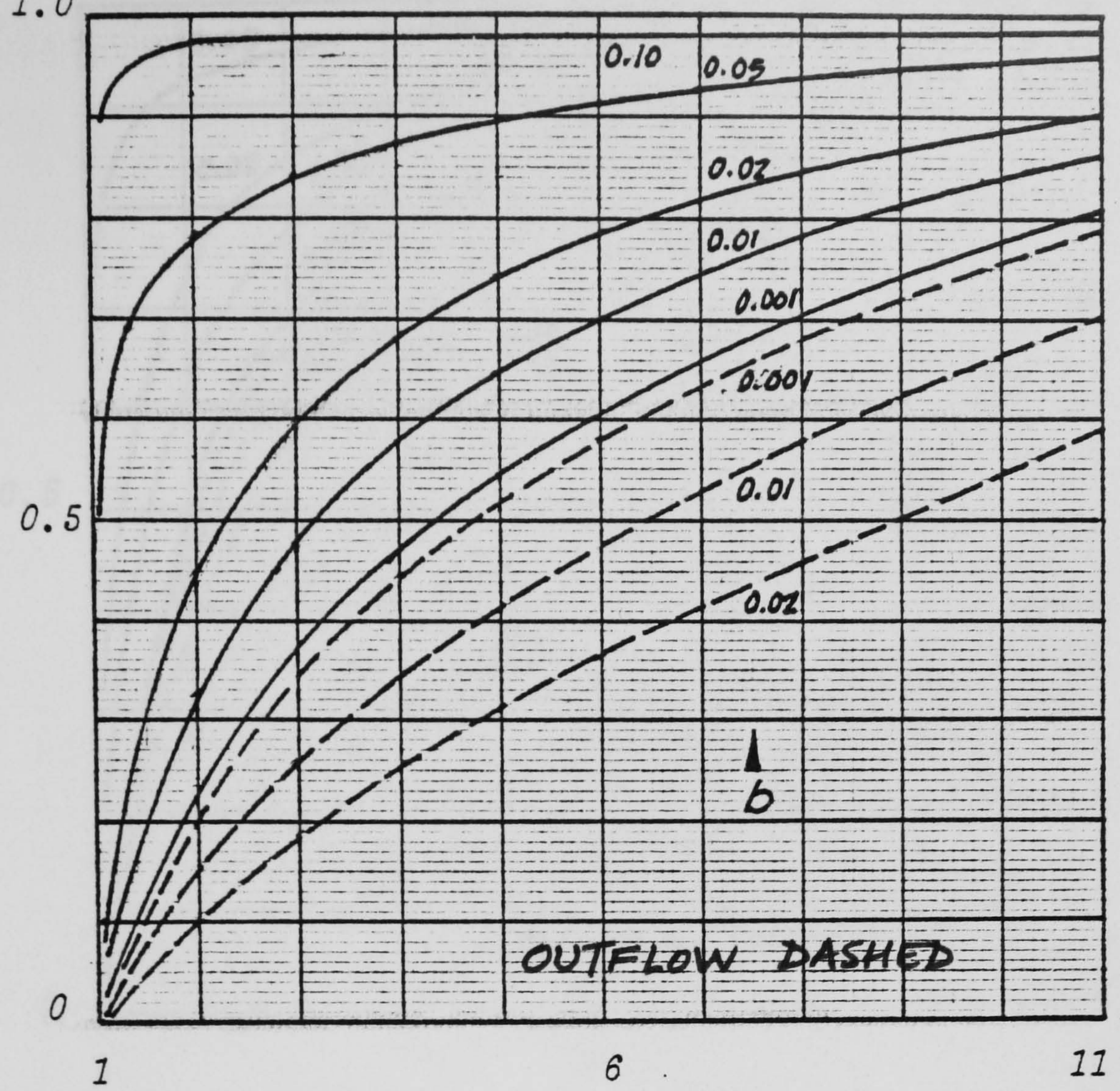
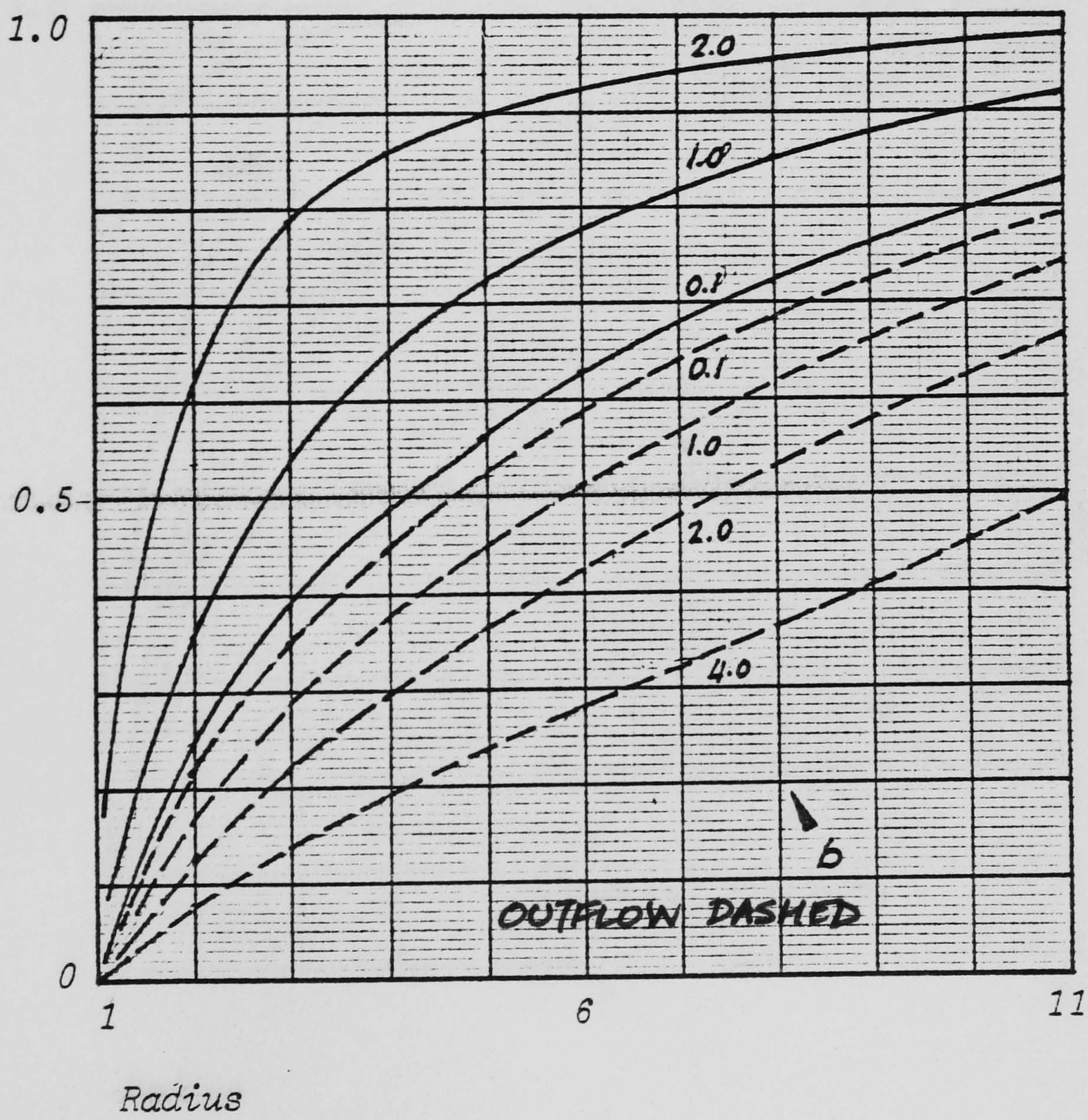


Figure 2.17. Predictions of the simple model - horizontal seepage

"Logarithmic law"



"Power law"



The ordinate direction for outflow cases must be reversed from that for inflow.

Figure 2.18. Predictions of the simple model - axisymmetric seepage

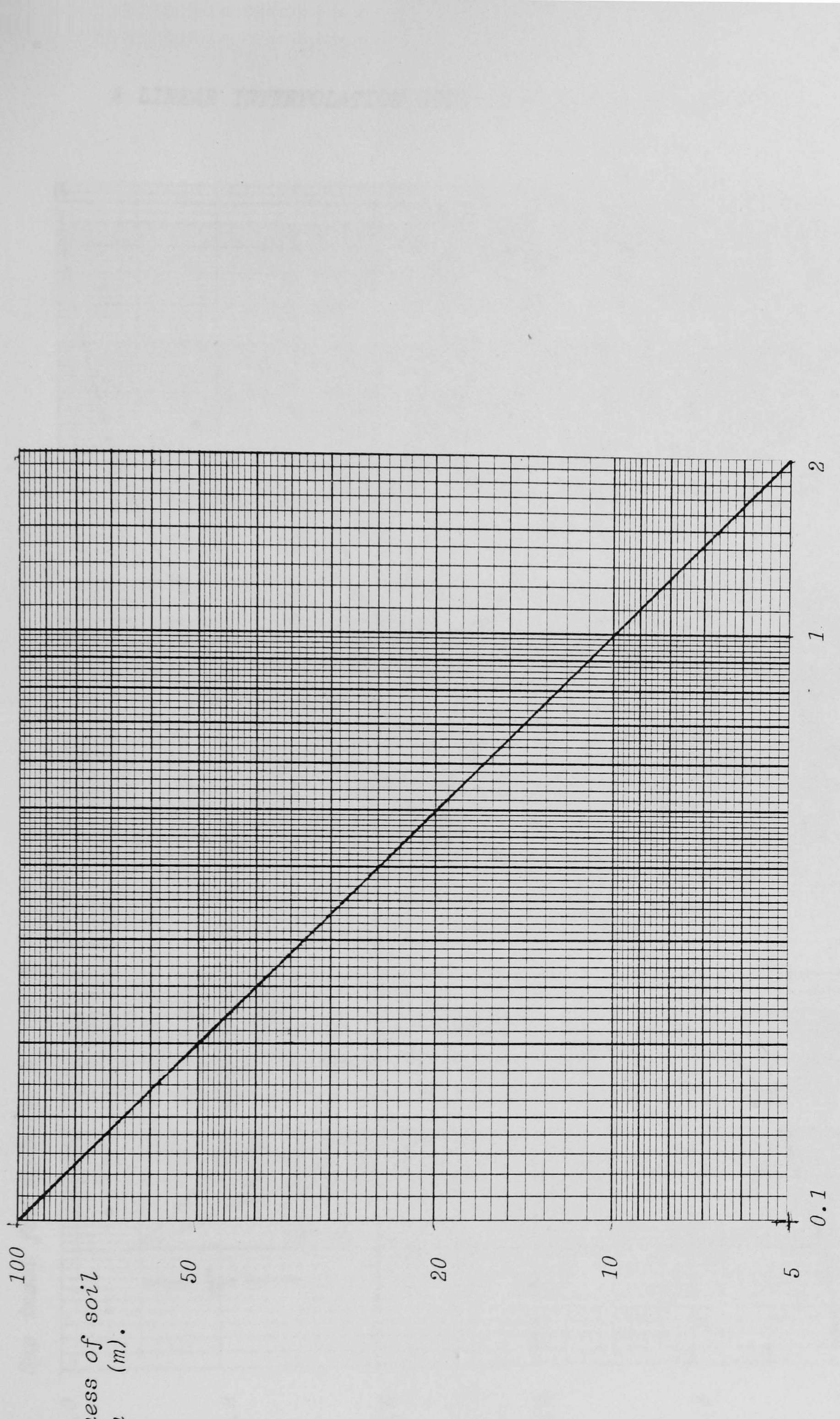


Figure 2.20. Influence of scale on the parametric study of vertical underdrained seepage in a soil with effective stress dependent permeability.

A LINEAR INTERPOLATION WITH $(1 - D_u)$ MAY BE APPLIED

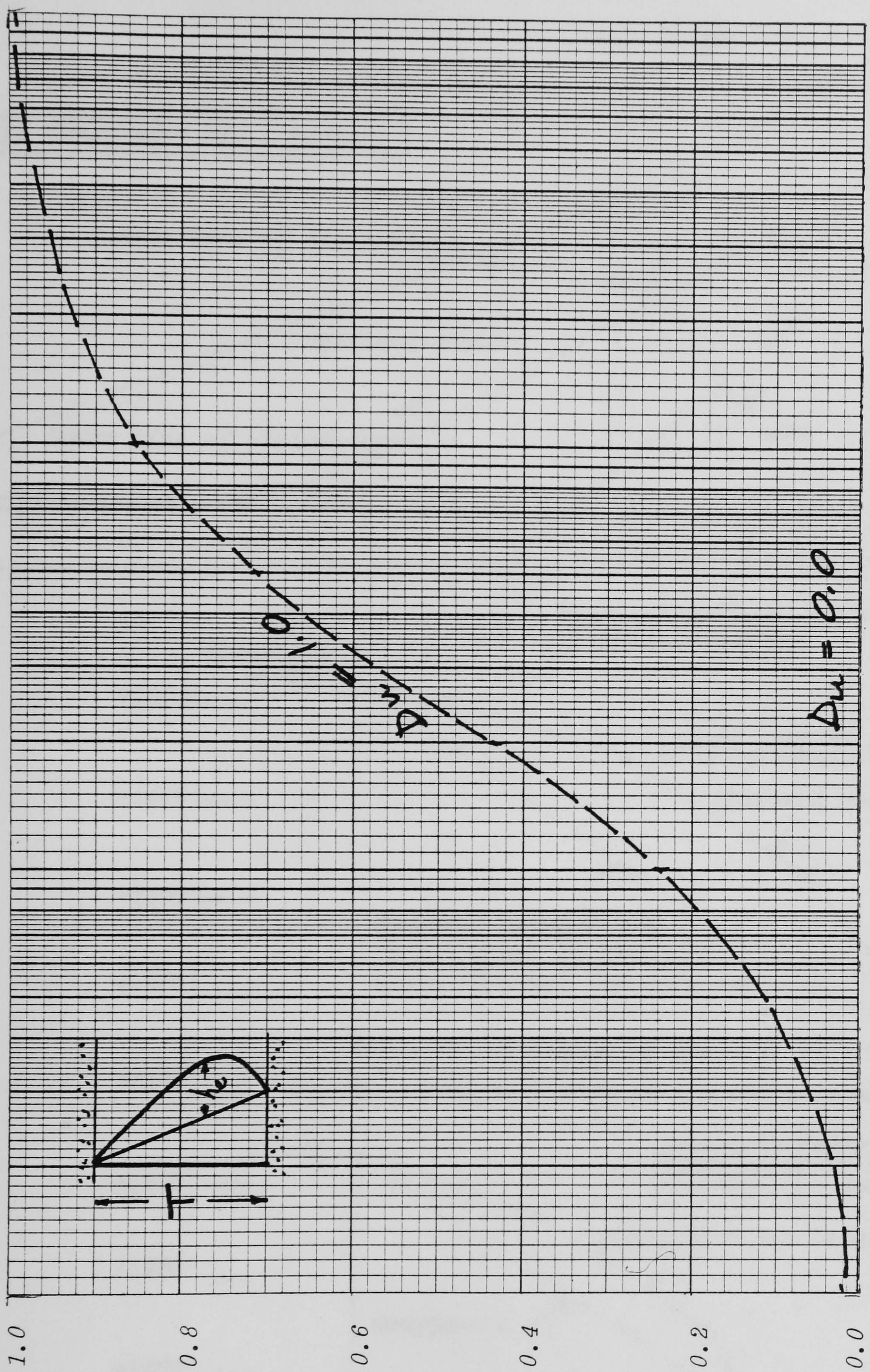
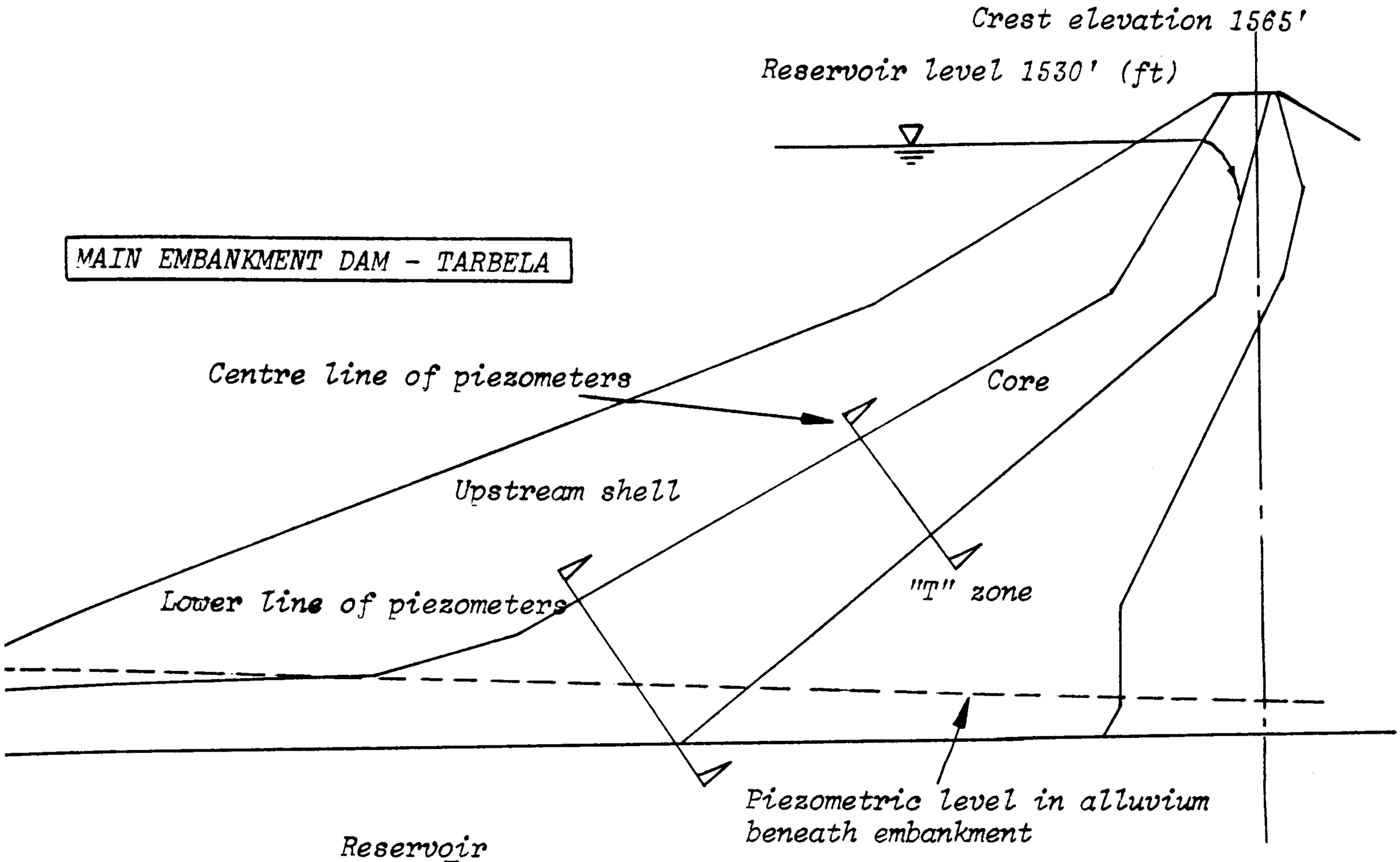
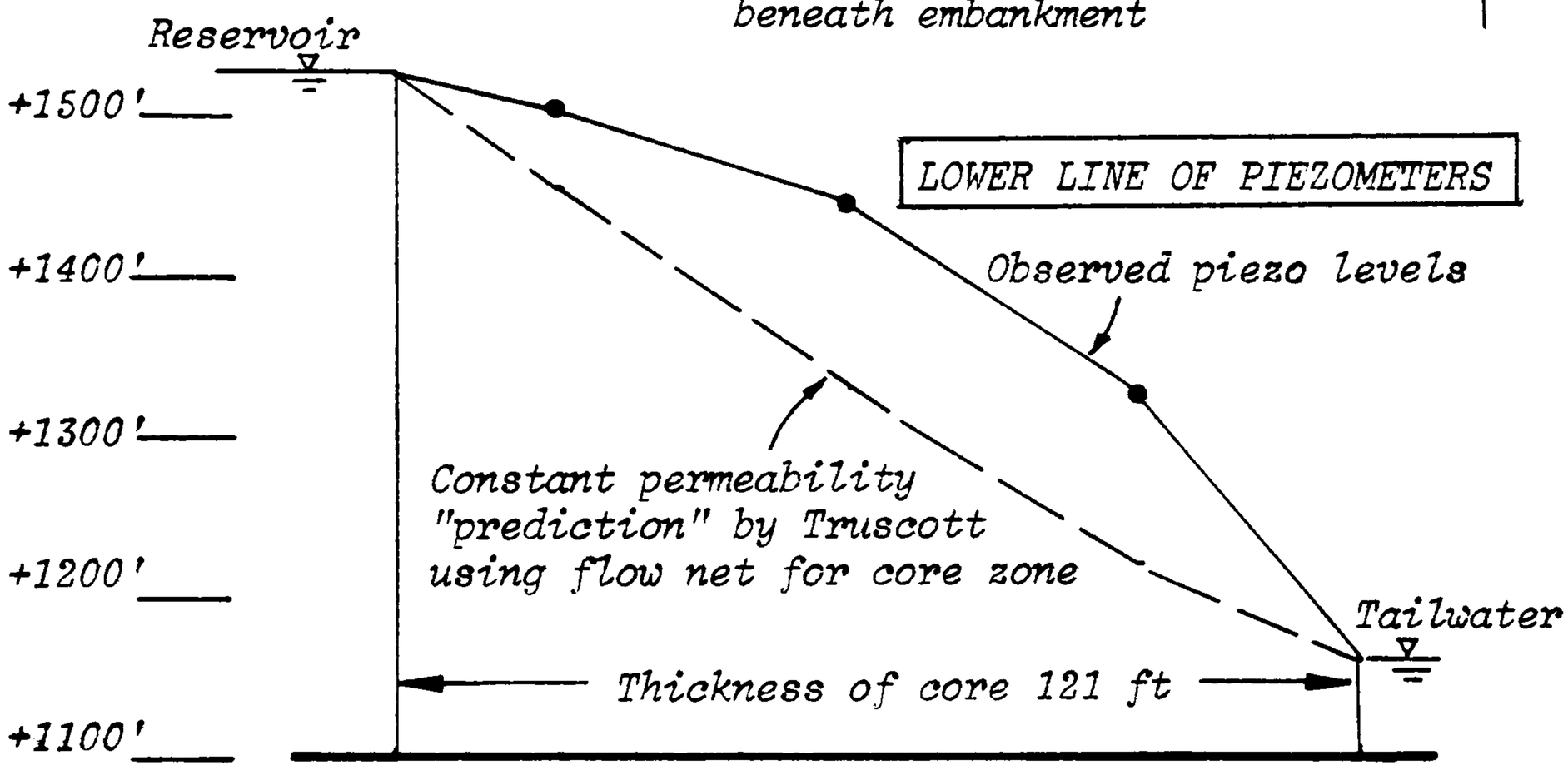


Figure 2.21. Influence of scale and of the b value on the pore pressure distribution: vertical underdrained seepage using effective stress dependent permeability. (Log law).





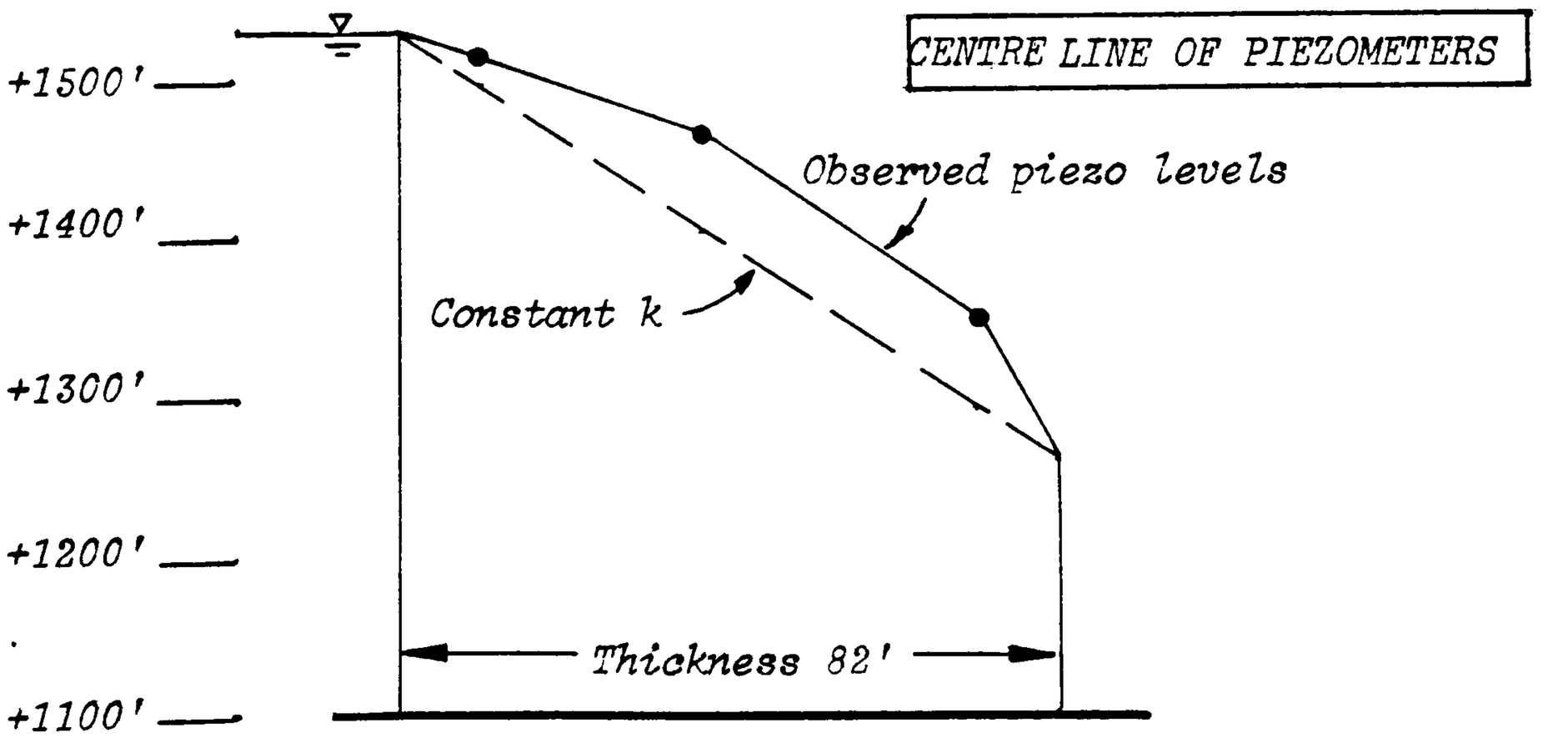


Figure 2.22. Pore pressures in the core of Tarbela Dam. (After Truscott, 1977).

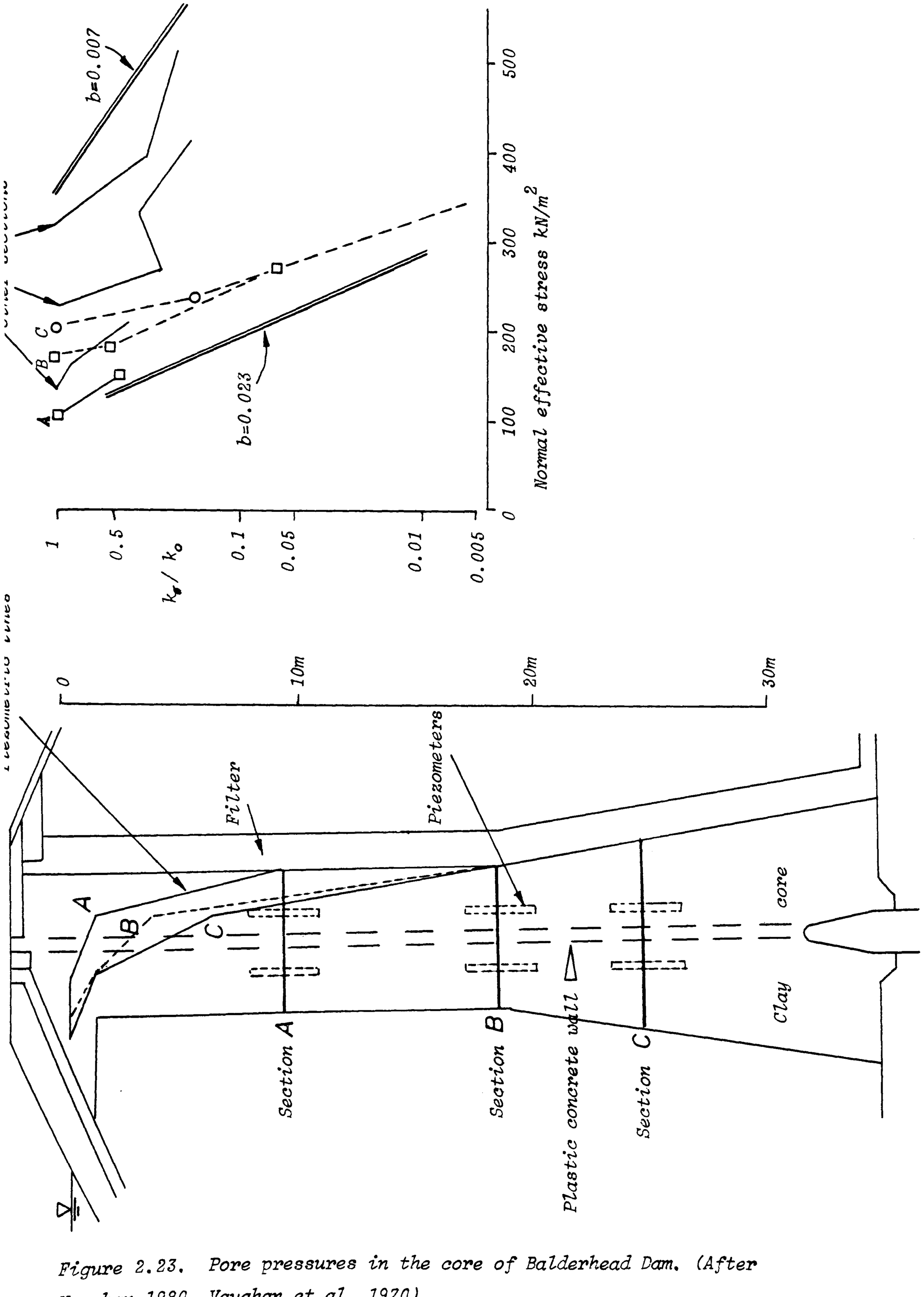


Figure 2.23. Pore pressures in the core of Balderhead Dam. (After Vaughan 1980, Vaughan et al. 1970).

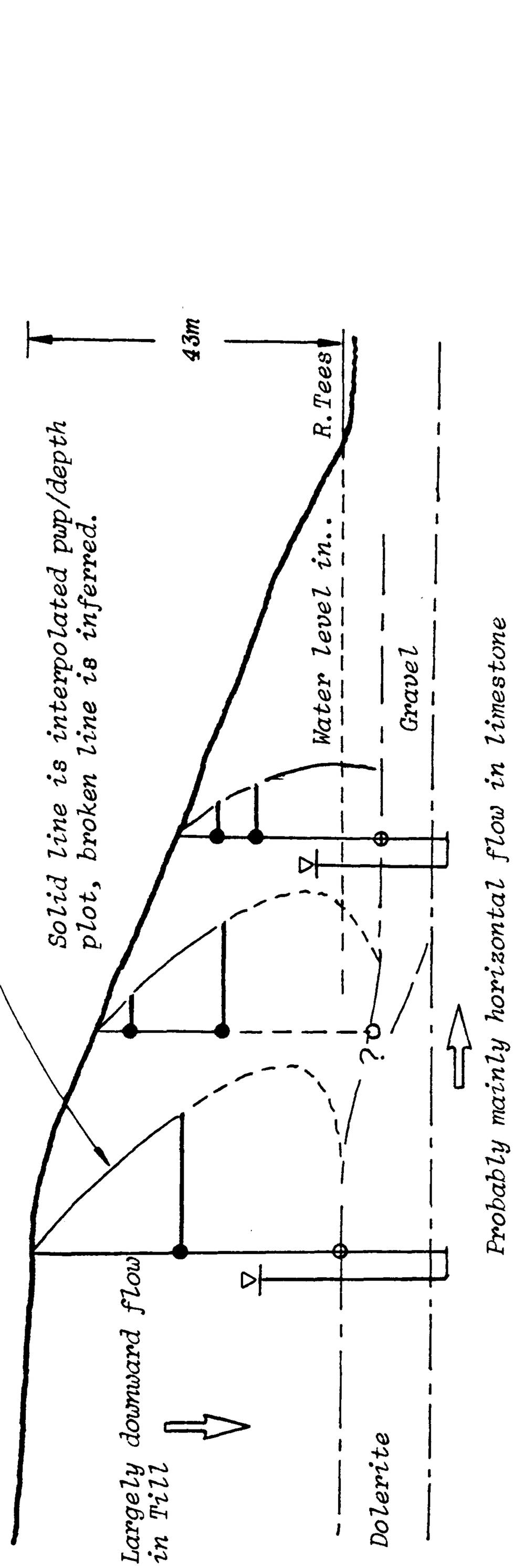


Figure 2.24. Pore Pressure Distribution in the Till Slopes at Cow Green Dam Abutment. (After Vaughan & Walbancke, 1973).

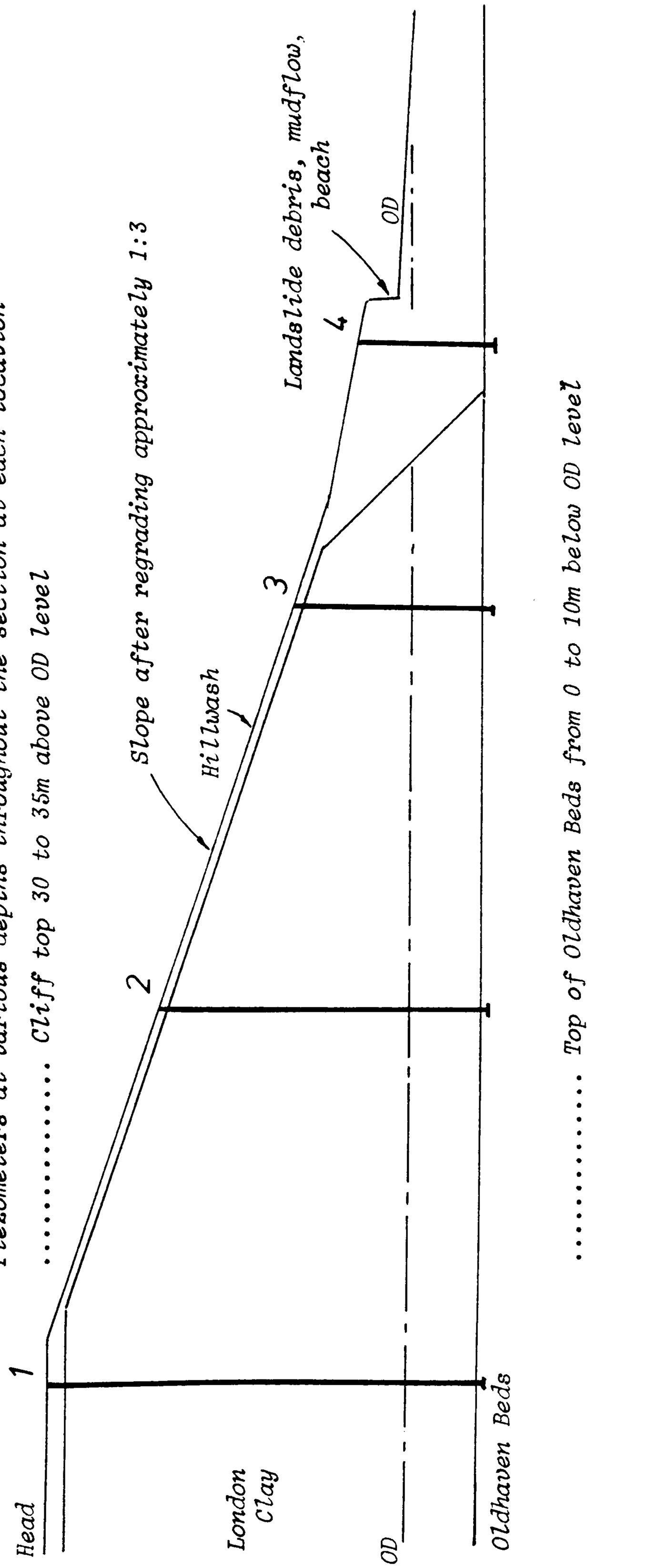


Figure 2.25. Sketch cross section of the Herne Bay cliffs showing typical piezometer locations. (After Bromhead, 1972).

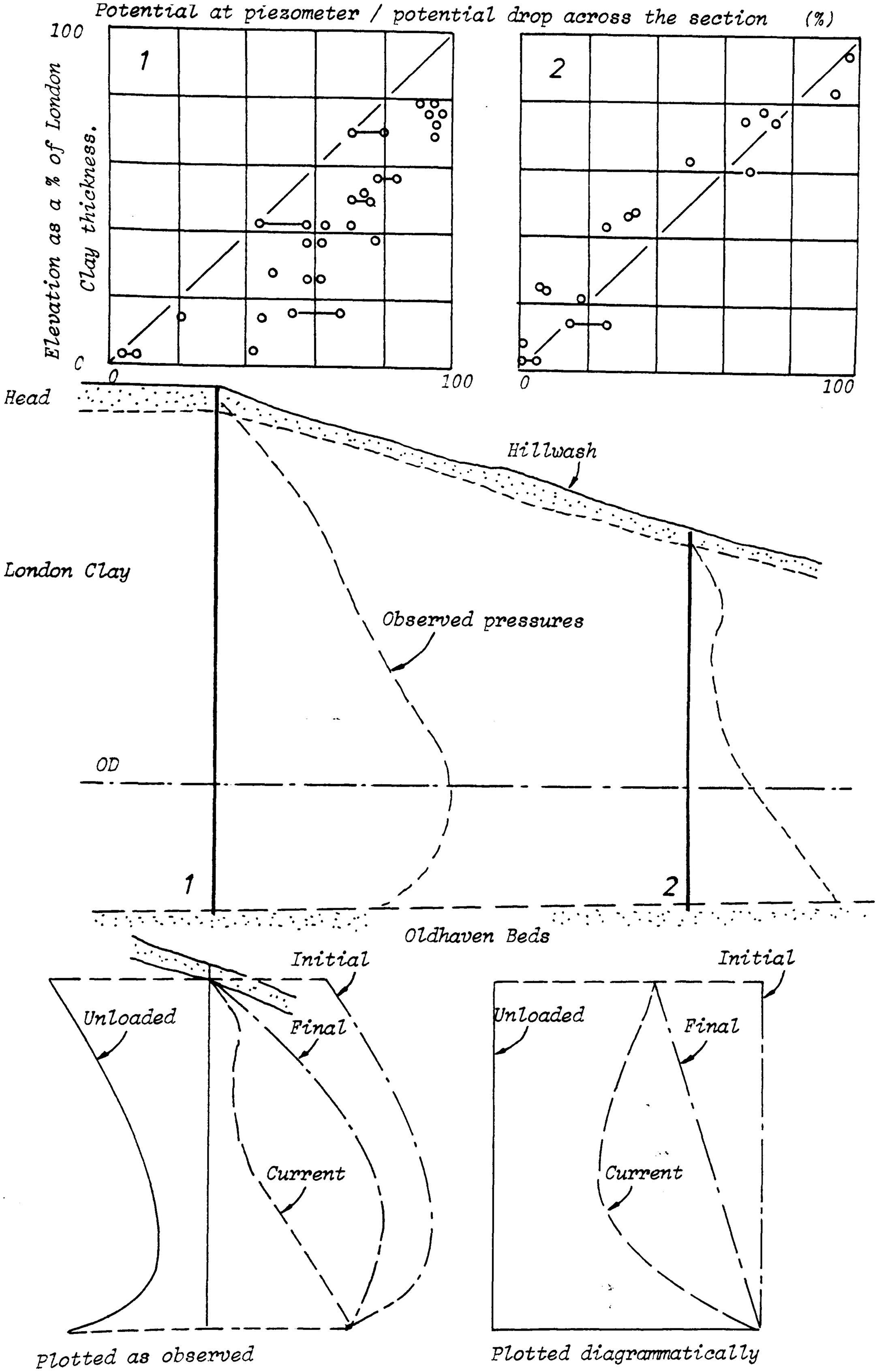
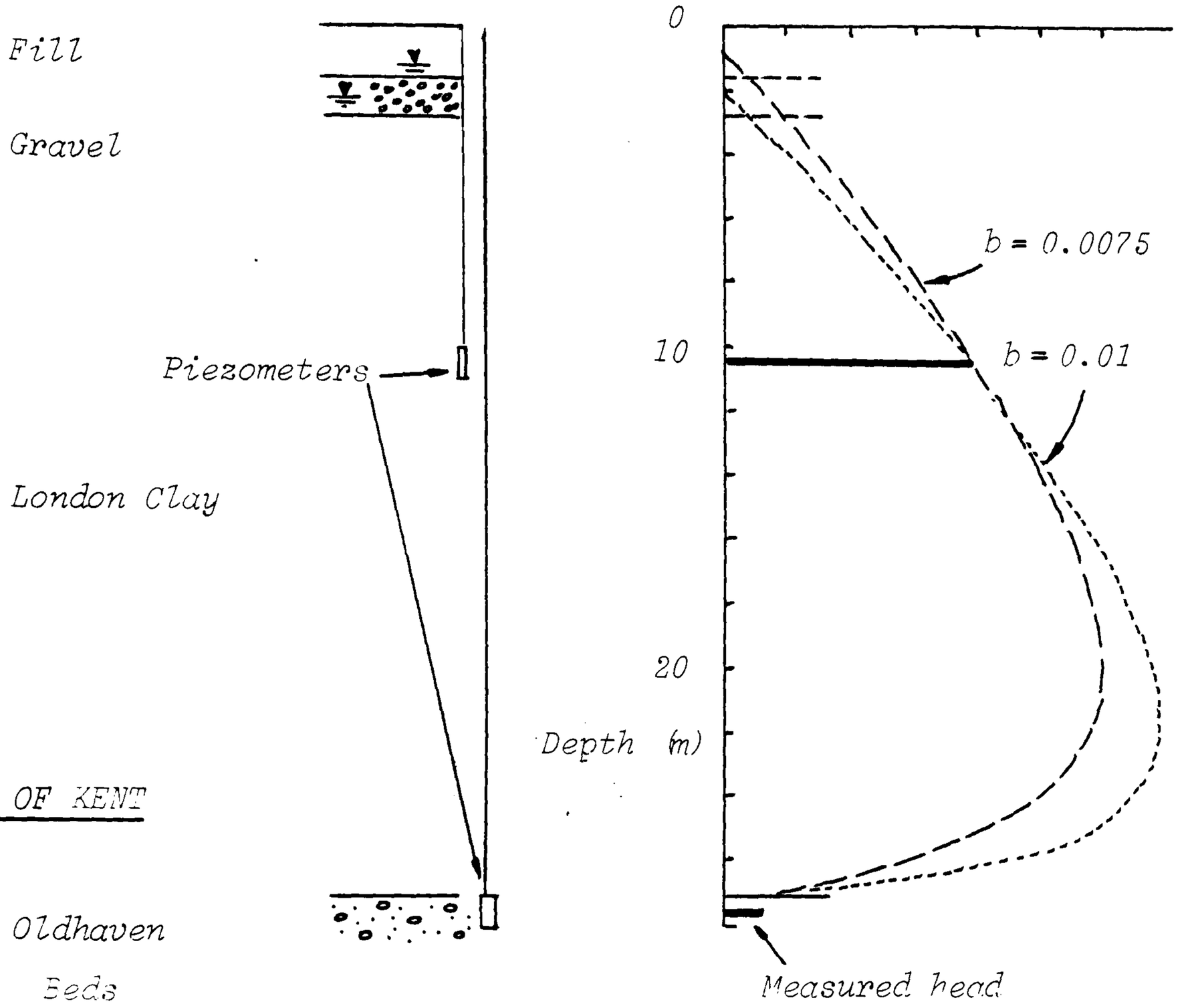
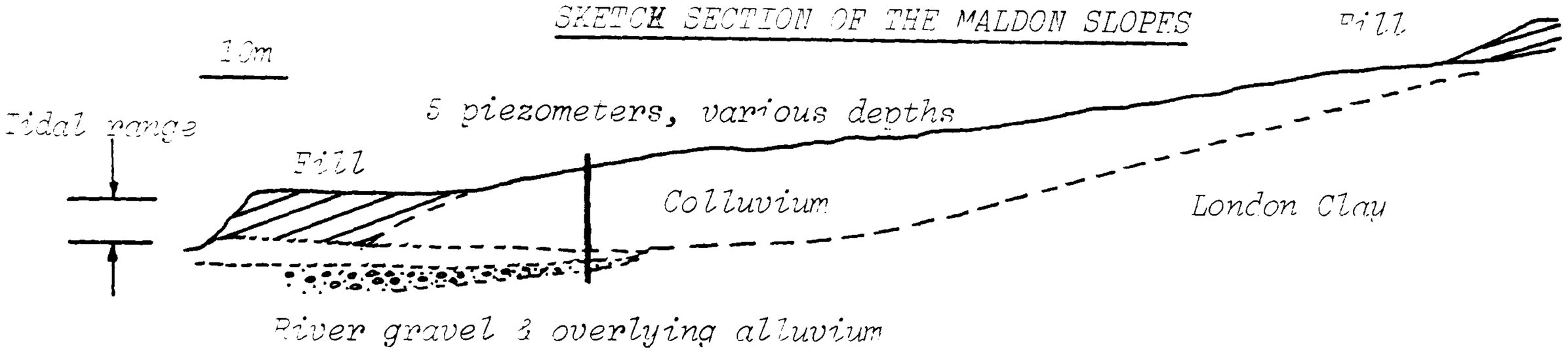


Figure 2.26. Typical pore water pressure conditions in the slopes at Herne Bay. (After Bromhead 1972).



UNIVERSITY OF KENT

SKETCH SECTION OF THE MALDON SLOPES



PORE PRESSURES AT MALDON

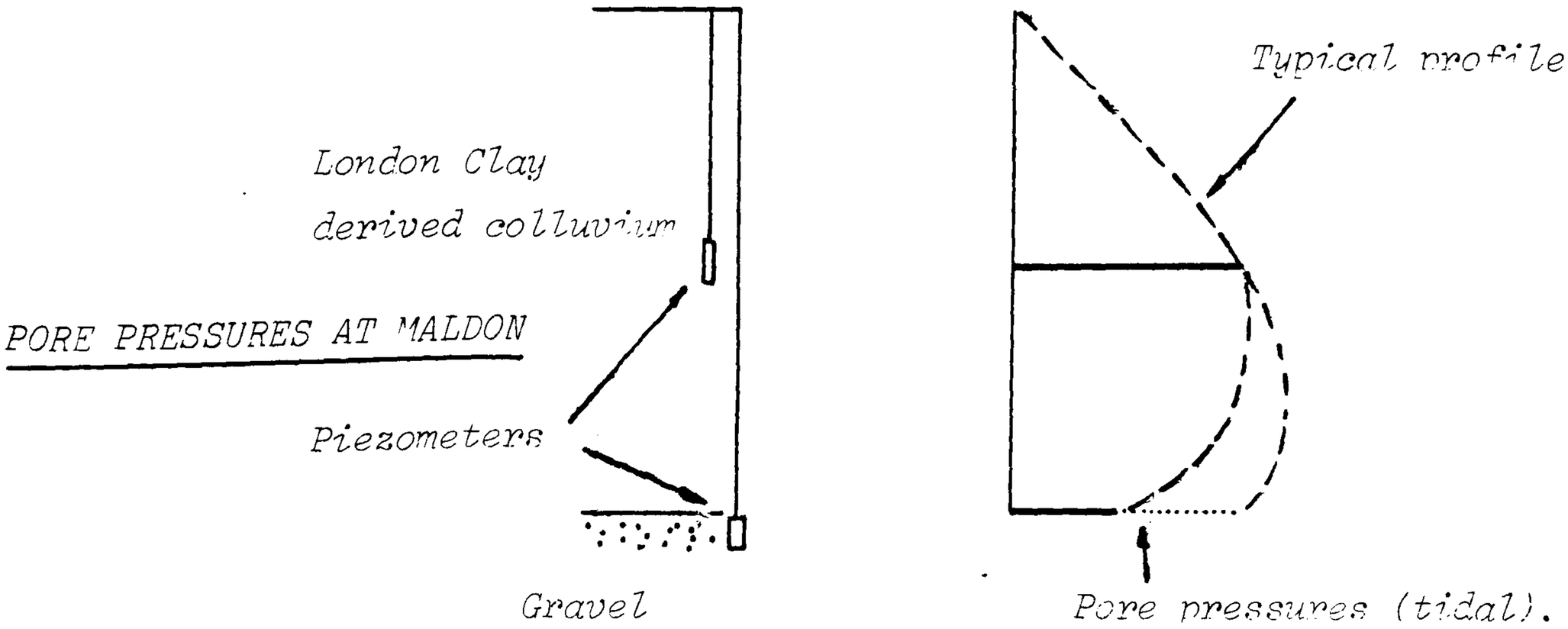


Figure 2.27. Field pore pressure/depth curves at the University of Kent, and at Maldon (Essex).

CHAPTER 3 - FINITE ELEMENT MODELS FOR SEEPAGE

3.1. Introduction

The finite element method has been applied to the solution of steady seepage and similar field problems for a considerable period of time and a large body of literature exists. However, the pioneering paper appears to be by Zienkiwicz and Cheung (1965) in which the theory is developed. This work was later developed to take into account soil and fluid compressibility in a variety of consolidation models. Broadly speaking, these consolidation models can be classified as *coupled* (and largely similar to Biot's theoretical model) or as *uncoupled* (and thus comparable to the Terzaghi-Rendulic consolidation model). Since except for the trivial one dimensional case, the uncoupled models are useless in the prediction of deformations during the consolidation process, much of the recent research has concentrated on coupled solutions. However, uncoupled solutions do appear to give a reasonable prediction of pore water dissipation (omitting of course the results of coupling such as the Mandel Cryer effect) and in view of their greater simplicity have been used to the exclusion of coupled models in this work. The basis for the finite element programs used is the theory outlined by Zienkiwicz and Parekh (1970) and given in brief below.

It is an easy matter to extend the method to cover arbitrary distributions of permeability and compressibility and the principles involved are outlined in Section 3.5.

3.2. Energy Basis of the Theory

If we define the total energy per unit weight of water (i.e. total head, H) at a point in the seepage domain as:-

$$H = z + \frac{u}{\gamma_w} + \frac{v^2}{2g}$$

in which z is the elevation head, u/γ_w the pressure head & $v^2/2g$ the velocity head, it is usually found that the velocity term is negligible and the total head which now contains potential energy terms only, may be renamed *potential* ϕ i.e.:-

$$\phi = z + \frac{u}{\gamma_w} \quad \underline{\text{or}} \quad z + h_w$$

Considering a cuboid soil element with sides inclined parallel to the axes of permeability, (see Figure 3.1) then considering the work done per unit time, in one of these orthogonal directions x, ΔW_x we have:-

ΔW_x = average driving pressure x area x velocity

$$= \frac{\partial p}{\partial x} \cdot \frac{dx}{2} \cdot dy \quad dz \cdot \quad v_x$$

Now with $\frac{\partial p}{\partial x} = \gamma_w \frac{\partial \phi}{\partial x}$ and $v_x = -k_x \frac{\partial \phi}{\partial x}$

we have

$$2.\ \Delta W_x = -\gamma_w\ k_x \left(\frac{\partial \phi}{\partial x}\right)^2 dx\ dy\ dz$$

Hence the work done *per unit volume* in all three orthogonal permeability directions is:-

$$\frac{\Delta W_1}{V} = \frac{-\gamma_w}{2}\left(k_x\left(\frac{\partial \phi}{\partial x}\right)^2 + k_y\left(\frac{\partial \phi}{\partial y}\right)^2 + k_2\left(\frac{\partial \phi}{\partial z}\right)^2\right)$$

and throughout the whole domain of volume

$$W_1 = \frac{-\gamma_w}{2}\int_{vol} k_x\left(\frac{\partial \phi}{\partial x}\right)^2 + k_y\left(\frac{\partial \phi}{\partial y}\right)^2 + k_2\left(\frac{\partial \phi}{\partial z}\right)^2 d\,vol$$

If water enters or leaves the seepage domain by crossing one of its boundaries, energy is contributed or lost. Thus the total energy dissipation rate must include for this. With a known flow rate of q per unit area per unit time from a boundary at an unknown potential ϕ, this contribution is:-

$$W_2 = -\gamma_w q \phi \qquad \text{per unit area}$$

or $$= -\int_{SR} q \cdot \phi \cdot \gamma_w \, d.\,\text{area}$$

Where SR is the part of the surface area of the problem where this activity is taking place.

Since natural systems tend to be conservative we expect the rate of dissipation of energy per unit time throughout the region to be a minimum and the finite element problem is one of minimising the sum $W_1 + W_2$ *

3.3. Finite Elements

A finite element is a subregion of the seepage domain which has a finite (as opposed to infinitesmal) size. Around the boundary of the element are a number of characteristic points (nodes) at which the potential is to be evaluated. The potential at any point in the element can be obtained from the nodal values by interpolation, i.e.:-

$$\phi_{xyz} = [N]\{\phi\}^e = [N_1 \; N_2 \; \cdots] \begin{Bmatrix} \phi_1 \\ \phi_2 \\ \vdots \end{Bmatrix}$$

where each term N_i is itself a function of the coordinates (xyz). Since the nodal values of potential are independent of the coordinates of the sampling point, the gradient of potential must be

$$\frac{\partial \phi}{\partial x} \text{ at } xyz = \left[\frac{\partial N}{\partial x}\right]\{\phi\}^e$$

and similarly for $\frac{\partial \phi}{\partial y}$, $\frac{\partial \phi}{\partial z}$

---

*The author is indebted to Dr. A. Skinner for this derivation. ie pp 72-74.

By subdividing the region into elements the evaluation of the integrals in the expression for energy dissipation:-

$$W = \frac{\gamma_w}{2}\int_{VR} k_x\left(\frac{\partial\phi}{\partial x}\right)^2 + k_y\left(\frac{\partial\phi}{\partial y}\right)^2 + k_z\left(\frac{\partial\phi}{\partial z}\right)^2 dVol \; + \; \gamma_w\int_{SR} q_i\phi \; darea$$

can be seen as the summation of similar, but more restricted, integrations in each element i.e.:-

$$W = \frac{\gamma_w}{2}\sum_1^{NE}\int_{VE} k_x\left(\frac{\partial\phi}{\partial x}\right)^2 ----- \; dVol \; + \; \gamma_w\sum_1^{NS}\int_{SE} q_i\phi \; darea$$

For a minimum in the rate of energy dissipation in the seepage regime, change of potential at any point (or node) will cause an increase in W. Hence the derivative of W with respect to the potential at node i is zero, i.e.:-

$$\frac{\partial W}{\partial\phi_i} = 0 = \sum_1^{NE}\int_{VE} k_x\cdot\frac{\partial\phi}{\partial x}\cdot\frac{\partial}{\partial\phi_i}\left(\frac{\partial\phi}{\partial x}\right) + ----- \; dVol$$
$$+ \sum_1^{NS'}\int_{SE} q_i\frac{\partial\phi}{\partial\phi_i} \; darea$$

Since node i is not connected to every element or surface in the subdivided region, but only to a subset NE' and NS' respectively of these, the summation need only be over these elements and surfaces.

Now, in any particular element

$$\frac{\partial}{\partial\phi_i}\left(\frac{\partial\phi}{\partial x}\right) = \frac{\partial N_i}{\partial x}$$

and

$$\frac{\partial\phi}{\partial\phi_i} = N_i$$

so that when all possible $\frac{\partial W}{\partial\phi_i}$ terms are considered we have a

matrix equation

$$\frac{\partial W}{\partial \{\phi\}} = \{0\} = [H]\{\phi\} + \{F\}$$

where each term in the matrix $[H]$ is the sum of contributions h_{ij} from each element connected both to node i and to node j

$$H_{ij} = \sum_{1}^{NE'} h_{ij} = \sum_{1}^{NE'} \int_{VE} k_x \frac{\partial N_i}{\partial x} \frac{\partial N_j}{\partial x} + \ldots\ldots\ldots \; dvol$$

and the vector $\{F\}$ is the sum of terms f_i from each part of the surface adjacent to node i

$$F_i = \sum_{1}^{NS'} f_i = \sum_{1}^{NS'} \int_{SE} q \, N_i \; darea$$

The so called stiffness matrix for an element could be written as:-

$$[K]^e = \int_{VE} [B']^T [D'] [B'] \; dvol$$

where

$$[D'] = \begin{bmatrix} k_{x'} & 0 & 0 \\ 0 & k_{y'} & 0 \\ 0 & 0 & k_{z'} \end{bmatrix} \quad \text{and} \quad [B'] = [B_1' \quad B_2' \quad \ldots\ldots]$$

in which

$$B_i' = \begin{bmatrix} \frac{\partial N_i}{\partial x'} & \frac{\partial N_i}{\partial y'} & \frac{\partial N_i}{\partial z'} \end{bmatrix}^T$$

and where x' y' z' are the *principal permeability axes* and also the *local coordinate directions* for the element. Alternatively, the same form $\int [B]^T [D][B]$ may be retained but with:-

$$[D] = \begin{bmatrix} k_{xx} & k_{xy} & k_{xz} \\ k_{yx} & k_{yy} & k_{yz} \\ k_{zx} & k_{zy} & k_{zz} \end{bmatrix}$$

and B_i is a slope matrix as above but this time expressed in terms of the overall or *global* coordinate system. Should the global and local coordinate systems be orientated arbitrarily then $[D]$ can be recovered from $[D']$ by the appropriate transformation matrix $[T]$ thus:-

$$[D] = [T]^T [D'] [T]$$

For simple elements, and indeed for many complex elements, it is simpler to transform the element geometry into the appropriate system, but where the permeability directions vary through an element the matrix must be found for each Gauss Point.

The seepage velocities can be found from:-

$$\{v\} = \begin{Bmatrix} v_x \\ v_y \\ v_z \end{Bmatrix} = -[D][B]\{\phi\}^e$$

3.4. Treatment of the "Known Potential" and "Known Flow" Boundaries

Possible boundary conditions for a seepage domain are shown in Figure 3.2. These include the following types:-

(a) and (c) Segments of boundary where the value of the potential is known *a priori*. If the whole segment has the same potential, then the velocity in the direction along, or tangential to, the boundary segment is zero. The unknown here is the potential gradient normal to the boundary, or rate of fluid transport across it.

(b) A boundary segment where the seepage quantity through the boundary is known. The commonest form of this is where this quantity is zero - an *impermeable* boundary. In this case, the unknown quantities are the boundary potentials.

(d) A part of the boundary where there is a combination of the two conditions a. and b., that is, there is no flow across the boundary and its potential is known to be equal to its elevation. The problem here is the determination of the *position* of this "free surface".

(e) The final commonly encountered field boundary condition is the seepage face. Here, the potential is equal to the elevation, the position of the seepage face is known - but there may be a discharge across it. The length of such a face depends on the interrelation of the seepage face and free surface.

The potential formulation for the finite element seepage analysis given above is quite capable of dealing with the first two of these types, yielding the appropriate unknown values as a part of the solution. Classes of problem definable in terms of these two boundary conditions alone are termed "confined". Dealing with the other two presents more problems.

In many cases, however, it is not necessary to consider free surfaces and seepage surfaces in order to arrive at an acceptable solution. For example, the combination of N. European climatic conditions and a clay soil will render the free surface idea largely redundant; as the upper boundary, exposed to the atmosphere, can be dealt with as a known potential boundary without appreciable loss of accuracy. In conditions equivalent to summer drought, this surface potential may have to imply a soil suction (Vaughan & Walbancke, 1973; Black, Croney & Jacobs, 1958).

A "known potential" boundary condition is analogous to a "known displacement" condition in structural analysis, and a wide variety of techniques able to deal with this are well established throughout the field of matrix methods in engineering mechanics (e.g. Zienkiwicz 1972 for a summary). It should be noted that a "reaction to earth" in such a case is the nodal in- or out-flow rate in the seepage analysis. The technique adopted in computer programs used in this research nulls the rows and columns of the stiffness matrix corresponding to the prescribed degree of freedom except for the value of 1.0 which is left as the principal diagonal. The appropriate element of the forcing vector of flow rates is then modified to yield the correct potential on back substitution.

In general, the treatment of "known flow" conditions is simpler as the product of flow rate and nodal shape function is integrated numerically over each element surface to produce an equivalent nodal "force" added into the forcing vector. $\{F\}$.

3.5. Treatment of the "Free Surface"

In situations where the free surface must be represented, there are a variety of techniques for so doing. Each of these present some difficulties in implementation and these are dealt with below:-

(a) Iterative, Variable Stiffness, Variable Geometry Methods

The first two of these methods can most simply be described as iterative, variable stiffness, variable geometry techniques. Basically, an assumption is made as to where the free surface is, and either boundary condition a. (known potential) or b. (no flow) is assumed. Then, with the complete regime defined, a simple, "confined" solution is produced. The appropriate results, of flow rate or boundary potential respectively, are then examined to see if the free surface conditions d. are satisfied; and if not, then the position of the free surface is modified and another trial solution attempted. It is this modification that poses problems for the programmer.

Since the complete mesh of finite elements, or at least an appreciable part of it, has its geometry altered in each iteration, new stiffness matrices must be formed, assembled and solved. Hence the terms iterative, variable stiffness, variable geometry in the description of these techniques.

Perhaps the simplest of the two techniques is to set the "no flow" condition on the trial "free surface". Then this is by definition a flow line and the nodal potentials derived from the confined solution can be compared to the node elevations. Taylor and Brown, 1967, describe this sort of process.

The alternative is to set the "known potential" on the trial position of the free surface and check the "reactions" or flow rates across this boundary given by the confined solution against the desired "no flow" condition. A number of authors have used this method (e.g. France, Parekh, Peters & Taylor, 1971), particularly since it lends itself to non-steady free surface seepage where the instantaneous velocity of the free surface may be related to this flow rate and the free surface is *not* a flow line during the process.

Most of the papers devoted to iterative, variable stiffness, variable geometry, techniques use simple illustrative examples. If these are chosen wisely, the algorithm for iteratively modifying the mesh is a simple one. For example in Figure 3.3 a., it is only necessary to shift the nodes of the outermost band of elements. It is also essential to avoid vertical or overhanging mesh segments above the upstream water level (X in Figure 3.3 b.) and "corners" in the trial free surface (Y in Figure 3.3. b.). In order to have the simple algorithm one must also know the exit point of the free surface. However, realistic examples are not so amenable to simple treatment.

We must, therefore, introduce the concept of MASTER, SLAVE and INDEPENDENT nodes. A master node is one actually on the free surface. It may, however, be constrained to move along a fixed path, such as the edge of a drainage layer, or the interface between soil strata.

A slave node is constrained to follow the movements of a particular master node. Independent nodes are those whose position is unaffected by the movement of the free surface. Given that nodes are defined in this way, that the allowable movement directions are prescribed for all master nodes, and the slave nodes are adequately referenced to their masters, then the iterative process can be automated (Fig. 3.3. c.).

The final problem arises if master and/or slave nodes cross over into a region of elements defined by independent nodes. In this case, the whole or part of a subregion of the mesh comprising a particular material type is "wiped out" and this usually requires additional alterations to the mesh, this time of a non-routine kind. Manual intervention at this stage is desirable to prevent otherwise inordinately heavy demands being made on computing resources (Fig. 3.3. d.).

Kealy and Busch (1971) avoid the problem of having to define the types of nodes by making extensive use of automatic mesh generation in their (strictly speaking, Taylor & Brown's) computer program. The node numbers from which the mesh was originally generated are "remembered". After nodes on the free surface have been corrected, the whole mesh is regenerated from the new coordinates of the "remembered" nodes. Fairly drastic mesh modifications can be acoommodated by this means, but it is vital to generate the data in columns of elements, rather than rows, for the best results. Elimination of a complete zone is indicated by the areas of certain elements becoming negative.

Some authors treat the seepage face as an extension of the free surface. While in the main this does not give rise to serious errors, it is not strictly correct, and it is more sensible to introduce a thin layer (Fig. 3.3) on to the edge of the mesh of greatly increased permeability to deflect flow lines as they emerge from the main part of the mesh. This is unnecessary if the latter of the two techniques is used, but may nevertheless simplify the overall algorithm since the programme will not therefore need to differentiate between free surfaces and seepage faces.

(b) Iterative, Variable Stiffness, Variable Properties Method

This section shows how by using simple techniques it is impractical to obtain a realistic free surface seepage solution by manipulating the permeability coefficients.

Essentially, the basis of an iterative, variable stiffness, variable properties method is to provide a seepage domain with the appropriate boundary conditions, perform a confined analysis and on the basis of an inspection of the results of such an analysis to modify the solution in some way, submitting the mesh with its new properties to a further analysis and so on until clearly defined subregions emerge, one with positive pressure heads, and the other with negative pressure heads. Ideally the final picture would be that of Figure 3.5 in which the flow line separating the two subregions would in every way satisfy the conditions of a free surface. Algorithms for modifying the permeabilities or for injecting a self equilibrating set of nodal flow rates (Bromhead 1976) would appear by analogy with techniques that have been successfully applied in structural methanics to be possible routes to a solution that does not require a variable geometry.

However, in a confined solution, with the upper seepage domain boundary, Figure 3.5. treated as impermeable, it appears to be the curvature of the equipotentials forced by the proximity of the boundary itself that distorts the zero pressure line away from the ideal "free surface" position. Desai 1976, for example, is only one of the authors who has commented on this apparent closeness.

Examining the ideal solution, Figure 3.5., in more depth, we find a number of geometrically similar figures for the equipotential and flow lines in the *positive pore water pressure* subregion. The continuation of the equipotentials into the *negative pore water pressure* subregion maintains the geometrical similarity.

Thus, by pushing the no flow boundaries sufficiently far from the region of interest so that their actual shape has little effect on the flow in the positive pore water pressure subregion (Fig. 3.5) *we could perhaps arrive at a state where the zero pressure line coincides with the ideal free surface line to all practical intents and purposes.*

While this argument is persuasive for simple, homogeneous cases, it is not necessarily so for arbitrarily zoned domains. Some trials of this have been carried out without success. This may, however, be due to the effects of the entry point singularity (Figure 4.3.a.).

(c) Iterative, Constant Stiffness Methods

These depend on adding an internally equilibrated system of flows to certain of the nodes of the mesh to force the solution into obeying some conditions *vis a vis* the position of the zero pressure line, or the velocity vector magnitudes and/or directions, for example, in the negative pore water pressure subregion. In essence, they force the boundary conditions to conform to those of the idealised diagram Figure 3.5. As of the present, none of the methods is completely satisfactory.

3.6. Variations of Permeability

Naturally sedimented soils have an inherent anisotropy due to their bedding and one of the principal permeability axes will lie in a direction perpendicular to the bedding plane. The other two axes will lie in the bedding plane and almost invariably it will be found that permeability in the bedding plane is independent of direction. Following sedimentation, a variety of geological processes may act to modify the values and possibly the directions of the principal permeabilities, but inevitably, three orthogonal principal permeability axes will be found. In laminated soils the effect of stress rotations on the principal permeability directions is likely to be quite limited since the intrinsic anisotropy in soil permeability is inherently more important than a stress induced anisotropy. However, in some

soils it is likely that they assume an anisotropy due to their consolidation under anisotropic effective stress conditions. Changes in the magnitude and direction of the effective stresses will therefore result in changes in the magnitude and direction of the permeability axes, with a corresponding effect on the seepage regime.

A variety of possibilities for introducing the effective stress dependence of permeability can be considered:-

(a) A complete interaction of stress with permeability giving rise to changes in both the magnitude and direction of the principal permeability axes.

(b) A situation in which the permeability axes do not change direction but the permeability magnitudes all change either:-

    (i) in response to changes in effective stress normal to the permeability axis,

    or

    (ii) in response to some averaged effect of all the effective stress changes.

(c) A case where certain of the permeability components remain unchanged but others respond to changes in a particular effective stress, for example, that normal to the permeability axis considered.

Possibility (a) can immediately be discarded on the grounds that the laws governing this type of interaction are virtually unexplored and the effort in programming a solution would be fruitless in view of the absence of suitable parameters for field situations. In cases (b) and (c) we have no rotation of permeability axes with rotation of principal stress and strain axes, and these situations are somewhat simpler than the other case.

3.7. Anisotropic and Non-Homogeneous Permeability

The finite element method can accommodate fairly arbitrary variations in permeability and in the directions of the principal permeability axes. With simple elements, these factors are taken as constant across each element with a possibly abrupt change of properties across an inter-element boundary. In the numerically integrated elements used in this research it is possible to have a greater degree of smoothness in the variation of these factors, the magnitudes and directions of permeability coefficients being defined by some function and thus capable of being evaluated at each Gauss integrating point. The [D] matrix is therefore evaluated afresh at each Gauss point as the contribution from that point to the element "stiffness" and other matrices is evaluated. Higher order functions than the element shape functions can be specified for these variations but in a global sense this higher order variation is followed only in an approximate, piecewise, fashion.

3.8. Effective Stress-Permeability Relationships and the Finite Element Solution

In Chapter 2 the use of effective stress dependent permeabilities in seepage analysis has been introduced and treated by means of closed form analytical solutions and a simple one dimensional finite difference model. For two and three dimensional work an alternative method is necessary, and the advantages of the finite element method for seepage analysis in homogenous soils lead to its adoption as a vehicle for the effective stress dependent permeability solutions.

Tests have been made using the finite element theory for a variety of effective stress-permeability functions including the "logarithmic" and "power-law" functions of Chapter 2. In these, the vertical total stress has been taken to be the dominant one - this is equivalent to assuming K_o to be unity* - and the permeability - effective stress relationships used are shown in Figure 3.6.

*In: $k = ae^{-b(\sigma')_{mean}}$

The finite element technique for dealing with effective stress dependent permeability is a simple, explicit iterative method. In the computer data, the coefficients for the nominated effective stress-permeability relationships are input in the place of ordinary permeability coefficients, and where the normal data would end, additional information on the total stresses in the soil must be provided. This takes the form of the three principal stresses and must be provided for each Gauss point. These are then averaged, since all the work described here has been done with the average total stress. Average stresses could be input (in principle) but the program was written with the provision of these stresses from (say) a non-linear finite element stress analysis, and they would therefore be available on a Gauss point basis, and be a full set of all the principal stresses. However, in much of the present work, the total stresses have been evaluated manually using simple rules appropriate to the one-dimensional cases used.

The first step in the analysis is the assumption of a set of potentials and hence pore water pressures throughout the mesh. As a preliminary estimate, the pore water pressures are taken as zero at each node point. Thus, when the element stiffness matrices are evaluated and the permeability coefficient is found at each Gauss point from the stored stress average, the pore water pressure interpolated from the nodal potentials (with a level correction applied for the Gauss point elevation) and the nominated permeability - effective stress law.

Following the formation of these stiffness matrices the assembly and solution processes proceed in the ordinary way to yield a new set of nodal potential values. From these, an integral of the potential over the volume of the mesh is evaluated using stored weighting factors for each node, *viz.*

$$\int_{VR} \phi \, dvol = \sum_{1}^{NE} \int_{VE} \phi \, dvol$$

$$= \sum_{1}^{NE} \sum_{i=1}^{NG} \sum_{j=1}^{NG} W_i \, W_j \, [N]^T \{\phi\}^e |J|$$

$$= [\lambda]^T \{\phi\}$$

NG is the number of Gauss points and W_i and W_j are the appropriate weighting factors.

in which the λ factors are the appropriately combined weighting coefficients evaluated for each node on an element by element basis.

For the second iteration, the potentials derived from the first iteration are used to define the permeabilities during the stiffness formation phase, and the process repeated as before. The new potential integral is compared with the old one, and if significant differences are found, then the process is repeated. Convergence is assumed when fluctuations in the potential integral have slowed down to an acceptable level.

In the following section (3.9), the testing and evaluation of this finite element method is described in detail and it is seen that complex accele rator techniques are not required. Most of the matrices are of fairly low rank and the formation, assembly and solution processes are rapid.

3.9. Testing the Effective Stress Dependent Seepage Model

Test 1: A 10 m high column of unit cross sectional area, comprising ten identical 8 noded isoparametric elements was devised to represent a wholly underdrained (D_u = 1) soil layer, and a permeability model in which the permeability k was a function of

mean effective stress:

$$\ln k = a - b\sigma'$$

An analytical model has been developed for this case and this provides a control on the final finite element solution. This analytical solution shows a distribution of pore water pressures with depth that is independent of the parameter a (Section 2.3).

Figure 3.8 shows the results of the six finite element test runs, and the analytical results are also plotted for comparison where these are not identical to the finite element results. It will be noted that for small b values, the finite element method yields answers that are identical to the analytical solution but that as b is increased, discrepancies appear. These differences between the numerical and analytical results arise where the potentials and hence permeabilities are most rapidly varying, and are the result of the simple parabolic element's inability to adequately represent the rapid variation of permeability with the coarse subdivision into elements chosen for this test. Selection of a finer overall mesh of elements, or one graded finer in this region, largely overcomes the problem.

Convergence in every case was rapid with a stable distribution of potentials being reached by the fourth iteration. The tests with the highest and lowest b values appeared to converge most rapidly, there was a small tendency to "overshoot" with b values in the middle of the range. These convergence characteristics can be seen most easily in Figure 3.9 which is a plot of the integral of potential over the whole finite element mesh vs. the number of iterations. Although it is possible for the value of this integral to remain constant while the actual potentials fluctuate wildly, that is an extremely unlikely occurrence, and the usefulness of this parameter as a guide to the rapidity of convergence is unimpaired.

As a severe test on the method, the initial conditions selected for the iterative process were that the potential at every node was taken as zero. A more rapid convergence can be obtained by starting with the potential at each node equal to its elevation (by inference having zero pore water pressure) or even from a preliminary finite element analysis using constant permeabilities (in the present case, these latter two possibilities are identical, but in general they will not be so).

Test 1a: An additional element was inserted at the base of the mesh to try to overcome the problem of the too rapid variation of permeability in this region. Some improvement in the relative agreement of the analytical and numerical solutions was noted. It is felt that excellent agreement is obtained for *reasonable* permeability laws - in the extreme case of b = 1.0, the permeability changes by about thirty orders of magnitude in the bottom 0.1 m!

Test 2: The second test is of horizontal flow with constant total stress. This is of course less severe than the vertical gravity flow of tests 1 and 1a and is furthermore, more amenable to analytical solution (Walbancke, 1976). A ten element, 10 m long flow channel has been used in the model, for which the cases of b = 0.001, 0.01, 0.02, 0.05, 0.1 and 1.0 have been considered. Excellent agreement with the analytical solution is again obtained, generally to well within ½% at any point, and much better for the smaller b values. At the high (0.1 to 1.0) b values there is some larger discrepancy but this is not so marked as in the vertical seepage. It is, however, quite noticeable that there is a pronounced oscillation in the integral used to monitor the iteration in the mid range of b values and that as many as 10 iterations can be necessary to secure a reliable result.

Conclusions from the Simple Tests: It appears that the *variable stiffness* approach adopted here is capable of yielding very accurate results within a coarse mesh. Few problems of stability arise - when permeability is weakly dependent on effective stress, the solution in the limit degenerates to the constant permeability case; and in the other limit, the onset of instability occurs long after the bounds of reasonable soil behaviour have been passed. Furthermore, since the stiffness matrices are of fairly low rank and are thus simple to form, assemble and solve, the computer time

and storage requirements of the variable stiffness approach (which are excessive when it is used in a stress analysis context and have led to the adoption of other techniques mainly from the consideration of the efficient use of computer resources) are not unduly large. Virtually all of this work has been completed using the minimum level (i.e. J1, "instant turnround") of computer resource available at Imperial College.

This oscillation was investigated with the graded meshes shown in Figure 3.10. In this case it was not found that finer subdivision increased the rate of convergence. In fact, increasing fineness of subdivision degraded the convergence characteristics (Figure 3.12). On closer inspection it was found that the finer subdivision only served to aggravate a condition which implied an apparent reversal of flow direction in the extreme edge element. This effect is analogous to the oscillations that sometimes arise in a time stepping consolidation solution when using this element, and is the direct result of the incompleteness of the shape functions used. Further discussion of this point is deferred to Section 4.4.

A general point, worthy of discussion, is the degradation of the solution as the b parameter is increased, followed by an apparent reversal of this trend. However, this is more apparent than real. It is the result of the 8 noded, parabolic element being unable to accommodate the very rapid change in potential close to the boundary at all accurately. Instead, it responds by trying to do so as best it can, but being restricted to a second order variation of potential across itself has to do this in a very approximate way. Plotting only the nodal values of potential is quite misleading, as can be seen from Figure 3.10 which shows the internal, or Gauss point, values as well; and hence reveals the true potential distribution in the last element (the b = 0.10 and b = 1.0 cases with horizontal flow have been chosen to illustrate the effect).

Note also that this effect is not due to the iterative effective stress dependent permeability method, but is an intrinsic property of this element; which is revealed elsewhere when the potential gradients are high, such as for example near a drainage boundary during the early stages in a consolidation solution.

As the b parameter is increased in magnitude we find analytically that virtually all the potential changes in the solution occur near the lower potential boundary. In the finite element solution we find the same effect, which is understandable since the permeability in the last element will be much lower, often by several orders of magnitude, than elsewhere in the mesh. The final element does exhibit the parabolic potential distribution noted above, but should we ignore this and plot only the nodal values we find reasonable apparent agreement! However, further increase in b causes only small changes in the finite element potential variation whereas the analytical solution shows a continual progression. Ultimately, for very large b, the agreement between finite element and analytical solutions is controlled solely by the size and shape of the last element. This effect is shown in Figure 3.10.

Unfortunately, it seems that in refining the finite element mesh we give rise to a progressively increasing instability in the solution process. This can be seen in the plot (Figure 3.12) of the potential integral $\int \phi$ dvol vs. the iteration No. As the mesh is progressively refined in the region of the drainage boundary, the amplitude of oscillation of the integral becomes larger, and more cycles of iteration are necessary to obtain the ultimate solution. In general terms this reflects the greater number of degrees of freedom involved, allowing a more complex oscillation in this potential integral as well as allowing an ultimately more accurate representation of the potential variation. Further discussion on this point is reserved until Section 4, under the heading "Element Induced Potential Oscillation".

If it were possible to more accurately specify the initial potentials in the problem (we do, after all, start from fairly arbitrary values) then the iteration would presumably be more rapid, but a certain loss of generality would result. This has not been explored since it is felt to be of little direct applicability since the whole problem only arises for impractical values of the b parameter.

In two dimensional cases where large potential gradients exist in two dimensions, this "best fit paraboloid" is even more severely peaked with the result that for large negative effective stress conditions are predicted and the function $-b\sigma'$ becomes large and positive,

ultimately exceeding the critical value for which $e^{-5\sigma'}$ can be respresented in the computer (note that at Imperial College e^{196} can be evaluated giving about 10^{276}). Long before this condition is reached, however, the solution has become worthless on purely practical terms.

3.10. Finite Elements Graphical Output

One of the major problems in the use of finite element methods for geotechnical analysis is the sheer volume of output that has to be processed. This is particularly the case when a large mesh is used or when a number of consecutive analyses are run. The latter case is very common when a time dependent process is being analysed or in the development stage of an iterative method. In principle, the analyst has two ways of presenting his results:-

Firstly, in the form of diagrams showing the behaviour at one or more *characteristic points*,

or

Secondly, as diagrams showing the *full-field* behaviour.

An example of the first type of presentation is to plot a selection of *stress paths;* and the second method is illustrated with the example of *flow nets* or pictures showing the deformation of the finite element mesh to an appropriately exaggerated scale. On the whole, the amount of work involved in plotting the *characteristic points'* results is much less than that for graphing the *full-field* pictures, and a consistent application of the latter techniques will usually require the use of a computer graphics program. Since this research is exclusively concerned with forms of seepage, and the results of the various analyses are not only best appreciated as *full-field* pictures, but are also conventionally depicted as such (in the form of *flow nets*), the use of computer graphics has been considerable.

Many of the individual techniques have been described elsewhere (e.g. Zienkiewicz 1972), but the program used in this work offers a selection of computer graphics techniques for checking the correctness of finite element mesh data and for processing or presenting the results of the analysis in a *full-field* form. It would be inappropriate here to discuss the full range of facilities offered by this program, except insofar as they are used for the diagrams in this thesis.

The facilities of FEGRAF used in the diagrams are as follows:-

1. Plotting finite element meshes. The principle is to trace the outline of each element in turn, using the optional facilities of indicating the position and numbering of the nodes, or of indicating the element numbers. Element meshes without numbers are also used as bases for the presentation of analysis results.

2. Plotting "exploded" finite element meshes. The principle here is as above but with a small gap left between each element. This enables the connectivity of the various elements to be seen at a glance.

3. Plotting the outlines of meshes. Thus the internal lines of the mesh do not confuse the issue.

4. Annotating the mesh with textual data.

5. Plotting contours. In the present case these are equipotentials, or contours of nodally defined potential (or equipotential). The contouring algorithm is very simple and provided that the mesh is finely subdivided where potentials vary most rapidly it provides acceptable results. In detail, in each n-noded element, the sub-set of nodal potentials is extracted, and the value at the element centroid is evaluated by shape function interpolation. Subsequently, the element is treated as n triangular sub-elements within which a purely linear variation of potential is assumed. Thus as an equipotential passes through an element it is seen on the plot as a series of straight line segments in each sub-element.

In exceptional cases, data defined at Gauss integrating points is contoured. This data is extrapolated linearly to the peripheral nodes of the element where the individual element contributions are averaged. These averaged nodal values are then treated as if they were nodally defined data *ab initio*.

6. The final data presentation method is the annotation of the plot with actual numerical values. These are scaled to lie between $\pm$ 1.0 and the appropriate multiplying power of 10 is output. It is often found that compiling results into this full-field format facilitates the later extraction of values for plots of the behaviour at *characteristic points*.

Figure 3.13 shows an example of each of these forms. It should be noted, however, that the contour plot (equipotentials) is *less* smooth than the finite element results, as a result of the simple algorithm used to plot the contours. This contrasts with manual flow nets drawn from finite element results which are often *more* smooth than the data really justifies.

3.11. De Mello's Work

The neglect of the effective stress dependent element of permeability on the development of seepage in soils is more surprising than the results of the effect itself, particularly since in every case to have an effective stress dependent permeability leads to higher pore water pressures and hence degraded strength and deformation properties than would be the case if the permeability were constant. Hence, the constant permeability case is *unsafe* (although by an amount that may, in many situations, be safely left out of consideration).

De Mello (1977) in his Rankine lecture clearly shows this. He first shows how, by the insertion of a chimney drain into an otherwise homogenous earth dam, the engineer "changes the statistical universe" in respect of seepage erosion of the downstream face of such a dam and then goes on to investigate the influence of permeability variations in the upstream shoulder of the dam. It is, however, clear from certain of his figures (notably his Figure 17) that he has considered an

ab initio distribution of permeabilities in this shoulder related to the *total* stress due to the self weight of the dam (this despite his Figure 11 in which he clearly shows permeability a function of effective stress). The coupling of pore water pressure with permeability has been sidestepped, as incidentally has the influence of reservoir pressures acting on the upstream face on the total stresses in the dam. Thus, De Mello's model is only an approximation to the correct solution. Nevertheless, his numerical results fit well with the observations of this thesis, and may be taken as further confirmation for the conclusion that it is by and large the *magnitude* of the permeability change and the fact that this is distributed through the seepage domain, rather than exactly *how* it is distributed, that controls the seepage pore water pressures.

3.12. Morgenstern & Guther's Approach

At a comparatively late stage in the preparation of this thesis, a paper by Morgenstern & Guther (1972) was discovered. This covers some of the ground of the earlier sections of this Chapter.

Broadly speaking, Morgenstern and Guther adopt the procedure shown diagrammatically in Figure 3.7. Their solution *is* coupled to the stress analysis, so that they do carry out step (h), the alteration of the total streses as a result of changed body forces, as the seepage regime alters. The seepage and stress analyses are performed in separate (but coupled) programs.

The effective stress permeability function chosen in their work is similar to the "power-law" function and takes the form:-

$$k = \frac{\alpha}{(J_1 + \beta)^n}$$

In which J_1 is the first effective stress invariant (equivalent to the mean effective stress) and α, β and n are the appropriate coefficients. Permeabilities are assumed isotropic and permeability rotations due to principal effective stress direction changes are ignored.

An additional feature of interest in the Morgenstern and Guther approach is that they are solving free surface problems with a variable mesh geometry in the seepage domain. They therefore have to have additional elements above the free water surface (also with a variable geometry) for the stress analysis, but do keep the same mesh as the seepage analysis below this internal free surface. The procedure is therefore:-

(a) Guess a free surface.
(b) Analyse stresses.
(c) Analyse seepage using current position of free surface.
(d) Adjust position of free surface by Taylor and Brown's (1967) method (presumably using permeabilities found in the previous stress analysis cycle, since although this is not perfectly clear from the text, their Figure 1 would seem to be fairly conclusive).
(e) Repeat steps (b), (c) and (d) until no further changes in the free surface position are required.

Among the conclusions is that the phreatic surface is higher when an effective stress dependent permeability relationship is taken than when a constant permeability is used in the analysis. In some cases the differences are substantial and have a destabilising effect on slopes. This conclusion is consistent with the compressing of the equipotentials near an exit face found using the writers own model. They also observe that their parametric study cannot be normalised as the results are strongly scale dependent.

Additionally, the elements used by Morgenstern and Guther are unlikely to suffer from the oscillating behaviour noted above in Section 3.9 and treated extensively below in Section 4.4 which are a feature of the parabolic serendipity elements used in this research (the Taylor & Brown → Kealy & Busch → Morgenstern and Guther program uses linear triangle elements or quadrilaterals made up from four linear triangle elements with the internal node eliminated from the system of equations at the time of assembly). While these elements are perfectly adequate

for one-degree-of-freedom-per-node seepage analysis, they need very fine mesh subdivision at stress concentrations to yield accurate stresses. Since the configuration selected by Morgenstern and Guther has such an intense stress concentrator in the corner of the excavation and a linear elastic stress-strain behaviour (which readily permits intense stress concentrations to appear) has been assumed, one must retain reservations about the accuracy and practicability of the solutions near the seepage exit point. Furthermore, the use of movements in the computed free surface position is neither necessarily an indicator that internal permeability - stress - potential readjustments are complete, nor is it of any use in confined seepage problems. However, in contrast to the Morgenstern and Guther work, the confined seepage problem is computationally trivial.

3.13. Summary

The well established finite element method, particularly when more sophisticated elements are used, is ideal for routine seepage analysis. Most types of boundary conditions are simply accommodated in the basic method and the only one posing any problems at all (the free surface) can be handled using one of several iterative techniques. In the context of the present work, the method directly solves problems where the permeability coefficients vary in space in a pre-defined way although it should be noted that high order functions for the variation of the permeability coefficients are treated as piece-wise continuous where the order of variation across any "piece" (i.e. element) is the shape function order for that element. (All elements used herein are isoparametric, virtually all of the 8 noded, serendipity kind).

A technique for dealing with seepage where the permeability is a known function of effective stress, given the initial total stress field, has been developed. This is an iterative technique the results of which correlate closely with those obtained from both closed form solutions and alternative numerical techniques. The occasional convergence problems have been investigated and have been found to arise principally from the characteristics of the element chosen for use.

Computer programs incorporating most of these features have been developed. These are supplemented by an auxiliary, computer graphics, program which simplifies the presentation of finite element results in two dimensions.

It should be noted that there is an alternative formulation for seepage in terms of a stream function rather than a potential. This alternative formulation readily lends itself to *adaptive* finite elements where the unknowns are connected with the shape of the element (i.e. coordinates) and the stream function is known (e.g. Liam Finn, 1980), thus simplifying computation of the position of free surfaces. Unfortunately, since the process of deriving pore water pressures is involved, *stream function* elements are not so readily suited to effective stress dependent properties analysis as are *potential* elements.

Principal permeability (and hence local coordinate) directions.

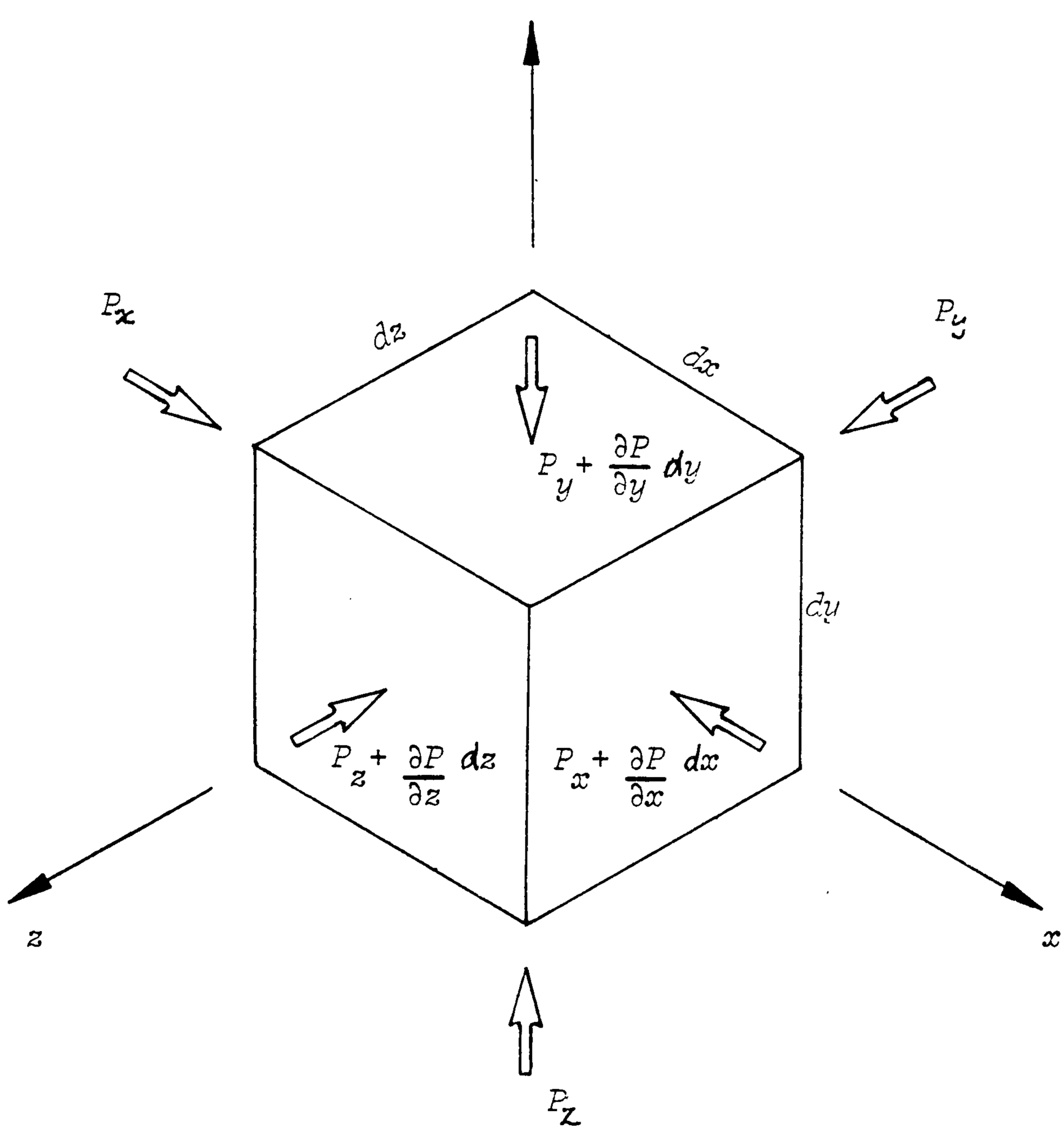
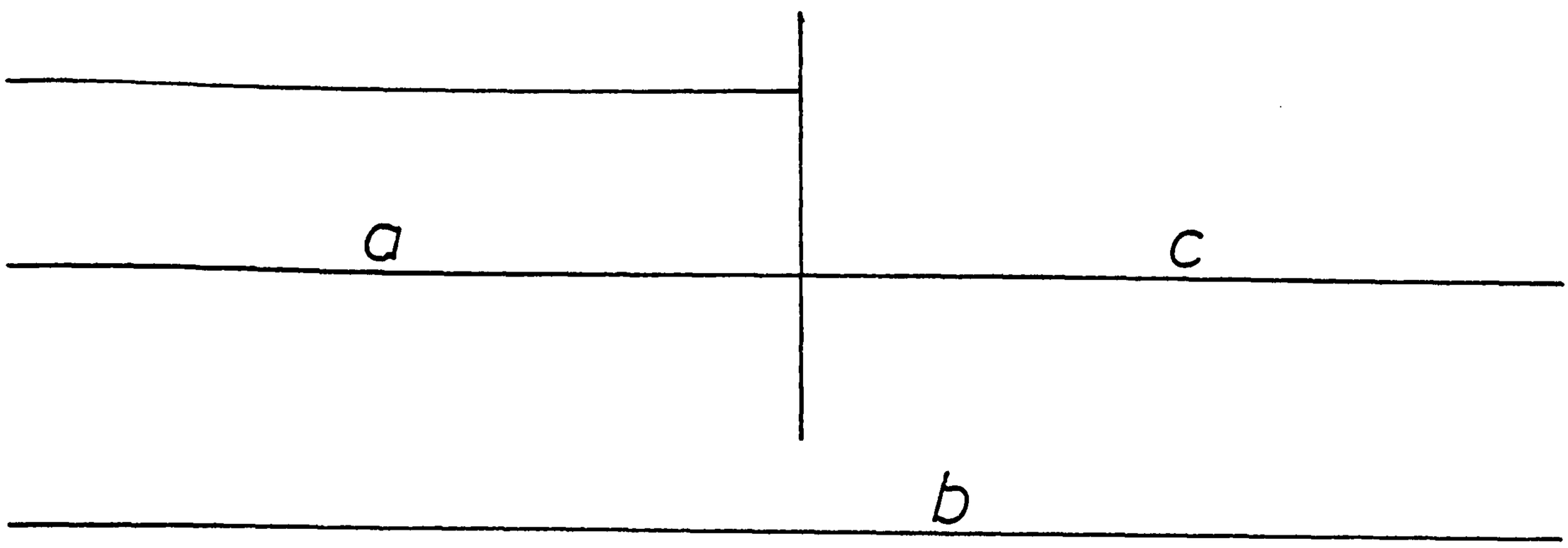
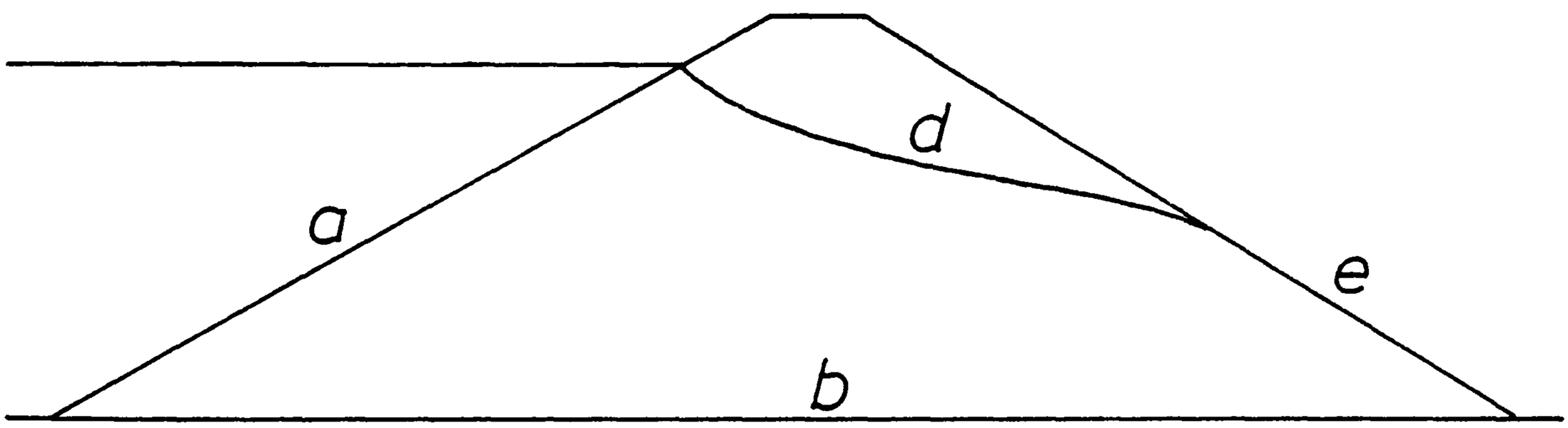


Figure 3.1. Pore fluid pressures acting on an infinitesimal soil element.



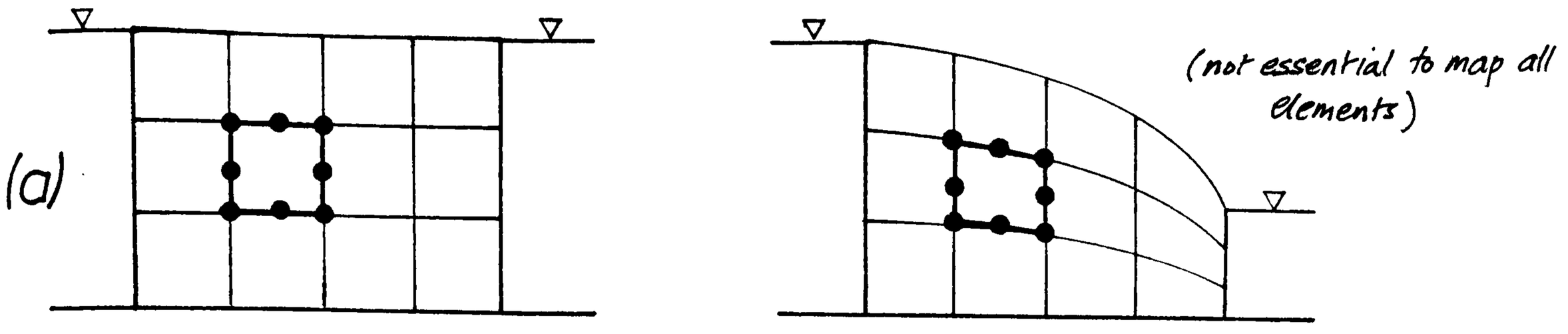
"Confined" problem



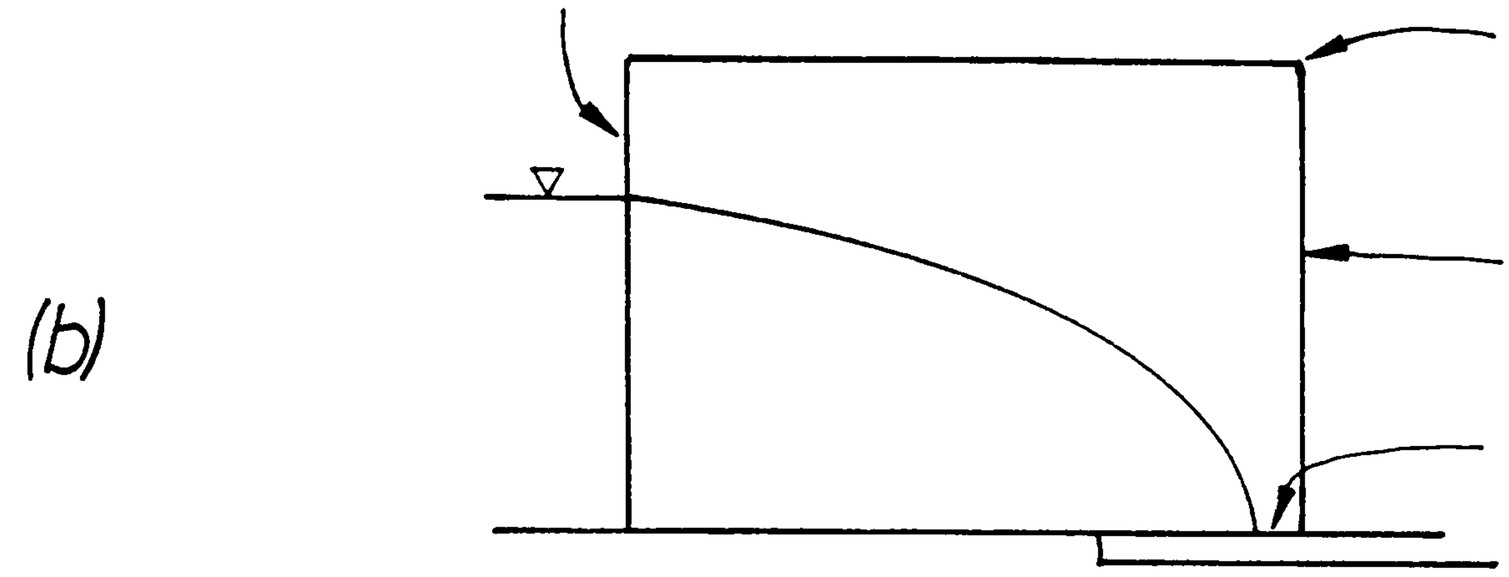
"Unconfined" problem

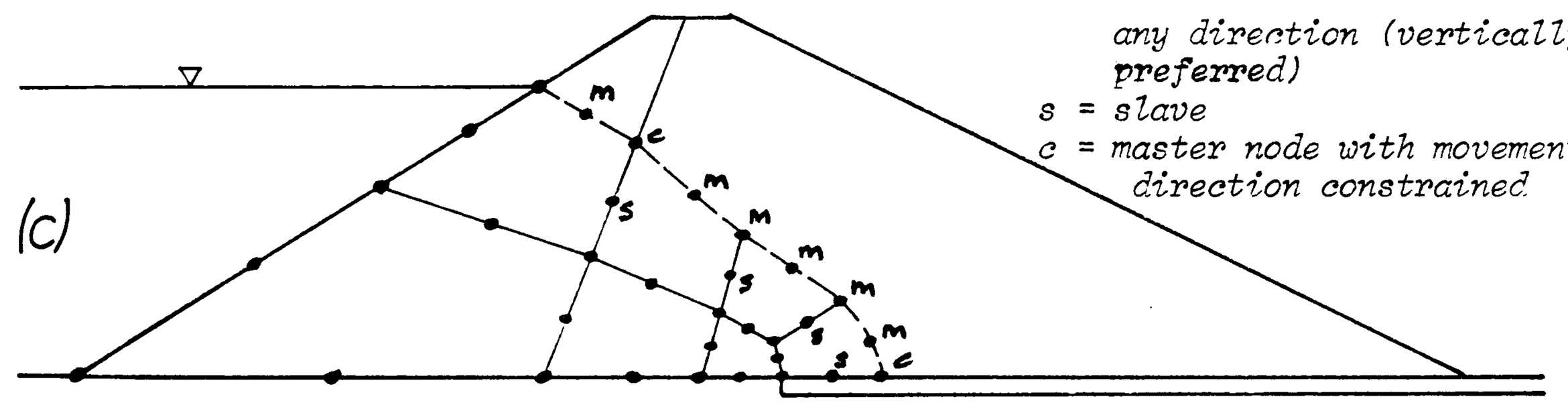
a, c	equipotential
b	impermeable
d	free surface
e	seepage surface

Figure 3.2. Types of boundary condition in seepage analysis.



Simple mesh transformation needed to solve the problem.





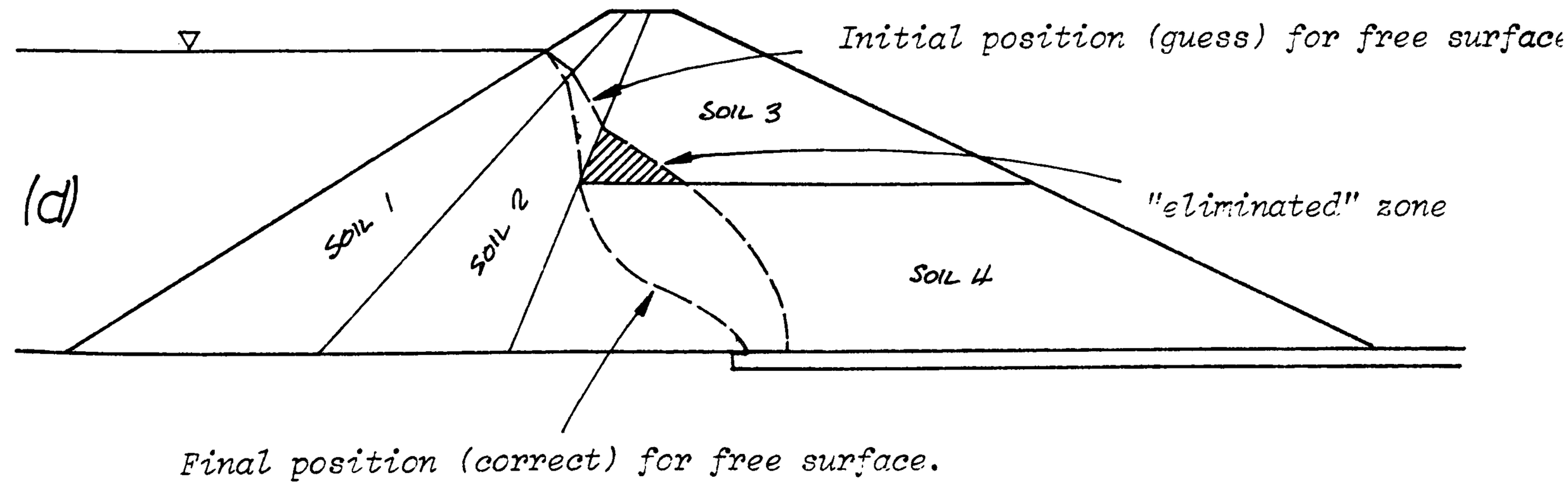
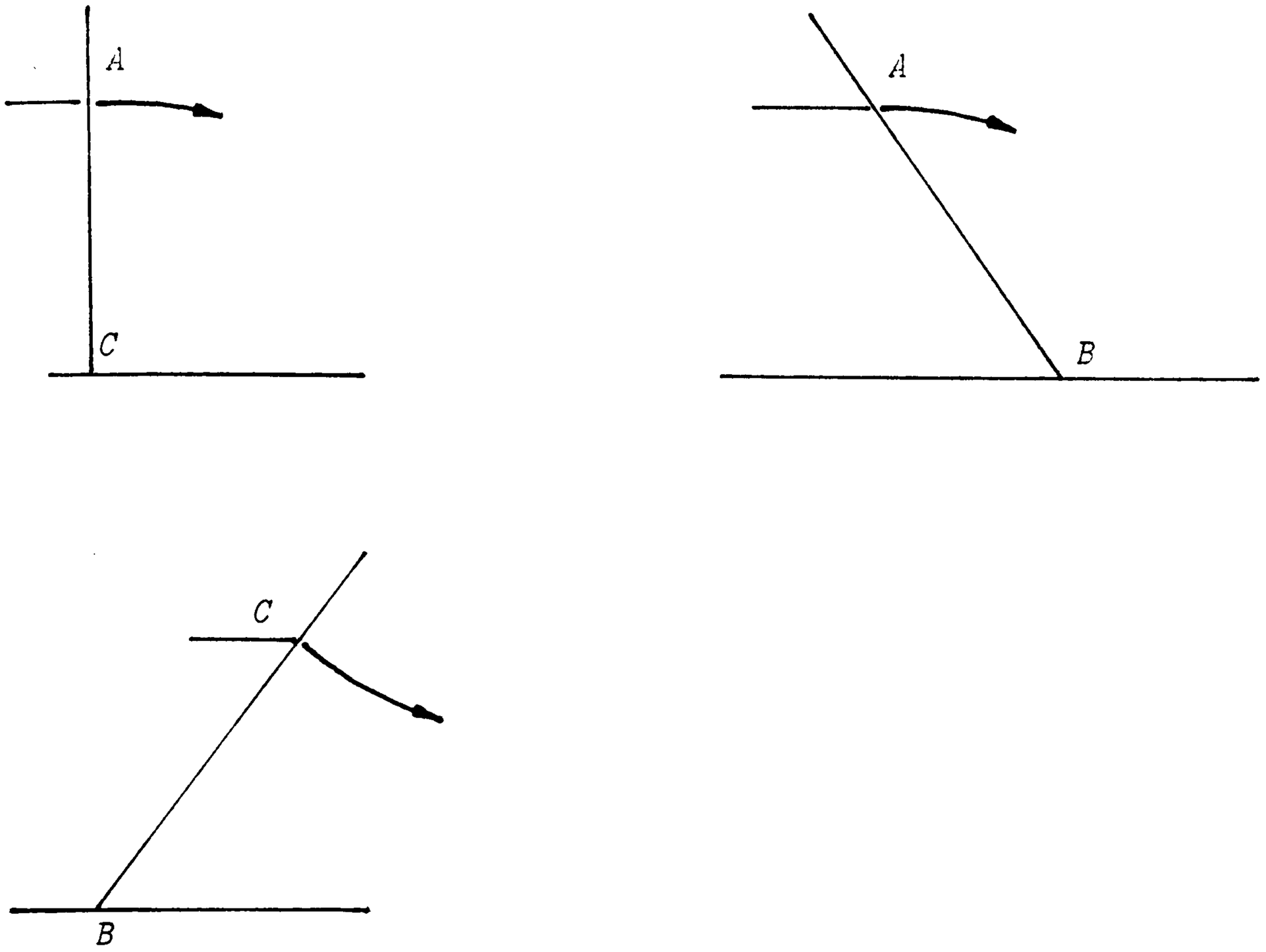
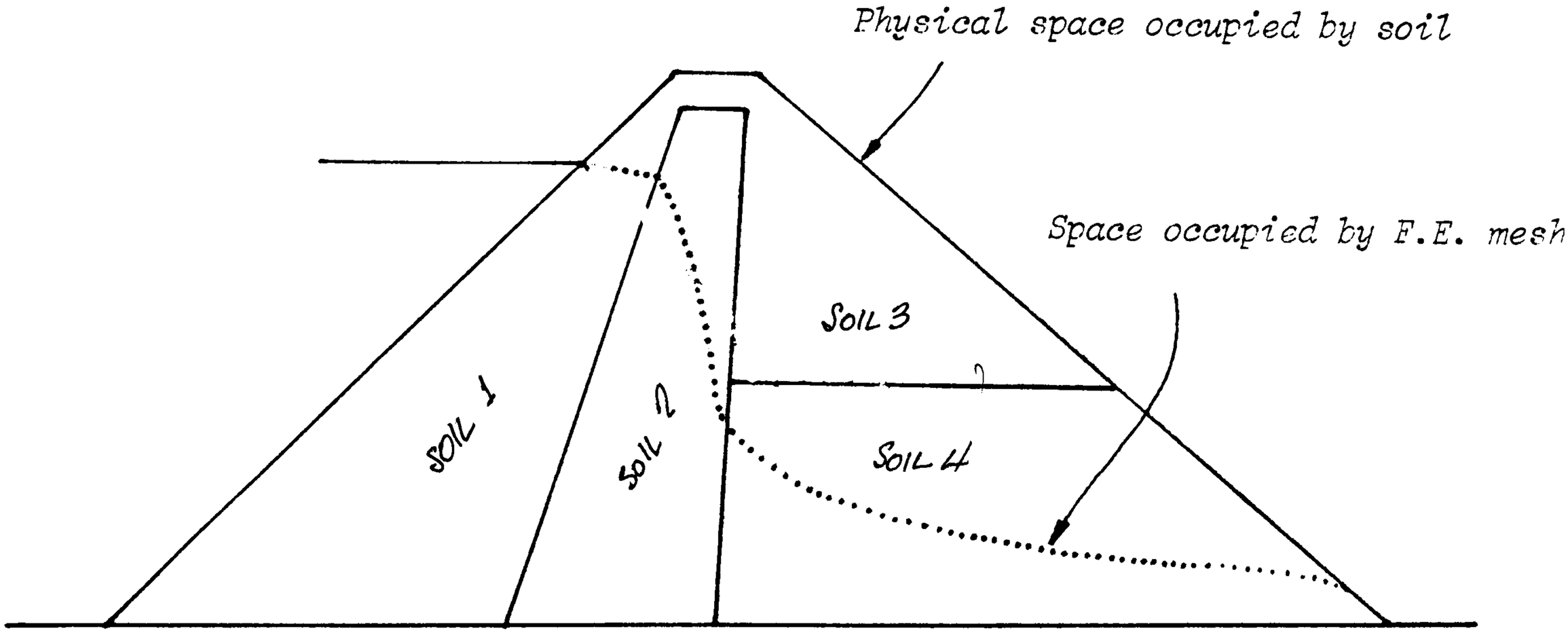


Figure 3.3. Aspects of the simulation of free surfaces with the finite element method.



Internal singularities (stagnation points) do not affect f.e. solution at all - neither do the entry conditions at "B" above. This is because these points are not considered explicitly in the solution (i.e. no Gauss point appears at "B"). If an infinitely fine subdivision is taken in this region a problem will arise. However, at "A", the velocity vector must be horizontal and hence its magnitude must be zero as the potential gradient is the same as the gradient of the free surface. Points "C" are not singular.

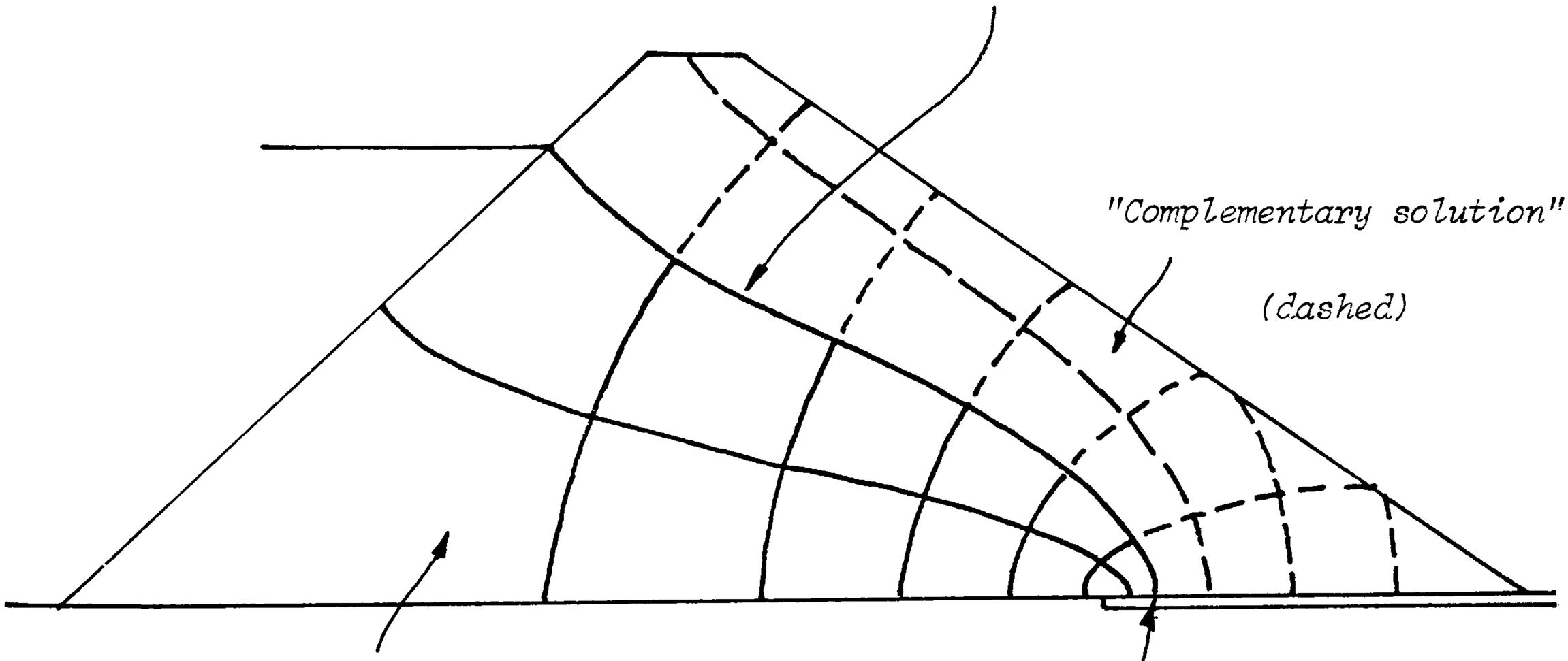
Figure 3.4. The positions of "entry singularities" and their importance in free surface analysis.



QUESTION: Can a solution be obtained in the whole region occupied by soil - i.e. within the initially defined geometry? (See also Fig 3.3).

(Drawn for homogenous case)

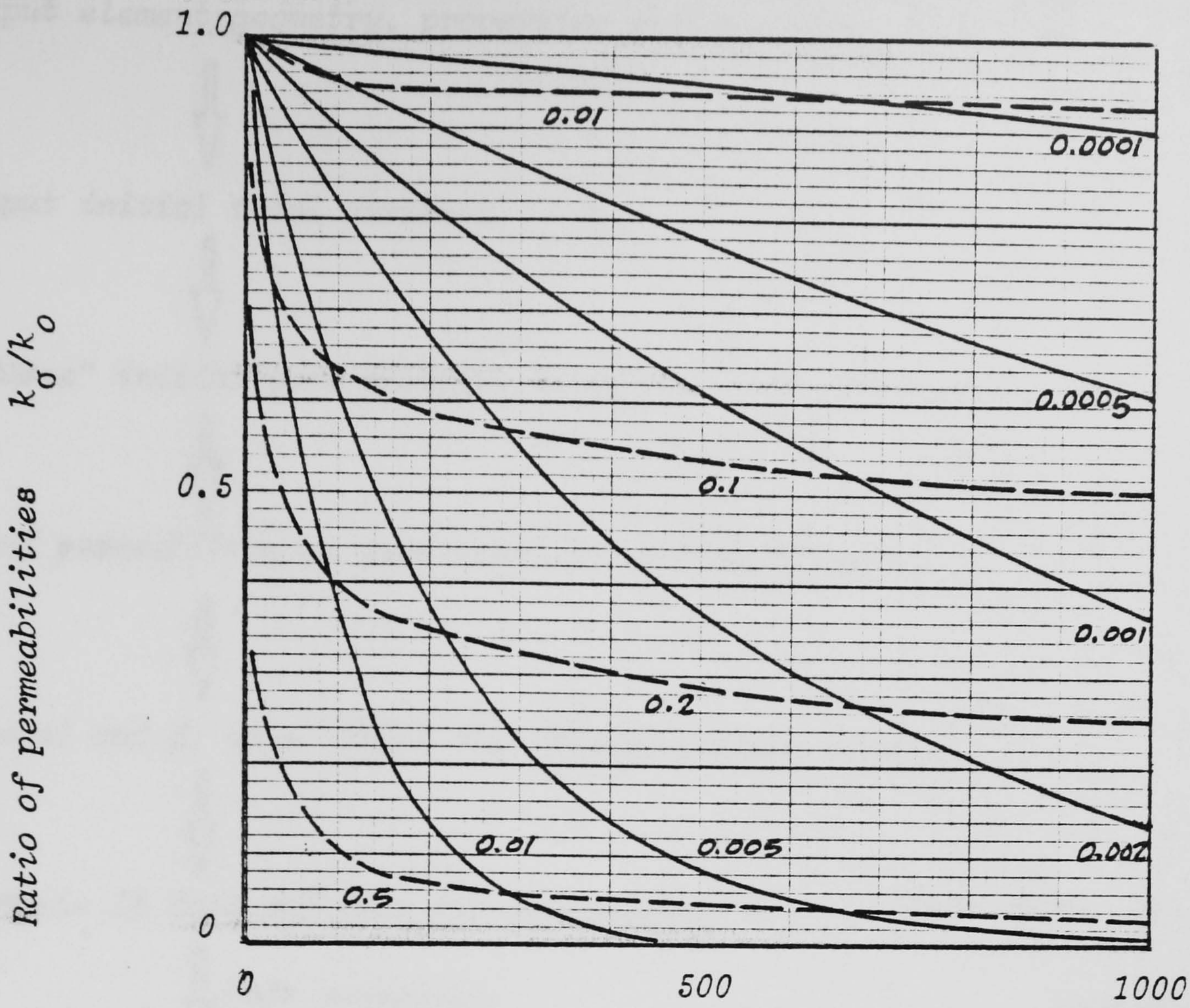
Satisfies conditions $\phi = y$, $v_n = 0$



Desired solution (solid)

Locating this point is difficult in variable geometry methods.

Figure 3.5. Fundamental basis of "constant stiffness" method.



Legend

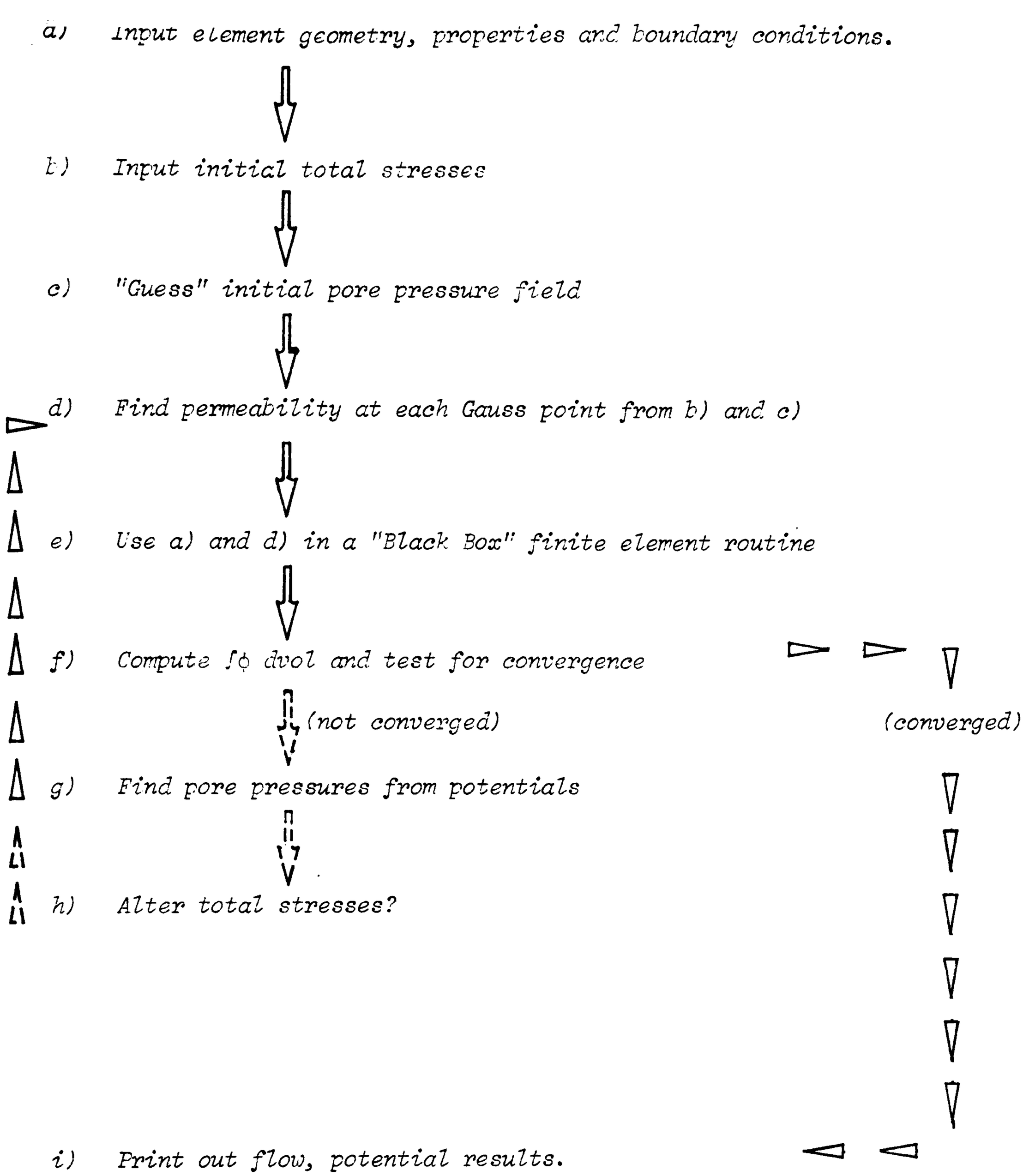
k_σ = *permeability at effective stress* σ'.

k_o = *permeability at zero effective stress.*

Solid line: "logarithmic" law.

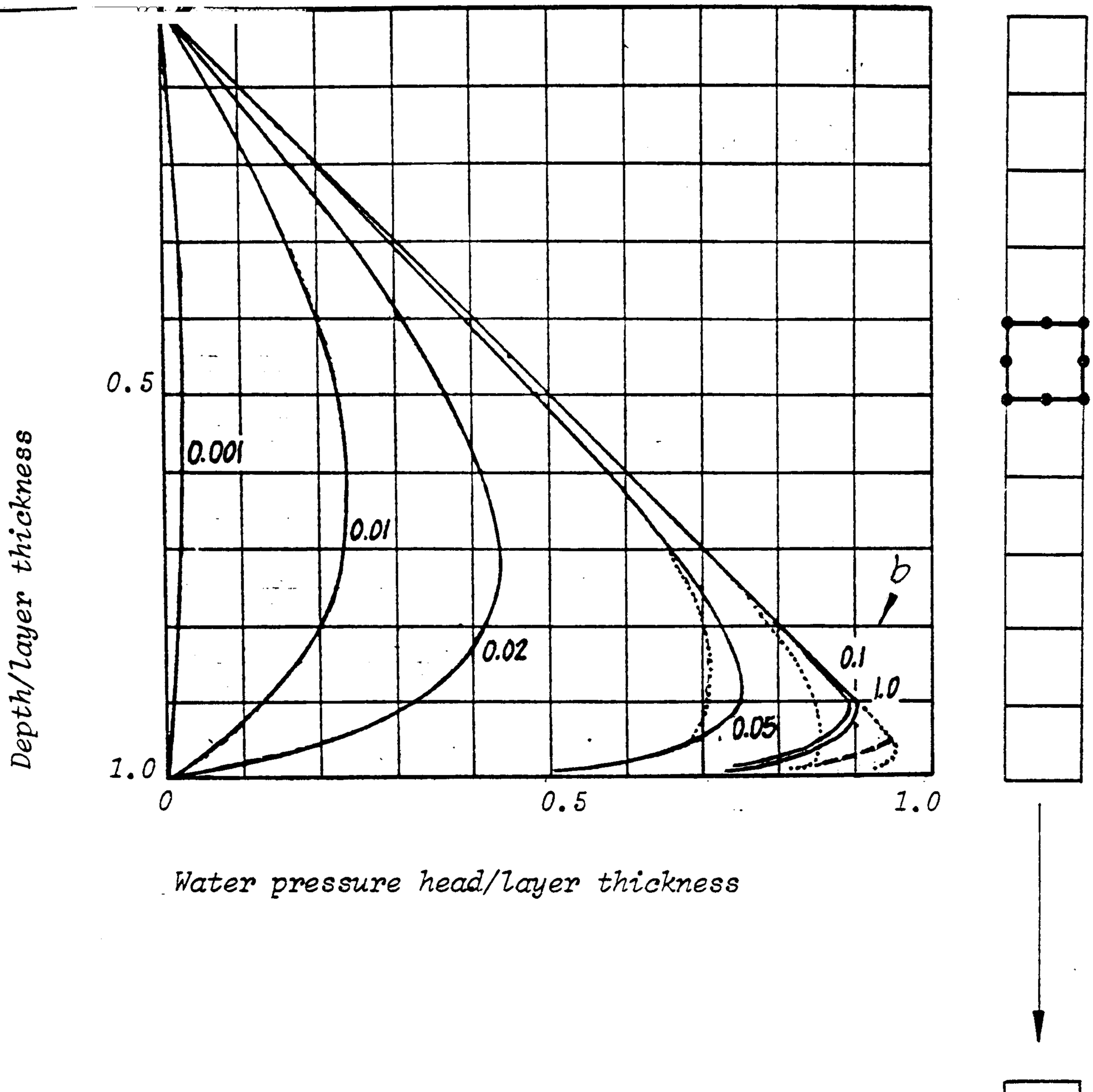
Broken line: "Power law".

Figure 3.6. Effective stress - permeability relationships.



NB. Step d) is performed within step e). The test in step f) is made manually. Using step h) has not been explored.

Figure 3.7. Principles of the finite element model.



Final element subdivision for "special" analysis

——— *Finite element results*

..... *Analytical results/(where not identical to above)*

---- *Finite element results - special analysis*

Figure 3.8. Finite Elements Test 1: Comparison of finite element and analytical results (cf. Figure 2.6).

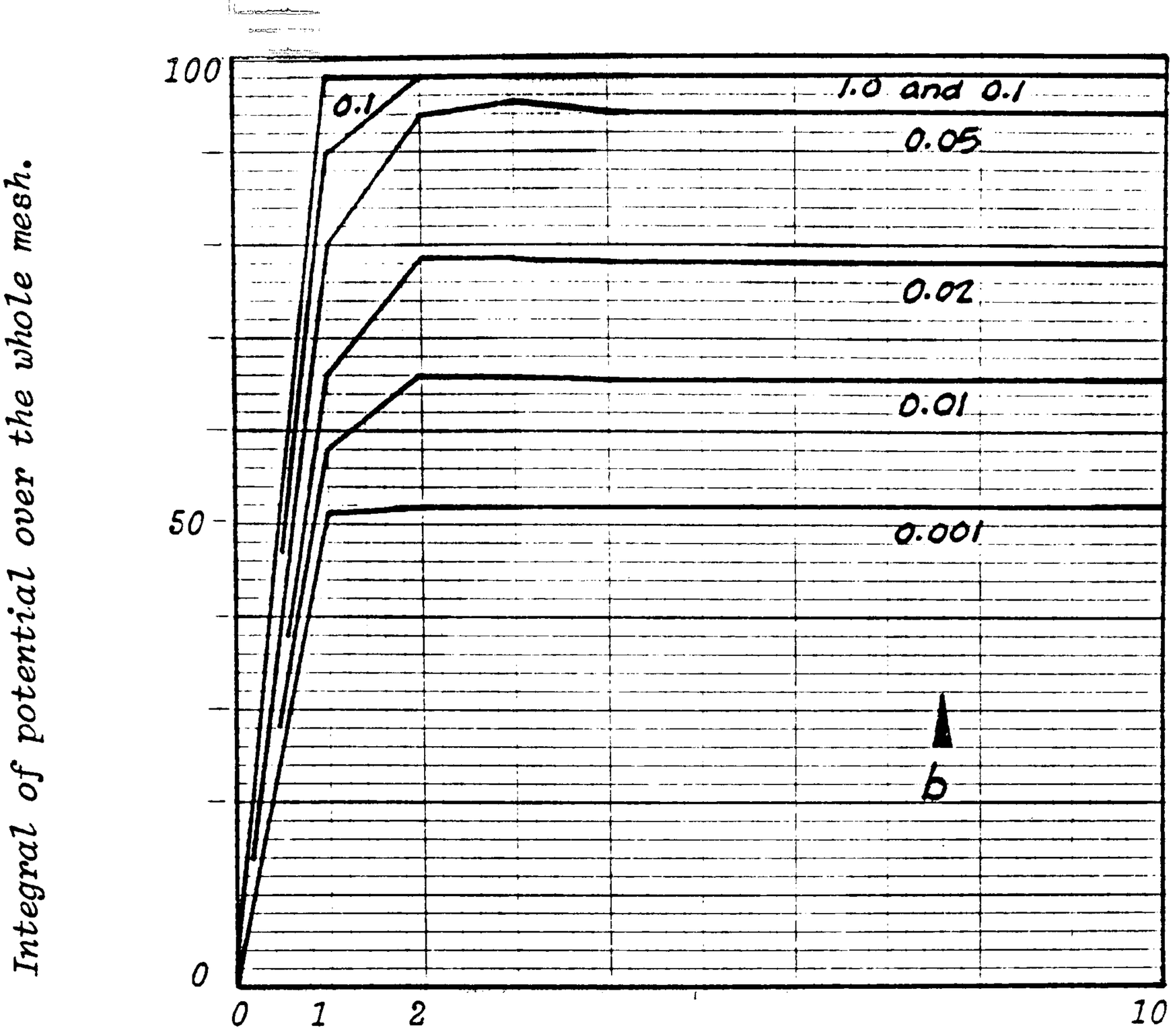
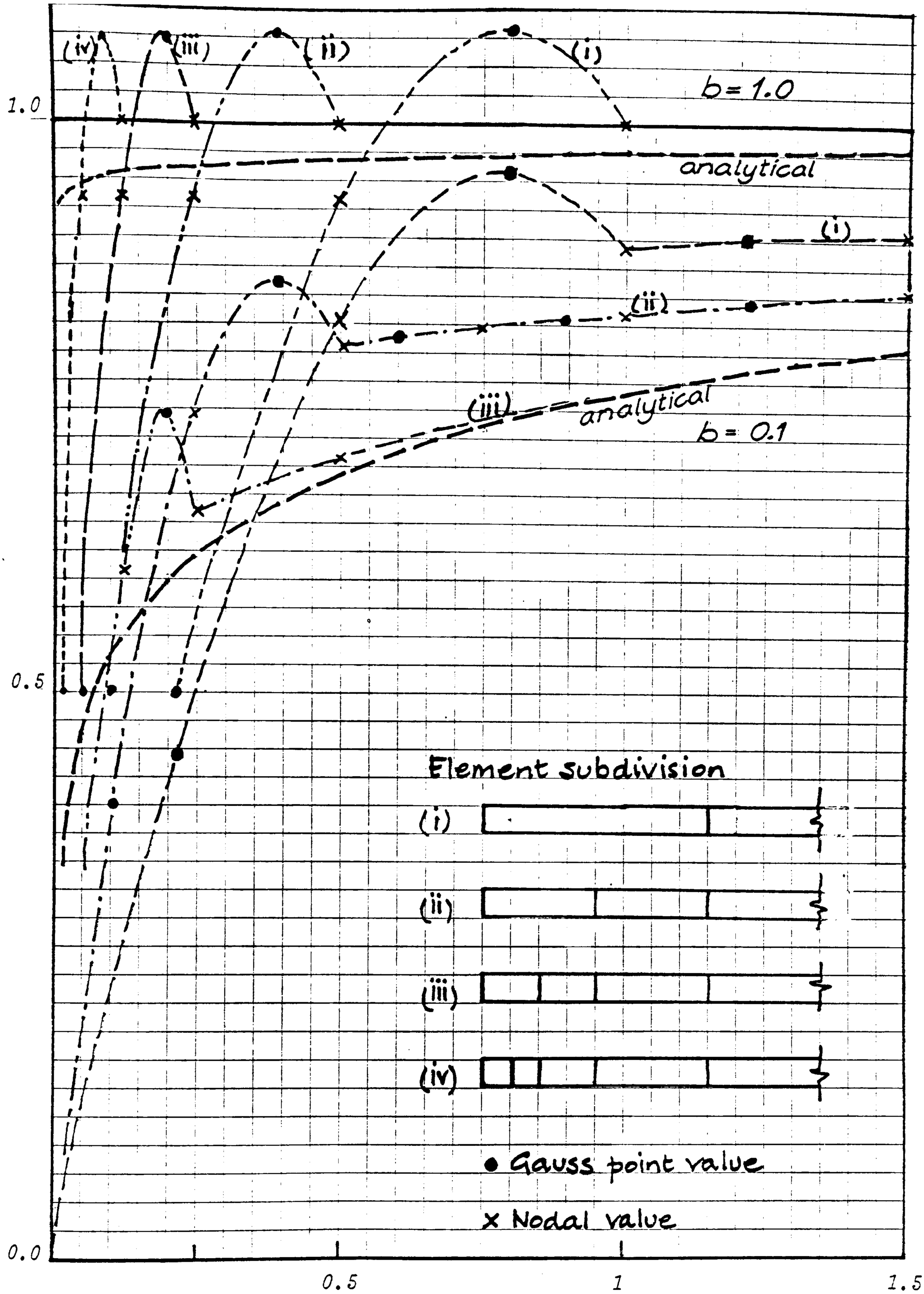
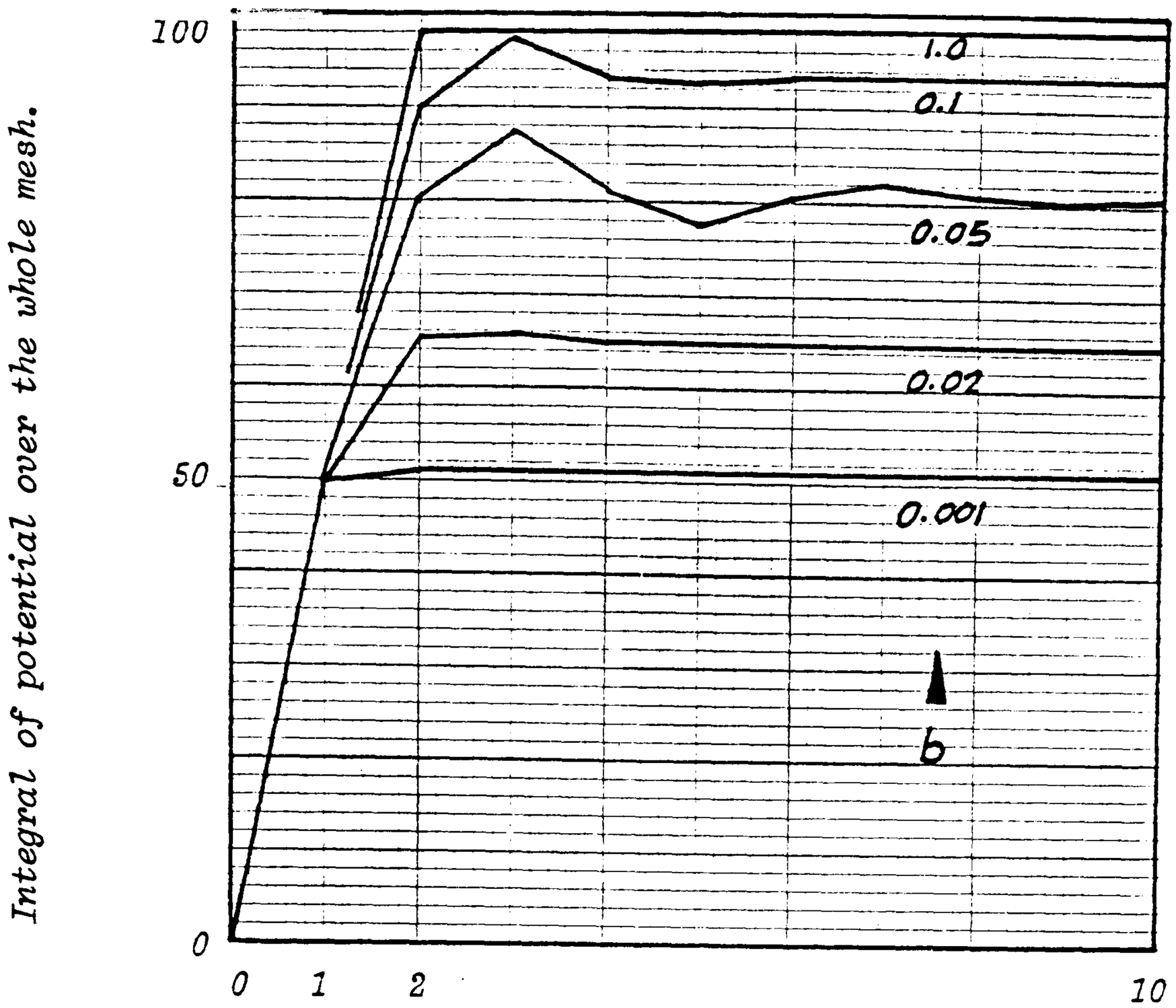


Figure 3.9. Convergence of finite element technique: Vertical, underdrained seepage.



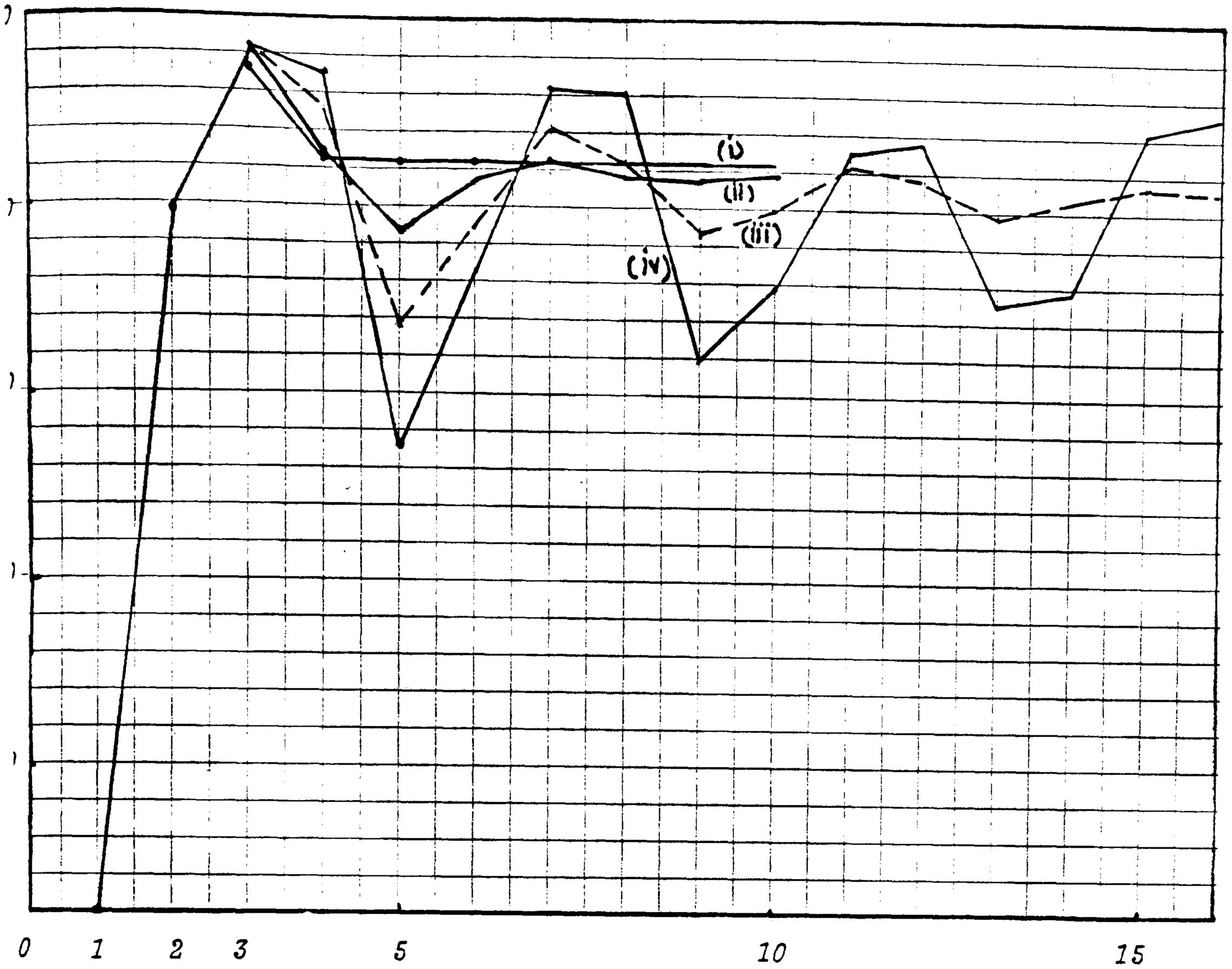
Distance from boundary: 1 = length of largest element

Figure 3.10. Finite Elements Test 2: Actual potentials close to downstream boundary



NB *The oscillation in the b = 0.05 case can be worsened with a poor mesh of elements.*

Figure 3.11. Convergence of finite element technique. Horizcntal seepage.



The markings on the plots (i), (ii), (iii) & (iv) refer to the finite element meshes shown in Figure 3.10.

Figure 3.12. Oscillation of the $\int\Phi$ dvol with increasing element subdivision

Horizontal seepage (cf Figure 2.10 for mesh and overall problem details).

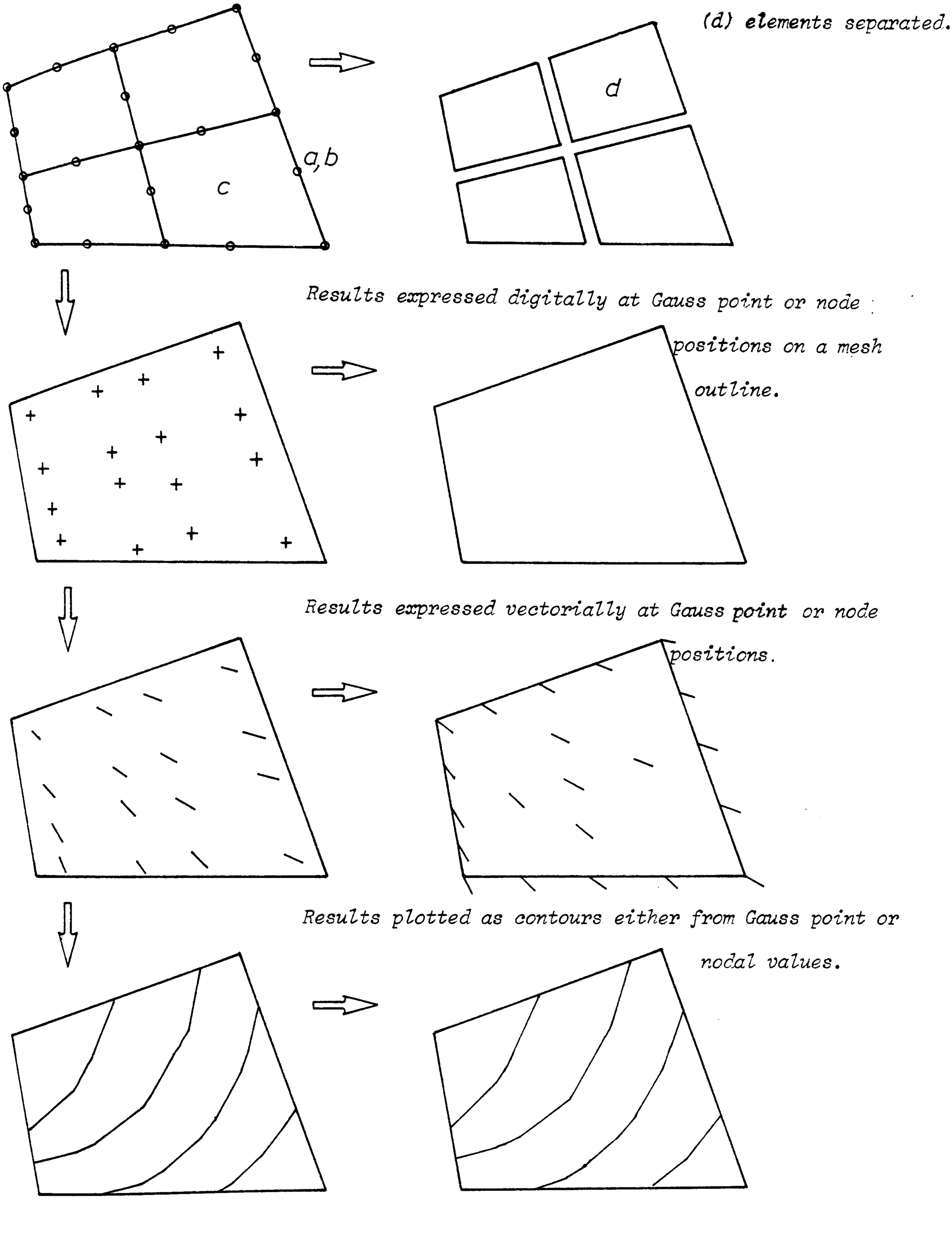


Figure 3.13. Facilities available through the finite element graphics program.

CHAPTER 4 - FINITE ELEMENT MODELS FOR PORE WATER PRESSURE DISSIPATION

4.1. Introduction

Transient problems in seepage analysis arise from two basic sources: the desaturation of the soil due to the drainage of water from its pores (or the converse if ground water levels are rising), and the change in fluid storage in a soil as a result of soil skeleton and/or pore fluid compressibility. In principal, both effects could act simultaneously, but in practice it is found that one effect will predominate. Finite element analysis techniques exist for the solution of both categories of problem.

In the former class of problems, the Neuman & Witherspoon (1971) approach (*vide* Section 3.5a) may be applied, with the instantaneous velocity of the free surface (which is not a flow line in this case) being given by the product of the soil porosity and the fluid velocity at the edge of the problem. The whole problem is basically the response of a free surface seepage regime in an incompressible soil to changed hydraulic boundary conditions.

The latter class of problems in generally termed "consolidation" or "dissipation".

In consolidation problems there are both changes in the fluid pressures and in the volume* of the soil. The theory of consolidation is thus simultaneously of importance to the prediction of stability and deformation. In broad terms, the parameters that govern consolidation behaviour are the permeability of the soil, and the compressibility of the soil skeleton or of the pore fluid. It is the way in which the second of these aspects is treated that gives rise to the different predictions of *coupled* and *uncoupled* consolidation solutions.

It is appropriate now to investigate the influence of changes of these parameters on the process of consolidation, particularly the influence of the dependence of these parameters on effective stress

*ie change in void volume

(as in the previous chapter) since they are both commonly held to be functions of effective stress.

Consolidation processes may be initiated by *either* total stress changes on the boundary of the seepage domain (setting up an out-of-equilibrium set of undrained pore water pressures which must dissipate) *or* by altered hydraulic boundary conditions.

4.2. Coupled and Uncoupled Solutions

In an uncoupled solution the total stress field once established is independent of the progress in dissipating pore pressures, but in a coupled solution the dissipation of pore pressures may give rise to total stress readjustments which in turn may cause undrained pore pressure changes elsewhere in the soil. An example of this is the radial consolidation of a soil cylinder (say in the triaxial apparatus) due to radial drainage from the periphery. Assuming an initially uniform pore pressure in the sample, the early stages of drainage will cause the outside of the sample to decrease in volume, compressing the centre of the sample as a result of which is subject to an undrained pore pressure increase. This is an instance of the so called "Mandel-Cryer effect".

Hence the soil elements in a coupled solution follow a somewhat different stress history to equivalent soil elements in an uncoupled solution. This gives rise to different predictions for the rate and magnitude of settlement and for the rate of pore pressure dissipation for the two different approaches.

In the context of an analysis of the problem, uncoupled theories provide much less complex numerical task than do the coupled theories. For example, in an uncoupled finite element solution there is only one unknown per node - the potential (or pore water pressure) - whereas in coupled work there are three (two displacements as well as the potential). Thus for an eight

noded element, the size of stiffness matrix increases from 8 x 8 to 24 x 24, a ninefold increase, before the increased complexity of the coefficients in the "elastic" part of this matrix is taken into account. The bandwidth and rank of the global stiffness matrix also increase in due proportion. There is therefore every incentive to economise on the use of computer resources by using the uncoupled approach wherever possible, unless the inaccuracies of this approach degrade the value of the results to an unacceptable level.

It is convenient, therefore, to discover that both methods yield the same answer in the case of one dimensional flow and settlement (with isotropic, homogenous and constant parameters). Accordingly, in the work described here, in which an uncoupled theory is used, the parametric studies are all of one dimensional cases.

It is believed that the broad conclusions from this parametric study are largely true when applied in two and three dimensional situations, using a coupled approach. The proof of this (or otherwise) is left to others.

4.3. Consolidation in a Soil with Effective Stress Dependent Permeability and Compressibility

Finite element model

Zienkiewicz and Parekh (1970) present a finite element model for the solution of a variety of problems, including consolidation, using the Swansea isoparametric element family. A computer program based on their approach was used as the basis for the work described below. The matrix solution scheme came direct from the thesis by Parekh (1965) (with the correction of the deliberate error designed to trap would-be plagiarists) and the incorporation of the more advanced isoparametric elements.

The problem can be stated in the following matrix form:-

$$[H]\{\phi\} + [G]\left\{\frac{d\phi}{dt}\right\} = \{F\}$$

where $[H]$, $\{\phi\}$ and $\{F\}$ are as discussed previously (Section 3.2) and the matrix terms $[G]$ and $\{d\phi/dt\}$ are introduced to allow for compressibility effects. Each term in the $[G]$ matrix is evaluated from element contributions, i.e.

$$G_{ij} = \sum_{1}^{NE'} g_{ij}^{e} = \sum_{1}^{NE'} \int_{VE} m_r \gamma_w N_i N_j \, dv$$

where NE' is the number of elements connected to node i *and* to node j. Zienkiewicz and Parekh consider a "finite element" in time, but they use the simpler central *finite difference* time step. This latter procedure has been used with considerable success (Bromhead, 1972) and consequently is used here.

Taking the centre of a time step of length δt between $t-\delta t$ and t:-

$$[H]\{\phi\}_{t-\frac{\delta t}{2}} + [G]\left(\frac{\{\phi\}_t - \{\phi\}_{t-\delta t}}{\delta t}\right) = \{F\}_{t-\frac{\delta t}{2}}$$

Assuming the potentials to vary linearly over the time step, $t-\delta t$ to t:-

$$\{\phi\}_{t-\frac{\delta t}{2}} = \frac{1}{2}\left(\{\phi\}_t + \{\phi\}_{t-\delta t}\right)$$

Rearranging these expressions:-

$$\left([H] + \frac{2}{\delta t}[G]\right)\{\phi\}_{t-\frac{\delta t}{2}} = \frac{2}{\delta t}[H]\{\phi\}_{t-\delta t} + \{F\}_{t-\frac{\delta t}{2}}$$

Or

$$[K]\{\phi\}_{t-\frac{\delta t}{2}} = \{P\}_{t-\frac{\delta t}{2}}$$

which is analogous to a steady (or even a structural stiffness method) solution where $[K]$, the stiffness matrix, remains invariant and the forcing load vector $\{P\}$ changes with each time step but in every case is a function of the potentials existing at the nodes of the finite element mesh at the commencement of the step. The full set of nodal potentials at the end of the time step can then be found from the starting and mid-step values thus:-

$$\{\phi\}_t = 2\{\phi\}_{t-\frac{\delta t}{2}} - \{\phi\}_{t-\delta t}$$

Unfortunately, the Zienkiewicz and Parekh model can only work if the permeability and compressibility values remain constant and has the further restriction that the time steps remain the same length. It is of course permissible to stop the process midway through and re-start with different soil properties or time steps but this requires a reformulation of the element stiffness matrices, re-assembly and re-decomposition.

If the time penalty for this additional work is not unacceptable, an alternative scheme largely based upon Zienkiewicz and Parekh's method presents itself, and this is to accept each time step as a

"complete problem", reformulating and resolving the equations for each time step. This means that the time steps can be of any length. We are still subject to the condition that the material properties do not alter, but this condition is now *for the duration of each time step only*. If the time steps are small during the period in which the potentials vary most rapidly then we can take our effective stress dependent compressibility and permeability laws and the program will follow them in an approximate, stepwise fashion.

Time Steps: Taking constant time steps, and a constant compressibility and permeability use of this procedure increases computation time by some 20%. If, however, varying time steps are used, the equivalent consolidation process can be followed with a nett computation time saving. For simplicity, time steps are assumed either constant or to increase in magnitude so that the nth time step Δt_n is given by:-

$$\Delta t_n = t_n - t_{n-1}$$

where

$$t_n = \Delta t_0 \cdot 10^{n\alpha}$$

in which α controls how many time steps there are per $\log_{10}$ cycle of time and Δt_0 is a basic time step size parameter. We usually find that there is an upper limit to the size of time step which must not be exceeded even in the later stages, and the program allows an upper limit to be set on the time step sizes.

Tests: Since there is a lack of published solutions even for the simple *steady* seepage in soil with an effective stress permeability, there are no realistic tests that can be made. However, with constant permeability and compressibility coefficients and a one dimensional doubly drained case the Terzaghi-Rendulic solution applies and the pore water pressure distributions given by the constant and varying size time step finite element solutions can

be compared to that. It is found that the numerical scheme gives very good results in both cases, although for a fuller discussion Parekh (1965) and Zienkiewicz and Parekh (1970) should be consulted.

4.4. *Element Induced Potential Oscillations*

One point worthy of note at this juncture is the element induced oscillation in potentials. This has been discussed briefly earlier in the discussion on the testing of the steady seepage effective stress permeability finite element model and is considered here in the context of the Zienkiewicz and Parekh model. In a "run" with say initially homogeneous initial conditions we tend to model the domain with boundary conditions on its *extreme edge nodes*. The edge elements then interpolate parabolically (in the case of the efficient second order element) as is shown in Figure 4.1. At the first row of Gauss Points, the potential *value* is of a reasonable size with the potential *gradients* in the correct direction, but the opposite is the case at the second row of Gauss points. As the time stepping proceeds, a wave of increased potential penetrates the mesh as illustrated in Figure 4.1 (b. and c.). The effect of this is magnified if permeabilities are increased when the potential rises (as in the effective stress permeability model). This oscillation can be largely suppressed by using the following artifice, without adversely affecting the overall quality of the solution.

We wish to find the highest potential value for a second row node without implying an adverse potential or potential gradient at the second row of Gauss points. This can be done by considering the geometry of the parabolic variation of potential across the element, remembering of course, always to work in the parent coordinate system.

(a) Correct initial potentials at nodes and Gauss points from the second rank of elements inwards and potential gradients

in the correct *direction* in the first rank of elements (Figure 4.2(a)).

$$\phi_2 = 0.75(\phi_3 - \phi_1) + \phi_1$$

This effectively assumes an *accelerated* consolidation for early times.

(b) Correct initial potentials as above, but a zero potential gradient at the second row of Gauss Points (Figure 4.2.(b)).

$$\phi_2 = (0.5 + 0.25\sqrt{3})(\phi_3 - \phi_1) + \phi_1$$

$$= 0.9330(\phi_3 - \phi_1) + \phi_1$$

The initial potential at the Gauss point will be incorrect, but this will not affect a constant properties solution at all, and can be allowed for in the effective stress model by having a cut-off for the maximum and minimum allowed permeability and compressibility values.

(c) Correct initial potential and zero potential gradient at the second row of Gauss points. This implies incorrect initial potentials and/or potential gradients at other Gauss points and/or nodes and will not be proceeded with (Figure 4.2.(c)).

It is of course more complicated if a two or three dimensional situation is contemplated, or alternatively if a non uniform initial distribution of potentials is contemplated especially as in the latter case the "ripple" of increased potential may be damped out by larger scale effects. Nevertheless the same general principles apply.

Reverting to the steady seepage iterative effective stress solution method the reason for the numerical instability can be seen to result from the situation where change in the potential in the second row nodes causes the potential gradient in the second row of Gauss points to reverse in direction. This effect is more apparent where the total stresses are constant than where they increase towards the boundary.

A trial of options (a) and (b) above was made and compared with the orthodox treatment. The element mesh used had 10 of the parabolic elements and 53 nodes and represented a doubly drained column of soil. (Figure 4.3). The Zienkiewicz and Parekh (constant k & m_v) model was used. The simple initial conditions caused a wave of potential increase 5.6% of the total potential change in the problem to build up. Using option (b) the solution was improved but there was still a wave of potential increase - this time reaching a maximum of 0.2% of the total potential change in the problem. With option (a) for the initial conditions, the positive potential wave was only 0.04%. However, especially in the early stages these initial conditions tended to cause an overestimate of the amount of consolidation (which is true of all the test runs) due to the potentials dissipating across the first row element in the first time step. This can only be reduced by taking a very narrow first row element.

The size of the time step is of importance in obtaining as little oscillation as possible in the solution. This is illustrated in Figures 4.4. and 4.5. Taking Zienkiewicz and Parekh's constant time steps it is seen that even with very large steps for which the solution is effectively worthless due to the magnitude of the oscillations the median line is still an accurate estimate of the true dissipation behaviour. There is a threshold step size for a given degree of accuracy in individual potential values and a smaller value below which the iteration procedure is monotonic. However, the time step size required for a given accuracy in individual potentials is very much smaller than is required for an equivalent accuracy in average dissipation rates.

If effective stress dependent properties are used, the early oscillation is wilder. It is reassuring that the "constant properties" solution has such a stable trend and by inference, within the oscillations that are observed, the non-linear properties solution is likely to be similarly stable.

4.5. *Previous Work*

The problem of consolidation in soils with varying properties has received a great deal of attention. Edelman (1953a) treats a soil where the modulus of elasticity is proportional to depth whereas Martins (1965) and Schiffman & Gibson (1964) concentrate on variations in the permeability coefficient with depth. Poskitt (1971) presents a finite difference scheme for non-linear properties. These authors concentrate on one dimensional work.

In both the Edelman and the Schiffman and Gibson papers, the analyses presented dissipate an initially uniform (with depth) excess pore water pressure vertically. Edelman allows drainage from the top surface of his soil layer, with an impermeable bedrock base. Both the initial and final pore water pressure distributions are therefore linear with depth. Schiffman and Gibson allow double drainage, but are dissipating to a final state of no overall underdrainage, so once again the initial and final pore pressures are linear with depth. Furthermore, in both cases, the coefficients of permeability and compressibility, whatever their variation, are independent of the actual magnitude of pore pressure. It is therefore quite natural for these authors to work in terms of excess pore water pressure as this is the conventional treatment and is correct in these particular cases. In general, and as will be seen in the following, it is incorrect to do so.

There is now a growing body of literature in the field of heat flow analysis where the material properties are a function of the field variable (in that case the temperature). For example, Aguirre Ramirez & Oden 1973 and Comini *et al* 1974 specifically include temperature dependency in thermal conductivity, heat capacity, rate of internal heat generation and heat transfer coefficients.

These solutions embrace a variety of complicated functions including step-wise continuous conductivity-temperature relationships, in some models (Comini *et al* 1974) even including latent heat effects so that the growth of freezing or thawing fronts can be predicted.

4.6. Effective Stress Permeability and Compressibility Relationships

In the finite element approach to the solution of dissipation with effective stress permeability and compressibility presented here, the total stresses are input at Gauss points at the start of the process and assumed not to vary. When the "stiffness" and "load" matrices are formed, these total stresses and the initial pore pressure conditions are combined to yield initial effective stresses from which the current permeability and compressibility values are evaluated. These parameters are then assumed to be operative *throughout* the current time step, but are re-evaluated for the next time step.

It is found that if the time steps are kept small while the potentials (and hence material parameters) are varying most rapidly, a smooth progression in the dissipation of the potentials is obtained. This is thought to be simpler than following the procedures of non-linear stress analysis; for example, carrying out a *pilot solution* to establish the likely range of variation of pore pressures in the next step so that parameters appropriate to the likely median can be selected for a proper solution.

In principle, either the permeability, or the compressibility (or both) can vary with increasing effective stress. Likely variations in the coefficient of permeability have been described in the previous chapter, and the function used most widely in that section (the "logarithmic law") has been carried over into this section. This law predicts a decrease in permeability with increasing effective stress, which is in accord with both field and laboratory evidence. On the other hand, the variation in compressibility with effective stress is a better documented phenomenon, but some inconsistencies arise.

Take, for instance, the linear voids ratio-effective stress plot typical of an overconsolidated soil (for a small stress range). This yields a single, constant, value for m_v. Alternatively, a straight line on a voids ratio *log* effective stress plot implies a decreasing modulus of volume change with increasing effective stress.

C_v may *increase* with increasing effective stress (e.g. Bishop & Al-Dahir 1970) where the rate of decrease of m_v with effective stress is larger than the rate of decrease of k.

The work described in the following sections makes one of two assumptions regarding m_v.

(a) Assuming m_v is a constant regardless of the way in which k varies

(b) Assuming that m_v varies in the same way as k does so that c_v remains constant.

From this, inferences are drawn (by interpolation) on what happens if m_v decreases with effective stress less rapidly than k does, and (by extrapolation) what happens if the changes in m_v are more rapid than those in k.

Hence a "logarithmic law" has been chosen for m_v variations despite there being no real justification for this on theoretical or experimental grounds.

4.7. Parametric Study - One Dimensional Dissipation

The first parametric study carried out with the dissipation model investigates the problem of one dimensional dissipation of pore water pressures. It is divided into two parts: firstly, a study where the total stress is constant (Figure 4.7) which crudely

represents a horizontal slice through a vertical dam core for example; and secondly, a study where the total stress varies with depth (Figure 4.8). Basically, these cases are analogous to the steady state seepage cases of Sections 2.3 and 2.4.

Taking the horizontal seepage case first it must be realised that there are at least six separate basic problems to be analysed:

(a) Swelling from an initially constant potential distribution to a steady state seepage condition,

(b) Consolidating from an initially constant potential distribution to a steady state seepage condition,

(c) Swelling from an already established steady seepage state to a uniform potential,

(d) Consolidating from an already established steady seepage state to a uniform potential,

(e) Consolidating from one set of uniform potentials to another.

(f) Swelling from one set of uniform potentials to another.

Since in a consolidating problem the permeabilities are reducing progressively in space and time, whereas in a swelling problem the permeabilities increase progressively there is no longer the symmetry between consolidating from state A to state B and swelling from state B back to state A that it is conventional to expect in the simple dissipation solutions. Furthermore, it is no longer possible to simply identify the initial and final pore water pressure distributions and to dissipate this excess pore pressure for two reasons: firstly, it may not be possible to identify the final steady state pore water pressure distribution *a priori* without a non-linear analysis potentially as complex as the "consolidation" solution itself, and secondly, (which is probably the more important of the two on *theoretical* as distinct from *practical* grounds) the actual values of the total pore water pressure govern the instantaneous values of the consolidation parameters themselves.

Where vertical flow is concerned, there are additional complexities. There is, for a start, the asymmetry between consolidating and swelling solutions noted previously. In addition, the effect of a stimulus applied at one end of the problem is different to the effect of that stimulus applied at the other end. This can best be seen in a diagrammatic form in Figures 4.6 to 4.8.

Very little purpose would be served by making an exhaustive series of analyses with all the various cases, since the practical difficulties of presenting the results in such a way as to be of most use in engineering practice are almost insurmountable. Instead, it has been decided that certain cases and effects should be explored to discover in what ways the results differ from the conventional solutions.

Table 4.1. Brief Outline of Parametric Study - Horizontal Flow

CONSOL - 1	F.E. Analysis of Simple Terzaghi problems, using Zienkiewicz & Parekh approach constant k, m_v and Δt. Constant total stress field.		
CONSOL - 2	Simple Terzaghi problem with constant k and m_v but with varying Δt. Constant total stress field.		
CONSOL - 3 a & b	As CONSOL - 1 but with slightly varied initial conditions in the edge elements.		
CONSOL - 4 to 7	Constant total stress field, varying k and m_v but with C_v remaining constant		
4	b = 0.01	h_w = 100 m	
5	0.005	100 m	
6	0.001	100 m	
7	0.01	10 m	
CONSOL - 8 to 13	Constant total stress field, varying k but constant m_v		
8	b = 0.01	h_w = 100 m	= 100kN/m^2
9	0.005	100 m	1000
10	0.001	100 m	1000
11	0.001	10 m	1000
12	0.001	1 m	1000
13	0.001	10 m	200kN/m^2

Horizontal Flow:

Some test runs of one dimension, doubly drained, consolidation with horizontal flow were made to test the influence of the assumption in the finite element model. A 10 m column of soil comprising 10 elements was again used (Figure 4.8) and initially constant total stress conditions were used. Both permeability and compressibility were taken as effective stress dependent but in such a way as to keep the apparent C_v constant. In order to over-stimulate the model and thus magnify any effects that might occur, an excess pore water pressure head of 100 m of water was used, together with very fiercely effective stress dependent parameters (b = 0.01).

Consolidation was dramatically delayed, and for 50% dissipation at the mid-plane of the soil column this solution took 11.6 times longer. Some other cases were also attempted (Table 4.2., and Figures 4.9 to 4.13 inclusive).

Table 4.2. Time Lag for 50% Mid-Plane Dissipation. Constant Cv Assumption

RUN	b	h_w(m)	TIME LAG FACTOR *	COMMENTS
CONSOL - 1 to 3	0.00	100	1.0	Identical to standard Terzaghi solution.
CONSOL - 4	0.01	100	11.6	C_v constant
CONSOL - 5	0.005	100	3.16	C_v constant
CONSOL - 6	0.001	100	1.28	C_v constant
CONSOL - 7	0.01	10	1.28	Identical result to CONSOL - 6

The 50% mid-plane dissipation point was chosen as a criterion for the assessment of the *time lag factor* because by this time the element induced potential oscillations have largely died out (they sometimes reappear in the final stages of solution) and also because of the great reliance often placed on the 50% consolidation point for fixing C_v on a laboratory test curve.

Schiffman and Gibson, 1964, have considered the case where the permeability varies in space but the compressibility remains constant. The analogue of this in the present series is to take the permeability to be a function of effective stress and to resolve the consolidation problem with constant compressibility. The same mesh and exaggerated Δh_w as in the earlier series was also taken, with the results summarised in Table 4.3.

* See p 128

Table 4.3. Time Lag for 50% Mid-Plane Dissipation. Constant m_v Assumption

RUN	b	h_w(m)	TIME LAG FACTOR	COMMENTS
CONSOL - 8	0.01	100	231.6	
CONSOL - 9	0.005	100	15.26	
CONSOL - 10	0.001	100	1.73	
CONSOL - 11	0.001	10	7.53	
CONSOL - 12	0.001	10	1.16	
CONSOL - 13	0.001	1	1.00	

Broadly speaking, the effective stress dependency in the model has remarkably little effect on the solution for reasonable levels of stress increase and low degrees of stress dependency *in a constant total stress field.* That this is not necessarily the case elsewhere is discussed below.

For the purposes of Table 4.2 and 4.3., it is convenient to introduce a time lag factor (T.L.F.)

where this is defined as

$$\text{T.L.F.} = \frac{t_{50}\ (\text{varying k, } m_v \text{ solution})}{t_{50}\ (\text{constant k, } m_v \text{ solution})}$$

In this, the t_{50} for the varying parameters solution is the time for 50% average pore water pressure dissipation taken from the appropriate plot and the t_{50} for the constant properties solution comes from the Terzaghi solution with the parameters identical to the initial values in the varying properties model.

The concept of a time lag factor is not of general use when defined in this way, since where the total stress varies throughout the model being dissipated, there are an infinity of possible initial values. Where this is the case (as below) the constant properties parameters are taken to be the values yielded by the nominated effective stress-property relationship at zero effective stress. Even this is hardly universal, since not only may there be no part of the model actually at zero effective stress (indicating that the selected properties are inappropriate to all parts of the model) but in the general case the nominated law may yield an indeterminate result (through hydraulic fracture or other mechanisms) at this point.

The results of this series of analyses are plotted in Figures 4.9 to 4.13 inclusive. Figures 4.9 and 4.10 show how the average degree of pore pressure dissipation increases with time (time on a logarithmic scale) for the constant C_v and constant m_v assumptions. In the latter case, the degree of pore pressure dissipation and the percentage of the total volume change are identical, but in the constant C_v case where m_v alters, this is not so. A third diagram, Figure 4.11 shows how the percentage volume change progresses in the constant C_v model.

Rather than use volume change measurements, the progress of a consolidation process is often monitored by pore water pressure measurements at the centre of a doubly drained soil specimen, or at the opposite end, if singly drained. This is typical of the situation in a triaxial dissipation test for instance. The "mid-plane" pore pressure dissipation curves for these two series of analyses are therefore given in Figures 4.12 and 4.13, once again expressed in terms of a percentage dissipation against logarithm of time plot. (The time scale also shows a time factor defined in the conventional way and using the *initial* coefficient of consolidation or the coefficient used to define the T.L.F. In each case the time factor is one quarter of the indicated time on the plots).

For this situation the three important variables are:-

(i) the b. parameter,
(ii) the initial excess pore water pressure head Δh_w,
(iii) the average total stress level σ

In the limited range of test solutions the following broad conclusions are demonstrated.

(i) Increasing the b. parameter flattens the curve and shifts it bodily to the right hand (or increased time) portion of the graph. (Δh_w and σ keptconstant). This is because the permeabilities are reduced all through the section.

(ii) Decreasing the excess pore water pressure head Δh_w steepens the curve and shifts it to the right, but all the curves for given b and σ values coalesce at large times. The decel eration in consolidation is due to decreased permeabilities as a result of the increased initial effective stresses.

(iii) Changing the total stress but keeping Δh_w and b constant causes a shift in the curve (to the right with increasing total stress) but no rotation or change in gradient on the plot. This relationship arises from the constant ratio between the two permeabilities at all times for two analyses run at different total stresses but all other things being equal.

It should be noted, however, that these effects are deliberately exaggerated in these analyses by the selection of high values for each parameter. At the sort of stress levels encountered in the field, the effects would be very small indeed.

By inference it is assumed that the effect of *swelling*, that is increasing the pore water pressures in the section, would be to move the consolidation curves to the left, with broadly similar (but of opposite sense) shifts to those resulting from the effective

stress dependency in the consolidating cases. This effect has not been tested since pore water pressure increments of the same magnitude as the decrements in the consolidating case would bring much of the mesh into a negative effective stress state of large magnitude*, and small pore pressure increments would lead to small, scarcely detectable, shifts as in the other series of analyses.

Vertical Flow

In Chapter 2, the final steady state pore water pressure in an underdrained soil layer with effective stress dependent permeability has been investigated. The classical approach (e.g. Wilson & Grace, 1942) is to assume a linear pore water pressure/depth profile before underdrainage commences, and from the Chapter 2 work on steady pore pressure distributions, this can only be the case if the initial conditions correspond to a zero degree of underdrainage. Suppose, however, that this is really so, and that the ground water table in the underlying aquifer is "suddenly" drawn down. (Suddenly is a relative term, and an acquifer depleted steadily over a 50 to 100 year timescale may still represent a "sudden" draw down to an overlying clay layer of low permeability). With an effective stress dependent (or even depth dependent) permeability, the ultimate steady state pore pressure depth distribution cannot be linear, but will be bowed. In this type of soil it is therefore quite wrong to draw initial and final straight line pore pressure depth plots and to dissipate only the triangular "excess" pore pressure between these two lines. Account must be taken of the actual magnitudes of the potentials since it is these, not merely the excess pressures, which govern the instantaneous values of the consolidation parameters; and furthermore, given general arbitrary functions for the interaction of these parameters with the level of effective stress, the final steady pore water pressure depth plot may be unknown.

**With the law for the effective stress dependency of the consolidation parameters selected for these analyses the properties are given by a function which is continuous throughout the positive and negative effective stress ranges. This is not necessarily the case with every relationship and this argument is more valid in general than this particular case would suggest.*

In this part of the parametric study, similar "logarithmic" laws for permeability and compressibility to those used in the horizontal dissipation case have been used. In addition, the 10 element, 10 m high soil column, finite element mesh with initially hydrostatic pore water pressure conditions has been taken as the appropriate model. It should be noted that in this type of problem it is unrealistic to exaggerate the amount of pore pressure to be dissipated and the results (plotted in Figures 4.14 to 4.16 inclusive) are correspondingly quite muted in comparison with other results.

The final part of the parametric study investigates doubly drained dissipation of an initially constant excess pore water pressure. This is broadly similar in concept to the first part of this study, using as it does an exaggerated pore water pressure increment to over stimulate the model and produce large effects. The results are plotted in Figures 4.17 to 4.19 inclusive. It should be noted that the concept of a "mid-plane" dissipation curve is of little value, as this is no longer the position of maximum excess pore pressure, or of zero potential gradient as in the simple constant properties solution.

The following points should be noted:-

(a) Where m_v is not a constant, the percentage pore water pressure dissipation and percentage settlement are not the same.

(b) In general, neither the initial nor final pore water pressure distributions will be linear thus the present analyses are somewhat artificial and contrived.

(c) The effects on the rate of dissipation are usually quite small.

(d) There is no "symmetry" between equivalent or complimentary swelling and consolidation cases.

In all analyses *except* where the influence of different initial edge conditions was being investigated, an initial edge condition similar to that shown in Figure 4.2(a) was chosen in order to minimize the effects of so called "element induced potential oscillations".

Table 4.4. Brief Outline of Parametric Study - Vertical Flow

CONSOL - 14 to 19		Total stress field increasing linearly with depth. Initially hydrostatic pore water pressures but suddenly and completely underdrained.
		Varying k and m_v but the overall C_v a constant.
	14	b = 0.01
	15	b = 0.005
	16	b = 0.001
		Varying k but m_v remaining constant.
	17	b = 0.01
	18	b = 0.005
	19	b = 0.001
CONSOL - 20 to 25		Total stress field increasing linearly with depth. Initially constant excess over hydrostatic pore water pressures. Double drained.
		Varying k and m_v but the overall C_v a constant.
	20	b = 0.01 Δh_w = 10 m
	21	b = 0.005
	22	b = 0.001
		Varying k but m_v remaining constant.
	23	b = 0.01 Δh_w = 10 m
	24	b = 0.005
	25	b = 0.001

Settlements

The computation of settlements in the varying m_v cases is of some complexity. Defining m_v as:-

$$m_v = \frac{\text{d. (strain)}}{\text{d. (effective stress)}}$$

it is found that:-

$$\text{strain} = \int m_v \ \text{d. (effective stress)}$$

taking $m_v = ae^{-b\sigma'}$ in the special case considered,

$$\text{strain} = \frac{-a}{b} e^{-b\sigma'} + c$$

At $\sigma' = \sigma_o'$, strain is zero; hence

$$\text{strain} = \frac{a}{b} (e^{-b\sigma_o'} - e^{-b\sigma'})$$

The settlement of the ground surface is found by integrating this strain function through the soil thickness. This has been done by sampling potentials and stresses at the Gauss points and integrating numerically through the soil thickness. A separate program has been used for this, as the process is only valid for one dimensional cases and to include it in the finite element analysis would involve a certain loss of generality. It should be noted that the final expression for strain (above) is only valid for $b \neq 0$ as this is a restriction on the integration with respect to effective stress performed above.

A selection of volume change and settlement calculations based on these equations (and using the program described) are shown in Figures 4.11 (horizontal flow), 4.16 (vertical flow following sudden underdrainage and 4.19 (vertical flow with double drainage

of a uniform initial excess pore water pressure).

In general form, the settlement ρ_t (or volume change) is given by:-

$$\rho_t = \int_{\text{stratum thickness}} \int_{\text{effective stress change}} (m_v) \cdot d(\text{effective stress})$$

In order to evaluate a % settlement, the final effective stresses must be known. For the computations in the Figures mentioned above, the last pore pressures printed out by the finite element analysis program were used. These were not less than two time steps after the dissipation curve had flattened off at large times and were indistinguishable from the analytical solutions for steady seepage.

4.8. Parametric Study - Constant Head In Situ Permeability Test

This final test of the non-linear consolidation model is not a complete parametric study but only a short series of analyses to examine the influence of effective stress dependent properties on the rates of equalisation of flows into or out of a spherical piezometer during a constant head in situ permeability test. The theory for a spherical piezometer in a homogenous, infinite medium with constant properties is that the flow rate of q_t at time t is (after Gibson 1962):

$$q_t = 4\pi R k (\phi_p - \phi_0)\left(1 + a/\sqrt{\pi c_v t}\right)$$

It is conventional to measure flow rates at various times through the test, and a plot of q_t VS $1/\sqrt{t}$ should yield a straight line (Figure 4.20) which when extrapolated to infinite time has an intercept q_∞ on the q axis corresponding to a steady state seepage regime. The influence of an effective stress dependent permeability

on this q_{∞} has already been discussed in Section 2.5 *et seq.* Ideally the compressibility would also be obtained from the slope of this plot.

However, in practice it is usually found that the q VS $1/\sqrt{t}$ plot is not a straight line but is curved. Various effects have been invoked to explain this (Gibson 1970, Wilkinson 1968, Bishop and Al-Dahir 1970) including the following:-

(a) Hydraulic losses in the piezometer leads, resulting in a changing head at the piezometer tip throughout the test.

(b) Total stress changes in the soil accompanying the application of the head increment or decrement at the piezometer tip, as a result of which the initial pore water pressure conditions are non-uniform.

(c) Non-uniform initial pore water pressure conditions arising from incomplete equalisation of groundwater conditions after piezometer installation.

(d) Air in the ground, piezometer or measuring system.

(e) Different compressibility or permeability in a smeared zone around the piezometer tip.

(f) Mandel-Cryer effects or other, similar, conditions not predicted by an uncoupled theory.

The above is by no means an exhaustive list.

Yet another possibility is that the changes in permeability and/or compressibility during the test lead to the observed flow rate changes, and the series of analyses of this section were made to explore this possibility in a very preliminary way.

The model used in these analyses is shown in Figure 4.21 comprising 8 elements and 43 nodes. These are axisymmetric elements, and a half section through these is a 30^{o} wedge. Unless infinite elements are used it is not possible to model an infinite region, but the extreme boundary is 30 piezometer radii from the centre.

There is an analogous situation where the head is not held constant but varies, as for example when ground water conditions re-establish themselves after piezometer installation or after ground water conditions have been perturbed artificially. This includes the situation that arises at the end of a constant head test. Not only is the analysis intrinsically more complex, but it is stressed that the flow rates and/or piezometer head history is dependent on the initial conditions at the start of the falling or rising head test. When effective stress dependent soil properties are included, even the symmetry between rising and falling head tests (which start from the same initial conditions) vanishes. With this added complexity it is scarcely surprising that the constant head test is usually preferred in engineering practice. The reader is referred to Gibson's (1963) treatment of this test for constant material properties. However, in contrast to Gibson, Edelman (1953b) purports to show that the compressibility of the soil has no effect on rising or falling head tests. Bjerrum (1953) terms this "a dubious result"!

Table 4.5. Analyses of Spherically Symmetric Dissipation

SPHERE - 1 a, b, c	Analysis to examine agreement between FEM and Gibson's analytical solution. Constant k, m_v but varying Δt; swelling and consolidating.
SPHERE - 2	Swelling test, constant m_v; varying k, Δt:
a	b = 0.001 σ = 200 $\Delta\phi$ = + 5 m
b	b = 0.001
SPHERE - 3	Consolidating test, constant m_v; varying k, Δt;
a	b = 0.01 σ = 200 $\Delta\phi$ = -5 m
b	b = 0.001
SPHERE - 4	Analogous to SPHERE - 2a but with m_v varying in such a way as to keep C_v constant.
SPHERE - 5	As SPHERE - 4 but with consolidating conditions.

The ratio of flow rate in the complete sphere to that predicted by this finite element model is given by the ratio of their solid angles subtended at the centre of the sphere. In the case of the 30^0 wedge chosen (Figure 4.21) this ratio is:-

$$\frac{4\pi R^2}{2\pi R . R \sin 30^\circ} \qquad (= 4)$$

Hence the sphere flow rates should be 4 times those from the finite element results.

Flow rates at the prescribed potential boundary nodes are yielded by the "reactions to earth" computed as part of the solution process. The sum of the nodal flow rates at the surface of the piezometer cavity, corrected by the above factor, gives the total flow rate. Since the solution is obtained at the middle of a time step, then this flow rate should properly be considered to be an average flow rate over the whole interval. Since, however, the values are associated in the printout with the end-of-step potentials and the time of the end-of-step point then the writer has plotted the flow rate against the end-of-step time for convenience. Such errors as arise from this are imperceptible in cases where an analytical solution exists to check against.

At small time values, the flow through the other prescribed potential boundary are negligible, but with increasing times they approach the values for the flows from the piezometer cavity as steady seepage conditions become established. In principle, the cumulative flow from a boundary could be used to predict total volume change Δv (cf. Section 4.7. *"settlements"*) since:-

$$\Delta V = \int_0^t \int_{area} q_t \; d(\text{surface area}) . d(\text{time})$$

$$= \sum_{n=1}^{NT} q_n . \Delta t_n . \Delta A$$

where Δt_n is the time step length

and ΔA is the area through which the flow q_n is discharged.

However, ΔA may have to be established by numerical integration of shape function products on the element surfaces with curvilinear elements as used here, and so the process is not as simple as it would first appear. Furthermore, individual errors accumulate so that the results at large times may be unreliable.

An additional factor is that the flow rate value is crucially dependent on potential gradients at the edge of the mesh. These may fluctuate wildly for small individual nodal potential changes giving an oscillating result. This is largely damped out by an integration procedure as used previously.

For the piezometer flow problem the predicted flow rates can, of course, be used directly, but by a converse argument to the above a smoother flow/time curve might be obtained by computing the total volume of fluid released from, or imprisoned in, storage (by fluid or soil structure compressibility) corrected as necessary for steady (no volume change) flow conditions.

The eleven examples in the parametric study revealed the following effects:-

(a) For constant properties, the Gibson solution is reproduced yielding an effectively straight line on a q *VS* $1/\sqrt{t}$ plot. The results of swelling and consolidating tests are identical, but the size of the early time steps are important - large time steps tending to exaggerate early dissipation. (SPHERE - 1 a to c).

(b) Constant m_v solutions appear better behaved with early oscillation in flow rates rapidly damped out in comparison to varying m_v solutions. This is the result of the varying m_v cases having higher instantaneous C_v values (the gradients of the q *VS* $1/\sqrt{t}$ plot are flatter for the varying m_v cases which is the same effect) and so the time steps are relatively larger.

(c) Where the oscillations have died out (or where a median line is fitted through the oscillations) this is a straight line on the q *VS* $1/\sqrt{t}$ plot passing through a q_∞ value identical to that predicted by the closed form theory. This q value is dependent on the base k value and on the b parameter, boundary heads and total stress assumed.

(d) At large times the q *VS* $1/\sqrt{t}$ plots show a small, upward concave, curvature and tend to a slightly higher q_∞ value. This has been checked in one case (SPHERE - 2b) and found to be the influence of a finite sized soil region in which the piezometer is embedded.

(e) No curvature in the plots that can be attributed to effective stress dependency in the parameters has been detected.

(f) Some of the early oscillations in the flow rate values are the result of poor selection of initial potential conditions at the edge of the piezometer cavity. (*vide* Section 4.4). The modified initial edge conditions of Figure 4.2 are not strictly applicable since the elements are both "non-rectangular" and axi-symmetric.

From conclusion (e) above it may be inferred that the installation and testing of a piezometer in a layered or otherwise non-homogenous deposit may give rise to the sort of non-linear q *VS* $1/\sqrt{t}$ plots often obtained in practice. At early times the Gibson solution applies, but at larger times the zone of changed pore pressures has spread to the extreme edge of the soil in which the piezometer is installed. The nature of the adjacent soil then dominates the subsequent behaviour. If it is *more* permeable than that in contact with the piezometer, a concave upwards curvature results and if *less* permeable a concave downwards curvature is obtained. This is explained diagrammatically in Figure 4.23.

It should, in principle, be possible to estimate the size of the zone in which the piezometer is installed from the time taken to reach the departure from the Gibson straight line and also the properties of the surrounding material by an extension of the basic theory.

However, an important conclusion is that the q_∞ to be used for the estimation of the permeability of the material in contact with the piezometer should be extrapolated from the early time straight line portion of the q *VS* $1/\sqrt{t}$ plot and not the large time value. This contrasts markedly with Gibson's (1970) extension of his theory to include for the effects of A values in which total stresses and the resulting pore pressure changes adversely influence the shape of the plot at early times.

4.9. Summary

Effective stress dependency in the permeability causes significant changes in the dissipation behaviour only when the dependency function is unrealistically intense. As far as can be judged from the numerical results, the *percentage* settlements are totally independent of the dependency of the permeability and compressibility on effective stress. However, the *absolute* settlements depend strongly on both the variation of permeability with effective stress (which governs the final distribution of pore water pressures in the soil under steady seepage conditions, *vide* Chapters 2 and 3) and the variation of compressibility with effective stress (which governs the change in voids ratio or strain under the effective stress changes that occur).

The early stages in the consolidation analysis are important, and the stability of the solution can be increased by selecting initial conditions wisely. This is particularly important when using certain elements, the higher order (parabolic and cubic) serendipity quadrilateral elements being cases in point.

The final steady seepage flow rate in a constant head in-situ permeability test is not influenced by the compressibility. Consolidation solutions tend towards the steady solution (Section 2.5), and within the constraints of the numerical technique used, produce straight line q *vs* $1/\sqrt{t}$ plots. Some curvature in this plot may result from the region in which the test is performed being of finite size, and this effect is discussed extensively above.

tial conditions

of 1st time step

of 2nd time step

ite element mesh

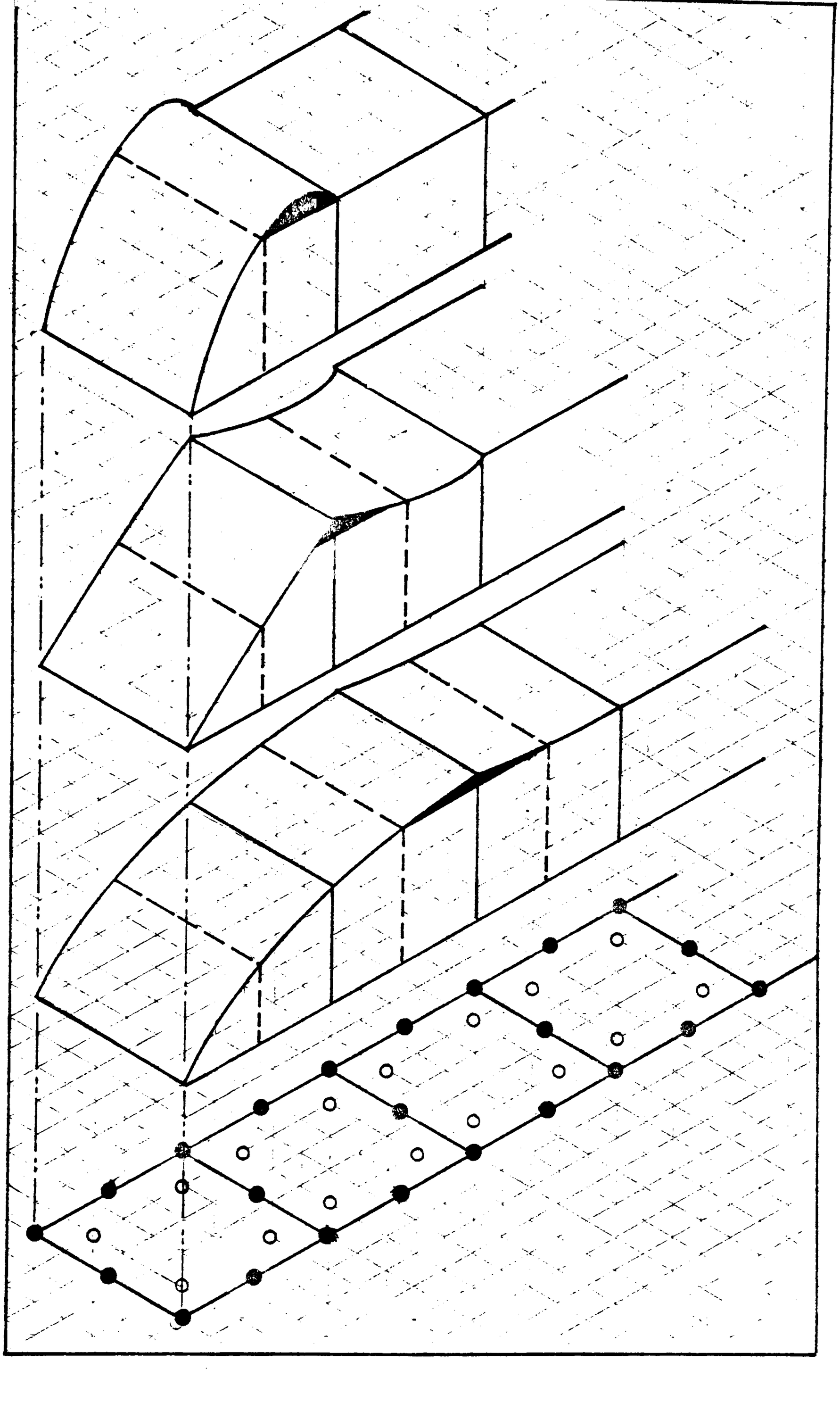


Figure 4.1. Illustration of "element induced" potential oscillation

(Solid black area is the wave of excess potential.)

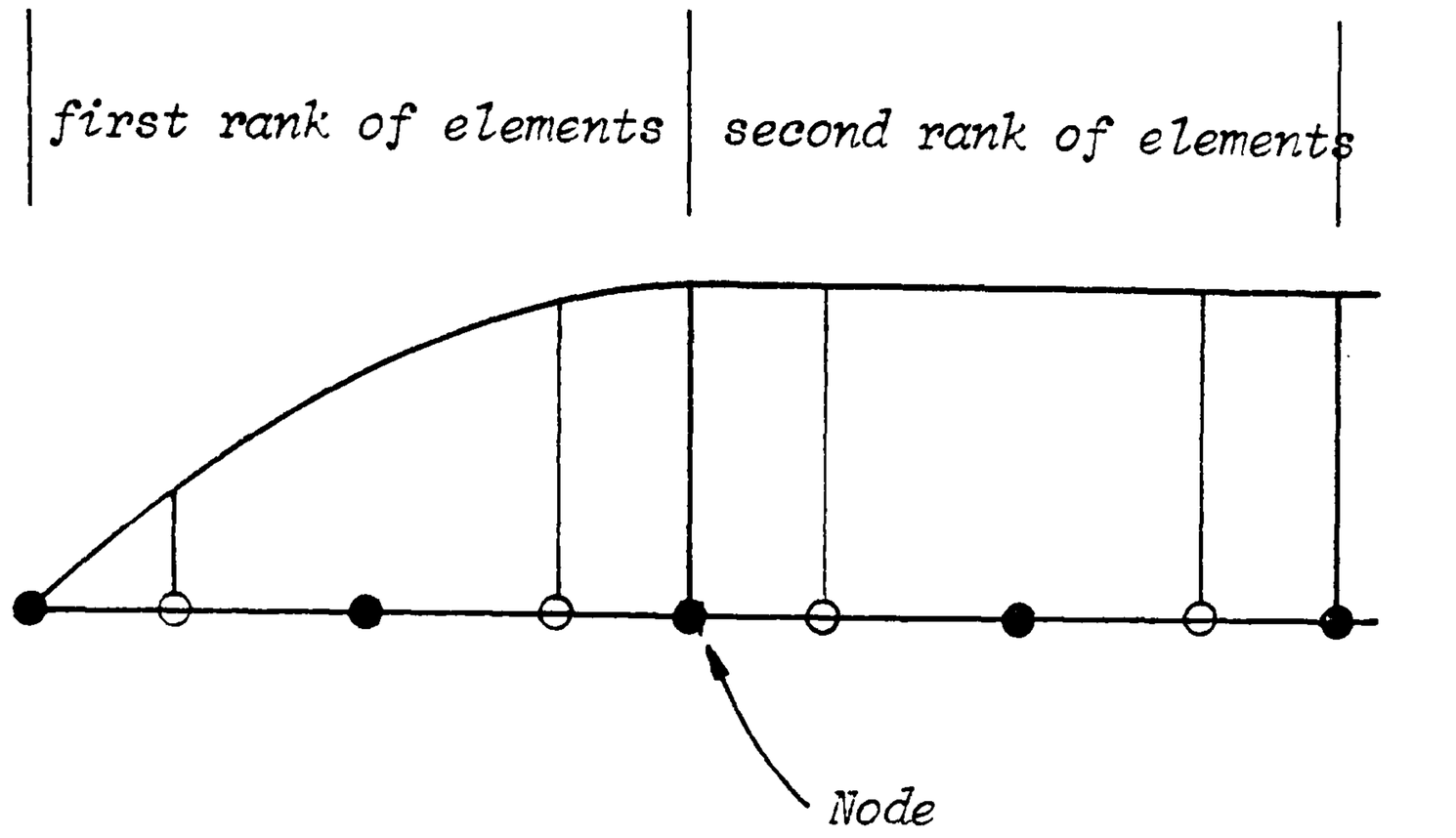
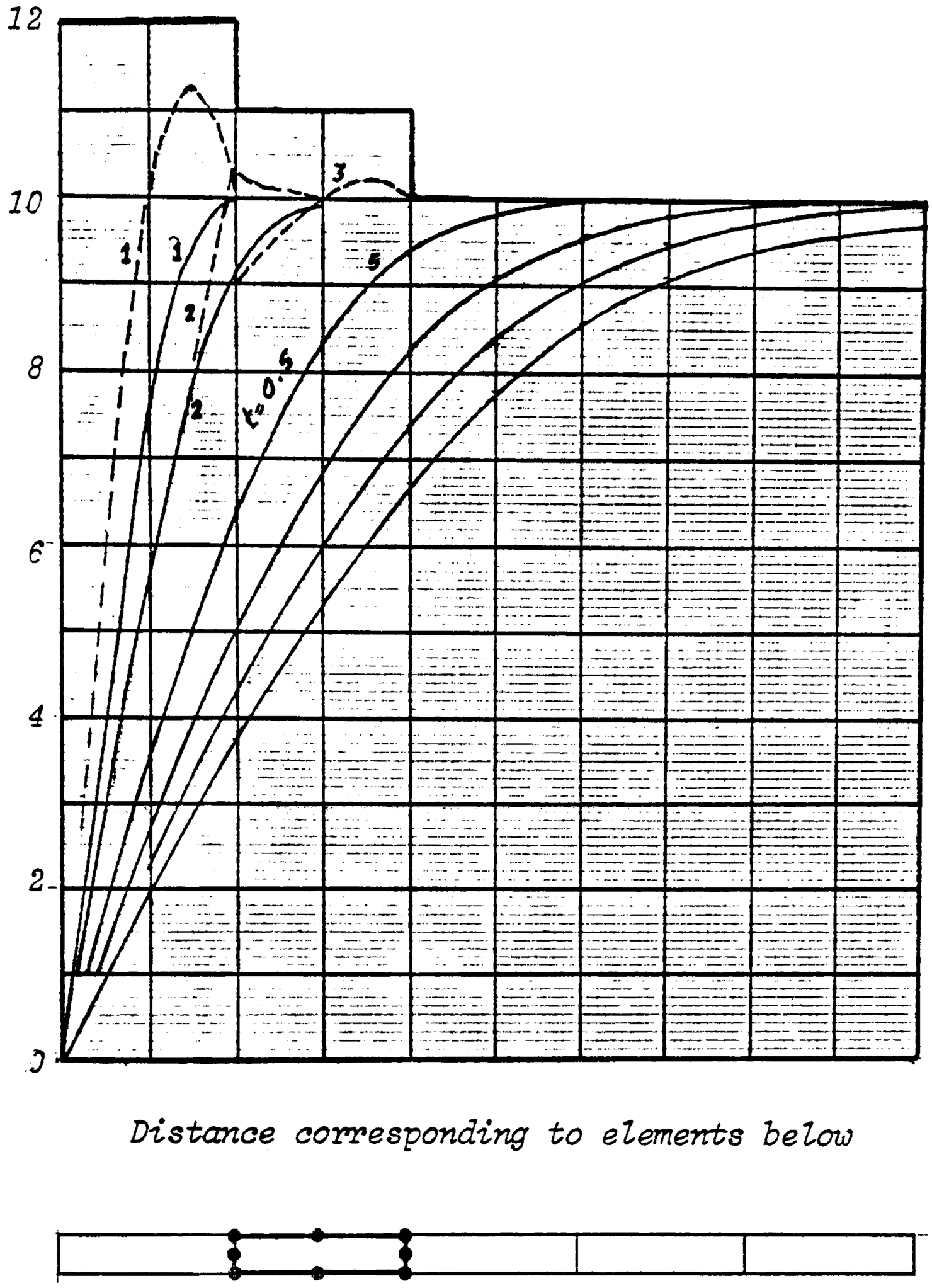


Figure 4.2. Alternative modelling of initial conditions close to known potential boundaries.



Legend

Solid line - isochrones for analyses using initial conditions case (a) from Fig. 4.2.

Dashed line - first three isochrones for most contrasting alternative initial conditions (case d).

Figure 4.3. Comparison of results yielded by different initial condition assumptions close to the drainage boundary.

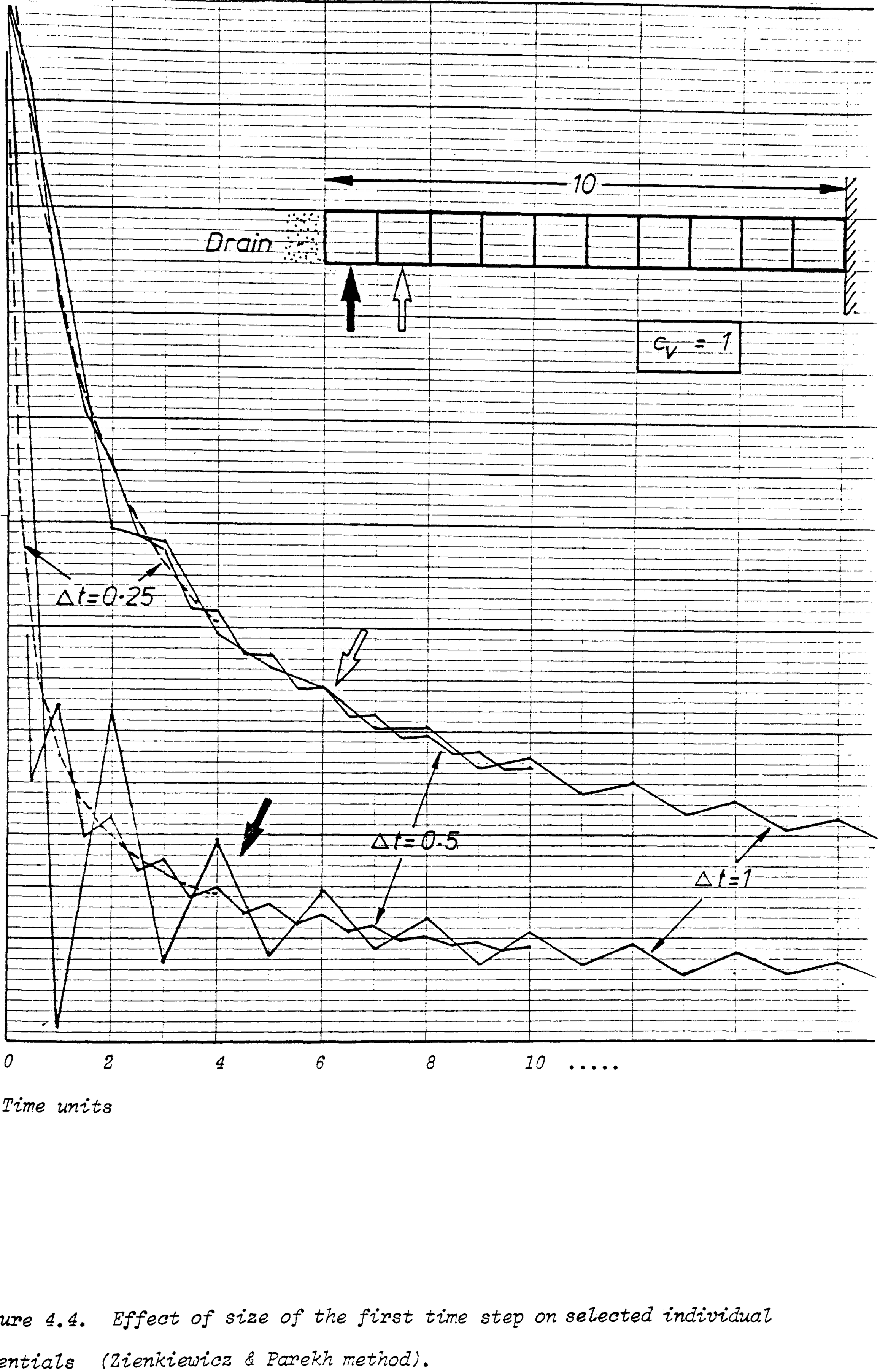


Figure 4.4. Effect of size of the first time step on selected individual potentials (Zienkiewicz & Parekh method).

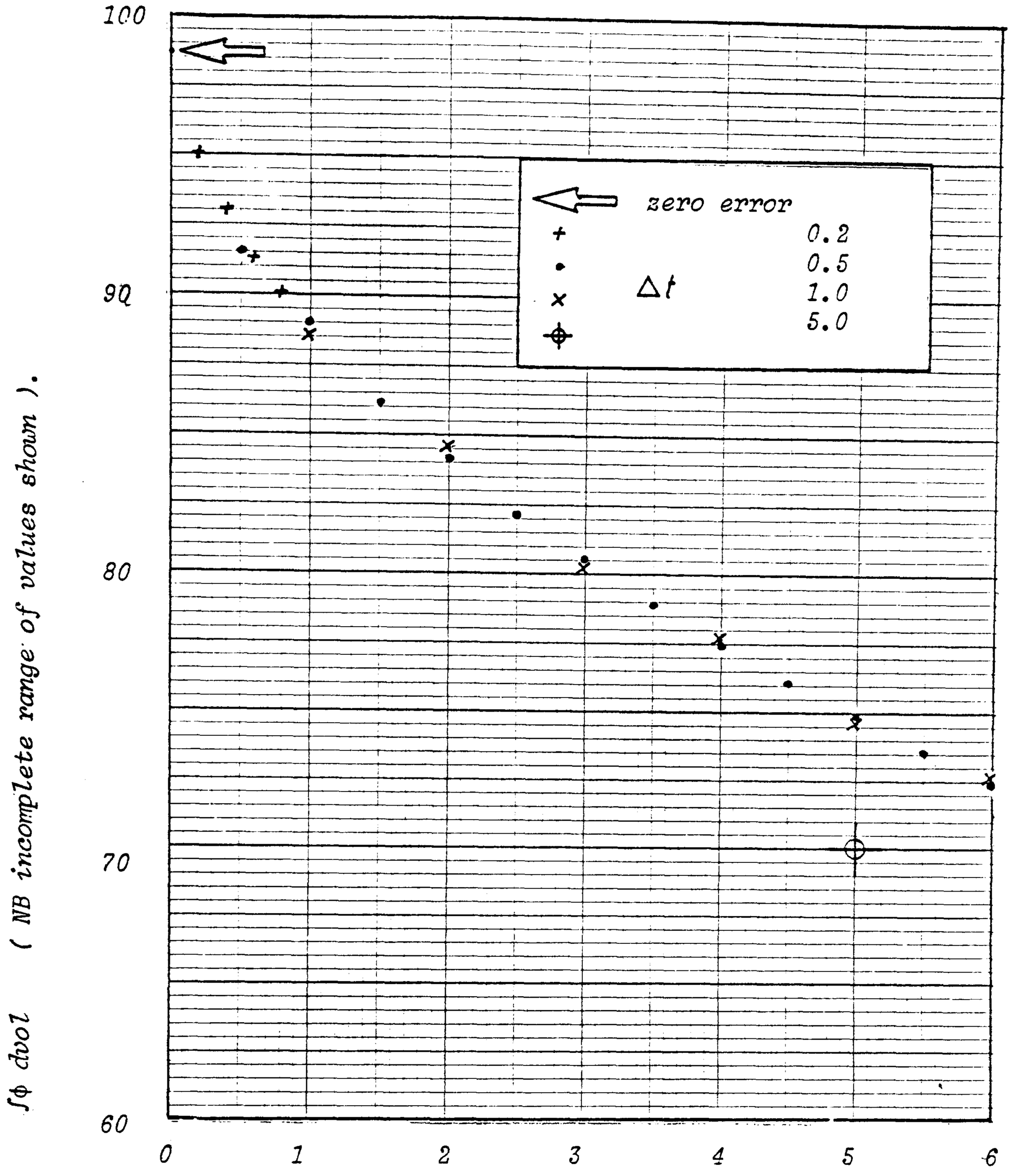
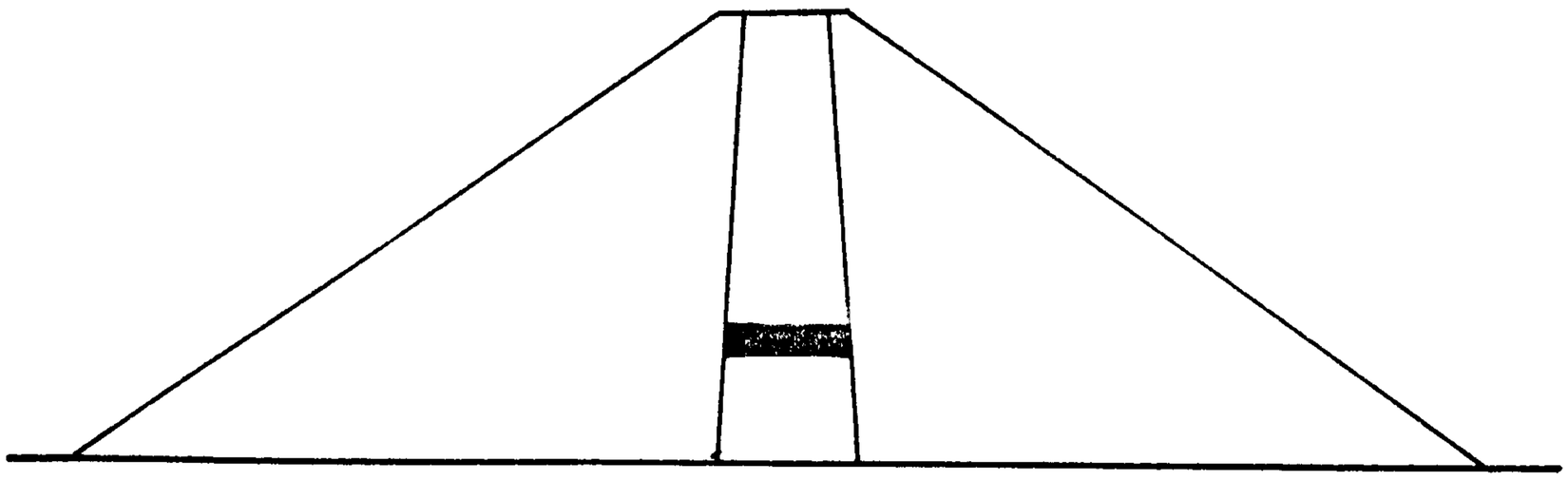


Figure 4.5. Effect of the size of the first time step on average dissipation of ∫φ dvol (Zienkiewicz & Parekh method).



Initial conditions *Final conditions*

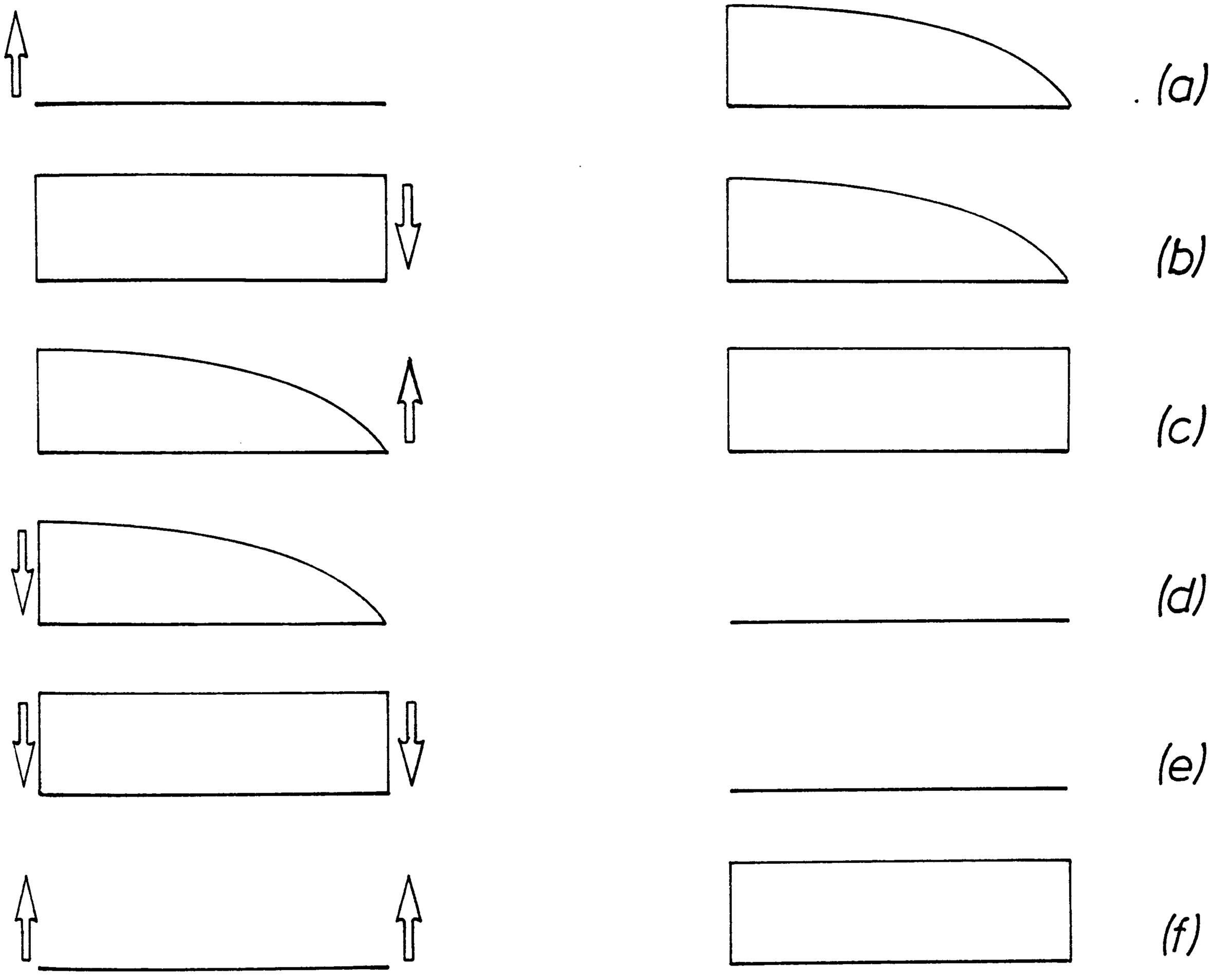


Figure 4.6. The six basic unique horizontal, one dimensional dissipation cases.

a) *Initial Conditions: (Assumed steady seepage)*

(i) *Hydrostatic.*
(ii) *Underdrained.*
(iii) *Artesian.*

b) *Change in hydraulic boundary conditions:*

(i) *Increase top pore pressure.*
(ii) *Decrease " " " .*
(iii) *Increase basal pore pressure.*
(iv) *Decrease " " " .*

c) *Add undrained pore pressures (and total stresses):*

(i) *Uniformly with depth.*
(ii) *Any distribution.*

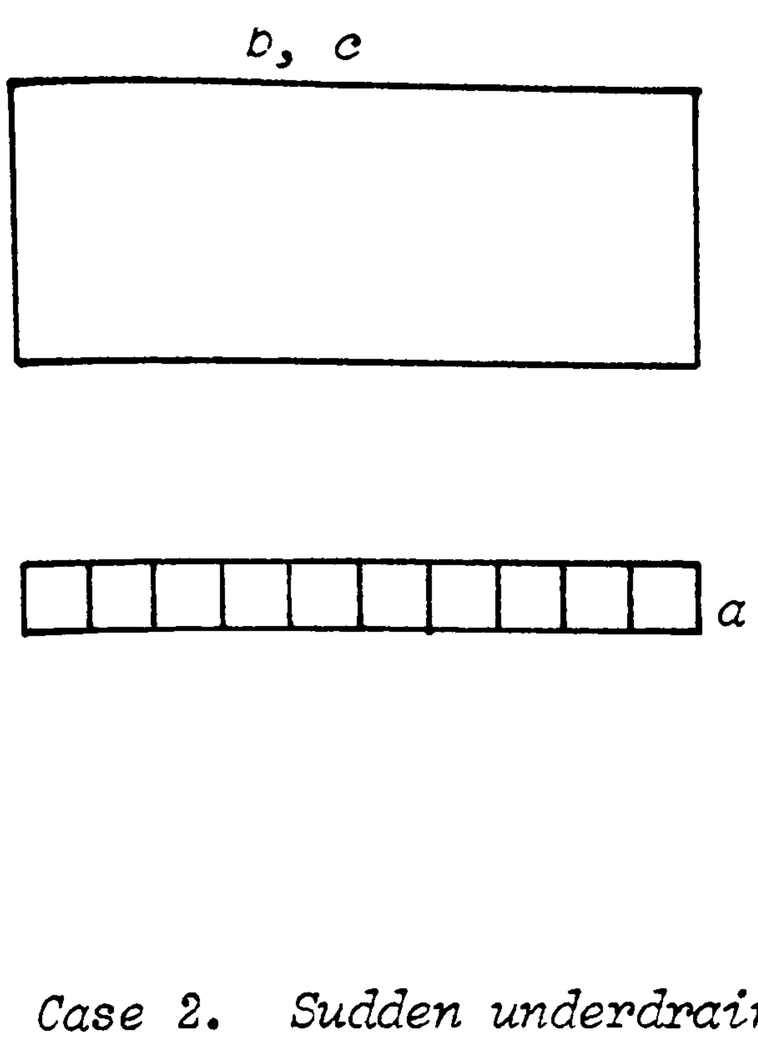
d) *Take either boundary as impermeable:*

(i) *Top (often unlikely).*
(ii) *Basal boundary (in this case pore water pressures increase hydrostatically with depth for both initial and final conditions).*
(iii) *Both taken as drainage boundaries.*

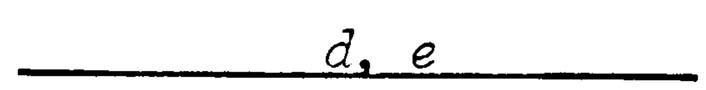
Permutations:

a x b x d(iii)		*12 separate cases*
a x b(i) and (ii) x d(iii)		*2*
a x b(iii) and (iv) x d(i)		*2*
No. of different cases where impetus for consolidation comes from hydraulic boundary condition changes	=	*14*
a(i) x c x d		*6*
a(ii) and (iii) x c x d(iii)		*4*
No. of different cases where internally generated undrained pore pressures cause consolidation	=	*10*

Figure 4.7. Basic, unique, one dimensional dissipation cases.
NB. the term "consolidation" used above includes swelling.



Case 1. Horizontal, doubly drained dissipation



Legend

a = mesh

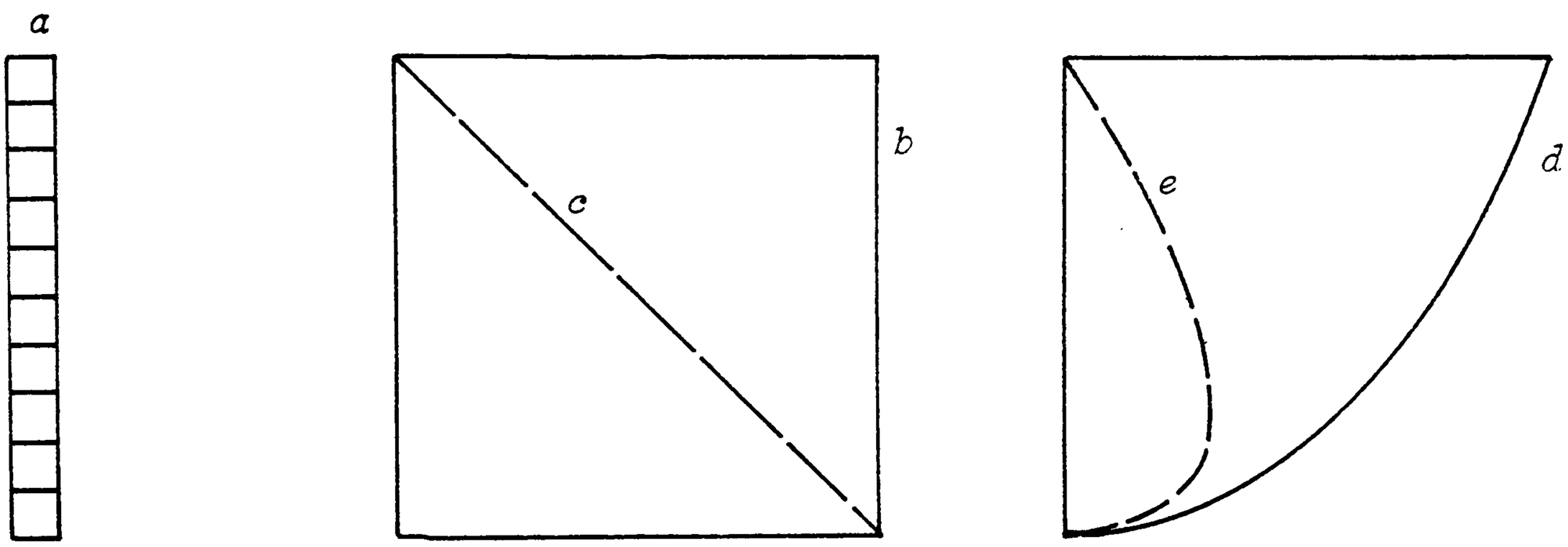
b = initial potential

c = initial pore water pressure

d = final potential

e = final pore water pressure

Case 2. Sudden underdrainage



Case 3. Vertical, doubly drained dissipation with constant initial excess pore pressure.

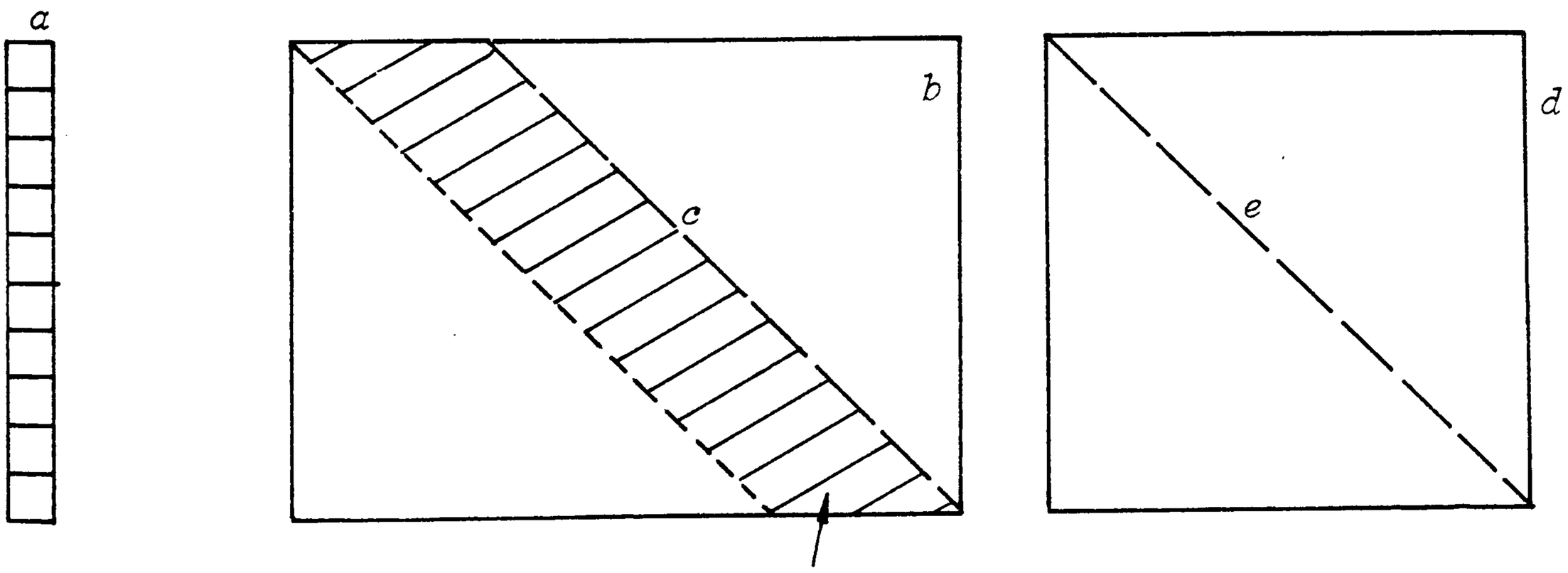


Figure 4.8. Key diagram: Cases considered in the parametric study.

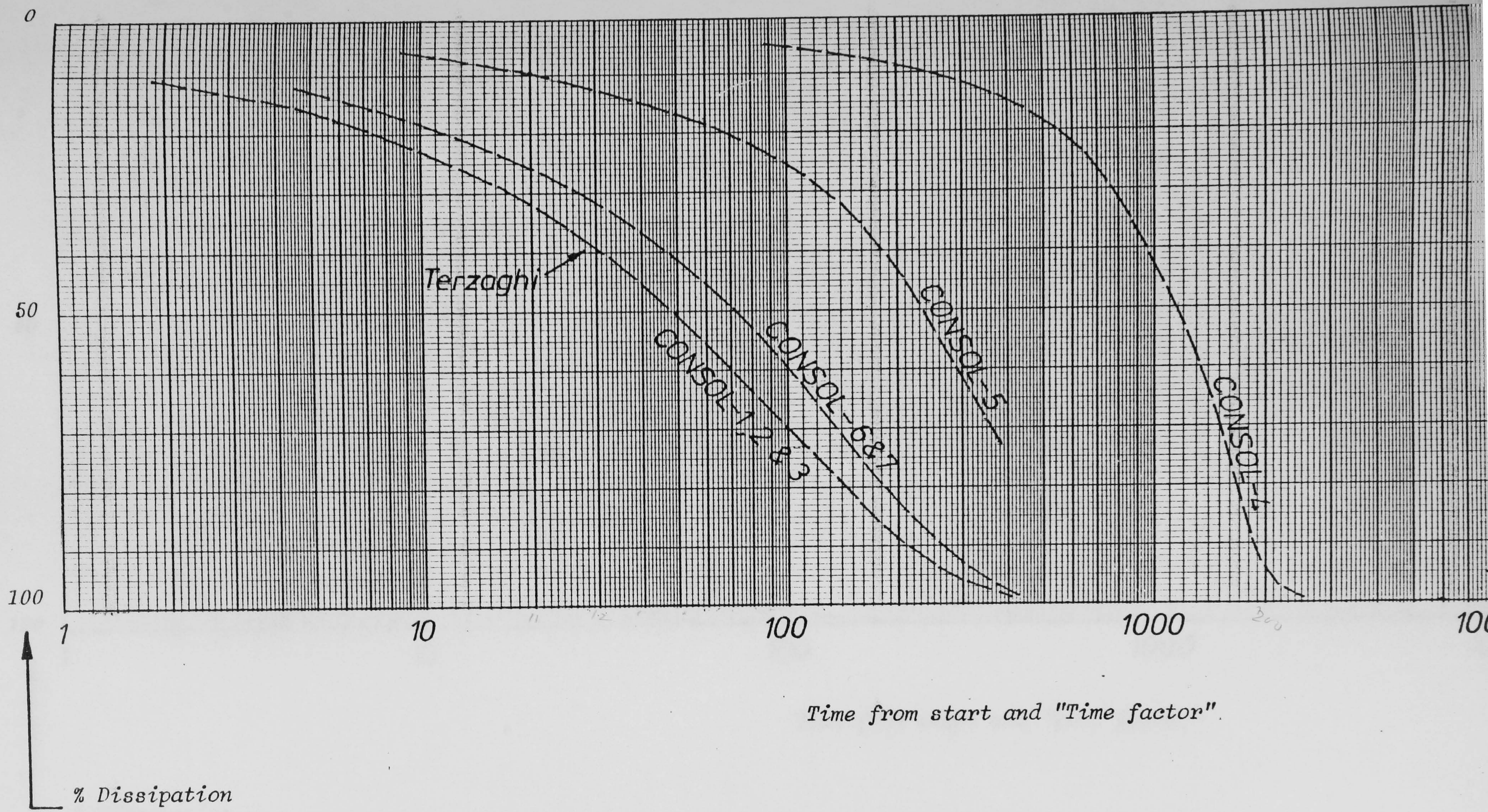


Figure 4.9. Average degree of pore water pressure dissipation, constant c_v model, horizontal flow.

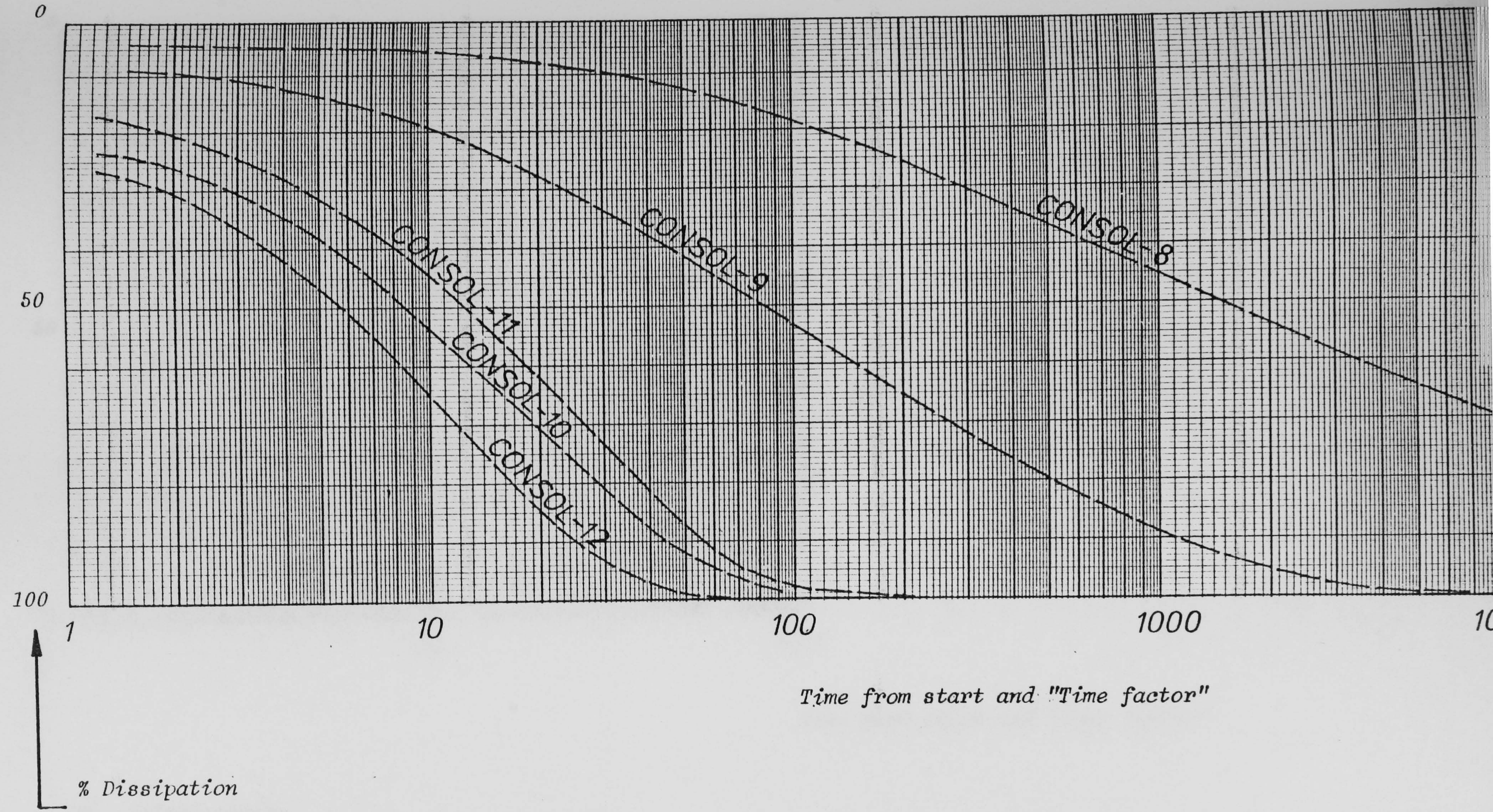


Figure 4.10. Average degree of pore water pressure dissipation, constant m_v model, horizontal flow. (NB in this case the average pwp dissipation and % volume change give rise to the same plots).

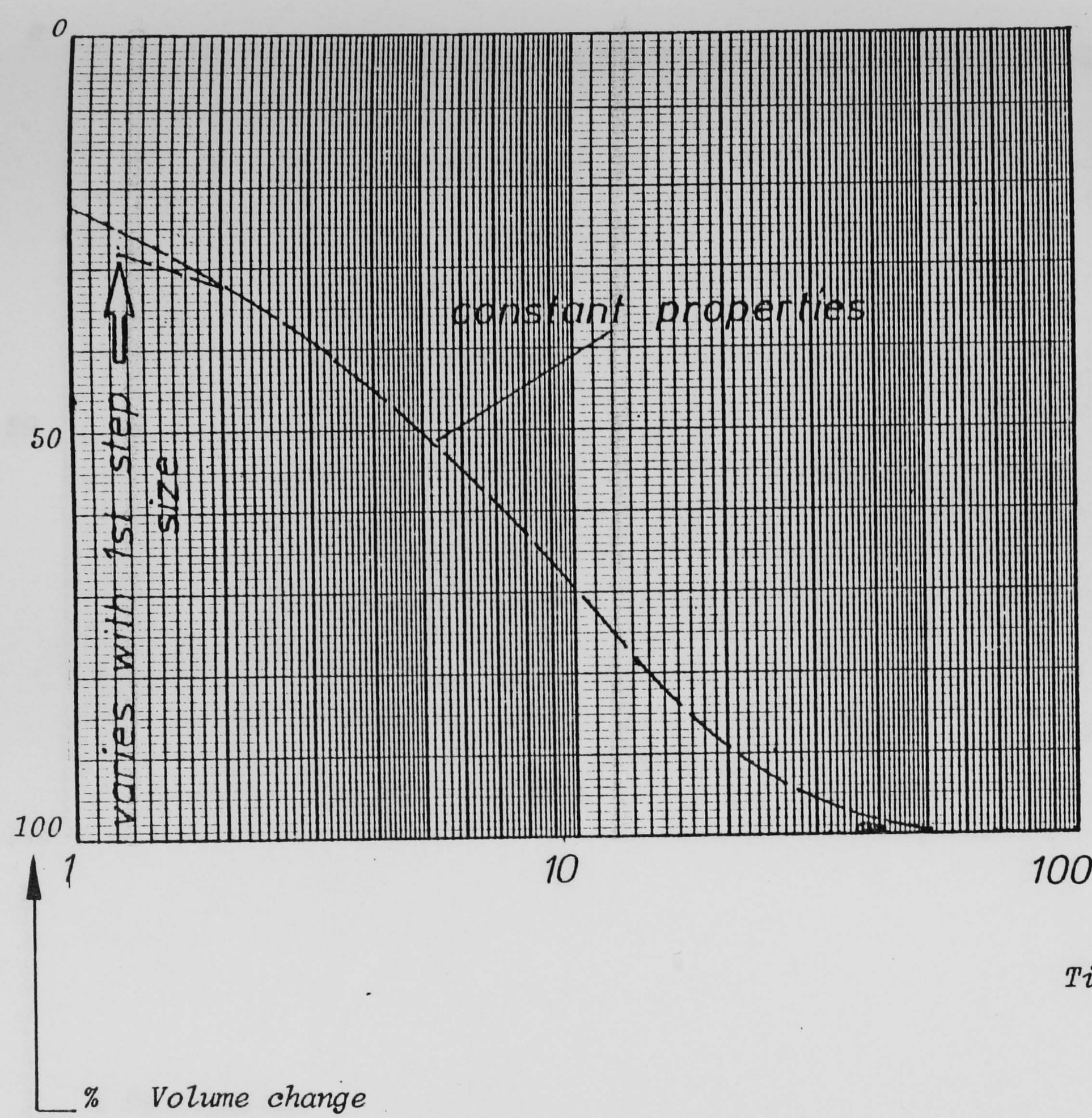


Figure 4.11. Average % volume change, constant c_v model, horizontal flow.

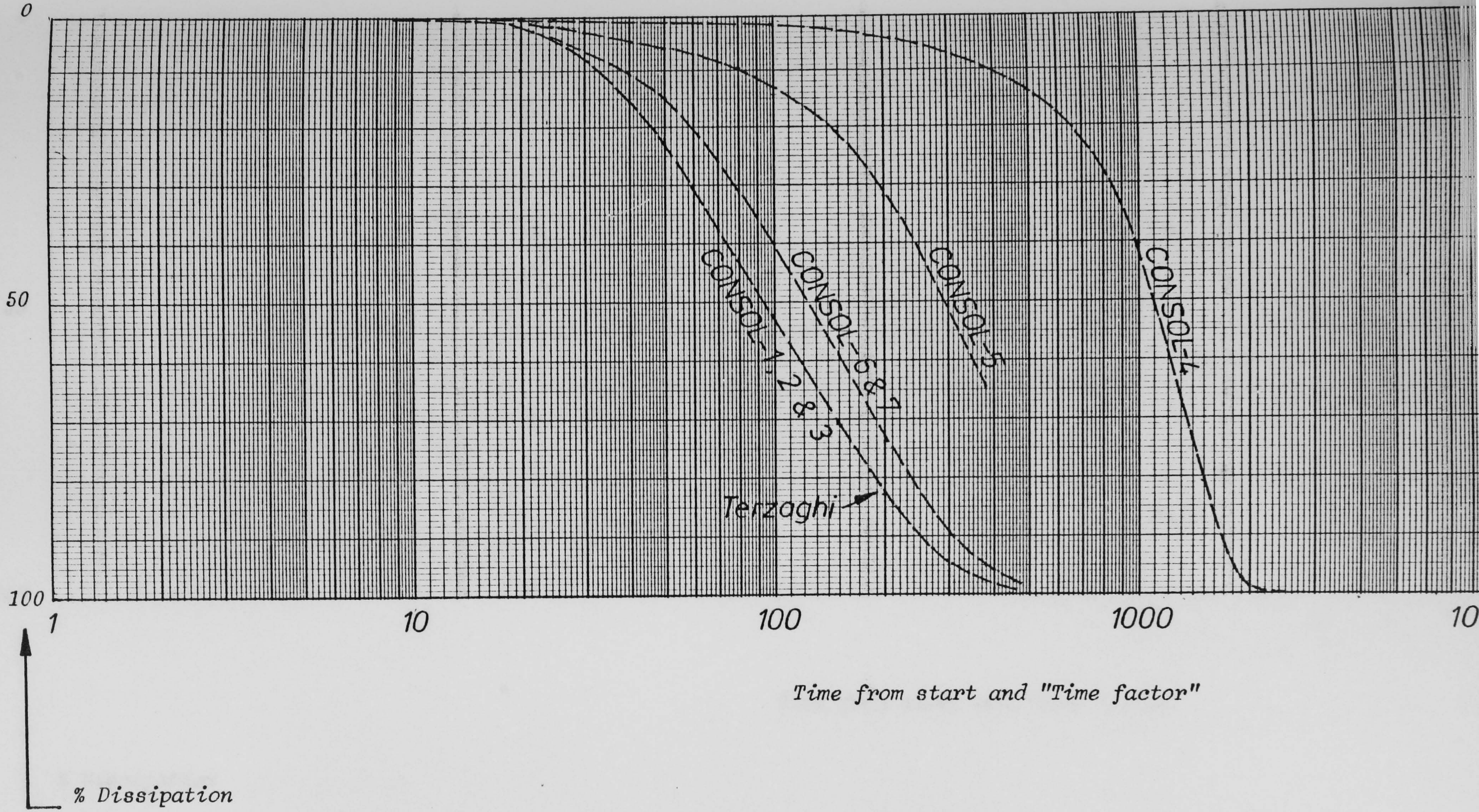


Figure 4.12. "Mid plane" pore pressure dissipation, constant c_v model, horizontal flow.

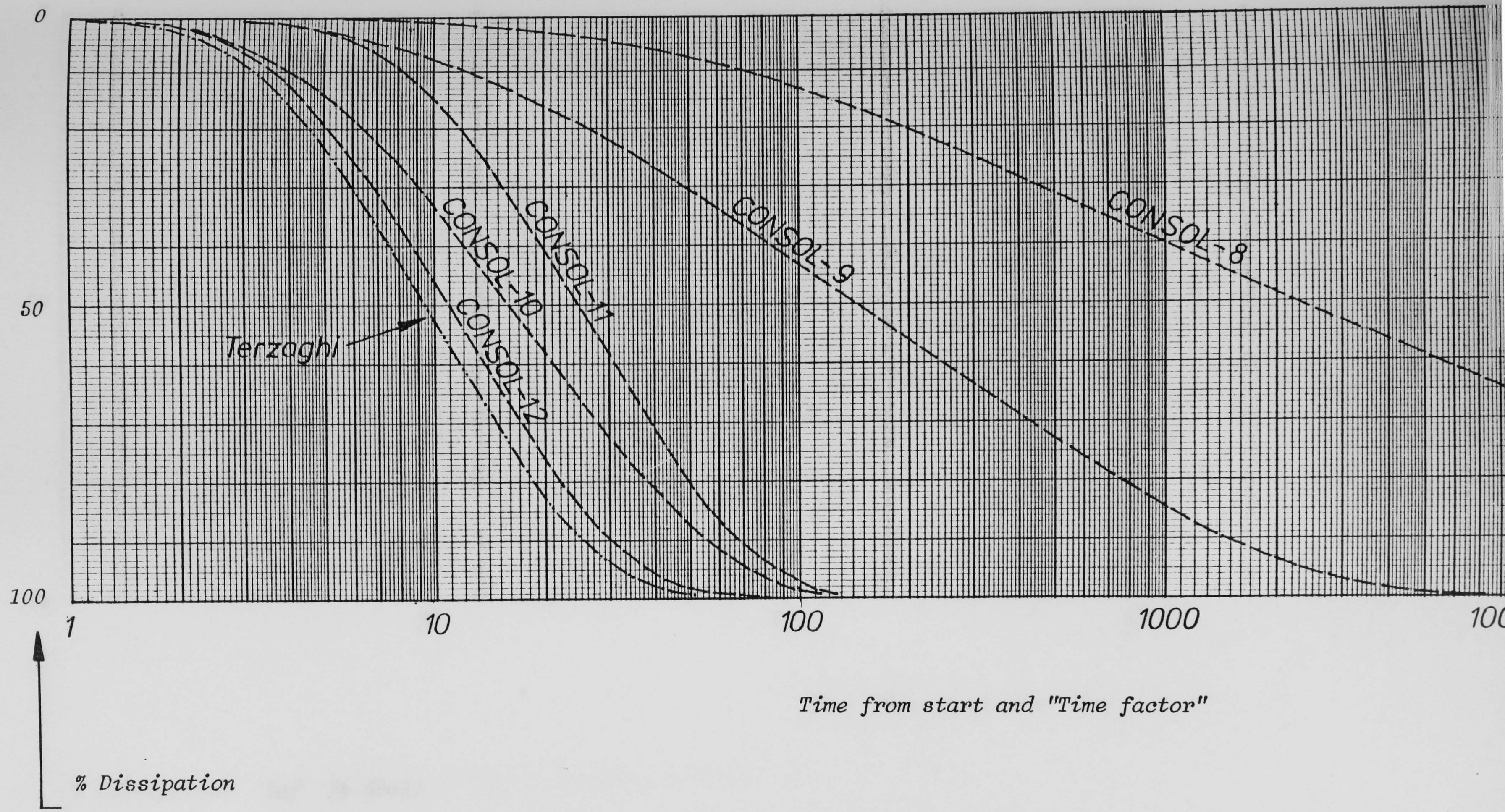


Figure 4.13. "Mid plane" pore pressure dissipation, constant m_v model, horizontal flow.

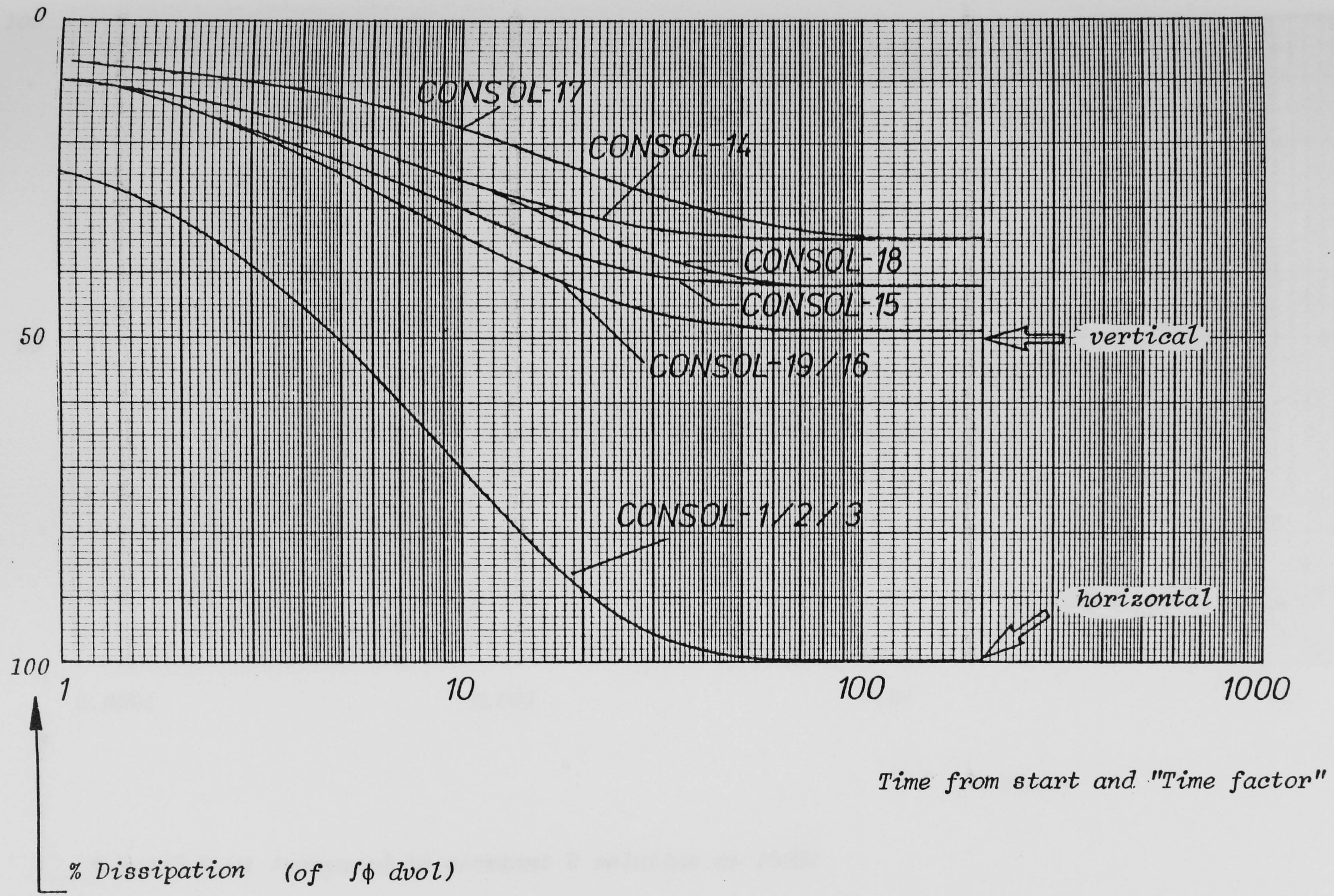


Figure 4.14. Dissipation rates in the underdrained problem for both constant c_v and constant m_v cases. NB even the "constant properties" solution goes to 50% ∫φdvol.

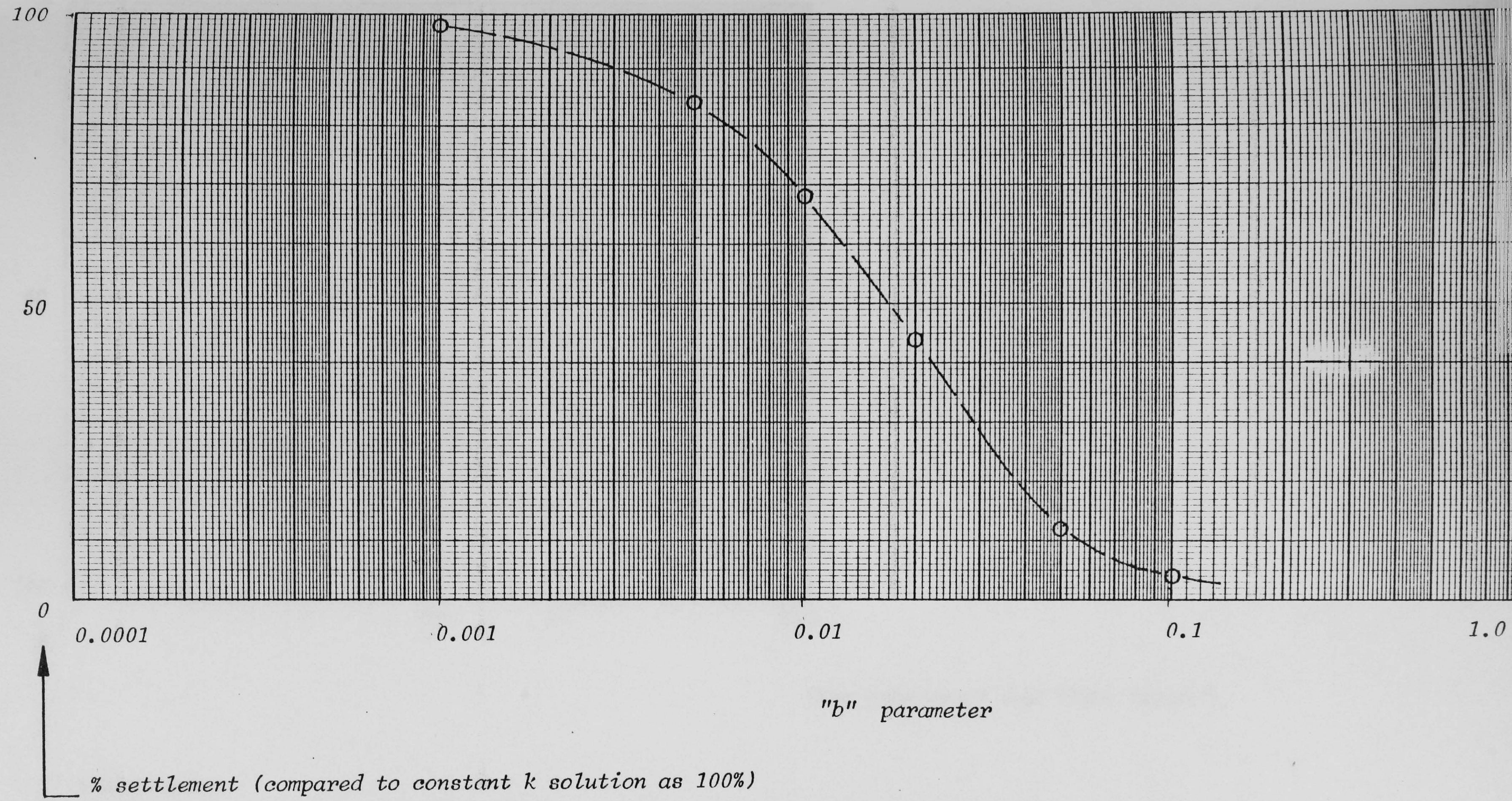


Figure 4.15. Final settlements in the effective stress dependent permeability solutions compared to the constant properties theory. Complete underdrainage.

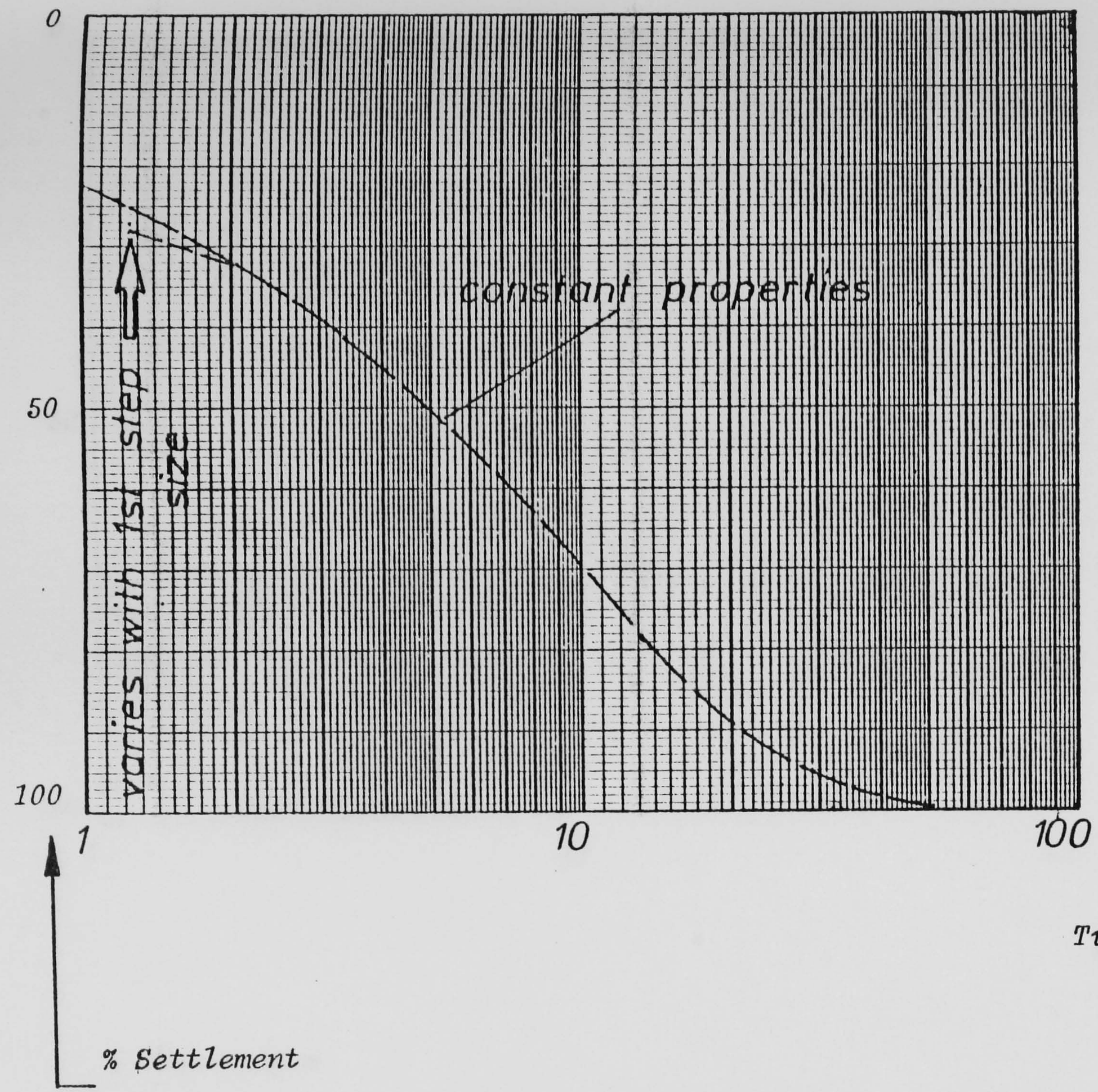


Figure 4.16. Average % settlement, constant c_v model. Vertical flow with sudden underdrainage.

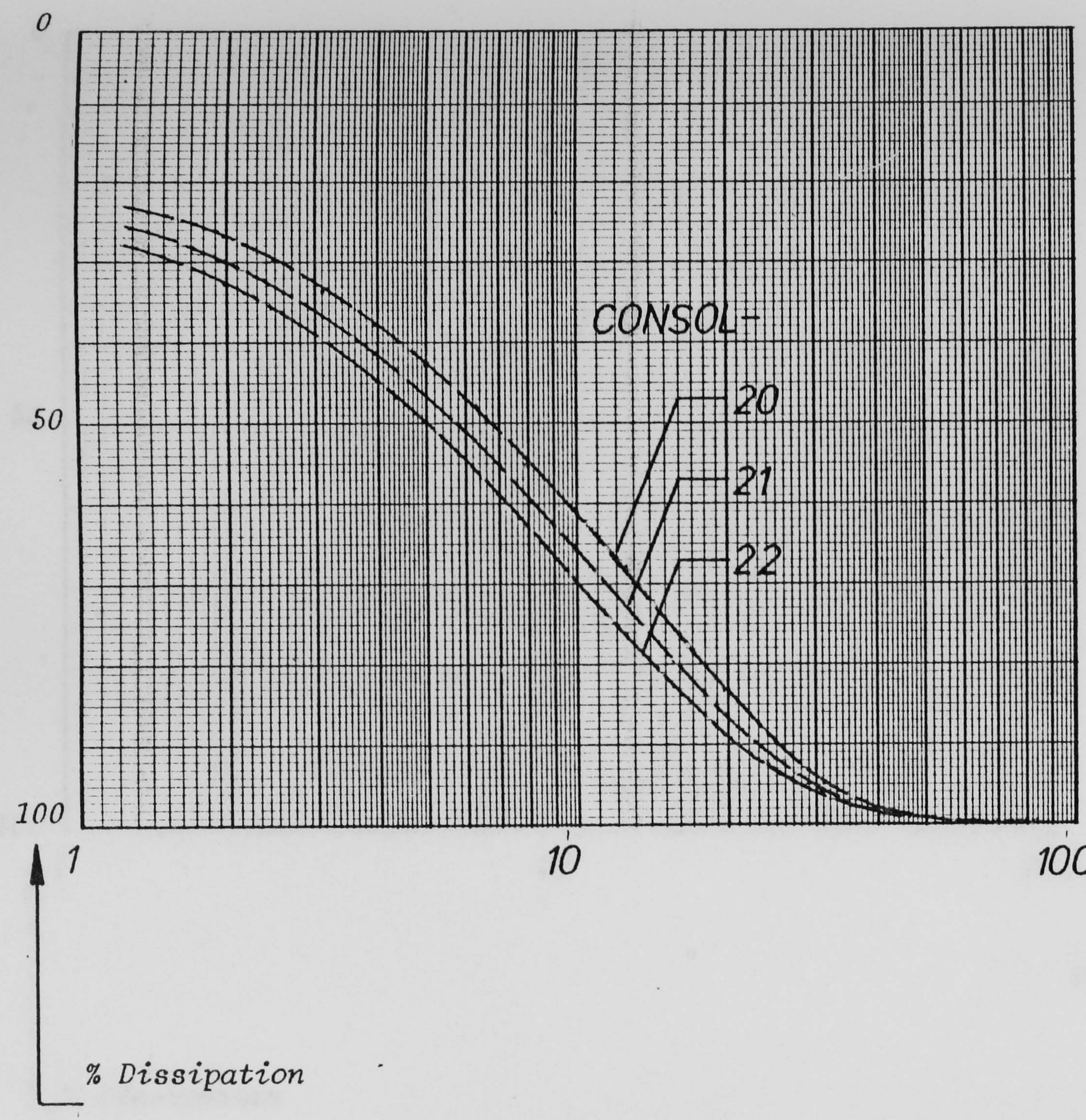


Figure 4.17. Average degree of pore water pressure dissipation, constant c_v model. Doubly drained vertical flow with a constant initial excess pore pressure.

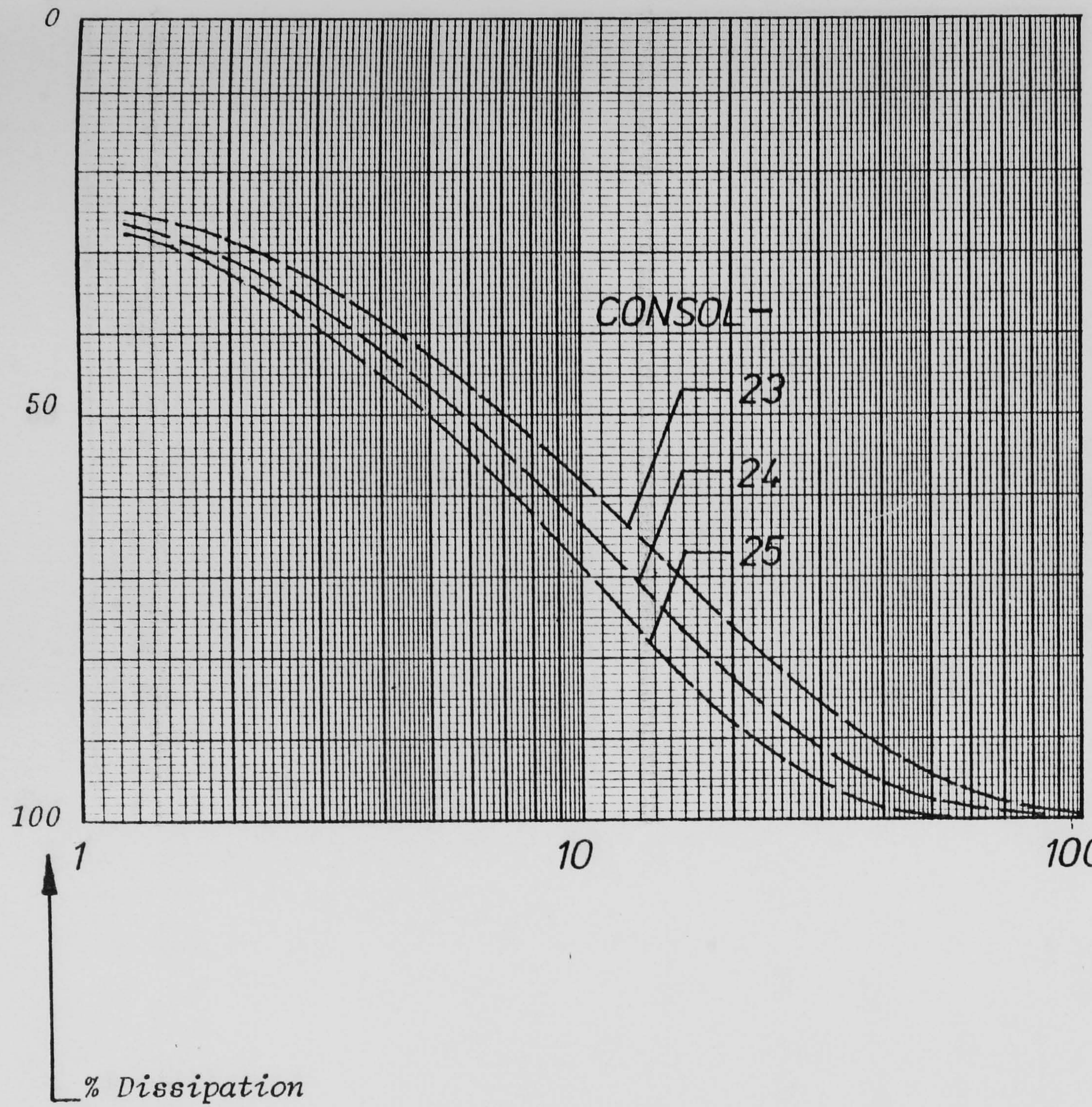


Figure 4.18. Average degree of pore water pressure dissipation, constant m_v model. Doubly drained vertical flow with a constant initial excess pore pressure.

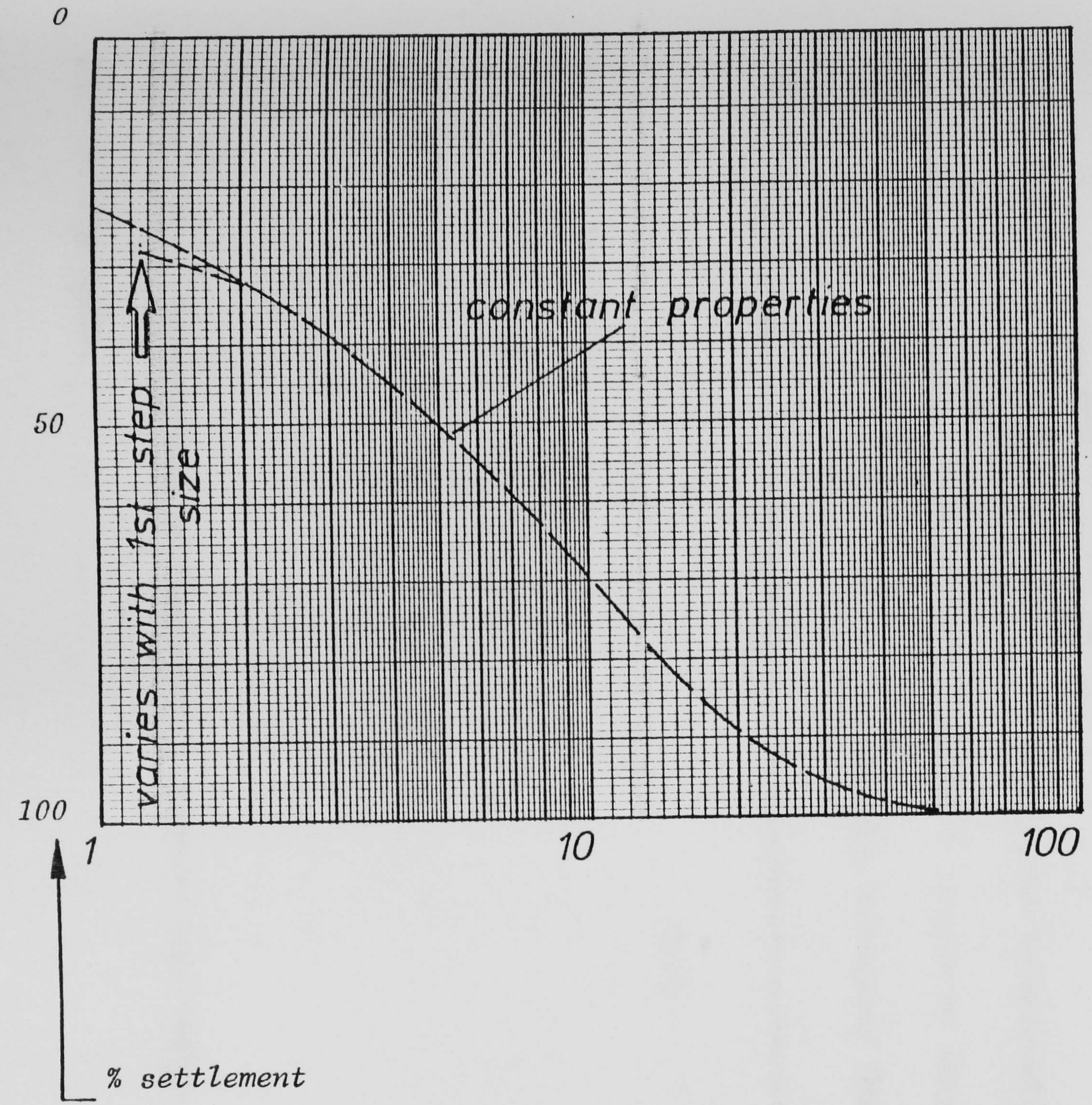


Figure 4.19. Average % settlement, constant c_v model. Doubly drained vertical flow with a constant initial excess pore water pressure.

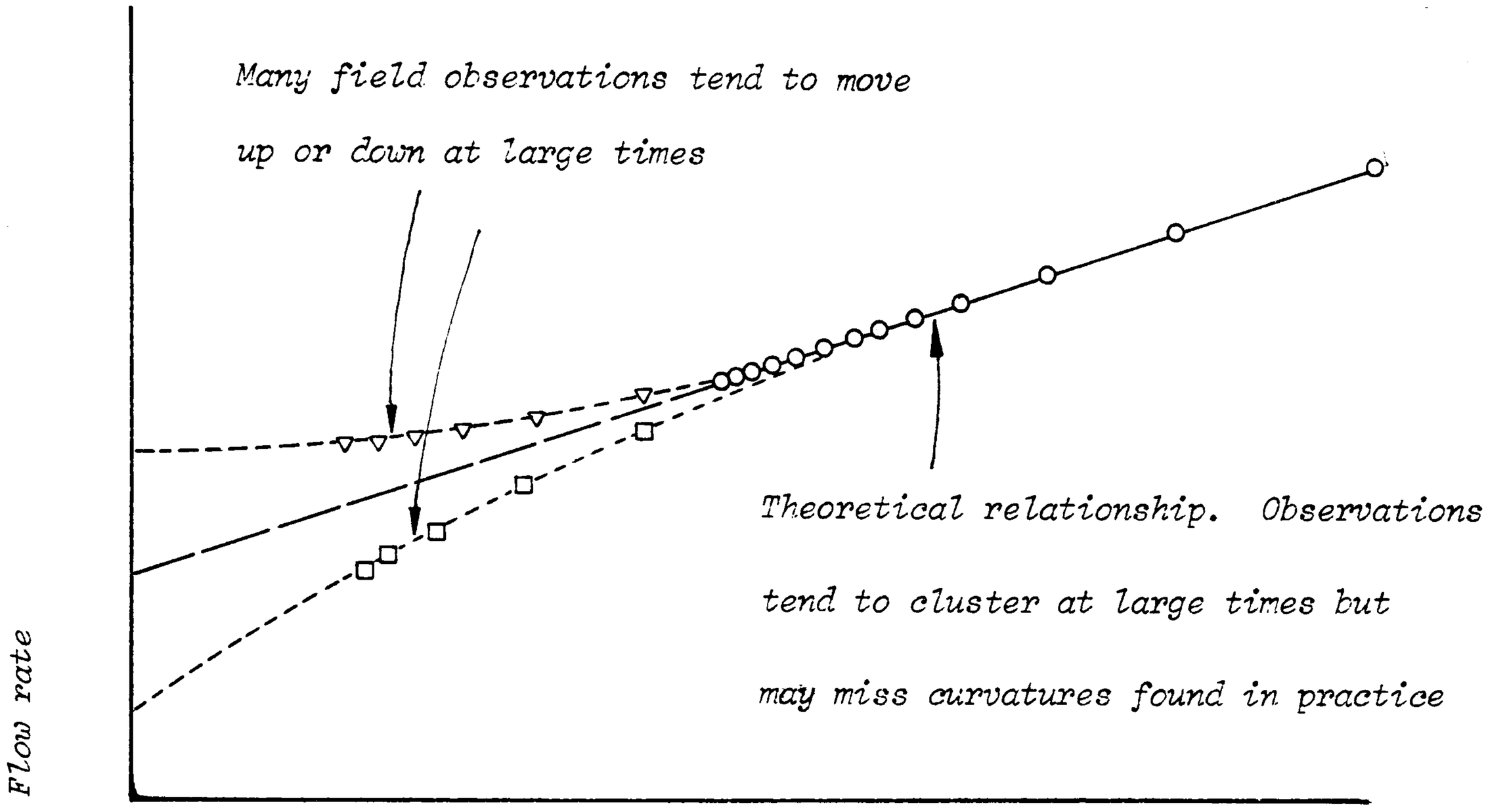


Figure 4.20. Observations of flow rate in constant head insitu permeability tests.

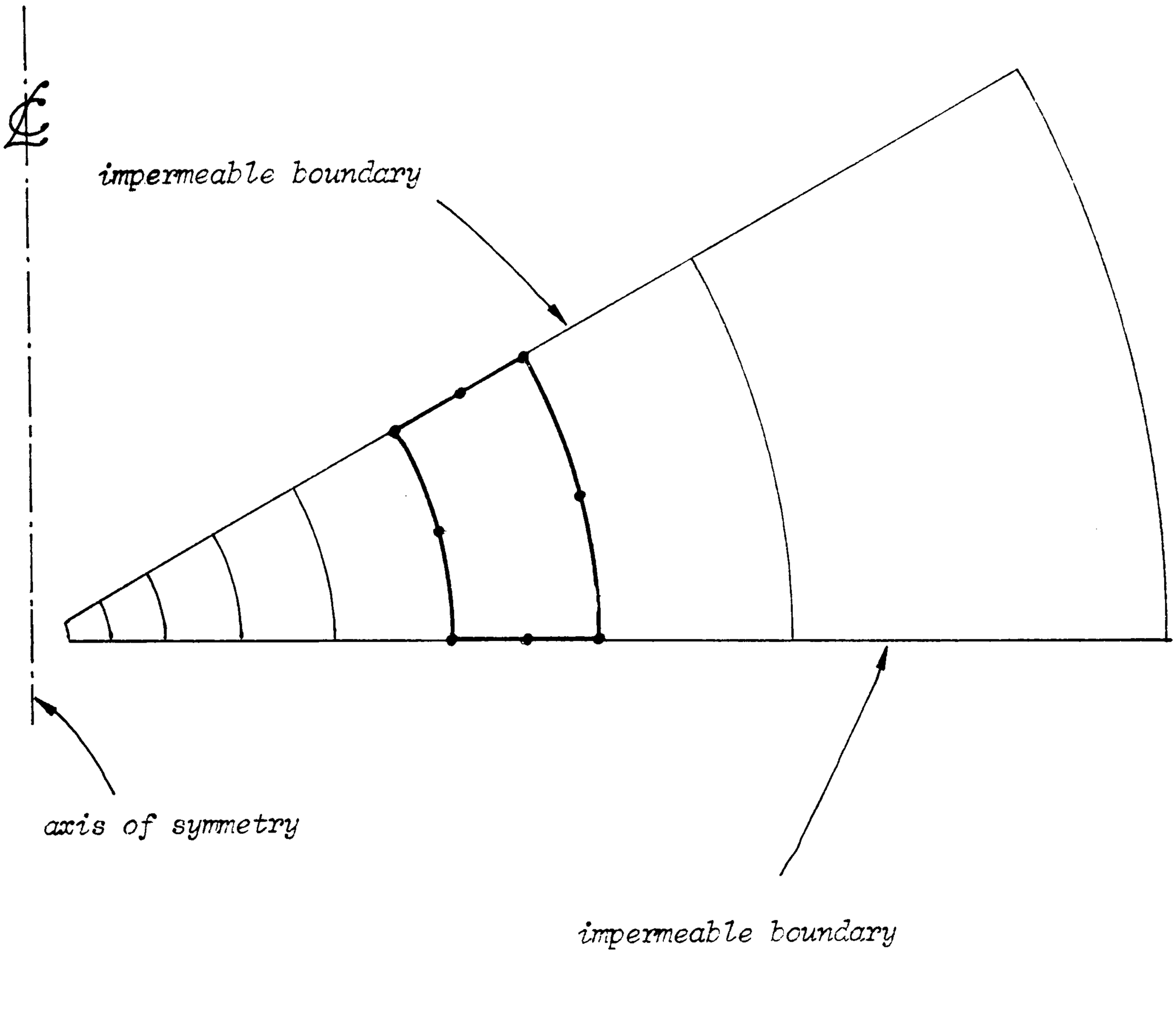
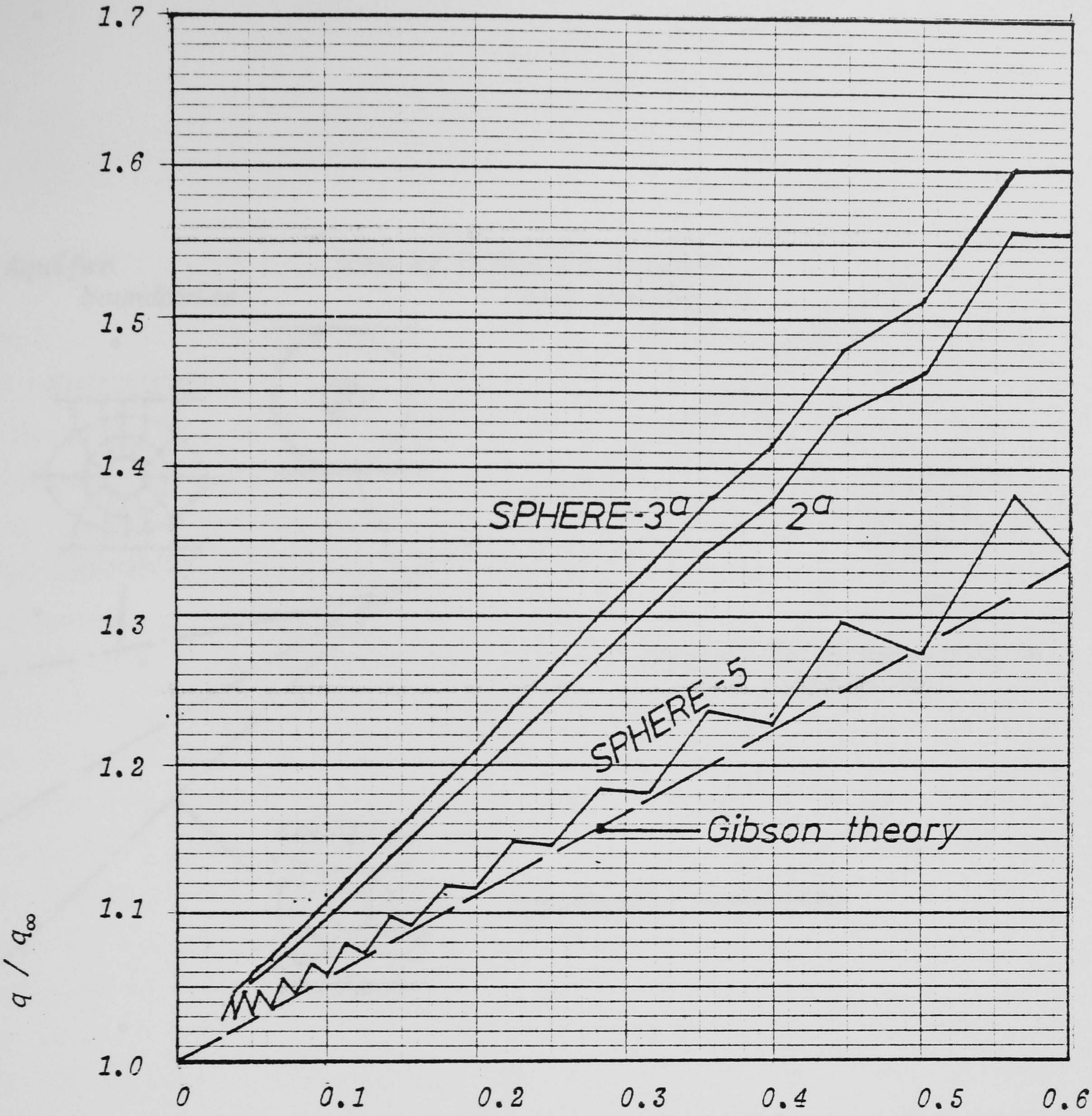


Figure 4.21 Finite element mesh used in analysis of spherically symmetric consolidation with effective stress dependent properties.



SPHERE-5 is the least "well-behaved" result and largely obscures the remaining results. These all lie close to the Gibson theory line.

Figure 4.22. Results of the parametric study of spherically symmetric seepage (constant head permeability test).

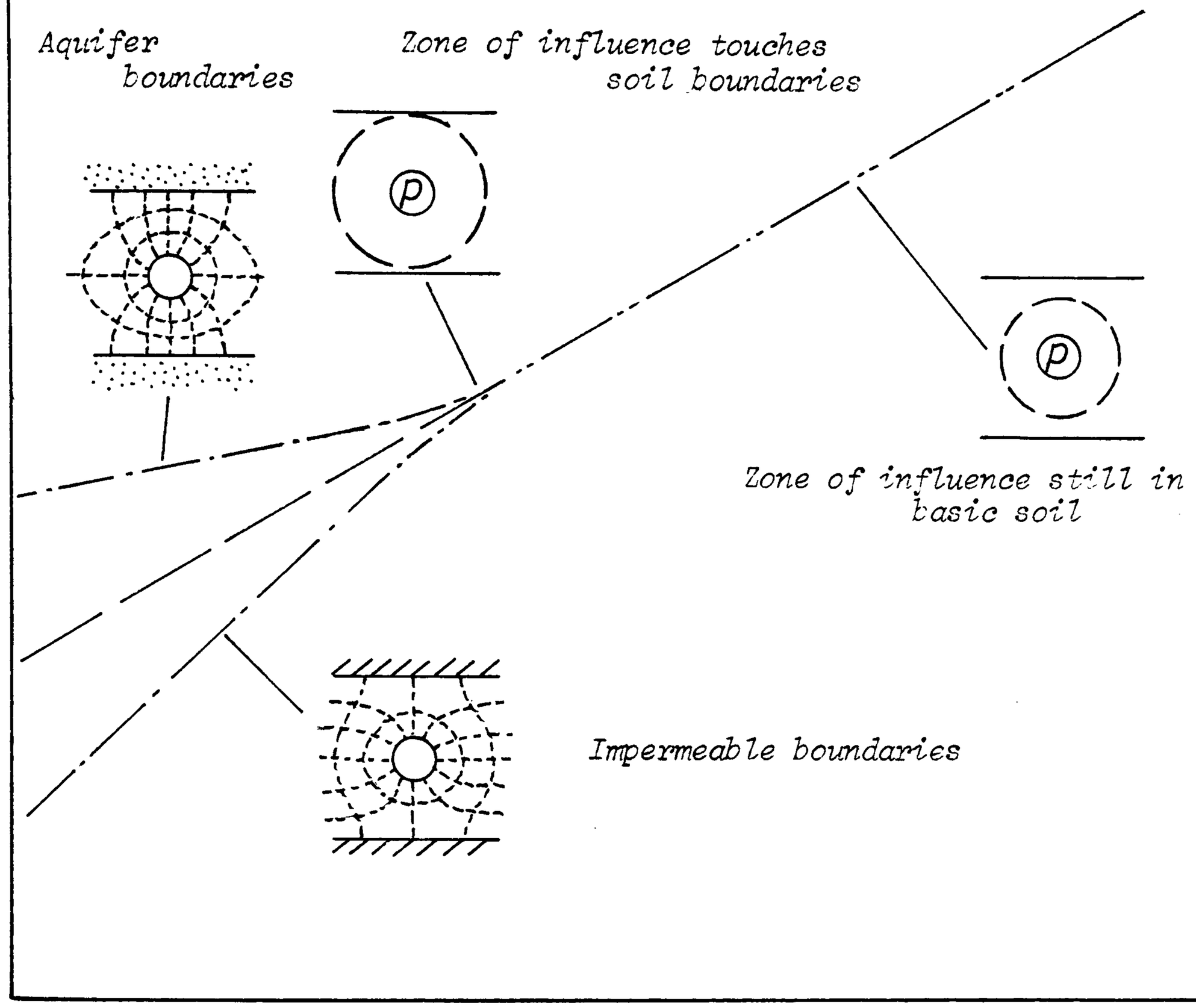


Figure 4.23. Possible explanation of curved q vs 1/√t plots

CHAPTER 5 - CONSTITUTIVE LAWS AND PARAMETERS FOR EFFECTIVE STRESS DEPENDENCY IN PERMEABILITY

5.1. Introduction and General Remarks

The solutions presented in Chapters 2 to 4 demonstrate a variety of important effects. Firstly, they show rapid changes in material properties close to drained boundaries in the seepage domain with a consequent increase in the potential gradient. Thus, the seepage flow rate, which is a combination of permeability and local potential gradient, is less sensitive to the intensity of effective stress dependence in the permeability than the permeability is to changes in effective stress across the seepage domain. It is therefore not possible to analyse the problem using a constant permeability theory (in terms of the overall hydraulic gradient) to yield an "average" permeability and to repeat the measurement with a different hydraulic gradient to obtain the variation of this average permeability with the changed effective stress conditions, since the magnitude of the computed average permeability will inevitably be wrong and the variation will usually also be incorrect. The exceptions to this may occur fortuitously in the case of the permeability magnitudes but the variation of permeability can be obtained only if the correct test procedure is followed. In this, the potential drop across the problem must be the same for every test and the changed effective stress conditions induced by altering the total stresses.

In the context of laboratory tests such as the triaxial test, where the total stress and pore water pressure can be varied at will, it is possible to arrange for this condition to be satisfied, but it is impossible in orthodox permeameters or oedometers. In the field, further difficulties arise if the changed effective stress conditions can only be obtained by altering a boundary potential (e.g. by using different heads in a constant head in situ permeability test). In a fill, it is possible to carry out tests at the same potential increment or decrement with respect to ambient pore water pressure

conditions on the same piezometer under increasing thicknesses of fill in a way that is impossible in a natural soil deposit where different total stresses can only be obtained by installing piezometers at different depths. Any variation in permeability detected in the latter case is also likely to be heavily influenced by lithological and stratigraphical factors as well as by the effects discussed above. An observed pore water pressure distribution may also yield information on the type of effective stress-permeability relationship, but cannot give information on the magnitude of permeability coefficients unless combined with some additional piece of evidence, for example a flow rate. It must also be reiterated at this point that the curved pore water pressure distributions that arise from variations of permeability in space either through inherent soil properties or as a result of an effective stress dependency do appear similar to conventional consolidation isochrones. It may take many years of regular observations in the field to decide whether or not the pore water pressure distribution is in fact steady although this observation need not be of pore water pressure directly but can be of some related physical quantity, e.g. settlement.

Published work which claims to have measured the variation of permeability with effective stress, or to have detected a field effect easily accounted for by such a relationship, needs to be considered in the light of the foregoing observations. Inevitably, due to the neglect of one or other factor, much of the published work is found to be less than completely satisfactory.

Walbancke, 1976, has briefly reviewed some of the more reliable field data on permeability variations with depth obtained in various soils evaluated by in situ permeability tests. Bishop and Al-Dhahir quote laboratory measured variations in permeability and compressibility with effective stress.

5.2. *Constitutive Laws*

The writer has followed Walbancke's (1976) lead as to the likely form of the effective stress - permeability relationship selecting two functions for investigation. Neither of the selected functions can properly simulate the very rapid increase of permeability in the vicinity of zero effective stress conditions (piping, hydraulic fracture, etc.). Taken with the range of parameters investigated in Chapter 2 and 3 they do, however, cover the range of likely permeability modifications resulting from effective stress increase. It is now clear that the exact form of the constitutive law selected is of much less importance than the overall magnitude of permeability change across the problem (e.g. Figures 2.16 - 2.19) and provided that the constitutive law selected for analysis bears some resemblance to the field relationship then the results of analysis will be sufficiently accurate for most engineering purposes.

5.3. *Suggestions for Further Work*

The simple, logical approach in accordance with the suggestions in Section 5.1 above is to measure the flow rate across a sample set up in a triaxial cell subject to a hydraulic gradient and to alter the total stress by cell pressure changes keeping the hydraulic boundary conditions fixed. After equilibration at each cell pressure the flow rate will be directly proportional to the new permeability. This approach is only valid for more permeable soils in which the flow rates are measurable (and in excess of membrane leakage). It is suggested that a series of these experiments be carried out to establish reasonable constitutive laws for the effective stress dependent permeability dependency and to discover reasonable bounds for the "intensity" parameters.

In soils with low permeability the flow rates will be too small to be measurable, and recourse must be made to an alternative procedure. It is suggested that measurements of pore water pressure through a sample (as above) using pore pressure probes could allow a fair

approximation to the operative constitutive law to be made, since the average total stress and average hydraulic gradient between each pair of pore pressure probes can simply be obtained. Since the permeability and hydraulic gradient must be inversely proportional if continuity is to be maintained, then the relationship between *relative* permeability and effective stress can be found. The analytical process for this is in essence the converse of the numerical technique in Section 2.7. It is further suggested that experiments be conducted on clay soils using this approach.

It seems from the work of Chapter 4 that volume change rates in dissipation are insensitive to the variation in the governing parameters during consolidation. This certainly needs to be explored further both theoretically and in the laboratory.

In situ constant head tests are not a good way of determining permeability - effective stress relationships except under fills where tests at different total stresses but subject to uniform hydraulic conditions can be carried out. Where this procedure has to a certain extent been followed, a degree of correlation between the effective stress changes and the measured permeability has been found but the investigations have not been sufficiently systematic to allow constitutive laws to be formulated.

Finally, experimental work is necessary to distinguish between the effects of stress induced and intrinsic (sedimentological) permeability anisotropy including how the magnitude and relative importance of each to the overall behaviour responds to changes in effective stress including rotation of the axes of the principal effective stresses from their original directions. The writer has no suggestions to offer as to how this latter effect might be investigated.

CHAPTER 6 - TRENCH AND COUNTERFORT DRAINS

6.1. Introduction

A widely used method for slope stabilisation is the construction of trenches filled with drainage materials and designed to reduce the pore water pressures in the slope. The term counterfort will be used to describe such drains which penetrate into solid ground below the soil layer which is being drained, and may therefore provide some mechanical buttressing to that soil layer; while the term trench drain will be reserved for the type of drain which does not thus penetrate and so contributes to stability only through a drainage action. In modern practice trench and counterfort drains are used mainly in stabilising shallow sliding soil layers (for example solifluction sheets) where comparatively modest reductions in piezometric pressure are sufficient to effect the desired increase in stability, the layer that is being drained in such a case is often much more permeable than the underlying soil, which may therefore be treated as an impermeable base. A less common use is in controlling pore water pressures near the surface of more homogenous natural or artificially created slopes to prevent instability developing. Frequently in such a case the soil which is being drained with trench drains may also be subject to a greater or lesser degree of underdrainage from a more permeable underlying layer. The third and least common use appears to be the interception of surface water flows. This would seem to be a form of drainage with a very short life expectancy with rapid siltation of the drains taking place. Ideally, the interception of surface and ground water flows should be separated, as indeed they are in many instances.

The origins of the counterfort drain, which seems to be the first of these types to have been used as a principal stabilisation measure, have not been explored in any depth, but Hutchinson (1977) reports that they were widely used in both France and England as long ago as the first half of the nineteenth century in both

embankments and cuttings, and it is felt that their invention however early must have been a recognition of the role of water and poor drainage in causing and maintaining slope instability. Designs reached a considerable degree of sophistication with the width of the counterforts increasing stepwise down slope to improve the stability of the clay between them, and the use of arches spanning between the counterforts is suggested by Collin (1846, in particular his plate III). Collin describes both masonry and 'stone' counterforts and clearly indicates in his text that the latter have a drainage effect. Collin also reports that sometimes the soil between the counterforts was excavated and re-compacted in thin layers, although this procedure was usually omitted (as in modern practice). There is perhaps an echo of this in modern attempts to destroy shear surfaces at residual strength in clays by breaking out and recompacting.

In early practice it was generally felt that drains which did not penetrate the seat of sliding were of little or no use (e.g. Whitley, 1880) and this opinion is still widely held. The basis for this belief is the emphasis on the mechanical buttressing effect, rather than on the drainage effect.

However, the development of a rational theory of the shear strength of soils based on Terzaghi's concept of effective stress has allowed the development of a theory for trench and counterfort drains.

6.2. *Approximate Theory*

At best, until the present, the design of trench drains for slope stabilisation in the U.K. has generally proceeded on a semi-empirical basis, and at the worst on an ineffectual *ad hoc* basis. Typically, in good practice, the average lowering of piezometric pressures required to produce the desired increase in safety factor has been calculated and the drains necessary to produce this effect

have been proportioned on the basis of experience or using a simple theory for the action of drains taken from the extensive, and mainly agriculturally biased, literature. Frequently, drainage alone is used, but in other cases it is used in conjunction with other forms of stabilisation measure. It is rare for the effect of drainage to be monitored closely, but a limited amount of case history data is available and this was reviewed by Hutchinson (1977). Even in the long term, the solution to a real and three dimensional trench drain problem is highly complex and unlikely ever to be amenable to a mathematical treatment with the following factors varying from site to site in an arbitrary manner:

a. intermittent recharge from infiltration
b. variable inflow of groundwater from upslope
c. non homogenous and anisotropic permeability (itself a function of effective stress)
d. the interplay between non-steady saturated and partially saturated flow
e. drain permeability and capacity.

Particularly with the factors a. and b. above being dependent on climatic conditions (with the known difficulties of prediction in that field) it is possible to state with some confidence that a full treatment will never be produced. The situation with regard to the *development* of the final flow regime is even more difficult with the stress relief effects accompanying excavation possibly having a dominant effect in the short term. In the following treatment of the way trench and counterfort drains modify the long term groundwater pressure in a soil slope, the long term steady state is dealt with in some depth, with a less deep treatment of the development of those long term pressures following.

Taking an initially horizontal ground surface and piezometric line in a soil with known permeability, with parallel trench drains of regular rectangular construction (as shown in the key diagram, Figure 6.1) it is possible to develop approximate solutions based

on appropriate analytical or numerical models. In every case the drains are assumed to be of sufficiently great length L upslope in comparison with their spacing so that a two dimensional approach is valid. In general, at each end of a run of drains, three dimensional effects will predominate and must be dealt with separately (Hutchinson, 1977). Definitions of the various symbols used will be found on the key diagram, Figure 6.1.

It has been possible to develop an analytical solution to the problem of counterfort drains in a soil resting on an impermeable base, and this treatment is given below (in Section 6.3) but in the main, the results have been obtained by means of a finite element technique, following in general terms the approach due to Hutchinson (1977) and suggested by Henkel (1957). In effect, we assume that a horizontal ponded surface exists at some depth (equivalent to $D - h_o$ in the key diagram)* below ground level. This approximation, which is probably not unreasonable for clay soils in temperate climates, enables a more general approach to be made by substituting h_o for D since infiltration in the partly saturated zone above the asssumed ponded surface may then be neglected. This assumption is implicit in all that follows in this section.

From the key figure, the following definitions and relationships can be drawn with respect to any horizontal plane although in particular we will concentrate on the plane cutting the drain inverts:-

(i) the average piezometric head, $\bar{h}$, on the plane between the drains can be expressed as:

$$\bar{h} = f_s h_m$$

in which f_s is a factor reflecting the shape of the relevant piezometric surface and h_m is the maximum piezometric head between the drains (by symmetry usually occurring at the drain centreline).

---

*The symbols D and H are used interchangeably for overall drain depth. The former of these is used principally in work which derives from Hutchinson and the latter in work arising from the closed form solution.

(ii) the average piezometric head, h_{av}, on the whole of the drain invert level plane is given by:-

$$h_{av} = \frac{h_d B + \bar{h} s}{A} \qquad (A = s + B)$$

where h_d is the piezometric head at the drain inverts and B is the width of the drains. It should be noted that in general (and for want of any firm data) h_d is assumed equal to zero, but need not be so, in particular where counterfort drains penetrate a permeable underlayer which is not fully underdrained. In the case where counterforts *penetrate* an impermeable underlayer all the measurements relating to drain invert layer should be made instead to the base of the layer which is being drained.

The expressions above do relate to horizontal ground. However, where the ground is inclined at an angle β to the horizontal, and with trench drains of high L/S ratio constructed down the line of steepest slope, the values of piezometric head are modified but may be represented by:-

$$\bar{h}' = \bar{h} \cos^2\beta \qquad h_o' = h_o \cos^2\beta$$

and

$$h_{av}' = h_{av} \cos^2\beta$$

Since most of the data is plotted in terms of for example $\bar{h}/h_o$, this will immediately be seen to be equivalent to $\bar{h}'/h_o'$ and the plots are valid for all β values.

Further parameters which are of use in the development of the following arguments are $\bar{\eta}$, the efficiency of the drains with respect to the intervening mass of soil defined as:-

$$\bar{\eta} = \frac{h_o' - \bar{h}'}{h_o'} \quad \text{or} \quad \frac{h_o - \bar{h}}{h_o}$$

and the overall drain efficiency η_{av} which is similarly defined by:-

$$\eta_{av} = \frac{h_o' - h_{av}'}{h_o'} \quad \text{or} \quad \frac{h_o - h_{av}}{h_o}$$

One may note the independence of either "η" on β ; and the fact that $\bar{\eta}$ and η_{av} become identical as the drain width B tends to zero.

6.3. *The Fully Penetrating Trench Drain - Analytical Solution*

Analytical solutions to most seepage problems even in cases where these actually exist are invariably complex and for most cases finite element (or other numerical) solutions are not only to be preferred on the grounds of simplicity but in many cases may require less computational effort. This is true of the case of seepage into drains which penetrate the full thickness of a soil layer down to an impermeable base. A solution to this problem is developed below, and compared to the finite element solutions used almost exclusively elsewhere to this work.

It should be noted that in an early discussion by Richardson (1908), where the whole problem was solved by the simple procedure of *flow net sketching*, an attempt to produce an analytical solution was abandoned because of the awkwardness of the boundary conditions which were formulated in terms of the rate of flow (or potential gradient) across the boundaries rather than in terms of the boundary potentials themselves. Once the problem is formulated in the correct terms, however, the solution follows as a matter of course.

The basis of the present solution is the Fourier solution to the flow of heat in a rectangular solid subject to an arbitrary distribution of temperature along one side and zero temperatures along the others

(Carslaw and Jaeger, 1947). The solution is developed using the analogy between the flow of heat (and resulting temperature distribution) and the flow of water through soil together with the superposition of various cases (allowable due to the linear nature of solutions to the Laplace equation).

Basic solution (Carslaw and Jaeger, 1947): A solution to the Laplace equation:

$$\frac{\partial^2 \phi}{\partial x^2} + \frac{\partial^2 \phi}{\partial y^2} = 0$$

is sought within the rectangular region $0 \leq x \leq s$ and $0 \leq y \leq b$ (Anisotropy in the permeability may either be dealt with at this level or by a scale transformation in the limits of the rectangle. This latter procedure will be assumed hereafter). The chosen solution must satisfy the boundary conditions that along the $y = 0$ boundary the potential ϕ is a function of x such that:

$$\phi = f(x) = \sum_{n=1}^{\infty} a_n \sin\left(\frac{n\pi x}{s}\right)$$

and is equal to zero on the other three boundaries. By the usual processes of Fourier analysis the coefficients a_n can be determined from:

$$a_n = \frac{2}{s} \int_0^s f(x') \sin\left(\frac{n\pi x'}{s}\right) dx'$$

A function that satisfies the various conditions is:

$$\phi_{xy} = \sum_{n=1}^{\infty} a_n \sin\left(\frac{n\pi x}{s}\right) \operatorname{Sinh}(b-y)\frac{n\pi}{s} \operatorname{Cosech}\left(\frac{n\pi b}{s}\right)$$

For the special case $f(x)$ = constant (K) we find:

$$\phi_{xy} = \frac{4K}{\pi} \sum_{n=1}^{\infty} \frac{1}{(2n-1)} \sin (2n-1)\frac{\pi x}{s} \sinh (2n-1)(b-y)\frac{\pi}{s} \operatorname{cosech}(2n-1)\frac{\pi b}{s}$$

(Carslaw & Jaeger express their solution in terms of summing from n = 0. Summing from n = 1 is more natural in terms of Fortran computer programming).

Boundary conditions: the impermeable boundary at the base of the soil layer (Figure 6.2) may be represented by an axis of symmetry in the seepage domain and the various boundary conditions can be represented as shown.

A. is a uniformly distributed boundary potential of value H/2 around all four sides of the seepage domain 'contributing' a potential of H/2 at every point.

B. is a boundary potential of H/2 uniformly distributed along the side y = 0, and C. a similar distribution along the side y = b.

D. and E. are the 'sawtooth' variations of potential between the limits of H/2 and -H/2 on the x = 0 and x = s sides.

Summing the effects of the various solutions at any point (x, y)

$$\phi_{xy} = \phi_{xy_A} + \phi_{xy_B} + \phi_{xy_C} + \phi_{xy_D} + \phi_{xy_E}$$

in which:

$$\phi_{xy_A} = H/2$$

$$\phi_{xy_B} = \frac{2H}{\pi} \sum_{n=1}^{\infty} \frac{1}{(2n-1)} \sin(2n-1)\frac{\pi x}{s} \sinh (2n-1)(b-y)\frac{\pi}{s} \operatorname{cosech}(2n-1)\frac{\pi b}{s}$$

$$\phi_{xy_C} = \frac{2H}{\pi} \sum_{n=1}^{\infty} \frac{1}{(2n-1)} \sin (2n-1)\frac{\pi x}{s} \sinh (2n-1)\frac{\pi y}{s} \operatorname{cosech} (2n-1)\frac{\pi b}{s}$$

'Sawtooth' side conditions: Representing the sawtooth function of the side boundary conditions D. and E. is a more complex matter. This function can be represented by the cosine series:

$$f(y) = \frac{8K}{\pi^2} \sum_{M=1}^{\infty} \frac{1}{(2m-1)^2} \cos 2(2m-1)\frac{\pi y}{b}$$

Hence,

$$a_n = \frac{2}{b} \cdot \frac{8K}{\pi^2} \int_0^b \sin \frac{n\pi y'}{b} \cdot \sum_{m=1}^{\infty} \frac{1}{(2m-1)^2} \cos 2(2m-1)\frac{\pi y'}{b} \cdot dy'$$

$$= \frac{16K}{b\pi^2} \sum_{m=1}^{\infty} \frac{1}{(2m-1)^2} \int_0^b \sin \frac{n\pi y'}{b} \cos 2(2m-1)\frac{\pi y'}{b} \cdot dy'$$

Now, the integral of a function of the form

$$\int \sin Ax \cos Bx \cdot dx \quad \text{is} \quad -\frac{\cos(A+B)x}{A+B} - \frac{\cos(A-B)x}{A-B}$$

thus

$$a_n = -\frac{8K}{\pi^3} \sum_{m=1}^{\infty} \frac{1}{(2m-1)^2} \cdot$$

$$\left[\frac{\cos\{n+2(2m-1)\}\frac{\pi y}{b}}{n+2(2m-1)} + \frac{\cos\{n-2(2m-1)\}\frac{\pi y}{b}}{n-2(2m-1)} \right]_0^b$$

It will be noted that at the lower limit of integration (0) the cosine terms both take the value -1 (regardless of the value of n) but at the upper limit (b) the cosine terms are 1 for even n or -1 for odd n. It is therefore possible to express a_n (for odd n only of course, since for even n, a_n = 0) as:

$$a_n = \frac{8K}{\pi^3} \sum_{m=1}^{\infty} \frac{1}{(2m-1)^2} \cdot \frac{4n}{n^2 - 4(2m-1)^2}$$

Rearranging so that all n are included:

$$a_n = \frac{32K}{\pi^3} \sum_{m=1}^{\infty} \frac{2n-1}{(2m-1)^2\left((2n-1)^2 - 4(2m-1)^2\right)}$$

which for $\frac{1}{2}$ = H/2 gives:

$$\phi_{xy_D} = \sum_{n=1}^{\infty} a_n \sin(2n-1)\frac{\pi y}{b} \sinh(2n-1)(s-x)\frac{\pi}{b} \operatorname{cosech}(2n-1)\frac{\pi s}{b}$$

and

$$\phi_{xy_E} = \sum_{n=1}^{\infty} a_n \sin(2n-1)\frac{\pi y}{b} \sinh(2n-1)\frac{\pi x}{b} \operatorname{cosech}(2n-1)\frac{\pi s}{b}$$

Numerical Solutions: Solutions summing the first 10, 25 and 50 terms of the series were evaluated using a computer program. There were a few% differences between the first two of the solutions, but the 25 and 50 term solutions were indistinguishable, and on the basis of this small test, it is probably adequate to sum only the first 25 terms or so to obtain a reasonable solution.

A number of cases for various drain spacing to depth ratios were compared to finite element solutions of the same problems, using fairly coarse meshes, (Figures 6.3 and 6.4). The results of the two different solutions are virtually identical, with a maximum difference of less than 2%, and generally better agreement. This general agreement shows how the finite element technique is capable of giving very accurate results even with coarse meshes of elements. The discrepancy between the analytical and numerical solutions is very localised at the level of the base of the drains where the equipotential lines are close together and more sharply curved than elsewhere in the mesh, a combination of factors which must have adverse effects in any numerical scheme and could in any case be overcome with an appropriate, graded, mesh of elements.

Not only were the finite element results found to be accurate, but the analyses were also found to be much more conservative of computer time than the evaluation of the terms in the series solution. Finite element methods have accordingly been used to obtain all the other two dimensional solutions in this work.

Potentially, two other useful results can also be derived from this basic solution. Firstly, the average pore water pressure at any depth in the soil can be obtained by integrating the potential across the chosen line, and then subtracting the appropriate elevation - this is the elevation measured from the $y = b/_2$ line.

Hence, since

$$\bar{\phi} = \frac{\int_0^s \phi \, dx}{s} = \frac{1}{s} \int_0^s \phi_A + \phi_B + \phi_C + \phi_D + \phi_E \, . \, dx$$

this can be written as:

$$\bar{\phi} = \bar{\phi}_A + (\bar{\phi}_B + \bar{\phi}_C) + (\bar{\phi}_D + \bar{\phi}_E)$$

Taking these groups one at a time,

$$\bar{\Phi}_A = H/2$$

$$(\bar{\Phi}_B + \bar{\Phi}_C) = -\frac{2H}{\pi^2}\sum_{n=1}^{\infty}\frac{1}{(2n-1)^2}\,\mathrm{Cosech}\,(2n-1)\frac{\pi b}{s}\cdot$$

$$\cdot\left\{\sinh(2n-1)\frac{\pi y}{s} + \sinh(2n-1)(b-y)\frac{\pi}{s}\right\}\cdot\left[\cosh(2n-1)\frac{\pi x}{s}\right]_0^s$$

Examining the square bracketed integral, we find that at the upper limit of integration, this has the value -1 for all n, and that it takes the value +1 for all n at the lower limit of integration. Thus, this group $(\bar{\Phi}_B + \bar{\Phi}_C)$ can be written as:-

$$\frac{4H}{\pi^2}\sum\frac{1}{(2n-1)^2}\,\mathrm{Cosech}\,(2n-1)\frac{\pi b}{s}\cdot\left\{\sinh(2n-1)\frac{\pi y}{s} + \sinh(2n-1)(b-y)\frac{\pi}{s}\right\}$$

The final group, $(\bar{\Phi}_D + \bar{\Phi}_E)$ can be treated similarly, yielding after integration:

$$(\bar{\Phi}_D + \bar{\Phi}_E) = \frac{16Hb}{\pi^4 s}\sum_{n=1}^{\infty}\frac{1}{(2n-1)}\sinh(2n-1)\frac{\pi y}{b}\,\mathrm{Cosech}\,(2n-1)\frac{\pi s}{b}\cdot$$

$$\left[\cosh(2n-1)\frac{\pi x}{b} - \cosh(2n-1)(s-x)\frac{\pi}{b}\right]_0^s$$

The square bracketed part of this simplifies to

$$2\left(\cosh(2n-1)\frac{\pi s}{b} - 1\right)$$

whence the result for $(\bar{\phi}_D + \bar{\phi}_E)$ can be written as:-

$$\frac{64H^2}{\pi^4 s} \sum_{n=1}^{\infty} \frac{a_n}{(2n-1)} \sin(2n-1)\frac{\pi y}{b} \operatorname{cosech}(2n-1)\frac{\pi s}{b} \left\{ \cosh(2n-1)\frac{\pi s}{b} - 1 \right\}$$

The average pore water pressure head $\bar{h}_w$ at the chosen level, a distance d below the ground level is thus:-

$$\bar{h}_w = \bar{\phi} - (H-d)$$

This has been evaluated for a number of drain spacing to depth ratios and plotted in Figure 6.5. There appears to be a little numerical roundoff problem at the lower end of the spacing/depth scale, but this has not been explored in view of the extremely limited practical applicability of those results.

A second result derived from the basic solution is the seepage quantity flowing through the soil from its wetted surface to the drain. Invoking Darcy's law, the total quantity is:

$$Q = -k \int_0^s \frac{\partial \phi}{\partial y} \text{ at } y=b \cdot dx$$

Now the first contributor, ϕ_A, to the overall potential has a zero derivative and can be neglected. The second two terms, ϕ_B and ϕ_C yield the following when differentiated:

$$\frac{\partial}{\partial y}(\phi_B + \phi_C) = -\frac{2H}{s} \sum_{n=1}^{\infty} \sin(2n-1)\frac{\pi x}{s} \cdot \operatorname{cosech}(2n-1)\frac{\pi b}{s} \cdot$$

$$\left\{ \cosh(2n-1)(b-y)\frac{\pi}{s} - \cosh(2n-1)\frac{\pi y}{s} \right\}$$

On integrating with respect to x we obtain I_1

$$I_1 = \frac{2H}{\pi} \sum_{n=1}^{\infty} \frac{1}{(2n-1)} \cdot \left[\cos (2n-1)\frac{\pi x}{s} \right]_0^s \cdot \operatorname{cosech}(2n-1)\frac{\pi b}{s} \cdot$$

$$\left\{ \cosh(2n-1)(b-y)\frac{\pi}{s} - \cosh(2n-1)\frac{\pi y}{s} \right\}$$

At y = b, one of the cosh terms takes the value 1, and when this is combined with the insertion of the integration limits for which the cos term has the values -1 (upper limit) and +1 (lower limit) the following result is obtained:

$$I_1 = -\frac{4H}{\pi} \sum_{n=1}^{\infty} \frac{1}{(2n-1)} \operatorname{cosech}(2n-1)\frac{\pi b}{s} \cdot \left(1 - \cosh(2n-1)\frac{\pi b}{s}\right)$$

A similar differentiation and integration procedure for the other two contributory potentials ϕ_D and ϕ_E produces:

$$\frac{\partial}{\partial y}(\phi_D + \phi_E) = \frac{\pi}{b} \sum_{n=1}^{\infty} a_n (2n-1) \cos(2n-1)\frac{\pi y}{b} \operatorname{cosech}(2n-1)\frac{\pi s}{b} \cdot$$

$$\left\{ \sinh(2n-1)(s-x)\frac{\pi}{b} + \sinh(2n-1)\frac{\pi x}{b} \right\}$$

Hence

$$I_2 = \sum_{n=1}^{\infty} a_n \cos(2n-1)\pi \operatorname{cosech}(2n-1)\frac{\pi s}{b} \cdot$$

$$\left[-\cosh(2n-1)(s-x)\frac{\pi}{b} + \cosh(2n-1)\frac{\pi x}{b} \right]_0^s$$

for which the result is:

$$2\sum_{n=1}^{\infty} a_n \cdot \cos(2n-1)\pi \cdot \operatorname{cosech}(2n-1)\frac{\pi s}{b} \cdot \left(\cosh(2n-1)\frac{\pi s}{b} - 1\right)$$

this always has
the value -1

The two terms can be simplified by means of the identity

$$\tanh\frac{A}{2} = \operatorname{cosech} A\,(\cosh A - 1)$$

into

$$I_1 = \frac{4H}{\pi}\sum_{n=1}^{\infty}\frac{1}{(2n-1)}\tanh(2n-1)\frac{\pi b}{2s}$$

and

$$I_2 = -2\sum_{n=1}^{\infty} a_n \tanh(2n-1)\frac{\pi s}{2b}$$

A parameter analogous to the ratio N_f/N_d obtained from the flow net sketching would be given by the result $(I_1 + I_2)/H$. Ideally, this would be evaluated for various s/H ratios as a design aid.

Unfortunately, I_1 is definitely a divergent series and I_2 is probably also divergent. This effect is the result of the singularity which appears at each corner of the square seepage domain for each of the constituent solutions B, C, D and E. Hence, despite the lack of singularity at these points in the assembled solution, no numerical solution can be obtained. Several thousand terms of each series have been summed, as it appeared that the *sum* of the two series might be convergent, but anomalous results were obtained (notably a complete reversal of flow direction at large s/H ratio s and a local reversal of the trend of the N_f/N_d vs. s/H plot in the vicinity of the point $s/H = 1$). Following the example of Richardson (1908) this approach has been given up as hopeless.

In the combined (A to E inclusive) solution, the singularities at the corner points vanish to be replaced by a single stagnation point at the centre of the seepage domain. It therefore appears that for finite s and H values, a finite flow rate must exist. The numerical difficulties arise from the locally infinite gradient values in the constituent solutions.

An alternative to the analytical integration procedure would appear to be to numerically integrate the gradient across the top of the seepage domain. Using a Gauss rule the gradient is not sampled at the troublesome corner points and the numerical problems are neatly side stepped. However, this approach is also not entirely free of convergence problems and has not been proceeded with. The flow through the soil is of course not the only factor to be considered in sizing the drains themselves and in selecting the grading for their infill. If gullying is to be prevented, the drains must carry the complete amount of precipitation on the slope, whether this is run off or infiltration. Run off is likely to put the larger loading on drain capacity unless it is sealed against ingress of surface water.

6.4. Effect of Fully and Partially Penetrating Drains on the Pore Water Pressures in a Soil Layer with Constant Permeability Resting On An Impermeable Base

Finite element analyses were carried out to determine the distribution of potentials as modified by trench and counterfort drains in a soil layer resting on an impermeable base, and from those potentials, the distribution of pore water pressures. The finite element meshes used were simple, rectangular arrays of 8 noded, isoparametric elements (Zienkiewicz, 1972) with no attempt made to map these into non-rectangular shapes, and the drains were simulated by imposing zero pore water pressure (i.e. potential equal to elevation) conditions on the appropriate part of the mesh. In practice, the width of individual drains tends to be small in comparison to the spacing and so in the parametric study the width of each drain has been taken to be zero. Later, when the case history data is examined, the actual drain widths are considered.

To investigate the influence of drain spacing, one can either produce fresh finite element meshes for each case; transform the geometry of a single original mesh; or use the transformation which results from the use of an anisotropic permeability. If the ratio of horizontal to vertical permeability is R_k then this is equvalent to multiplying the horizontal scale by the inverse of R_k and taking the permeability to be isotropic. It is then possible to consider the effects of anisotropic permeability and increasing drain spacing to depth ratio in the same analyses. Accordingly, all of the results are plotted in terms of the composite parameter $s/(h_o\sqrt{R_k})$ which for brevity will be referred to as R_s henceforth.

Analyses for R_s ratios of 1, 2, 3..... to 8 and for depth of layer to depth of drain ratios (n) of 1, 1.2, 1.5, 2, 3 and 4.5 have been made. Some irregularities begin to appear in the pore water pressure distributions for the larger R_s ratios due to an implicit distortion of the elements; but when pore water pressures are averaged across any section it is found that the fluctuations balance out and that they may safely be disregarded. The control on the acceptability of the solutions is, of course, the analytical solution for the n=1, or fully penetrating drain, case presented in section 6.3.

A composite diagram showing the meshes of finite elements used in the analysis of the various n ratios is shown as Figure 6.6.

The results of this series of analyses are presented graphically in Figures 6.7 to 6.11; the usefulness of these charts in geotechnical engineering design is believed to be virtually self evident.

The following broad conclusions may be drawn:-

(a) The average decrease in pore water pressure at any level between drain invert level and the base of the layer is most strongly dependent on the drain spacing parameter R_s.

(b) This average pore water pressure decrease is virtually the same at *any* depth below drain invert level, particularly when the drain spacing is small. Even with larger drain spacings, the reduction of the average decrease in pore water pressure with depth from drain invert level to the base of the layer is not very marked - the maximum difference between the average decrease in pore water pressure head at these two levels is only *ca.* 4% of the drain depth at the largest spacing (R_s = 8) considered.

(c) A given drain is more effective in a deep layer than in a shallow one in terms of this average reduction in pore water pressure, although the increase in this effect becomes imperceptible for depth ratios (n) greater than about 3. (This should not however be taken to imply that shallow drains would be more effective than deep ones in any given soil stratum - the deeper the drain is, the more effective it is regardless of all other factors).

6.5. *Effect of Partially Penetrating Drains on the Pore Water Pressures in a Partly Underdrained Soil Layer of Uniform Permeability*

The same finite element meshes used in the previous section were used to investigate the effect of partial underdrainage from the underlying soil layer. Once again depth ratios (n) of 1.2, 1.5, 3.0 and 4.5 were used and the boundary potentials at the base of the layer fixed at the appropriate values to give underdrainage ratios D_u of between 0.0 and 1.0 in steps of 0.25. It could readily be seen, however, that the potentials yielded in the solution were a linear function of D_u (this was tested exhaustively in the n = 1.2 case shown in Figure 6.12, and by random sampling elsewhere) and accordingly only the extreme case of D_u = 0 was solved for. The potentials (or pore water pressures, etc.) in any other case can be obtained by multiplying the value for D_u = 0 by the factor (1 - D_u (actual)).

The case for n = 1.0 is a limiting case and the values have to be obtained by inference. If the drain penetrates the underlying layer it must either alter the pressures in that layer or itself be overcome by them. In either case the drain and underlying layer boundary conditions are not independent as in the other cases - the solutions are therefore not strictly comparable. If, however, the drain does not penetrate the underlayer, n is not strictly 1.0. Nevertheless, by inspection of the curves for the other cases, an upper limit for the case of n = 1.0 has been drawn on the results diagram, Figure 6.13.

It may readily be seen that the drains are more effective in the deeper soil layers. In terms of actual pore water pressure reduction the more strongly underdrained the soil layer is the less the *absolute* reduction is, but in *relative* terms the reduction is independent of D_u. An additional noteworthy point is that neither at the top nor at the base of the layer do the drains have any effect on the mean pore water pressures - they have their maximum effectiveness at drain invert level.

In comparison with the impermeable base solutions, the ratio tends to be larger in the underdrained case. Hence the pore pressures adjacent to the drains for a given degree of centreline pore pressure depression are larger in the underdrained case than in the impermeable base case.

Overall drain efficiencies may be quite low if the underdrainage ratio is small since the pore water pressures are recharged from below; but strong underdrainage helps to such an extent that in the limit the drains serve no useful purpose and may dispensed with.

6.6. Analysis Where Permeability is Effective Stress Dependent

A small series of analyses were carried out using the effective stress dependent finite element model, as used for the one dimensional case studies and again using only the logarithmic based permeability - effective stress function. The s/H ratio of 2 was chosen, and since the results in this case are not totally independent of the unit weight of soil and size of the overall system, 5 m deep drains in a soil of unit weight 20 kN/m^3 were assumed.

As might be expected, the retarding effect of a permeability reduction immediately adjacent to the drain surface which arises from an effective stress - permeability relationship leads to a modified pore pressure distribution. Furthermore, unlike the case of anisotropic permeability, this problem cannot be solved merely by a linear mapping.* Thus the pore water pressure distribution at drain invert level shows much less drawdown close to the drain than does the constant permeability solution. This effect can lead to somewhat lower drain efficiencies than the homogeneous permeability theory would predict but in practice is likely to be offset by an increased horizontal permeability, if this exists.

Figures 6.14 and 6.15 show the results of the small parametric study which has been made.

It should be noted that any other effect which tends to reduce the permeability adjacent to a drain (for example, smearing the soil fabric and hence blocking off more permeable horizons) will give rise to a similar effect, as also may incomplete equilibration of the pore pressures to their post-drain installation steady state. The latter does depend, however, on the pore pressure response to total stresses during excavation as much as to hydraulic considerations.

**With anisotropic permeability and an unmapped zone of seepage, flow lines and equipotentials no longer cross at right angles. They do so when the flow net is mapped (e.g. Section 7.3). Flow lines and equipotentials remain orthogonal in the effective stress dependent permeability solution.*

The effect of an effective stress dependent permeability in the underdrained cases is to insulate the soil from the basal underdrain to a large degree and this has an additional adverse effect on the pore water pressures as well as impeding flow from the drains.

6.7. Field Data on Final Steady Pore Water Pressures Adjacent to Trench Drains

Hutchinson (1977) reviews the field data from eleven sites (Table 6.1. - his Table 1) and his review of this field data is presented in Figure 6.16. A few points should be noted. Firstly, it is probable that some of the apparent higher drain efficiencies are better accounted for by invoking a modest degree of underdrainage than anisotropic permeability (frequently, the pre-drain installation pore pressures are not known to any higher degree of accuracy). Secondly, the shape of the profile of pore water pressure heads at drain invert level is often flatter than the theory predicts. This may be due to residual pore pressures from undrained unloading of the slope or to lateral stress relief on installation (or also to a degree of underdrainage).

There is still, therefore, a great need for careful observations of pore water pressure in and around these drains if a more accurate analysis is to be developed.

6.8. Pore Water Pressure Changes on Installation of Trench Drains

The stress changes in a soil in which trench drains are cut follow a complex sequence and are dependent on a great many factors. An analysis using a non-linear* elastic method developed by Hamza (1976) was used for some preliminary analyses on a typical trench drain installation, but a systematic study was abandoned when it became evident how dependent the results were on not only the geometric properties of the trench excavation but also on the factors:-

a. In situ lateral stresses.
b. Pore pressure parameters.
c. Lateral stresses in the backfill (including the effect of compaction, Ingold, 1980).

---

was used in the analyses reported below.

Table 6.1. Details of Counterfort Drain Installations (after Hutchinson, 1977)

REF.NO.	SITE NAME	APPROX SLOPE	PRINCIPAL MATERIAL	DRAIN DETAILS					DRAIN PERFORMANCE PARAMETERS						
				B	D	S	h_o	S/h_o	hm	h	h_{av}	h_m/h_o	$\bar{\ }$	av	T years
1	Bredon Hill (Up Slip)	14^o	Upper Lias	.8	3.0	11.3	c.2.6	4.35	.90	.72*	.67*	.35	.72*	.74*	1.2
2	Sevenoaks (Lobe D)	7^o	Lr. Greensand over Wealden	.9	4.6	17.4	3.1	5.61	1.60	.95	.90	.52	.69	.71	2.2
3	Guildford (P402-4)	7^o	London Clay	.8	5.0	15.3	3.97	3.85	2.36	1.86	1.77	.59	.53	.55	10.5
4	Hodson (E1-2)	5^o	Gault Clay	.6	3.7	8.5	3.55	2.39	c.2.2	c.1.62	1.51	.62	.54	.57	1.5
5	Hodson (E3-4)	5^o	Gault Clay	.6	3.7	8.5	3.55	2.39	c.1.5	c.1.12	1.05	.42	.68	.70	1.5
6	Burderop Wood (16-9)	6^o	Gault Clay	.6	3.7	11.6	3.32	3.49	2.28	1.56	1.48	.69	.53	.55	1.6
7	Burderop Wood (K9-14)	6^o	Gault Clay	.6	3.7	25.0	2.90	8.86	c.2.35	1.93	1.88	.81	.33	.35	1.6
8	Boulby (N2-3)	14^o	Till	.5	5.2	11.0	4.86	2.26	2.52	2.02*	1.93*	.52	.58*	.60*	5.8
9	Boulby (T2)	15^o	Till	.5	5.5	6.0	2.9	2.07	1.0	.80*	.74*	.34	.72*	.74*	5.9
10	Barnsdale (D7-9)	11^o	Upper Lias	.7	3.5	11.3	2.77	4.08	1.35	.88	.83	.49	.68	.70	0.7
11	Barnsdale (D22-24)	7^o	Upper Lias	.7	5.0	11.3	3.43	3.29	3.0	2.41	2.27	.87	.30	.34	0.4

Notes: All dimensions in metres

*= estimated values, using an f_s value of 0.8

Selection of appropriate parameters in each of these three factors can lead to the prediction of increased or decreased pore water pressures in the soil.

The typical case selected for analysis was a trench drain installation with drains 4m deep, 1.2m wide and 10m centre-to-centre, in a 10m thick layer of soil. Symmetry has been used to restrict the size of problem to be analysed and the 44 element, 161 node problem is shown in Figure 6.17. This figure also shows the boundary conditions selected (horizontal fixity on the vertical boundaries and *rigid-rough* conditions on the bottom of the soil layer).

Stress changes accompanying excavation were computed using the release forces on the excavated sides. K_o, the coefficient of earth pressure at rest, was taken to be 1.0 for the calculation of the release forces. The changes in total stress were then converted into undrained pore water pressure changes using Henkel's (1960) α and β parameters - β was taken to be 1.0 as the soil was assumed saturated - and the influence of various α factors was investigated. (Since by far the major part of the stress change is due to horizontal releases the effect of different K_o factors can be visualised merely by scaling up the basic results).

To treat incompressibility in an elastic analysis requires the use of an infinite bulk modulus, or Poisson's ratio equal to one half. However, Bishop and Hight (1977) observe that an undrained analysis should be carried out with a slightly lower Poisson's ratio, confirming the previous practice which was to use a value close, but not equal, to the limiting 0.5 value. The particular element in use, and the high precision of the CDC6000 series computers in use at Imperial College allow a Poisson's ratio of very close to 0.5 (say 0.499) to be used (Hamza 1976, Naylor 1974). These analyses used 0.495.

The *value* of Young's modulus in a *stress* analysis with a constant, homogenous modulus is immaterial: in this case a value of 10^5 was used.

Figure 6.18 shows the pore water pressures following excavation predicted by the above analyses for α values of 0 and $\pm$ 0.5. These are extracted from the output at the element centroids (each value the average of the four adjacent Gauss point values) for the row of elements closest to the base of the drains, these elements being shaded in Figure 6.17.

A broadly similar picture is obtained at higher levels except that the centreline pore water pressures may remain virtually unchanged or even rise slightly.

The following conclusions were drawn on the basis of the solutions obtained:-

(a) the combination of K_o = 1 and α = 0 in this case brings the pore water pressures down to very approximately their steady seepage (long term) values, although this effect may largely vanish when the trench is backfilled.

(b) with large α factors the pore water pressures adjacent to the drains can rise where the effect of "mean total stress unloading" is more than offset by "shear stress loading".

(c) the nett effect is small unless either K_o for the backfill, or the α parameter for reloading, is markedly different than for excavation. Lateral stresses in compacted backfill may be very high (Ingold 1980).

The intermediate principal stress changes have an important bearing on the overall behaviour and on the magnitude of the undrained pore water pressure changes. This has been commented on in other connections by, for example, Lopes 1979.

6.9. Increase in Effectiveness of Counterfort Drain Installations With Time

If the reduction in pore water pressure between counterfort drains due to the effect of the stress relief accompanying excavation is ignored then the problem of estimating the increase in effectiveness as a function of time is considerably simplified. The initial and final pore water conditions are as shown diagrammatically in Figure 6.19 from which it can be seen that the amound of *excess* pore water pressure head to be dissipated (the difference between the initial and final conditions) varies across the whole problem in a complex way. Even with the simplifying assumption it is not at present possible to analyse this other than numerically. However, to complete a comprehensive parametric study of the problem using (say) the finite element method would be quite uneconomic in computer resources as a result of which the present philosophy of analysing specific cases from which more general inferences can be drawn has had to be adopted. Since thedangers of too great an extrapolation from limited data are well known this point will not be further laboured here.

Three cases were analysed using the constant properties Zienkiewicz and Parekh (1971) method and found that the time for 50% *equalisation* at the drain invert centreline was between 40% and 60% of the time for an equivalent degree of dissipation in a one dimensional case with a drainage path length equal to half the drain spacing.

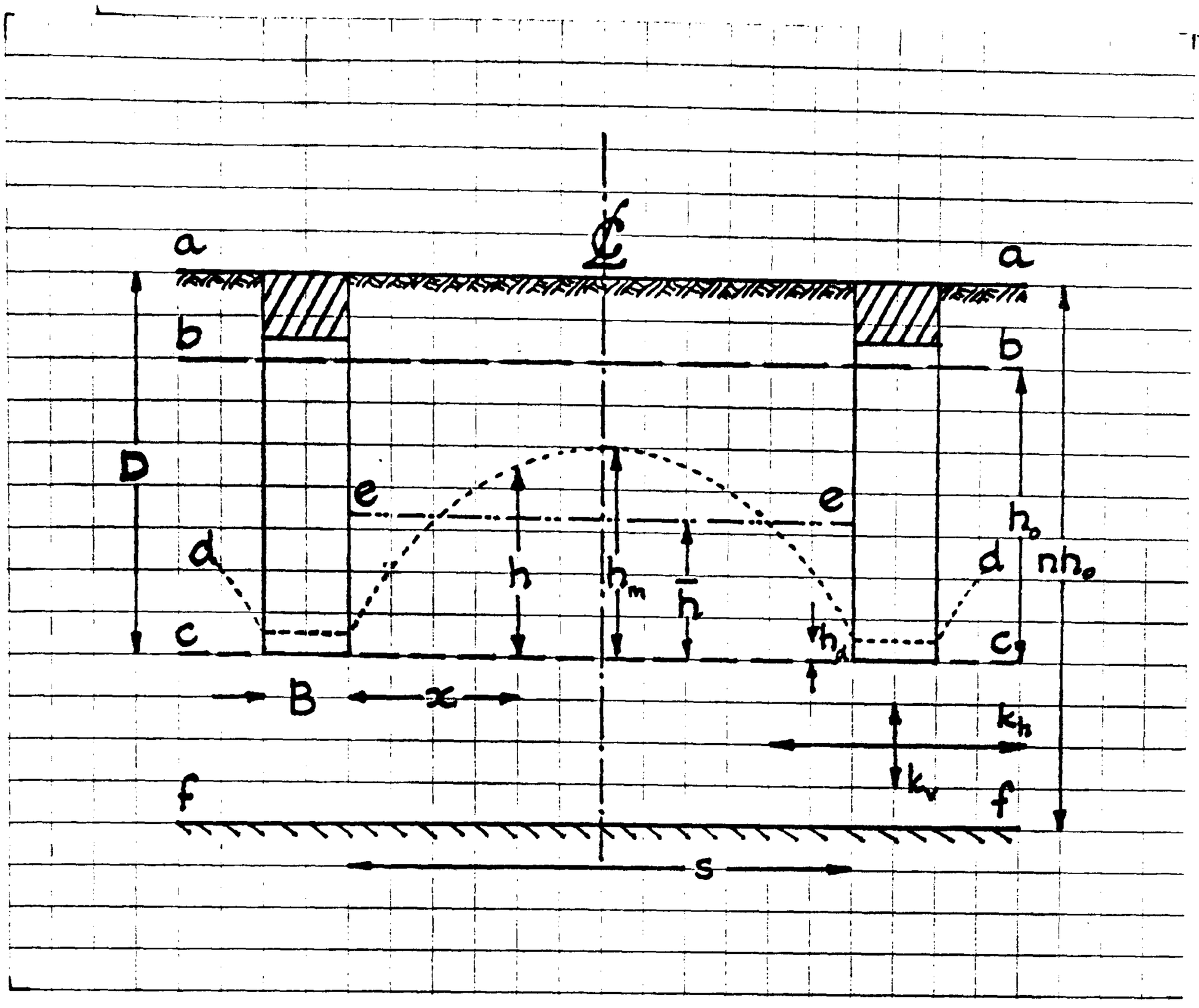
6.10. Conclusions

Henkel's (1957) general approach to the treatment of counterfort drains, particularly as further developed by Hutchinson (1976) has been followed to its logical conclusion with the aid of closed form analytical and numerical methods. These show that the pore water pressures are dependent on drain spacing and also on the depth of the layer in which the drains are installed and on the nature of the underlying soil. The influence of anisotropic permeability is to change the apparent drain spacing, an increased lateral permeability increasing drain efficiency.

The influence of an effective stress dependent permeability was briefly explored, and found to cause increased pore water pressures particularly adjacent to the drains where the rapid decrease in permeability forms a cut off to seepage.

Studies of the total stress and pore water pressure changes on the installation of trench drains and on the development of the steady state pore water pressures around such drains have been inconclusive in view of the large number of imponderable factors present.

However, Hutchinson's correlation of the limited field data with the theory shows that the general approach is reasonably satisfactory for predicting long term or steady seepage pore water pressures. It also confirms the findings of the numerical study that drain depths and spacings used in British construction practice lead to comparatively small drain efficiencies.



Legend:

a - a — *ground surface*

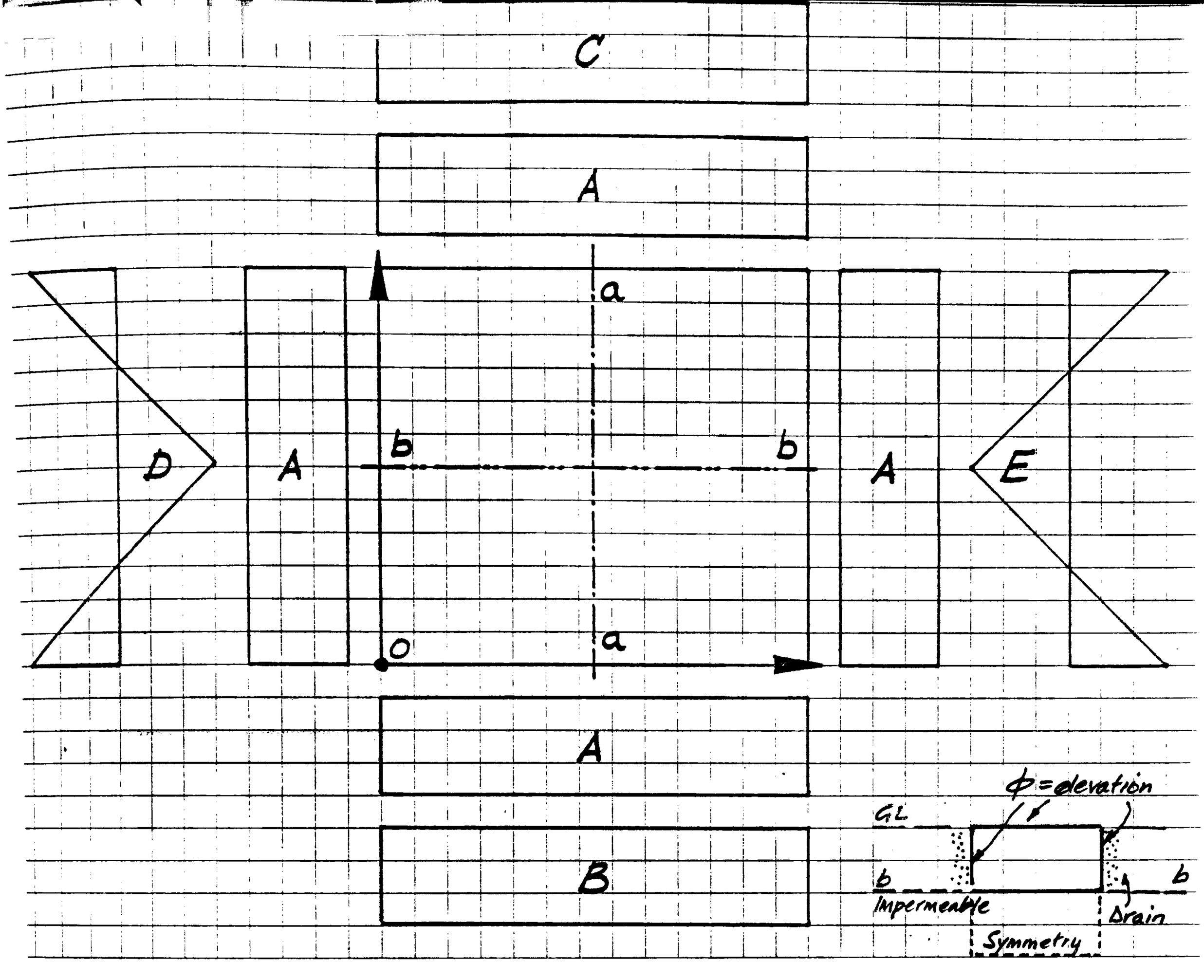
b - b — *original piezometric elevations for drain invert level c - c*

d - d and e - e — *are respectively the actual and average piezometric levels for drain invert level following the establishment of steady seepage conditions after drain installation.*

f - f — *base of soil layer being drained*

k_h, k_v — *horizontal and vertical permeability coefficients*

Figure 6.1. Key diagram: cross section through typical trench drain installation (generally after Hutchinson 1977).



Legend:

a - a	*line of symmetry equivalent to drain centre line*
b - b	*line of symmetry equivalent to impermeable base at drain invert level.*
O	*origin of coordinates, x coordinates running horizontally y coordinates running vertically.*
A,B,C,D,E	*See text.*

Figure 6.2. Schematic diagram showing distribution of boundary potentials used in the analytical solution.

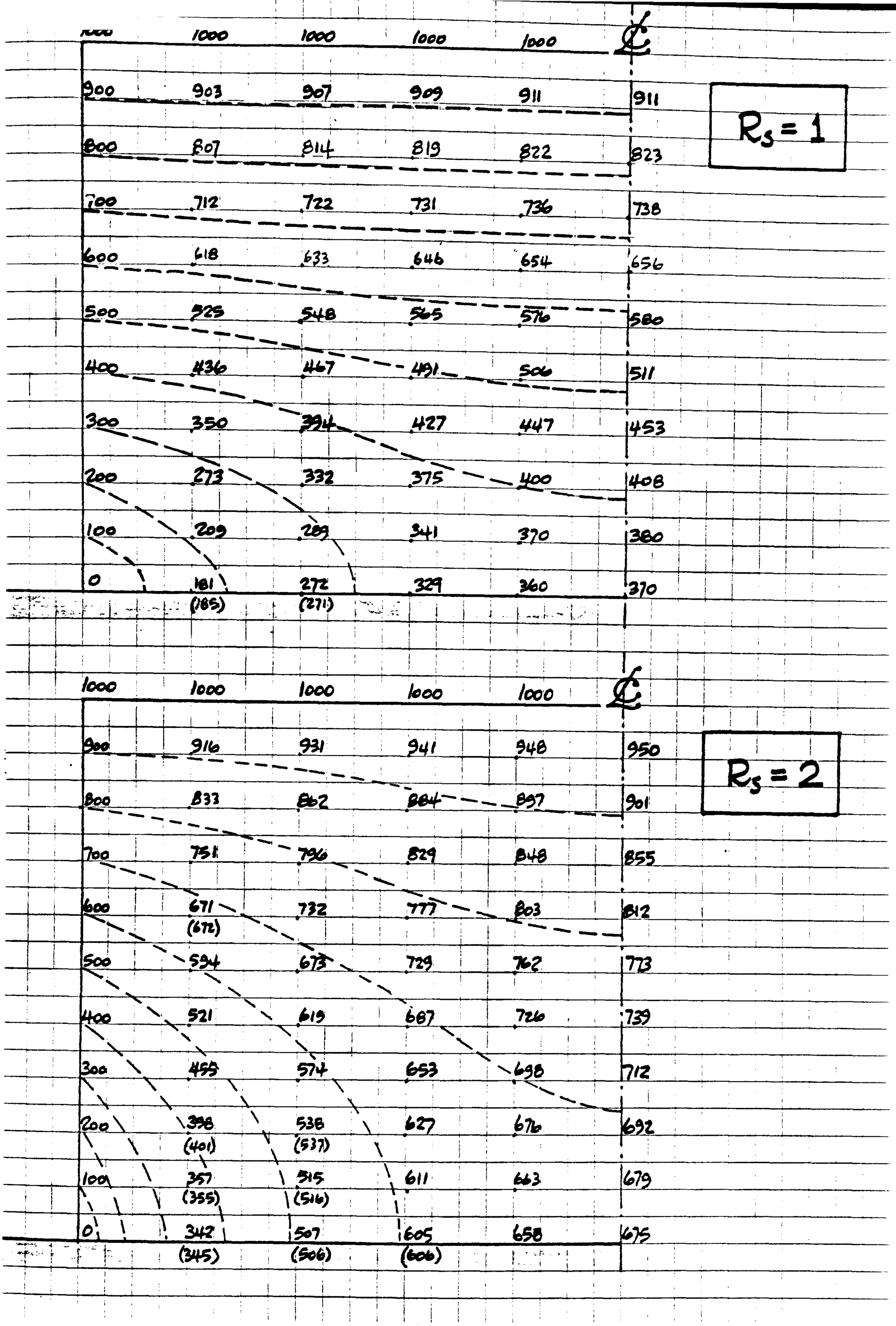


Figure 6.3. Comparison of Fourier & Finite Element Solutions to Richardson's Problem.

(Finite element values are shown in parenthesis when different to Fourier results.)

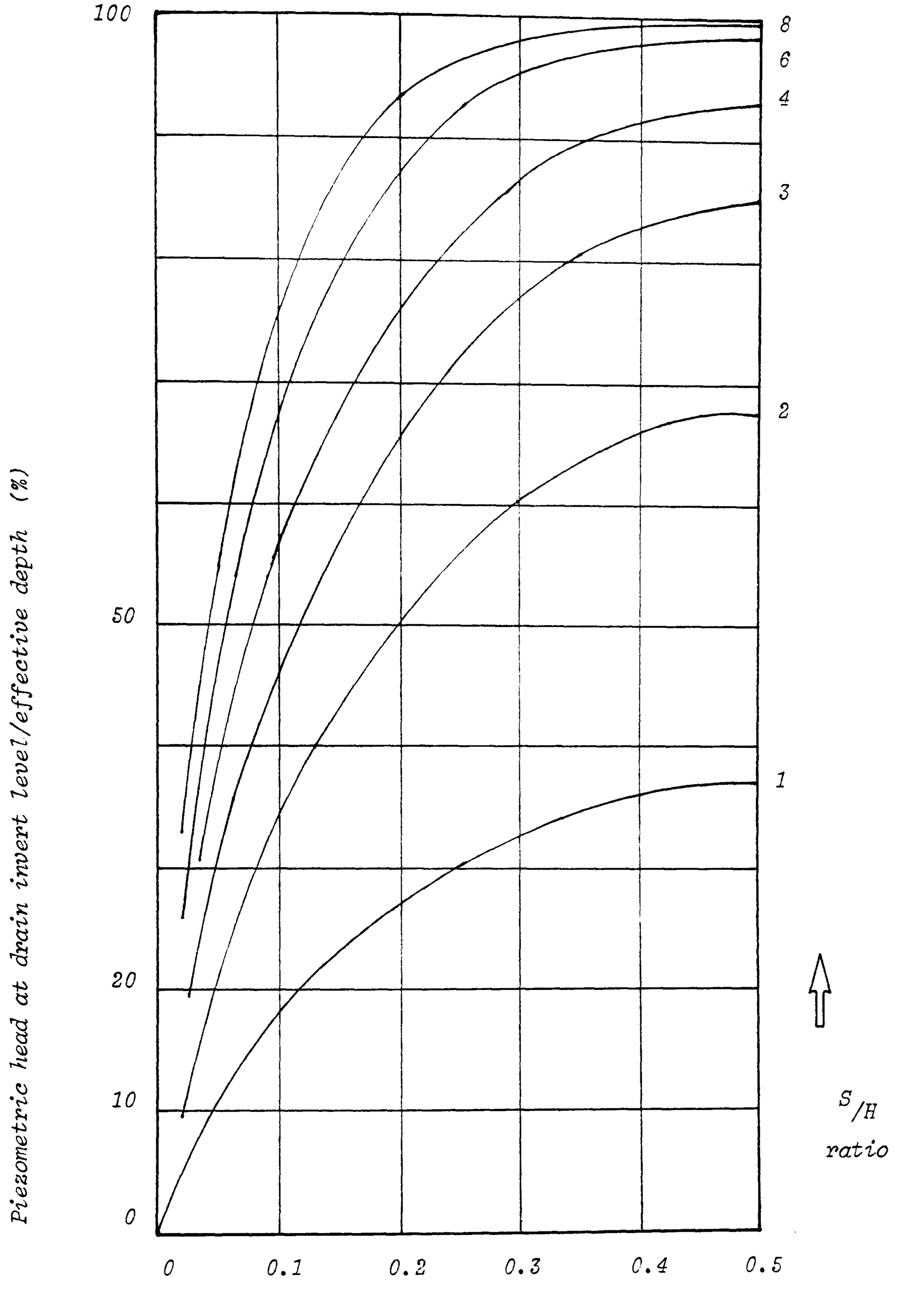


Figure 6.4. Summary of piezometric levels at drain invert level in the Richardson problem/Finite element and analytical solutions indistinguishable.

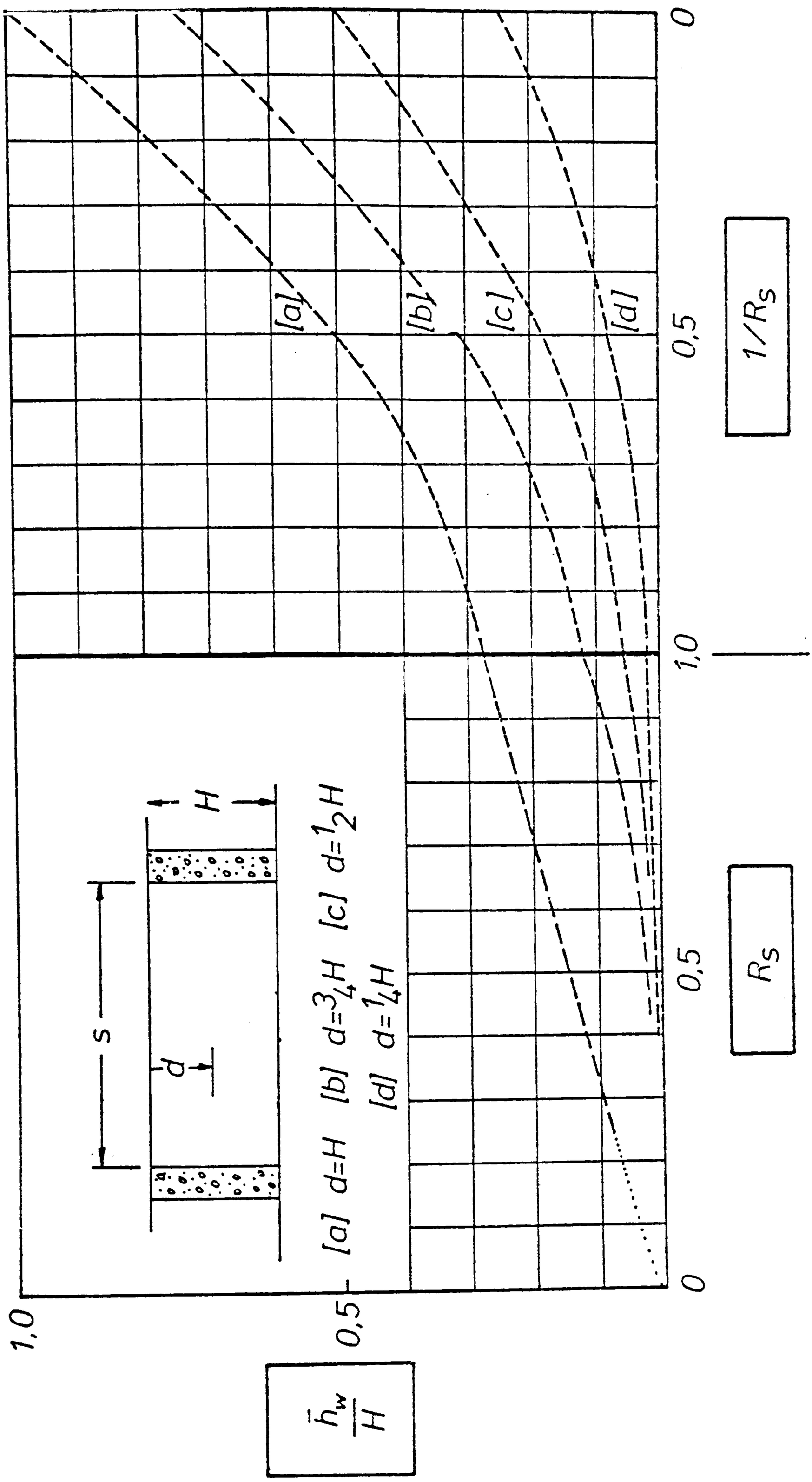


Figure 6.5. Influence of counterfort drains on the average pore water pressure at various depths in a counterfort drain installation. (Closed form solution).

No. of elements.	No. of nodes.
25	96
30	113
35	130
50	101
60	215

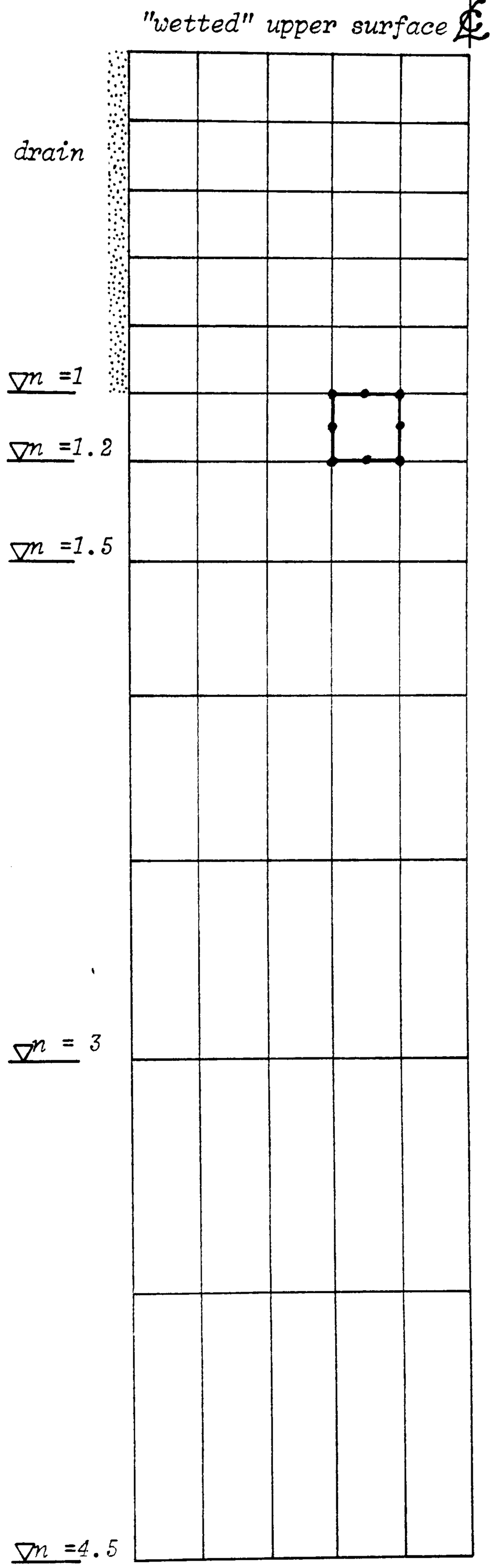


Figure 6.6. Finite element meshes used in parametric study of trench and counterfort drains.

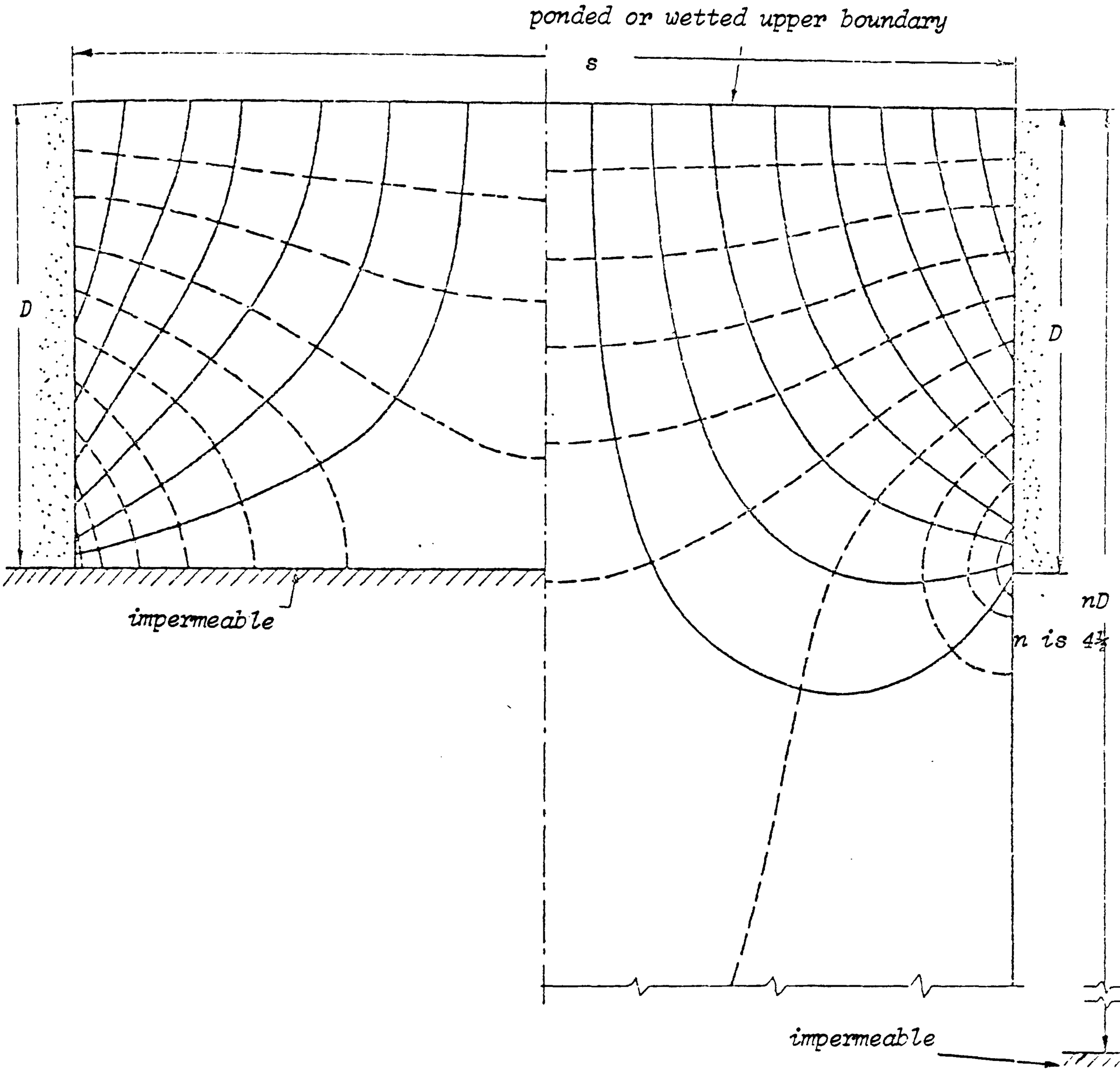


Figure 6.7. Typical flow nets derived from finite element analysis.

(Largely after Hutchinson, 1977)

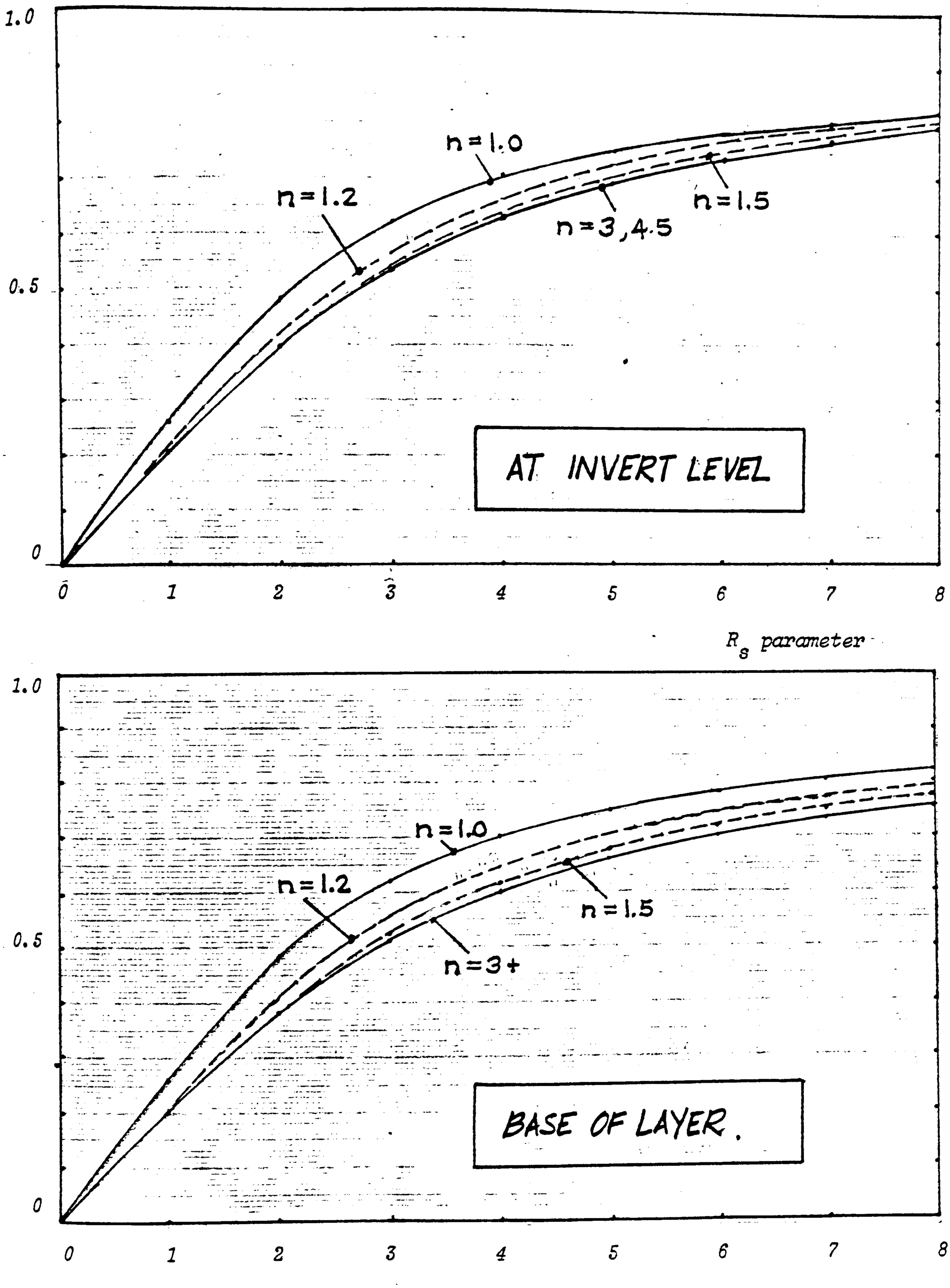
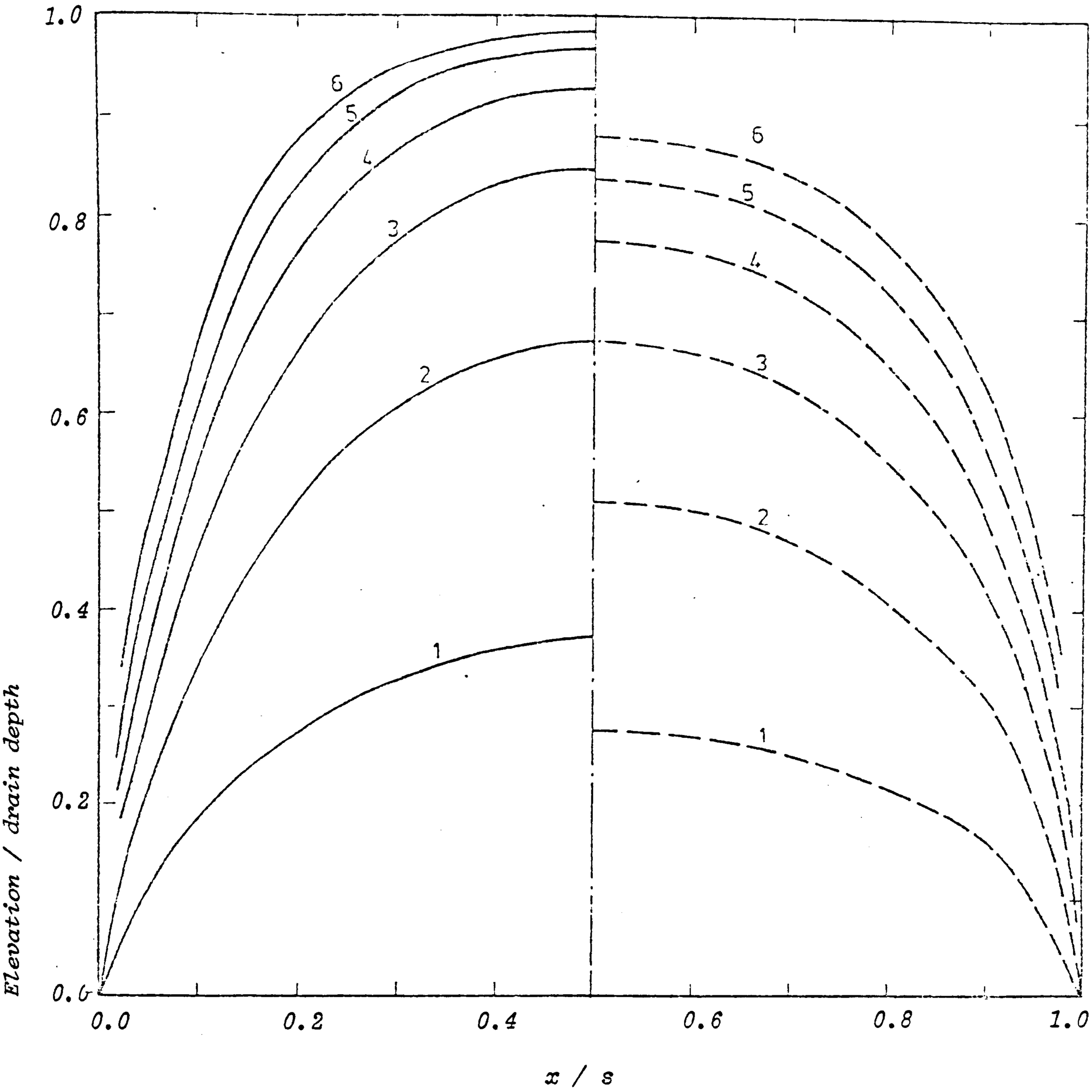


Figure 6.8. Trench drains - pore pressure reduction at various depths.



This side:

Fully penetrating drains

(n equal to 1)

This side:

Partly penetrating drains

(n equal to 4.5)

R_s is equal to the values marked against the individual lines.

Figure 6.9. Pore water pressures at drain invert level in trench drain installations with different depth factors (impermeable base).

Finite element results obtained at these intervals:

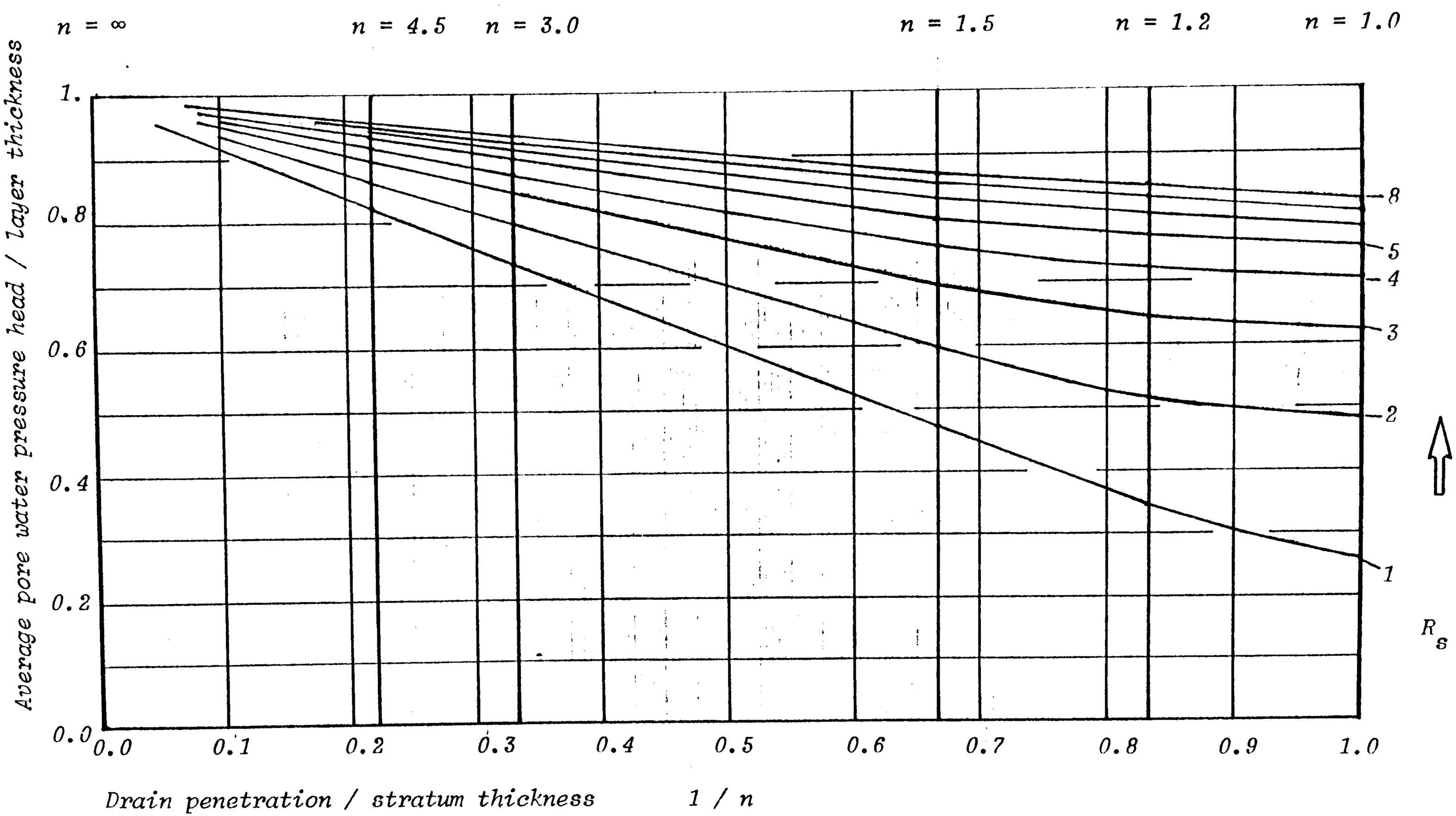


Figure 6.10. Impermeable base solution: average pore pressures at base of layer as a function of drain penetration.

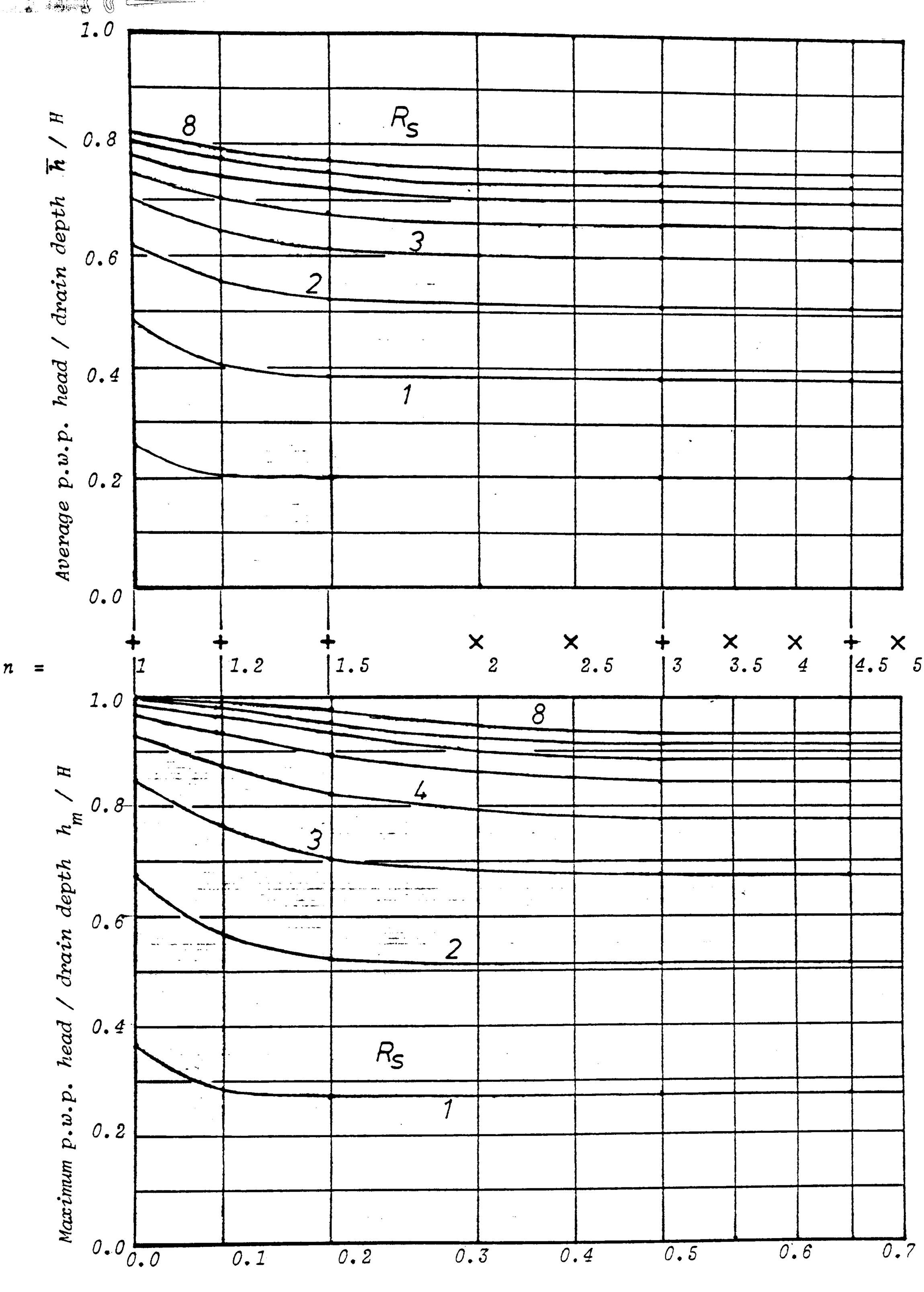


Figure 6.11. Impermeable base solution: average and maximum pore pressures at base of layer as a function of depth factor.

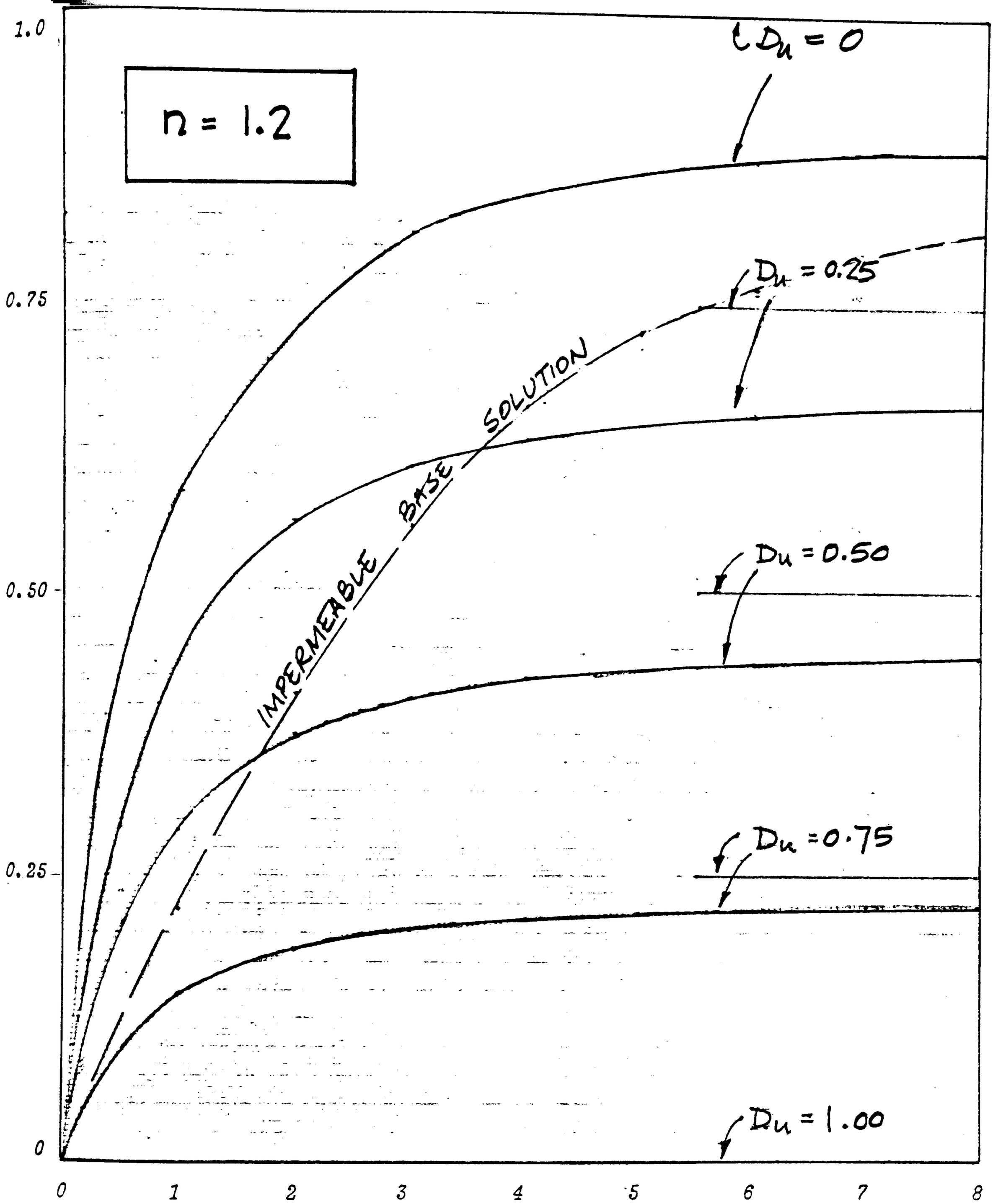
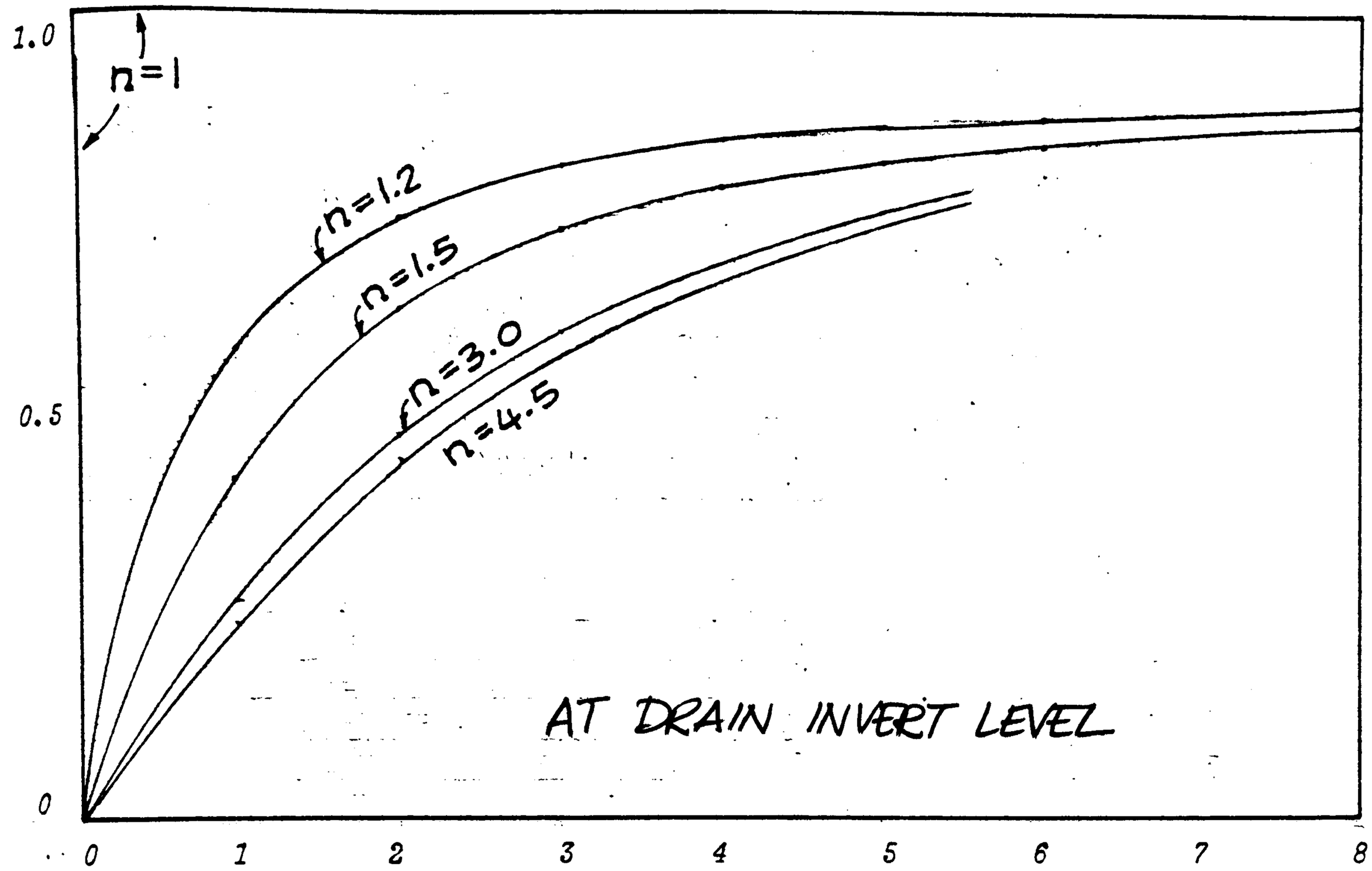


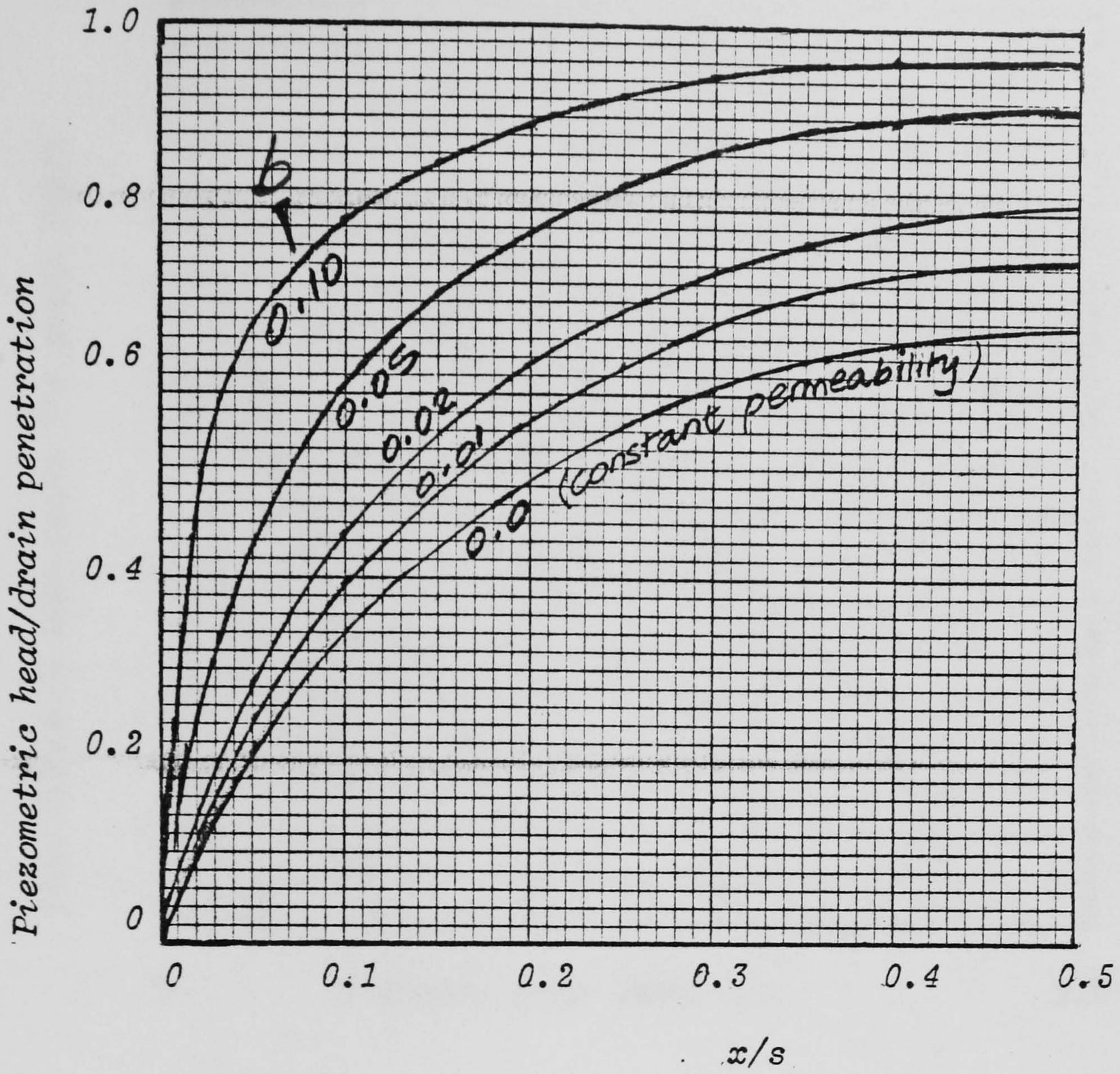
Figure 6.12. Effect of partly penetrating drains in an underdrained soil layer on pore pressures at drain invert level.



The effect for a different underdrainage ratio from the $D_u = 0$ case assumed in the above diagram can be found from:

$$\bar{h}/H = (1 - D_u)\ \bar{h}/H \text{ (from graph)}.$$

Figure 6.13. Effect of trench drains with different penetrations into a partly underdrained soil layer.



"LOG LAW"

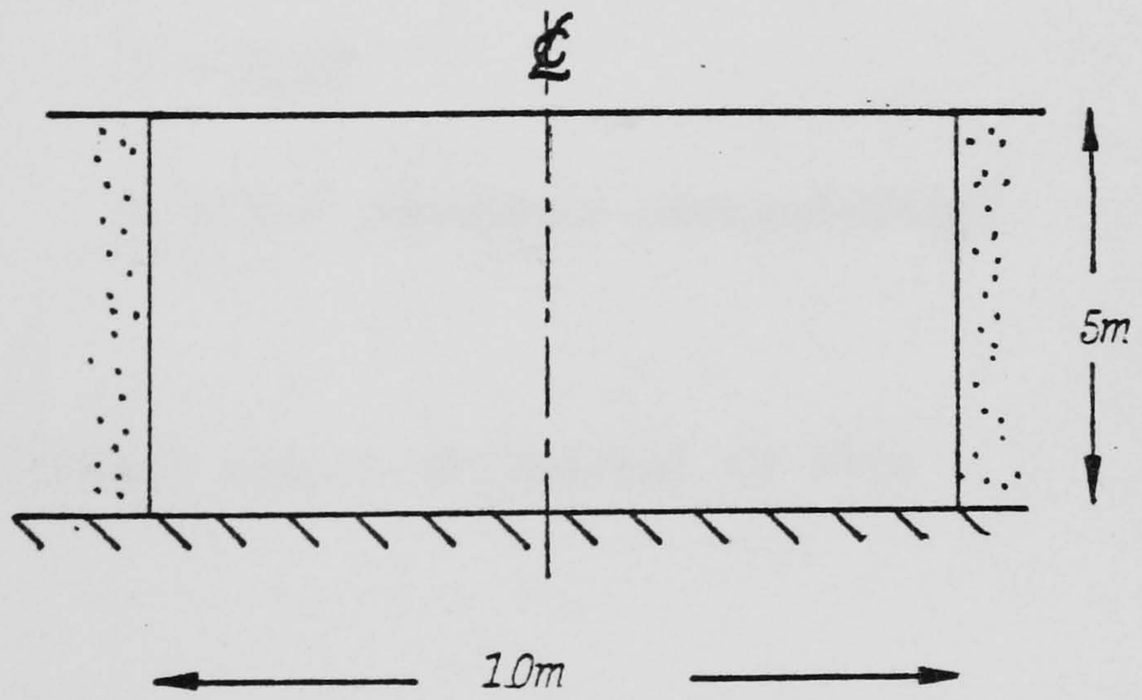
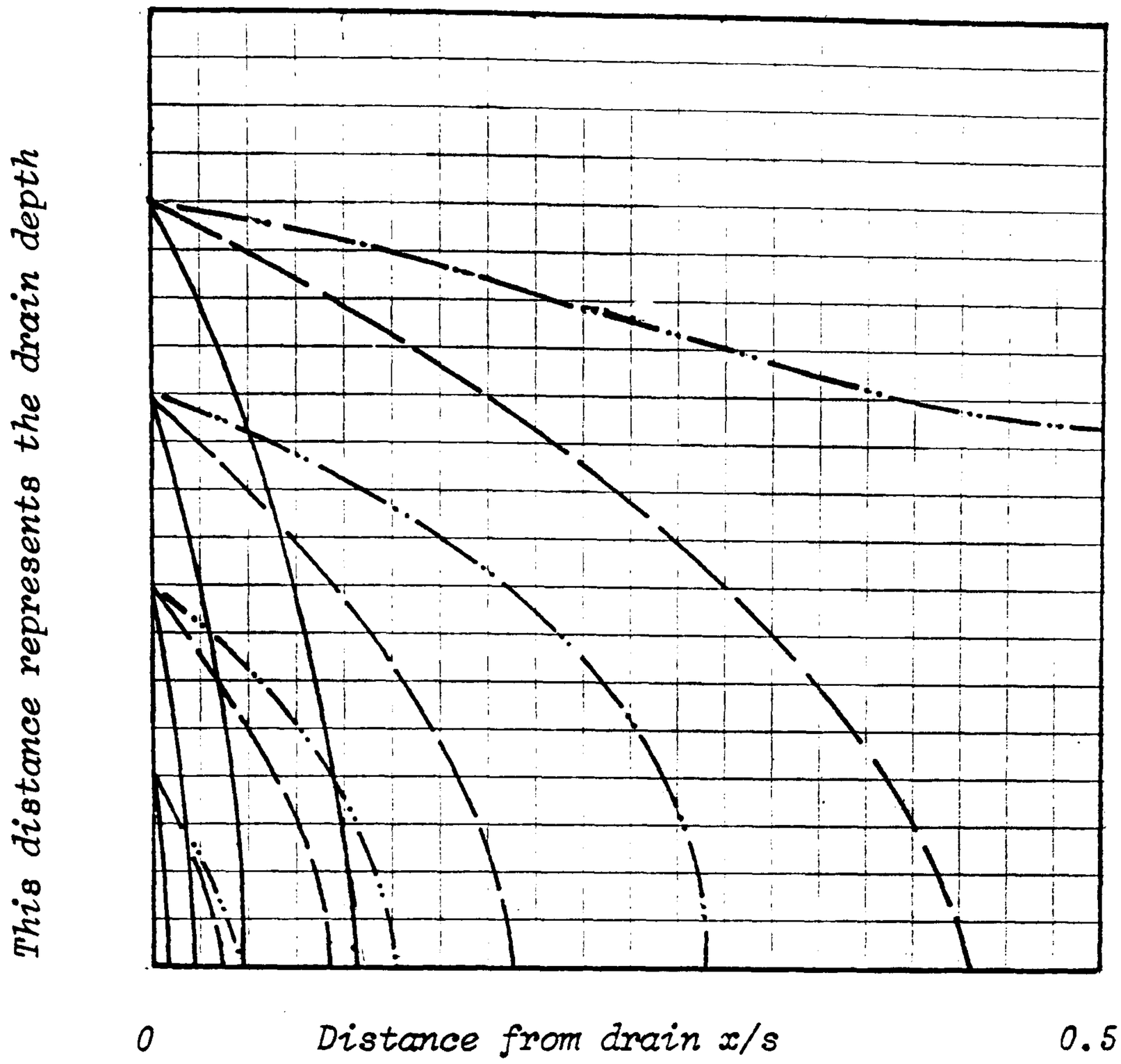


Figure 6.14. Flow where permeability is dependent on effective stress-piezometric heads at drain invert level.



Legend

———— *b = 0.1*

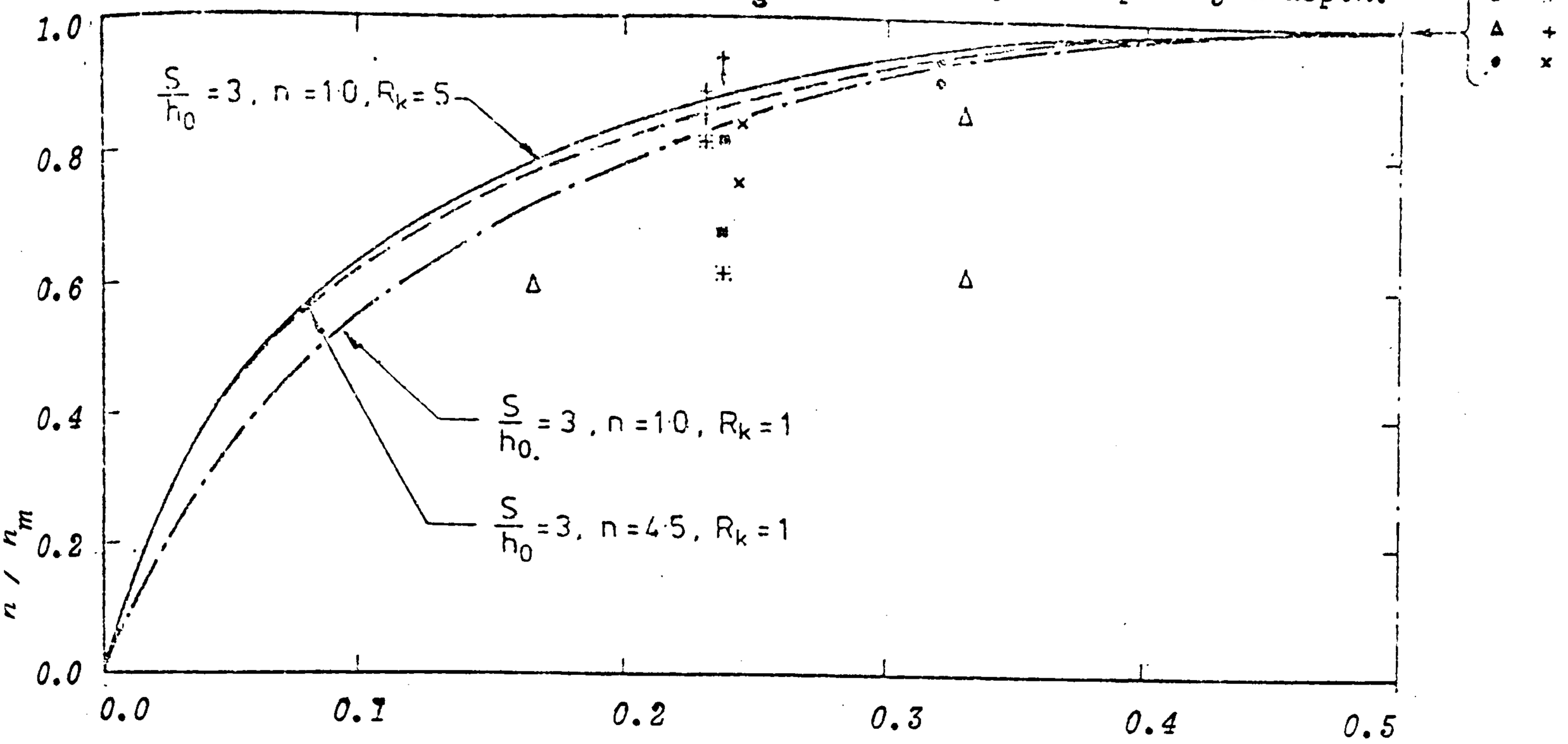
— — — *b = 0.02*

—··—··— *b = 0.0 (constant permeability)*

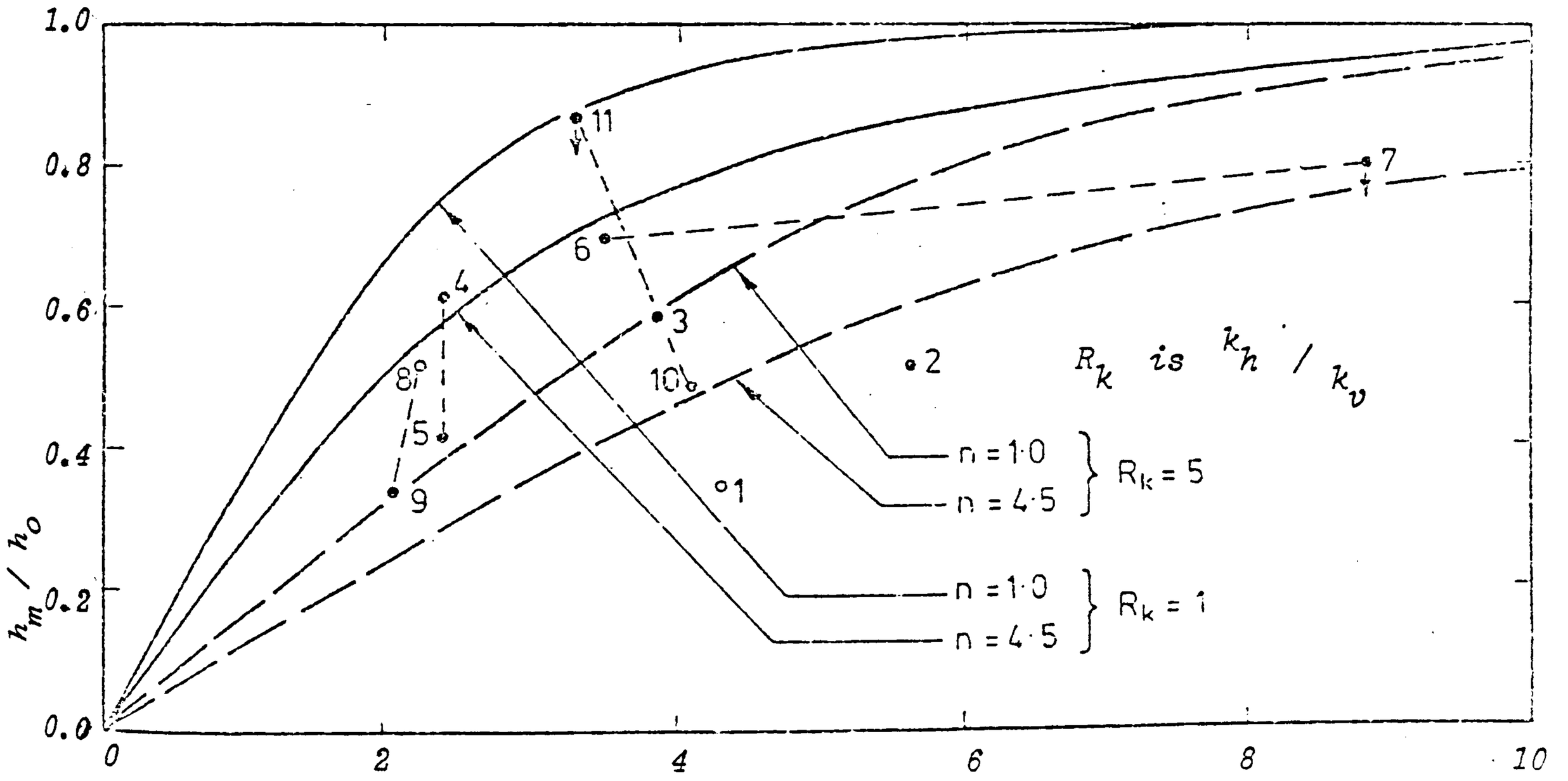
NB Flow lines and equipotentials remain orthogonal in this solution.

Figure 6.15. Equipotentials in the effective stress permeability analysis. (See also Fig. 6.14).

NB In these plots, which are for the impermeable base case, permeability anisotropy has been extracted from R_s leaving only the spacing & depth.



Relationship between maximum and average piezometric elevation.



Relationship between average piezometric head and effective drain depth.

Figure 6.16. Comparison of theory with field measurements of pore water pressure (after Hutchinson, 1977).

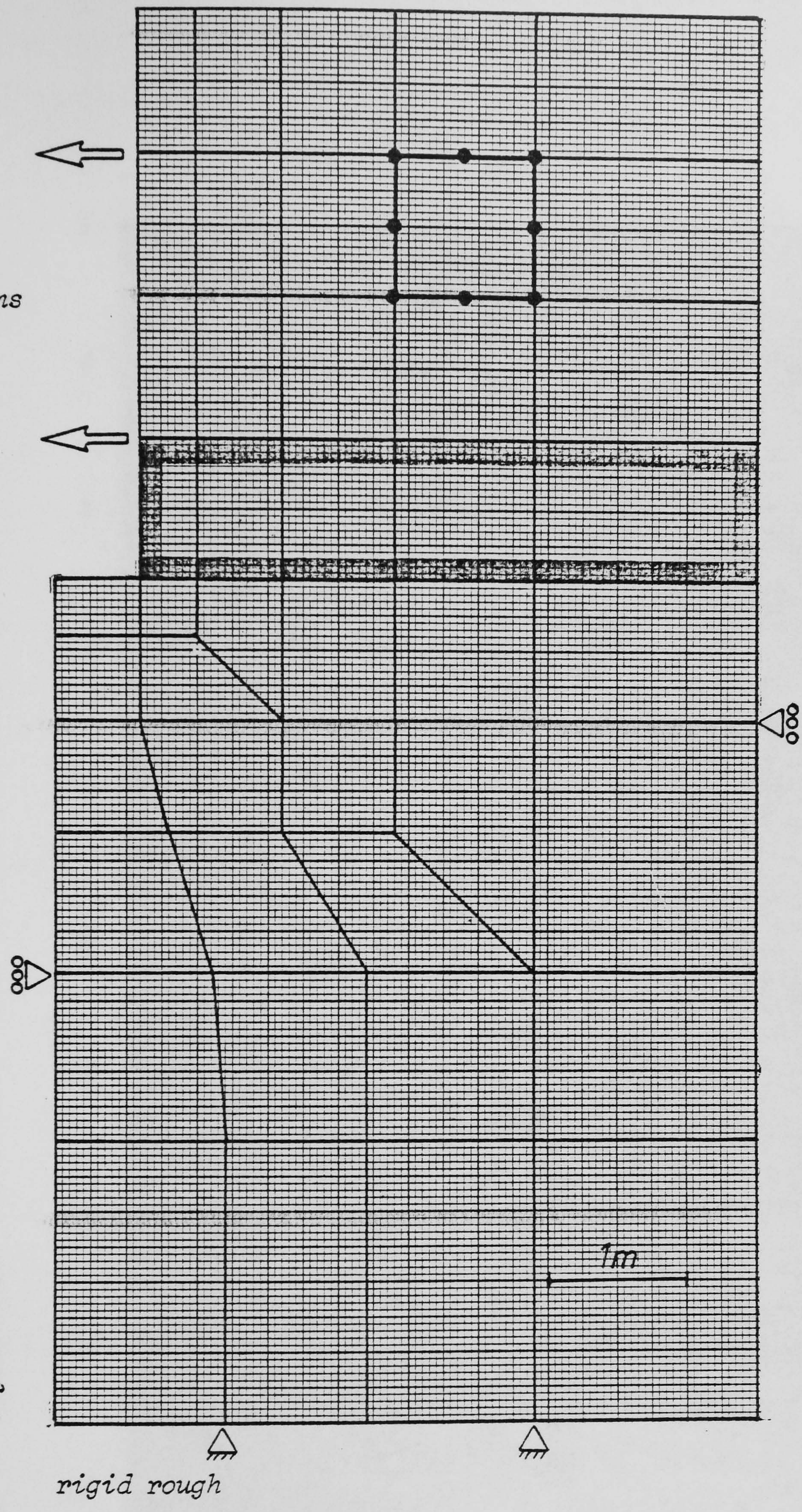


Figure 6.17. Finite element model for stress changes on installation of trench drains.

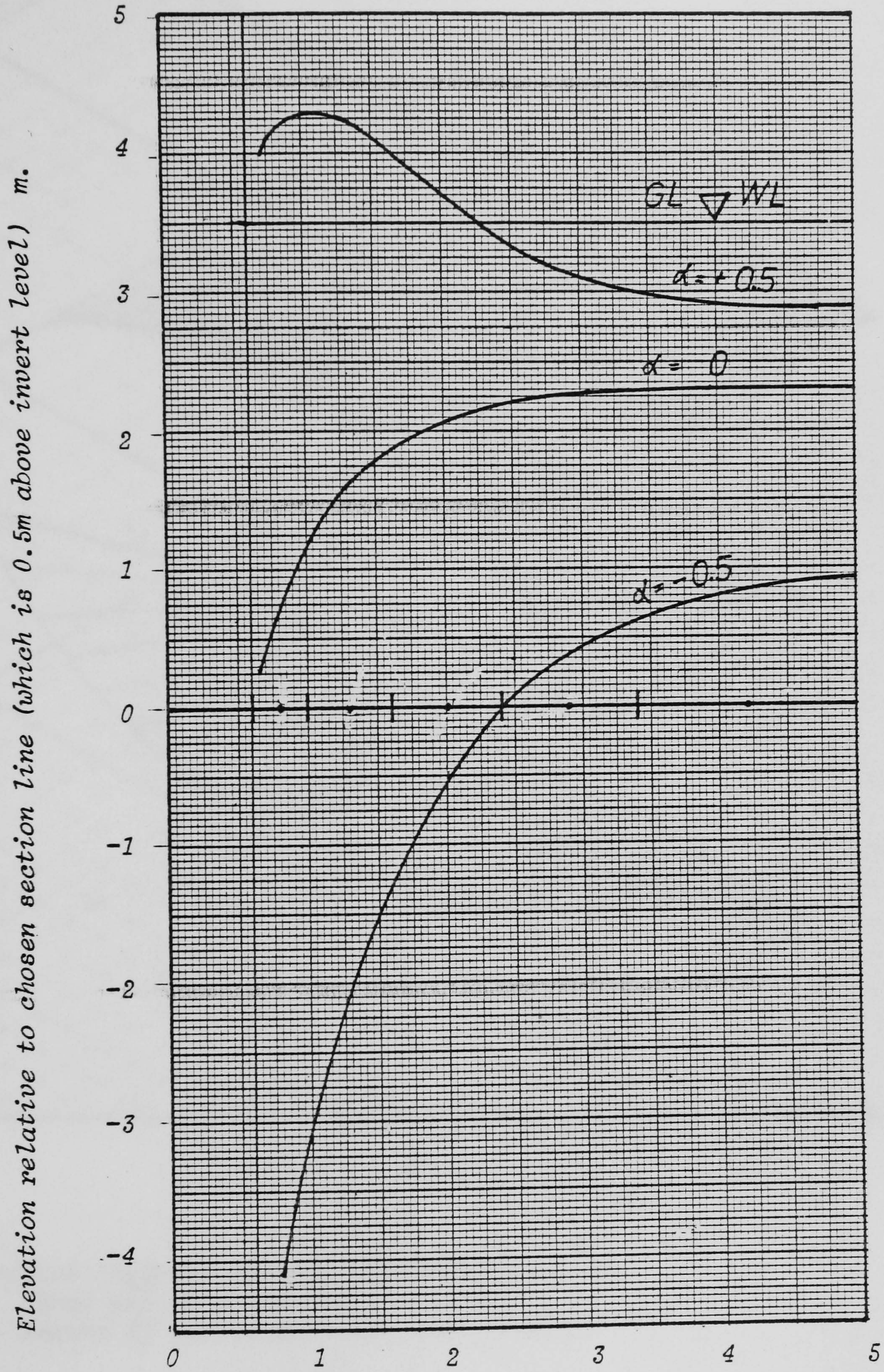
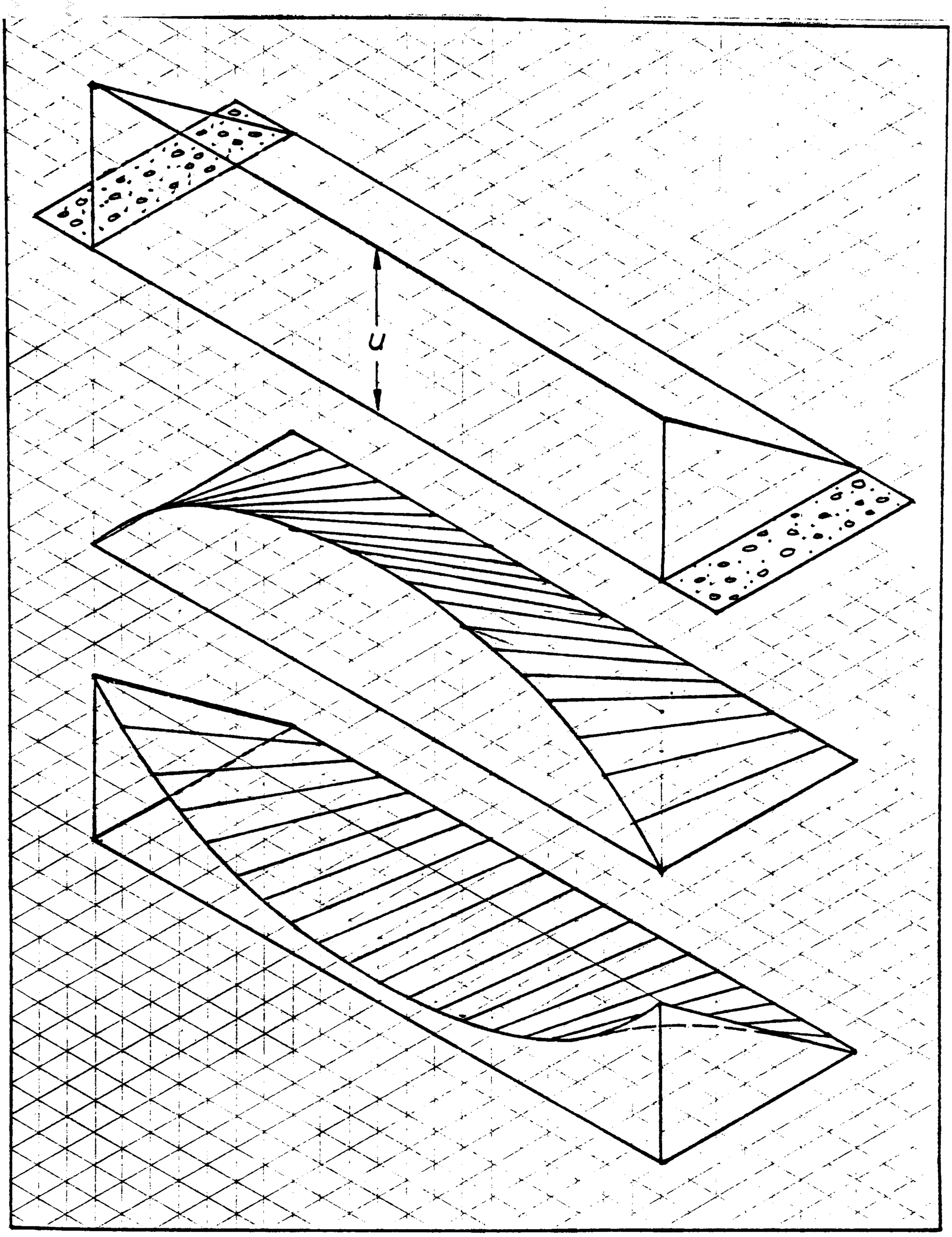
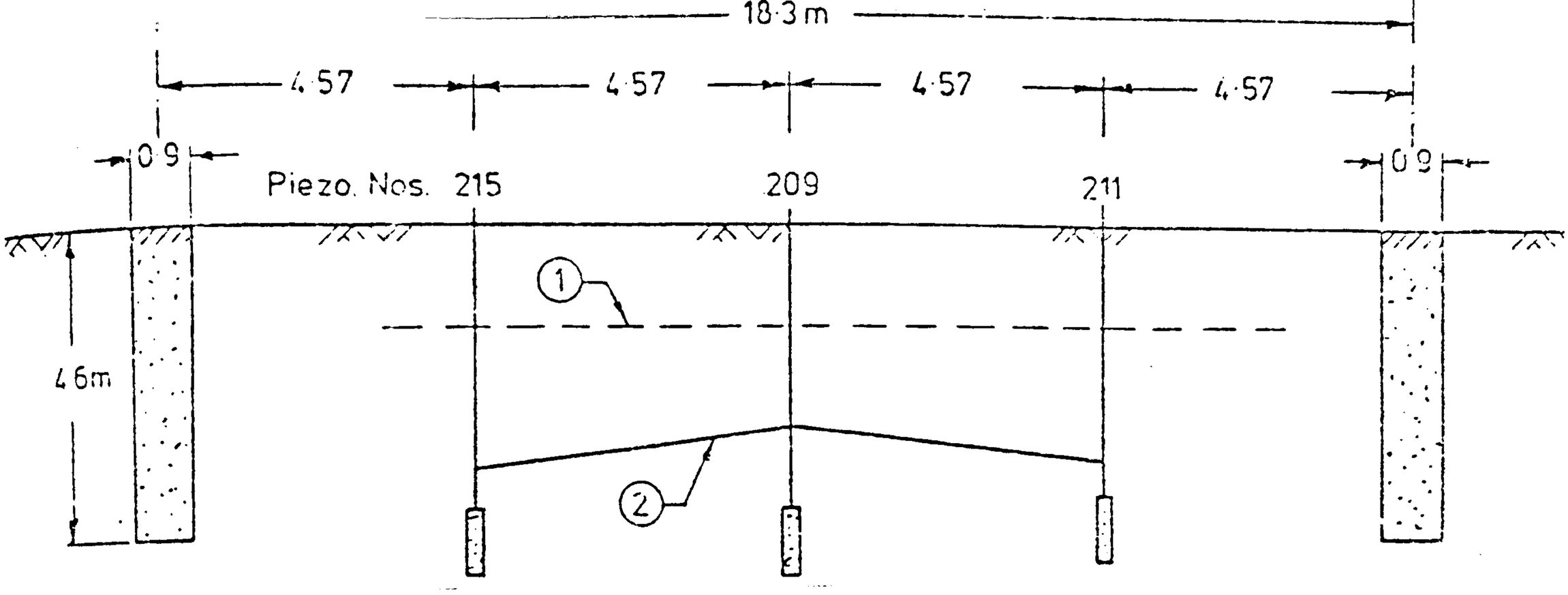


Figure 6.18. Typical calculated pore water pressures immediately after excavation of trench drains (from finite element analysis).

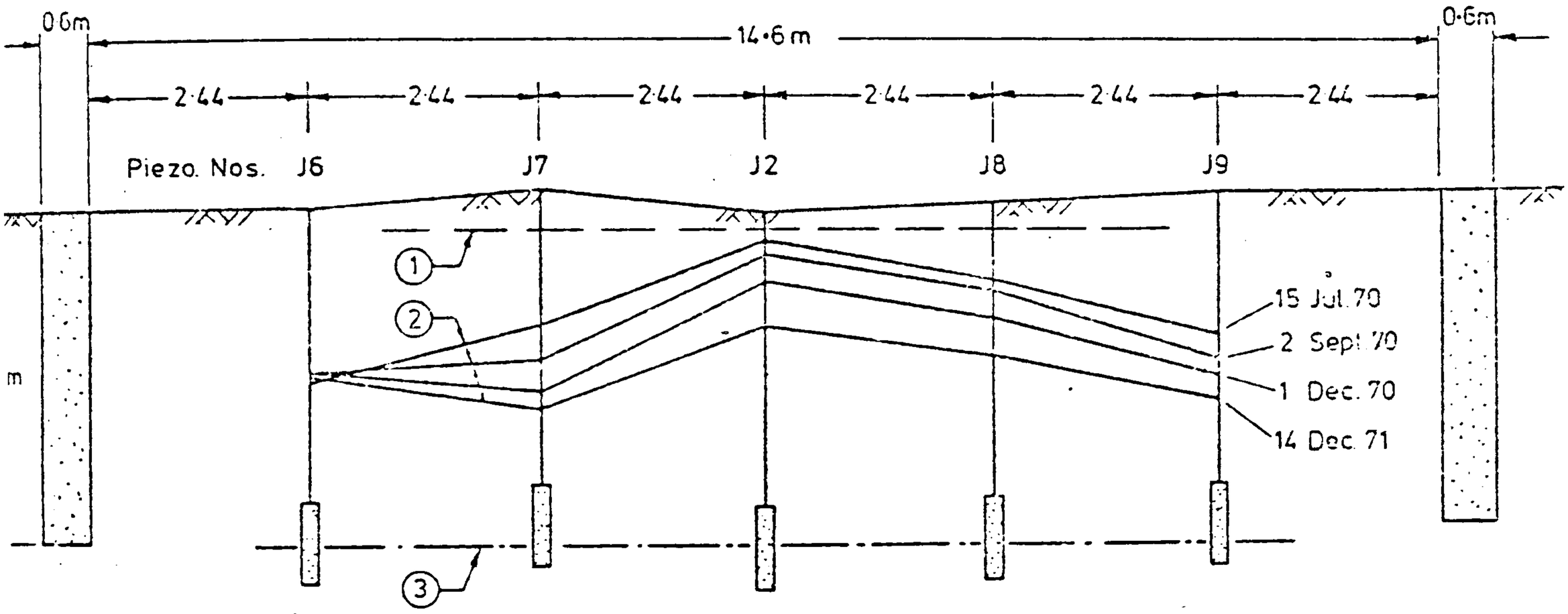


Top: Initial (hydrostatic) pwp distribution
Middle: Final pwp distribution
Bottom: Amount of pwp to be dissipated (excess)

Figure 6.19. Initial and final pore water pressure distributions in a counterfort drains installation.



Cross section of the Sevenoaks drains looking downslope. (1) is the approximate position of the original piezometric line. (2) is the position of the piezometric line after drainage.



Cross section of the drains at Burderop Wood. (1) is the original piezometric line. (2) are the various positions of the piezometric line following drainage. The slip surface is approximately at (3). (the drains were installed about 2 weeks before the upper line in (2) was measured).

Cross section of the drains at Guildford.

(1) is the original piezometric line (based on the "lost" piezometer P103.) (2) is the long term position about 10.5 years later.

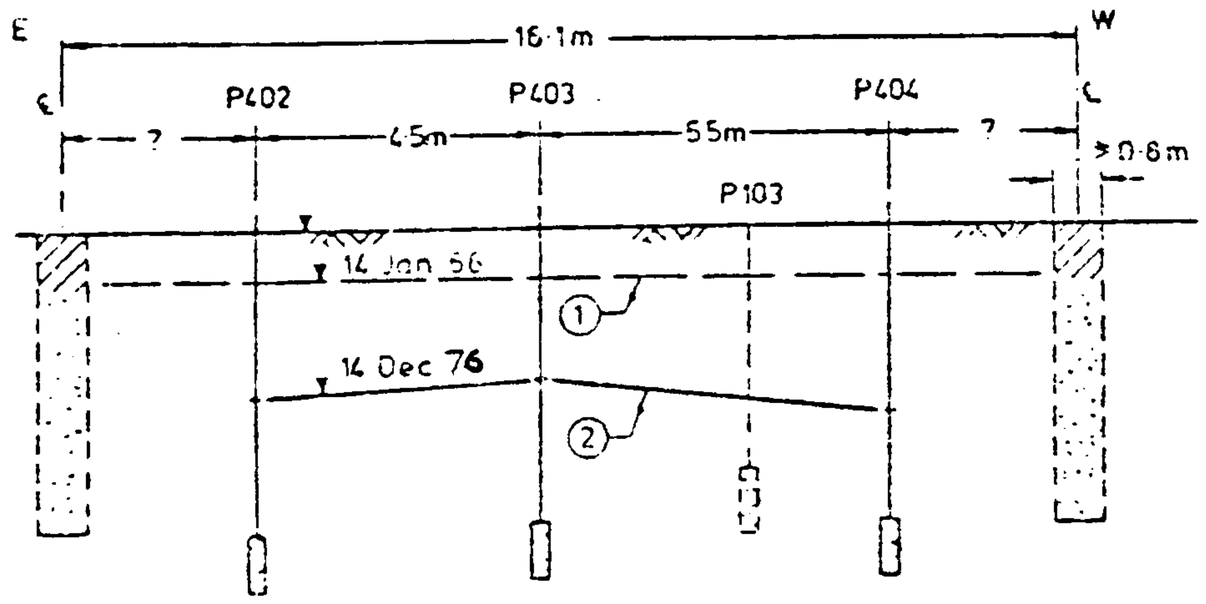


Figure 6.20. Field measurements of pore water pressure in trench drain installations (after Hutchinson, 1977).

CHAPTER 7 - PARAMETRIC STUDY OF SEEPAGE IN SLOPES

7.1. Introduction to the Parametric Study

Stability charts (e.g. Taylor 1937, Spencer 1968, Pilot & Moreau 1970, Janbu 1957, Bishop & Morgenstern 1960, Hoek & Bray 1977) are widely used in the design of earth slopes, particularly during early phases such as feasibility studies because of their ease and simplicity. However, those charts which are formulated in terms of effective stress need some data on the state of the pore water pressures in the slope, usually in the form of an average pore pressure ratio (r_u) parameter. Somewhat surprisingly, a number of field measurements (James 1970 , Walbancke 1976, Skempton 1970) appear to give an average pore pressure ratio of about 0.3, and the following parametric study was undertaken partly to see if there is any fundamental underlying reason for this. A second hypothesis that was tested by this parametric study was that if perhaps slight steepening of a slope served to reduce the pore water pressures sufficient to more than offset the decrease in stability resulting from the increased slope angle or if alternatively the average pore pressures increased greatly for modest increases in slope angle, then an explanation would be provided for the occurrence of slides in only part of an earth slope, the remainder appearing perfectly stable.

Furthermore, Vaughan and Walbancke, 1976, observe that in many cases the seepage conditions, and the seasonal variations in those conditions, can be quite adequately simulated by considering only one dimensional vertical flow, and the parametric study allows the limits to which this convenient approximation can be extended to be established on a rational basis. An additional commonplace assumption regarding seepage in long slopes is (at least in any colluvial mantle) that flow is parallel to the slope surface, and the limits of applicability for this are also explored.

7.2. Boundary Conditions

The boundary conditions for seepage in an earth slope are of vital importance to the resulting pore pressure distribution. The problem of the upper surface condition has been examined by Walbancke,1976, who finds that for clay slopes, in a temperate climate, zero pressure

conditions may be found at, or slightly below, ground level. This suggests that the treatment of the ground surface in a seepage analysis should be as a "wetted" boundary, albeit with an appropriate potential (implying pore water suction if need be). In contrast to this, many writers prefer to fit the pore pressure data to, or derive it from, sketched flow nets, often fragmentary in nature, with a clearly defined "free surface". Examples of this can be found in Skempton & Brown 1961, Hoek & Bray 1977, and in many texts.

In view of the practical difficulties accompanying the measurement of pore water pressures *above* the zero pressure line, and relating these values to the fluctuations of permeability once negative pore water pressures have to be considered, it is scarcely surprising that few results have been published, excepting of course, the results of Black *et al*, 1958, which demonstrate quite clearly how complex the problem is. It is probably much more acceptable in the present state-of-the-art to neglect the partly saturated and pore water suction zone, and thus work with a seepage regime that occupies but a part of the complete slope section (Figure 7.1).

The other boundary condition of major significance is that acting at the base of the soil stratum in which the slope is formed. Should this be inclined or contorted in any way, the pore water pressures throughout the section will be modified, but in the main (and particularly for slopes in deep soil deposits) the effect of the *shape* of this boundary will be of much less importance than its *nature*. In the present context, the term nature is used to describe whether or not the lower boundary is impermeable or permeable, and if the latter, what boundary potentials obtain. A truly impermeable basal boundary appears unlikely to occur in practice, but it may be a convenient fiction where a large decrease in permeability occurs rapidly with depth. However, as much of the applicability of the parametric study will be in the clay soil area, such a permeability decrease is improbable, and the "impermeable base" solution of comparatively limited value.

The alternative to the "impermeable base" assumption is the "permeable base" solution. Earlier, in the discussion on counterfort and trench drains, the influence of the value of this basal boundary potential was explored, as it was in Chapter 2, in which one dimensional seepage and the effects of underdrainage were dealt with at some length. However, in some of the major fields of application of counterfort drains, the "impermeable base" solution is more appropriate than the "permeable base" one, an example of this being where a (relatively permeable) colluvial mantle overlies a parent mass of (relatively impermeable) unweathered overconsolidated clay, and trench drains in the mantle to improve its overall stability are proposed. Should there be a layer of much greater permeability at the base of the mantle then the straightforward solution would be to tap this; thus simply underdraining the mantle and allowing trench drains to be dispensed with. However, it is accepted that this simplified view may not always appeal to the engineer, and trench drains installed notwithstanding (Skempton & Weekes 1976).

The view that the present author has taken (that the permeable base model is the more important of the two) contrasts strongly with that of most other workers who have considered the problem. However, their interests (e.g. Freeze & Witherspoon 1966, 1967) appear to lie with regional ground water hydrology, and on such a scale, that not only can an aquiclude be found at some depth, but also the concept of a free surface at the top of the saturated part of the aquifer may not be too far from the truth. (The writer still cannot, however, reconcile the idea of a free surface with an infiltration of meteoric water). Lafleur & Lefebvre 1980 compromise by taking a permeable basal stratum which is totally confined.

In relegating the impermeable base solution to a secondary role, it was noted that much of the application of this parametric study would be to clay soils. In complex sedimentary series these are frequently underlain by sandy facies (e.g. the London Clay of the London Basin by beds of the Woolwich & Reading Series; and the

Gault, which is at Folkestone underlain by Folkestone Beds and in Hampshire by the Carstone and Ferruginous Beds: Other examples are too numerous to mention) in which the potentials are variable within a large band. In the main, natural artesian conditions are rare, partly because of the lack of the necessary geological structures, but in many cases due to the exploitation of the aquifer with wells, and once again, the London Basin provides an excellent case of this (Wilson & Grace, 1942, Water Resources Board 1972). However, despite the fact that it may not be necessary to analyse many present-day situations with artesian conditions, it may well be necessary to invoke those conditions to satisfactorily explain natural features of considerable age such as the anomalous gravel filled pipes in the London area (widely described, but best summarised by Berry 1979) and explained by Hutchinson, 1980, as being eroded and infilled pingo roots. Thus, this possibility should not be overlooked. Local artesian conditions may also result in the vicinity of reservoir impounding, or can be induced by a deep excavation below the piezometric level in the basal aquifer. (Figure 7.1).

Various degrees of underdrainage down to complete (D_u = 1.0, Chapter 2)* underdrainage are possible, but the higher degrees of underdrainage almost invariably reflect a degree of artificial groundwater extraction. A reduction in permeability with depth (or with increasing effective stress) may quite effectively "insulate" the slope itself from its basal underdrain and this effect should not be neglected when using the results of this particular study.

One convenient feature of the underdrained solution is that due to the linear nature of solutions to the Laplace equation (solutions for different boundary conditions can be simply added to produce the solution for the combined boundary conditions), it is not

---

*When quoting the degree of underdrainage of a soil stratum, the writer will always imply that this is measured from the crest of the slope to the base of the stratum. It is therefore a global underdrainage ratio. This may be different to a local underdrainage ratio, measured from the toe of the slope, for example.

necessary to complete a full range of solutions for different degrees of underdrainage. The pore water pressure at any point for *complete* (Du = 1) underdrainage (and homogeneous permeability) being zero; and equal to some value u, with no underdrainage (Du = 0), then for an intermediate degree Du; the pore pressure is given by:

$$u_i = (1 - Du_i)u$$

This effect has been noted and further described in earlier sections (2.2) of this thesis.

Finally, the "side conditions" at the top and toe of the slope, and the distance of these away from the slope itself have some effect. This is minimised in the present study by treating them as impermeable and removing them as far away as practicable subject to conditions of overall economy in the use of finite elements in the solution.

7.3. Geometric Mapping

The finite element mesh used in the parametric study is shown in Figure 7.3. This basic mesh was used in all the analyses, and rather than going through the relatively arduous process of mapping the mesh geometry to cope with different slope inclinations and slope height to stratum thickness ratios, the mapping resulting from anisotropic and non homogeneous permeability in various zones has been used. Referring to the figure, zone 1 represents the earth slope and zone 4 the soil beneath the slope. By altering the ratio of horizontal to vertical permeability in zone 1, the effective slope angle is changed. The vertical permeability in this zone is kept constant throughout the study to provide a common base for all the various analyses. In zone 4, the horizontal permeability is always taken to be the same as in zone 1, and the ratio of vertical permeability in zone 4 to zone 1 alters the slope height to stratum thickness ratio. Permeability coefficients for the other zones are chosen to be compatible with zones 1 and 4.

The various permeability coefficients in each zone are related as follows:-

If the slope angle is 1 to m and the ratio of total stratum thickness to slope height is n then:-

$$Kx_1 = Ky_1/\sqrt{m}$$

$$Kx_4 = Kx_1$$

$$Ky_4 = (\sqrt{n-1})\ ky_1$$

$$Ky_2 = Ky_1$$

$$Ky_3 = Ky_5 = Ky_4$$

$$Kx_2 = Kx_3 = Kx_5 = 10\ Ky_1$$

Subscripts x and y relate to direction, the numbers relate to the zones.

The final condition removes the "side boundaries" a distance $\sqrt{10}$ times the slope height away from the slope toe and head. (A greater distortion than this was felt to be unacceptable with the particular mesh of elements used, and in any case unnecessary).

The writer acknowledges the assistance of a number of the students of the 1978/79 M.Sc group, who at the instigation of Dr. S. Cavounidis, undertook to run a number of the analyses in this study. Unfortunately, however, by the very nature of things, it was inevitable that some of these analyses would contain small errors, and those runs have been corrected and repeated. Table 7.1* indicates the range of the various parameters studied, while a selection of the results (plotted on both the "parent" and derived or mapped meshes, which also serve to show the nature of some of the transformations) are presented in Figures 7.4 A to E. It should of course be noted that while the "parent" mesh is the undistorted one in terms of the *finite element* data, it is the transformed one in terms of the field seepage problem.

*p224

7.4. Problems Arising From the Use of the Single Slope Model

Several problems arise from the use of a single finite element mesh to represent *all* the cases of slope angle and depth ratio. The first of these is that the extreme cases of n = 1.0 and n = ∞ cannot be analysed , and these are important "end points" on any graph (it should be noted that the graph, Figure 7.6., is plotted in terms of 1/n since this gives a more natural graph scale range of·from 0 to 1). While it is possible to extrapolate the other results to the end points, the accuracy of the finite element solution itself degrades as the elements are excessively distorted (the permeability transformation is effectively an element distortion) and the extrapolation has to be made from data which is subject to increasing error in the very direction of the extrapolation.

It is the degradation of the solution with increasing element distortion that is the second problem. This can be seen in the results plots (Figures 7.4 and 7.5) in the part of the section where the potentials vary most slowly. These erratic equipotential contours have not been "touched up" to produce a clearer and less ambiguous result since so to do would be to obscure the fact that the solution was already tending to be degraded for those distortions.

The way in which the n = 1 case is dealt with is to use a separate mesh (Figure 7.5 A & B). It should be noted that this case has been exhaustively examined by Sweeney (1970) with special reference to permeability variations with depth and the pore water pressures in the valley side slopes adjacent to Cow Green Dam.

In this n = 1 case, the potential in the basal underdraining layer cannot be constant unless it is also zero.

7.5. Analyses with Effective Stress Dependent Permeability

Problems where the permeability is effective stress dependent have solutions that are extremely *scale* dependent as well as being a function of the shape and type of the boundaries and the nominated stress-permeability function. Systematic, universally applicable, parametric studies are therefore not practical. (The simple mapping functions used above, section 7.3., no longer apply).

To demonstrate the effect of stress - permeability dependency on the seepage regimes in slopes a single model has been analysed. The details of the mesh and the solutions are shown on Figure 7.9. Underdrained and impermeable base solutions are made and plotted against constant permeability analyses for comparison. That the stress dependent cases exhibit relatively higher pore water pressures is immediately evident from the position of the equipotentials, but the effect is far more marked in the underdrained case than in the impermeable base solution.

For the above work the logarithmic stress - permeability function with a b parameter of 0.005 (equivalent at this scale to a twentyfold reduction of permeability across the greatest thickness of soil in underdrained case). The dominant total stresses have been taken to be the vertical ones and these are approximated by the thickness of soil above a particular point multiplied by the soil unit weight.

The salient pore water pressure depth profiles given on Figure 7.9 show how important the effective stress - permeability function is, and how its influence is particularly marked where underdrainage is present.

7.6. Sweeney's Model

In an M.Sc. thesis at Imperial College in 1970 Sweeney developed a simple method of analysing seepage in a zoned wedge of soil representing a stratified soil slope resting on an underdrained sub stratum (Figure 7.10). The key diagram shows a u = 0 upper boundary (i.e. potentials vary linearly along the slope face) and a linearly varying potential boundary at the base of the wedge.

If the soil is homogenous, then an equipotential is a straight line joining the two points of appropriate potential on the boundary. If the wedge is formed of two or more different soils then there must be a dogleg in the equipotential as flow is refracted across the soil boundary. The law governing this refraction is a simple function of the ratio of permeabilities on either side of the boundary and a dog legged line joining the two boundary potentials and yet satisfying this interface condition can be found by trial. Although in practical terms the more layers there are the more complex the problem is to solve, there are no additional theoretical complexities. It should be noted that a decreasing permeability with depth gives a bowed pore pressure depth profile (*cf* Chapter 2), and that the appropriate selection of boundary potentials and increasing permeability with depth can yield negative pore pressures throughout the whole slope section (See Section 7.9).

Unfortunately, Sweeney's model cannot be used for radial rather than circumferential* changes of permeability, since the method is based on the assumption that all equipotentials are geometrically similar. Thus effective stress dependent permeability cannot be included as the changes in total stress in the circumferential direction are larger at greater radii.

Sweeney's solution for a continuously varying permeability is naive and not soundly based in polar coordinate geometry.

The more marked the overall decrease in permeability is,the more the pore pressures and equipotentials close to the air face of the slope approach the infinite slope method's assumption of flow parallel to the slope.

Sweeney's results were verified by him using a lumped parameter electric analogue model. They can be obtained more easily by means of the finite element technique.

**The terms "circumferential" and "radial" are used in the sense of a polar coordinate system (r, θ) as denoting "constant r " and " constant θ " respectively.*

7.7. Results of the Parametric Study

The average potential in the triangular region (Zone 1 - Figure 7.4) which comprises the main body of the slope was evaluated by sampling the points on the equipotential plots with the aid of a transparent overlay mask at the points required by Hammer's integration rule for the triangle (below, and Figure 7.8). Since the datum for potentials is at the bottom of the slope and the maximum potential is at the crest of the slope, the average (sampled and weighted) potential can be non-dimensionalised by dividing by the slope height.

Next, the average pore water pressure can be found by subtracting the average elevation of Zone 1 (with respect to the datum) from the average potential. This elevation is $\frac{1}{3}$ of the slope height so the value to be subtracted, when non-dimensionalised as in the case of the potentials, becomes $\frac{1}{3}$.

The resulting values have been plotted in Figure 7.6 as points on a plot of "depthfactor n" against "slope angle", both axis parameters being modified so as to give convenient scale ranges. Equi-pore water pressure lines have been drawn for both the impermeable and permeable base solutions, the latter having no overall underdrainage.

The average pore pressure ratio $\bar{r}_u$ can be found by dividing this average pore pressure by a further parameter representing the average total stress in the slope, or more exactly by

$$\bar{r}_u = 3 \bar{R} \frac{\gamma_w}{\gamma}$$

where $\bar{R}$ is the non-dimensionalised pore pressure from Figure 7.6 and the average total stress divided by the slope height is given by $\gamma/3$

Table 7.1. Analyses Carried Out in Slope Seepage Parametric Study

SLOPE ANGLE =	1:1	1:2	1:3	1:4	1:5
DEPTH FACTOR n					
1*	✓	✓	✓	✓	✓
1.5	✓	✓	✓	✓	✓
2	✓	✓	✓	✓	✓
3	✓	✓	✓	✓	✓
6			✓		
11			✓		

**These analyses using a different mesh with a "wedge" of soil only. Compare to the results of Sweeney (1970).*

For $\gamma = 2\gamma_w$ the plot yields virtually the correct value for $\bar{r}_u$ of 0.5 for the impermeable base case when the slope angle is zero. This result is not duplicated with the permeable base solution and this may be the result of an invalid extrapolation.

A depth factor of 1 cannot validly be taken other than for complete underdrainage in the permeable base solution.

Care must therefore be exercised when using the extrapolation outside the range of the numerically evaluated points (shown by bold triangles on the plot). The equi-pore pressure lines are shown as a row of symbols as a reminder of this.

Calculation of the Average Pore Water Pressure Head in the Slope:
The parametric study indicates fairly uniform potential distributions in each case, and a simple, numerical integration scheme has been used within the triangularsubregion of the slope itself (the zone marked as "zone 1" in Figures 7.3 and 7.4 a to z inclusive). This scheme is detailed in Zienkiewicz (1972) p. 151, table 8.3 and credited to Hammer *et al* (1956) and comprises sampling points at the centroid, mid-points of the sides, and apices, with weights of 27/60, 8/60 and 3/60 respectively (See Figure 7.8). As all the slope transformations are linear, this integration is independent of whether the section is transformed or not.

The averaged pore water pressure is plotted as a function of the ratio average pore pressure head to slope height against slope angle and depth factor in Figure 7.6.

Notes on the Use of the Parametric Study in Practice:

The results of this parametric study can be used in routine slope design as follows:-

1. On a section through the proposed slope, select the mean depth to the zero pressure line, modified as appropriate for any special conditions, e.g. drains etc., at the toe and crest of the slope.

2. Perform any transformations for anisotropic permeability, or permeability varying with depth. (Do this tranformation for the part of the section *underneath* the zero pressure line).

3. From the transformed section, take off the slope inclination and depth factor.

4. Using these two factors, determine the average pore water pressure to slope height ratio from Figure 7.6 and hence evaluate the average pore water pressure head in the soil.

5. Using now the *real* slope height, determine the average vertical total stress.

6. Derive the average pore pressure ratio r_u and use this in orthodox slope stability charts to predict the stability of the slope.

This entire process is illustrated in Figure 7.7.

7.8. Lafleur and Lefebvre's Work

The results of a similar study to that described above have recently been published (Lafleur & Lefebvre 1980). They use the finite element method using Neuman and Witherspoon's (1970) method for analysing free surface problems. Their model is largely similar to that of Figure 7.1 but the complete slope is mantled by a zone of high permeability which they term "the upper aquifer". Beneath the soil comprising the slope is a "lower aquifer" which itself rests on an impermeable basal boundary. This lower aquifer is therefore *confined* (Figure 7.11, which draws heavily on their Figure 1) except in their analyses where the lower aquifer occupies a large proportion of the slope as well as underlying it.

The first important finding of their work is that for reasonable infiltration rates the water table was brought to the surface of the upper aquifer (implying run-off). They were therefore able to dispense with this refinement in the remainder of their analyses, taking the upper surface of the problem to be "wetted". This is in accord with the treatment given herein, which was decided upon on the basis of deduction, rather than trial.

Secondly, they find that seepage is effectively parallel to the slope at shallow depths and take this as support for the usual "flow parallel to the slope" assumption made in the infinite slope method of analysing shallow superficial slides.

In their parametric study, they take a depth of soil equal to twice the slope height, and consider different ratios of lower aquifer thickness to total thickness. The lower aquifer is taken to be ten times more permeable than the soil above. This has the effect of decreasing the effective soil thickness to slope height ratio and furthermore establishes a more efficient horizontal connection at the base of the upper layer. This is best visualised by imagining the necessary scale transformation. It is therefore only their "no aquifer" case that is strictly comparable with any part of the study described in previous sections, although one or two other cases are possibly analogous and could be compared if the relative permeability/space transformations were sorted out. The Lafleur and Lefebvre analyses are all of the impermeable base kind in the context of the writer's parametric study. However, the strong upward hydraulic gradient patterns at the toe of the slope found in Section 7.7 are repeated here, but are exacerbated as the lower aquifer thickness increases. A complete change occurs when the lower aquifer thickness is such that it is no longer confined - after this,it has the effect of *underdraining* the slope and the pore pressure conditions become greatly improved.

A second part of the paper shows the effect of the different seepage regimes on the factor of safety evaluated using slip circles. It is not surprising that where the lower aquifer is punctured, and the artesian pressures in it released, the factor of safety rises substantially.

The third, and largest part of the paper is devoted to four case histories. In the first of these, there *is* underdrainage overall (i.e. it is not an "impermeable base" solution) and the slope-forming clays are sub-divided into three layers. Since the permeability decreases in the deeper layers, substantial *perched water table* effects are found (*cf* my Chapter 2). The strong underdrainage leads to flow being largely vertical in character.

In the remaining three case histories, the geometry is more complex than in the initial parametric study, but they are to all intents and purposes the same problem. The agreement between observed and predicted piezometric heads is good, although in one case anisotropic permeabilities have to be invoked to obtain this good fit.

In conclusion, Lafleur and Lefebvre have demonstrated important effects, confirmed by the writer's own parametric study.

7.9. Permeability Changing with Depth

Much of this thesis is concerned with the variations of permeability with effective stress and the details of the analytical methods needed to deal with this case. This, in an underdrained field situation leads to a perched ground water table effect with a hydrostatic pore pressure/depth distribution over part of the thickness of soil and an intense draw down at the base. On the whole, this can be simulated by an *a priori* subdivision of the soil into layers of pre-defined permeability with the physically lowermost strata having the lowest permeability; this may be a realistic assumption if the soil is layered in that way.

A paradoxical situation arises if, in an underdrained soil layer, with a slope formed in its upper surface, the permeability *increases* with depth. Consider again the completely underdrained soil column of Section 2. If now, instead of a decreasing permeability with depth, we have an increasing permeability, it is found that for continuity a decreasing hydraulic gradient with depth is required. This can only be achieved with negative pore water pressures in the profile.

Not only does the geotechnical engineer have a great reluctance to rely on negative pore water pressures for the stability of his slopes, but also in cases where they are predicted, it is found that the conventional free surface cannot be found, or takes up a position which is not physically realistic.

This will be illustrated by a case study rather than a parametric study, and is an analysis of a tailings dam at Choppington Brickworks, Cheshire. The problem was first posed by J. Mawditt of Bullen & Partners

and the analyses were carried out using Taylor & Brown's (1967) method under the auspices of Structures & Computers Ltd., whose director Dr. P. K. T. Lim and Mr. Mawditt the writer thanks for permission to include this study in the thesis.

A stylised cross section of this tailings dam in shown in Figure 7.12 and the permeabilities of the three strata increase by a factor of 10 (i.e. the lowermost stratum is 100 times more permeable than the dam fill. The site is perfectly underdrained by underground workings. After numerous trials, no free surface linking the head- and tail-water could be found. This was initially thought to be the result of the eclipse of part of the finite element mesh in the iteration (Section 3.5), and so the problem was re-analysed with constant permeability. Unacceptable mesh distortions still occurred, and on following the process with a slow convergence factor it was found that the seepage regime was attemting to bifurcate (Figure 7.12) and form two independent flow nets. These could only be made to coalesce if a permeability anisotropy of more than 200 times was assumed ($k_h > k_v$). Very much greater relative permeability anisotropies were required to bring the free surface into the main part of the slope.

Even with high relative anisotropy in the strata a stable free surface position could not be found when the stratified, increasing permeability with depth, properties were re-introduced. The problem was then analysed with the wetted boundary condition assumed on the air face of the dam. In this analysis, extensive zones of negative pore water pressure were predicted. It is felt that these account for the convergence problems as it should be observed that in the constant permeability, bifurcated flow patterns, seepage is largely in the vertical direction and the zero pore pressure free surface condition is incompatible with the negative pore water pressures predicted in vertical seepage earlier in this section.

Lafleur and Lefebvre (1980) do not find these negative pore water pressures since the only case of theirs which is totally underdrained (their Site No. 1 - Hull) has a decreasing permeability with depth. Furthermore, their second case (Saint-Urbain) and their case study with an outcropping lower aquifer only has *local* rather than complete underdrainage. The confined nature of the lower aquifer in their remaining two cases also acts against the effect.

The influence of an *effective stress dependent* permeability (and also where the permeability decreases with depth) can be described as follows:

(a) Lafleur and Lefebvre's model, lower aquifer fully confined:

The downward flow zone from the crest of the slope enlarges due to the increased impedance to flow at the base of this zone. At the toe, although the size of the artesian flow zone is laterally compressed, the pore water pressures are relatively unaltered.

(b) Same model as (a), lower aquifer outcrops:

The perched water table effect in the upper soil is exaggerated.

(c) Same model as (a), no lower aquifer:

The results are similar to (a) except that it is harder to differentiate between the dlownflow and upflow zones. Equipotentials are shifted downflow in every case and pore water pressures do rise under the slope toe. There is, of course, a transition between (a) and (c) when the aquifer thickness is small.

(d) Section 7.3 model, impermeable base:

As (c).

(e) Section 7.3 model, no (or moderate) underdrainage

As (a).

(f) Section 7.3 model, strong underdrainage

As (b) but more intense.

7.10. Comparison of the Theory with Field Measurements

The parametric study and the analyses using effective stress dependent permeability show how important it is to establish the hydraulic boundary conditions at the base of the soil layer in which the slope is formed. When computing the pore pressures at depth this is far more important than the precise nature of the boundary conditions assumed for the air face of the slope.

At Herne Bay in Kent (Ove Arup & Partners 1970, Bayley 1971) the partly underdrained slope was systematically instrumented with piezometers. In broad terms the equipotentials obtained were similar to the lowest diagram in Figure 7.9 except that the pore water pressures under the slope face still reveal the effects of the undrained unloading of excavations due to landsliding, marine erosion and regrading as part of a cliff stabilisation scheme (Bromhead 1972). It is not clear whether the pore water pressure depth profiles obtained at that site were the result of an effective stress dependent permeability or the result of intrinsic properties of the soil. Since the transition from the London Clay into the underlying Oldhaven Beds is accompanied by an increasing fraction of fine sands and silts, the latter explanation appears less likely.

Walbancke, 1976, investigated a variety of slopes but with comparatively shallo borings to find evidence for the incomplete equilibration of pore water pressures. These did not penetrate far enough to reveal the position of the interface with more permeable strata at depth nor did they establish the value of the potential at that position.

Lafleur & Lefebvre, 1980, compare the results of their own parametric study with field measurements at four sites. This is discussed in detail in the previous section (above).

Finally, James' (1970) observation of an average r_u of about 0.3 in numerous piezometric measurements in London Clay slopes (principally railway cuttings). This value can easily be obtained approximately from Figures 7.6 and 7.7 taking say a 10m high slope with the zero pressure line about a metre below the surface and a depth factor greater than 2, and β about 1:3.

7.11. Pore Pressure Changes Accompanying Excavation and Equilibration Rates

A number of authors have analysed excavations in soil with various stress-strain relationships to attempt to follow progressive failure from the pioneering work of Dunlop & Duncan 1970 to the present. To simulate delayed failure of excavation sidslopes a variety of mechanisms have been proposed, the most convincing being Vaughan & Walbancke's (1976) treatment of the problem in terms of the equalisation of stress induced pore water suctions. At the instigation of Dr. Vaughan and with the aid of Dr. Walbancke one of Walbanckes case histories was analysed firstly by a linear elastic finite element method to discover the stress changes accompanying excavation (done as a single stage, admissable for stresses in the linear elastic case, Lopes 1979). Pore pressure changes were computed using Henkel's α parameter, averaged at nodes, added to an initially steady no-flow pore pressures and dissipated by Zienkiewicz & Parekh's method. (Bromhead 1972) "Constant strain" triangular elements were used for both the stress and dissipation analyses.

The opportunity has been taken to re-appraise these analyses since the slope model used was similar to that used for the steady seepage analyses in the present work since there might be some advantage in following the general approach using more sophisticated elements

and so forth. In the event it was found that the major problems were not those associated with the elements used especially in the dissipation analysis. The broad conclusions were as follows:-

(a) The stress changes produced were crucially dependent on the nature of the stress and displacement boundaries selected and on their position (Gibson 1974) reports extreme instances of the role of the boundary conditions on settlements where the modulus varies with depth).

(b) The use of a linear elastic model will imply undrained failure of even fairly stiff overconsolidated soils. The magnitude of these failed zones depends on the in-situ K_o value before excavation begins.

(c) Since due to the factors in (a) and (b) above soil elements do not follow the correct total stress path (and in fact move into inadmissable parts of the total stress space) the pore pressures predicted are largely incorrect.

On the basis of the first three conclusions above it was felt that a non-linear stress analysis was called for and some attempt made to link the pore pressure changes to the total stress path followed.

(d) The constant strain triangle is unsuited to stress analysis as it leads to stress jumps of considerable magnitude between elements (unless very large numbers of elements are used).

(e) Despite the foregoing the dissipation analysis showed that significant pore pressure changes were still taking place at considerable times after excavation - with parameters selected to be appropriate to the London Clay the times for equalisation to be largely complete were larger than the timescale for delayed failure.

(f) The pore pressure regime to which the pore pressures in the slope equalised were highly dependent on the seepage boundary conditions selected, but the overall timescale was independent of this.

In the light of Chapter 2 and parts of this Chapter, conclusion (f) can be extended to include the effects of permeability variations particularly those due to changes in effective stress.

The extent and nature of computations necessary to improve on the earlier conclusions lying outside the central theme at present being explored have led to this not being further dealt with.

7.12. Conclusions

The parametric study shows that steady, equilibrated pore water pressures in slopes are highly dependent on the degree of underdrainage into underlying soils, but if the underlying soils are impermeable the pore water pressures are largely independent of slope angle and that an average pore pressure ratio of about 0.25 - 0.30 is found.

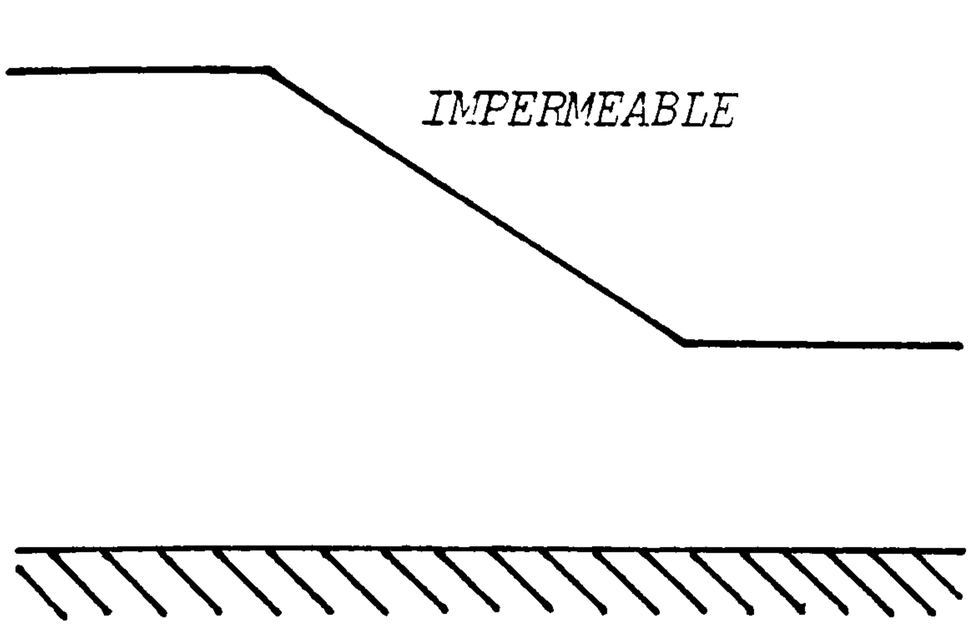
By "insulating" the slope from the influence of any underdrainage, the effect of a permeability that decreases with depth or which is dependent on the magnitude of effective stress is to make the seepage regime in the slope approach the "impermeable base" case.

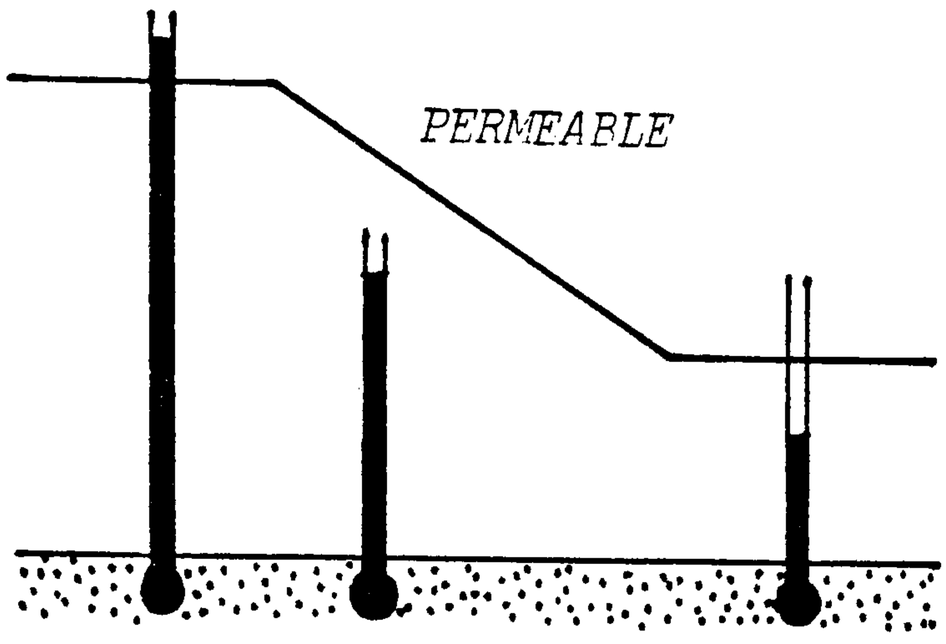
On deductive, physical and numerical grounds the wetted upper boundary case is more appropriate to the analysis of seepage in clay slopes than is the free surface case. Computational difficulties may attend the use of iterative techniques for locating the free surface if the permeability increases with depth in an underdrained situation.

In many cases flow close to the air face of the soil tends to be parallel to the slope.

Vaughan and Walbancke's conclusion is found only to be valid for very strong degrees of underdrainage or where the permeability increases with depth.

Basal boundary conditions

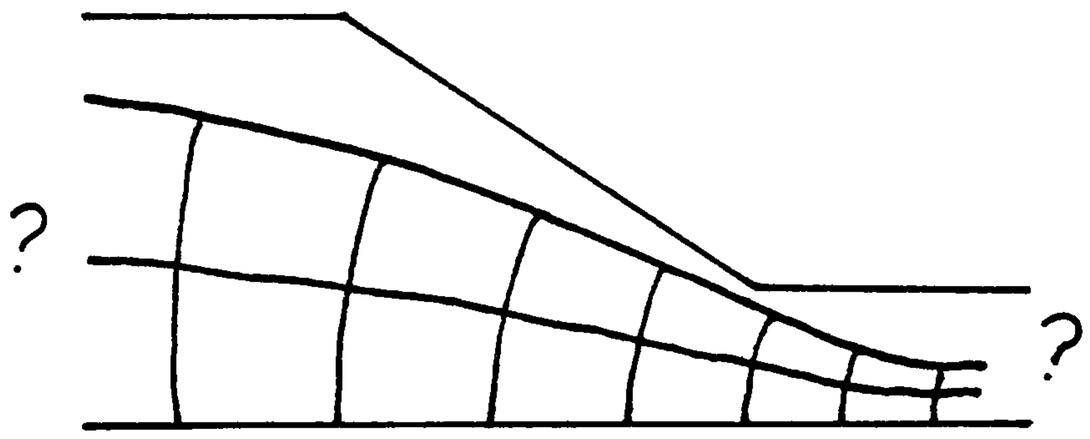




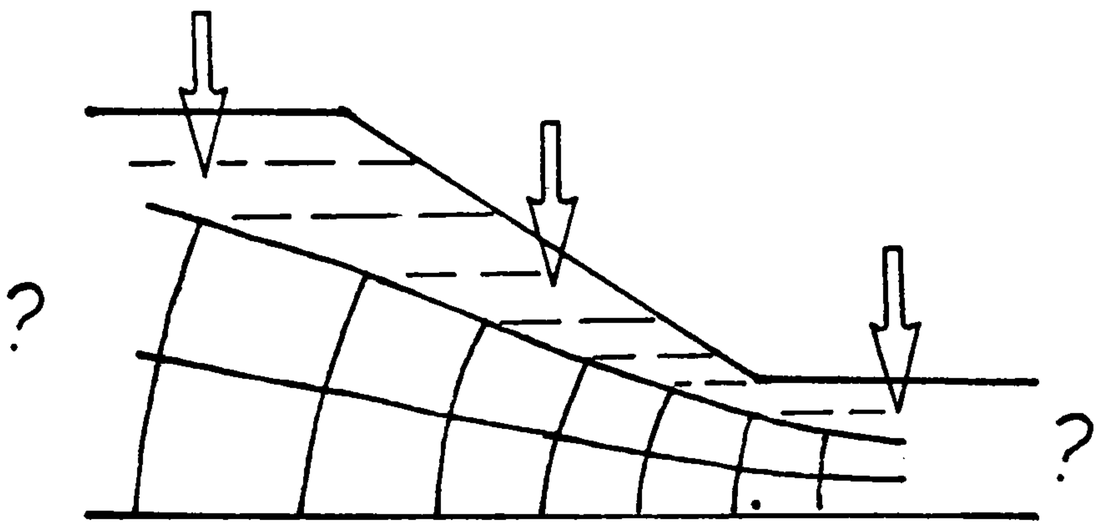
Artesian *Underdrained*

Transitional

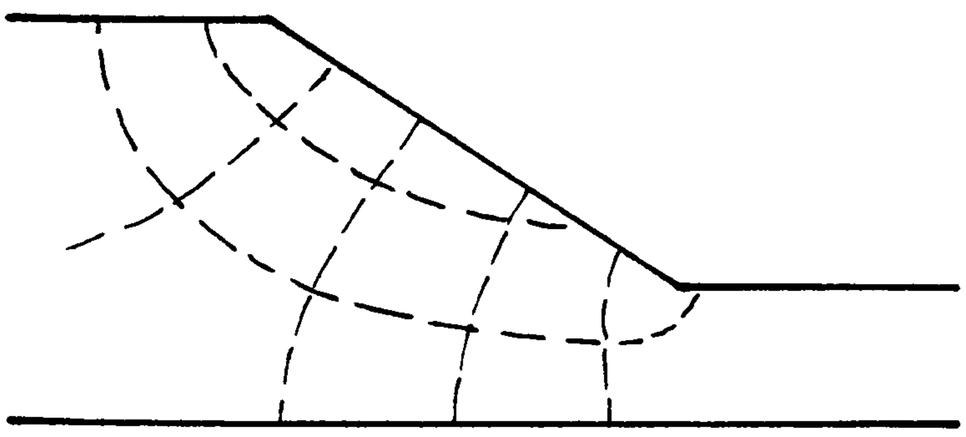
Surface boundary conditions



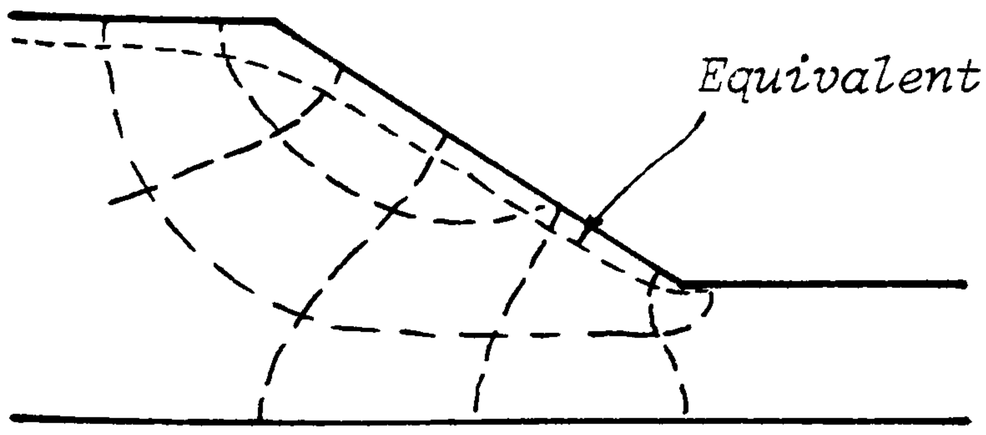
Free surface - involves cross flow



Infiltration through partly saturated zone.



Wetted boundary, u = 0



Wetted boundary, u < 0

Figure 7.1. Seepage in slopes and boundary conditions.

Flow nets are diagrammatic and based on the impermeable base case.

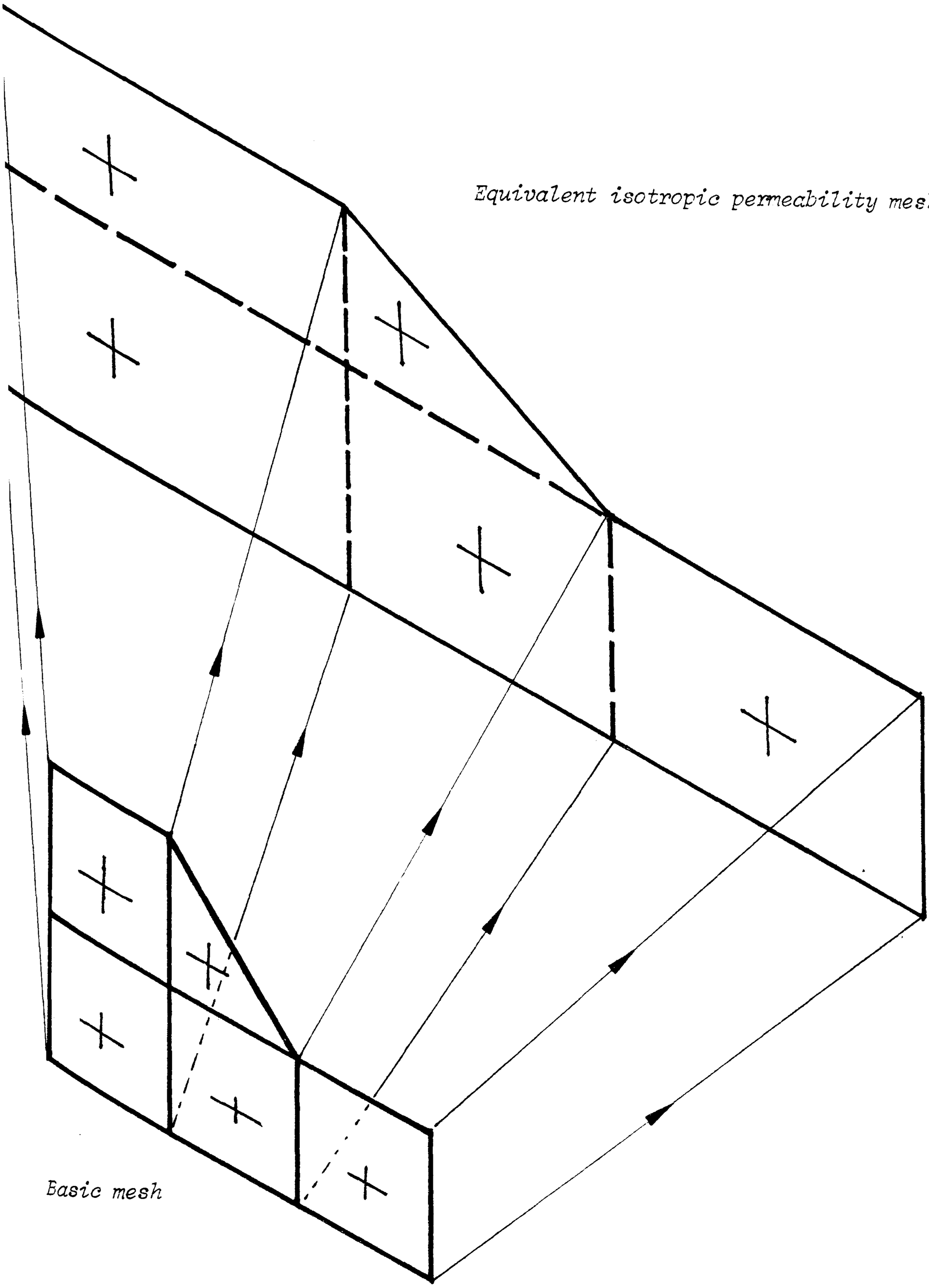


Figure 7.2. Use of non-homogenous permeability to transform the geometry of a single finite element mesh. (See section 7.3).

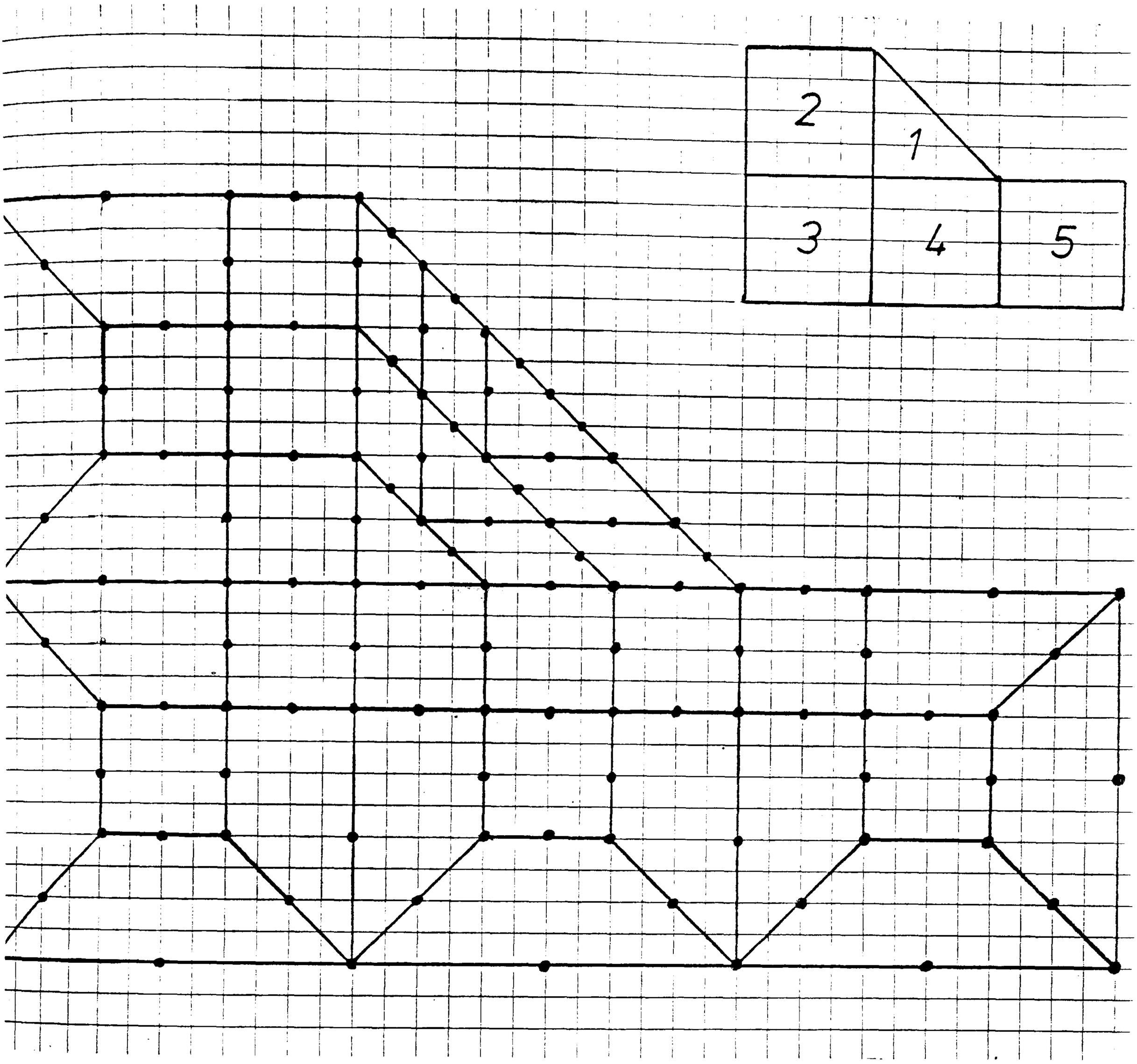


Figure 7.3. *Basic finite element mesh and zoning convention for parametric study.*

See Table 7.1 and Figures 7.2 & 7.3 for an explanation of the range of this parametric study, and for details of the parameters and transformations used.

All the results have been plotted automatically on to the basic (ie untransformed) finite element mesh.

Equipotentials at 10% potential drops are plotted. Figs 7.4 & 7.5

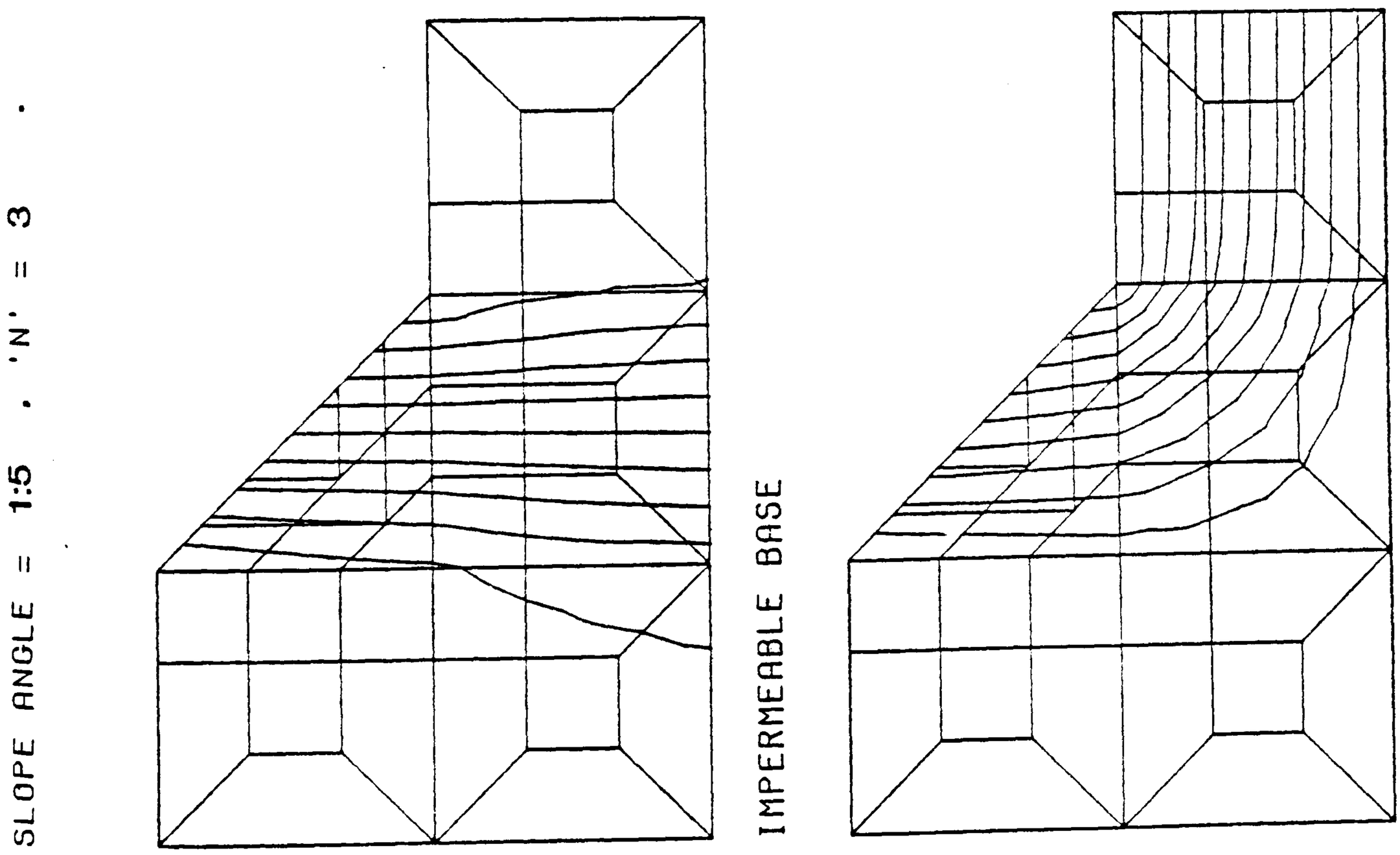
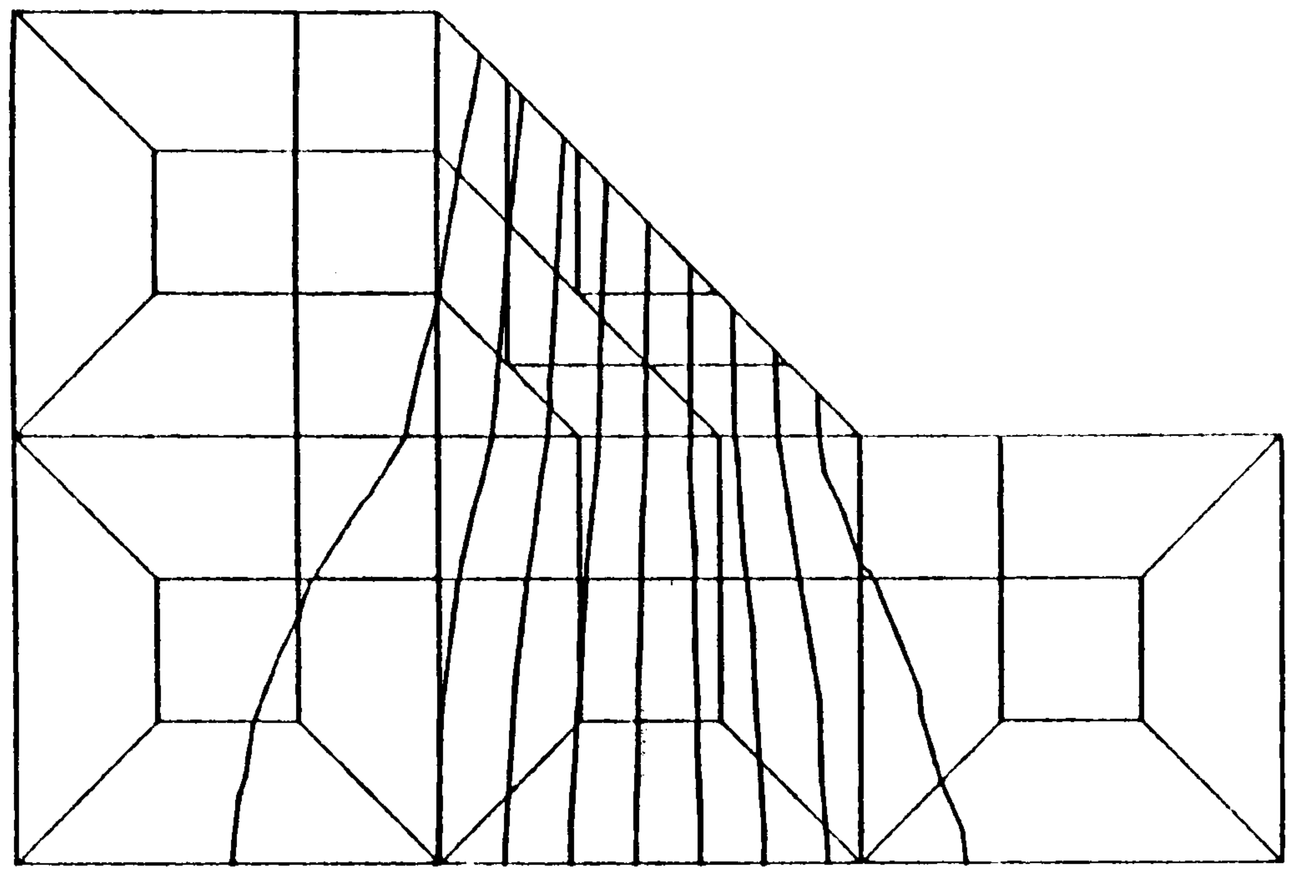
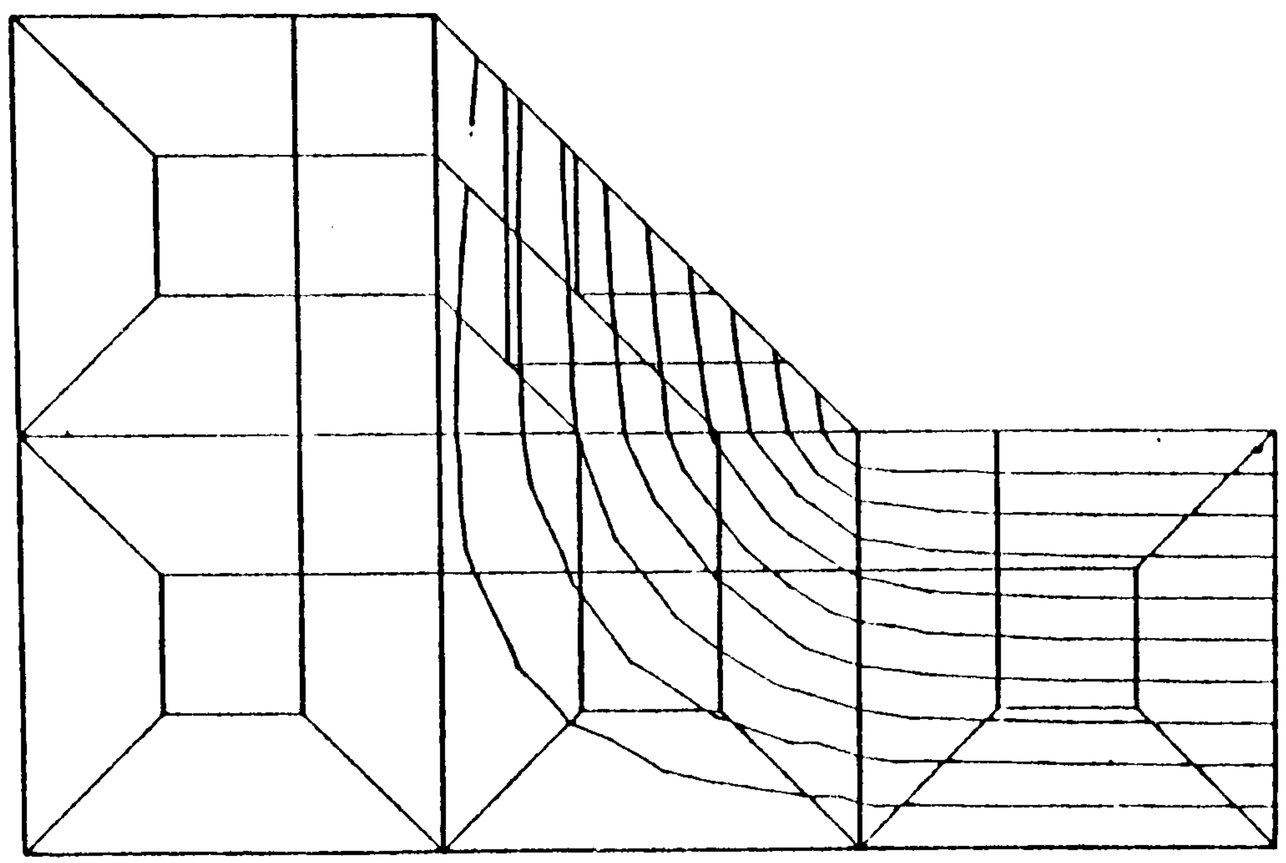


Figure 7.4. (A) Seepage in slopes: main parametric study.

SLOPE ANGLE = 1:4 . 'N' = 3 .

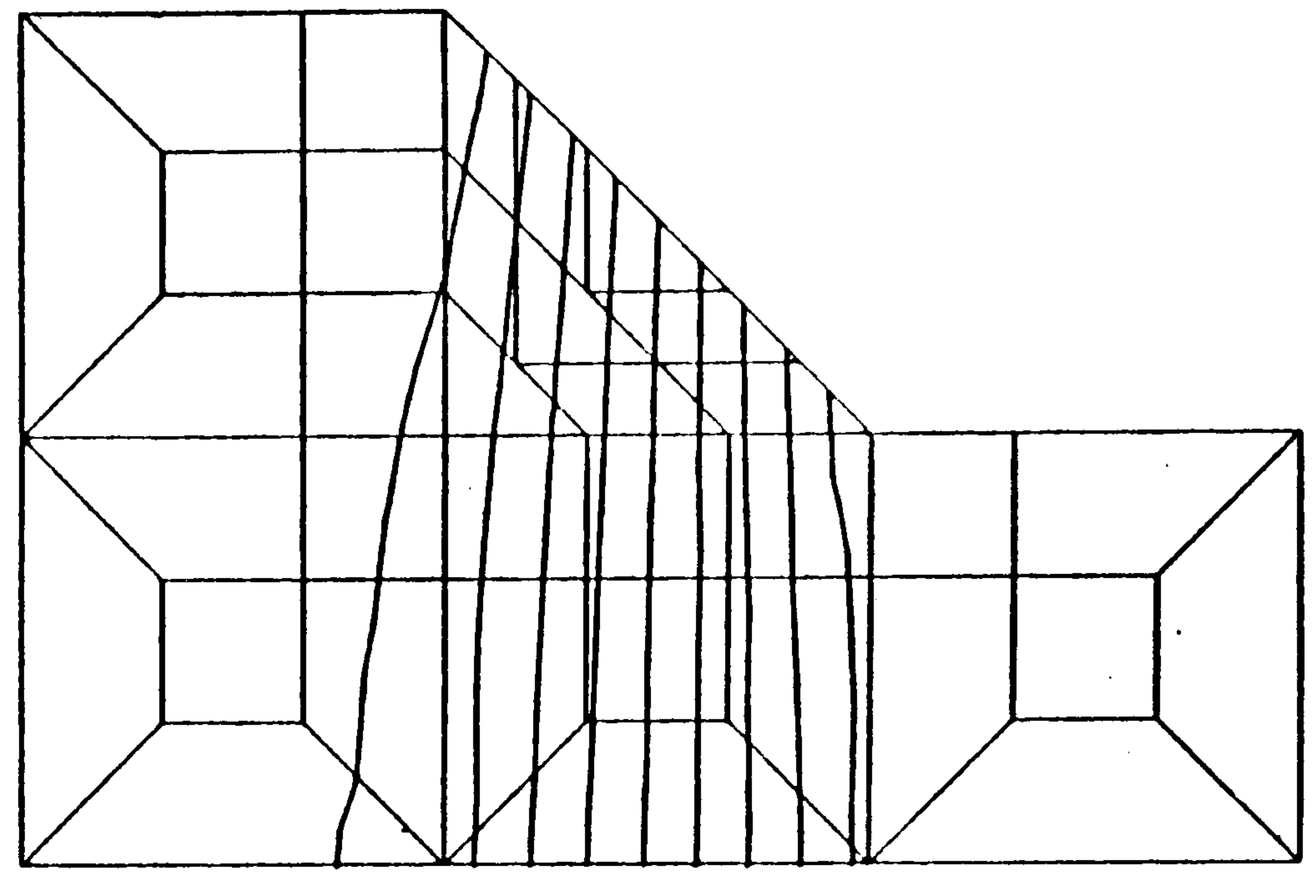


IMPERMEABLE BASE

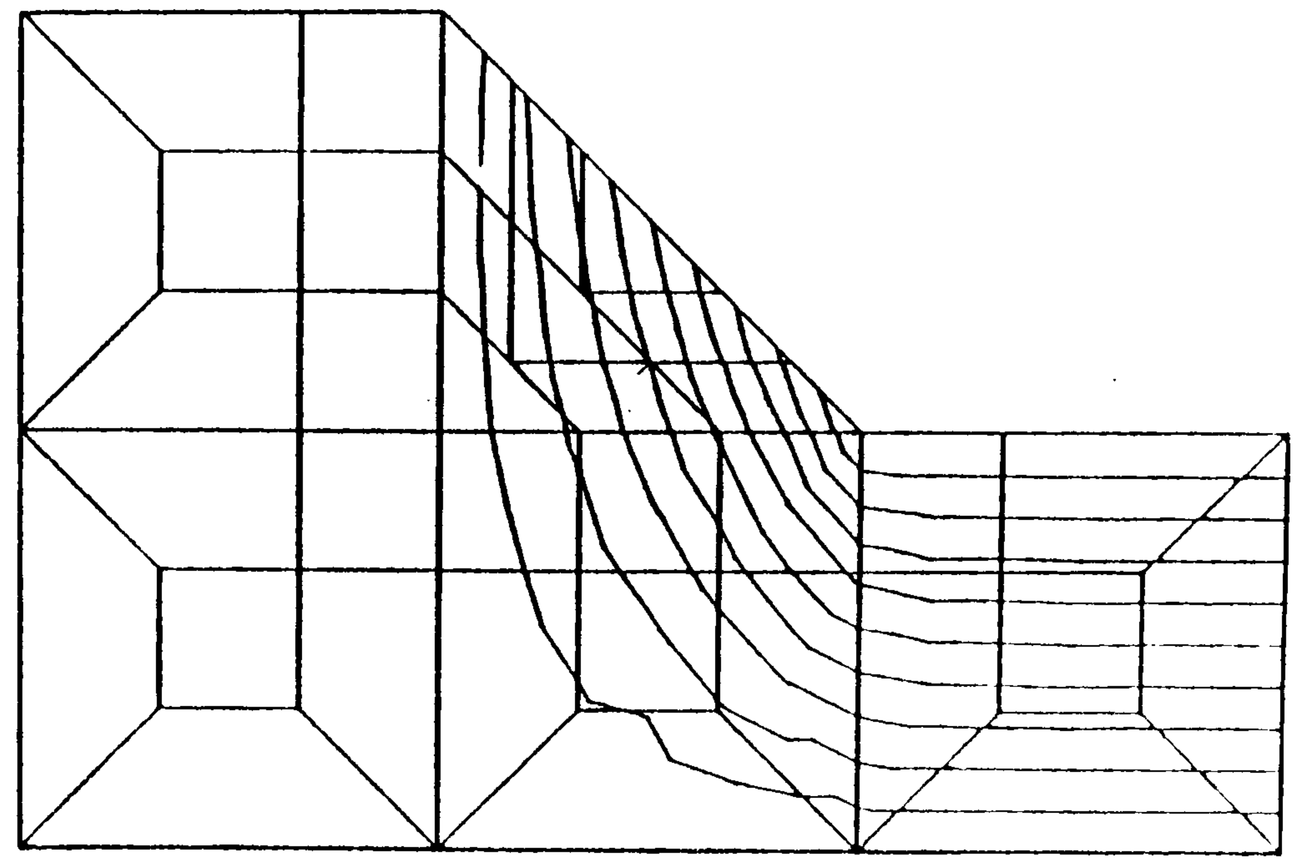


NO UNDERDRAINAGE

SLOPE ANGLE = 1:4 . 'N' = 2 .



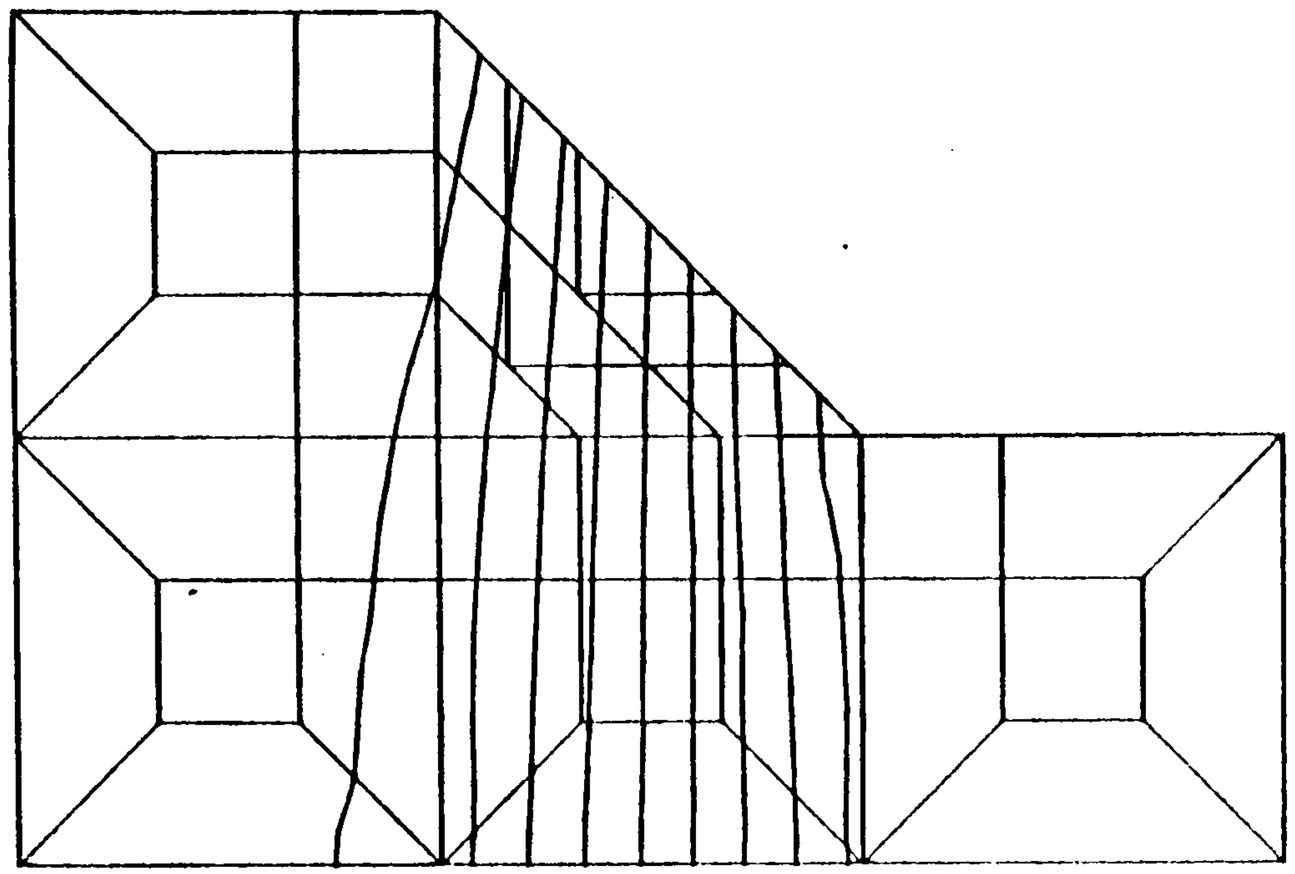
IMPERMEABLE BASE



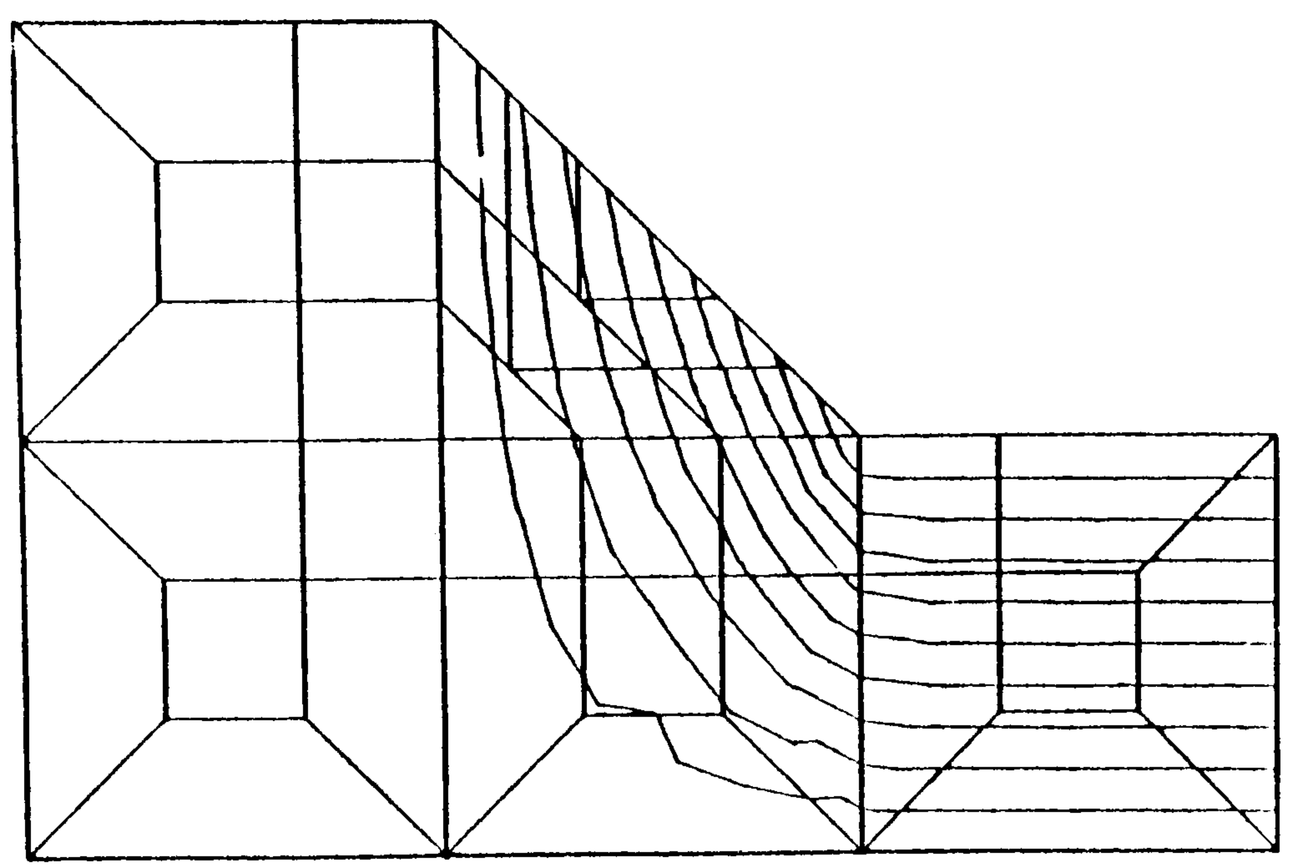
NO UNDERDRAINAGE

Figure 7.4. (B) Seepage in slopes: main parametric study.

SLOPE ANGLE = 1:5 , 'N' = 2 .

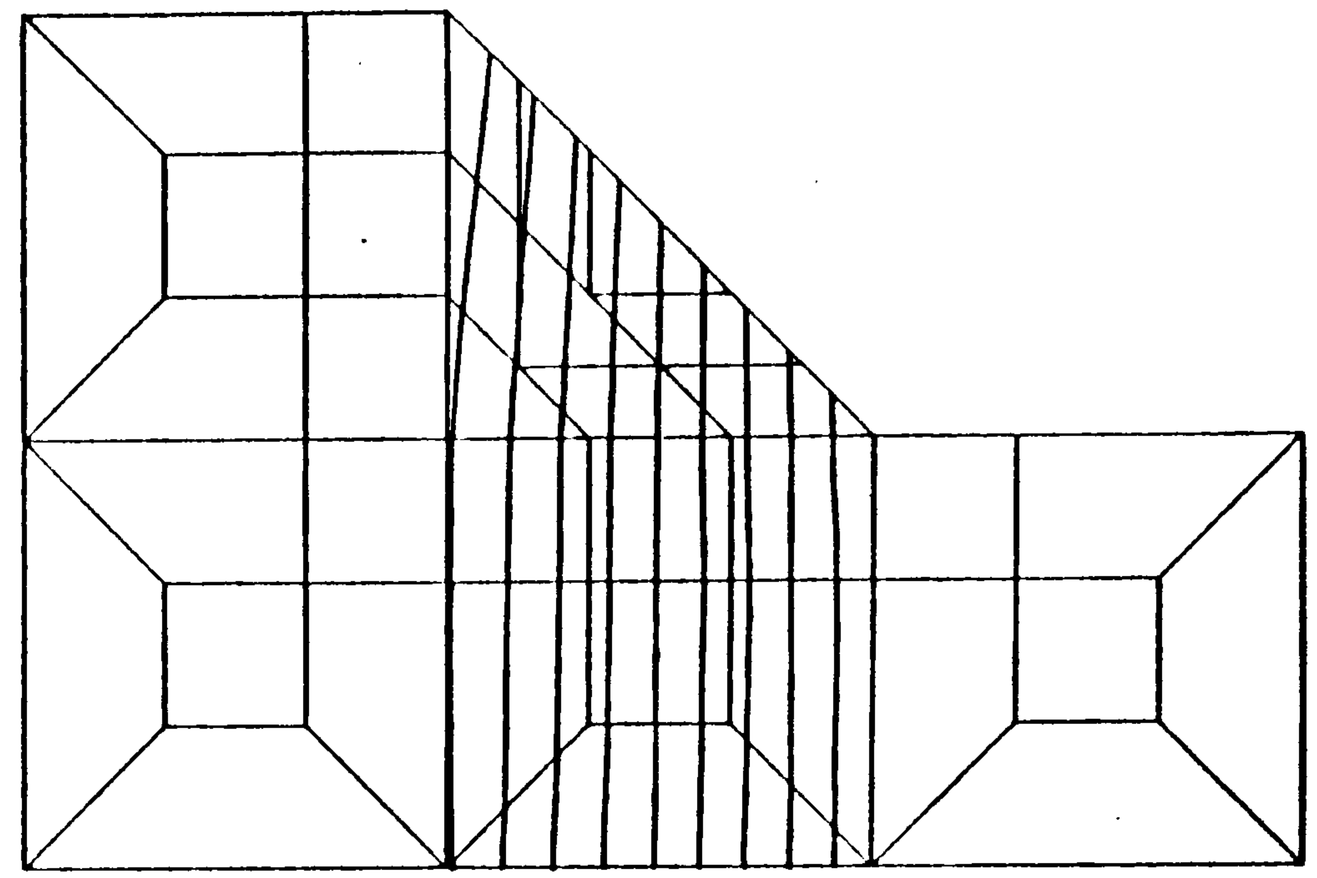


IMPERMEABLE BASE

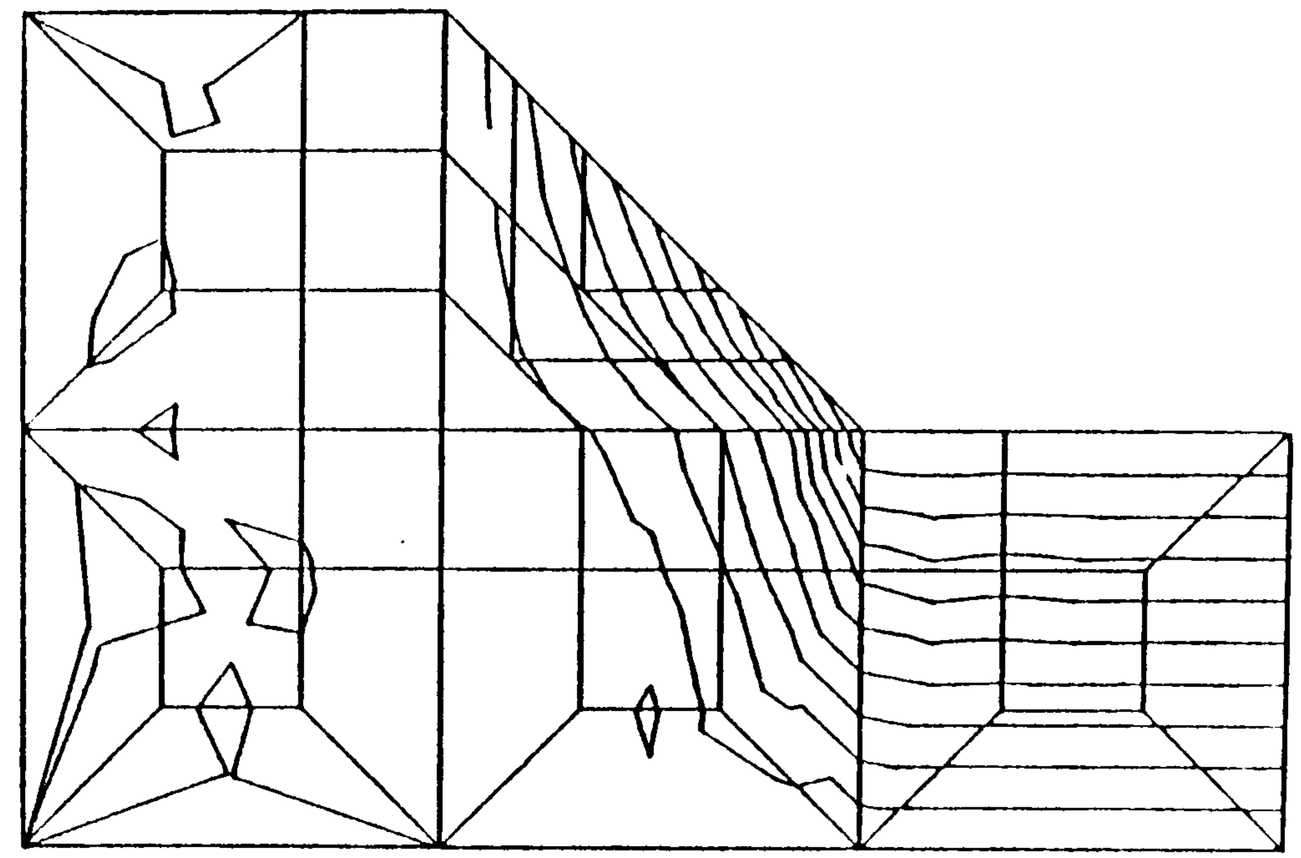


NO UNDERDRAINAGE

SLOPE ANGLE = 1:5 . 'N' = 1.5 .



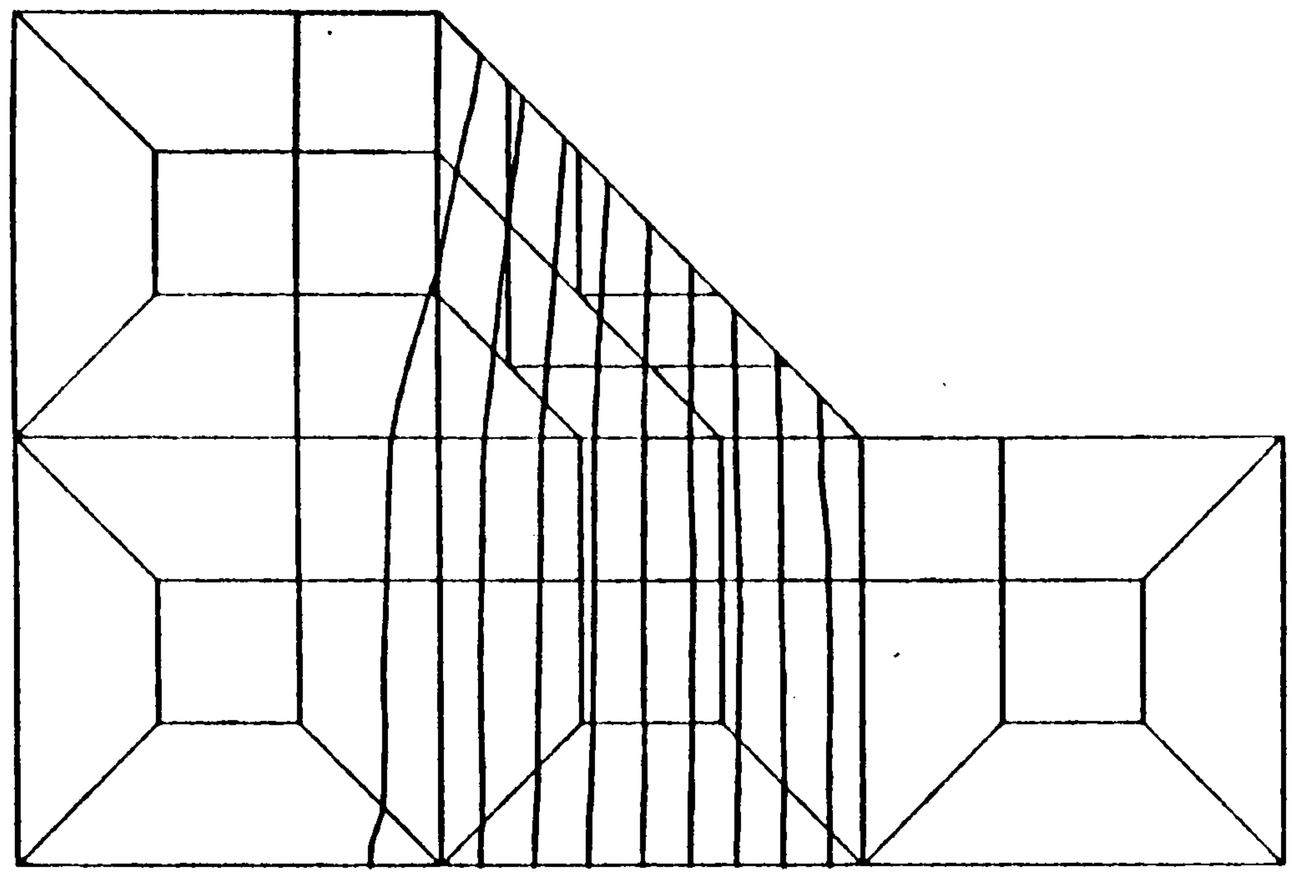
IMPERMEABLE BASE



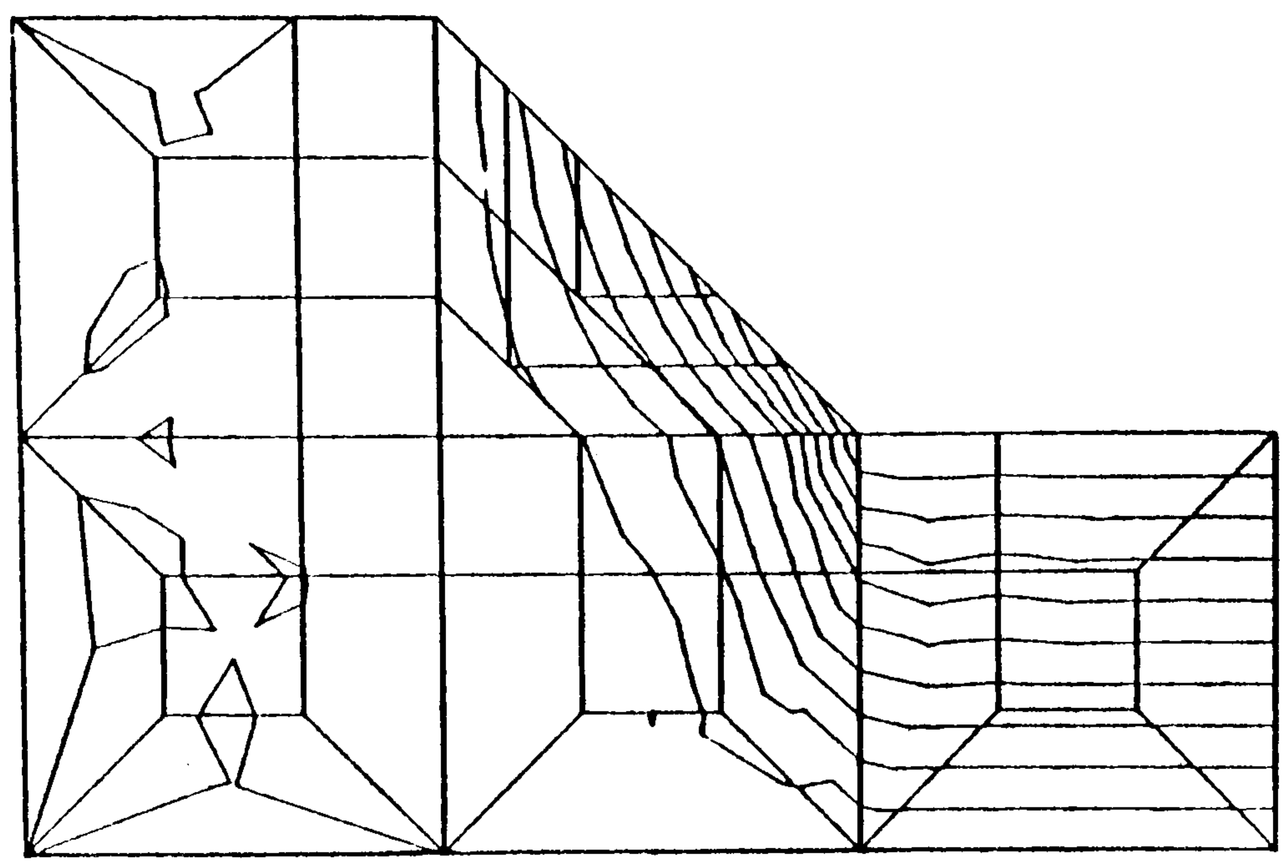
NO UNDERDRAINAGE

Figure 7.4. (C) Seepage in slopes: main parametric study.

SLOPE ANGLE = 1:4 . 'N' = 1.5 .

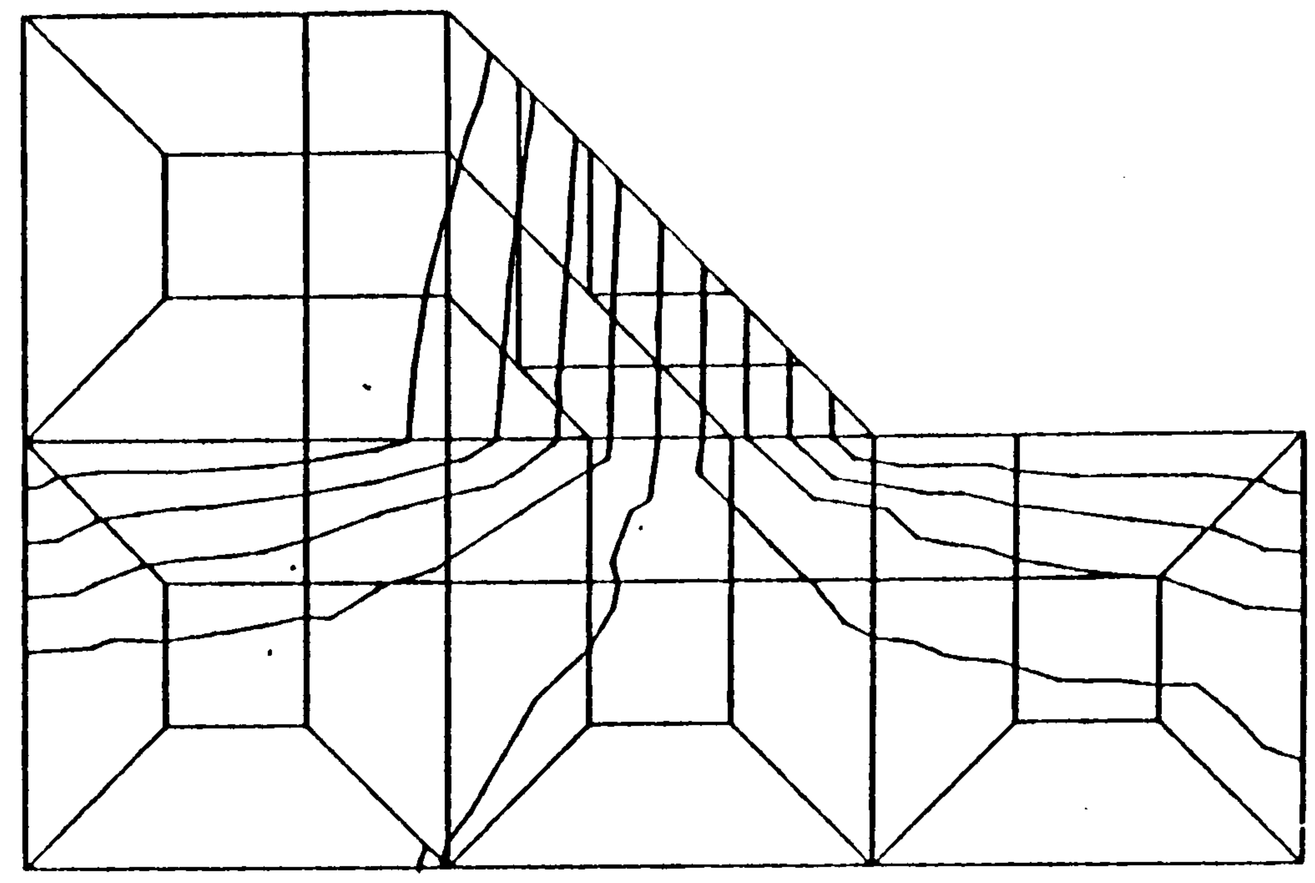


IMPERMEABLE BASE

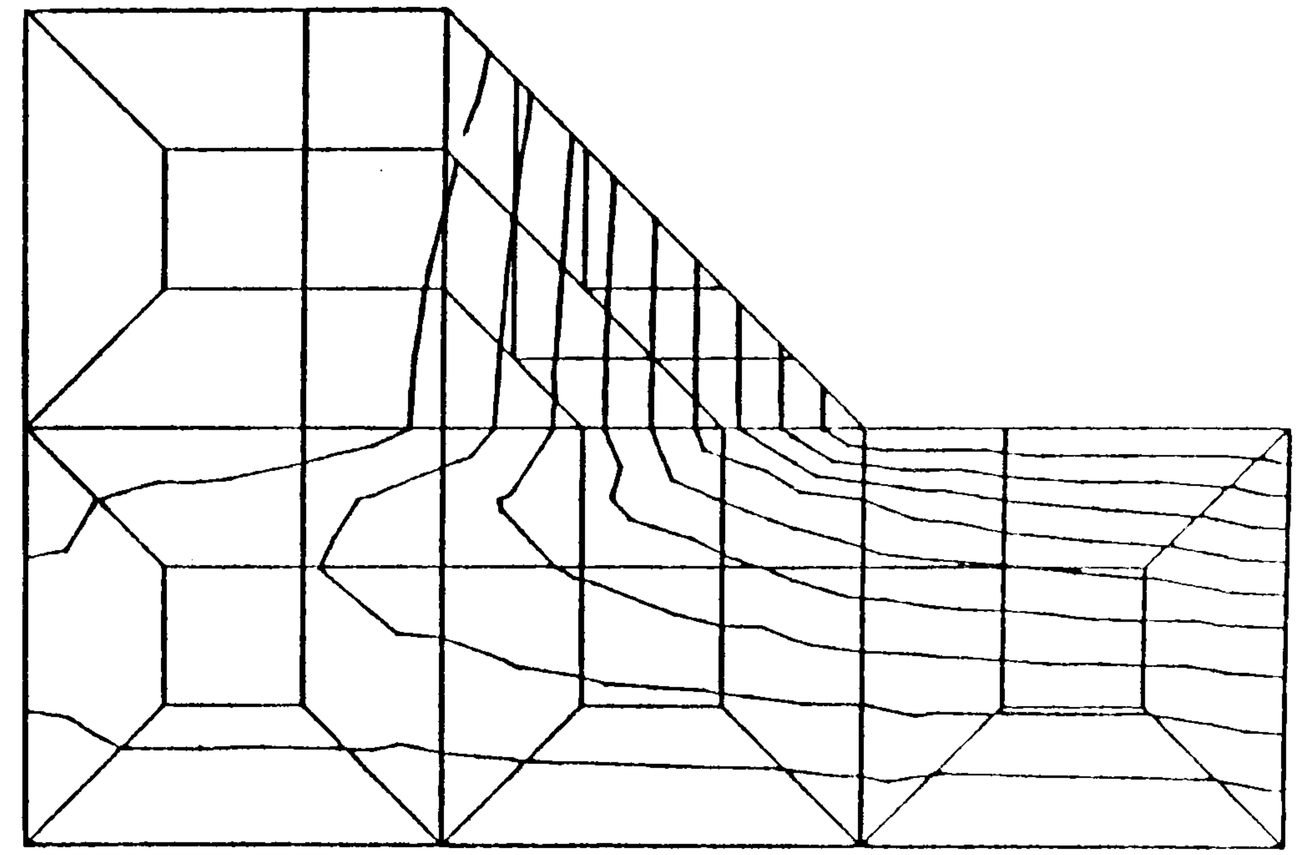


NO UNDERDRAINAGE

SLOPE ANGLE = 1:3 . 'N' = 11 .



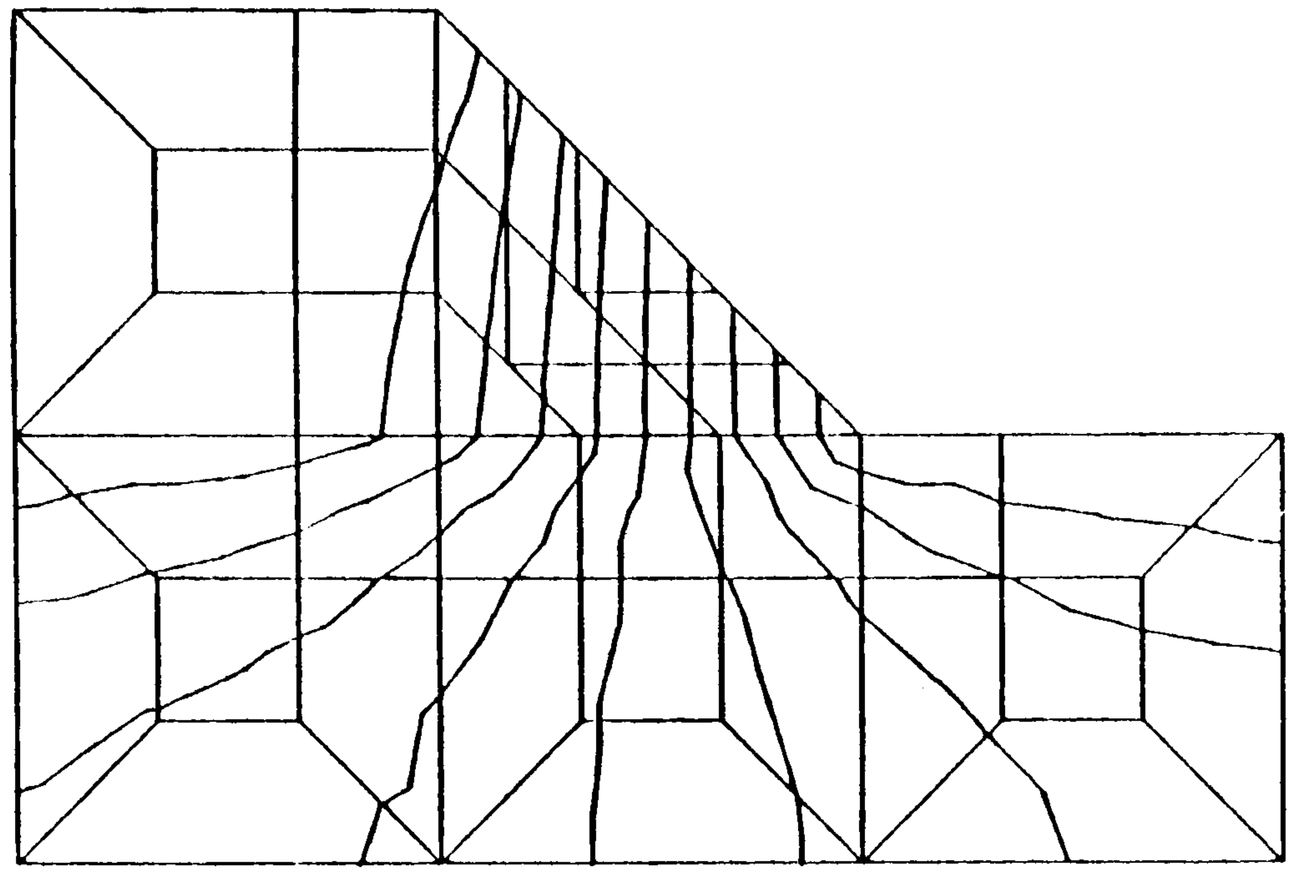
IMPERMEABLE BASE



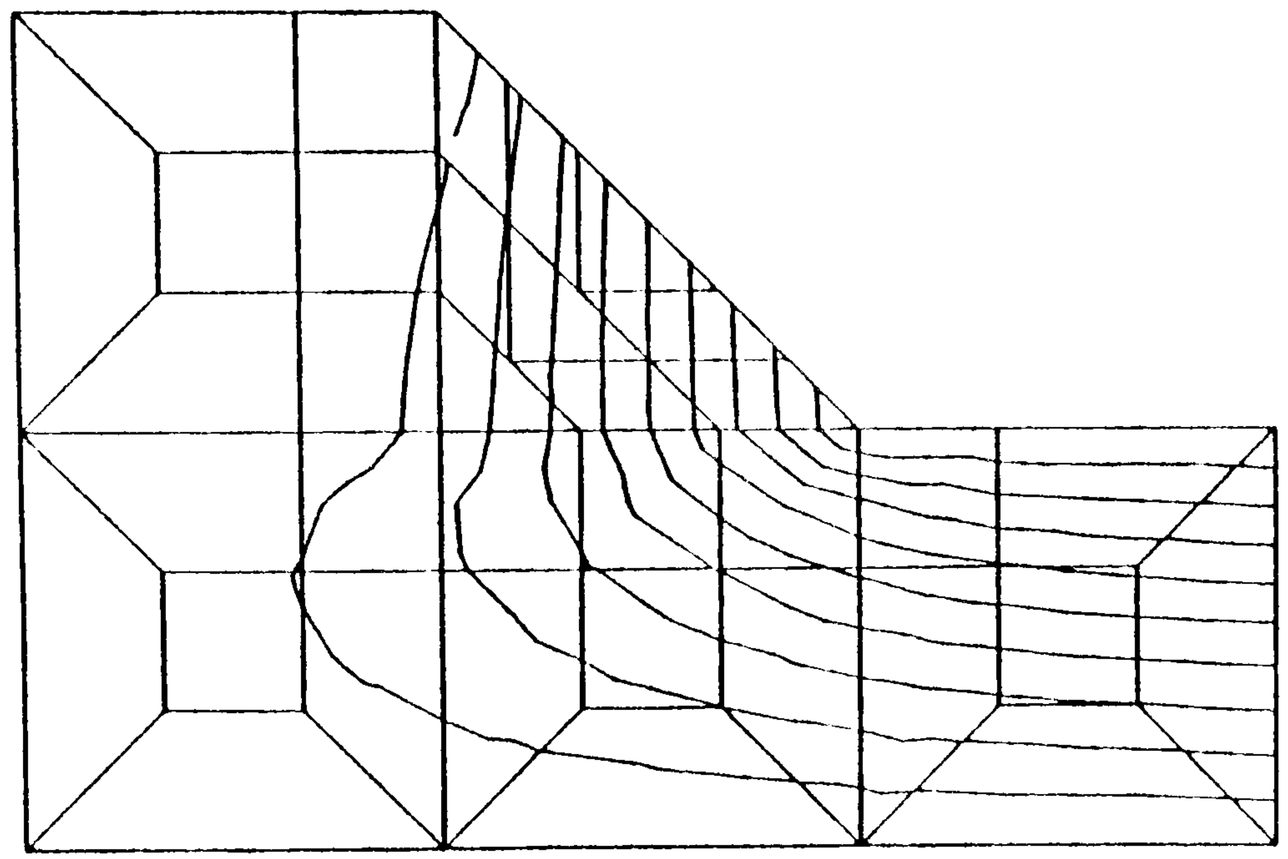
NO UNDERDRAINAGE

Figure 7.4. (D) Seepage in slopes: main parametric study.

SLOPE ANGLE = 1:3 . 'N' = 6 .

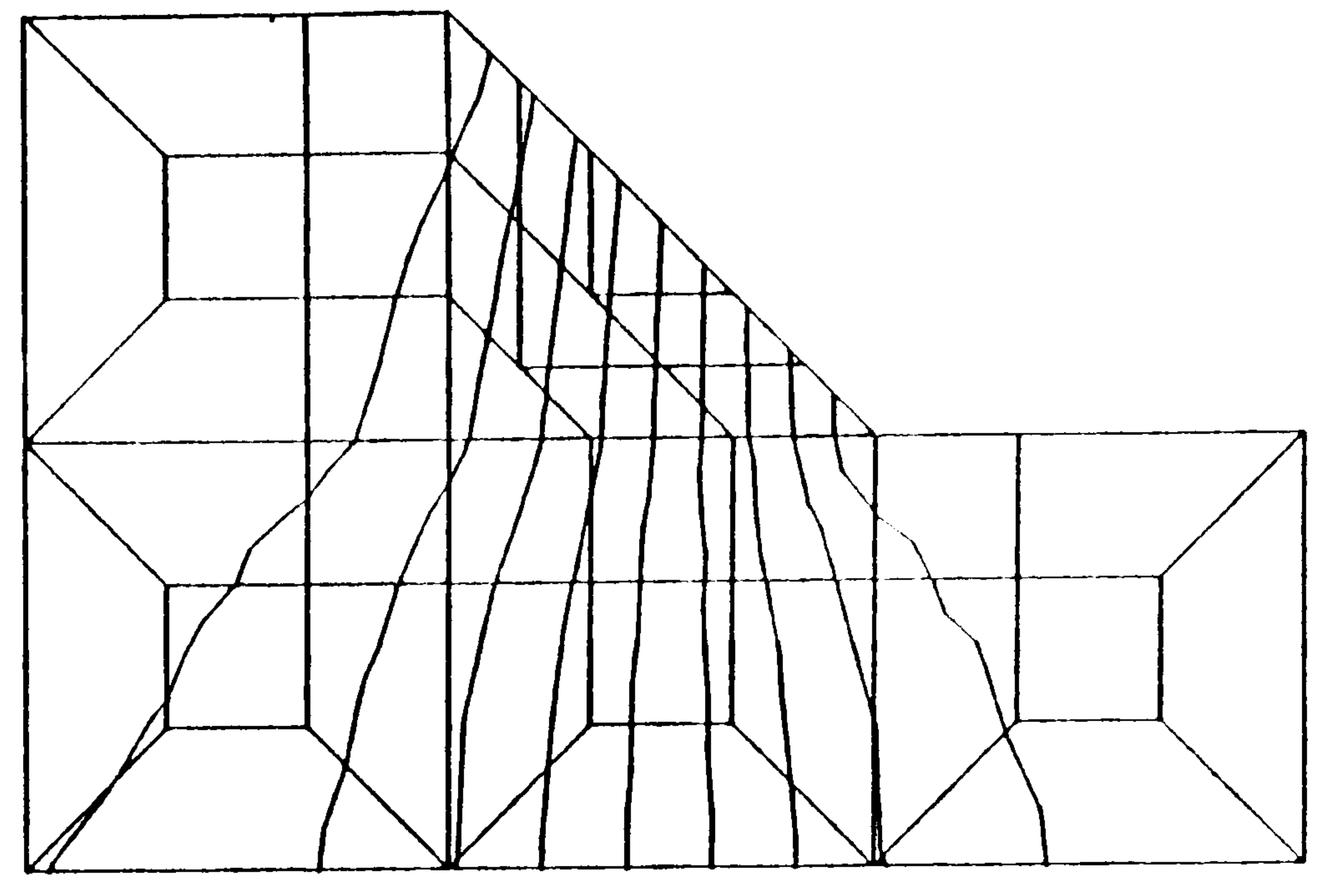


IMPERMEABLE BASE

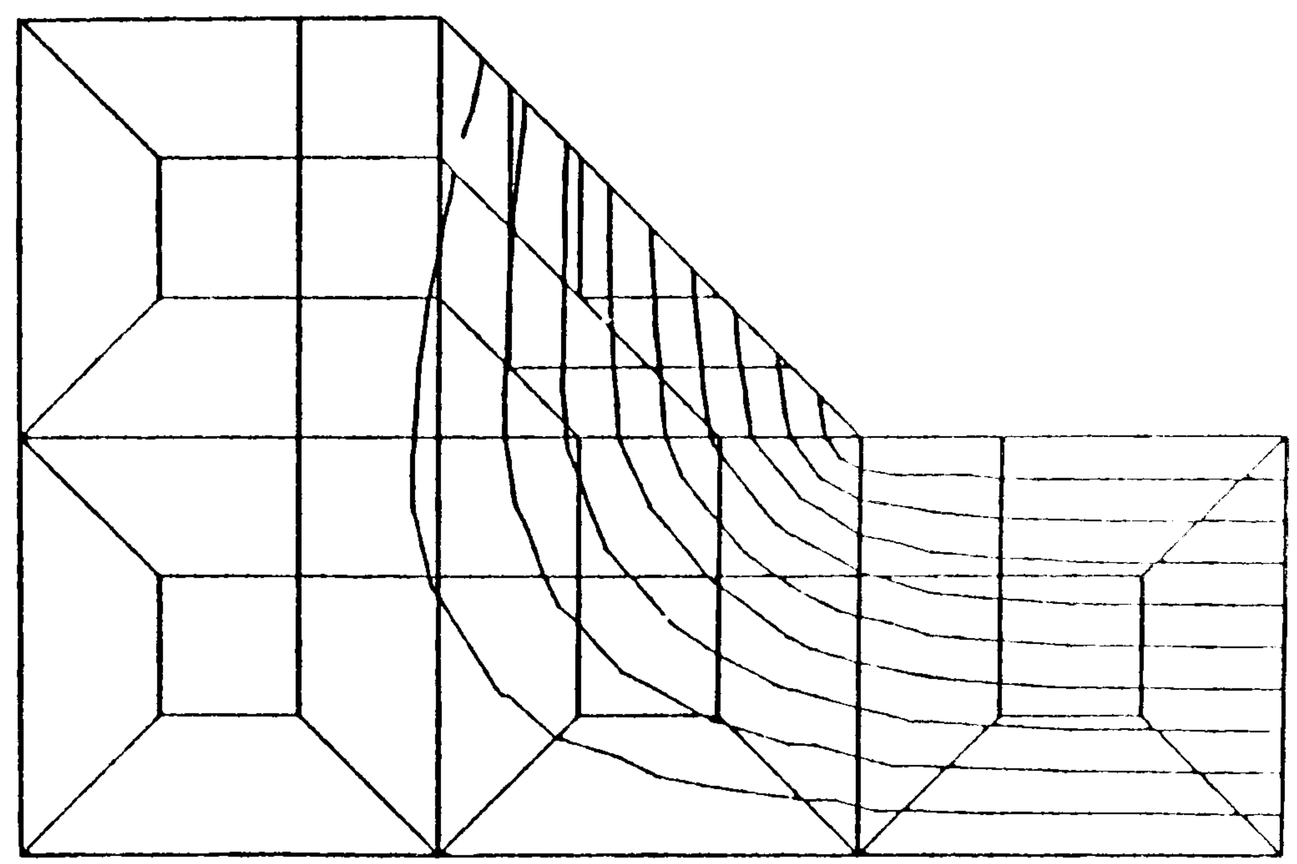


NO UNDERDRAINAGE

SLOPE ANGLE = 1:3 . 'N' = 3 .



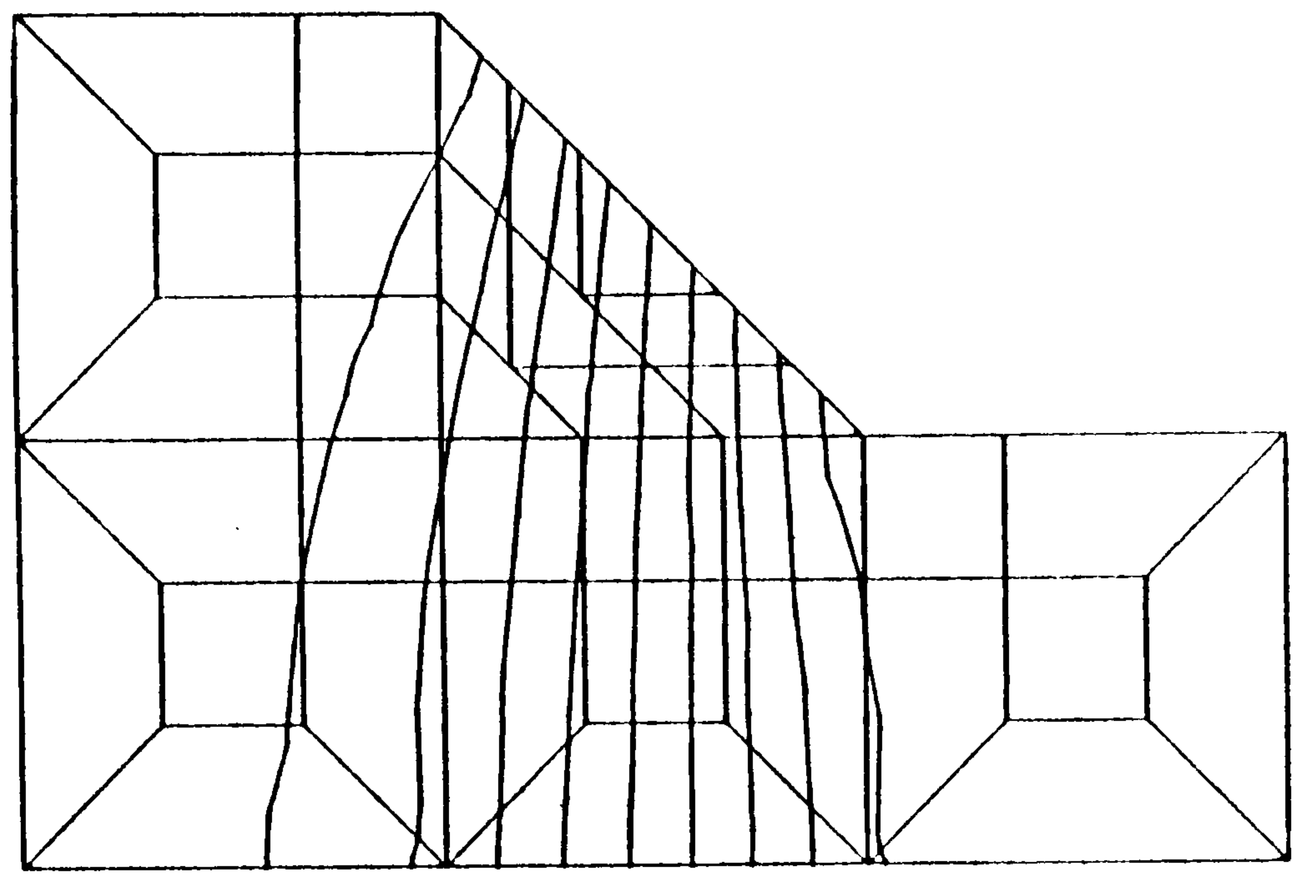
IMPERMEABLE BASE



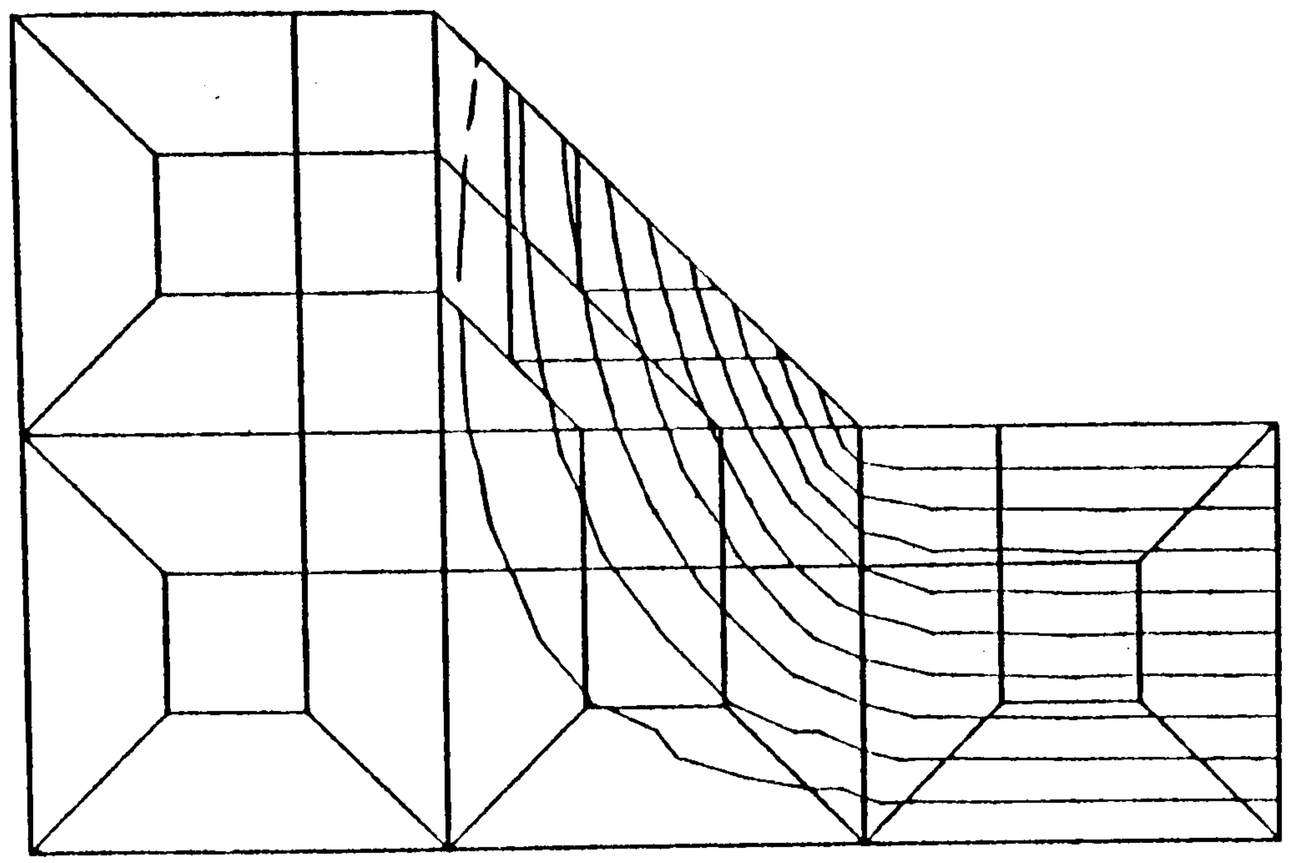
NO UNDERDRAINAGE

Figure 7.4. (E) Seepage in slopes: main parametric study.

SLOPE ANGLE = 1:3 . 'N' = 2 .

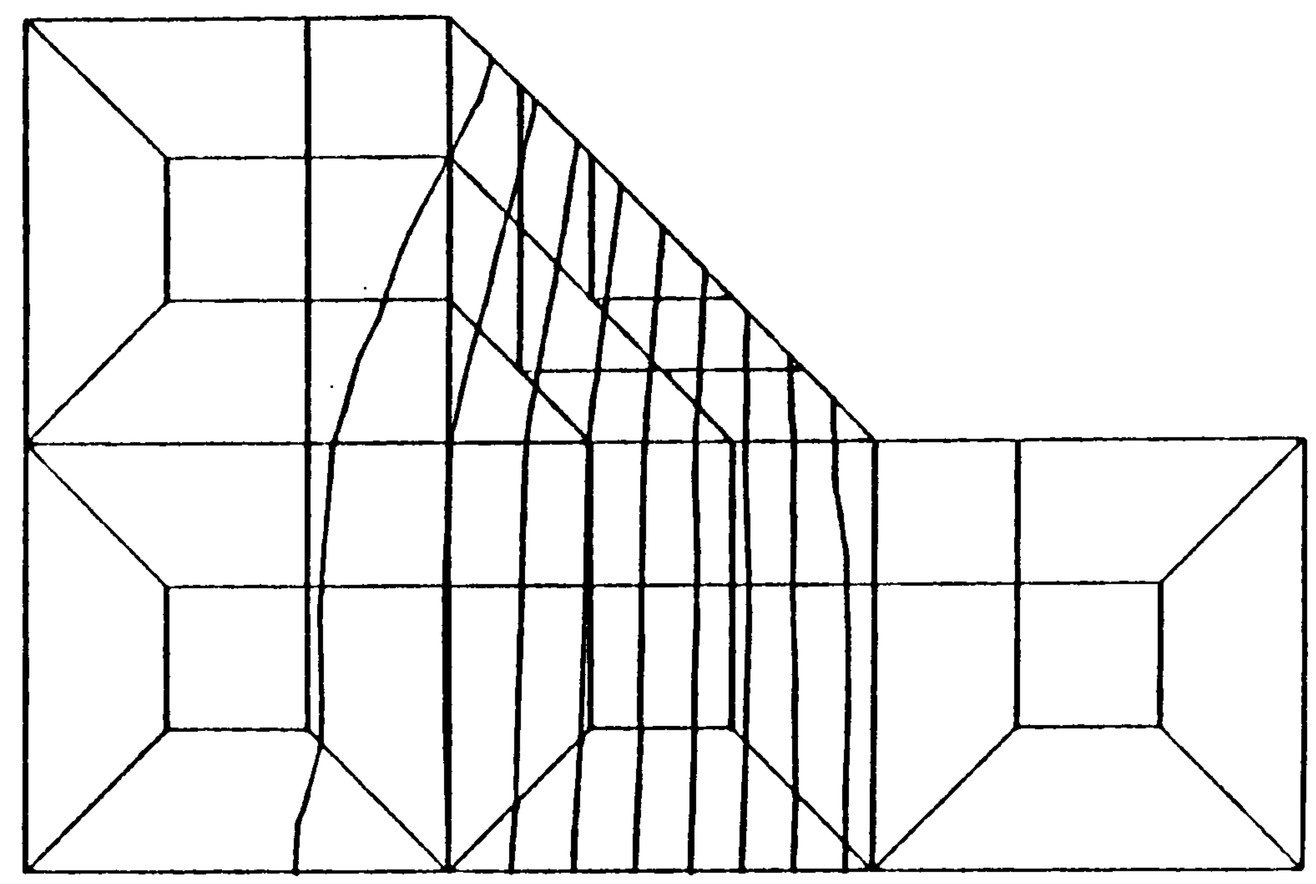


IMPERMEABLE BASE

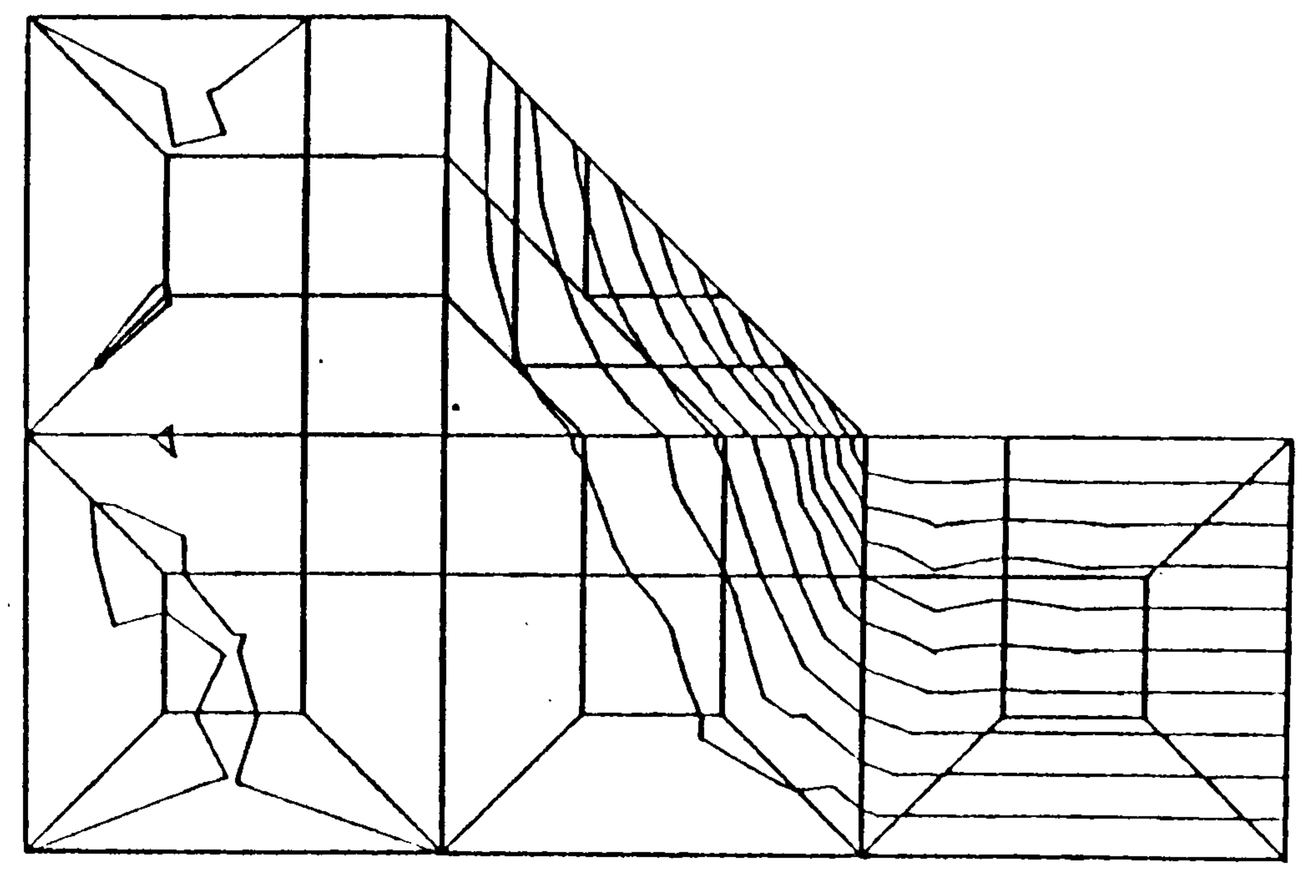


NO UNDERDRAINAGE

SLOPE ANGLE = 1:3 . 'N' = 1.5 .



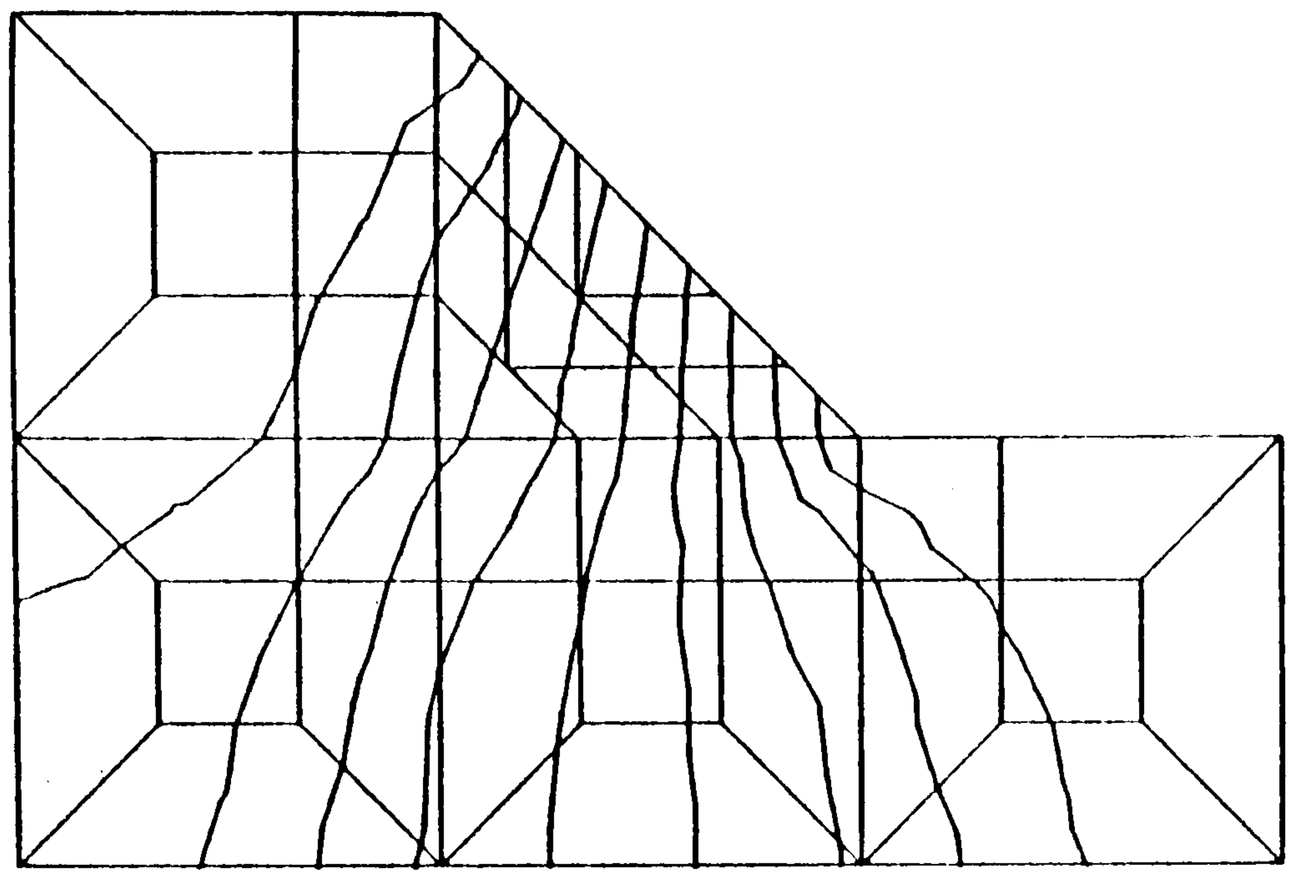
IMPERMEABLE BASE



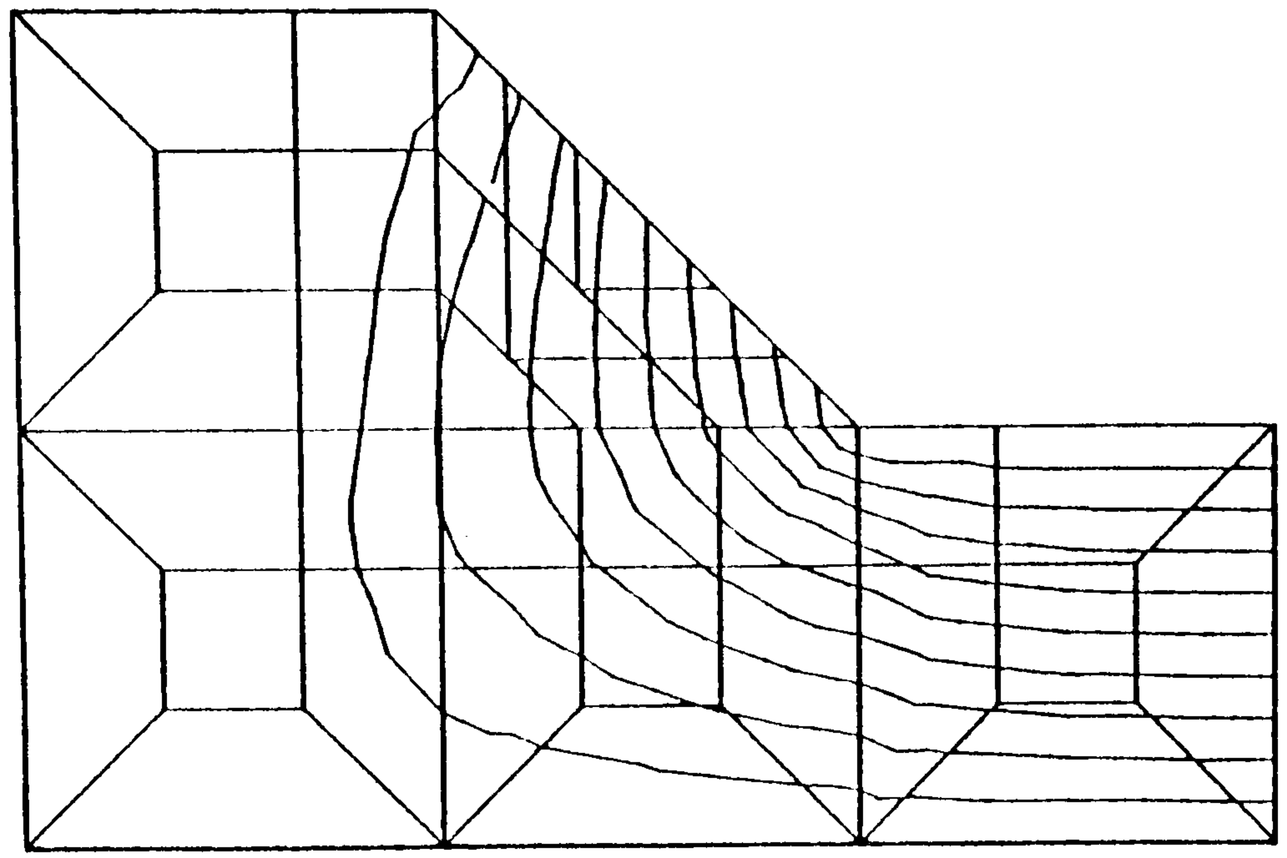
NO UNDERDRAINAGE

Figure 7.4. (E) Seepage in slopes: main parametric study.

SLOPE ANGLE = 1:2 . 'N' = 3 .

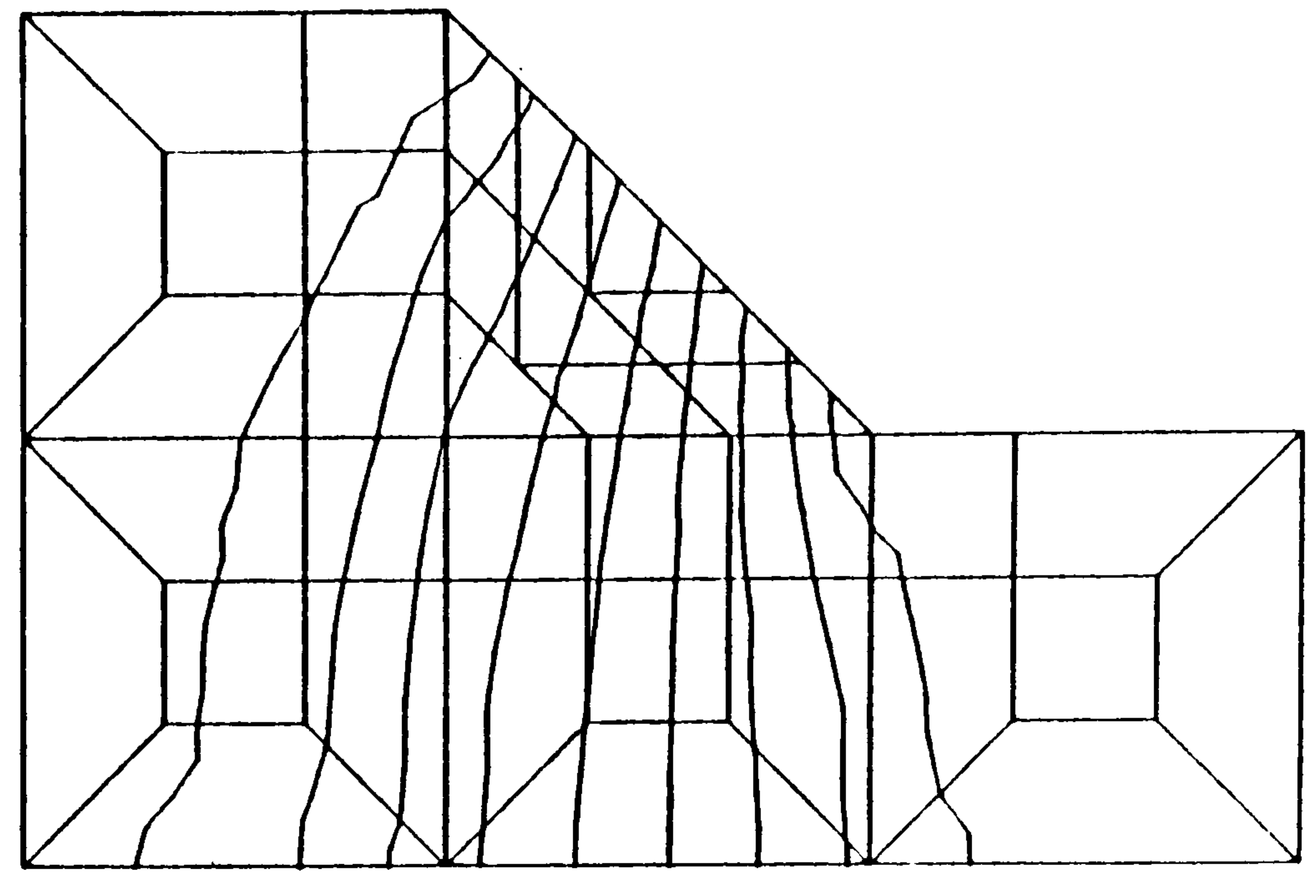


IMPERMEABLE BASE

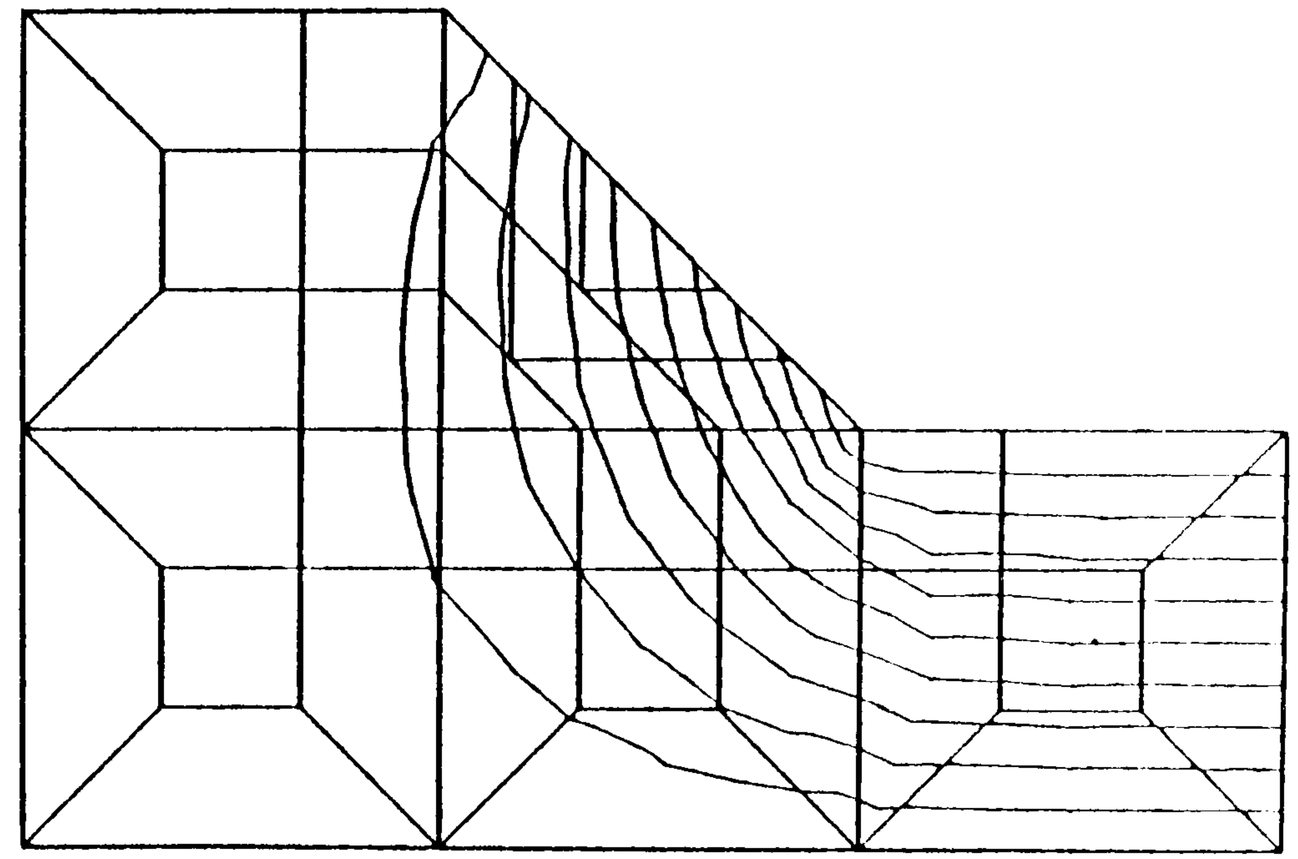


NO UNDERDRAINAGE

SLOPE ANGLE = 1:2 . 'N' = 2 .



IMPERMEABLE BASE



NO UNDERDRAINAGE

Figure 7.4. (G) Seepage in slopes: main parametric study.

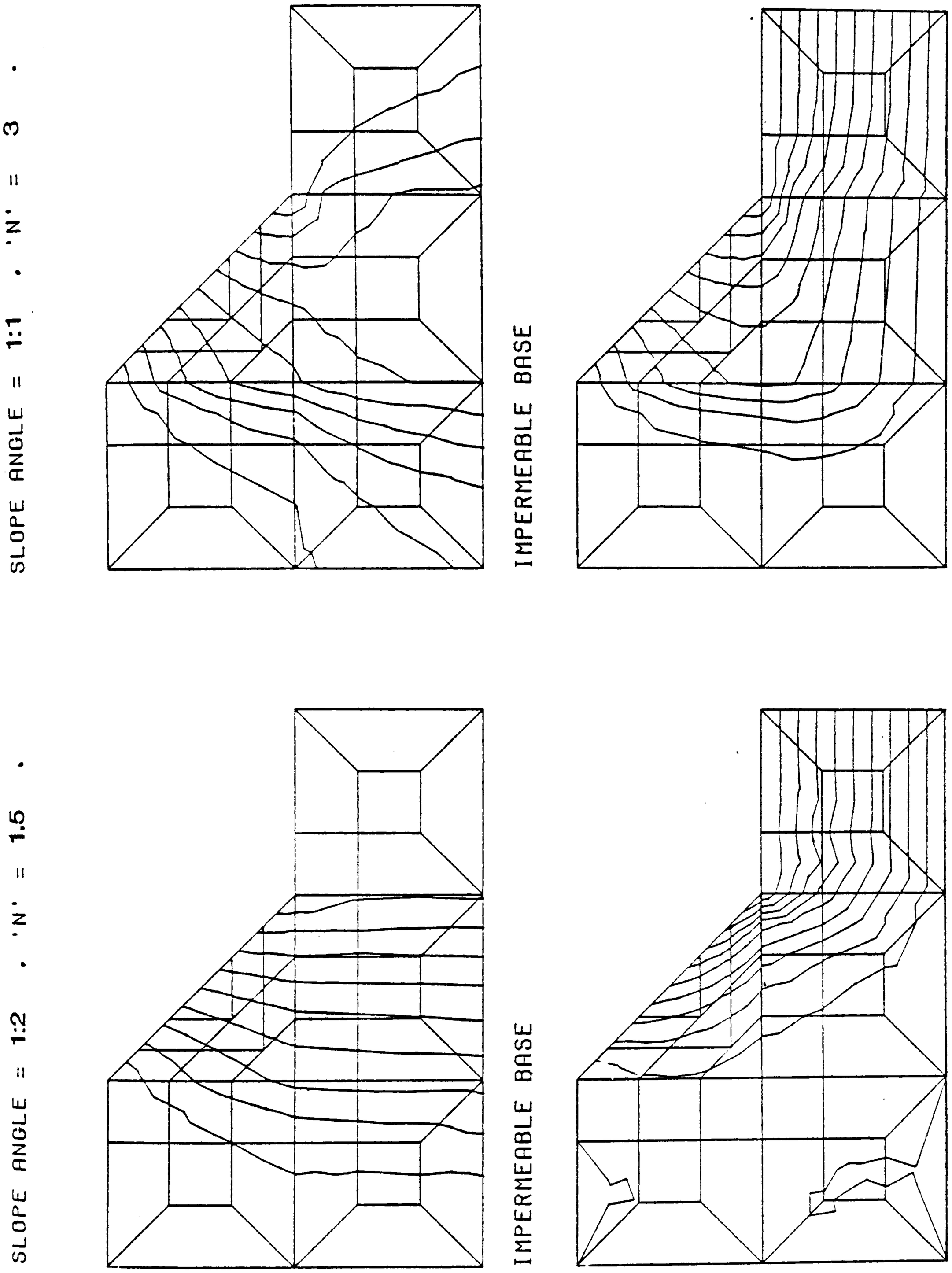
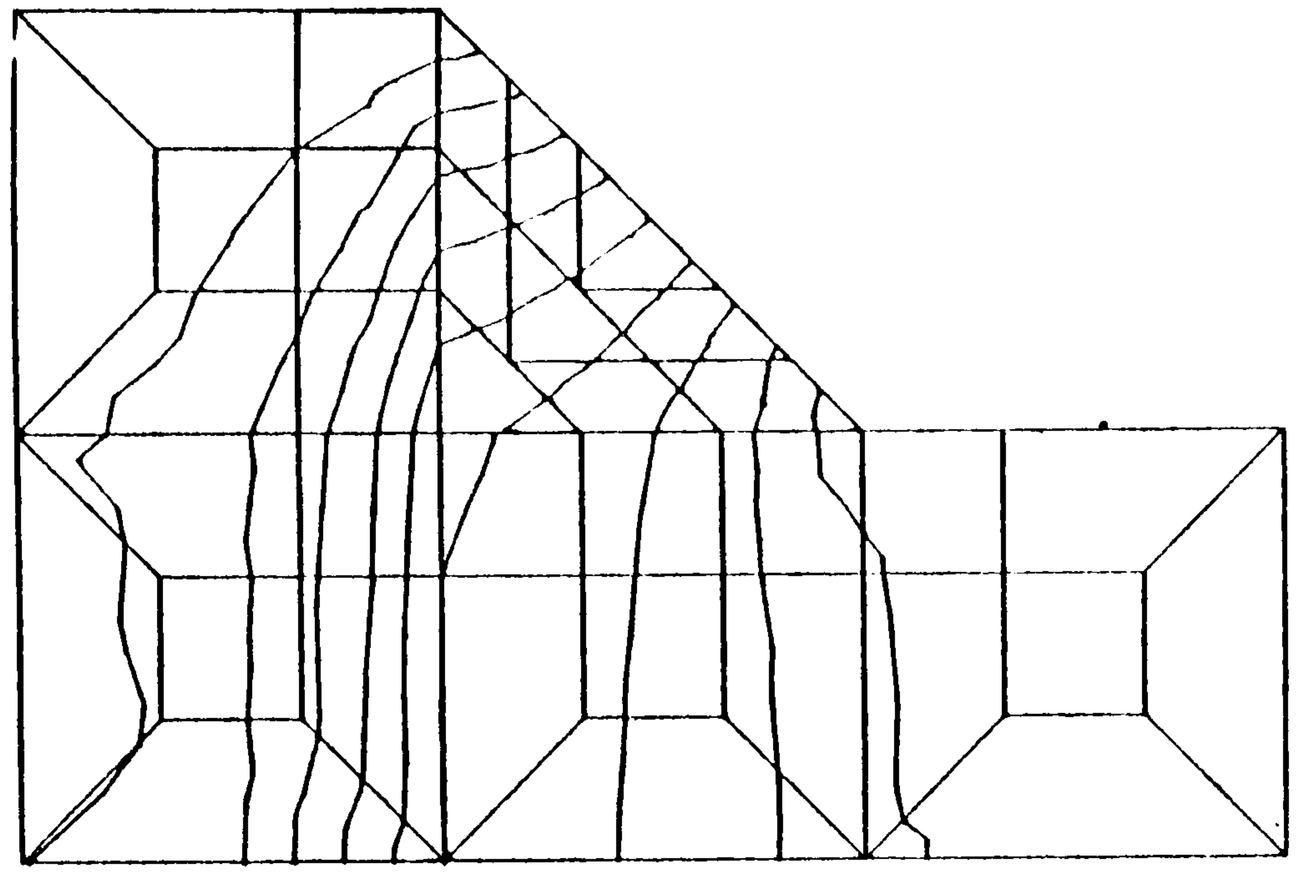
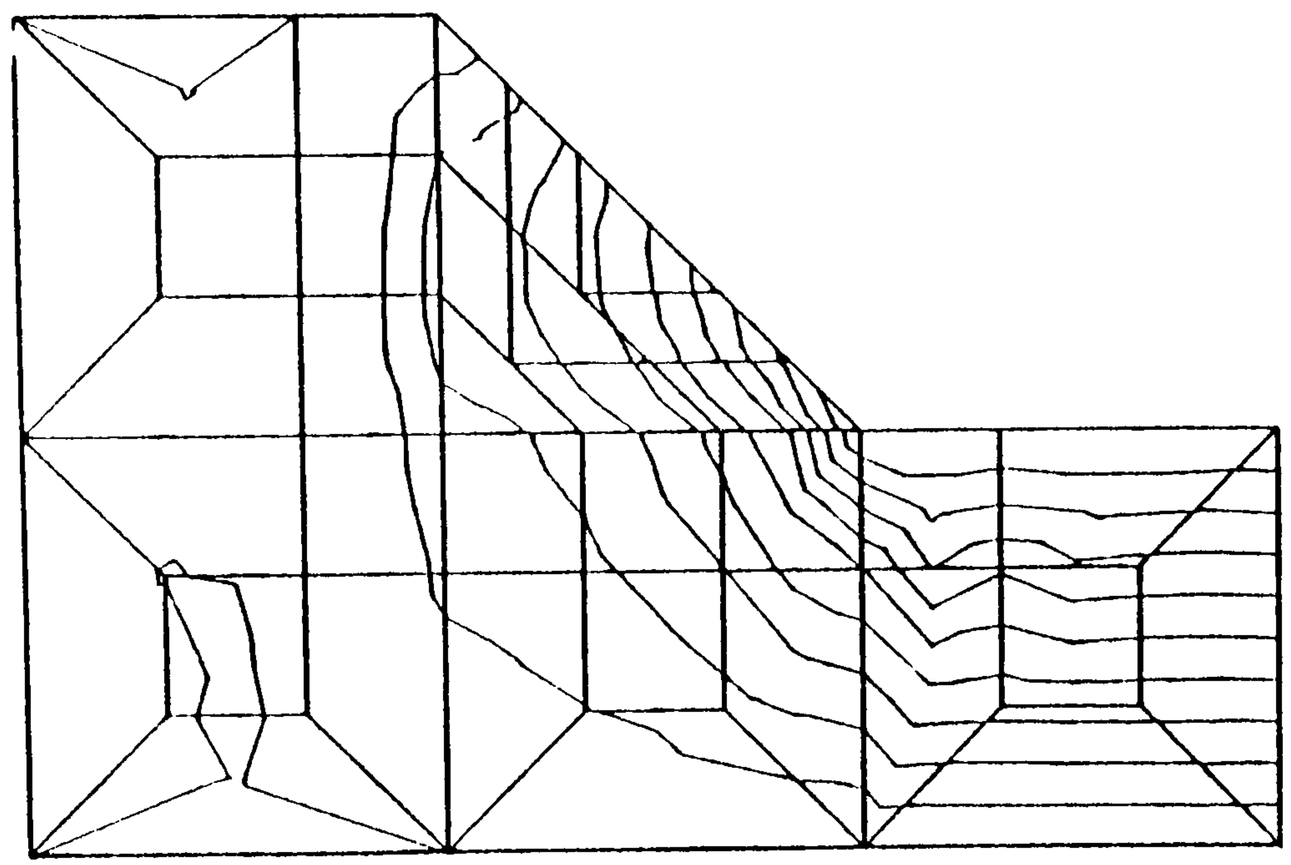


Figure 7.4. (H) Seepage in slopes: main parametric study.

SLOPE ANGLE = 1:1 . 'N' = 1.5 .

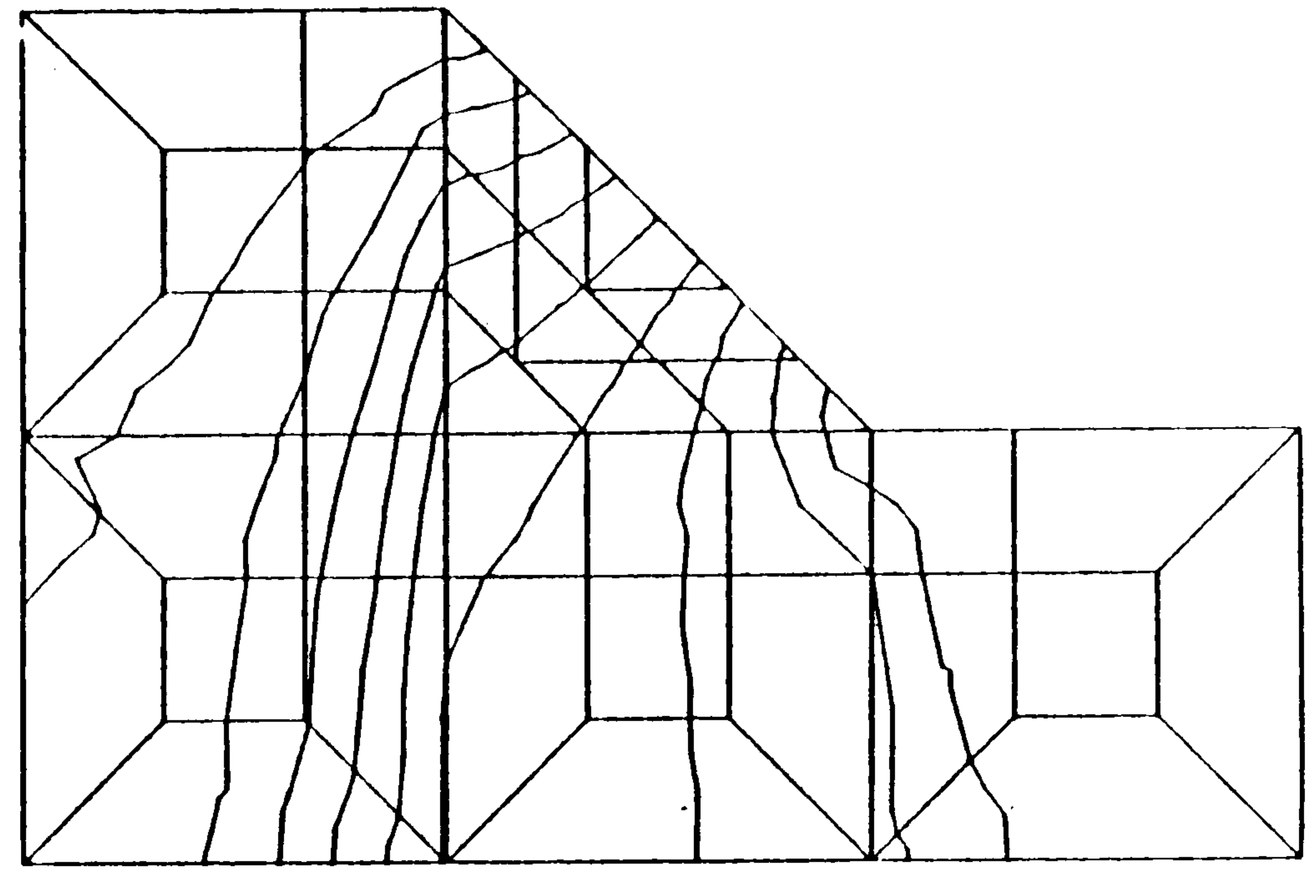


IMPERMEABLE BASE

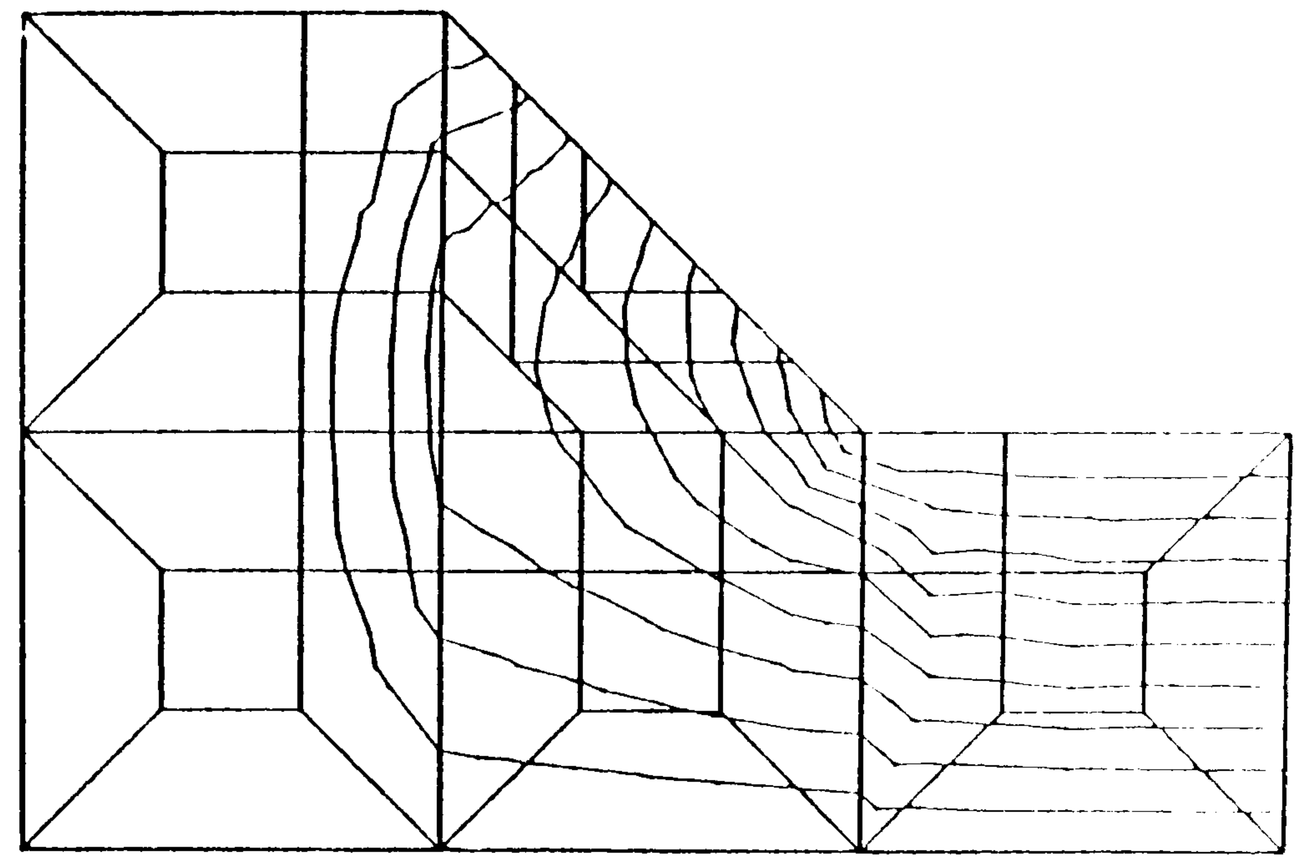


NO UNDERDRAINAGE

SLOPE ANGLE = 1:1 . 'N' = 2 .



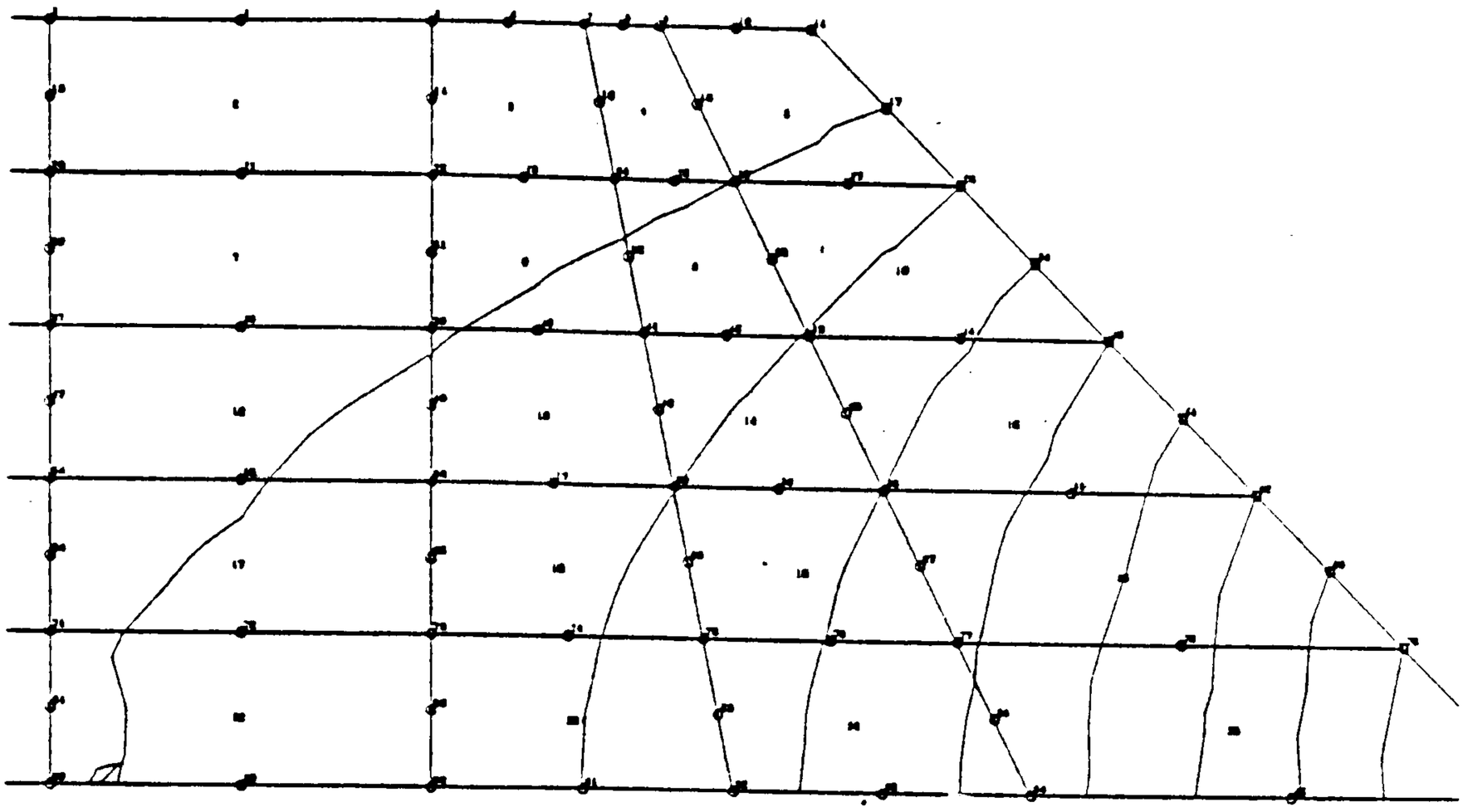
IMPERMEABLE BASE



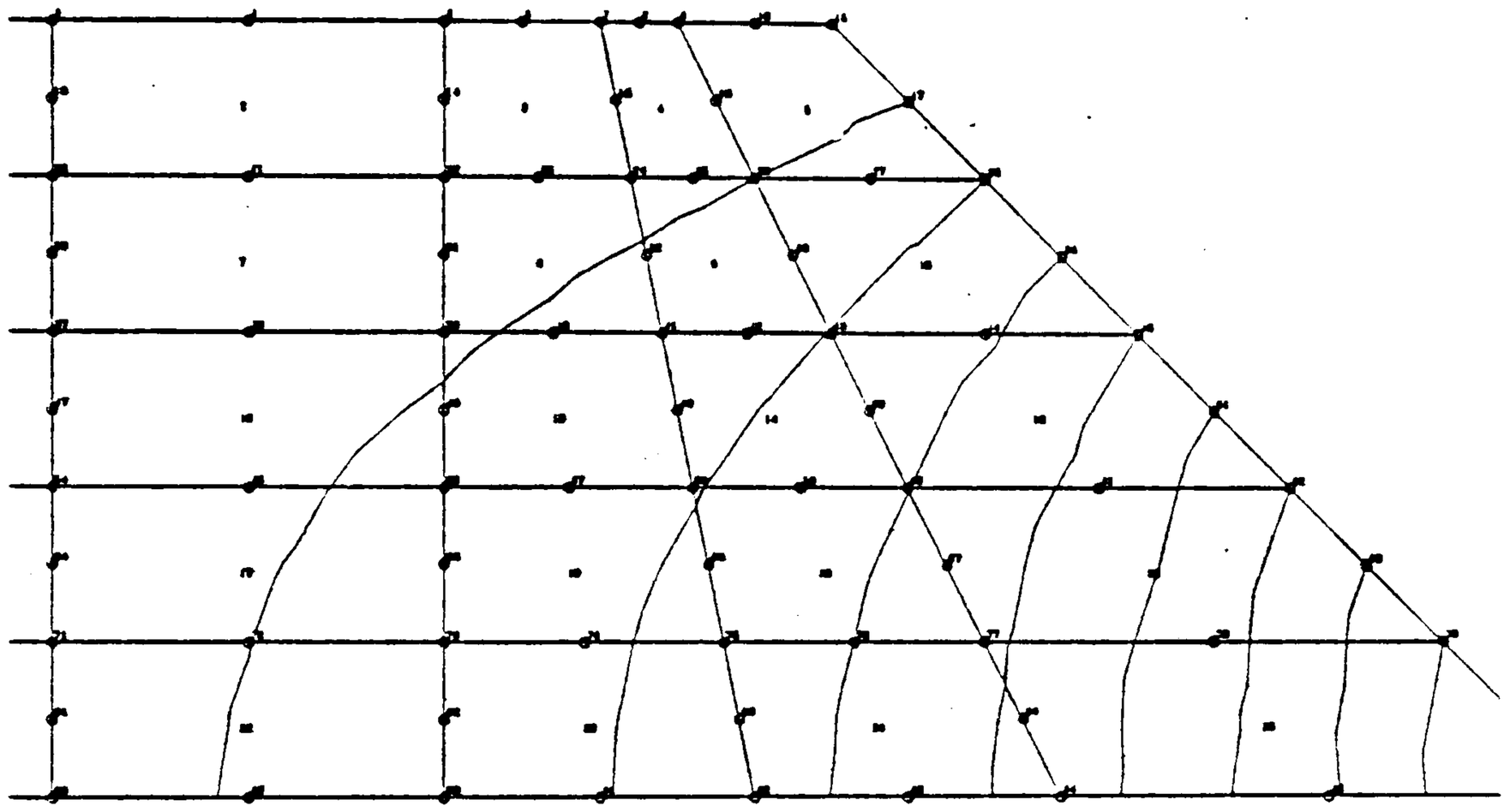
NO UNDERDRAINAGE

Figure 7.4. (I) Seepage in slopes: main parameters studied.

1 in 1



1 in 2



1 in 3

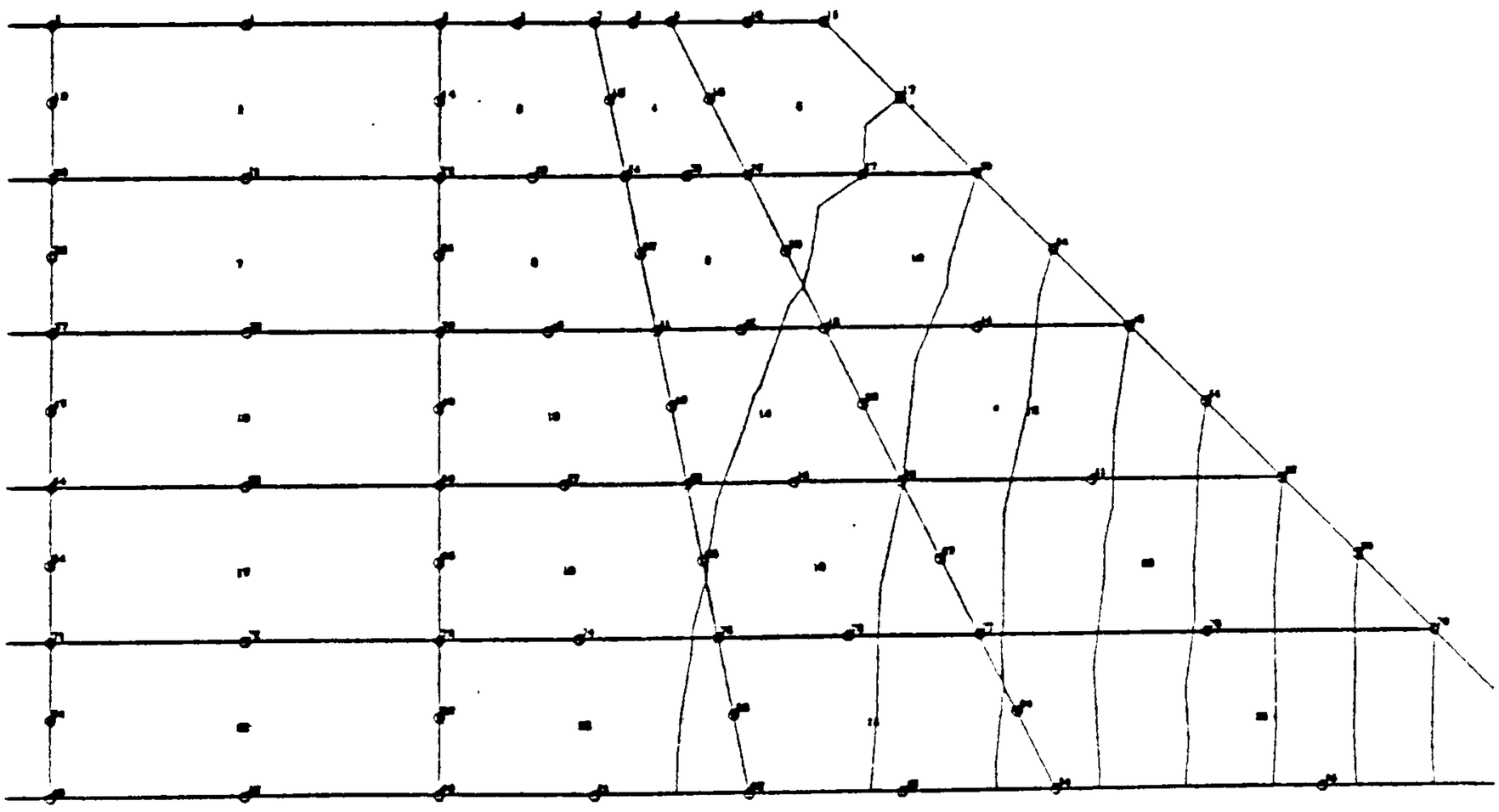
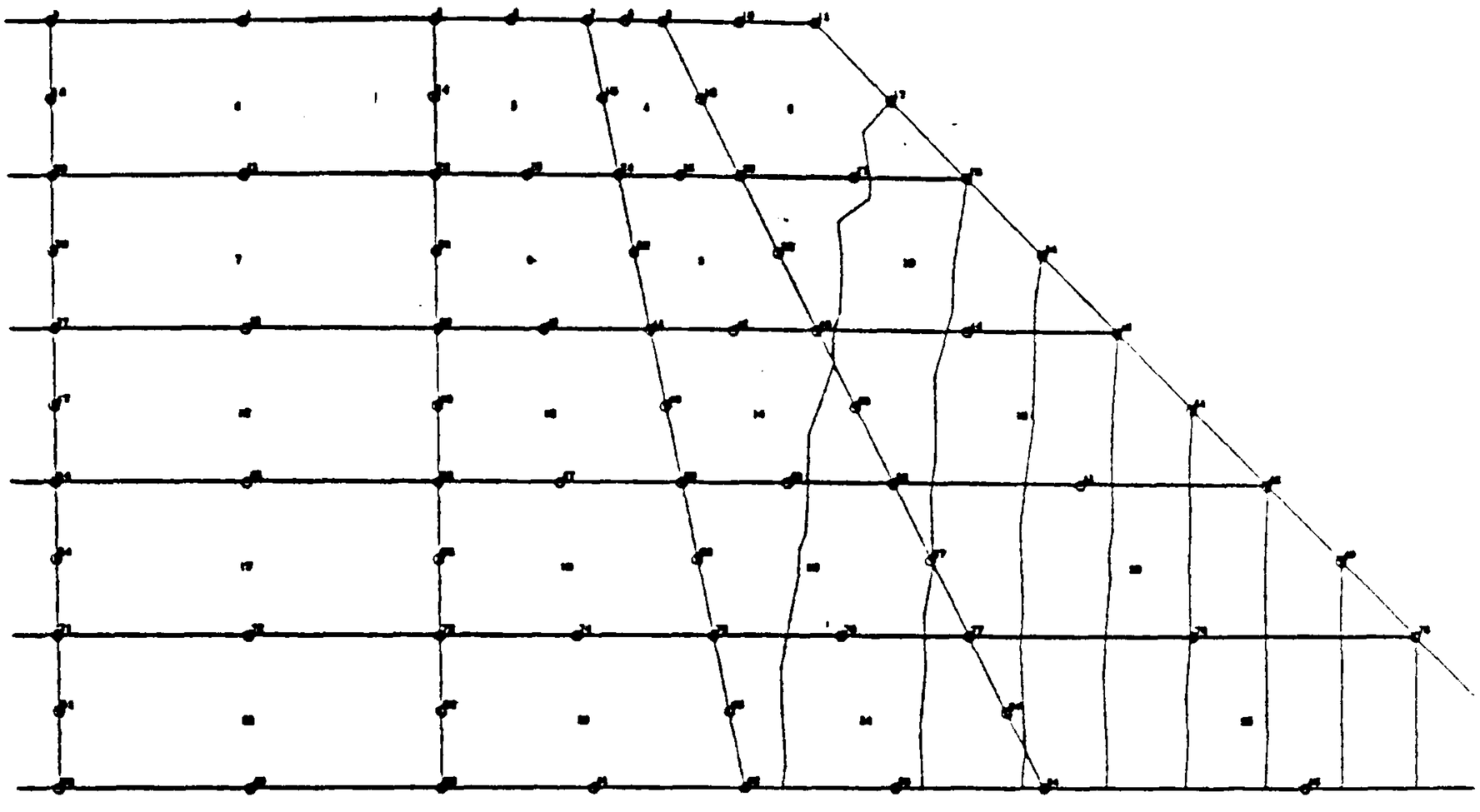
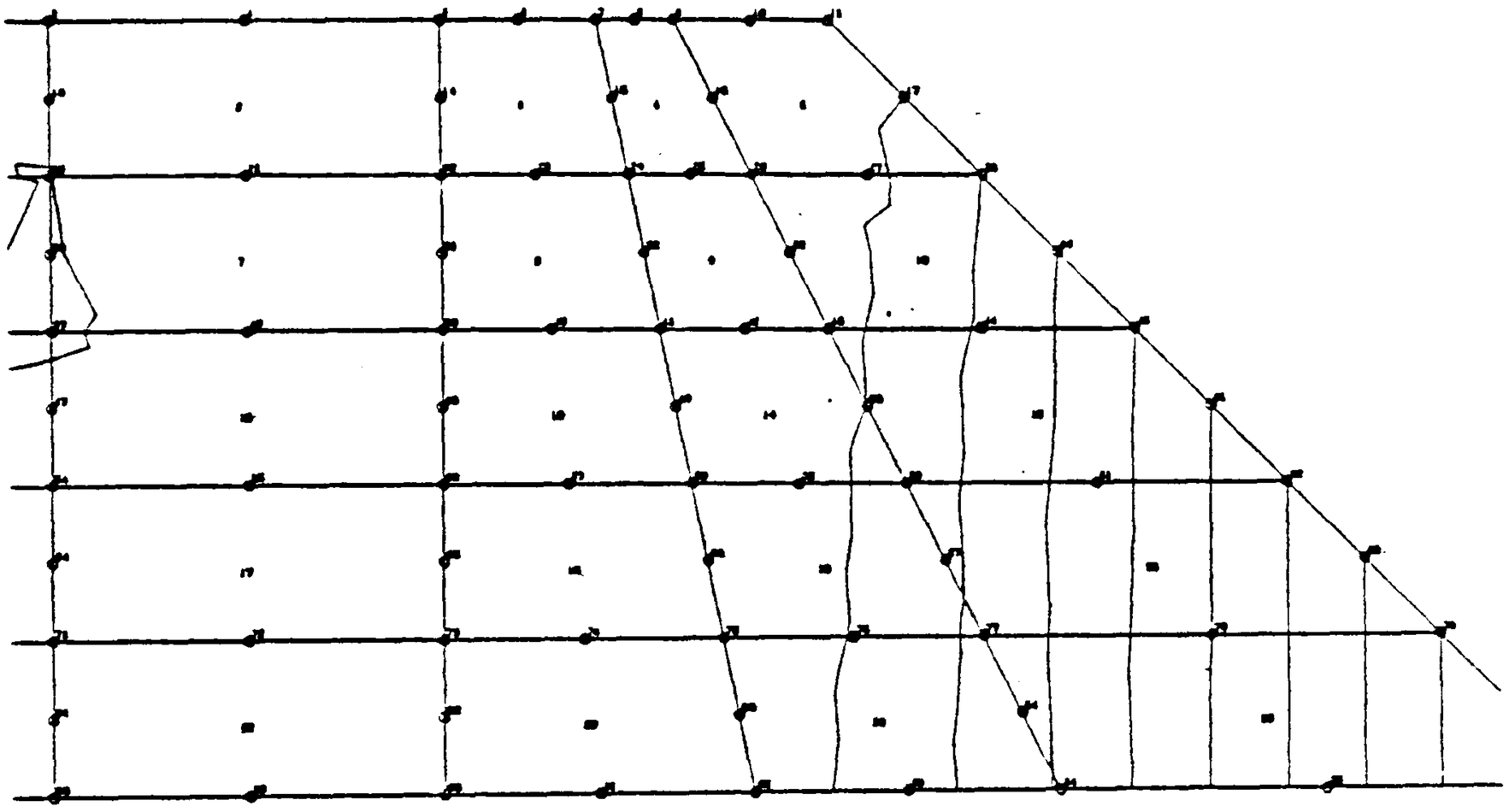


Figure 7.5. (A) Seepage in slopes: subsidiary parametric study.

1 in 4



1 in 5



1 in 6

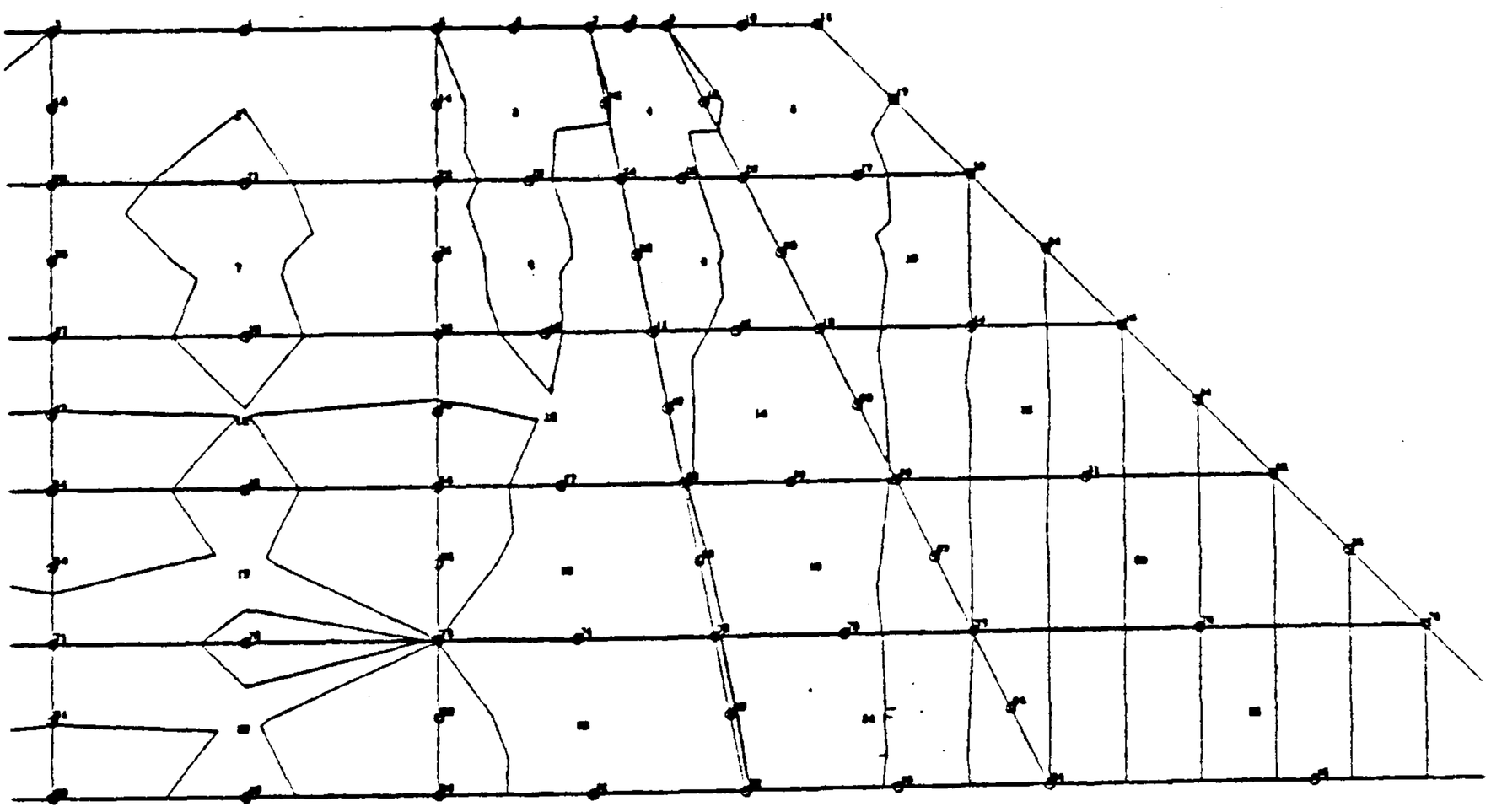
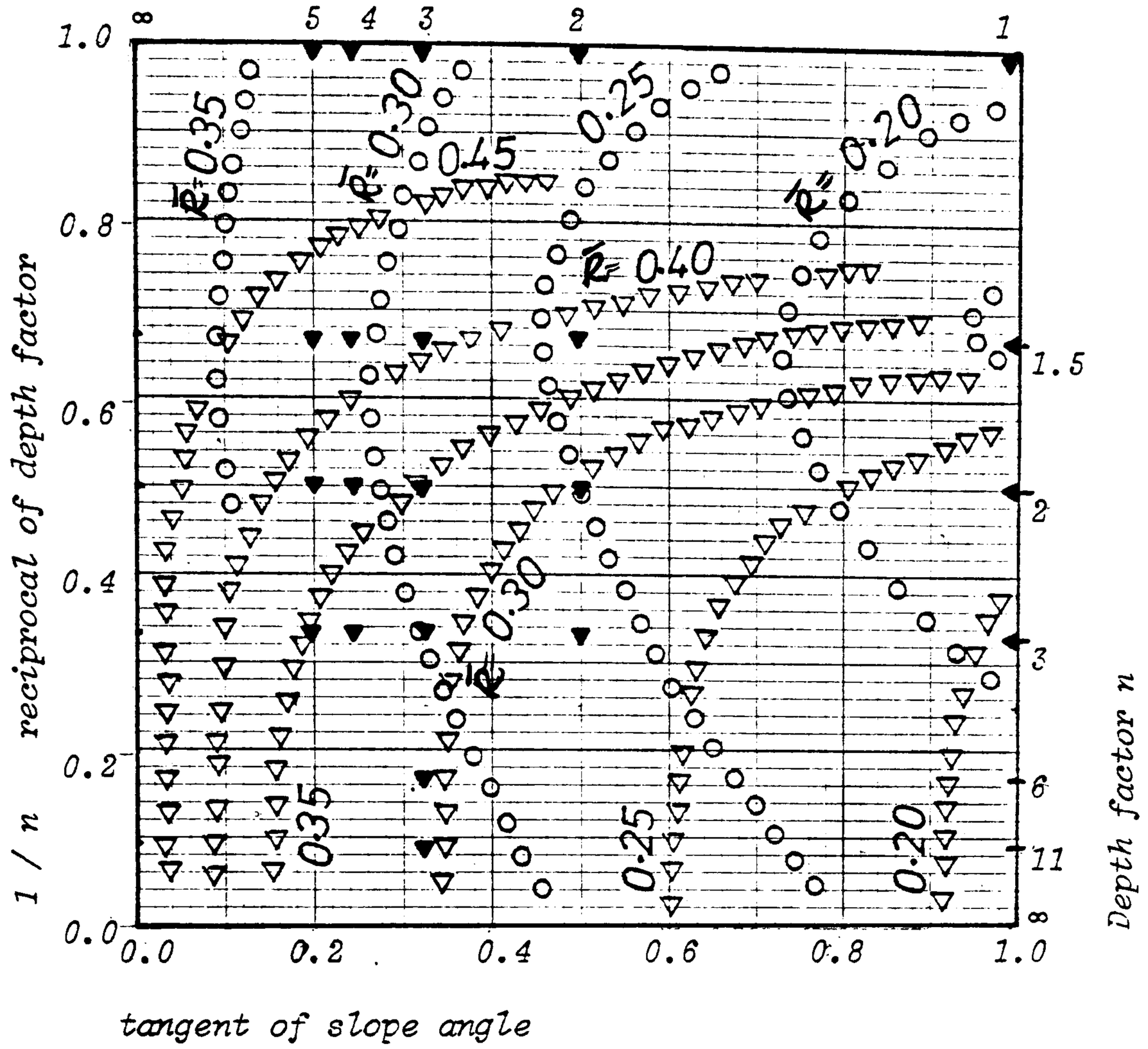


Figure 7.5. (B) Seepage in slopes: subsidiary parametric study.



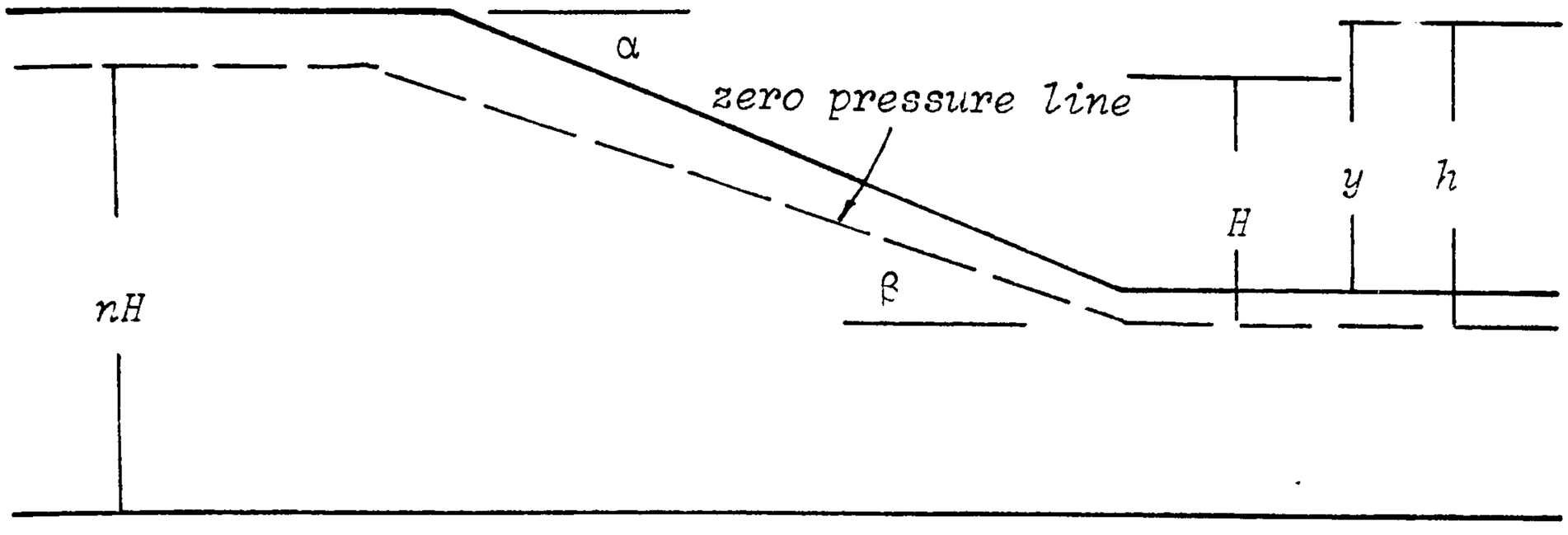
See page 225 & Fig 7.7.

○○○○○ ..... *Impermeable base solution*

▽▽▽▽▽▽ ..... *Permeable base solution - no overall underdrainage*

▼ ..... *Numerically evaluated result at this point*

Figure 7.6. Average pore water pressures in slopes - a summary of the parametric study.



Impermeable, or with $u = \gamma_w h_w$

a) Average pore water pressure head from Fig. 7.6 using H, β & n.

b) If permeable base problem $D_u = \dfrac{nH - h_w}{nH}$

c) Average pore water pressure head now multiplied by $(1-D_u)$ *to evaluate* $\overline{R}$

d) Neglecting any negative pore water pressures, the average pore pressure ratio r_u *is given by:*

$$r_u = (\overline{R} \,.\, 3\ \gamma_w\ H) \,/\, (\gamma\ h)$$

e) Use stability charts with α, y, r_u*, c', φ' & γ to calculate factor of safety against sliding.*

Figure 7.7. Use of the slope model in routine design & analysis.

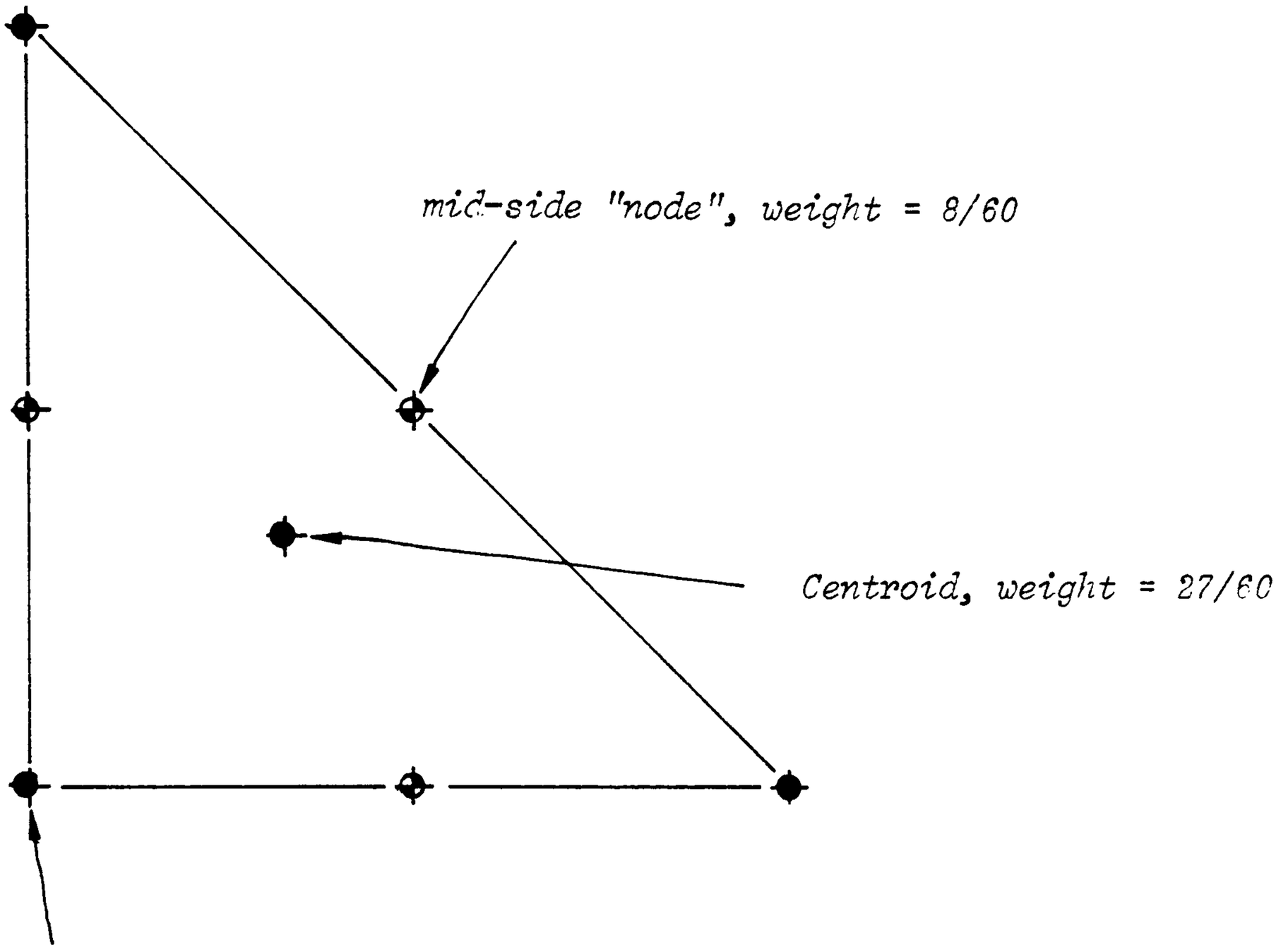


Figure 7.8. Hammer's integration rule for a triangle.

(based on data in Zienkiewicz 1972).

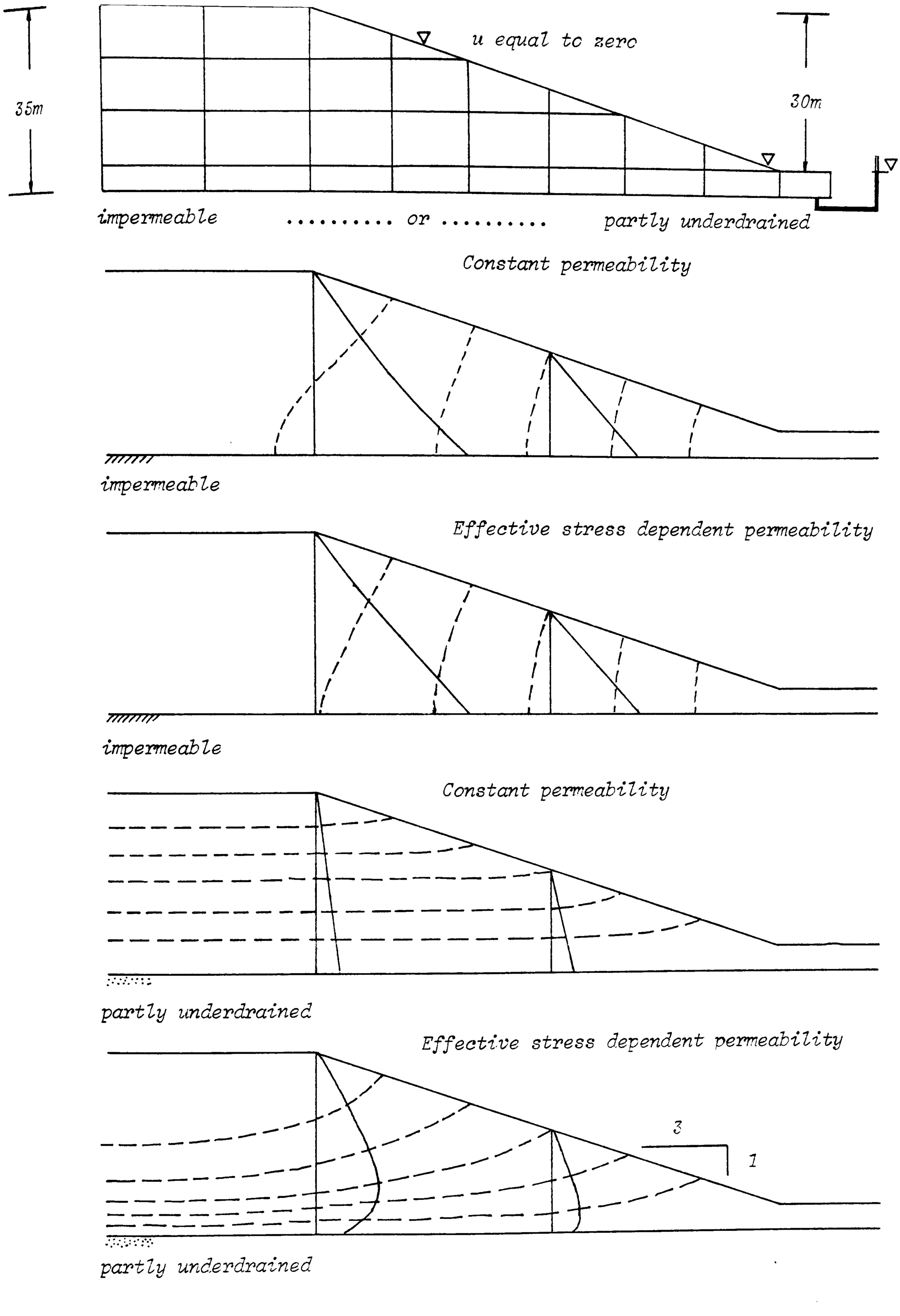


Figure 7.9. Influence of an effective stress permeability on seepage in earth slopes.

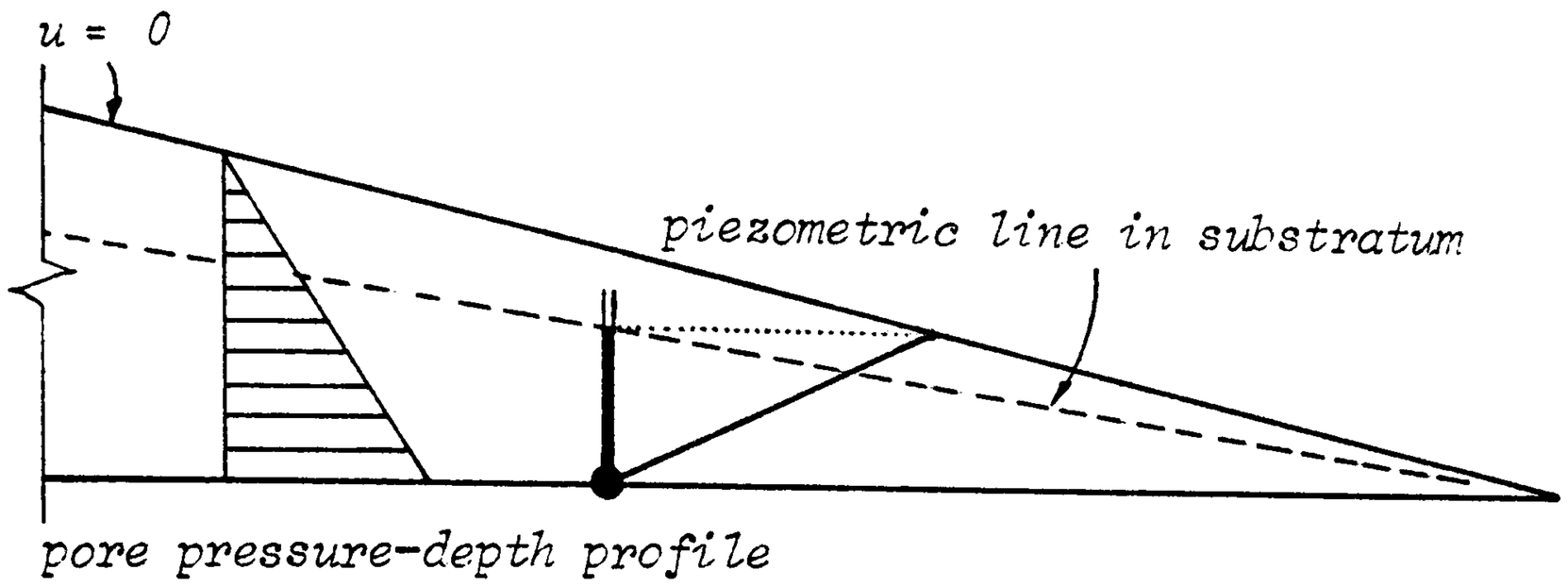


Figure 7.10. Sweeney's (1970) model for seepage in a slope.

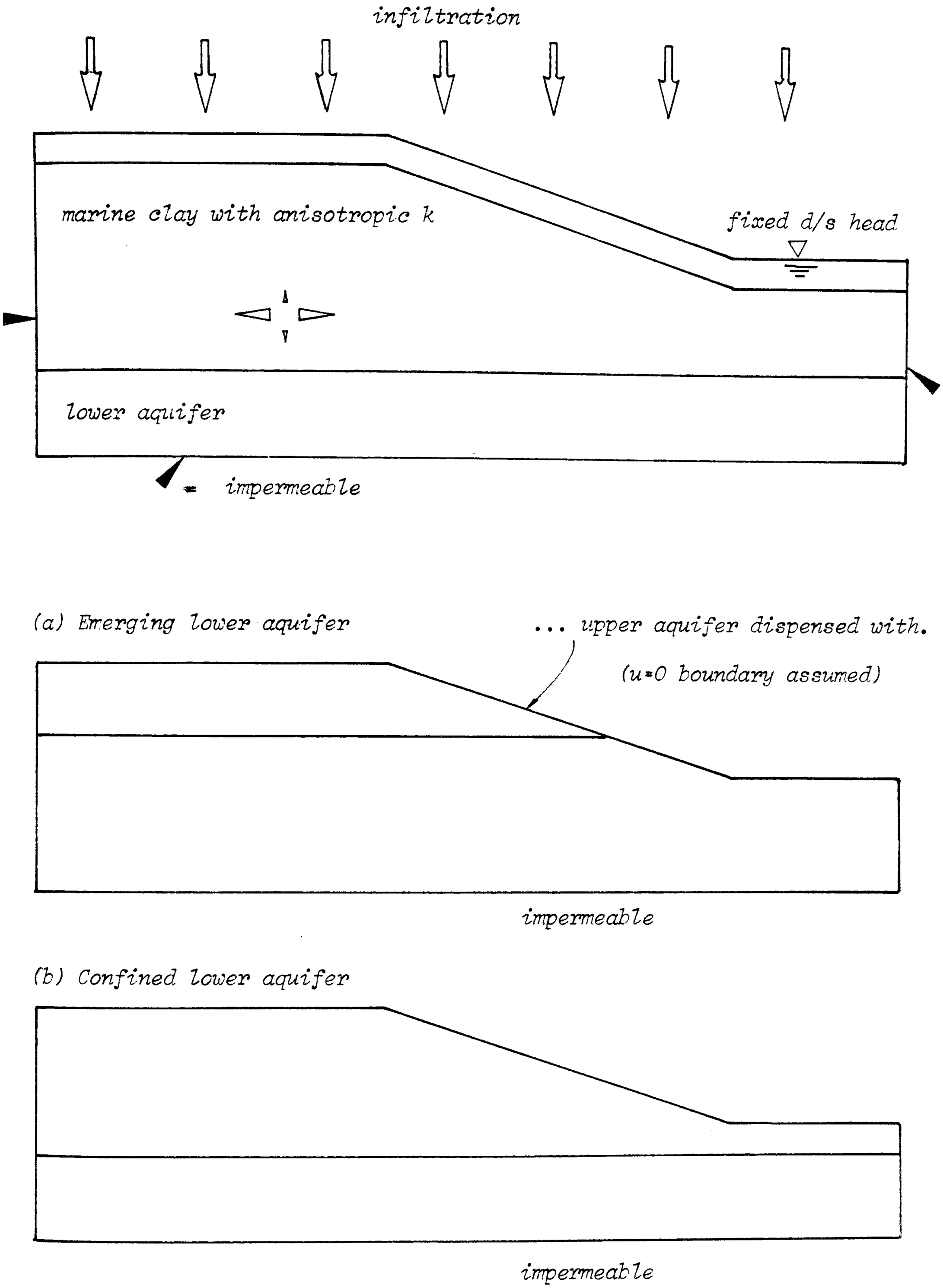


Figure 7.11. Basic concepts in the work of Lafleur & Lefebvre (1980).

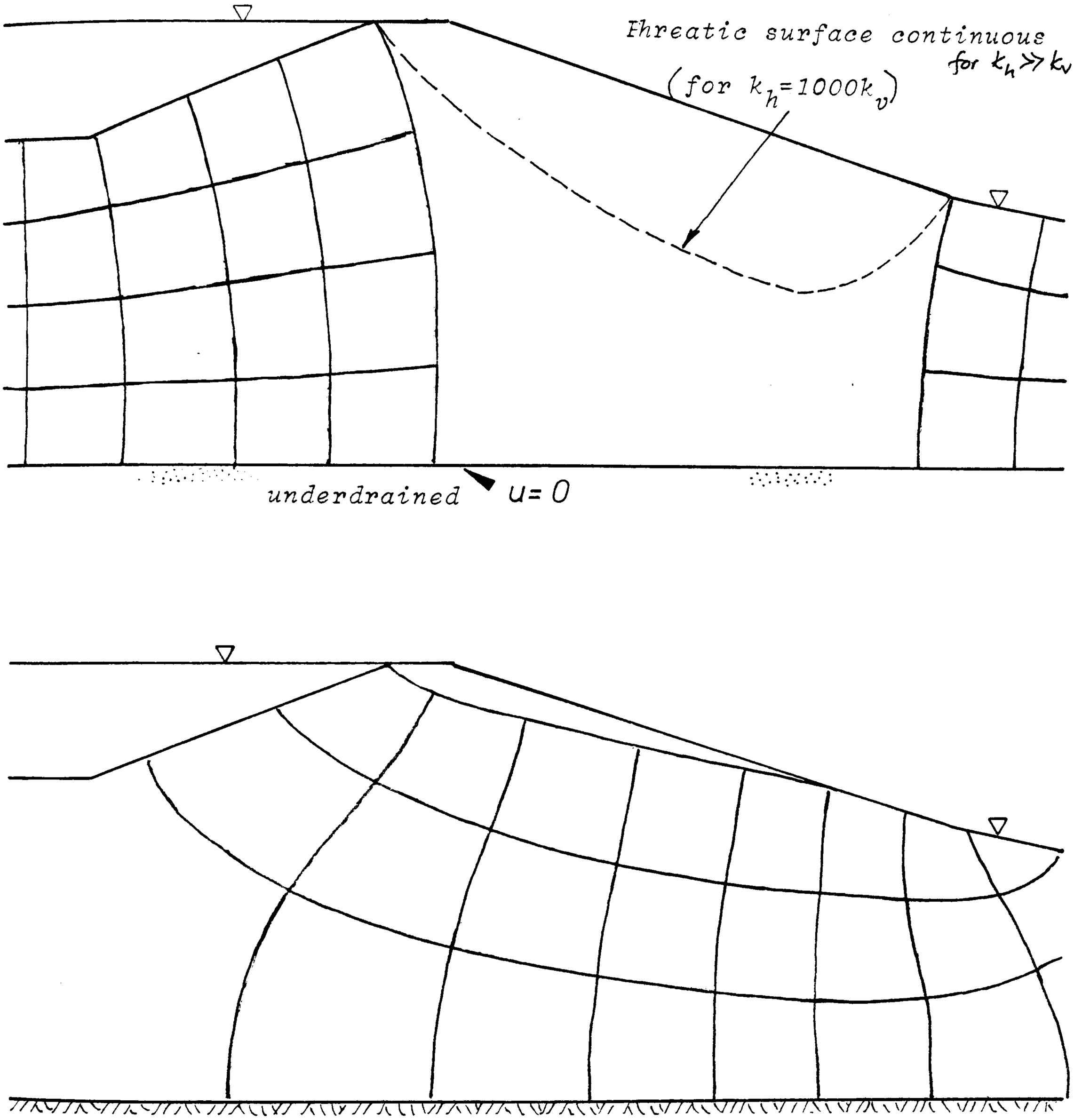


Figure 7.12. Constant permeability solutions for tailings dam.

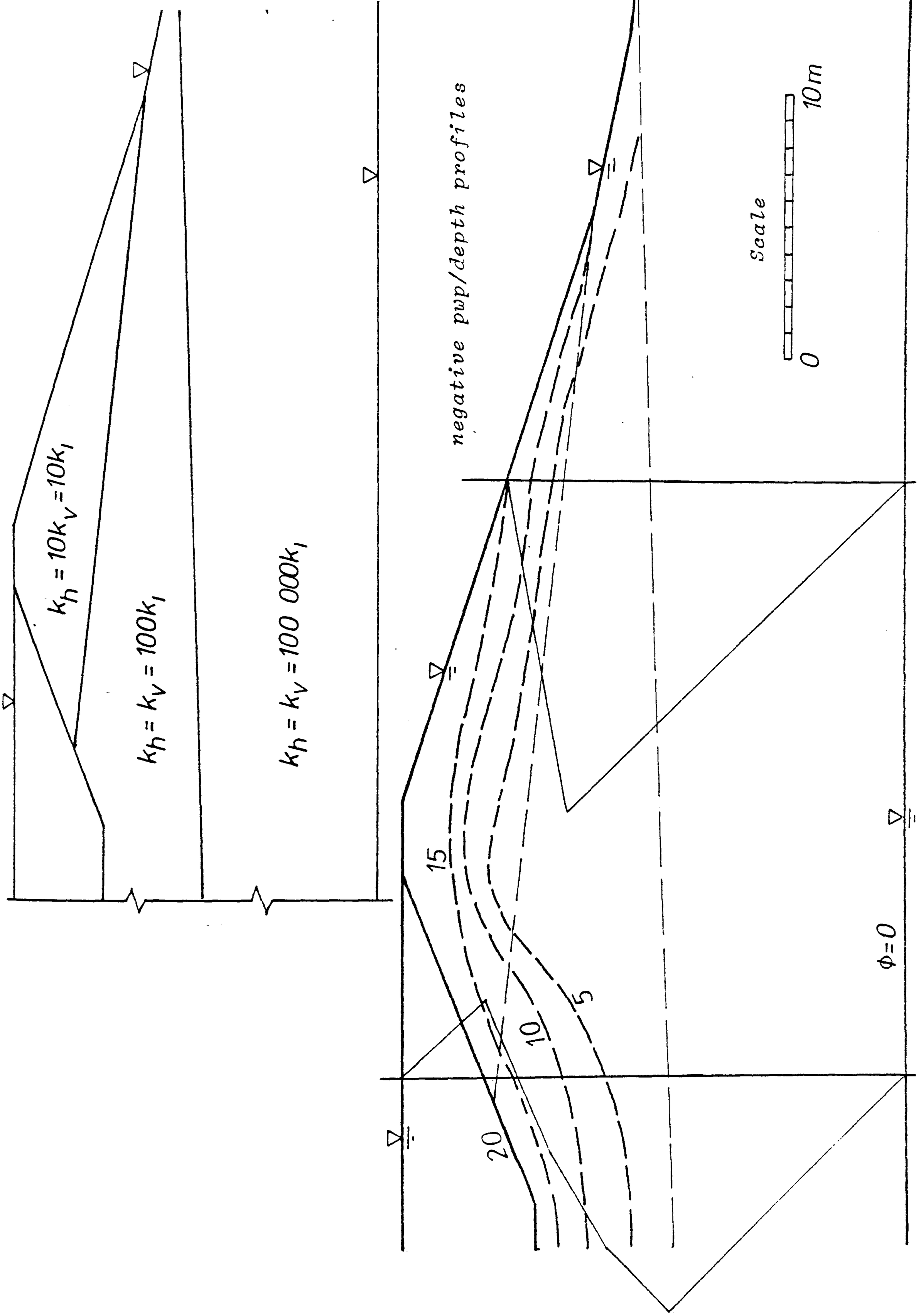


Figure 7.13. Tailings dam with increasing permeability with depth - wetted boundary solution.

CHAPTER 8 - CONCLUSIONS

8.1. Methods of Analysis of Seepage and Consolidation

The author's preference for the finite element method as a vehicle for computation in seepage and consolidation is self evident at this point. It is necessary to point out that this preference is influenced by the following factors:-

(a) the ease with which arbitrarily zoned problems may be represented,

(b) the ease with which anisotropic parameters are handled,

(c) the ability of the method to yield detailed information over part of the problem (using a graded mesh) without enormous costs in computational resources,

(d) the physical significance of results computed at intermediate stages of the analysis process, so that non-linear behaviour can be simulated and understood in a simple iterative way.

Despite the apparent advantages which other methods may appear to offer in certain cases, the finite element method is still an unparallelled general analysis tool. Its usefulness in seepage analysis is still not fully realised, however, and the literature on practical case studies or on systematic parametric studies is still in its infancy.

At the outset, this research concentrated on the use of the 8-noded, parabolic serendipity element devised at Swansea, since this element offers advantages of simplicity and compatability with other finite element work at Imperial College and was already programmed by the author and available for use. Some difficulties were experienced in its use in cases (both due to rapid potential variations across an element near a boundary) of consolidation and steady seepage with a non-linear permeability. It is now thought that the 9-noded,

parabolic Lagrangian element would confer advantages over the Serendipity element in suppressing this behaviour as the shape functions are more complete. This element also offers advantages where the automatic generation of element meshes is an important consideration.

Analytical, or closed form, solutions have considerable aesthetic appeal. It is also a widely held view that the existence of a closed form solution simplifies the computation necessary for a parametric study. This may well be true if the end result of the computation is a single value such as a flow rate, but it is sometimes found, as it was here, that the computation of field values using the closed form solution is in fact more, not less, costly in computer resources than a numerical model. Furthermore the closed form solution can often be in terms of a slowly converging series with significant numerical problems associated with its evaluation.

8.2. Realistic Simulation of Field Boundary Conditions

The finite element method is capable of handling all types of boundary conditions so far postulated for seepage either directly or through some iterative process (Section 3.4). Truly impermeable boundaries are a convenient fiction which may be invoked if the permeabilities on each side of an interface differ by two or more orders of magnitude; and a similar permeability ratio, but of the opposite sense, combined with appropriate pore pressure conditions permits an interface to be treated as an equipotential.

Boundary conditions along air faces of the seepage regime are the major source of difficulty. The so called "free surface seepage" can only develop in coarse grained soils and may be obscured by capillarity, which latter effect will dominate in seepage in very fine grained soils. In these cases, the assumption of a "wetted surface", at zero pressure, perhaps some depth below the true ground surface, is a better model for predicting the overall pore pressure distribution. Neither of these yields anything like the

correct pore pressures close to the air face, but in the main these are of interest only to soil physicists and are best predicted by soil physicist's models of seepage in the partly saturated zone.

Lafleur and Lefebvre (1980) using the finite element method, have shown that the existence of a higher permeability mantle on the slope renders a free surface approach an unnecessary complication. Additionally, it may not be possible to predict a position for the free surface (that satisfies geotechnical engineers' prejudice) in certain cases, notably where there is a significant increase of permeability with depth.

8.3. The Use of Non-Linear Models in Seepage

Non-linear models for steady seepage have hitherto been little used, and the literature is scanty. Nevertheless, the present studies confirm the importance of permeability variations on the distribution of potentials in a seepage regime. This effect is largest where the permeability changes take place *in the direction of* seepage (i.e. along a flow line) rather than at right angles to that direction. Typically, a permeability variation resulting from a change in effective stress is an important effect of this sort whereas permeability variations resulting from weathering or stratigraphical changes will only be found to meet this criterion on a very restricted range of cases.

Analytical, or closed form, solutions to seepage in soils with an effective stress dependent permeability have been developed, but only for a limited number of simple cases. Numerical solutions of varying degrees of complexity are presented in this thesis. The simplest of these is applicable only to one dimensional cases, but is capable of dealing with effective stress - permeability relationships for which the analytical solutions are not available; the most complex is an iterative finite element technique tested and used for two dimensional work but equally as applicable to three dimensional problems. All the results from the numerical

techniques have been compared to the closed form solutions with a remakable degree of correspondence.

Non-linear models are much more widely used in the analysis of consolidation processes. However, the element of non-linearity considered is usually in the stress-strain behaviour (or compressibility) and not in the permeability. This is thought to reflect the importance placed by modern researchers on the correct prediction of ground movements and demands a "coupled" solution. However, "uncoupled" solutions are quite adequate for computing pore water pressure dissipation rates (and indeed, in certain circumstances, yield identical pore pressure and deformation results to the more sophisticated coupled methods) and the effects of non-linearity in the permeability, notably a dependency on effective stress levels, have been explored in a limited number of cases by means of an iterative finite element technique. This technique is a simple extension of the work described above on steady state seepage combined with an existing, uncoupled, consolidation theory.

The fundamental findings of this section are that whereas even a modest amount of effective stress dependency in the permeability can strongly influence the distribution of potentials in the steady state seepage regime, even quite strong effective stress dependency in permeability *or* compressibility have comparatively little influence on the *overall* rates of pore water pressure equilibration. Locally, of course, the relative values and rates of equilibration may be considerably different from those predicted by a simple theory.

Final settlement magnitudes depend on the overall pore pressure change and hence do reflect non-linearity in the properties.

Finally, it is observed that the relationship between permeability and effective stress can only be observed correctly if the tests are carried out under similar hydraulic conditions and the effective stresses changed by altering the total stress conditions.

8.4. Trench and Counterfort Drains

The approach to the analysis of seepage around trench and counterfort drains pioneered by earlier writers has been pursued by means of a parametric study using a finite element model. This parametric study has been "proved" in comparison with an especially developed closed form solution, and close agreement found for the cases which could be compared. All the results are presented in the form of design charts which are immediately applicable to the design of drain installations.

One of the most important features of trench drain installations found during this study is that for maximum effectiveness, the drain spacing to depth ratio must be fairly small, much smaller in fact than is conventional in routine work in this country. It also emerges from a study of instrumented trench drain installations that the theory is broadly in agreement with the observations; but that on the whole the performance of trench drain installations is rarely monitored to the necessary degree of accuracy.

Some work on the influence of effective stress dependent permeability has been carried out. This demonstrates that the effect is to *increase* the effective or apparent spacing to depth ratio in contrast to the effect of anisotropic permeability (usually is higher in the horizontal than vertical direction) which serves to *decrease* the spacing to depth ratio.

A small parametric study into the pore pressure changes accompanying excavation and the development of the final steady state pore water pressure regime has been less conclusive, and a satisfactory explanation of the piezometer records from certain of the case histories, which indicate anomalous behaviour in the first seasonal cycle after these trench drains were installed, has yet to be found.

8.5. Seepage in Slopes

The small parametric study of seepage in slopes has a number of important results. Firstly, it shows that for soil slopes without significant underdrainage, seepage is largely horizontal and that the average pore water pressure ratio r_u is about 0.3 in all cases. Thus the findings of James (1970) in this respect are not merely fortuitous. They indicate that he was most probably reporting field measurements of pore water pressure in slopes that were fully equilibrated.

When the slope is subject to underdrainage, the pore water pressure conditions are considerably modified, but it does not reach the essentially one dimensional, vertical flow condition described by Walbancke (1976) unless it is subject to a considerable degree of underdrainage or unless it has a small depth of soil to slope height ratio. The influence of a decrease in permeability with depth or with effective stress in an underdrained slope is to make the seepage conditions approach those for the impermeable bedrock case. This can be most easily visualised by means of Sweeney's (1970) wedge model for seepage in an underdrained slope with a varying permeability.

Whatever the case as regards the boundary conditions, the use of a permeability which depends on effective stress in analysis leads to increased pore water pressures being predicted at the toe of the slope with a consequent reduction in calculated stability.

8.6. General Observations

The work in this thesis shows how far ahead of laboratory and field measurements are the various numerical analysis techniques. Further field measurements to verify the detailed results of the parametric study are a potentially fruitful source for further research, as is an extensive programme in the laboratory to define the true nature

of the relationship between permeability and effective stress. In particular, the way that principal permeability axes respond to rotations in the principal stress directions has hitherto received no attention. It would also be of great practical significance to fully understand the relative importance of *intrinsic* (soil fabric dominated) permeability anisotropy and that imposed on the soil by the stress system under which the soil is consolidated.

REFERENCES

Aguirre, Ramirez, G. & Oden, J. T. (1973)
Finite Element Techniques applied to heat conduction in solids with termperature dependent thermal conductivity
Int. Jnl. Num. Meth. in Engng., 7, 345-356

Al-Dhahir, Z.A., Kennard, M.F., & Morgenstern, N.R. (1970)
Observations on Pore Water Pressures Beneath the Ash Lagoon Embankments at Fiddler's Ferry Power Station
Proc. Conf. on the In Situ Testing of Soils & Rocks, 265-276

Bayley, M. J. (1971)
Cliff Stability at Herne Bay
Civ. Engng. & Publ. Wks. Rev. 63, 860-861

Biot, M.A. (1955)
Theory of Elasticity and Consolidation for a Porous Anisotropic Solid
Jnl. Appl. Phys. 26, 182-185

Bishop, A.W., & Al-Dhahir, Z.A., (1970)
Some Comparisons Between Laboratory Tests, In Situ Tests and Full Scale Performance with Special Reference to Permeability and Coefficient of Consolidation
Proc. Conf. on the In Situ Testing of Soils & Rocks, 251-264

Bishop, A.W. & Morgenstern, N.R. (1960)
Stability Coefficients for Earth Slopes
Geotechnique 10, 192-147

Bishop, A.W. & Hight, D. W. (1977)
The Value of Poisson's Ratio in Saturated Soils and Rocks Stressed Under Undrained Conditions
Geotechnique, 27, 3, 369-384

Biot, M. A. (1941)
General Theory of Three-Dimensional Consolidation
Jnl. Appl. Phys., 12, 155-164

Bjerrum, L. (1953)
General Report (especially p. 367)
Proc. 3rd Int. Conf. Soil Mechs. & Fndn. Engng, 2, 362-371

Black, W. P. M., Croney, D. & Jacobs, J. C. (1958)
Field Studies of the Movement of Soil Moisture
Road Res. Tech. Paper No. 41, HMSO

Boehmer, J. W. & Christian, J. T. (1969)
Plane Strain Consolidation by Finite Elements
MIT Dept. of Civil Engineering Research Rept. R69-60 Soil Mechanics Publ. No. 243

Bromhead, E. N. (1972)
A Study of Some Aspects of Time Dependent Failure of Cuttings in Overconsolidated Clays with Special Reference to Transient Pore Water Pressure Effects
M.Sc., Dissertation, Imperial College

Bromhead, E.N. (1976)
Discussion on Desai (1976)
Int. Jnl. Num. Meth. in Engng, 11, 908-909

Carslaw, H.S. & Jaeger, J.C. (1959)
Conduction of Heat in Solids
Clarendon Press, Oxford (2nd Edn.)

Chowdhury, R.N. & King, G.J.W. (1972)
Non-Linear Seepage in Isotropic and Anisotropic Porous Media
Proc. I.C.E. (Supplementary Vol.), 53, 100

Collin, A. (1846)
Recherches Experimentales Sur Les Glissements Spontanes des Terrains Argileux
Paris: Casilian - Goeury et V. Dalmont

Comini, G., DelGuidice, S., Lewis, R. W., & Zienkiewicz, O.C. (1974)
Finite Element Solution of Non-Linear Heat Conduction Problems with Special Reference to Phase Change
Int. Jnl. Num. Meth. in Engng., 8, 613-624

Darcy (1956)
Les Fontaines Publiques de la Ville de Dijon
Publ. V. Dalmont, Paris

De Mello , V.F.B. (1977)
Reflections on Design Decisions of Practical Significance to Embankments Dams
Geotechnique, 27, 279-355

Desai, C.S. (1976)
Finite Element Residual Schemes for Unconfined Flow
Int. Jnl. Num. Meth. in Engng, 10, 1415-1418

Dunlop, P., & Duncan, J. M. (1970)
Development of Failure Around Excavated Slopes
Trans. Am. Soc. C.E., 69, SM2, 471-493

Edelman, Ir. T. (1953a)
The Consolidation of a Layer Which Modulus of Elasticity is Proportional to the Depth
Prc. 3rd Int. Conf. Soil Mechs. & Fndn. Engng, 1, 358-361

Edelman, Ir. T. (1953b)
The Influence of Compressibility of Soil on Some Problems of Ground Water Flow
Proc. 3rd Int. Conf. Soil Mechs. & Fndn. Engng, 2, 219-223

Ellis-Jones, C.R. (1978)
Private communication on the subject of the stability of the Downs Hill, Maldon; supported by various reports to The Maldon District Council on the same subject.

Finn, W. D. L. (1967)
Finite Element Analysis of Seepage Through Dams
Proc. A.S.C.E. Jnl. Soil Mech. Div., 93, 41-48

Finn, W. D. L. & Varoglu, E. (1980)
A Variational Formulation of Free-Surface and Moving Boundary Problems Incorporating Adaptive Finite Elements
Proc. 1st Int. Conf. on Numerical Meth. for Non-Linear Problems, 623-648

France, P.W., Parekh, C.J., Peters, J.C. & Taylor, C. (1971)
Numerical Analysis of Free Surface Seepage Problems
Jnl. of Irr. & Drain. Div. A.S.C.E., 97, IRI, 165-179

Freeze, R.A. & Witherspoon, P.A. (1966)
Theoretical Analysis of Regional Groundwater Flow, I: Analytical and Numerical Solutions to the Mathematical Model
Water Resources Res., 2, 641-656

Freeze, R.A. & Witherspoon, P.A. (1967)
Theoretical Analysis of Regional Groundwater Flow, II: Effect of Water Table Configuration and Subsurface Permeability Variations
Water Resources Res., 3, 623-634

Gambolati, G. (1975)
Use of the Over-Relaxation Technqiue in the Simulation of Large Ground Water Basins by the Finite Element Method
Int. Jnl. Num. Meth. in Engng, 9, 219-233

Ghaboussi, J. & Wilson, E.L. (1972)
Flow of Compressible Fluid in Porous Elastic Media
In. Jnl. Num. Meth. in Engng, 4, 419-442

Gibson, R.E. (1963)
An Analysis of System Flexibility and Its Effect on Time Lag in Pore Water Pressure Measurements
Geotechnique, 13, 1-11

Gibson, R. E. (1966)
A Note on the Constant Head Test to Measure Soil Permeability In-Situ
Geotechnique, 16, 256-259

Gibson, R.E., (1970)
An Extension to the Theory of the Constant Head In-Situ Permeability Test
Geotechnique, 20, 193-197

Gibson, R. E. (1974)
The Analytical Method in Soil Mechanics
Geotechnique, 24, 113-140

Hammer, P.C., Marlowe, O.P., & Stroud, A.H. (1956)
Numerical Integration Over Simplexes & Cones
Math. Tables Aids Comp., 10, 130-137 (Ref. by Zienkiewiz (1972))

Hamza, M.M.A.F., (1976)
Analysis of Embankment Dams Using Non-Linear Finite Element Method
Ph.D. Thesis, Imperial College

Henkel, D.J. (1957)
Investigations of Two Long Term Failures in London Clay Slopes at Wood Green & Northolt
Proc. 4th Int. Conf. Soil Mechs. & Fndn. Engng, 2, 315-320

Henkel, D.J. (1960)
The Shear Strength of Saturated Remoulded Clays
Proc. Conf. on Shear Strength of Cohesive Soils, Boulder, Colorado

Herbert, R. (1967)
Discussion on Timlin (1966)
Geotechnique, 17, 72

Herbert, R. & Rushton, K.R. (1966)
Ground Water Flow Studies by Resistance Networks
Geotechnique, 16, 53-75

Hodge, R.A.L. & Freeze, R.A. (1977)
Groundwater Flow Systems and Slope Stability
Can. Geotech. Jnl., 14, 466-476

Hoek, E. & Bray, J.W. (1977)
Rock Slope Engineering (2nd Edn.)
Inst. Min. & Metal, London

Hutchinson, J.N. (1977)
Assessment of the Effectiveness of Corrective Measures in Relation to Geological Conditions and Types of Slope Movements
Bull.Int. Assoc. of Engng. Geol, 16, 131-155

Hutchinson, J.N., Bromhead, E.N. & Lupini, J.F. (1980)
Additional Observations on the Folkestone Warren Landslides
Q. Jnl. Eng. Geol., 13, 1-32

Hutchinson, J.N. (1980)
Possible Late Quaternary Pingo Remnants in Central London
Nature, 284, 253-255

Hwang, C.T., Morgenstern, N.R. & Murray, D.W. (1972)
Application of the Finite Element Method to Consolidation Problems
Proc. Symp. Appl. of the F.E. Method in Geotechn. Eng. U.S. Army W.E.S. 739-764

Ingold, T.S. (1980)
Lateral Earth Pressures - A Reconsideration
Ground Engineering, 13, May, 39-43

Irmay, S. (1953)
Saturated Steady Flow in Non-Homogenous Media & Its Applications to Earth Embankments, Wells, Drains.
Proc. 3rd Int. Conf. Soil Mechs., & Fndn Engng, 2, 259-263

James, P.M. (1970)
Time Effects and Progressive Failure in Clay Slopes
Ph.D. Thesis, Imperial College, London

Janbu, N. (1957)
Stability Analysis of Slopes with Dimensionless Parameters
Harvard University Soil Mechanics Series No. 46

Kealy, C.D. & Busch, R.A. (1971)
Determining Seepage Characteristics of Mill-Tailings Dams by the Finite Element Method
U.S. Bureau of Mines Report RI7477

Lafleur, J. & Lefebvre, G. (1980)
Groundwater Regime Associated with Slope Stability in Champlain Clay Deposits
Can. Geotech. Jnl., 17, 44-53

Laim Finn, W.D.
See Finn, W.D.L. (This author styles himself in both modes)

Mandel, J. (1953)
Consolidation des Sols (Etude Mathematique)
Geotechnique, 3, 287-299

Martins, J.B. (1965)
Consolidation of a Clay Layer of Non-Uniform Coefficient of Permeability
Proc. 6th Int. Conf. Soil Mechns, & Fndn. Engng, 1, 308-312

Morgenstern, N.R. & Guther, H. (1972)
Seepage into an Excavation in a Medium Possessing Stress Dependent Permeability
Proc. Symp. on Percolation Through Fissured Rock Int. Soc. Rock Mechs. & Int. Assoc. Eng. Geol., Stuttgart, T2-C, 1-15

Naylor, D.J. (1974)
Stresses in Nearly Incompressible Material by Finite Elements with Application to the Calculation of Excess Pore Water Pressure
Int. Jnl. Num. Meth. in Engng, 8, 443-460

Neuman, S.P. & Witherspoon, P.A. (1970)
Finite Element Method of Analysing Steady Seepage with a Free Surface
Water Resources Res., 6, No.3, 889-897

Neuman, S.P. & Witherspoon, P.A. (1971)
Analysis of Non-Steady Flow with a Free Surface Using the Finite Element Method
Jnl. of Water Resources Res., 7, No.3, 611-623

Padovan, J. (1974)
Semi Analytical Finite Element Procedure for Conduction in Anisotropic Axisymmetric Solids
Int. Jnl. Num. Meth. in Engng, 8, 295-310

Parekh, C.J. (1965)
A Finite Element Solution for Transient Field Problems
M.Sc. Thesis, Swansea University

Parekh, C.J. (1969)
Finite Element Solution System
Ph.D. Thesis, University of Swansea

Pilot, G. & Moreau, M. (1973)
La Stabilite des Remblais Sur Sols Mous
Editions Eyrolles, Paris

Poskitt, T.J. (1971)
The Numerical Solution of Non-Linear Consolidation Problems
Int. Jnl. for Num. Meth. in Engng, 3, 5-11

Richardson, L.F. (1908)
The Lines of Flow of Water in Saturated Soils
Scient. Proc. Roy. Dublin Soc. Vol XI, No. XXVII, pp 295-316

Sandhu, R.S. & Wilson, E.L. (1969)
Finite Element Analysis of Seepage in Elastic Media
ASCE Jnl. Eng. Mechs. Div. 95, 285-312

Schiffman, R.L. (1958)
Consolidating of Soil Under Time Dependent Loading and Varying Permeability
Proc. Hwy. Res. Bd., 37, 584-617

Schiffman, R.L. & Gibson, R.E. (1964)
Consolidation of Non-Homogenous Clay Layers
Prc. ASCE Jnl. Soil Mechs. & Fndns Div, 90, 1-30

Skempton, A. W. (1954)
The Pore Pressure Coefficients A & B
Geotechnique, 4, 143-147

Skempton, A.W. & Brown, J. D. (1961)
A Landslide in Boulder Clay at Selset, Yorkshire
Geotechnique, 11, 280-293

Skempton, A.W. & Henkel, D.J. (1961)
Field Observations on Pore Pressures in London Clay
Proc. Conf. on Pore Pressure & Suction in Soils, 81-84

Skempton, A. W. (1970)
First Time Slidesin Overconsolidated Clays
Geotechnique, 20, 320-324

Skempton, A.W. and Weekes, A. G. (1976)
The Quaternary History of the Lower Greensand Escarpment and Weald
Clay Vale near Sevenoaks, Kent
Phil. Trans. Roy. Soc. London A 283, 493-526

Spencer, E. E. (1967)
A Method of the Analysis of the Stability of Embankments Assuming
Parallel Inter-Slice Forces.
Geotechnique, 17, 11-26

Starr, M.R., Skipp, B.O., & Clarke, D. A. (1969)
Three-Dimensional Analogue Used for Relief Well Design in the Mangla
Dam Project
Geotechnique, 19,87-100

Sweeney, M. (1970)
Pore Pressures in a Non-Uniform Clay Slope by Theory and Electrical
Resistance Analogue
M.Sc. Dissertation, Imperial College

Taylor, D.W. (1937)
Stability of Earth Slopes
Jnl. Boston Soc. Civ. Engrs, 24, 197-246

Taylor, R. L. & Brown, C.B. (1967)
Darcy Flow Solutions with a Free Surface
Proc. A.S.C.E. Jnl. Hyd. Div, 93, 25-33

Tomlin, G. R. (1970)
Seepage Analysis Through Zoned Anisotropic Soils by Computer
Geotechnique, 16, 220-230

Truscott, E.G. (1977)
Behaviour of Embankment Dams
Ph.D. Thesis, Imperial College

Vaughan, P.R. & Walbancke, H.J. (1973)
Pore Pressure Changes and Delayed Failure of Cutting Slopes in
Overconsolidated Clay
Geotechnique, 23, 531-539

Volker, R.E. (1969)
Non-Linear Flow in Porous Media by Finite Elements
Proc. A.S.C.E. Jnl. Hyd. Div., 95, 2093-2114

Walbancke, H.J. (1976)
Pore Pressure in Embankments and Cuttings
Ph.D. Thesis, Imperial College

Water Resources Board (1972)
The Hydrogeology of the London Basin with Special Reference to
Artificial Recharge
Water Resources Board 1972

Whitley, H.M. (1880)
Earthwork Slips on the Castle Eden and Stockton Railway
Min. Proc. Instn. Civil Engrs. 62, 280-284

Wilkinson, W.B. (1968)
Constant Head In-Situ Permeability Tests in Clay Strata
Geotechnique, 18, 172-194

Wilkinson, W.B., Barden, L. & Rocke, G. (1970)
An Assessment of In-Situ and Laboratory Tests in Predicting the Pore Pressure in an Earth Dam
Proc. Conf. on the In-Situ Testing of Soils & Rocks, 277-293

Wilson, G. and Grace, H. (1942)
The Settlement of London Due to Underdrainage of the London Clay
Jnl. Inst. Civ. Engrs, 19, 100-127

Zienkiewicz, O.C. (1972)
The Finite Element Method in Engineering Mechanics (2nd Ed.)
Wiley International

Zienkiewicz, O. C., & Cheung, Y.K. (1965)
Finite Elements in the Solution of Field Problems
The Engineer, 220, 507-520

Zienkiewicz, O.C., Mayer, P. & Cheung, Y.K. (1966)
Solution of Anisotropic Seepage by Finite Elements
Proc. A.S.C.E. Jnl. Eng. Mechs. Div, 92, 111-142

Zienkiewicz, O.C. & Parekh, C.J. (1970)
Transient Field Problems: Two Dimensional and Three Dimensional Analysis by Isoparametric Finite Elements.
Int. Jnl. for Num. Meth. in Engng, 2, 61-71

Additional References:

Bayley, M.J. (1972)
Cliff Stability at Herne Bay
Civil Engineering & Public Works Review, 63, 860-861

Berry, F.G. (1979)
Late Quaternary Scour-hollows & Related Features in Central London
Q. Jnl of Eng. Geol., 12, 9-29

Bromhead,E.N. (1978)
Large Landslides in London Clay at Herne Bay, Kent
Q. Jnl of Eng. Geol.,11, 291-304

Lopes, F.de R. (1979)
The Undrained Bearing Capacity of Piles & Plates Studied by
The Finite Element Method
PhD Thesis, Imperial College

Ove Arup & Partners. (1970,1971)
Herne Bay East Cliff Stability Study
Unpublished Consulting Reports: Vols 1, 2 & 3

Vaughan, P.R., Kluth, D.J.,Leanard & Pradoura,H.H.M. (1970)
Cracking & Erosion of the Rolled Clay Core of Balderhead Dam
and the Remedial Works Adopted for its Repair
Trans. 10th Int. Cong. Large Dams, Montreal, 3,73-93

Vaughan, P.R. & Walbancke,H.J. (1973)
The Stability of Cut and Fill Slopes in Boulder Clay
Midland Soc. Soil Mech. & Foundn Eng., Birmingham. 270-272

Vaughan, P.R. (1980)
Personal Communication

IMPERIAL COLLEGE

Collected Papers

EDWARD NICHOLAS BROMHEAD

Supplement to Ph.D. Thesis

October, 1980

CONTENTS

1. Introduction

2. Large Landslides in London Clay at Herne Bay, Kent

3. A Simple Ring Shear Apparatus

4. Factors Affecting the Transition Between the Various Types of Mass Movement in Coastal Cliffs Consisting Largely of Overconsolidated Clay, with Special Reference to Southern England.

5. Additional Observations on the Folkestone Warren Landslides (with J. N. Hutchinson and J. F. Lupini)

6. Solutions for Seepage in Soils With An Effective Stress Dependent Permeability (with P. R. Vaughan)

7. Cliff Recession on the Isle of Wight S.W. Coast (with J. N. Hutchinson and M. P. Chandler)

1. Introduction

The regulations of the University of London for the award of the degree of Doctor of Philosophy permit candidates to submit additional documentary material to support theses in their submission. This volume contains a number of papers published, or approved for publication, during the candidates' registration, together with some brief explanatory notes on each one.

2. "Large Landslides in London Clay at Herne Bay, Kent" QJEG 1978

This paper summarised stability analysis results for three large coastal landslides in London Clay, together with a potted history of each one. The author believes that the back analysis data given in this paper significantly extends knowledge of the field residual strength of London Clay in both quantitative and qualitative terms.

3. "A Simple Ring Shear Apparatus" Ground Eng. 1979

The device described in this paper was designed by the author and built under his direction at Kingston Polytechnic. It is intended to provide a laboratory measurement of residual strength to an accuracy, and within a timescale, appropriate to the commercial testing laboratory; and it is not intended to supplant the Imperial College designed device for fundamental research into residual strength. Experience shows that the device fulfils its design objectives, and the machine has been enthusiastically accepted in industry in both the United Kingdom and abroad.

4. "Factors Affecting the Transition Between the Various Types of Mass Movement in Coastal Cliffs Consisting Largely of Overconsolidated Clay, with Special Reference to Southern England" QJEG 1979

This paper draws on the previously published work of J. N. Hutchinson to attempt to provide a more general picture for the reasons underlying the change from one type of mass movement behaviour than the previously accepted tripartite classification based on the severity of marine erosion.

The paper was presented at the Regional Conference of the Engineering Group of the Geological Society held in Southampton University in September 1978.

5. "Additional Observations on the Folkestone Warren Landslides"
QJEG 1980

In this long paper, the historical data on the various mass movements at Folkestone Warren is reviewed and the back analyses reconsidered in the light of this review. It is found that previously held opinions on the sequence of events and their cause are largely erroneous and the paper sets the record straight. The reasons for the unusually large (30m+) displacements of the 1915 slide are discussed. Selected samples of Gault Clay are tested in ring shear both at Imperial College and at Kingston Polytechnic (as part of the proving trials fo the simple ring shear apparatus - see Section 2) with remarkable correlation between the two test series.

While in a multiply authored paper it is not possible to accurately accredit work to individual authors, the contribution of the present writer was in the new stability analyses and in one series of ring shear tests. The latter were, however, not made by the writer personally, but were carried out under his immediate supervision.

This paper was also presented at the 1978 Engineering Geology Group (of the Geological Society) Regional Conference at Southampton.

6. "Solutions for Seepage in Soils with An Effective Stress Dependent Permeability" Proc. 1st Int. Conf on Numerical Meth. in Non-linear Problems, Swansea 1980

This paper summarises the subject matter of Chapters 2 and 3 of this thesis. It was presented at a conference held at Swansea University in September 1980.

7. "Cliff Recession on the Isle of Wight S.W. Coast" Proc. ICSMFE, Stockholm 1981

This paper has been selected by the BGS sub-committee for presentation at the forthcoming Stockholme ICSMFE. The writer's contribution to this multiply authored paper lies in aspects of the fieldwork, computer stability analysis and soil strength testing.

The importance of this paper is in the clear description of the mechanics of cliff retreat at this highly active location.

Q. Jl Engng Geol. 1978 Vol 11 pp. 291–304, 10 figs., 5 tables, 3 plates. Printed in Northern Ireland.

Large landslides in London Clay at Herne Bay, Kent

E. N. Bromhead

School of Civil Engineering, Kingston Polytechnic, Canbury Park Road, Kingston.

Summary

Stability analyses of three large coastal landslides in the London Clay cliffs east of Herne Bay in Kent are presented together with summarised accounts of the investigations which made them possible. The results of these analyses are then compared with the results from other field and laboratory studies of residual strength and slope stability in London Clay.

Introduction

The residual strength of a soil is an important parameter, being of fundamental importance both to the behaviour of existing landslides (Skempton 1964) and to the problem of progressive failure (Bishop 1971). An important step in the understanding of residual strength came with the development of the ring shear apparatus, with which Bishop *et al.* (1971) demonstrated that very large relative displacements of the soil on each side of a developing shear surface were often essential to develop the true residual strength: previous measurements in other apparatus using pre-cut shear planes or multiple reversals, generally tended to over-estimate this strength.

However, many field studies, including those of natural slopes (Skempton & Delory 1957, Hutchinson 1967) and of failures of cutting slopes and retaining walls (James 1970) suggest higher values for the residual strength *in situ* than implied by the ring shear test. This may be due either to inadequate field measurements of pore water pressure or due to 'size effects'. This latter phenomenon is the result of comparing relatively small scale instability in the field, where shear and normal effective stress levels are of small magnitude, with laboratory tests more usually carried out at higher stress levels, since the accuracy of tests at lower stress levels is notoriously low due to difficulties in absolute measurement. Where the test results, themselves, are dependent on the stress levels applied, the correlation with analyses of field situations becomes highly speculative. The comparative lack of adequate field evidence has stimulated the presentation of the case histories of three large landslides in the coastal London Clay cliffs at Herne Bay in Kent, the scale of which makes their analysis less sensitive to the factors described above.

Location and geology

Herne Bay is on the north Kent coast, near the easternmost edge of the London Clay outcrop (Fig. 1). Extending for several miles from the town in an easterly direction are coastal cliffs which rise quickly to a maximum elevation of 40 m above Ordnance Datum, but are generally a few metres lower. In recent years, these cliffs have been subjected to extensive coast defence and cliff stabilisation work and now bear little resemblance to their former appearance when they were the site of several large landslides and numerous mudslides (Hutchinson 1970).

The succession in the cliffs is:

Head up to 3 m.
London Clay approximately 30 m.
Oldhaven Beds not exposed at the sites of the landslides.

The Oldhaven Beds comprise compact, silty fine sands of a grey colour which weathers brown within several years of exposure. They outcrop in the beach eastward from about grid reference TR198686 and dip westwards at about 2 degrees. A transition zone of up to 3 m in thickness, in which occasional silty clay layers become of increasing importance, marks the base of the London Clay, a stiff, fissured, overconsolidated clay of Eocene Age. Overlying the London Clay is Head, comprising clayey sands and gravels, locally achieving thicknesses of 3 m, but more generally existing only as a sparse cover. In the extreme east, where the Oldhaven Beds form steep cliffs, the London Clay is in some places entirely absent.

Although the Oldhaven Beds contain occasional lamellibranchs, they are comparatively barren of micro-fossils, in direct contrast with the overlying London Clay which has a rich micro-fossil population providing several useful marker bands (Hughes 1970). However, since the micro-fossils tend to be pyritised, they are easily damaged by weathering, not only when exposed in the beach, but also in the uppermost 10 m of the London Clay where oxidation has led to the soil becoming brown in colour. Beneath the most highly weathered zone, a further transitional zone about 15 m in thickness is present and through this the colour changes from brown, through an olive colour to the characteristic blue–grey of unweathered London Clay. Gypsum crystals formed during the weathering

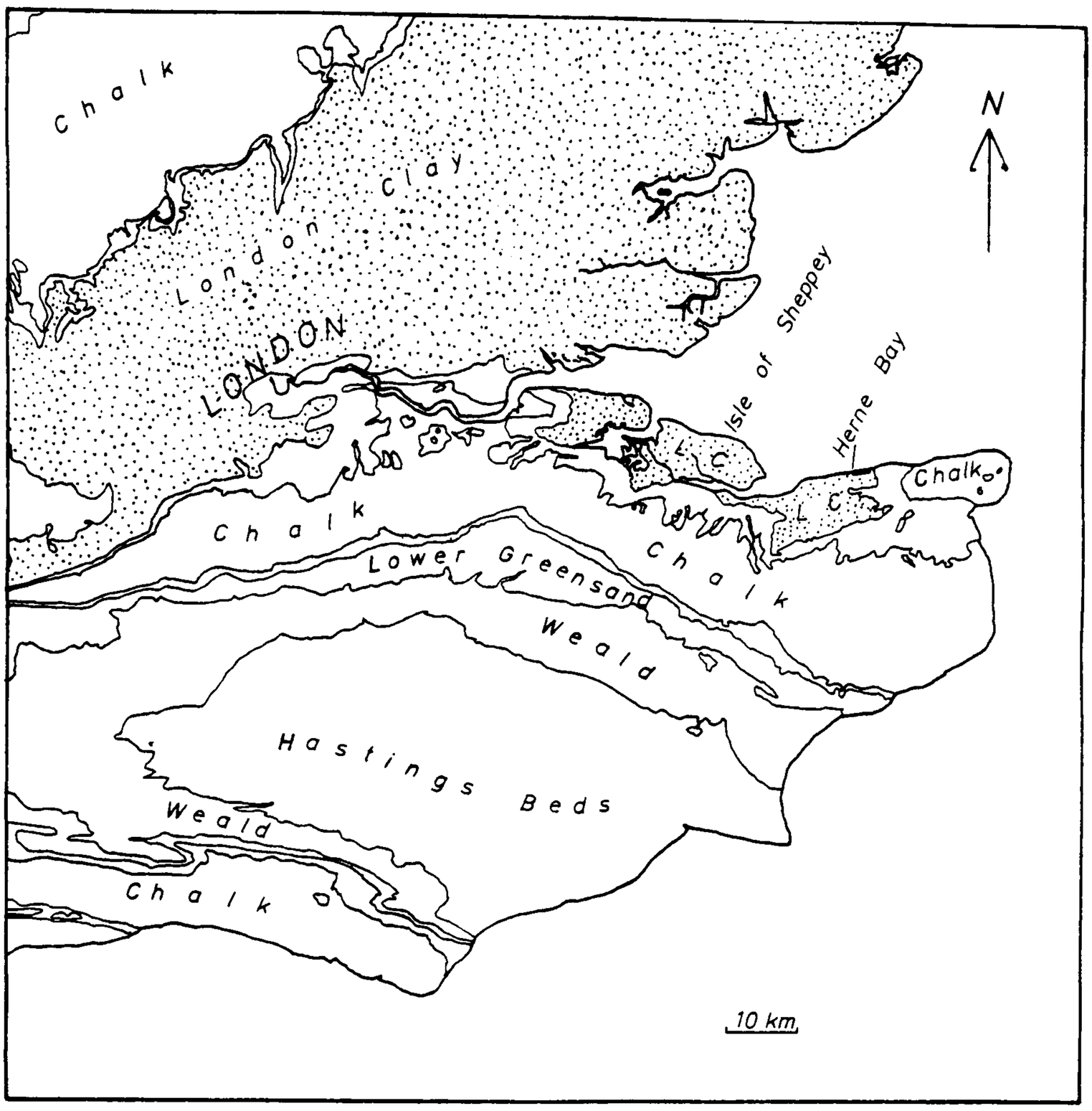


FIG. 1. Solid geology of southeast England showing the extent of the London Clay outcrop and the location of Herne Bay.

process are common in the uppermost levels. Weathering inwards from the face of the cliff is negligible since, until recently, the rates of surface transport have been rapid; but there are localities where the surface layers of the slope consisting mainly of old mudslide materials have been stabilised *in situ* by means of shallow drainage trenches.

Accompanying the weathering and erosion of the cliffs have been changes in the fissure structure within the clay (Bayley 1972, Tchalenko 1968); but on the whole the London Clay exhibits a uniformity of appearance at corresponding horizons across the whole site. The ranges of plasticity indices and moisture contents are small and are listed in Table 1.

Mechanism of coastal recession

In the past, the cliffs have been degraded principally by a process of mudslide formation and erosion, with the transported materials being removed by marine action at beach level. Mudslides at this locality have been described in detail (Hutchinson 1970), and on

TABLE 1. Average geotechnical properties of the London Clay at Herne Bay

Soil type	Natural water content %	Liquid limit	Plastic limit	Unit weight kg/m^3	Clay fraction
Brown London Clay	25–30	85–95	22–29		67–72
Blue London Clay	24–30	80–95	22–32	1765–2000	60–70 (in middle 50's at depth)
Mudslide	30–45+	—	—		—

the basis of this and observations elsewhere, a mechanism by which such mudslides keep moving down low-angle slopes was proposed (Hutchinson & Bhandari 1971). This mechanism is one of *undrained loading*, with frequent small falls or slips of material from a steep rear scarp behind a mudslide on to the head of the slide, contributing to instability not only by their weight, but also by raising the water pressures along the back part of the slip surface. Once mudslide activity is started, it can only be self-supporting if falls from the rear scarp are frequent enough, and where the cliff is capped with thick, relatively sandy head deposits the rear scarps may be too well drained and stable to maintain the mudslides. Without the protection of mudslide tongues pushing seaward each winter and flattening the overall slope of the cliff, the sea attacks the cliff toe, precipitating a deep-seated rotational type of landslide when the cliff is sufficiently oversteepened, It is very noticeable that the three sections of cliff at Herne Bay capped by the greatest thicknesses of Head are also occupied by the remains of deep-seated landslides. In the high London Clay cliffs of the north coast of the Isle of Sheppey (Fig. 1), which is 20 km to the west and capped with much more extensive Head, deep-seated landslides are more prevalent and mudslides are only a secondary agent of mass transport.

Previous investigations

In the 1930's, both to improve the amenities of Herne Bay as a holiday resort and as a means of unemployment relief, a seawall and a number of small buildings were constructed along the toe of the cliffs. Cliff instability, perhaps worsened by these activities, held up construction until a stabilisation scheme described in detail by Duvivier (1940) and comprising regrading, drainage and extensive further construction of reinforced concrete retaining walls was carried out. These remedial works were preceded by an extensive borehole investigation, extending well to the east of the stabilised area since it was intended to augment the seawall and cliff stabilisation as and when funds became available. The deep-seated nature of one old landslide in the stabilised area was not recognised at the time, and the regrading and drainage carried out were insufficient to prevent continued movement, causing further damage to the seawall, which was subsequently rebuilt in 1962–3. At this time, several areas of local and superficial instability that had occurred in the upper parts of the cliffs were repaired and the stabilised area was extended approximately 70 m eastwards.

The overall situation in the untreated area worsened with the occurrence of another deep-seated slip in 1953, and a further scheme for coast protection and cliff stabilisation was accordingly prepared and undertaken in the period 1969–72 (described by Allan 1968). Coincident with this work, an independent investigation (Bayley 1972) was carried out to assess the efficacy of the proposed works. The slip surfaces of the large landslides were found by the visual inspection of borehole samples, and the identification was corroborated by an examination of the micropalaeontological succession (Hughes 1970) making use of the micro-fossil succession identified and used previously for this purpose by Hutchinson & Hughes (1968). During this investigation some 82 piezometers were installed. The majority of these were located to provide a profile of pore-water pressures at each of four locations along six chosen sections, twenty in or just below the deep-seated slips and a further fifty at locations where there had not been any deep-seated movement. These piezometers were read approximately monthly for about two years, and the highest value observed during this period (1969–71) taken for use in this study. Bayley (*op. cit.*) also commented on the still continuing superficial instability in the area stabilised in 1937 using an approach due to Skempton (1970) where the decrease in strength with time is treated as 'softening'.

In addition to the above mentioned studies, Hutchinson (1965*b*), in an extensive investigation of the natural degradation processes, catalogued each area of coastal instability in Kent including the east cliffs at Herne Bay, described here.

Beacon Hill landslide

The remains of the westernmost of the three large landslides (KD 70 in Hutchinson's survey) lie in a cup-shaped hollow at the base of the cliffs just below the crest of Beacon Hill, at Ordnance Survey grid reference TR 189 685 (see Fig. 2). It was movement of this landslide which caused the most serious damage to the works in 1937 and prompted the first stabilisation measures. That these were not completely successful in this instance is evidenced by the continuing slow movements which caused the seawall to bulge outwards. Demolition and reconstruction of this stretch of wall was carried out in the period 1962–3 (Bayley 1972). On the completion of this work, movements continued, although possibly at a somewhat slower rate, and the wall still forms a noticeable salient at this point. Some of this offset has been attributed to a setting out error; but much is due to slow slipping. A periodic survey initiated by Hutchinson (1965*b*) of the deformation of the promenade reveals annual deformation rates occasionally in excess of 25 mm. It is not known whether this is reflected in the inclinometers installed in 1969–70 and described by Bayley, who reports that a sewer, found during the works of 1962, had deviated some 11 ft (3.5 m) from its presumed initally straight position between installation in 1908 and rediscovery. This represents an annual rate of 60 mm, but a major part of this probably occurred

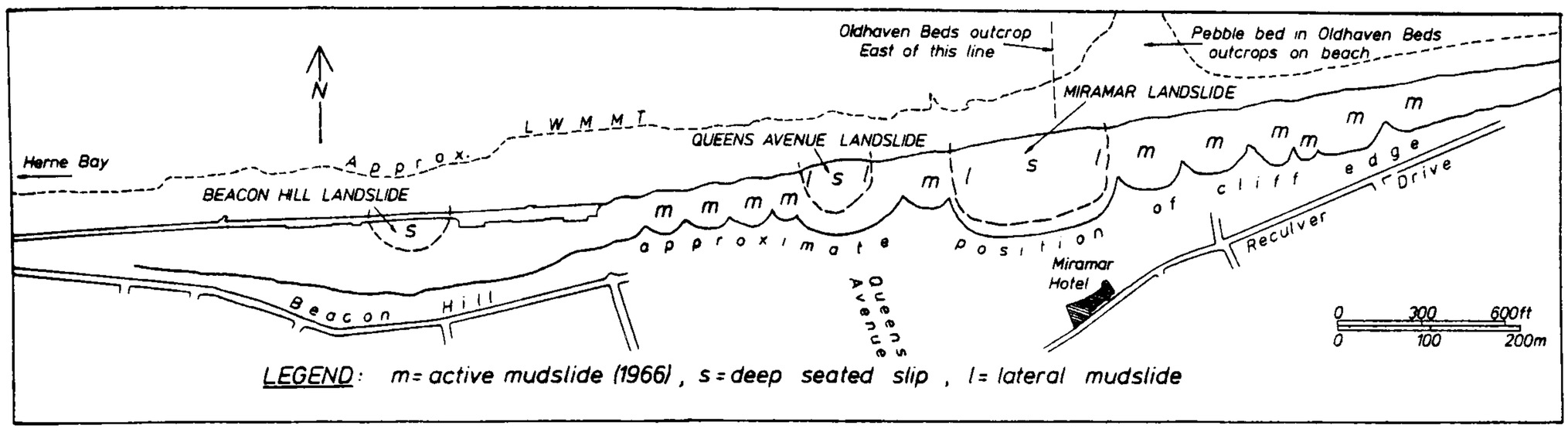


FIG. 2. Plan of the east cliffs at Herne Bay showing the locations of the major sites of instability.

before the remedial works were undertaken and may, therefore, be a gross over-estimate of the current deformation rate.

Bayley gives a section through this landslide (shown in Fig. 3), from which it may be seen that the slip surface is very nearly a circular arc in section. This is attributable to the comparatively great depth below sea-level of the underlying Oldhaven Beds. From the stratigraphical evidence within the section itself, and the position of the centre of the 'best fit' slip circle, a total rotation of 25° (equivalent to a displacement around the slip surface of 50 m) has been estimated. This is consistent with the gaps in the micropalaeontological succession found by Hughes (1970) and reported by Bayley.

Previous attempts at analysis of this landslide had been attempted by Wise (1957) who noted deep tension cracks at the position shown on the section, and a toe heave '70 yards seawards of the wall' in the autumn of 1956, but his under-estimate of the scale of the movements throws serious doubt on the validity of his calculations. These tension cracks are in the vicinity of cracks noted at other times and at a position which corresponds to a change in the gradient of the slope, defining the position of the upper end of the slip surface quite well. The position of the toe is less determinate, but it is probably seaward of the end of the longest groynes (which have not apparently suffered distortion), a position entirely in accordance with the best fit slip circle. On one old drawing through this area, the position of an alleged toe heave was noted, but a number of visits to the shore have failed to reveal any signs of this, probably since the area is considerably mantled by littoral deposits. From these and other surface features (Fig. 4), the depth-to-length and width-to-length ratios are estimated to be 0.14 and 1.10 respectively.

Stability analyses of this slip have been undertaken using two methods: firstly the semi-rigorous method described by Bishop (1955) has been used on the 'best fit' slip circle; and secondly, the Morgenstern & Price (1965) method has been used on the slip surface that diverges from the best fit slip circle to meet with Wise's tension cracks and to provide a slightly flat 'sole' along the interface with the Oldhaven Beds. Bayley quotes the results of an analysis by Kenney's

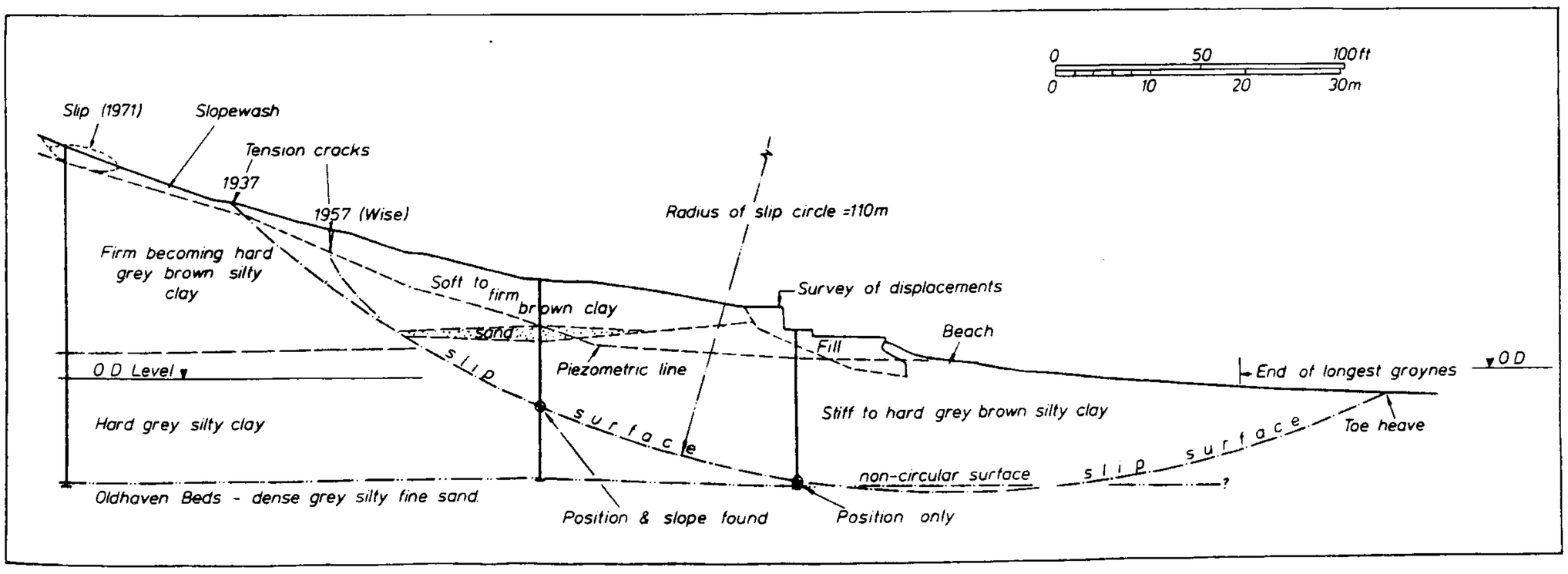


FIG. 3. Section through Beacon Hill landslide. (After Bayley 1972). The position of this section is shown on Fig. 4.

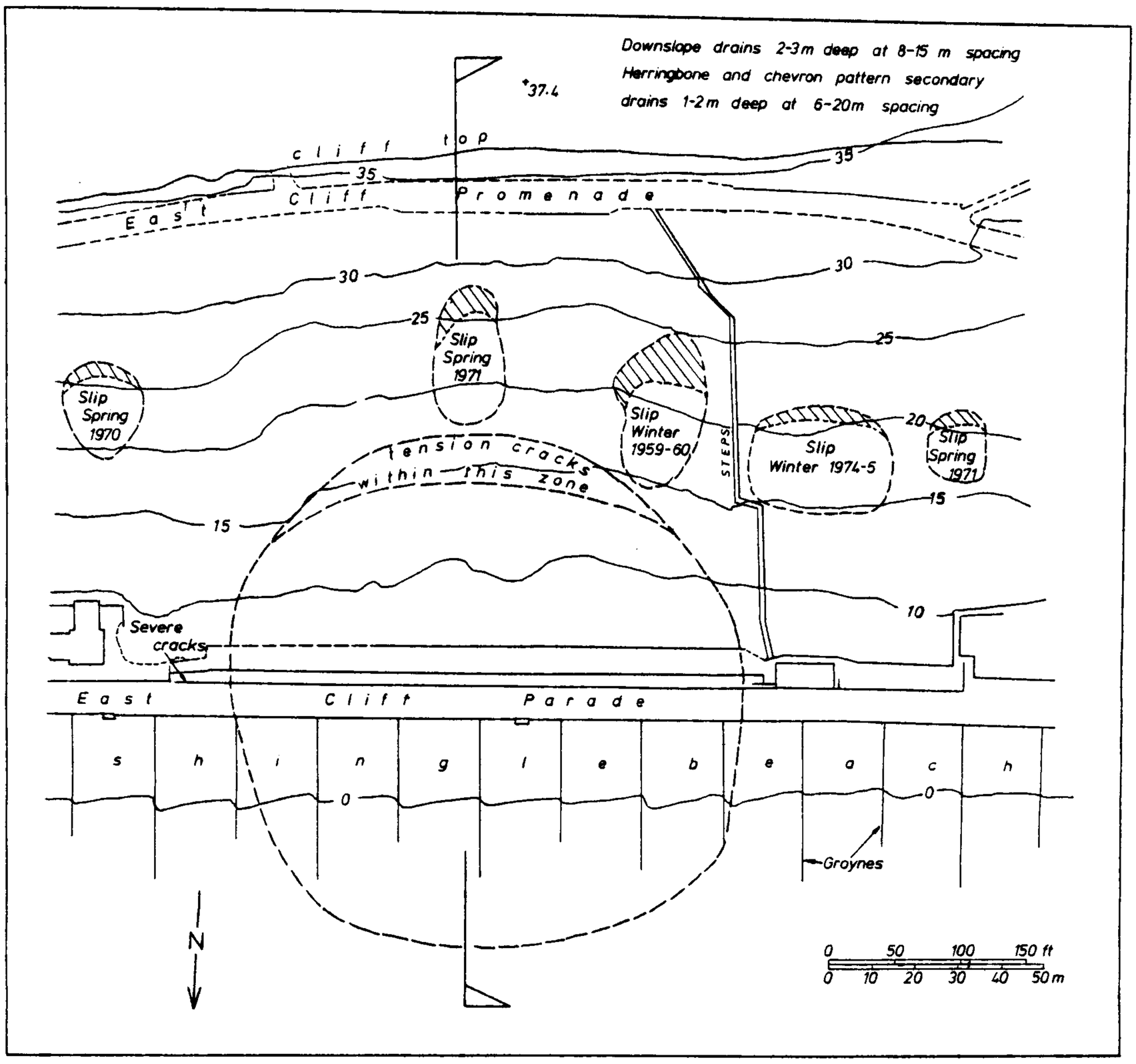


FIG. 4. Contour plan of Beacon Hill landslide. (Based on an original air survey by Meridian Airmaps Ltd.). Contours are marked in metres.

(1956) method in which the mobilised angle of shearing resistance was found to be 14.1° for this slip surface. The results of these analyses compare favourably, revealing a mobilised angle of shearing resistance of 14.7° at an average normal effective stress of about 100 kN/m^2, and they are tabulated in Table 2. Pore water pressures were derived from observations of three piezometers in, and nine piezometers adjacent to, the slipped mass on this section.

It appears from the evidence in early editions of the Ordnance Survey that there have been only small coast line changes at this location and the first movements of this slip must therefore predate the middle 19th century. With only comparatively small changes

TABLE 2. Slope Stability analyses: Beacon Hill landslide

Method	Average pore water pressure ratio r_u	ϕ'_r for equilibrium	Average shear stress kN/m^2	Average normal effective stress kN/m^2	Comments
Bishop's semi-rigorous	0.43	14.7°	28.2	107.5	Best fit slip circle radius = 110 m
Morgenstern and Price	0.43	14.8°	28.5	107.5	Slight divergence from circle, flat 'sole' and rear tension cracks.

Bayley quotes a value of ϕ'_r of 14.1° obtained using Kenney's method.

in profile throughout this period, re-construction and analysis of previous configurations was not found to be practicable.

Queen's Avenue landslide

Approximately 600 m eastward from the Beacon Hill landslide is the remnant of another mass movement (O.S. grid reference TR 195 685; Fig. 2). This site has recently been subjected to extensive regrading, but as shown in Fig. 5, it previously comprised the eroded remains of a large landslide at the base of a deep indentation in the cliff line. The first movements are reported to have occurred in conditions following a tidal surge in 1896, and evidence from the Ordnance Survey provides indirect support to this date by showing the slip on the following series map. Continuous movements probably occurred from that time until about 1969 since, not only does this slip lie well eastward of the end of the 1937 concrete seawall and groynes, but surface indications (notably depressions marking the site of tension cracks) in evidence for several years, also suggest that deep-seated movements continued during the construction activities. This slip has the code number K72 in Hutchinson's (1965*b*) survey.

Fig. 6 is a cross-section through this landslide showing the ground profiles before and after regrading. Both cases have been analysed by means of Morgenstern & Price's method (and the results presented in Table 3), but since the pore water pressures in this landslip were first measured some months after regrading and have been used in both analyses, the results for both cases are probably conservative because there is evidence that movements have now ceased and that the remedial works have taken effect. Residual angles of shearing resistance of about $12\frac{1}{2}°$ at average normal effective stresses in the range 103 to 113 kN/m^2 are mobilised. The d/L and B/L ratios are respectively 0.15 and 1.30. As in the case of the

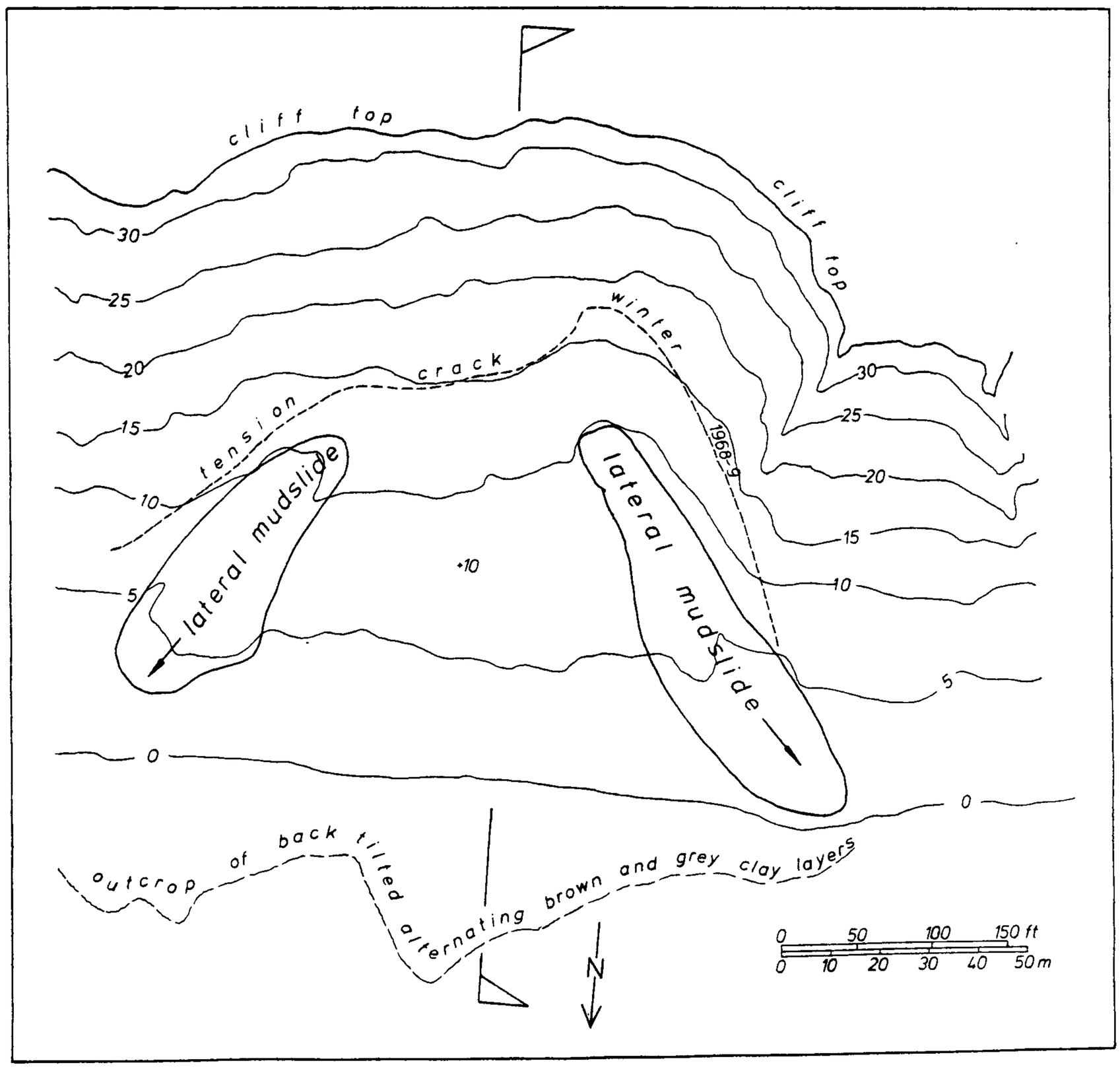


FIG. 5. Contour plan of Queen's Avenue landslide. (Based on an original air survey by Meridian Airmaps Ltd.). Contours are marked in metres.

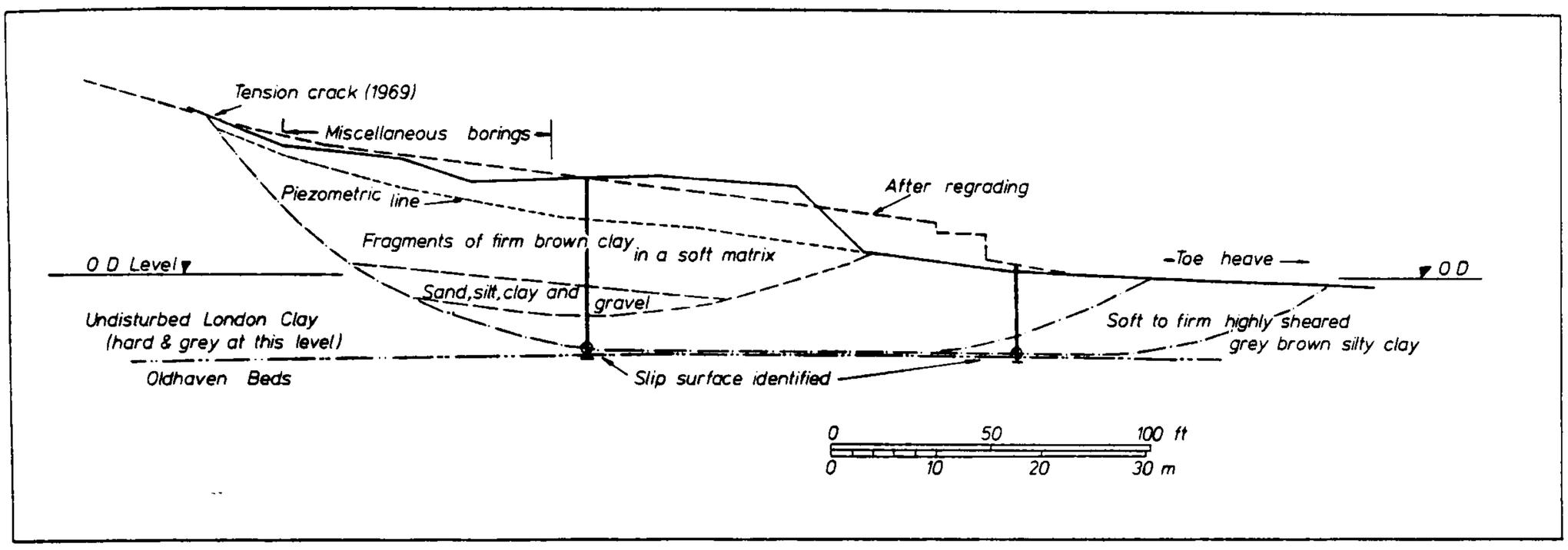


FIG. 6. Section through Queen's Avenue landslide. The position of this section is shown on Fig. 5.

Beacon Hill landslide, calculations have been carried out for the centre line section, since although sufficient information was obtained to contour the rear-most half of the slip surface from Bayley's and other investigations, the pore water pressure data to allow the analysis of other sections are not available. The pore water pressures used in the analyses have been derived from three piezometers in, and six piezometers adjacent to, the slip mass on this section. Displacements of the slip surface are at least 30 m.

Miramar landslide

Further eastward still, the Oldhaven Beds outcrop on the seashore and rise until near Bishopstone Glen they comprise the major part of the cliffs (Figs. 2 and 7). Coinciding with the outcrop of the Oldhaven Beds on the foreshore is an area of particular interest, since within the time-scale of the Ordnance Survey two large slips have occurred there, the first of which was completely eroded by the sea, precipitating the second (coded K73 by Hutchinson). Interest is engendered on a number of counts, namely:

a. the most recent slip has been covered by frequent aerial photography;
b. the complete degradation cycle for two slips at virtually identical sites can be studied;
c. the slip is of a long, bench-like character so that 'end effects' do not enter into the analysis;
d. the slip surface itself is highly non-circular and the distortions accompanying slipping were manifestly evident at the surface.

Between the first (1872) and second (1898) series of the Ordnance Survey, great changes appear to have taken place along this stretch of the coast line at Herne Bay, the earlier map showing the slope to be fairly even and well vegetated but breaking up into land slips at the time of the later map. Hutchinson (1965*b*) discusses this, the interpretation in terms of physical processes is not at present clear. However, the cliffs at the position of the Miramar landslide are shown considerably to seaward of their present position, and at some time between the two series, a major

TABLE 3. Slope stability analyses: Queen's Avenue slip

Profile	Average pore water pressure ratio r_u	ϕ'_r for equilibrium	Average shear stress kN/m^2	Average normal effective stress kN/m^2	Comments
1966 before regrading	0.36	12.5°	22.9	103.3	Pore water pressures are those measured after regrading, during 1969–70
1970 (and present) after regrading	0.34	12.3°	24.6	112.9	Currently appears stable.

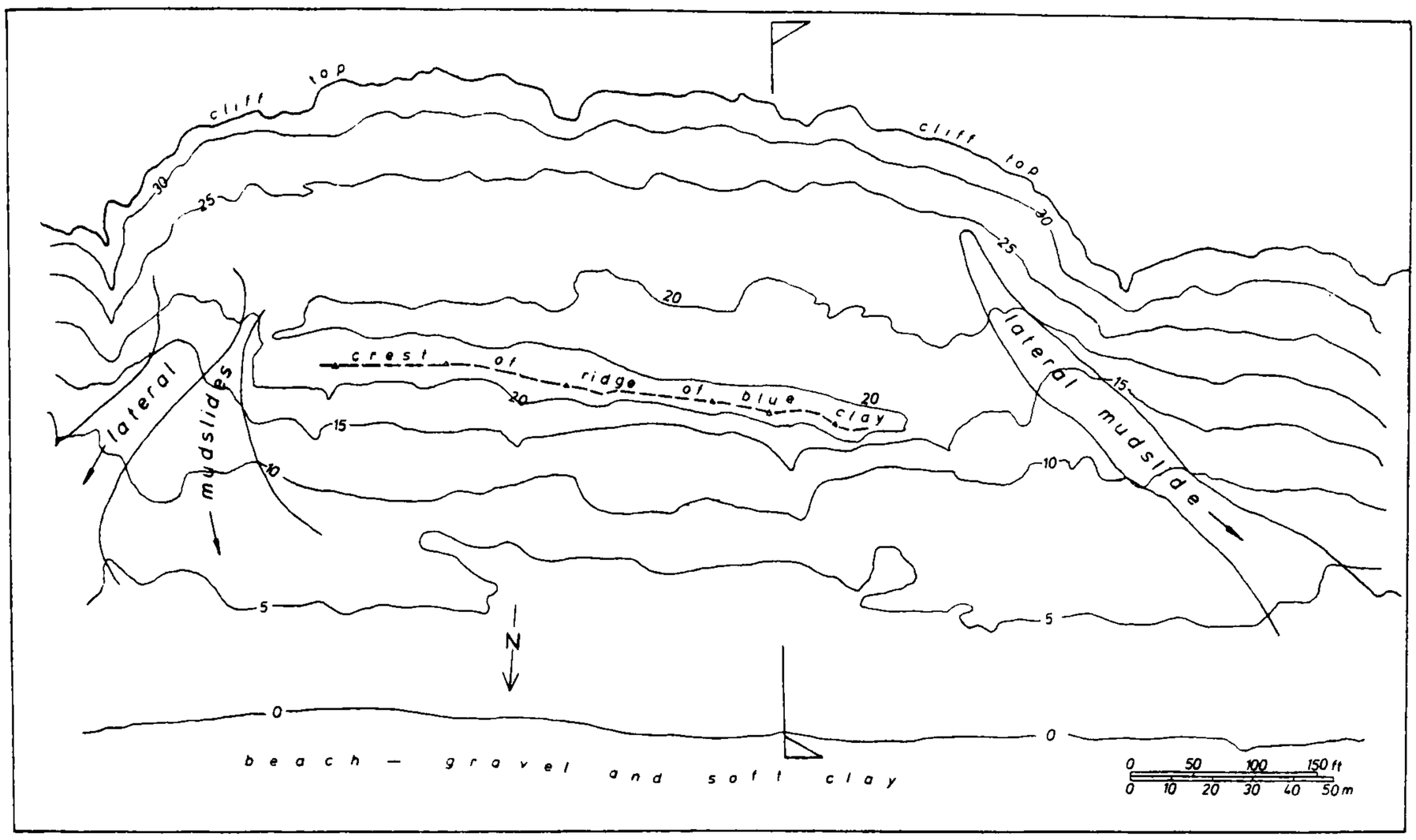


FIG. 7. Contour plan of Mirimar landslide. (Based on an original air survey by Meridian Airmpas Ltd.). Contours are marked in metres.

cliff failure took place (Hutchinson 1965*b*, on the basis of local records, places this in 1883) with the loss of about 20 m along approximately 100 m of cliff. The O.S. second edition clearly shows a ridge and graben structure, similar to that of the second landslide discussed below. By the time of the third series (1906), the ridge moved seawards some 12 m and had moved more at its western end than elsewhere. Later, at the survey for the fourth series (1933) no traces of this landslide were mapped and this probably accounts for Duvivier's apparent neglect of the instability at this site. Cliff-top interceptor drains installed in the pre-war works were terminated in the centre of this area and discharged downslope into the sea.

Early in the morning of 4 February 1953, another major landslide took place involving the same stretch of cliff. This time about a 25 m width of cliff top was lost, and photographs (Pl. 1 and 2) taken several days later, reveal this slipping down between sharply dipping sliding surfaces to form a near-horizontal graben structure, while the original cliff face was pushed forward intact to form a sharp crested ridge. The unusual features here are a function of the internal distortion within the sliding mass itself. During the slip, the debris at the bottom of the cliff (remnants of the earlier landslide) was considerably disturbed, and this material probably suffered local instability causing the pronounced heave near the toe, evident in air photographs taken in 1956. It could also be seen in these photographs that the ridge had moved seawards some 10 m, showing preferential movements at the western end in the manner of the earlier slip. Subsequently, additional movement of the ridge took place, amounting to a further 15 m in the period 1956–66. Large mudflows formed at each end of the landslide, fed by the erosion of the rear scarp and emerged around the ends of the intact block (Pl. 3).

Hutchinson (1965*a*,*b*) carried out an initial examination of this landslide and made a preliminary analysis of the first movements. He later (Hutchinson & Hughes 1968) established that a gap in the micropalaeontological succession was commensurate with a total displacement of nearly 18 m along the rear part of the slip surface. His section (1968) was taken normal to the position of the ridge, and not parallel to the direction of slipping in the first movements as are the sections in Figs. 8 and 9, which accounts for the small differences between the two. The positions of the sections are shown in Fig. 7 which is a site plan of the topography in 1966.

Considerable movements of this landslide were still occurring in the period following the air survey in 1966 up until regrading was well advanced, and the rate of movement was such that cross sections at the same location at fairly closely spaced intervals in time are markedly different (Fig. 8 and 9) and analyses of the following configurations were undertaken to attempt to define the residual strength mobilised at the various stages:

a. situation immedately after failure;
b. profile determined from air survey in 1956;
c. profile determined from air survey in 1966;
d. regraded profile.

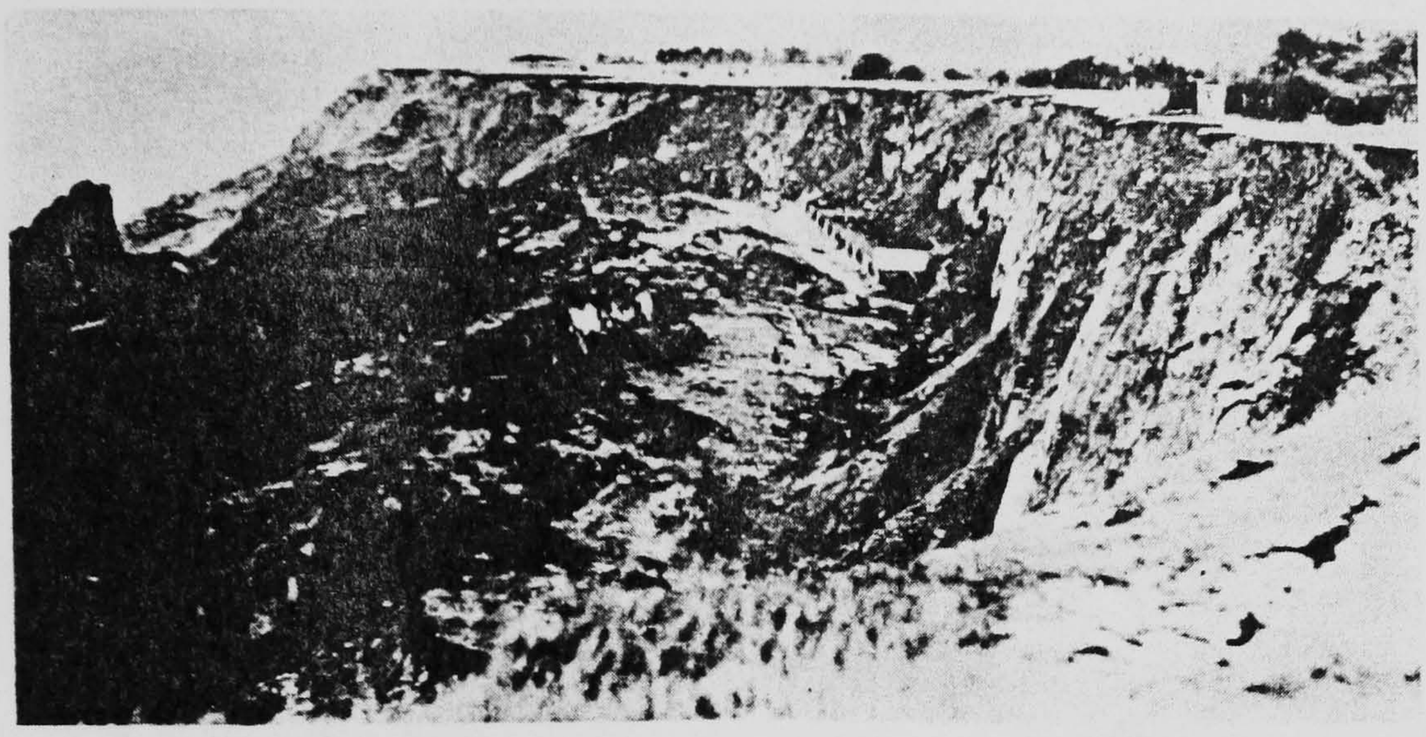


PLATE 1. Miramar landslide from the west, two days after failure showing steep slip surfaces. (Photo courtesy The Kent Messenger.)

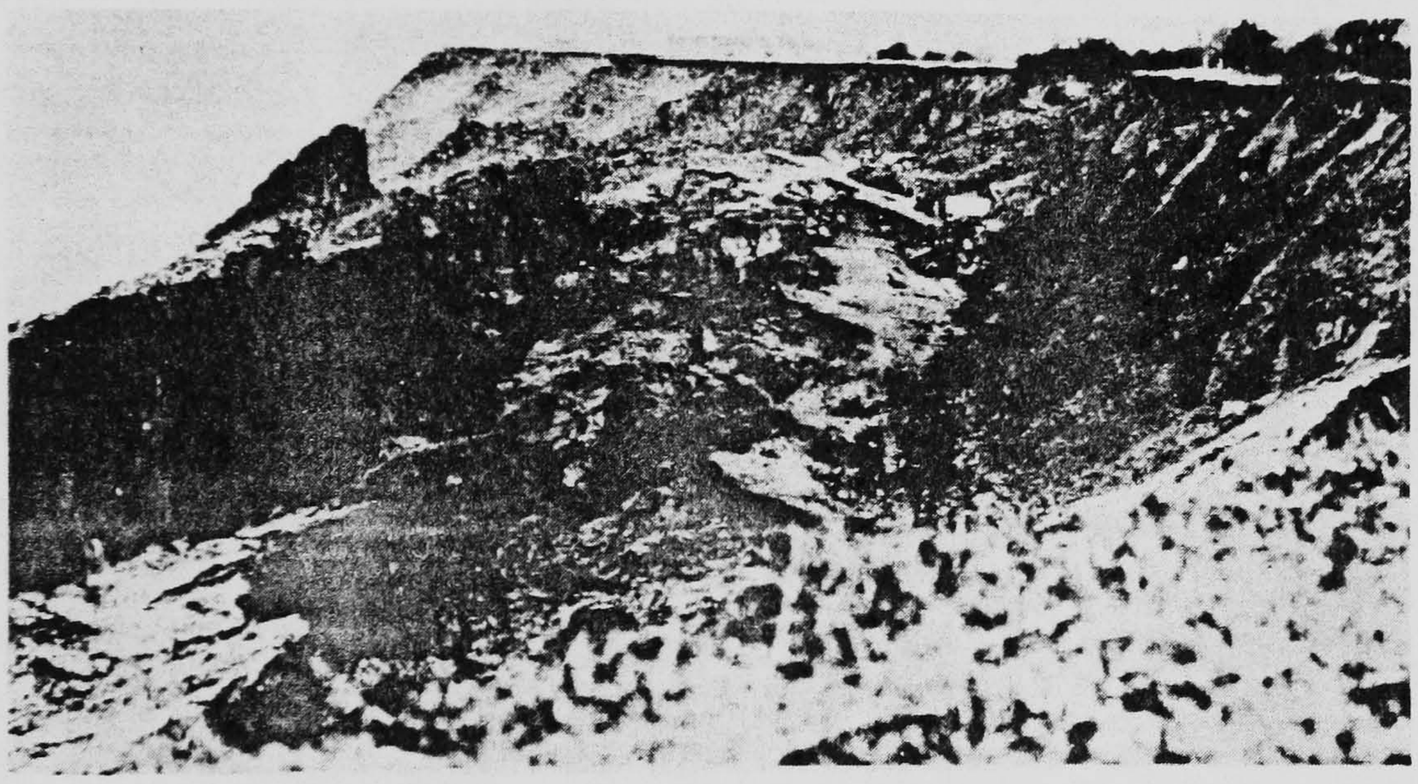


PLATE 2. Miramar landslide from the west, twenty days after failure showing rapid onset of degradation. (Photo courtesy The Kent Messenger.)

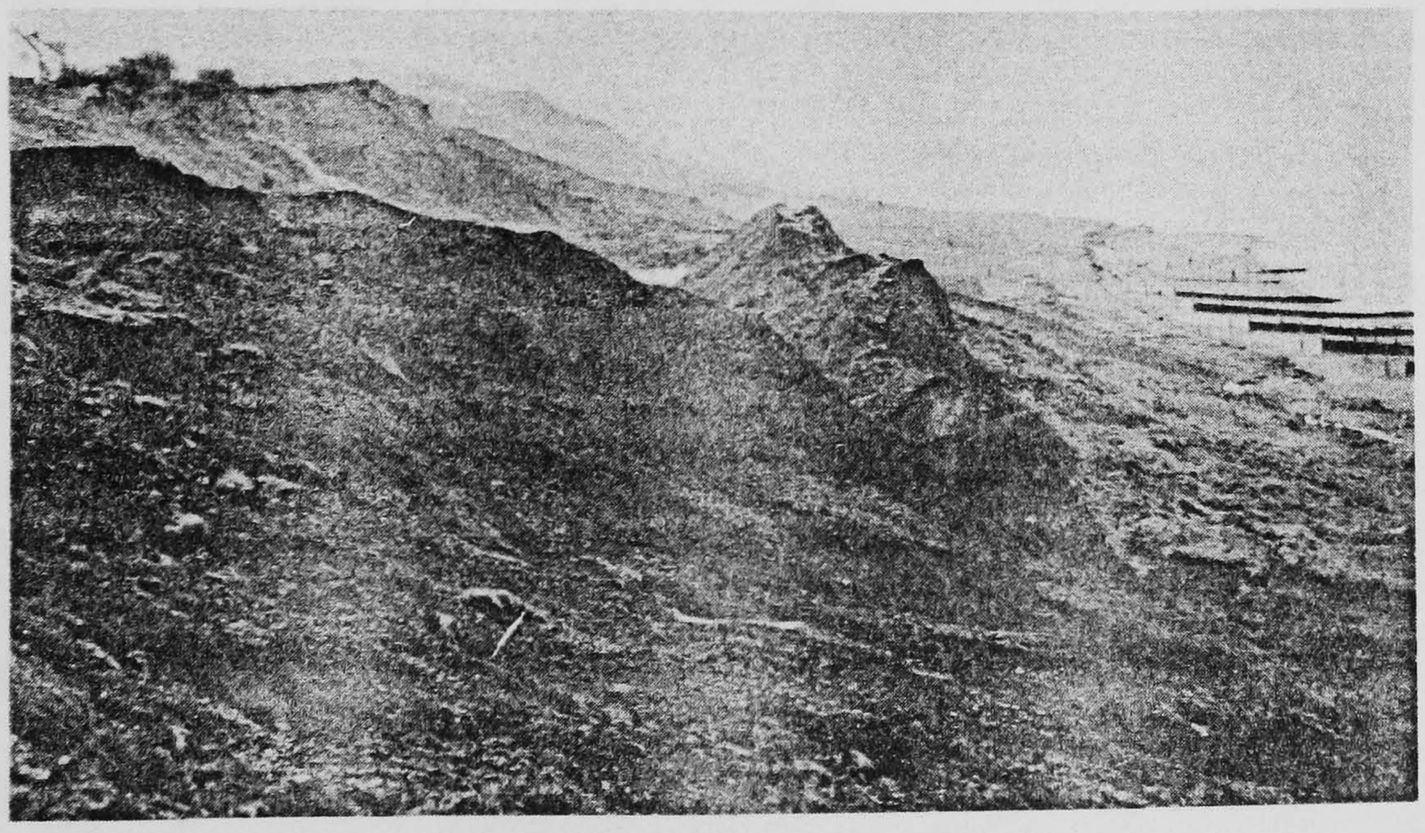


PLATE 3. Miramar landslide from the east, winter 1969-70.

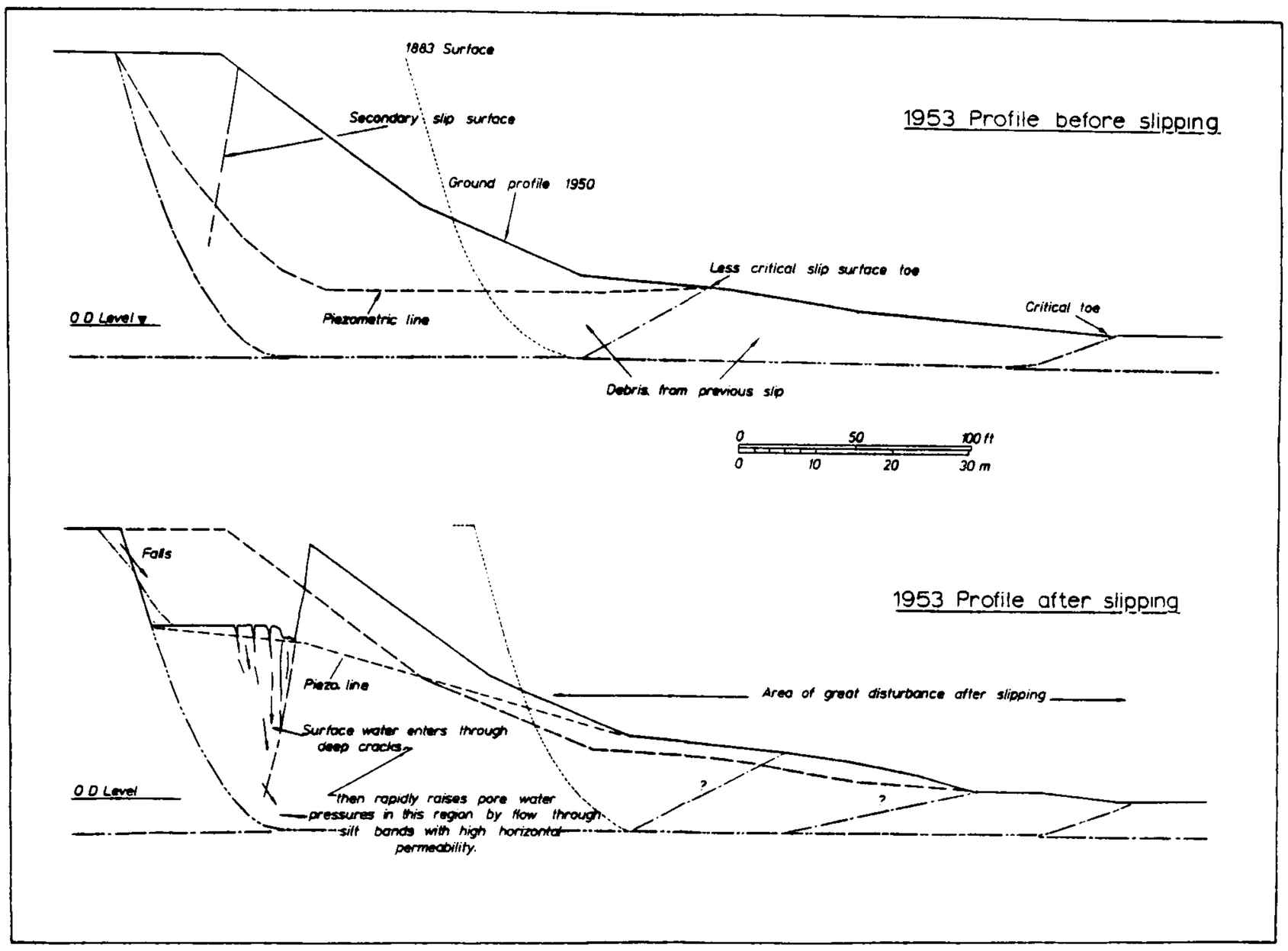


FIG. 8. Sections through the Miramar landslide showing the mechanism of the first movements, 1953. The position of these sections is shown on Fig. 7.

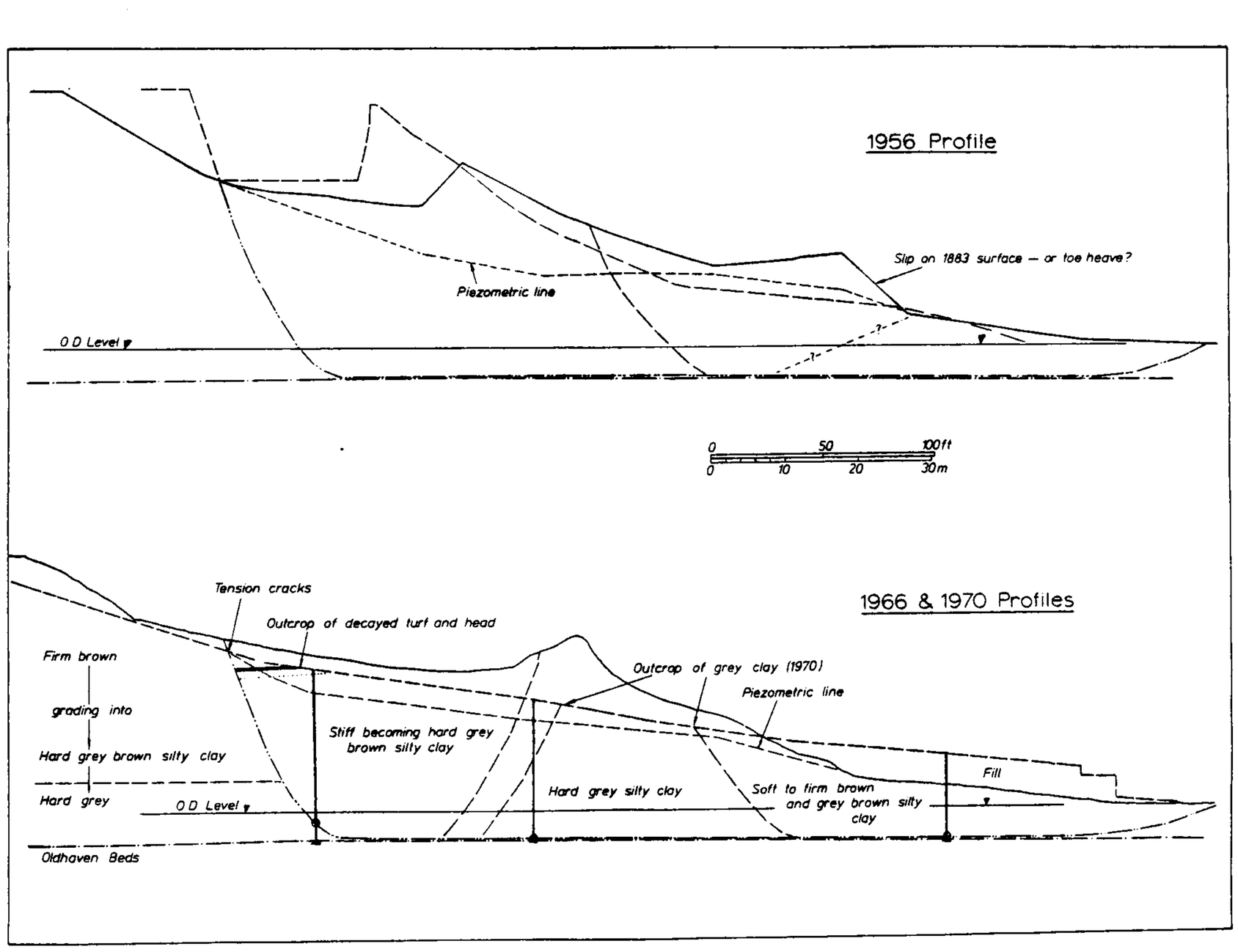


FIG. 9. Sections through the Miramar landslide showing erosion and regrading, 1956–70.

The first of these sections was compiled on the basis of an air survey of 1950, the photographic evidence being taken shortly after slipping. It was assumed that the total erosion was small and that there was no gross volume change accompanying the first movements. A second section was determined from an air survey of 1956, using a mirror stereoscope and parallax bar. Finally, the last two sections were produced from accurate air surveys commissioned in connection with the recent coast stabilisation activities. Naturally, the comparative accuracy of the first two of these sections is poor compared to the later ones, but an accuracy of perhaps ± 2 m on the position and level of the salient points is nevertheless entirely adequate. There would seem, at first glance, to be some inconsistency in the sections as the cross-sectional area appears to increase, instead of decreasing due to erosion, with the passage of time. This is most probably due to the rotation of the slipped mass in plan, and to a much lesser extent, to the bulking of materials when they have slipped and increased their moisture content and air voids. The d/L ratio has varied between 0.21 and 0.17, with a B/L ratio of 1.6 that makes the problem very amenable to conventional plane strain stability analyses.

Pore water pressures were determined from six piezometers in, and ten piezometers adjacent to the slip mass, whose installation has been described by Bayley (1972) and Bromhead (1972). Assessments of the pore water pressures in the early profiles has been made on the basis of a comparison between pore water pressures in the slip itself and those in the undisturbed clay at adjacent locations, together with a somewhat subjective assessment of the rate of inflow of surface water. The results of the four analyses are tabulated in Table 4 and indicate residual angles of shearing resistance in the 10.8° to 12.3° range at very high average normal effective stresses of about 150 kN/m^2.

As the profile along the chosen section before the onset of major movements had been surveyed from the 1950 air photographs it was entirely natural to attempt an analysis of the first instability to determine the 'peak' or 'first time' shear strength parameters mobilised in the previously unsheared London Clay. In contrast to all the other analyses described above in which the distribution of shear strength around the slip surface was known (i.e. all at residual strength), and in which the pore water pressures were directly measured or inferred on the basis of direct measurements, the 'first time movement' analysis was the subject of a certain amount of conjecture.

From the section (Fig. 8) it can be seen that the slip surface passes through not only undisturbed London Clay but also through the remnants of the earlier slide. It was established that the residual angle of shearing resistance appropriate to the effective stress level along the old slip surface was approximately 11° and that slip surfaces rising steeply through the slip debris were, in general, less critical than those passing along the flat slip surface just above the contact with the Oldhaven Beds. In all subsequent analyses this most critical toe was used. An assessment of pore water pressures in adjacent locations where undisturbed clay was present to the full height of the cliffs, revealed very consistent distributions of pore water pressure with depth and the mean distribution was chosen.

An analysis of the complete section was then carried out (once again using the Morgenstern–Price procedure) in order to evaluate the mean shear strength parameters mobilised along the remainder of the slip surface. These were found to be 'fully softened' strength parameters of $c' = 0$, $\phi' = 20°$. Chandler & Skempton (1974) determine first-time slide parameters for small slips in London Clay, and show that although cohesion c' is considerably reduced, it still has an appreciable, although small, value. Thus the author's finding of $c' = 0$, $\phi = 20°$ is not in agreement with the latest work, (although equal to the now superseded results of Skempton 1970). Clearly, some small amendment in the stability calculations (such as the proportion of the shear surface at the first-time value versus that at the residual value as shown in Table 5, or in the chosen residual value itself) would

TABLE 4. Slope stability analyses: Miramar Landslide (residual strength)

Profile	Average pore water pressure ratio r_u	ϕ'_r for equilibrium	Average shear stress kN/m^2	Average normal effective stress kN/m^2	Comments
1953	0.40	12.3°	32.6	148.8	Pore water pressures somewhat speculative.
1956	0.38	10.8°	29.4	154.4	
1966	0.37	11.5°	29.6	145.1	Pore water pressures measured 1969–70.
1970 (and present)	0.43	11.6°	25.3	122.8	Currently appears stable except at toe where seawall shows distress.

TABLE 5. Slope stability analyses: Miramar landslide (first-time failure)

Zone of slip surface / Type of analysis	1883 slip debris* Parameters	1883 slip debris* Average stresses	Sole	Steep rear part Parameters	Steep rear part Average stresses
'Progressive failure'	← Combined →		Shear = 18.8 kN/m² Normal = 96.9 kN/m² Effective	$c' = 21.6$ kN/m² $\phi' = 20°$	Shear = 56.4 kN/m² Normal = 97.0 kN/m² Effective
'Fully softened'	$c' = 0$ $\phi' = 11°$	Shear = 14.1 kN/m² Normal = 72.6 kN/m² Effective	← Combined →		
			$c' = 0$ $\phi' = 20°$		Shear = 78.6 kN/m² Normal = 216.0 kN/m² Effective

* Most critical slip surface passes right along 1883 slip surface. Alternative toe positions are invariably less critical due to their steep rise.

alter the parameters by the small amount needed to give the same result.

Since the 'fully softened' approach is an empirical one, and a true understanding of the first-time failure behaviour of slopes in overconsolidated clays seems more likely to arise from investigation of progressive failure, a modified model was developed. Bishop (1971) shows that a model with part of a slip surface at peak and part at residual is equally as valid as one in which there is a uniform mobilisation of an intermediate strength. However in a soil mass there are only a limited number of ways in which such non-uniform strain distributions can develop without causing serious deformations at the ground surface (of which none appear to have been observed in the present case). One such way is for stress relief due to erosion to have caused large strains at the base of the London Clay which is very close to sea-level at this location. In the limit, the occurrence of strains causing the strength to drop to residual over much of the London Clay–Oldhaven Beds interface is a possibility. Taking this into account in the stability analysis and using the appropriate residual strength, it was found that the shear strength parameters required for equilibrium over the remainder of the slip surface were $c' = 21.6$ kN/m² and $\phi' = 20°$. It should be noted, however, that any combination of parameters satisfying equilibrium with the shear and normal effective stresses quoted in Table 5 would be equally as valid. Strengths of at least this magnitude are required for stability elsewhere in the Herne Bay cliffs.

Interpretation based on a variable residual strength

Fig. 10 is a collation of the results of stability analyses for residual strength of London Clay. Average shear stress versus average normal effective stress along the actual slip surface is shown. Each result is plotted as a bold mark on the chart, and this information is supplemented by the results of cut plane and

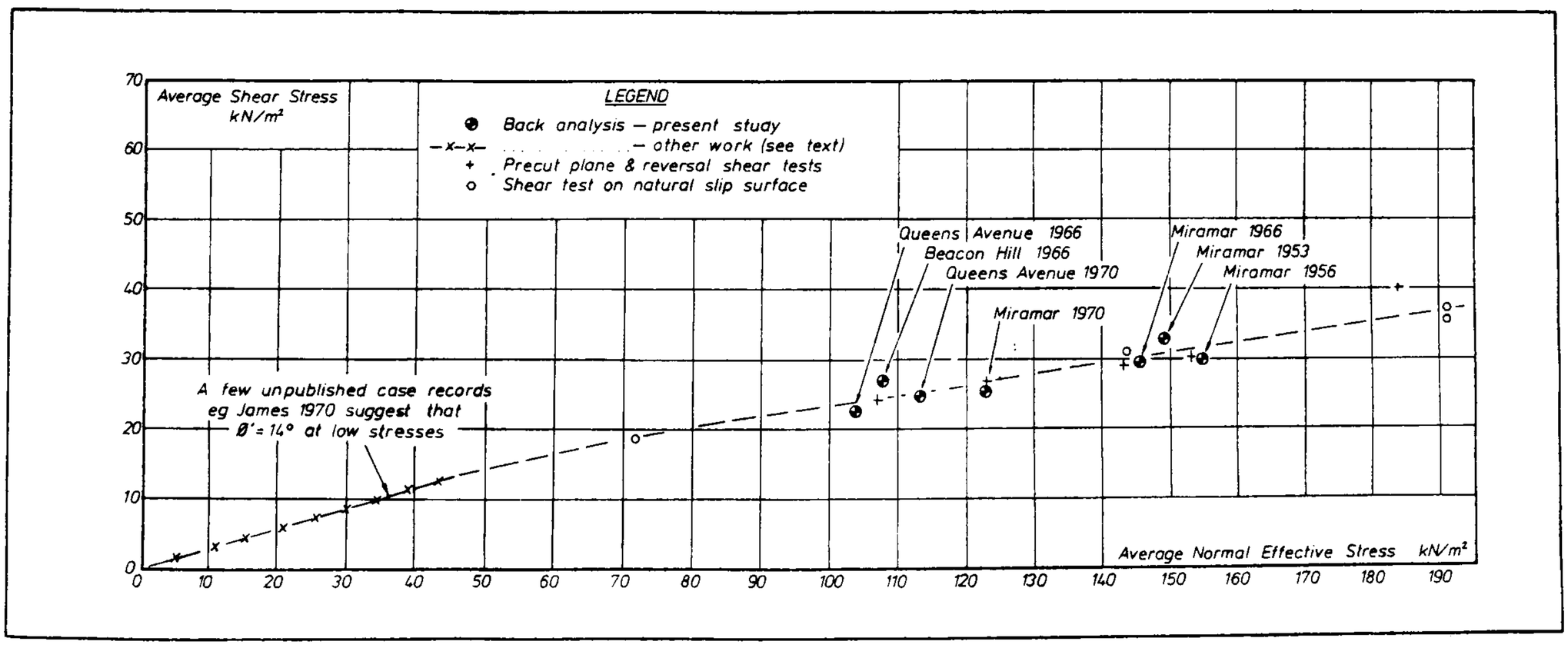


FIG. 10. Residual strength envelope for London Clay by back analysis and laboratory testing.

reversal shear-box test results (carried out as part of this investigation or presented by Bishop *et al.* 1971). Laboratory test data are shown by a smaller symbol. There is quite good agreement between the shear-box tests and back analysis. The curvature of the envelope is striking (if one is prepared to accept the limited back analysis data from James (1970) that ϕ'_r is about 14° at low effective stresses). However, the data are scant, and when the variation of plasticity, mineralogy and lithology of the London Clay is taken into account perhaps it is surprising that there should be any agreement at all. There is evidence that the residual angle of shearing resistance appears to be normal stress dependent; this probably indicates the influence both of the stress dependency of the parameter ϕ'_r in the brown, weathered clay, and the increasing proportion of blue or grey unweathered clay (with its lower residual shearing resistance) in the deeper and larger scale landslides in which the highest effective stress levels are found. Chandler (1977) notes a similar effect in Lias Clay.

Interpretation based on a constant residual strength

The approach adopted by Bayley (1972) was to accept the value for the residual shear strength parameter ϕ'_r from the Beacon Hill slip as a base value since that landslide is most certainly in a state of limiting equilibrium (with very small annual displacements during the period in which pore water pressures were actually measured). For the other two cases, pore water pressures were measured after stabilisation. Since these now give every indication of stability, his approach was to assess the amount by which the factor of safety (defined as the ratio of available to mobilised shear stress) exceeds unity by calculating the available shear strength by means of the base value (from Beacon Hill). Thus, the existence of a single, unique value for the parameter ϕ'_r was assumed. From this it may be inferred that either the pore water pressures acting on the slip surfaces of the other two slips must have been greatly reduced by the regrading and drainage work—or the factor of safety before the recent works must have been in excess of unity.

That the latter alternative is untenable is shown both by the tension cracks appearing during the regrading of the Queen's Avenue landslide and the continuing movement of the Miramar ridge between the air survey of 1966 and regrading in 1970.

However, the major movements may have taken place intermittantly and the overall impression of instability may be attributable to the lateral mudslides and other superficial slipping.

Furthermore, in both cases (particularly so in the case of the Miramar landslide) the pore pressures on the slip surface are controlled to a great extent by the mean water level in the Oldhaven Beds (in which the pore water pressures are tidal) along the flat 'sole' of the slip surface. It is this dependency that has allowed the measured pore water pressures to be used in the analysis of profiles before and after regrading, and to aid in the assessment of pore water pressures in the early profiles for the Miramar landslide.

The main effect of the drainage and regrading appears, therefore, to have been confined to reducing the pore water pressures along the slip surface where it is well above the Oldhaven Beds (to each side of the centre line section in the case of the Queen's Avenue landslide). In the Miramar landslide, where end effects must be smaller due to the long bench-like nature of the slip, drainage may well have increased stability by stiffening the remnants of the graben block so that additional work would need to be done in order to allow the internal distortions that would have to accompany further slipping. From a visual examination of the site it appears certain that the marginal improvements in overall stability have been effective and future movements, if any, will be small in magnitude or superficial in character.

Other limitations

The remaining approach is, of course, to discard limit equilibrium analysis altogether on the grounds of the unquantifiable inaccuracies introduced by the neglect of end effects and the internal work required for non-circular slips to be kinematically admissable mechanisms. If account is taken of these factors it follows from a process of intuitive argument that the true mobilised shear resistance of the soil is, in fact, less than that predicted using an uncorrected limit analysis, which must reinforce the earlier conclusions of this discussion. One can, however, still justify the use of back calculated residual strength parameters in each case since the evaluated parameter must contain an allowance for end effects and internal work requirements that will be applicable even after remedial works for stabilisation have been carried out (unless these involve gross changes to the geometry of the slip surface). Calculated 'improvements' in stability will be more realistic than the absolute calculated values of factor of safety.

Other forms of instability

It should not be imagined that the deep-seated instability described above is all that has occurred at Herne Bay. During stabilisation in the period 1969–71 there were at least three instances of slipping during the regrading of the easternmost length of cliffs, and since then there have been two failures of the sheet piled seawall. In the period since the war, there have been many cases of small-scale slipping in the area treated in the 1930's, in the main confined to the upper part of the cliffs. Further cliff stabilisation work

has been carried out in an attempt to prevent future instability in this region.

References

ALLAN, A. R. 1968. Coast protection and stabilisation at Herne Bay. *Civ. Engng publ. Wks Rev.* **63,** 860–1.

BAYLEY, M. J. 1972. Cliff stability at Herne Bay. *Civ. Engng publ. Wks Rev.* **67,** 788–92.

BISHOP, A. W. 1955. The use of the slip circle in the stability analysis of earth slopes. *Géotechnique* **5,** 7–17.

——1971. The influence of progressive failure on the choice of the method of stability analysis. *Géotechnique* **21,** 168–72.

——, GREEN, G. E., GARGA, V. K., ANDERSEN, A. & BROWN, J. D. 1971. A new ring shear apparatus and its application to the measurement of residual strength. *Géotechnique* **21,** 273–328.

BROMHEAD, E. N. 1972. A large coastal landslide at Herne Bay, Kent. *Arup J.* **7,** 12–14.

CHANDLER, R. J. 1977. Back analysis techniques for slope stabilisation works: a case record. *Géotechnique* **27,** 479–95.

—— & SKEMPTON, A. W. 1974. The design of permanent cutting slopes in fissured clays. *Géotechnique* **24,** 457–66.

DUVIVIER, J. 1940. Cliff stabilisation works in London Clay. *J. Instn civ. Engrs* **14,** paper 5233.

HUGHES, M. J. 1970. Herne Bay stability study—report on the stratigraphical micropalaeontology. *Rept. Inst. Geol. Sci. Palaeont. Dept.* PD/70/3.

HUTCHINSON, J. N. 1965*a*. *The stability of cliffs composed of soft rocks with particular reference to the coasts of SE England.* Thesis, Ph.D., Univ. of Cambridge (unpubl).

—— 1965*b*. A survey of the coastal landslides of Kent. *Build. Res. Sta. Note* EN/35/65.

—— 1967. The free degradation of London Clay cliffs. *Proc. Geotech. Conf., Oslo* **1,** 113–8.

—— 1970. A coastal mudflow on the London Clay cliffs at Beltinge, north Kent. *Géotechnique* **20,** 412–38.

—— 1973. The response of London Clay cliffs to differing rates of Toe Erosion. *Geologia Applicata E Idrogeologia* **8,** 221–40.

—— & BHANDARI, R. K. 1971. Undrained loading—a fundamental mechanism of mudflows and other mass movements. *Géotechnique* **21,** 353–8.

—— & HUGHES, M. J. 1968. The application of micropalaeontology to the location of a deep seated slip surface in the London Clay. *Géotechnique* **18,** 508–10.

JAMES, P. M. 1970. *Time effects and progressive failure in clay slopes.* Thesis, Ph.D., Imperial College, London Univ. (unpubl.).

KENNEY, T. C. 1956. *An examination of the methods for calculating slope stability.* Thesis, M.Sc., Imperial College, London Univ. (unpubl.).

MORGENSTERN, N. R. & PRICE, V. E. 1965. A method for calculating the stability of general slip surfaces. *Géotechnique* **15,** 79–93.

—— &—— 1967. A numerical method for solving the equations of stability of general slip surfaces. *Comput. J.* **9,** 388–93.

SKEMPTON, A. W. 1964. Long term stability of clay slopes. *Géotechnique* **14,** 77–101.

—— 1970. First time slides in overconsolidated clays. *Géotechnique* **20,** 320–4.

—— & DELORY, F. A. 1957. Stability of natural slopes in London Clay. *Proc. 4th Int. Conf. Soil Mech.* **2,** 378–81.

TCHALENKO, J. S. 1968. The microstructure of London Clay. *Q. Jl Engng Geol.* **1,** 155–68.

WISE, E. V. A. 1957. *The stability of natural slopes in overconsolidated fissured clay.* Thesis, M.Sc., Imperial College, London Univ. (unpubl.).

A simple ring shear apparatus

by E. N. BROMHEAD*, MSc, DIC, BSc, CEng, MICE

THE HITHERTO EXPENSIVE and time-consuming nature of ring shear tests to determine the residual strength of soils has prevented the test from becoming a routine procedure in commercial laboratories. This has had the result that the ideal "three-pronged attack" on landslip problems by

(*a*) back analysis,
(*b*) ring shear tests on representative strata, and
(*c*) direct shear tests on actual slip surfaces,

is rarely fully developed. Since a number of studies have shown that the ring shear tests may possibly provide the lower bound strengths in any investigation, this omission is of concern.

However, ring shear testing cannot become a routine procedure outside the research laboratory until a simple, robust, inexpensive apparatus which has a fairly large potential through-put of tests in the working week is developed. This Paper describes such a device, which has recently been built and evaluated at the School of Civil Engineering, Kingston Polytechnic and which in its fully developed form is now available commercially.

Description and general principle

An annular soil sample 5mm thick with inner and outer diameters of 70mm and 100mm respectively is confined radially between concentric rings. It is compressed vertically between porous bronze loading platens by means of a lever loading system and dead weights.

In the prototype this lever system was adapted from a proprietary 5:1 ratio hanger system complete with lever levelling jack originally part of a direct shear apparatus. This system was, however, deleted from that manufacturer's range along with the machine in question and replaced by a new machine with a 10:1 ratio counterweighted system. Accordingly, the production machines were adapted to use the new components.

A rotation is imparted to the base plate and lower platen by means of a variable speed motor and gearbox driving through a worm drive. This causes the sample to shear, the shear surface forming close to the upper platen (which is artificially roughened to prevent slip at the platen/soil interface).

The settlement of the upper platen during consolidation or shear can be monitored by means of a sensitive dial gauge bearing on the top of the load hanger.

Torque transmitted through the sample is reacted by a pair of matched load measuring devices (sensitive proving rings in the prototype) bearing on a cross arm.

Fig. 1 shows both the prototype and production shear cells in partly sectioned elevation.

Sample preparation

The lower porous platen and confining rings are assembled and a remoulded sample kneaded into the annular cavity. The top of the sample is then struck off level with the top of the confining rings, and the upper platen placed in position, located on the centring pin, which is well greased. With the water bath (which is a push fit over the 'O'-ring seal) in position, the sample is flooded with distilled water. If a very soft sample has been prepared, it is quite important to allow time for it to come into equilibrium under the load of the upper platen and then under the load of each item of the lever loading system, since if too much load is applied too quickly there may be excessive 'squeeze' or loss of soil through the clearance between the upper platen and confining rings. However, with some soils, it may be preferable to get a load on to the sample to prevent swelling.

The sample is then consolidated under loads which provide the desired normal effective stress on horizontal planes, and the coefficient of consolidation can be evaluated by monitoring the vertical settlement. When the soil is fully consolidated it may be sheared at the appropriate rate.

Developments from the prototype

It was found that the absence of a clutch mechanism in the prototype led to considerable difficulty being experienced with setting up and with gear changing. The lack of manual control over the rotation was another source of annoyance. A pin wheel clutch and handwheel were therefore added to the worm drive in the production device.

During the initial trials, it was found that with the original "built up" design for the confining rings, platens and centring pin, it was almost inevitable that cumulative manufacturing tolerances gave rise to an eccentricity in alignment. Accordingly, the production machines are built around the central drive shaft and this problem does not arise. The opportunity was taken to combine the confining rings and lower platen and also to improve the general drainage ducts. This composite assembly is positively located on the central shaft and held down by knurled nuts. Sample preparation is aided by the simplicity with which the platen/confining ring assembly can be removed from the water bath.

For tests at low normal stresses the torque transmitted through the sample may be quite small and it was found that the proving rings lacked sufficient sensitivity. The production units have the proving rings mounted in turrets with quick release clamps so that the effective length of the torque arm can be changed at will, and the torque arm was redesigned with positive stops at two positions so that the rings could be brought to bear at similar radii without measurement. These turrets also allow a variety of load cells to be fitted, and they swing out of the way for sample preparation.

Other detail design improvements include a more compact drive (again identical with that for the appropriate proprietary direct shear machine) and the provision of a scale of degrees so that the amount of rotation can be seen at a glance. Fig. 2 is a photograph showing the general arrangement.

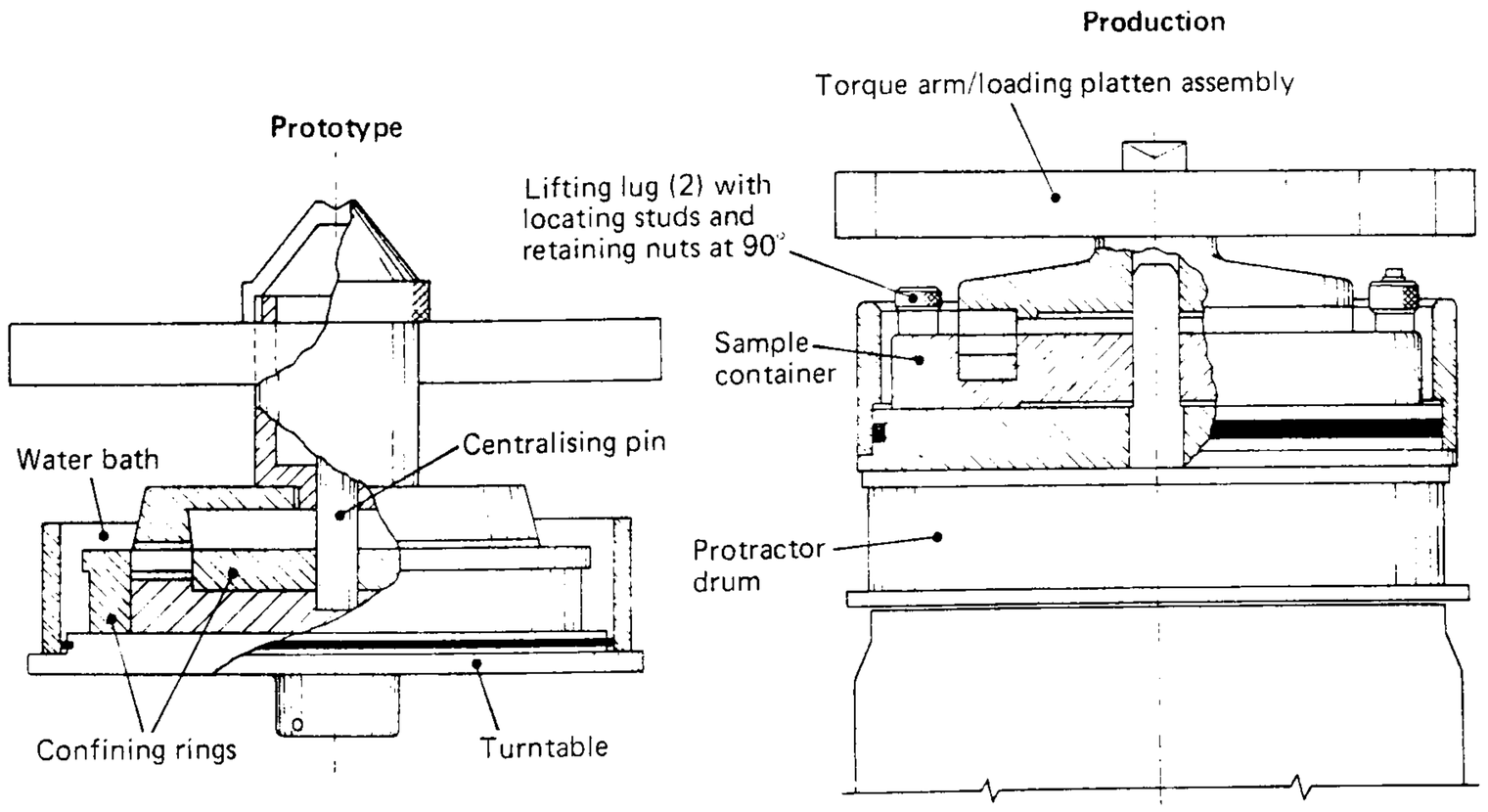


Fig. 1. Partly sectioned general elevations comparing the prototype and production models

*Senior Lecturer, Kingston Polytechnic, Kingston upon Thames, Surrey

Interpretation of results

Bishop *et al.* (1972) discuss the influence of a variety of distributions of shear stress across the sample in a ring shear test on the measured torque and hence on the angle of shearing resistance calculated assuming a uniform shear stress distribution. In some cases, errors of about 10% may arise. It is, however, much more likely that the distribution is close to the uniform one particularly where the sample is narrow in comparison to its diameter.

Conventionally, we take a uniform shear stress when residual strength has been reached and hence the torque T transmitted through the sample is given by:

$$T = \tfrac{2}{3}\pi\,(R_2^3 - R_1^3)\tau$$

where R_1 and R_2 are respectively inner and outer sample radii. (It should be noted that the non-uniform strain distribution greatly encourages progressive failure in brittle soils and it is therefore unlikely that any ring shear apparatus will give a reliable peak shear strength. The brittleness index cannot therefore be fully defined on the basis of ring shear tests alone).

Since the torque is given by the mean load on the proving rings (or load cells) multiplied by the distance between them:

i.e. $$T = (F_1 + F_2)L/2$$

Thus:

$$\tau = \frac{3\,(F_1 + F_2)L}{4\pi\,(R_2^3 - R_1^3)}$$

The normal effective stress σ' is given by:

$$\sigma' = \frac{P}{\pi\,(R_2^2 - R_1^2)}$$

where P is the total vertical load

Hence:

$$\tau/\sigma' = \tan\phi' = \frac{3\,(F_1+F_2)\,(R_2^2 - R_1^2)L}{4\,(R_2^3 - R_1^3)P}$$

Sources of error

The errors that can arise in the use of this apparatus do so from:

(*a*) inaccuracies in load measurement,
(*b*) friction on the centring pin,
(*c*) binding between the upper platen and the confining rings due to tilting, or 'squeezed' soil becoming trapped,
(*d*) side friction if the slip surface forms below the top platen/soil interface, and
(*e*) the possible non-uniform mobilisation of shear stress across the sample.

The apparatus was originally designed to use commercial grade proving rings and these are of course quite adequate for most purposes. Their accuracy is fairly limited at low loads and for tests on very weak materials or at very low normal effective stress it may be necessary to resort to more sensitive electrical load cells, but an alternative method of overcoming the problem is to adjust the proving rings so that they react closer to the axis of the device. This increases the loads to be carried and brings them into a better part of the proving ring's working range.

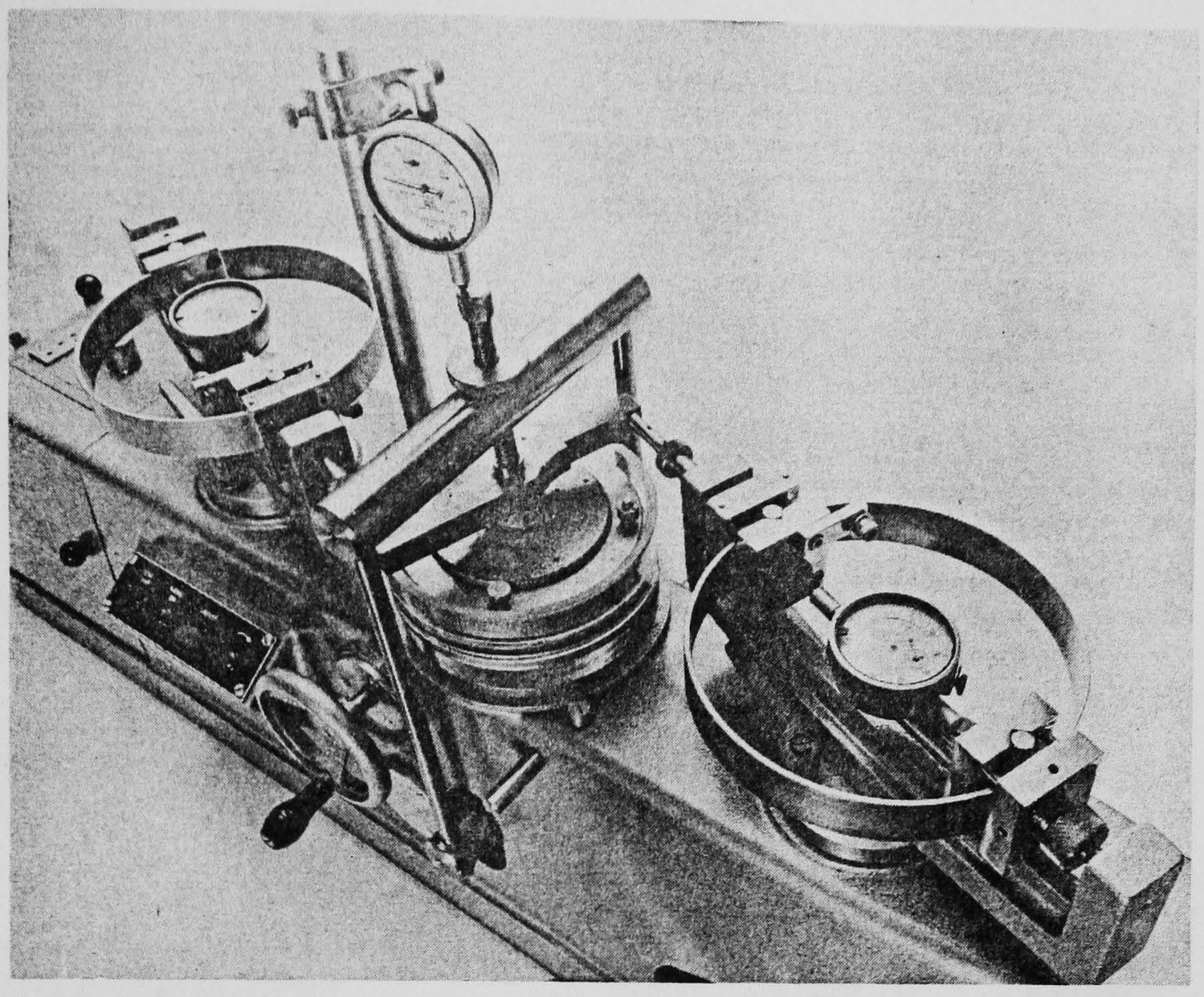


Fig. 2. Photograph showing general arrangement of production machines

Differences in the stiffnesses of the proving rings can throw an unbalanced load onto the centring pin and cause friction. This will also be affected by uneven settlement of the loading platen. However, such friction will have two components — one tending to reduce the normal load carried by the soil sample and the other tending to increase the torque transmitted to the proving rings. The effects are therefore largely self-compensating, as in fact are all the similar types of side friction noted as (*b*) and (*c*) above. Furthermore, the likely unbalanced loads will only give rise to small amounts of torque due to friction if the centring pin is lightly greased and of an appropriate diameter. The possibility of tilting and its resulting effects is reduced by the presence of the centring pin. In the prototype the taper of the loading platen was designed to prevent 'squeezed' soil from being trapped but was found to be an unnecessary refinement. Soil extruded from the outside of the sample can of course be removed during the test with a soft brush or a jet of water from a wash bottle.

In practice it is found that the main slip surface forms close to the upper platen, but that other slip surfaces can and do form more deeply in the soil. It seems unlikely, therefore, that side friction on the confining rings is a significant factor.

Smear type ring shear devices, particularly those of very simple construction are apparently more subject to these relatively unquantifiable effects than the Imperial College device. However, a systematic study by La Gatta (1970) showed that the largest potential source of error was in the assumption of uniform mobilisation of shear stress on the slip surface, and this is also found to be so in the present case.

Selection of appropriate strain rate

In this apparatus, the sample is so thin (and double drained) that extremely rapid rates of shear are possible while still allowing full drainage to occur. However, higher rates of shear may induce rheological or viscous shear strength elements.

One method of ensuring that the results are obtained in terms of effective stresses is to test so slowly that the sample is fully drained at all times through the peak (which is of course a remoulded peak since even if an "undisturbed" sample is used, its upper surface is remoulded during preparation) and on to the residual state. This is a fairly slow process even in the present device.

An alternative and more rapid procedure is as follows:

(*i*) Consolidate the sample to the first normal load, and monitor settlement to determine the time for full consolidation (t_b).
(*ii*) Shear the sample undrained for about 5 revolutions to form a shear surface; release the torque.
(*iii*) Reconsolidate to rid the sample of undrained pore water pressures from (*ii*) above; the value for t_b can be updated from this stage in some tests.
(*iv*) Select a shearing rate and shear the sample on the pre-formed slip surface A flat topped stress strain curve usually results and providing that the sample is sheared for a time at least as long as t_b and the measured shear stress does not change we can be sure that the sample is fully drained. The shear rate can be changed at this point to investigate viscous effects.
(*v*) The sample is then re-consolidated to the next normal effective stress, providing a new value for t_b, and the procedure of step (*iv*) followed.

This process is quite simply explained to technicians with minimal skills and has been found by experience to give results identical with those of the first method.

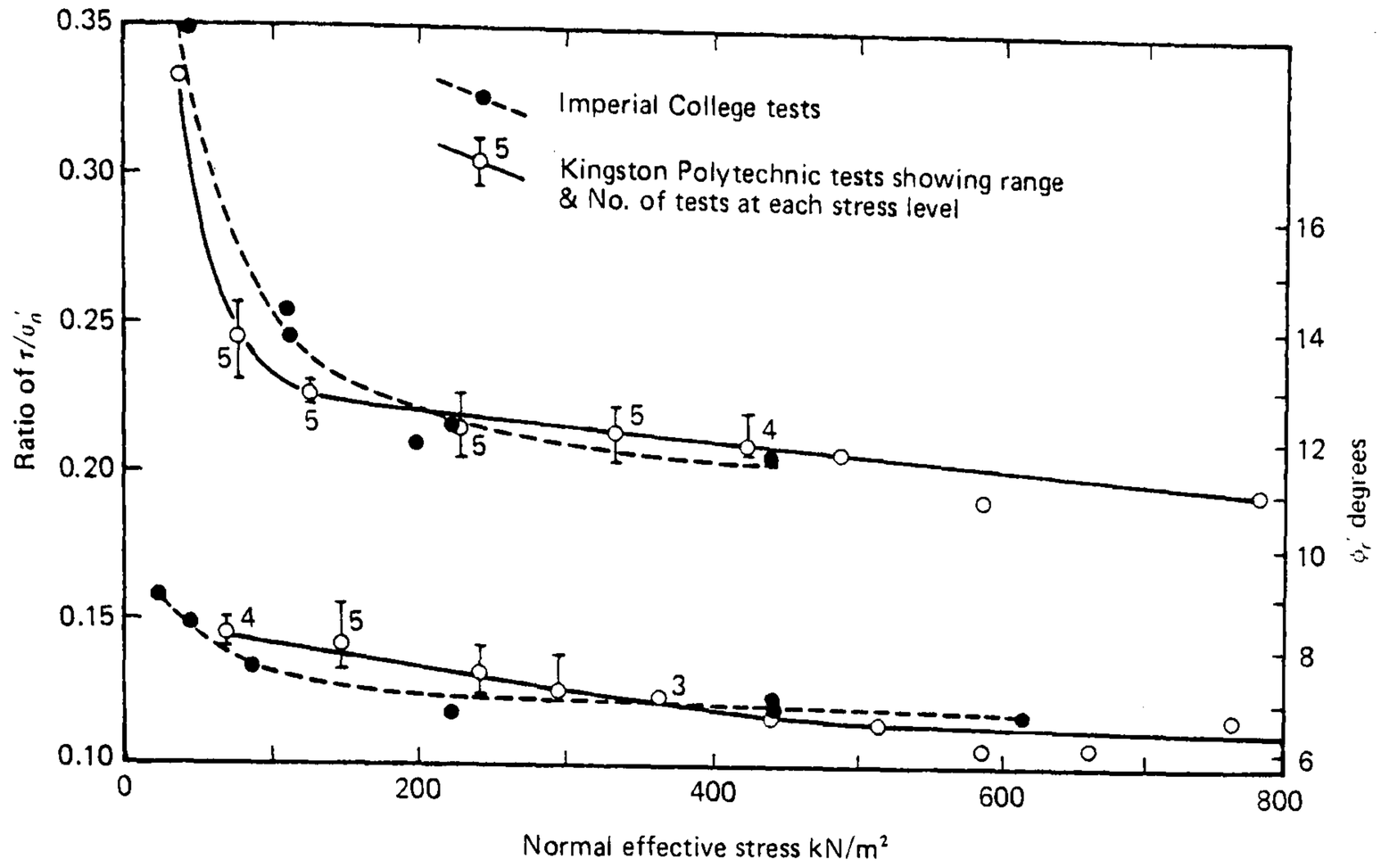


Fig. 3. Comparison of results of ring shear tests on Gault clay (from the formation at Folkestone Warren) in the Imperial College and the present machines

Volume changes during shear

Settlement of the upper loading platen (which may be monitored by means of the single sensitive vertical dial gauge) has two components: the dilation or contraction of the soil due to shear and the loss of material due to 'squeeze'. In practice it is impossible to separate these two.

Practical experience

Proving tests have been carried out on a number of soils, mainly clays, from southern England. An interesting comparison between the present machine and the Imperial College ring shear machine described by Bishop *et al.* (1971) was provided by tests on the high and low liquid limit Gault Clay samples from Folkestone Warren (Hutchinson *et al.*, 1979) where it was only possible to separate the two sets of results by plotting them to a large scale on the demanding ϕ_r' *vs.* normal effective stress diagram (Fig. 3).

In the past it has been felt that ring shear test results tended to underestimate the field mobilised shear strength. It would certainly appear to be so from the limited number of published records. However, with the expensive and lengthy process of establishing a full ring shear strength envelope in the laboratory it is rare for more than a single ring shear test to be carried out, usually on a sample selected to have the highest liquid limit. It would rightly be recognised as absurd to correlate field conditions with a single triaxial test, or for that matter with any single soil test, due to the natural variation of soil properties over any site and a similar situation in relation to ring shear tests should be recognised. It is surely time to accord the ring shear test equal treatment. Two tests over a range of four or five normal stresses can usually be carried out within a normal working week.

The prototype was constructed from mild steel and although a variety of platings including passivated cadmium and nickel were tried, the components suffered from some corrosion. This is being overcome by the use of flat chromed brass, bronze or stainless steel as appropriate.

It has been found that the roughness of the upper platen is a significant factor if the soil has an appreciable silt fraction, but for clays is of much lesser importance.

Conclusions

This new ring shear apparatus is simple in design and inexpensive in construction. Tests on both remoulded and 'undisturbed' samples can be made quite rapidly and the results are comparable with those obtained from much more sophisticated equipment.

Comparing the construction with a direct shear (shear box) apparatus, it will be seen that they have much in common. Although the ring shear has some extra components, the capital costs for the two devices are broadly similar, and due to the simplicity of operation of the ring shear, running costs need not be excessive.

In view of this it is expected that ring shear testing to determine the residual strength parameters of soils will become a routine operation in commercial testing laboratories.

Acknowledgements

The prototype was built in the School of Civil Engineering, Kingston Polytechnic largely by Mr. R. Stevens, Senior Technician, and a number of the proving tests were performed by Mr. A. Harris, Mr. R. B. Higginson and Mr. N. D. Lambert. The author is grateful to Mr J. F. Lupini and Professor J. N. Hutchinson of Imperial College for permission to quote the results of the comparative test. He would like to acknowledge the help of the design staff of Wykeham Farrance Engineering Ltd. especially that of Mr. G. Pelling.

References

Bishop, A. W., Green, G. E., Garga, V. K., Andresen, A., & Brown, J. D. (1971): 'A new ring shear apparatus and its application to the measurement of residual strength'. Geotechnique **21**, No. 4, 273-328.

La Gatta, D. P. (1970): 'Residual strength of clays and clay-shales by rotation shear tests'. Harvard Soil Mechanics Series No. 86, Cambridge. Massachusetts.

Hutchinson, J. N., Bromhead, E. N., & Lupini, J. F. (1979): 'Additional observations on the coastal landslides of Folkestone Warren'. Q. J1. Eng. Geol. *in press*.

Q. Jl Engng Geol. 1979 Vol. 12 pp. 291–300. Printed in Northern Ireland

Factors affecting the transition between the various types of mass movement in coastal cliffs consisting largely of overconsolidated clay with special reference to Southern England

E. N. Bromhead

School of Civil Engineering, Kingston Polytechnic, Canbury Park Road, Kingston upon Thames, Surrey.

Summary

At present, the most widely accepted hypothesis for the transition from mudsliding to deep-seated rotational slipping as the dominant agent of mass transport in actively eroding clay cliffs is that the transition depends on the rate of marine erosion at the toe of the slope. This paper explores an alternative theory, that the transition from one type of behaviour to another depends largely on the nature of the materials at the crest of the slope and to a lesser, but still important, extent on the groundwater hydrology.

The main argument behind this alternative theory is that the presence of stronger soil strata at the crest of the slope inhibits the mudslide behaviour that would otherwise occur and hence form a toe-protecting 'mudslide barrier'. This allows marine action to erode the toe of the slope directly, causing it to be oversteepened, and ultimately precipitates a deep-seated rotational landslide. Where the coastal cliffs are capped with thick, hard and jointed caprock the slides tend to be of the multiple rotational kind.

Introduction

Cliffs of overconsolidated clays are a common feature of the coasts of southern and eastern England, and in a series of works, Hutchinson (1965 and subsequently) undertook a survey of these. It was found that there was a strong dependence of slide types and processes in these cliffs on the intensity of marine erosion at their foot, conveniently divisible into strong, medium, and zero categories (Hutchinson 1968, 1973). This latter category (zero erosion) is the case of an abandoned cliff which undergoes 'free degradation' solely under the influence of weathering and climate, a process examined exhaustively at Hadleigh, Essex by Hutchinson & Gostelow (1976) but which lies entirely outside the scope of this paper.

Despite the convenience of this tripartite categorization, there is an accumulating body of evidence to suggest that the correlation of slide processes with erosion rate is largely fortuitous and that any such subdivision should rather distinguish between 'active' and 'inactive' types, with subcategories in each type based on other factors. Unfortunately, most of this evidence is observational rather than quantitative and it is therefore difficult to be conclusive. However, it is hoped that the following recapitulation of the fundamental mechanics of the various slide types will adequately demonstrate that the type of mass movement is most strongly controlled by the properties of the soil forming the head of the slope and by the groundwater hydrology in that material—the rate of erosion at the toe being a secondary consideration.

By and large, there are two important types of slope degradation behaviour under active marine erosion, and for convenience in this account they will be referred to as type *MS* and type *DR* slopes, where the terms *MS* and *DR* imply that the dominant mode of mass movement takes place either by relatively shallow, essentially translational mudsliding (*MS*), or by deep-seated rotational landsliding (*DR*). An important subgroup of type *DR* slopes is that in which the landslides are multiple *and* retrogressive. Such landslides are usually found in slopes with a thick caprock (Hutchinson 1968*a*).

Type *MS* slopes

Type *MS* slopes present an appearance similar to that shown in cross-section in Fig. 1. This comprises one or more repetitions of a basic unit, which in turn is a steep head slope and a much flatter front slope. The head slope of the upper unit is unstable and so provides a continual change of debris from small falls or slides which accumulates and 'feeds' the mudslide proper which occupies the flatter front slope. In a multiple configuration, spillage from upper mudslides supplements that falling from the head slope. Hutchinson (1970) draws attention to the very low-angle slopes of these mudslides and advances a mechanism of *undrained loading* to account for this; the general idea is further developed by Hutchinson & Bhandari (1971). The importance of this process to the present thesis is explored below.

Where the cliff is occupied entirely by mudslides, these form a series of semi-circular embayments (termed 'corries' in earlier work—a misnomer which carried the 'mud glacier' (Lacey 1929) analogy to the extreme) in the cliff top which retreat with the retreat of the cliff line and change little in shape or size. This retreat is seasonal, and is fastest in the late winter or early spring. The mudslides themselves also have their greatest activity at this time of year and form tongues which can extend far across the beach when the slides

0481–2085/79/1000–0281$02.00 © 1979 The Geological Society

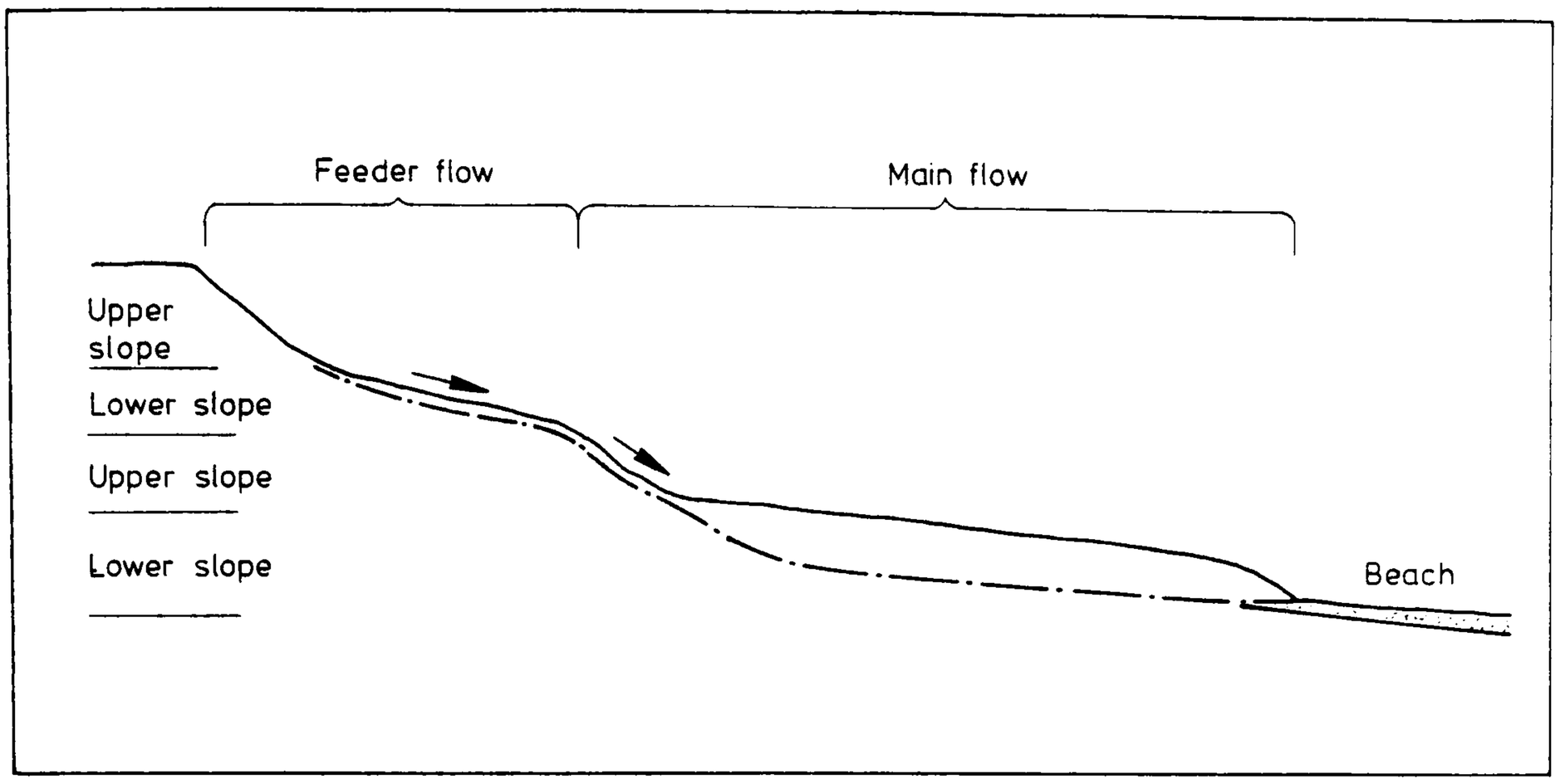


FIG. 1. Section through a typical, two unit, type *MS* slope; (after Hutchinson 1970).

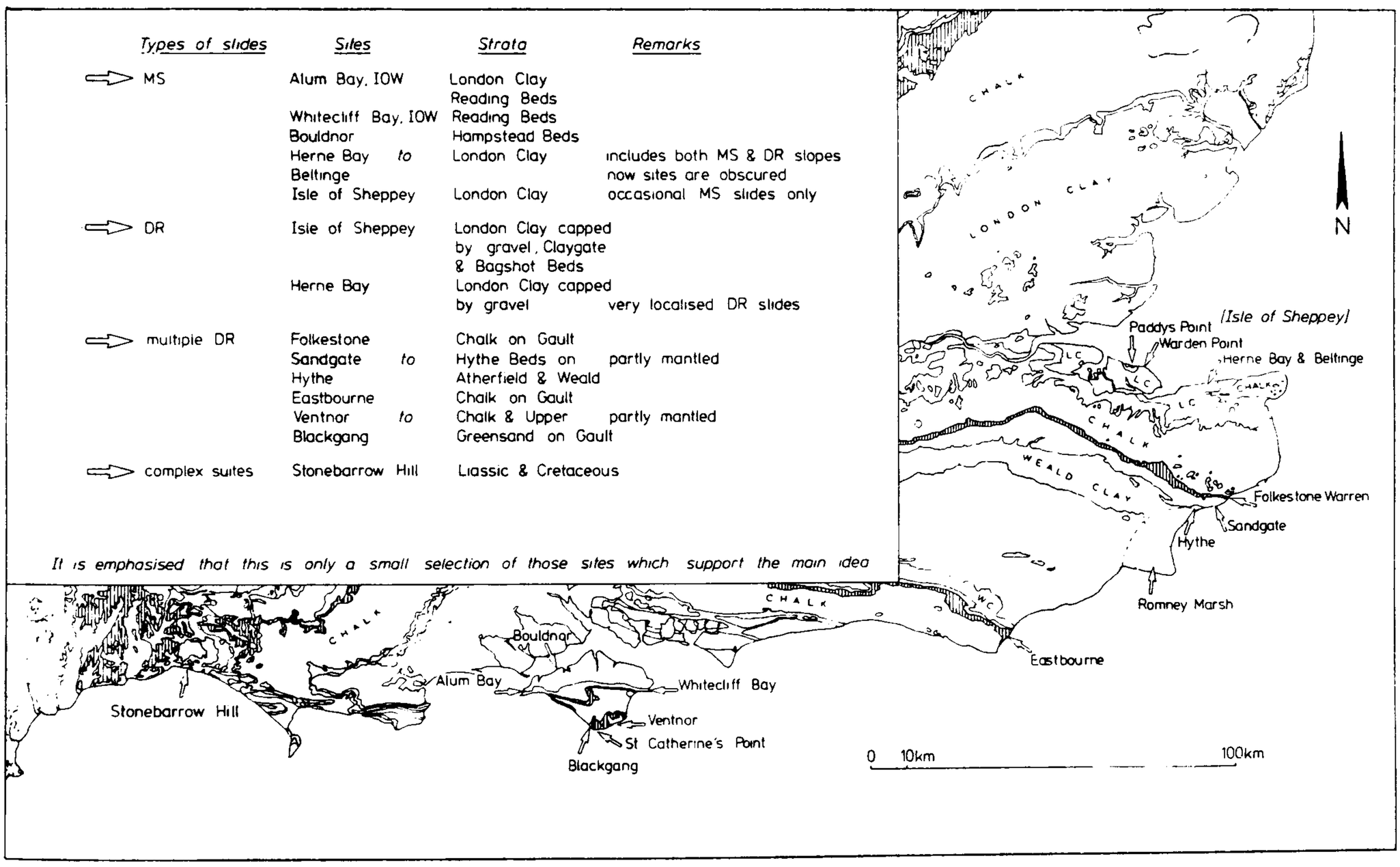


FIG. 2. Location map showing the locations of the various sites discussed in the text as type examples.

are most active. During the summer, when there is little or no movement, the tongue may be eroded back towards the general line of the cliff foot.

Many of the slopes of London Clay on both sides of the Thames (Fig. 2) were formerly the site of extensive mudslides, but most of these have been destroyed by stabilization works. Perhaps the best examples were those of the East Cliffs stretching from Herne Bay to Beltinge, the western part of which was stabilized in 1939 leaving a stretch of cliffs below the Lees, Beltinge as the classic example (Fig. 3); this had extremely evenly spaced corries up until 1969 when they

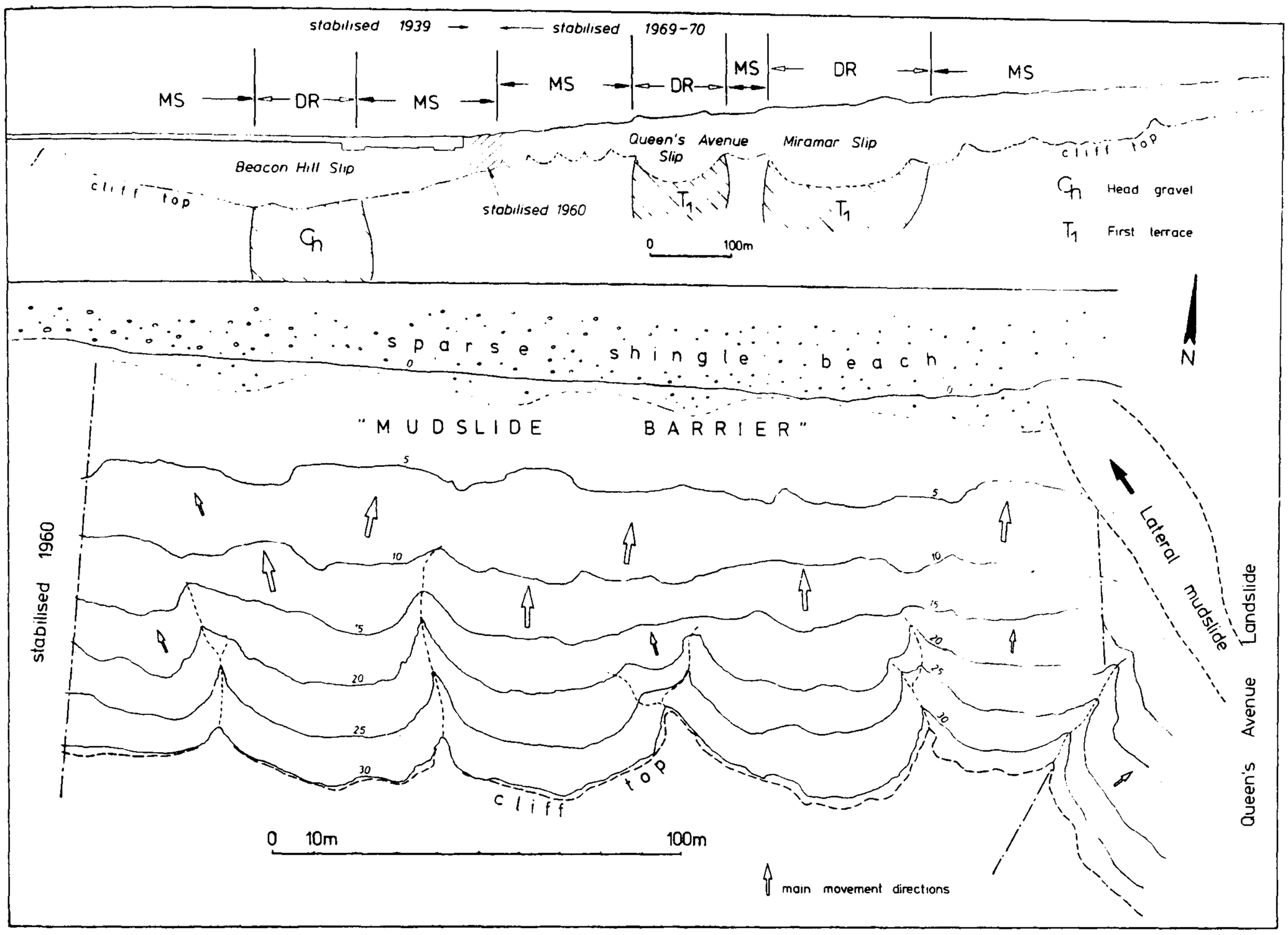


FIG. 3. Plan of the mudslide complex at The Lees, Beltinge, showing the exemplar type *MS* slope prior to regrading and drainage in 1969. The inset map shows how type *DR* and type *MS* behaviour alternates along the coast.

too were treated with regrading and shallow drainage works. Hutchinson (1970) describes a mudslide in these East Cliffs a little to the east of the Lees, and the type section (Fig. 1) draws heavily on his accurately surveyed and investigated cross-section. Less well developed mudslides were formerly also to be found in the West Cliff and Studd Hill to the west of Herne Bay until they too were stabilized.

At present, the best developed mudslides occur sporadically along the north coast of the Isle of Sheppey. If secondary forms, parasitic on deeper slides in the London Clay, are ignored it is usually found that these mudslides owe their origin to natural or artificial surface drainage discharging over the crest of the cliff. The cliffs between Queenborough and Minster are also occupied predominantly by mudslides.

Other ideal type *MS* slopes are to be found on the Isle of Wight at Bouldnor (Hutchinson & Bhandari 1971) which have been inactive recently; in the outcrop of the London Clay at Alum Bay, and in the Reading Beds at Alum and Whitecliff Bays. The Reading Beds mudslides are of considerable age (that at Alum Bay being reported as in existence over 70 years ago), but the London Clay mudslides seem to have developed over the last year or so.

Undrained loading

Hutchinson (1970) drew attention to the ability of the lower parts of mudslides to advance by shearing on extremely low-angle slopes, in many cases flatter than those corresponding to a state of limiting equilibrium for residual strength and groundwater coincident with, and flowing parallel to, the slope surface. By means of piezometric observations in a number of mudslides Hutchinson & Bhandari (1971) confirmed that there were considerable excess pore water pressures in the mudslide debris and that these were largely brought about by the essentially undrained loading of the headward parts of slide by the debris from the steeper slopes at the rear. This situation is explained diagrammatically in Fig. 4.

Hutchinson & Bhandari's measurements of pore water pressures intermediate between hydrostatic and

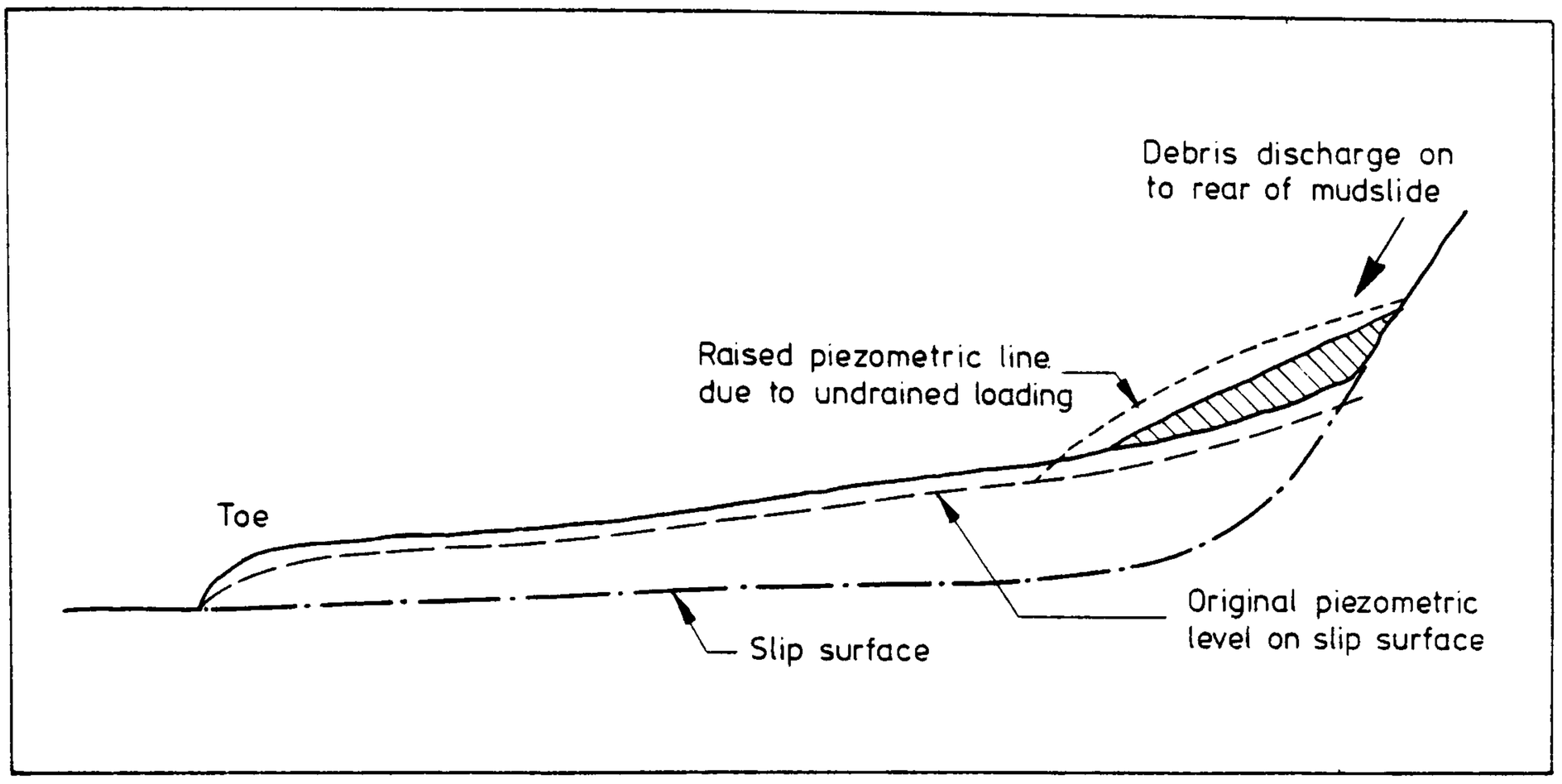


FIG. 4. Section through an accumulation mudslide showing the influence of undrained loading on the pore water pressures in a part of the slide; (after Hutchinson & Bhandari 1971).

geostatic values in a mudslide have been accepted as reasonably characteristic for winter conditions. An attempt to measure summer piezometric pressures was made with a Casagrande Standpipe piezometer 2 m deep in a mudslide at Warden Point in the summer of 1974. This remained dry throughout the summer and before any piezometric levels were detected was lost either through vandalism or by being buried when the mudslide started moving again.

Critical rates of supply

On examination of the behaviour of a mudslide throughout the seasonal cycle, it is found that the factor of safety against sliding is quite high in the summer when not only are the piezometric pressures depressed but falls and slips at the head of the slide are uncommon, and therefore the piezometric pressures are not supplemented by undrained pore water pressures. In the winter, with *only* the increased groundwater levels, a small but nevertheless important reserve of safety still exists and it takes the additional undrained loading effect to stimulate movement. If, however, the effect of toe erosion on a mudslide with winter piezometric conditions is considered, but without undrained loading, it is found that this must be extremely severe to reduce the factor of safety against sliding to unity; conversely, the amount of undrained loading for a similar effect is usually quite small. It therefore seems that the prime factor in re-starting the mudslide is this amount of undrained loading, the supply of which depends ultimately on the condition of the soil at the crest of the slope.

In order to demonstrate these effects, a series of stability analyses on the Beltinge mudslide described by Hutchinson (1970) have been made. These are summarized in Table 1, taking as a base for $F = 1$ the situation with full undrained loading.

There is however, a critical or threshold value for the rate at which material must be discharged on to the head of a mudslide to maintain a continual movement, and this will hereafter be referred to as a critical supply rate. If the discharge is in excess of this critical supply rate, the mudslide responds by a change in profile and a greater advance at the toe. All changes in the rate of supply can cause fluctuations in the mudslide profile and its rate of movement, but once the supply of debris falls below the critical supply rate, the mudslide stops moving (although a small time-lag necessary to dissipate existing undrained pore water pressures may occur). It is usually the case that mudslides cease to move when climatic conditions improve in late spring and remain dormant well into the follow-

TABLE 1. *Comparison of stability at various times for mudslide in Fig. 5 (Flow II, Beltinge; Hutchinson 1970)*

Case	Factor of safety
Full undrained loading: (taken as base)	1.00(F_u)
Drained loading:	
Winter pore water pressures only	1.10
Summer pore water pressures	1.65
Amount of toe erosion to reduce FS to 1.00	
Summer pore water pressure	37 m
Winter pore water pressures	20 m

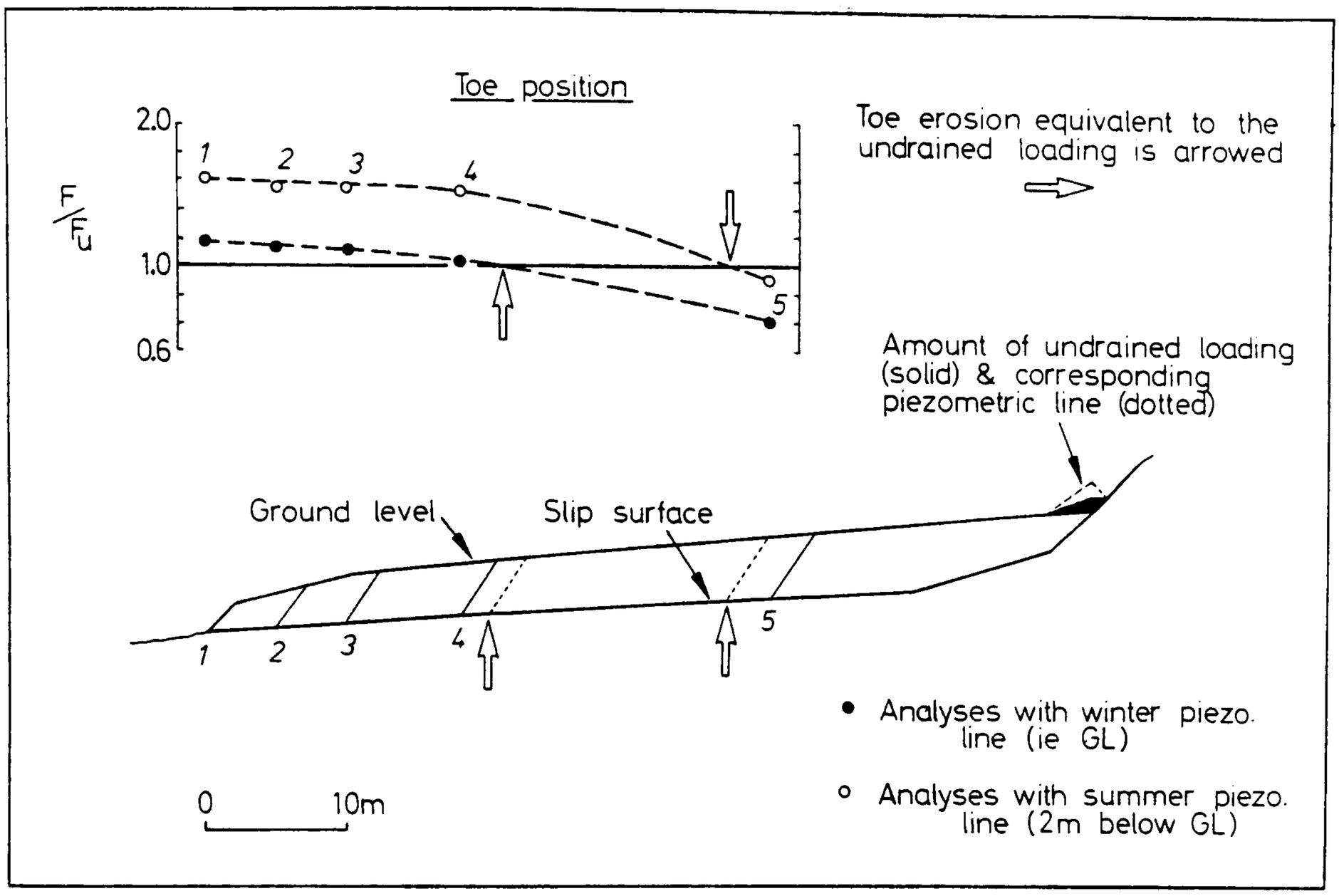


FIG. 5. Stability analyses demonstrating the relative importance of toe erosion and undrained loading. Flow II from Beltinge (Hutchinson 1970) has been chosen for these comparative analyses. The amount of undrained loading is purely nominal.

ing autumn, only being rejuvenated by heavy winter rainfall. They are seemingly unaffected by the erosion occurring during the summer.

Having defined this critical rate of supply it is now appropriate to examine the erosion conditions at the toe of the slope. It will be immediately apparent that with a less than critical rate of supply, the mudslides will not move and marine erosion can waste away the tongues and attack the intact clay behind, over-steepening the whole slope and bringing about deep-seated, rotational slides. This process has been termed 'breaching the mudslide barrier' (Hutchinson 1968). Furthermore, even with some mudslide movement, erosion can be severe enough to have this effect and it is only when the debris supply exceeds a second threshold value that a mudslide barrier of sufficient depth and activity to withstand the appropriate erosion can be built up.

As the cliff recedes, the type, extent, and thickness of materials capping the slope and exposed on the cliff face change. If these materials are water bearing, loose, sandy or gravelly soils, they provide a ready source of supply and the average slope angle of the cliff may flatten rapidly. This agrees with the observations of Lacey (1929) that the presence of such Head will stimulate mudslides. However, it should not be overlooked that too rapid flattening of the slope may result in the 'exhaustion' of this source of supply and the cessation of mudslides, with such mudslide barrier as exists being broken through at some later date. In such a case, the mudslides cannot be rejuvenated and a change in behaviour from type *MS* to type *DR* is the result. A similar ultimate result will be experienced if the cliff-top materials are too strong or well drained to support the appropriate critical rate of supply of debris.

Exploring the opposite end of the spectrum, it will be seen that in a cliff experiencing type *DR* behaviour, eating back into a soil or stratum more capable of maintaining the critical rate of supply can change the behaviour to type *MS* as the rear scarp mudslides never become exhausted and as the debris of the last deep-seated slide is eroded away a mudslide barrier can be established.

No actual example of this has yet been observed, probably because the length of time over which observations have been maintained is too short and because the number of available sites is dwindling. Furthermore, the transitional forms, if they do exist, would presumably be mistaken for one or other of the basic forms. Furthermore, the author is not aware of any site where erosion has caused markedly different cliff-top conditions to be revealed and where such a transition might be expected.

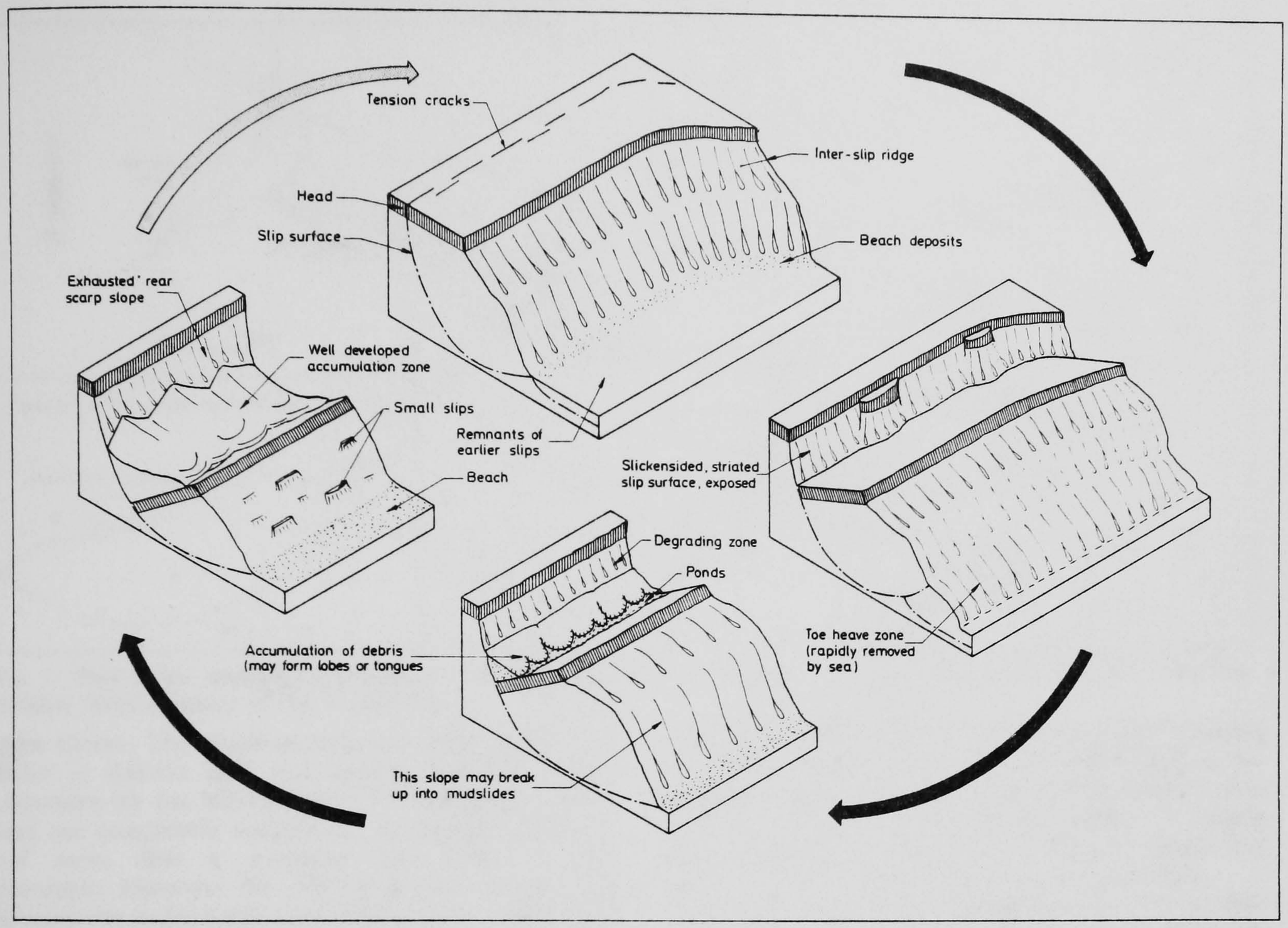


FIG. 6. Block diagrams showing the nature of the landsliding cycle of a type *DR* slope. The two block diagrams in the foreground are foreshortened for economy of space.

Type *DR* slopes

The other important type of coastal mass movement is the deep-seated, rotational kind. Following over-steepening of the cliff, a deep-seated slide will occur. This invariably leaves a steep landward scarp which rapidly degrades, with the accumulation of debris on the back-tilted former cliff-top. Together with marine attack at the toe, this undrained loading of the head of the slide keeps it in motion, albeit quite slowly. In the later stages of the process, rear scarp degradation is very slow but the accumulated debris feeds mudslides which spill out around the sides of the slide mass, which is ultimately eroded away leaving the essentially bi-linear slope profile which precedes a further deep-seated slip. This process is illustrated in Fig. 6 which draws heavily on Fig. 3 of Hutchinson (1973). It should be noted that to the casual observer the bi-linear slope form is very similar to that of a type *MS* slope, especially during the summer when there is little mudslide activity in either type. However, the upper part of a type *DR* slope in these later stages is generally more even, supports vegetation, and does not have the feeder flows and corries of the type *MS* slope; its lower part is free from mudslide tongues.

An important factor in the type *DR* slope is the inhibition of mudslide activity in the upper slopes as they are flattened. This comes about by the control of the supply of potential undrained loading material by stronger soil strata at the crest of the slope, a process which can be seen quite clearly in the rear scarps of the type *DR* slides near Paddy's Point on the Isle of Sheppey, some of which are apparently quite old and relatively slightly degraded. Unfortunately, the age of many of these slides makes them poor type examples.

As was the case for type *MS* slopes, many good examples (such as those at Herne Bay) have been destroyed. The best existing examples are those of the North Sheppey coast in the vicinity of Warden Point and further west, (Fig. 2).

At Warden Point (Fig. 7) there is a fine series of deep-seated rotational slides, easily accessible by road. A number of houses on this road have been lost over the cliff in recent years, and coastal recession has been

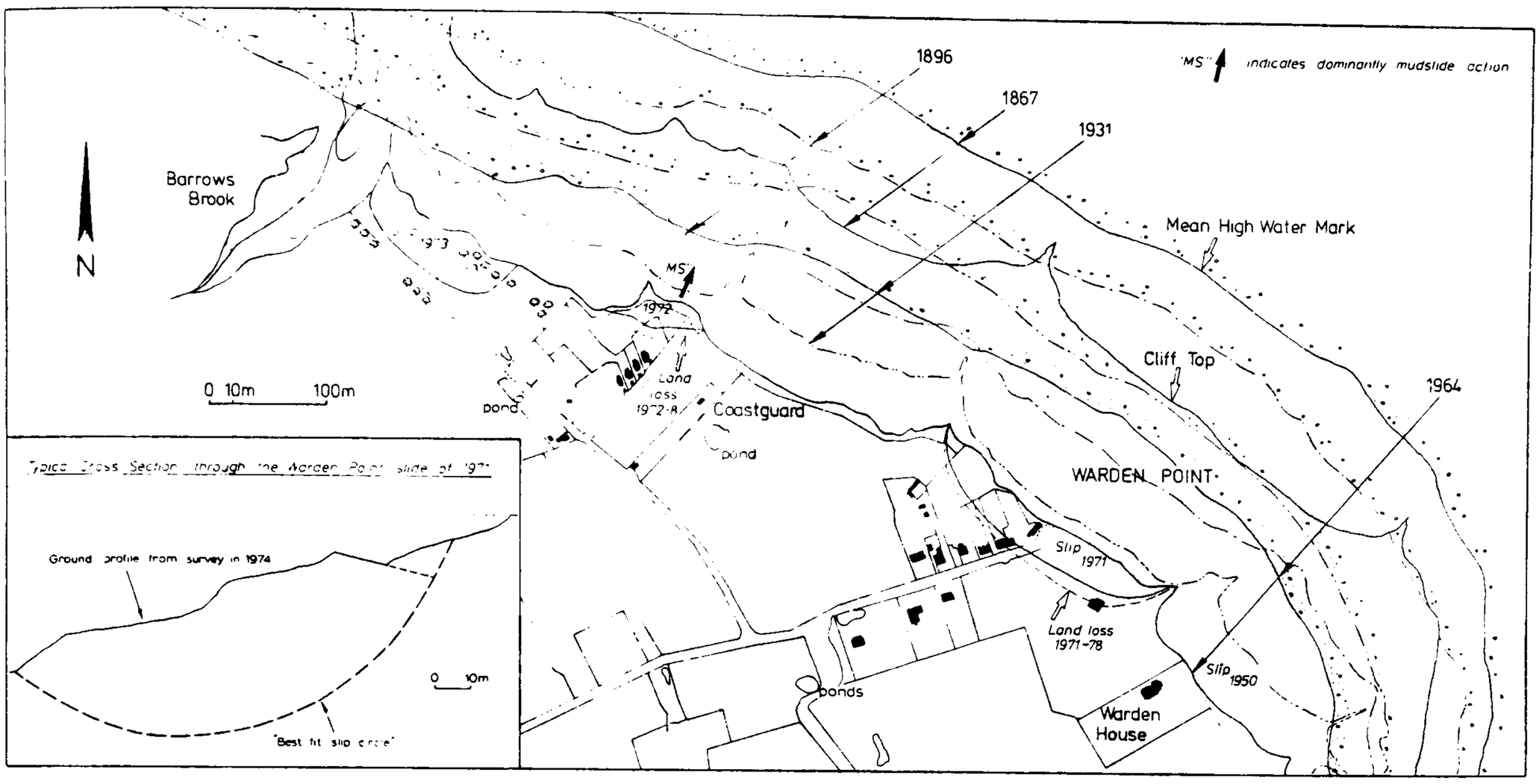


FIG. 7. Plan of the landslides and erosion at Warden Point, Isle of Sheppey, showing the exemplar type *DR* slope. The detailed block diagrams of Fig. 6 apply here.

quite severe. The Head capping the slopes at Warden Point is thinner and less evenly distributed than elsewhere on the North Sheppey Coast and is therefore not completely satisfactory as an ideal example, but more data is available here (Fig. 7) than elsewhere. However the original ground surface rises towards the present cliff edge implying the existence of a former hill at this location which, in common with other high ground on Sheppey, would probably have been capped with Head, Claygate and/or Bagshot Beds. Recent slides appear to extend smaller distances along the coast and to take smaller 'bites' into the cliff top than formerly, so it would appear from the 25 inch OS maps; this probably reflects the decreased cliff height and thickness of cappings as the hill was eroded away. One final pointer to the existence of this 'Warden Hill' is the former location of St. James's Church, Warden Point. Many other old churches in this area are built on high ground such as that of Minster.

An interesting feature of the deep-seated rotational slides at Herne Bay (where *DR* and *MS* type slopes each occupied a part of the East Cliffs) was that as the underlying sandy beds (the Oldhaven Beds) rose to beach level and higher, the landslide slip surfaces changed from an almost classic circular arc section to a flat-soled, non-circular section (Bromhead 1978). This is thought to be due to the strain concentrating effect of the interface between the overconsolidated clay and its more rigid underlying sand.

Previous theory

The most widely known and accepted theory relating to these types of slide behaviour is that of Hutchinson (1968, 1973) who ascribes the control to the intensity of marine erosion. Unfortunately, this work is intended to apply only to cliffs of similar height, composed wholly of London Clay and subject to largely similar climatic conditions. This naturally leaves toe erosion intensity as the only remaining variable.

However, toe erosion intensity and the rate of cliff-top retreat are not necessarily the same thing, although the latter has been used as a pointer to the former. The height of the cliff and movement of the toe are the other important factors in gauging the masses shifted, and if for example the toe advances as much as the crest retreats, then this cannot be put forward as a case where rapid erosion is being experienced. This situation has occurred in the vicinity of Paddy's Point on the Isle of Sheppey.

A second important factor is the temporal position of the observer. The later stages in a type *DR* recession cycle look so similar to type *MS* behaviour that if the *DR* cycle is of long duration (and our best evidence can only go back to the first editions of the Ordance Survey maps) it may not be evident that the cliff is subject to *DR* behaviour at all. On the other hand, if the same period of observation corresponds to the early part of a similarly long-period type *DR* cycle, the observer can only report a rate which includes the initially large 'bite' and subsequent rapid rear scarp degradation. The average rate of erosion will therefore be overestimated and a false picture obtained. The evidence of erosion intensity when based solely on cliff-top position as shown on early maps must therefore be viewed with suspicion, especially when used as the sole or principal criterion.

Furthermore, when both type *DR* and type *MS*

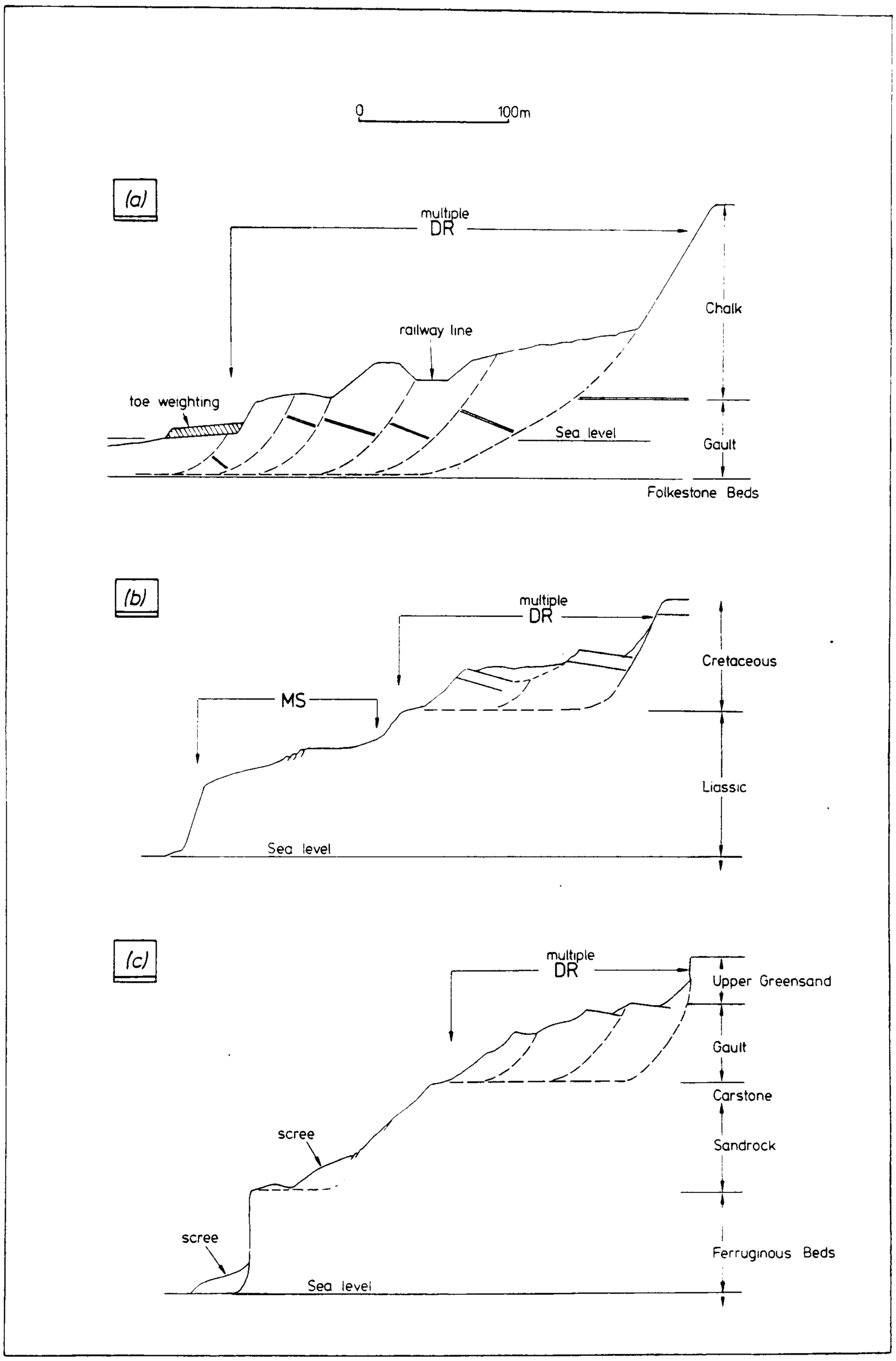


FIG. 8. Sketch sections through typical slopes with multiple *DR* slides.
a Folkestone Warren; *b* Stonebarrow Hill (after Brunsden 1973); *c* Blackgang, Isle of Wight.

behaviour are found in the same stretch of coastal cliffs which are straight or slightly curved in plan, this poses a serious problem for the erosion rate theory. It may just be possible that marine erosion can be locally concentrated, perhaps by refraction of waves by very localized beach features, but it seems an unnecessarily overcomplicated extension to the mechanism. Often, a mudslide is found in a row of deep-seated slides and inevitably this is found on closer inspection to be the result of local soil and ground- or surface-water conditions at the head of the slope. The reverse situation is less commonly found, (but the temporal position of the observer may of course be an important factor here); however, at Herne Bay (Bromhead 1978) three deep-seated landslides were found in a stretch of cliffs occupied mainly by mudsliding. The positions of these correspond precisely to the outcrops of Head shown on the 6 inch geological map (Fig. 3).

System theory approach

Brunsden (1973) stresses the applicability of system theory to the study of mass movements, and with reference to coastal landslides and mudslides explains the conceptual framework within which the theory may be applied.

This system model for a mudslide demonstrates that the rates of input and throughput, when considered in relation to the amount of debris storage in the slide itself, are the critical regulators in the system and that the output from the system, although an important factor through negative feedback, is by no means as important as the erosion rate theory implies.

Multiple rotational slides

It is interesting to examine the behaviour of cliffs where the crest is very much stronger than the body of the slope, i.e. forming a caprock. Such cliffs are usually fronted by an undercliff of multiple deep-seated rotational failures, for example: Folkstone Warren, the Isle of Wight, and various locations in Dorset and elsewhere. The presence of the cap rock almost totally inhibits the rear scarp degradation process.

It would appear that the fundamental difference between a caprock slope with multiple *DR* slides and a simple *DR* slope is a function of the degree of control over the failure of slabs of the caprock exercised by its joint distribution and orientation. This would certainly appear to be the case at Folkestone Warren (Fig. 2) and this is discussed by Hutchinson *et al.* (1979). Other excellent examples of slopes with multiple *DR* slides are to be found along the south coast of the Isle of Wight with perhaps the clearest example just west of St. Catherines Point (Fig. 8).

The coastal landslides in the vicinity of Paddy's Point on the Isle of Sheppey, where the London Clay is capped with Claygate and Bagshot Beds may be a transitional form between the type *DR* behaviour seen elsewhere at Sheppey and the multiple type *DR* slides characteristic of a caprock slope.

'Caprock' slopes apparently without multiple *DR* slides

A number of slopes on the coast of southern England have a caprock but appear not to have multiple *DR* slides, for example the Hythe Beds escarpment from Aldington to Hythe and Sandgate. These slopes have quite a low inclination, support only sporadic, small-scale shallow sliding, and appear to be analogues of the abandoned cliff of London Clay at Hadleigh (Hutchinson & Gostelow 1976). The presence of the Flandrian Romney Marsh at the toe of the western part of this escarpment completes the resemblance.

However, closer examination reveals a number of very degraded rotational slides west of Hythe and cambering in a valley to the east, together suggesting a considerable age for this slope. At Sandgate where, despite the presence of a sea wall, marine attack is still active, multiple *DR* slips are *mantled* by later solifluted material. It may well be that similar slides could be exhumed at other places along this abandoned cliff if the erosion were to strip off the mantle.

Complex suites of different landslide types

Occasionally, in a high cliff with varied lithology, the slide types in different parts of the slope will reflect the lithologies present. It is worth examining these slopes in some detail for the further light that they throw on the present hypothesis. Two further factors complicate matters. The first of these is the ease with which silts and sands are eroded by seepage and the washed out materials tend to obscure other forms of instability; the second is the influence of even quite thin hard ledges on any mudslide activity.

Examples of such complex suites are as shown in diagrams b & c of Fig. 8 where multiple *DR* slips occur at the top of the suite with mudslides occupying the lower slopes. In both cases, the multiple *DR* slides are in a section of the cliff with a caprock. This would seem to confirm that the caprock is the dominant factor.

Conclusion

As it stands, the present evidence supports the general conclusion that the type of slide behaviour in a cliff mainly composed of overconsolidated clays and subject to marine erosion is controlled to as great an extent by the type of material and the hydrological conditions at the crest as by the intensity of the erosion.

It is suggested here that if the crest is broadly

similar in nature to the rest of the slope, then mudsliding is the dominant form of mass movement, whereas on the other hand, if the crest is stronger or better drained, then deep-seated, rotational failures occur in a well defined cycle. The presence of a very much stronger caprock, particularly if allied with a strong basal bed, modifies the deep-seated rotational slips into multiple rotational slips.

ACKNOWLEDGMENTS. The author would like to gratefully acknowledge the fundamental contribution to this subject of Professor J. N. Hutchinson (reflected in the reference list), and to thank the Building Research Establishment for access to Hutchinson's (unpublished) coastal landslide survey. In addition he would like to mention the help of Messrs D. L. Medley, M. J. Whitwell, S. J. Lee, and R. D. Curtis with field reconnaissance work. The staff at the British Library Map Room have been of great assistance in the review of the old Ordnance Survey plans.

References

BROMHEAD, E. N. 1978. Large landslides in London Clay at Herne Bay, Kent. *Q. J. eng. Geol. London.* **11,** 291–304.

BRUNSDEN, D. 1973. The application of system theory to the study of mass movement. *Geol. appl. Idrogeol. Univ. Bari.* **8,** 185–207.

HUTCHINSON, J. N. 1965. A survey of the coastal landslides of Kent. *BRS Note EN 35/65.* Building Research Station.

—— 1968. Field meeting on the coastal landslides of Kent, 1st–3rd July, 1966. *Proc. geol. Assoc. London.* **79,** 227–237.

—— 1968*a*. Mass movement. *In: The Encyclopaedia of Geomorphology*, Reinhold

—— 1970. A coastal mudflow on the London Clay Cliffs at Beltinge, North Kent. *Geotechnique. London.* **20,** (4), 412–38.

—— 1973. The response of London Clay cliffs to differing rates of toe erosion. *Geol. appl. Idrogeol. Univ. Bari.* **8,** 221–39.

——, & BHANDARI, R. K. 1971. Undrained loading, a fundamental mechanism of mudflows and other mass movements. *Geotechnique. London.* **21,** (4), 353–8.

——, & GOSTELOW, T. P. 1976. The development of an abandoned cliff in London Clay at Hadleigh, Essex. *Philos. Trans. R. Soc. London. A* **283,** 557–604.

——, BROMHEAD, E. N. & LUPINI, J. F. 1979. Additional observations on the Folkestone Warren landslides.

LACEY, J. M. 1929. Littoral drift along the north-east coast of Kent, and the erosion of the Beltinge Cliffs near Herne Bay. *ICE Selected Eng. Papers No. 72.*

Q. J. eng. Geol. London, 1980 Vol. 13 pp. 1–31 Printed in Northern Ireland.

Additional observations on the Folkestone Warren landslides

J. N. Hutchinson, E. N. Bromhead* & J. F. Lupini

Department of Civil Engineering, Imperial College, London SW7 2BU.
*School of Civil Engineering, Kingston Polytechnic, Canbury Park Road, Kingston-upon-Thames, Surrey KT2 6LA.

Summary

The Folkestone Warren landslides are first compared to the landslides at geologically related sites on the northern coast of France and the southern coast of England. Additional historical data is then presented on the Warren landslides, particularly that of 1915, and the influence on these of the interruption of littoral drift produced by the Folkestone Harbour works is examined. An indication is also given of other considerable mass shiftings which have taken place in the Warren since the early nineteenth century. A preliminary morphological study is made, the features being linked, where possible, with the historical data. The degree to which the frequent Chalk falls from the High Cliff are controlled by the joint pattern is briefly examined and the recent subsurface investigations in the Horse's Head area are reviewed and discussed.

The existing back-analyses of the slips are critically re-examined in the light of the fresh historical and morphological data and additional back-analyses are carried out. Measurements of the residual strengths of the high and low liquid limit Gault are made, in two different ring shear machines, and compared with the combined results of the back-analyses.

Introduction

The first treatment of the Folkestone Warren landslides in terms of effective stresses appeared a decade ago (Hutchinson 1969). At that time the ring shear test as a method of determining residual strength in the laboratory was relatively unexplored and the residual strength data presented were thus derived entirely from cut-plane, 60 × 60 mm, direct shear box tests. Additional information is now available which has prompted the writing of this further paper. This comprises chiefly the following: (a) The results of a site investigation carried out for British Railways in the vicinity of the Horse's Head. (b) Drained ring shear test data on the Folkestone Warren Gault, carried out on the apparatus developed by Bishop *et al.* (1971). (c) Similar test data carried out on the apparatus developed by Bromhead (1979).

A more detailed review has also been made of some aspects of the history of the Warren; in particular of the 1915 slip and of the interruption of the littoral drift by the Folkestone Harbour works. The main loadings and unloadings which the landslides have undergone since the commencement of railway construction in about 1840 are identified and discussed. In the light of the foregoing, the opportunity has been taken to re-appraise and extend some of the earlier back-analyses. The values of residual strength thus derived are compared with those measured in ring shear. Preliminary work has also been done on the morphology of the Warren and on the influence of the joint pattern in the Chalk on the form and behaviour of the rear scarp of the landslides.

Geologically related sites

As shown in Fig. 1, coastal sites exhibiting the descending sequence Chalk, Upper Greensand (sandy facies) and Gault (clayey facies), and Lower Greensand are to be found at four places in the breached Weald–Boulonnais anticline, at three localities in the Isle of Wight and at several places further west in England and further south in France.

Of the four Weald–Boulonnais sites, Folkestone Warren (a) has by far the most extensive landslides. This is probably due mainly to the absence of the Upper Greensand there, the correspondingly large thickness of the argillaceous Gault (of *c.* 45 m), the low dip of the strata (of *c.* 1°) and the high relief. At Cow Gap, Eastbourne (b), the relief is much lower and the landslides there are relatively small.* On the Boulonnais coast the Gault is less clayey and only about 10–20 m thick, and the dip is up to 15° (Destombes & Shephard-Thorn 1971). The landslides at the French equivalents of Folkestone Warren and Cow Gap, between Cap Blanc Nez and Wissant (c) and near Hardelot (d) respectively, are thus of limited scale. Moreover, the southerly of these two sites, in the Forêt d'Hardelot, is now protected from the sea by an extensive system of littoral dunes. In the Le Havre region, the Gault is even thinner, and the coastal landslides (Masson 1976) may be controlled more by the underlying Kimmeridgian.

The E–W monocline running through the Isle of Wight gives rise to coastal exposures of the above sequence at Culver Cliff (e) and Compton Down (f). At both these, sites, however, the landslides are small and confined essentially to the Gault, chiefly as a

*The planed-off remnants of earlier slides may be seen at low tide in the foreshore on the east side of Beachy Head (Davies 1939, Kennedy 1969).

0481–2085/80/0100–0001$02.00 © 1980 The Geological Society

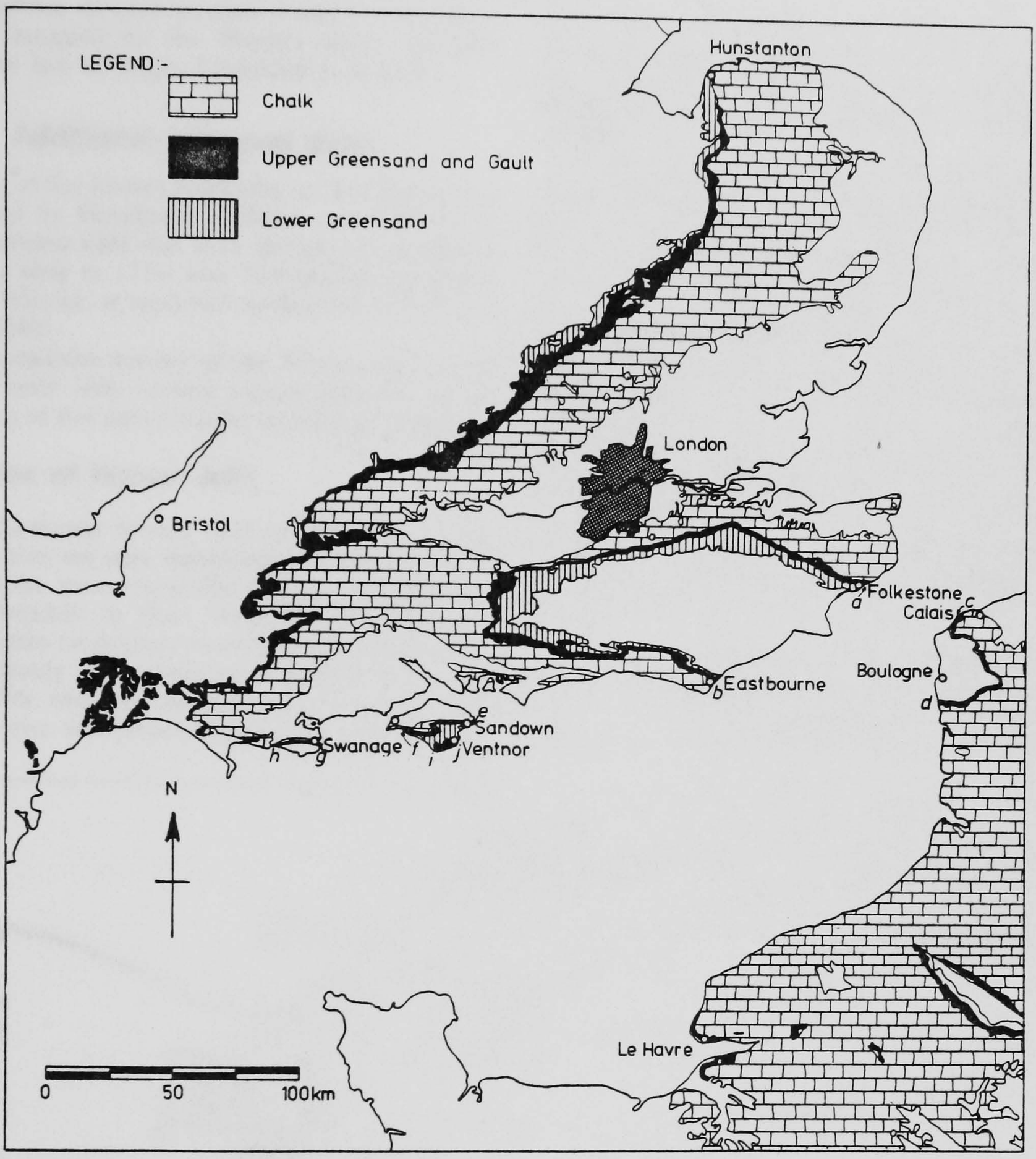


FIG. 1. Map showing the solid geology of south-east England and northern France. The coastal sites exhibiting the descending sequence of Chalk, Upper Greensand, Gault and Lower Greensand are indicated with the lower case letters a–j by which they are referred to in the text.

result of the high northerly dips (40–60°). Again, at the related Isle of Purbeck sites (g, h) no really extensive slips are developed, partly because of generally high northward dips and partly because of the tendency, already evident at Eastbourne, for the Gault facies of the Upper Greensand and Gault formation to thin and become sandier to the west. Furthermore, west of about Mupe Bay, the Upper Greensand and Gault begins to overstep the underlying strata until, in east Devon, it rests on the Trias (Wills 1929). Thus, although large coastal landslides involving the Chalk and the Upper Greensand and Gault exist in this last-mentioned area (Arber 1940), they are not close analogues of Folkestone Warren. To the north, in East Anglia, the Gault thins and changes in lithology, and is represented in the cliffs at Hunstanton only by 1.2 m of Hunstanton Red Rock (Chatwin 1961).

The closest analogy to the Folkestone Warren landslides is provided by the complex of landslides (i–j) which form the Undercliff of the south coast of the Isle of Wight (Hutchinson 1965*a*). This extends for about 12 km along the coast, compared with 3 km at the

Warren, and has an area between 5 and 6 times larger than that occupied by the Warren slides. Detailed work on the Isle of Wight Undercliff is in hand.

Additional historical data

The history of the known landslides at the Warren has been treated by Hutchinson (1965*b* and 1969). The earliest recorded slide was then thought to be that of 1765, but a slide in 1716 near Folkestone, and possibly in the Warren, is reported by Berryat (1756) and Roberts (1840).

A comprehensive history of the Warren will not be attempted here; only certain aspects relevant to the main themes of this paper will be treated, as follows.

Interruption of littoral drift

The predominant littoral drift on this part of the coast is towards the east. Interference with this drift in the Folkestone area, therefore, tends to deplete the beaches downdrift in East Wear Bay (Fig. 2) and hence stimulate landsliding in the Warren. Such interference probably took place on a modest scale from the late 17th century onwards, as a result of the various groynes and jetties which were built to form early havens at Folkestone (Folkestone Common Assembly Minute Books, 1670–1835). Major interference, however, dates from the construction of a masonry harbour there in the first decade of the 19th century.

The development of the modern Folkestone Harbour is outlined in Fig. 3. Construction began in about 1807; the West Pier was completed by 1810 and the Haven by 1820. By 1830, however, the harbour mouth was almost completely choked by sand and shingle and in 1842 the Folkestone Harbour Company went bankrupt. Shortly afterwards, the harbour was bought by the South Eastern Railway Company, who built a spur line to connect it to the Folkestone–Dover railway which was then under construction. From then on, successive extensions were carried out in order to produce shingle-free, deep water berths. In 1861–63 the Promenade Pier was built, initially of timber but stone cladded and extended in 1881–83 when it was renamed the New Pier. A further extension to this in an ESE direction was made in 1897–1905 (Bishop 1973).

The effect of these works was, of course, to trap the littoral drift on the west side of the western harbour arm. A water colour in Folkestone Museum shows a beach accumulating in that locality in about 1820. The

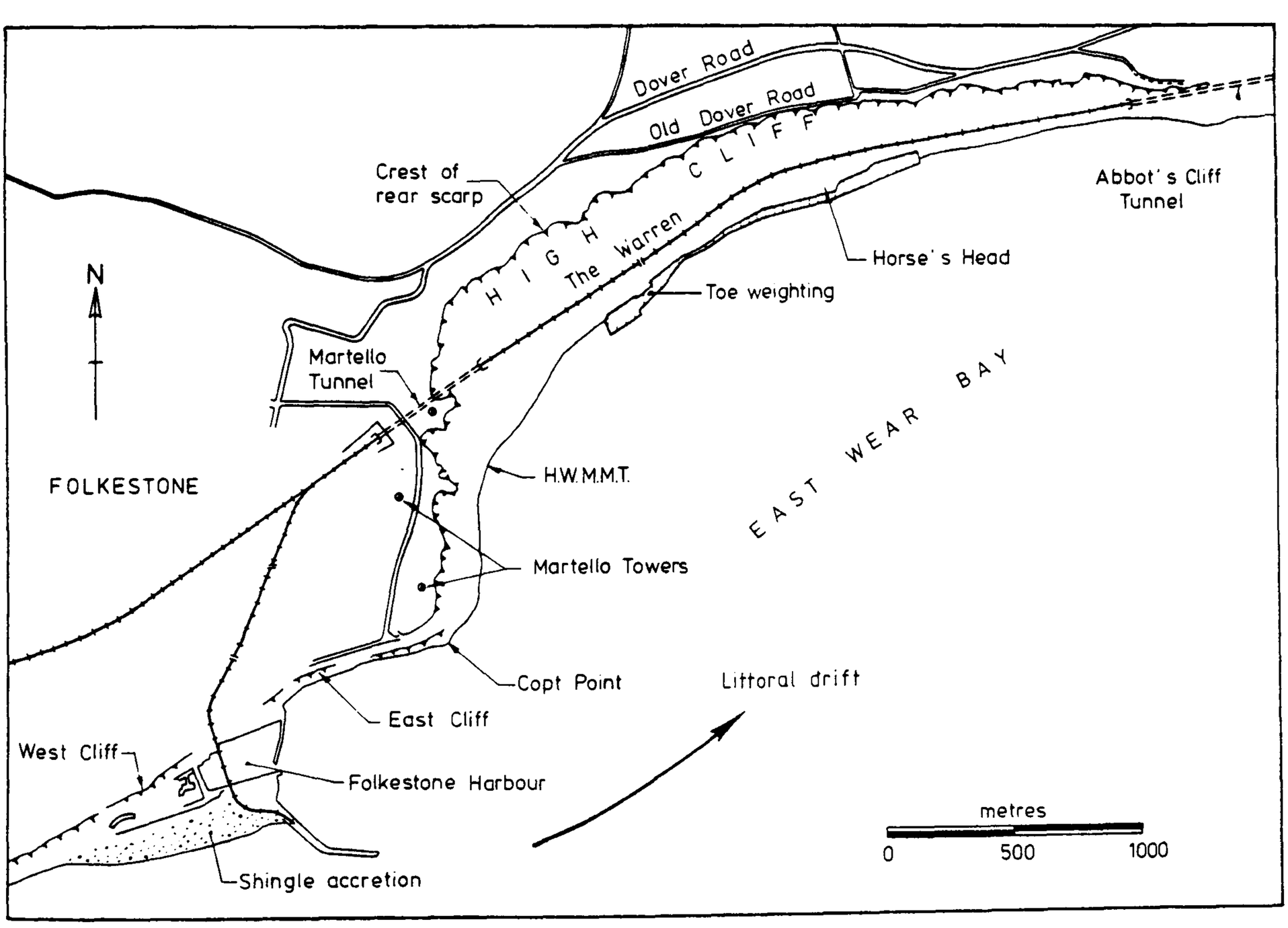


FIG. 2. General location map showing the relationship of Folkestone Warren to Copt Point and Folkestone Harbour.

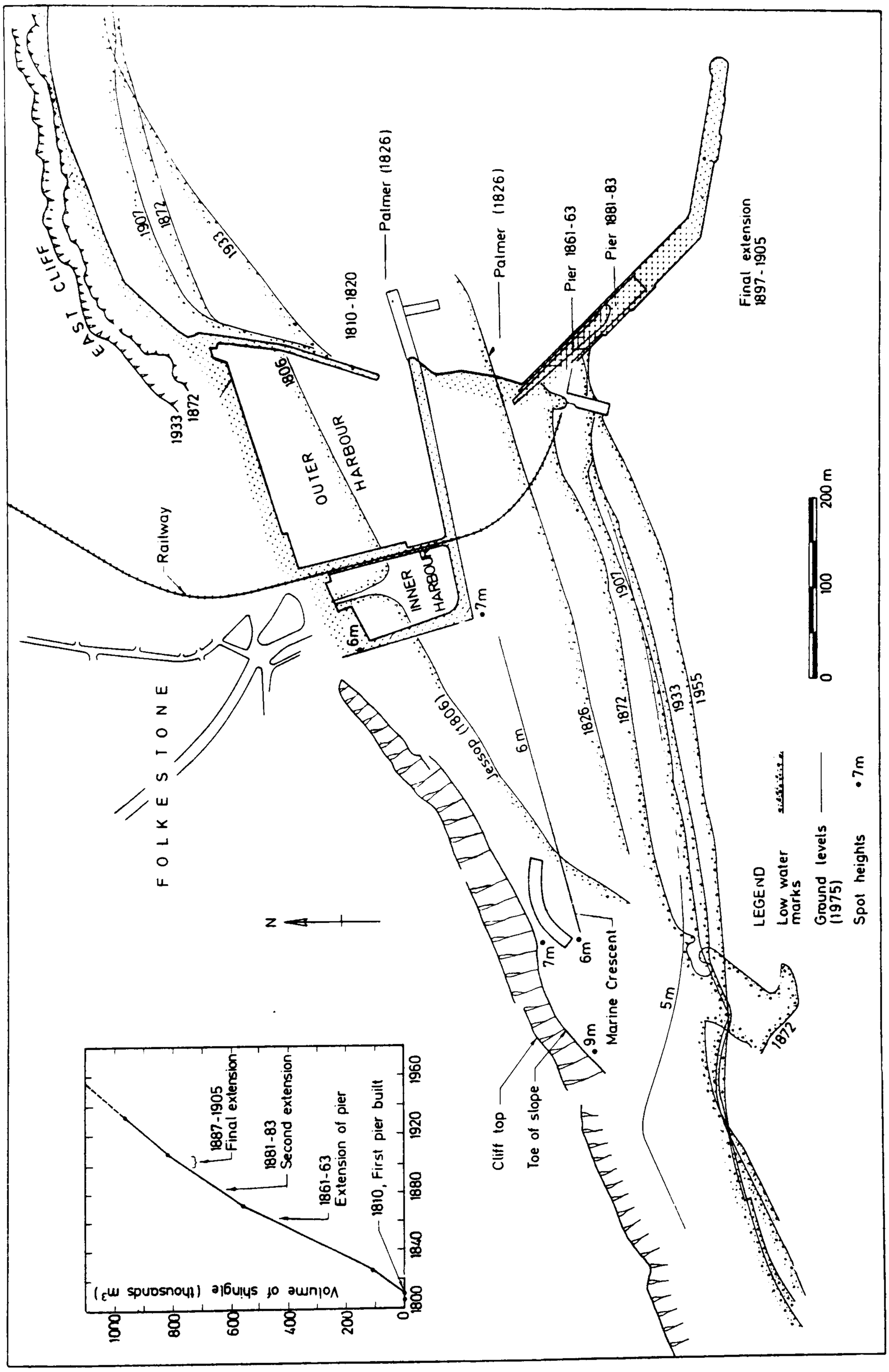


FIG. 3. Plan depicting the historical developments of Folkestone Harbour and the estimated quantity of shingle accumulated since 1806 above low water mark.

progress of this accumulation has been estimated from the available maps and plans, as shown in Fig. 3. An early stage in this process is described by Palmer (1834). Because of uncertainty with regard to the shape of the sea bed inshore before the construction of the harbour, the volumetric estimates refer only to accumulation above M.L.W. (taken as −2.40 m O. D. Newlyn) and thus underestimate the actual volume of beach.

The resulting depletion of beaches downdrift from Folkestone Harbour has been noted by several authors (e.g. Redman 1852; Drew 1864; Anon 1865, 1870; Mackie 1883; Wheeler 1902; Osman 1917). Mackie's account is particularly vivid: 'Beautiful as the Warren still is, it is not to be compared with the Warren of half a century ago. The ingenuity of our present generation, which has constructed a harbour where our forefathers utterly failed, has not been without effects which lovers of the grand and beautiful scenes of nature must regret. While the beach has accumulated to an enormous extent west of the harbour, the rugged form of Copt Point has crumbled away until nothing is left but the rocky foundation on which it stood, and year by year the Warren which nestled behind it grows less and less in extent, as the restless waves roll up and swallow it'.

This account appears only in the 2nd (1883) edition of Mackie's book, not in the 1st (1856) edition. This is concordant with the contemporary evidence (Drew 1864 and Anon 1865) that '. . . the sea having considerably gained on the shore at that point {by the new coastguard cottages in the Warren}, in consequence of the holding back of the shingle, from the carrying out of the new jetty at Folkestone' (Anon 1865). Evidence for strong beach erosion in the area at about this time is also provided by Sir J. Coode's report in 1871 (in Wheeler 1902) of the disappearance of an 80 yard wide shingle bank near Lydden Spout (about 5.5 km ENE of Folkestone Harbour). Subsequently Osman (1917) writes that 'all of us who are old enough to remember the Warren in the early eighties, before the stopping of the run of shingle by Folkestone Pier Extension . . .'.

The direct connection between the various extensions of the western arm of Folkestone Harbour and the accumulation of beach on its updrift side is clear (Fig. 3). The beach depletion downdrift, which is an inescapable consequence of this, is not recorded in similar detail, but from the few observations given above it is evident that significant erosion was already occurring in the Warren by 1864 and that this seems to have been intensified in 'the early eighties'.

If Wood's (1971) suggestion that the beach would deplete rapidly following cut-off of the littoral drift is accepted, it would seem likely, as indicated by Mackie and Osman, that these two phases of erosion can be related, respectively, to the construction of the Promenade Pier in 1861–63, and to its stone cladding and extension into the New Pier in 1881–83. Direct observations of erosion in the Warren resulting from the final extension of the New Pier in 1897–1905 are scanty, but its occurrence is implicit in the records of continuing accumulation of beach updrift (Fig. 3).

The chain of events discussed above, whereby successive extensions of Folkestone Harbour pier lead to increasing interference with the littoral drift with consequent beach accumulation to the west and depletion to the east, leads finally to the stimulation of landsliding in the Warren, as was realized by most of the authors quoted above. Accurate correlation is not possible, partly because of incomplete data and partly because the incidence of the landslides is influenced by factors such as ground-water, geotechnical conditions and tides, as well as by coastal erosion and the degree of defence against this. A possible interpretation of the available records, however, is given in Table 1.

From Table 1 various points emerge:

1. In the century preceding completion of the first stone pier in 1810 only two certain slides are known of in the Warren , with possibly one more. Lyon's description of Folkestone Warren in 1786 as 'pasture' also points to a relative stability during this period, which from Mackie's (1883) account can be inferred to have lasted until about 1833.

2. In the 105 years following the construction of the West pier in 1810, during which pier extensions were completed in 1863, 1883 and 1905, eight major slides occurred of which three were probably of a larger (M) type than had hitherto been recorded.

3. If each slide is associated with the last pier extension preceding it, four phases of increasing slide activity are evident, as detailed below:

1810–1862 Two R type slides took place 29 and 49 years after completion of the West Pier. No M type slides occurred in this period.

1863–1882 An R type slide took place 2–7 years after completion of the Promenade Pier and an M type after 14 years.

1883–1904 An R type slide occurred 3 years after completion of the New Pier and an M type after 13 years.

1905–1915 An R type slide occurred 1 year after completion of the final pier extension and an M type (the largest recorded) after 10 years.

4. There has been a period of reduced activity, with essentially only two, R type, slides since 1915. This is probably due to a combination of the great size and relatively large movements of the 1915 landslide and the considerable sea defence, toe weighting and drainage measures carried out subsequently.*

In summary, the evidence suggests that the successive extensions of Folkestone Harbour, particularly

*Some beach feeding at the western end of the Warren was also carried out for a number of years prior to 1939 (Toms 1948).

TABLE 1. *Possible correlations between the development of Folkestone Harbour and the incidence of major landslides in the Warren*

Folkestone Harbour development		Major slides* in the Warren		Approx. number of major slides in period	Elapse of years from completion of pier work to next major slide	
Description	Date of completion	Probable type†	Date		R type	M type
Various Small early havens		?	1716	1716 to 1809 (3)		
		?	1765			
		R	1800			
West Pier	1810					
		?	1839		29	
		R	1859		49	
Promenade Pier	1863			1810 to 1915 (8)		
		R	1865–1869		2–7	
		M	1877			14
New Pier	1883					
		R	1886		3	
		M	1896			13
Final extension	1905					
		R	1906		1	
		M	1915			10
		R	1936–1937	1916 to present (2)		
		R	1940–1947			

*Excludes Chalk falls.
†After Hutchinson (1969).

between 1810 and 1905, led to a progressive increase of landsliding in the Warren, which culminated in the great slide of 1915.

The 1915 landslip and associated events

The 1915 failure is complicated by the fact that several large Chalk falls from its rear scarp (the High Cliff) were associated with it. As noted by Hutchinson (1969), this introduces uncertainties into stability analyses of the 1915 undercliff. With the additional data now available it is appropriate to re-examine the development of the 1915 slip before attempting any reappraisal of its stability.

The mass movements under discussion all took place in the early evening of 19th December 1915. There was an unusually large number of eye-witnesses, comprising railway staff and passengers, soldiers on guard duty and local residents. The events occurred after dark, but there was a good moon.* A contemporary plan, showing the main slide displacements, Chalk falls and upheavals of the foreshore has recently been obtained from British Railways, Southern Region. This is reproduced in Fig. 4. The names of the various features referred to below are given there or on Fig. 5. No complete published account of the slide has been found and the following reconstruction of the events (see opposite) is based chiefly upon two contemporary newspaper accounts, Anon 1915*a* and Anon 1915*b* (abbreviated to X and Y, respectively).

*Two days before full moon.

Reconstruction of events

Time (G.M.T.)	Event
Shortly after 6.00 p.m.	Watchman noticed that there had been a subsidence in the line at the Martello Tunnel end of the Warren. Gave his red light to soldiers to stop the expected 6.10 p.m. from Ashford and went to telephone the station (X).
About 6.30	Start of big fall of the rear scarp at Steady Hole heard and seen by soldiers near Warren Halt (X, Y).
About 6.30†	Occupants of 'Eagle's Nest' notice ceiling cracking 'without any warning' (X).‡
Say about 6.35	They try to leave, find doors jammed and climb out through a window (X).
6.35	Platelayer arrives at Abbotscliff Signal Box and tells signalman to put all signals to danger because of the fall (at Steady hole) (X).
About 6.36–6.40	The three occupants of Eagle's Nest have reached the end of their garden when they see the start of the 'Great Fall' to the east of them (X). The cliffs to the west of them are also falling (Y).
About 6.35–6.40	Signalman, platelayer and three soldiers run from Abbotscliff Signal Box as cliffs behind it start to fall. Signalman feels rails go down 'quite a foot' as he leaves his box (X).
About 6.38–6.43	Start of the 'Great Fall' from the rear scarp near Capel Lane. This turned into a flow slide, buried the railway line under 40 feet of debris for a length of about 250 yards, and ran about $\frac{1}{4}$ mile out to sea (X).
Shortly after 6.45	The 6.10 Ashford to Dover train leaves Folkestone Junction Station, fortunately 'a little late', with about 130 passengers (X, Y).
About 6.50	The above train brakes suddenly as it emerges from Martello Tunnel into the Warren, on seeing soldiers with red lamps who report line blocked ahead (X).
About 6.50–7.10	Passengers wait in the train while engine and front carriages sink slowly down (X, Y) with the continuing movements of the M type slide.
About 7.10	Guard asks passengers to leave train, soldiers conduct them on foot back to Folkestone Junction through the Martello Tunnel (X).

From the above, the following pattern of failures appears likely:

approx. time	Event
By 6.00 p.m.	A slight sinking of the W end of the Warren undercliff had occurred.
6.30–6.35	(1) Fall at Steady Hole. (2) Slide of 'Eagle's Nest'.
By 6.35–6.40	Sinking of the undercliff had spread eastwards to Abbotscliff Signal Box.
6.40	The 'Great Fall' near Capel Lane.
6.40–7.00 or later	Continuing seaward, and generally downward, movements of virtually the whole Warren undercliff.

†At about 6.45 p.m. according to reference (Y), but this seems less reliable.

‡Details of the slide involving this house are given on page 10.

It is thus concluded that a renewal of movement of the M type slips forming the undercliff commenced at the western end of the Warren and spread eastwards. This disturbance triggered the three associated failures of the rear scarp in a west to east order, namely the Steady Hole fall, the Eagle's nest slide and the Great Fall. These, and particularly the former, further stimulated the movements of the undercliff.* Osman (1917) considered that the Steady Hole and Great Falls occurred in response to movements in the undercliff.

Two main factors probably brought about the renewal of movement in the undercliff:

(a) The continuing erosion in East Wear Bay, intensified by the extension of the New Pier completed in 1905 (discussed above).

(b) The unusually high rainfall of 1915 and especially its last 4 months. The rainfall at Folkestone, Cherry Gardens (about 4 km west of the Warren), from the start of records in 1868 to 1915, was as shown in Table 2.

In addition, the low tide (two days before Springs), which preceded the time when movement of the undercliff was first reported by about $1\frac{1}{4}$ hours, will probably have acted as the final trigger.

The facsimile of the contemporary plan of the 1915 slide, shown in Fig. 4, is probably the best existing record of its movements. It shows the area involved in the main slide, extending over 2350 m from south of the east end of the Martello Tunnel to a point about 520 m west of the west portal of the Abbotscliff Tunnel. From this point an area of more moderate movements formed an eastward extension of the slide, reaching to within about 260 m of the same Abbotscliff portal. The seaward displacements of the slide are well indicated by the railway lines. In the main slide the displacement is generally of the order of

*It should be stated that 'a geological expert' quoted by Anon 1915*b* , considered that the Steady Hole fall was the first event and that this triggered the movements of the undercliff which in turn brought about the two falls further east. This neglects the 6.00 p.m. observation.

TABLE 2. *Rainfall recorded at Folkestone, Cherry Gardens, for* 1915 (*Meteorological Office*)

Period	Rainfall (mm)	% of average of 1881–1915	Remarks
Year 1915	1019.8	138%	Highest annual 1868–1915
Sept–Dec. 1915	515.1	158%	Second highest 1868–1915*
Dec. 1915	203.2	256%	Highest December 1868–1915

*Highest for the four months September to December is 1896, the year of the preceding M type slip, with 518.7 mm

10–20 m, but increases to a maximum of about 50 m in the vicinity of Warren Halt, opposite the Steady Hole Chalk fall. Throughout the main slide, the rear scarp was marked by a considerable draw-down of the talus, except where modified or obscured by Chalk falls. In the eastward extension the rear scarp is formed by a crack with about 0.6 m settlement on its seaward side. These slides badly damaged the sea walls and destroyed all the drainage headings.

Both main and eastward extension slides were accompanied by an upward heaving of the foreshore, involving a strip which extended between about 140

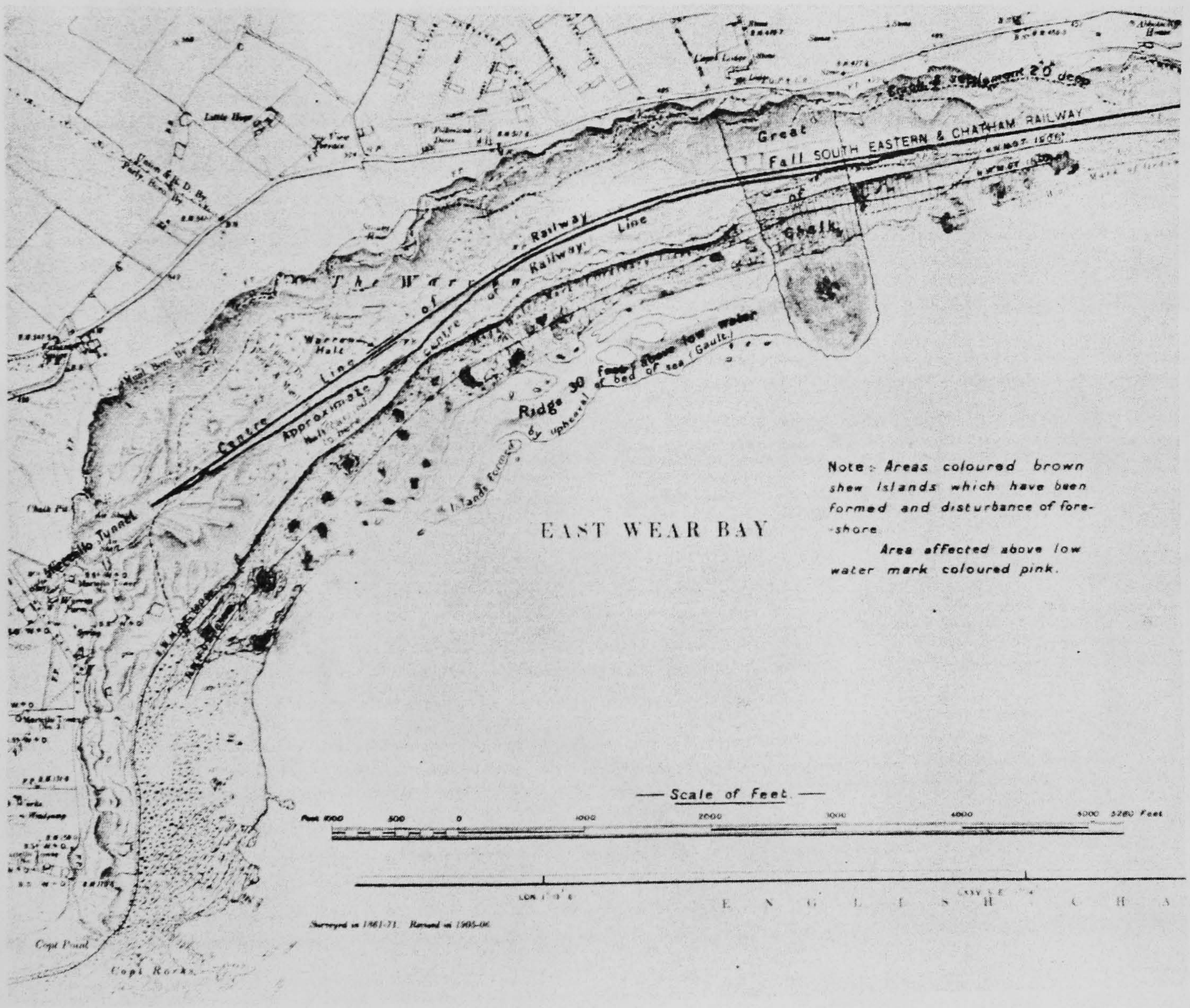


FIG. 4. A contemporary survey of the features produced by the 1915 slip (Acknowledgments to British Railways, Southern Region. Based upon the Ordnance Survey map of 1907).

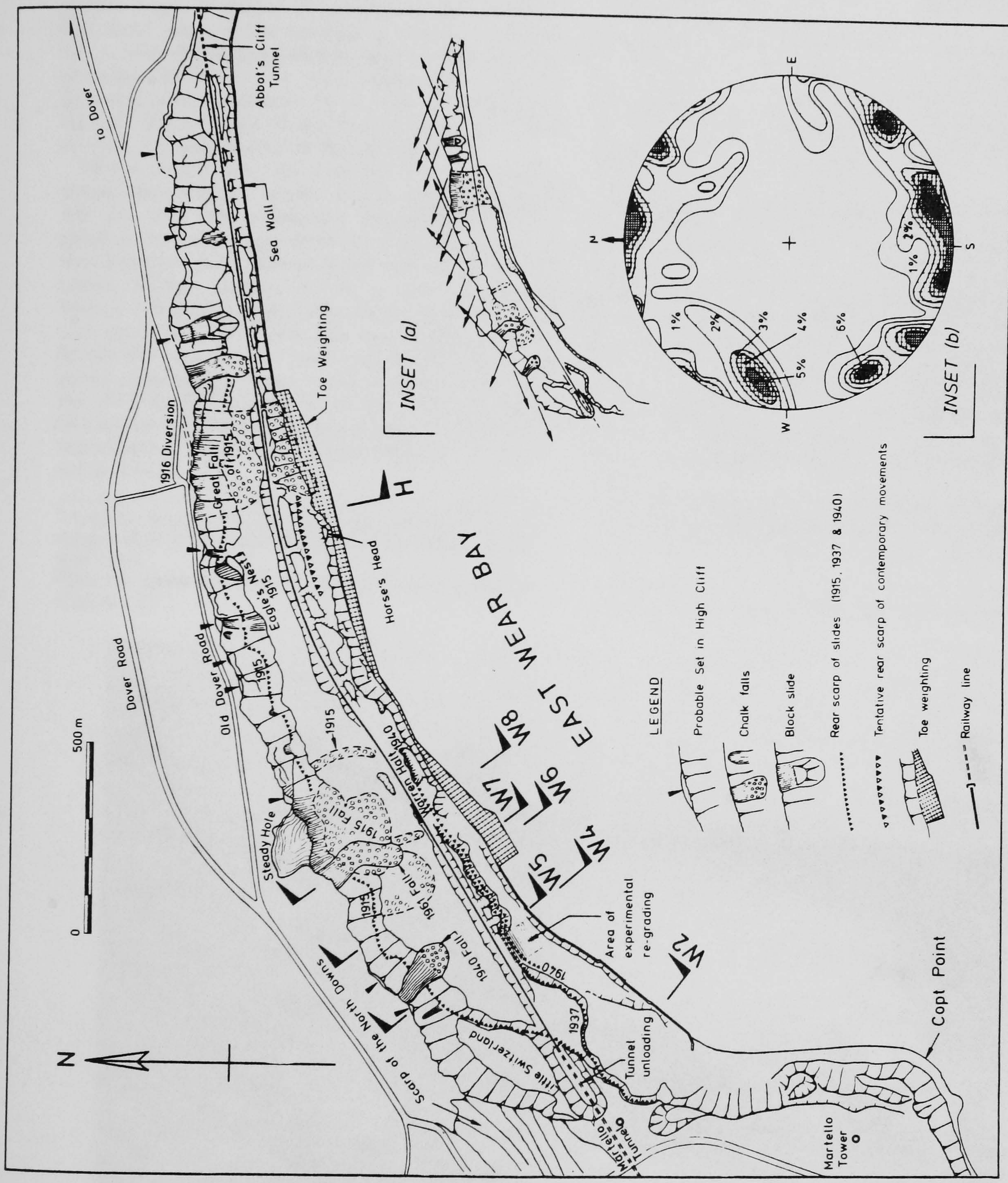


FIG. 5. Outline geomorphological map of the Warren, showing dated rockfalls from rear scarp and present traces of the dated R and M type slips. The major features of the Warren, and the positions of the cross-sections, are also shown. In inset (a), the main trend directions in the rear scarp are identified: these correspond roughly to the predominant joint directions shown in inset (b).

and 240 m out from the former shoreline (Fig. 4). In front of the central half of the main slip there was a second ridge of upheaved sea bed further seaward. The outer edge of this reached to between 260 and 350 m from the former shoreline and it had a width of generally 80–90 m. The inner and outer zones of upheaval were separated by a virtually continuous lagoon.* Photographs of the heaved foreshore, taken in 1915, are reproduced in Figs 6 and 7.

Of the three Chalk falls from the rear scarp that at Steady Hole was the largest. It took about 2 acres of cliff top land and obliterated Rakemere Pool.† Its speed of movement appears to have been moderate to slow however and it moved down virtually as a block (Anon 1915*a*), coming to rest at the rear of the Warren against the High Cliff, where it can be clearly seen today (Fig. 8). There had been a large crack in Steady Hole for over 30 years before 1915 and it had grown considerably larger in the period leading up to the 1915 landslip (Anon 1915*b*) but there is no record of a set having taken place before then. A chalk fall in this vicinity is reported by Toms (1948) to have occurred in 1912.

The house called 'Eagle's Nest' was built in 1911 on a small natural platform, some feet below the crest of the High Cliff, which had been formed by a set which occurred in 1896–97 (Anon 1915*a*, *b* & *c*). During the 1915 landslip this platform slid over 30 m down the High Cliff on a plane discontinuity inclined at 50–60° to the horizontal. The movements were so gentle that the house was scarcely damaged: it was eventually removed and built inland.‡ This slide can be seen on Fig. 9 and, in the distance, on Fig.10.

The 'Great Fall' (Fig. 10), although of smaller volume than the Steady Hole fall, was much more dramatic. The part of the High Cliff involved had set by 0.6–0.9 m on about 19th January 1877, just after the major renewal of movement in the Warren undercliff of 12th January of that year (Anon 1877). The eventual fall on 19th December 1915 was very rapid and transformed into a flow slide which buried the railway line over a width of about 250 m or more (Fig. 10) and ran about 400 m out to sea (Anon 1915*a*). A section through the debris of the fall is given by Osman (1917). A photograph of this is reproduced by Toms (1966).

The old main road between Dover and Foikestone was diverted, following damage by cracks which developed at the rear of the part of the High Cliff

*A similar feature was formed by the landslip of 25th December 1839 at Dowlands and Bindon (Conybeare & Buckland 1840).

†This was drained in 1914 by driving a heading beneath it (Osman 1917).

‡Not the modern house of this name in Steady Hole.



FIG. 6. View to the east of the sea cliff and heaved foreshore of the Warren, taken just after the 1915 slip. The partly eroded 'cape' of the debris of the Great Fall can be seen just beyond the Horse's Head. (Acknowledgments to British Railways, Southern Region).



FIG. 7. View to south west of the sea cliff and heaved foreshore of the Warren, taken just after the 1915 slip. (Acknowledgments to British Railways, Southern Region).

involved in the Great Fall. These cracks were 'nearly 4 inches wide' and the road was closed to vehicles (Anon 1915*b*). By 31st December the section of the cliff bounded by these cracks near Capel Lodge had set by nearly 0.6 m. A permanent diversion of the crest road around the affected area was opened in January 1916 (Anon 1916) (Fig. 11).

It is evident from both Figs 5 and 12 that the eastern end of the Martello Tunnel traverses the slipped mass which forms 'Little Switzerland'. In the 1877 landslip the easternmost 97 m of this tunnel gave way (Anon 1877). As a result 87 m of this length was opened out, in the same year, to form a cutting. In 1898, as a result of a further movement in the cliff over the Martello Tunnel, the east end of this tunnel was unloaded (Fig. 5) for a length of about 180 m, the spoil being dumped on the slopes east of the tunnel or in the sea (Toms 1948). During the 1915 landslip the Martello Tunnel was again cracked, at a point 165 m in from its east portal, that is at approximately the point where the tunnel passes out of slipped masses into *in situ* strata (Anon 1915*c*, Anon 1916).

Mass shifting in the Warren

The Warren is a dynamic feature which is continually being modified by mass shifting of various types and rates. The most rapid natural shifts of mass are brought about by the Chalk falls from the rear scarp. The R and M type slides move more slowly, but involve very large masses of material. Slower, but significant changes also take place on its littoral, by the accumulation and depletion of the beach and by both marine erosion of the seaward edge of the slipped masses and downward erosion of these where they form the foreshore.

Since at least the construction of the first modern harbour at Folkestone in the early 1800's these natural changes have been influenced by human interference: particularly after the commencement of railway construction through the Warren in about 1840. As discussed above, the effects of the developing harbour have been major. In addition the cuttings, and the spoil arising from these, have effected considerable changes in the disposition of masses in the Warren and form a background against which such measures as the toe weighting should be viewed. In general, our information on the topography of the Warren at various times is not adequate enough for us to trace these various changes with any precision. Nevertheless, some approximate figures can be arrived at, and these are summarized in Table 3. The qualitative effect of these changes on the factors of safety of the M and the R type slips can readily be appreciated from their

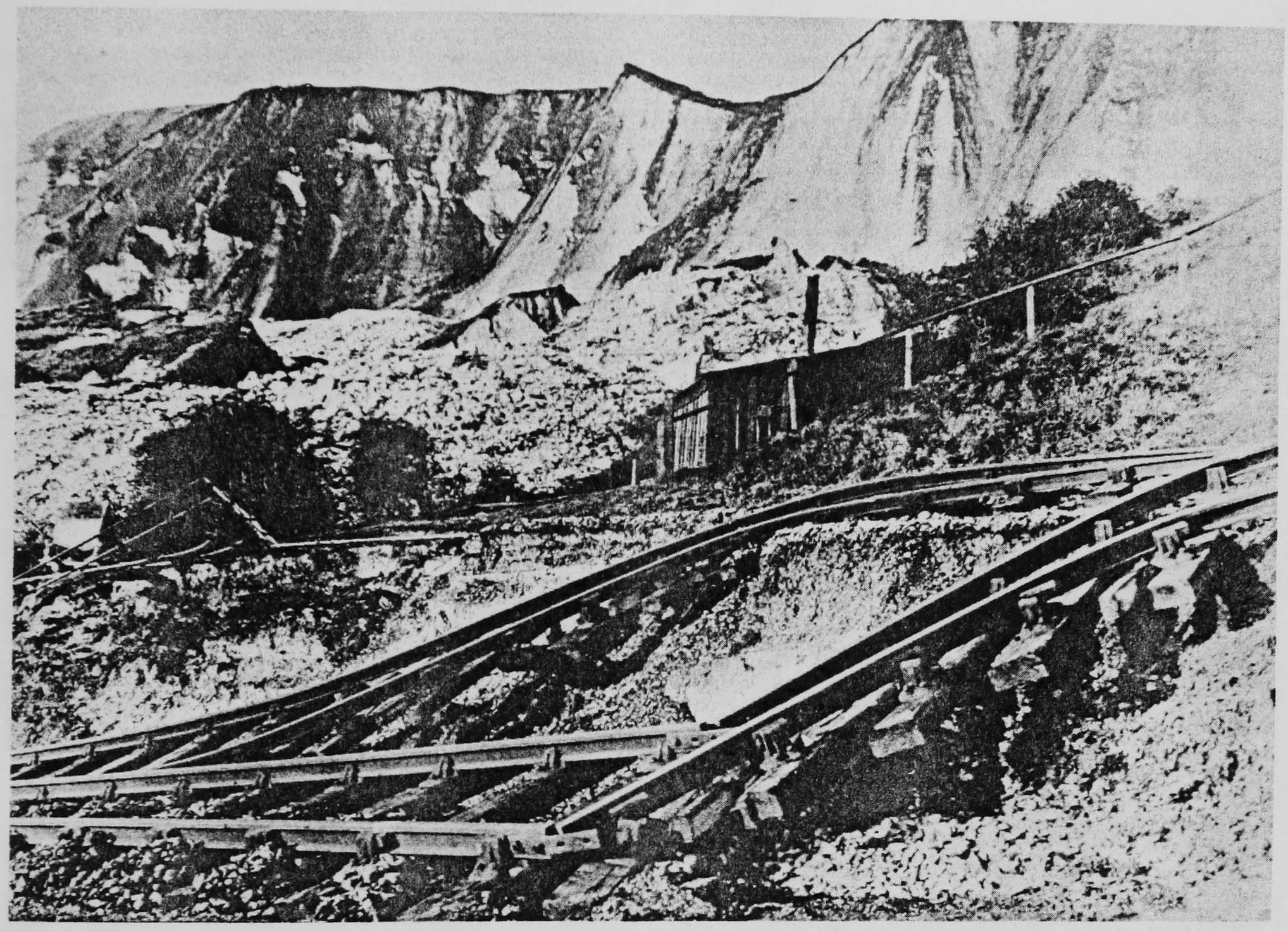


FIG. 8. The Steady Hole Fall of 1915, viewed westwards from about 250 m east of Warren Halt, taken shortly after its occurrence. (Acknowledgments to British Railways, Southern Region).

locations relative to the appropriate neutral points (Hutchinson 1977). Typical positions of the latter are shown on Fig. 16.

Outline morphology

General

At least until the construction of the sea wall and toe weighting, the Warren was in a state of dynamic equilibrium under the combined influence of its topography, geology, hydrology and its exposure to marine attack. This is reflected chiefly in the widening of the undercliff towards the west, which compensates, in the case of both R and M type renewals of movement and potential further retrogressions of the rear scarp, for the gradual reduction in passive resistance at the toe as the level of the Gault rises.

The multiple rotational nature of the Warren slips is best seen at their western end (Fig. 5), where the rear scarps of the R type slips of the 1930's and 1940's parallel both the associated rear scarp of the 1915 M type slip and the High Cliff above the ancient slide block of 'Little Switzerland'. Elsewhere, the multiple slide blocks are generally obscured by a mantle of Chalk debris derived from numerous falls from the High Cliff. These falls occur both sporadically and in association with deep-seated, M type renewals of movement in the undercliff.

On Fig. 5 are shown the debris accumulations that can be readily distinguished: these are dated where possible. The large concentration of debris in the vicinity of Steady Hole is striking (Figs 5, 11 and 12). Further east, just beyond Horse's Head, the area blanketed by the flow slide debris of the Great Fall of 1915 (Figs 4 & 5), and the associated fresher rear scarp, can be clearly distinguished on the aerial photograph of Fig. 11. An element of flow sliding is also evident in the debris of other falls, for example that in 1961 (Fig. 5).

Over most of its length, the High Cliff consists of a succession of broad, irregularly spaced buttresses, with their seaward faces inclined at a rather uniform angle of about 55° to the horizontal. At Steady Hole, the cliff line is broken by a depression, thought to be the headward remnant of a former branch dry valley. The upper parts of the cliff are fairly well vegetated but

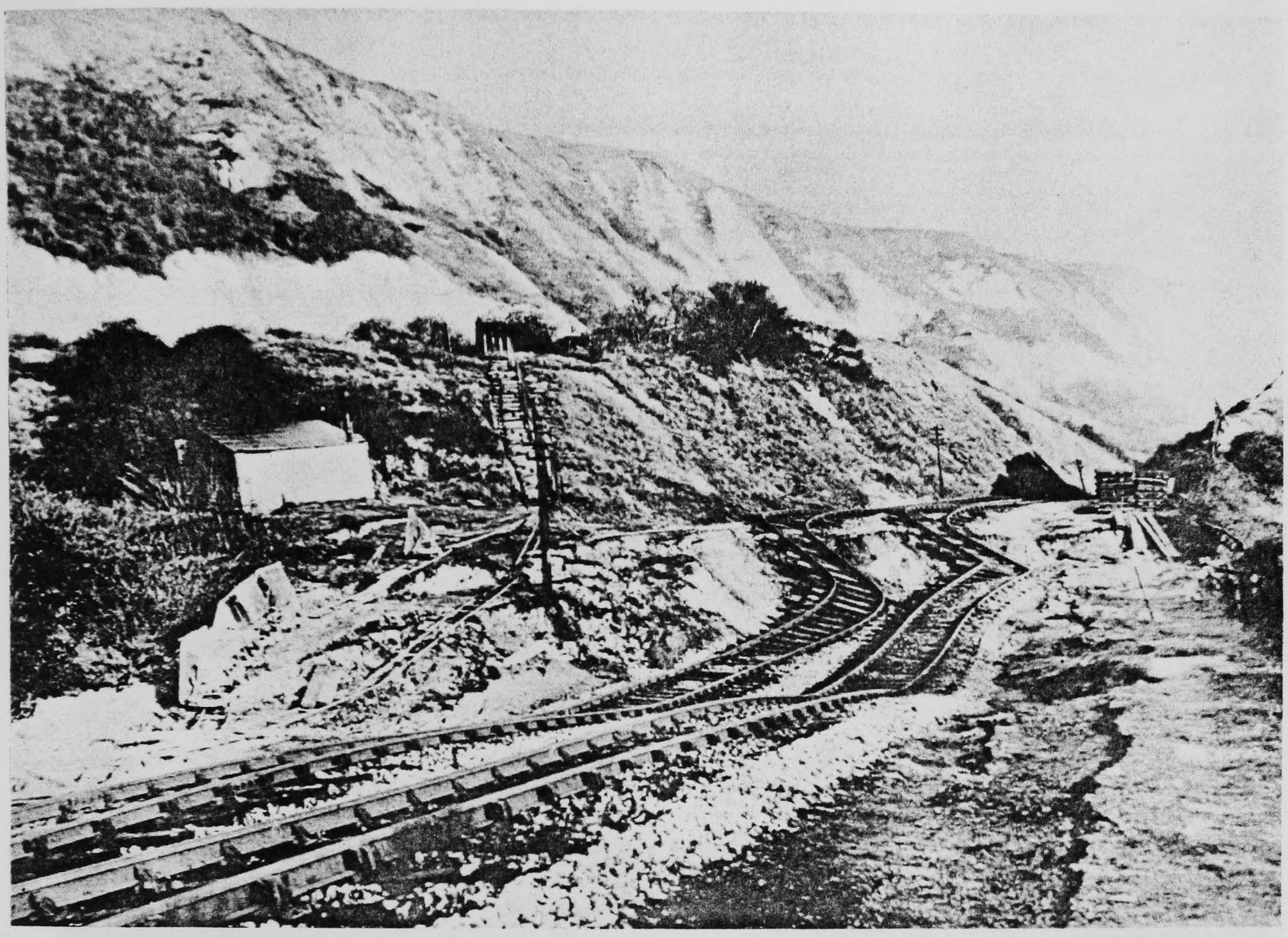


FIG. 9. The central part of the Warren, viewed eastwards from a point about 200 m east of the Warren Halt, shortly after the 1915 slip. The trace of the slip along the foot of the rear, scarp is clearly seen, and the Eagle's Nest can be discerned immediately above the central of the three telegraph poles. (Acknowledgements to British Railways, Southern Region).

much of its foot is freshened by the movements of the 1915 slip: the break in the talus can still be traced except where masked by later Chalks falls. By contrast, east of the Great Fall, the High Cliff appears more vegetated and less active. Indeed, in this area, the movements of the undercliff were generally less than 1 m. (Fig. 4). Sets affecting the High Cliff (Hutchinson 1969) are shown diagrammatically in Fig. 5.

The character of the sea cliff also changes along its length, with the effects of R type slides strongest at the western end and lessening gradually towards the east. Slight contemporary movements of the order of 1 m in the vicinity of Horse's Head are the most easterly R type slides recorded to date, and beyond this point it may well be that the R and M type slides coalesce. A noteworthy feature of the sea cliff generally is the great thickness of Chalk fall debris, with isolated instances of the multiple slide blocks being exposed as at Horse's Head.

Modification of the morphology by the various engineering works connected with the railway is considerable, as noted above.

Evidence of joint control in the rear scarp

In plan, the rear scarp of the Warren has a generally arcuate form, concave to seaward, with the degree of concavity increasing towards the west (Fig. 5). On closer inspection, it is found to be made up chiefly of three *en echelon* sets of essentially joint-controlled faces, A, B, and C (Fig. 5a), which trend at whole circle bearings of about 67°, 47° and 109°, respectively. These give the rear scarp in detail a somewhat saw-toothed appearance. Its general form (which is paralleled in the shape of East Wear Bay) reflects the tendency of the B sets of faces to become increasingly predominant over the A sets towards the west. Sets A and C also appear to control, respectively, the trends of the dry valleys and the scarp of the North Downs just inland. These joints are also likely to exert some control on the retrogression mechanism at the Warren, as suggested by Hutchinson (1969).

The field and historical evidence of chalk falls from the rear scarp suggests that these generally occur at the projecting corners of individual 'saw-teeth'. A



FIG. 10. The debris of the Great Fall viewed westwards from near the Abbotscliff Signal Box shortly after the 1915 slip. (Acknowledgments to British Railways, Southern Region).



FIG. 11. Oblique aerial view looking west, taken prior to 1942, showing the details of the eastern part of the Warren, particularly the rearward trace of the 1915 slip, the site of the Great Fall, the diverted coast road and the nature of the coastline before construction of the toe-weighting, (Acknowledgments to the Building Research Station, Watford).

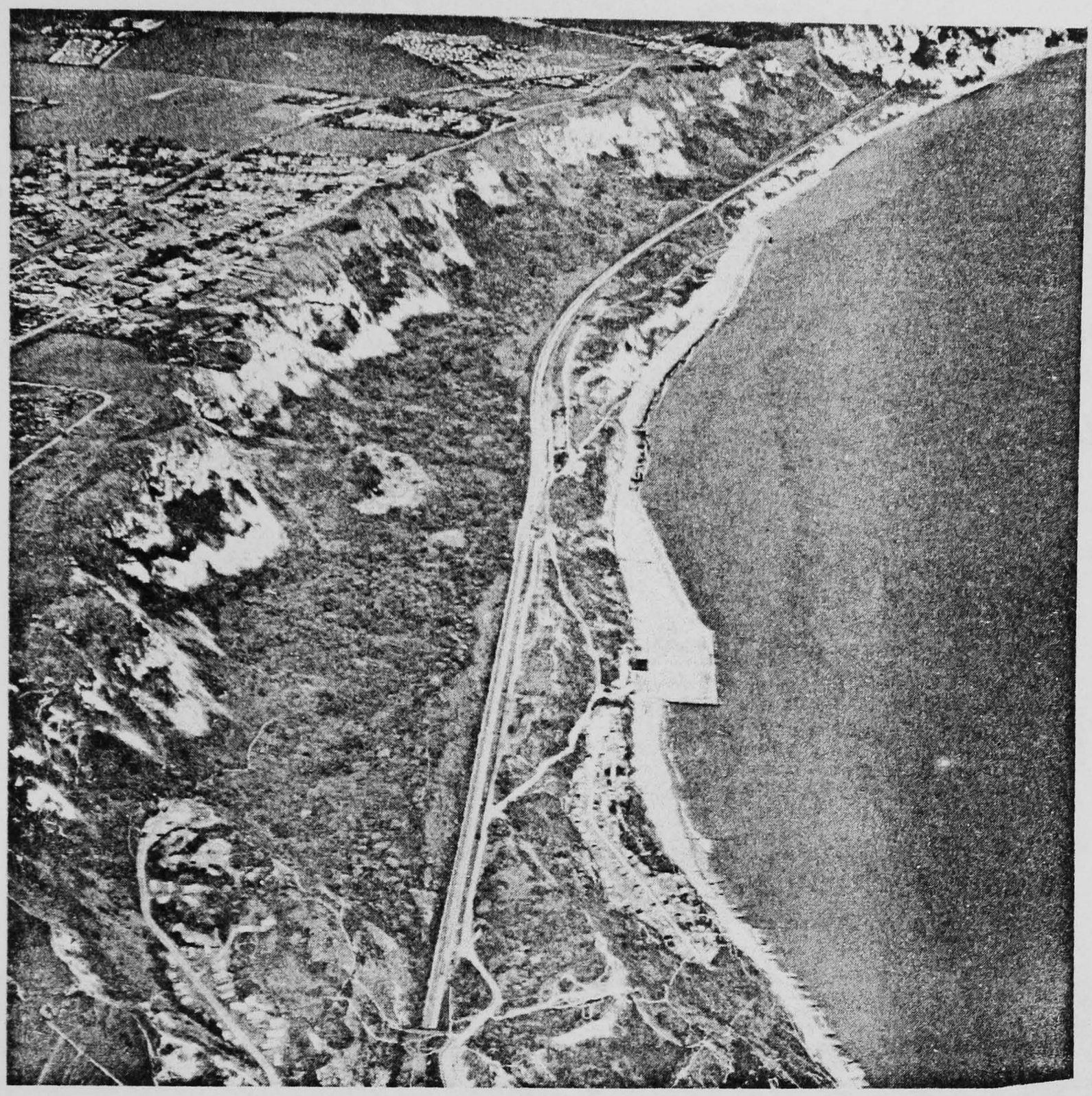


FIG. 12. Oblique aerial view looking North-east, taken in 1976, showing details of the western part of the Warren, particularly the Steady Hole Fall with the associated seaward deviation in the line of the railway, and the toe-weighting. (Acknowledgments to Professor J. K. S. St. Joseph, Director in Aerial Photography, University of Cambridge).

given mass of chalk between two major parallel joints of set A or B (one forming the cliff face, and one inland of this), thus tends, through successive falls, to 'unravel' from its exposed end. Commonly, this process appears to take from east to west, the size of each individual fall probably being largely controlled by the conjugate joint set C.

In an attempt to supplement the above trends, derived from the local morphology, with specific geological data, a pilot joint survey has been made in the area. This commenced on the rear scarp of the Warren, but because of the sparsity of readily accessible features there, was extended as far as the quarry below Sugarloaf Hill (*c.* TR 225 380) to the west and Abbot's Cliff (to *c.* TR 283 387) to the east. A rigorous sampling procedure was not followed and many of the largest and most dominant joints could not be reached. Attention was concentrated on the steeper discontinuities; sub-horizontal ones were not surveyed.

In all, 104 discontinuities (predominantly joints) were surveyed. The results were plotted on a lower hemisphere, equal-area, polar stereonet (Hoek & Bray 1977) and are summarized in the contours of Fig. 5b. These are in rough correspondence with the trends of faces A and B (Fig. 5a) but, probably through unrepresentative sampling, reflect only weakly that of faces C.

Recent investigations in The Horse's Head area

Since 1938 British Railways have kept a continuing check on movements within the Warren by precise triangulation and by observations within the drainage

TABLE 3. *Approximate estimates of some of the elements of mass shifting in the Warren since the early part of the nineteenth century*

Date	Event	Approx weight involved (Tonnes × 10^6)
1840–44	Excavation of rail cutting	2.2*
1810–present	Interception of littoral drift (above L.W.M.)	2.5†
1887 & 1898	Opening out the Martello tunnel.	0.4
late 1930's	Beach replenishment	'a large quantity' (Toms 1948)
1948–55	Toe weighting, sea defences	0.7
1915–16	Marine erosion of toe heave	*c.* 0.3–0.5
1915	M type slip	70–90
1936–present	R type slips	*c.* 10
1877–present	Chalk falls from the High Cliff	*c.* 2–3

*According to a manuscript section of 1851, held by British Rail at Waterloo, on which the quantities were agreed by Francis Tredwell, Contractor, and John Wright, Resident Engineer. The prices were 9d. per cubic yard in open cut (1, 085, 266 yd^3) and 1s.0d. per cubic yard in tunnel (257,465 yd^3). Rakemere Pool (there referred to as *Wraightmore* Pool) was partially filled during these works.

†This figure could be doubled if account is also taken of the volume trapped below low water mark (L.W.M).

headings. These have revealed that an area in the vicinity of the Horse's Head, and south of the railway (Fig. 5), has been moving slowly seawards. Since 1962 additional measurements have been made on the sea wall in this vicinity: these show that, in spite of the toe-weighting, this wall has moved a maximum of approximately 730 mm seaward between early April 1962 and mid-January 1978. In addition, from the completion of its construction in about 1954, (Viner-Brady 1955) to April 1962, the wall is estimated by British Railways to have moved about 178 mm seaward.

The area of greatest movement, just east of the Horse's Head, coincides with the location of the debris tongue of the 'Great Fall' of 1915 (Figs 4 & 5). The part of this which projected into the sea was rapidly eroded away and there is evidence that high rates of recession have continued in this area. A British Railways drawing (No. 10/2252 K/P31) shows the sea cliff between about 30 and 320 m east of the Horse's Head to have retreated by as much as 29 m from 1935–46 and 17 m from 1946–52. Viner-Brady (1955) also refers to continuing recession at this locality in 1953 as being a main reason for extending the sea wall and toe-weighting to the east.

The movements involving the Horse's Head were thought likely to represent a potential easterly extension of the 1940 slip, the latest significant slide (of R type) to have occurred in the Warren. Accordingly, in 1968, it was decided by British Railways to carry out a subsurface investigation of the area involved. Details of this are reported by Halcrow (1970): brief accounts are also given by Wood (1971, 1972). Three rotary boreholes were put down in 1969. Each was carried down into the Folkestone Beds, and two Casagrande piezometers were sealed into each hole; one within the Folkestone Beds (F) and the other within the overlying masses of slipped Gault (G) (Fig. 13). Slip indicators were provided in the deeper piezometer in each borehole. These and the piezometers were read (approximately once a week on average) from about 11th September 1969 until the deeper piezometer tubes were constricted by the continuing slow movements. Piezometer 3F constricted at a depth of 29.6 m in July 1972, and piezometer 2F at a depth of 28.2 m in September 1973. All readings were discontinued in June 1975. The slip surfaces shown on Section H (Fig. 13) are based on the above-mentioned evidence of constriction.

Plots of the available readings in piezometers 1F and 1G and 2F and 2G are shown in Fig. 14. The readings in piezometers 3F and 3G are similar to those in 2F and 2G. As noted by Hutchinson (1969), the piezometric levels in the Folkestone Beds in this vicinity are a little above mean sea level and respond fairly intimately to variations in tide levels (Fig. 15).

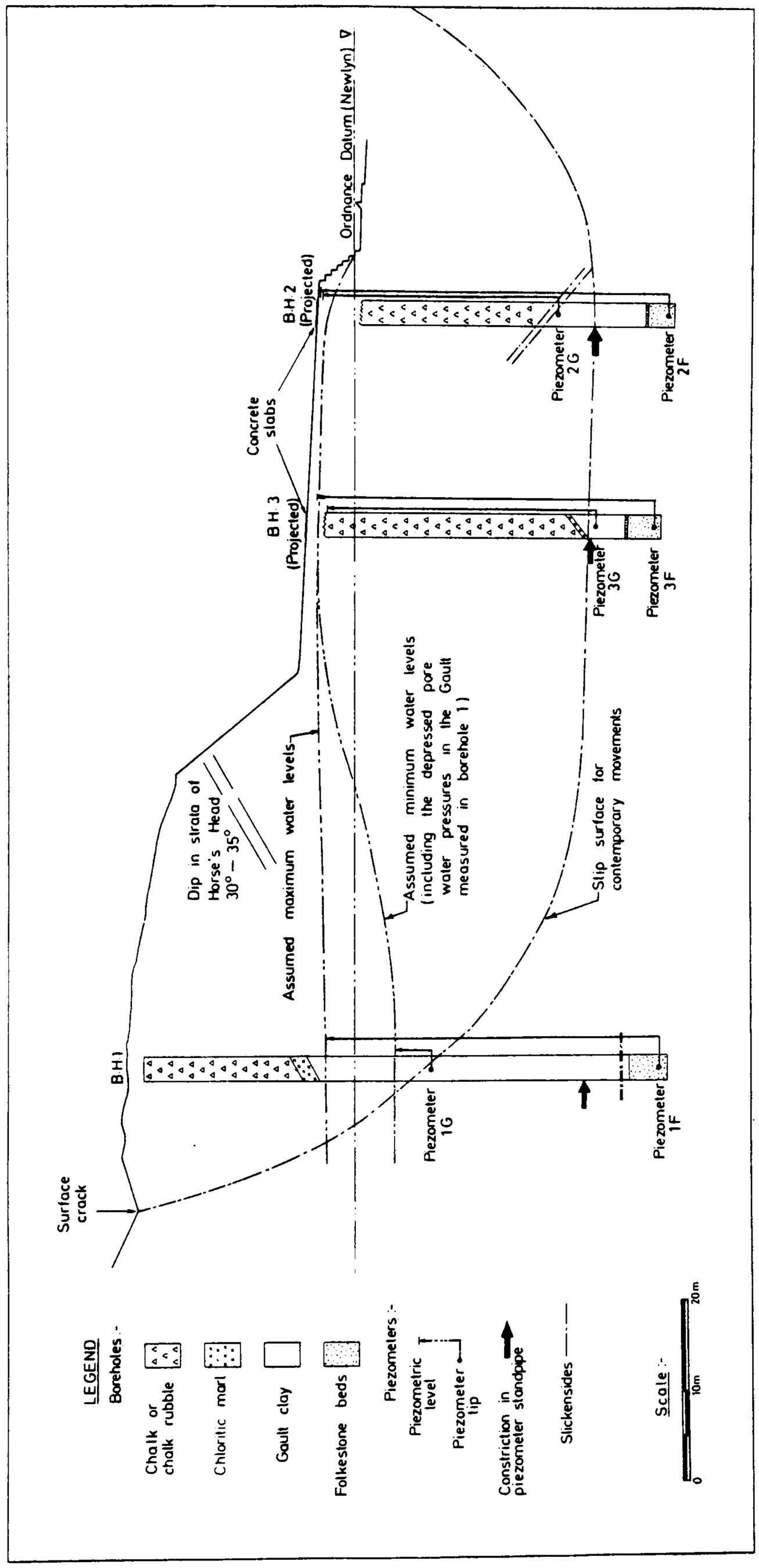


FIG. 13. Cross-section H through the R type slip in the vicinity of the Horse's Head, based largely on the data from Halcrow (1970).

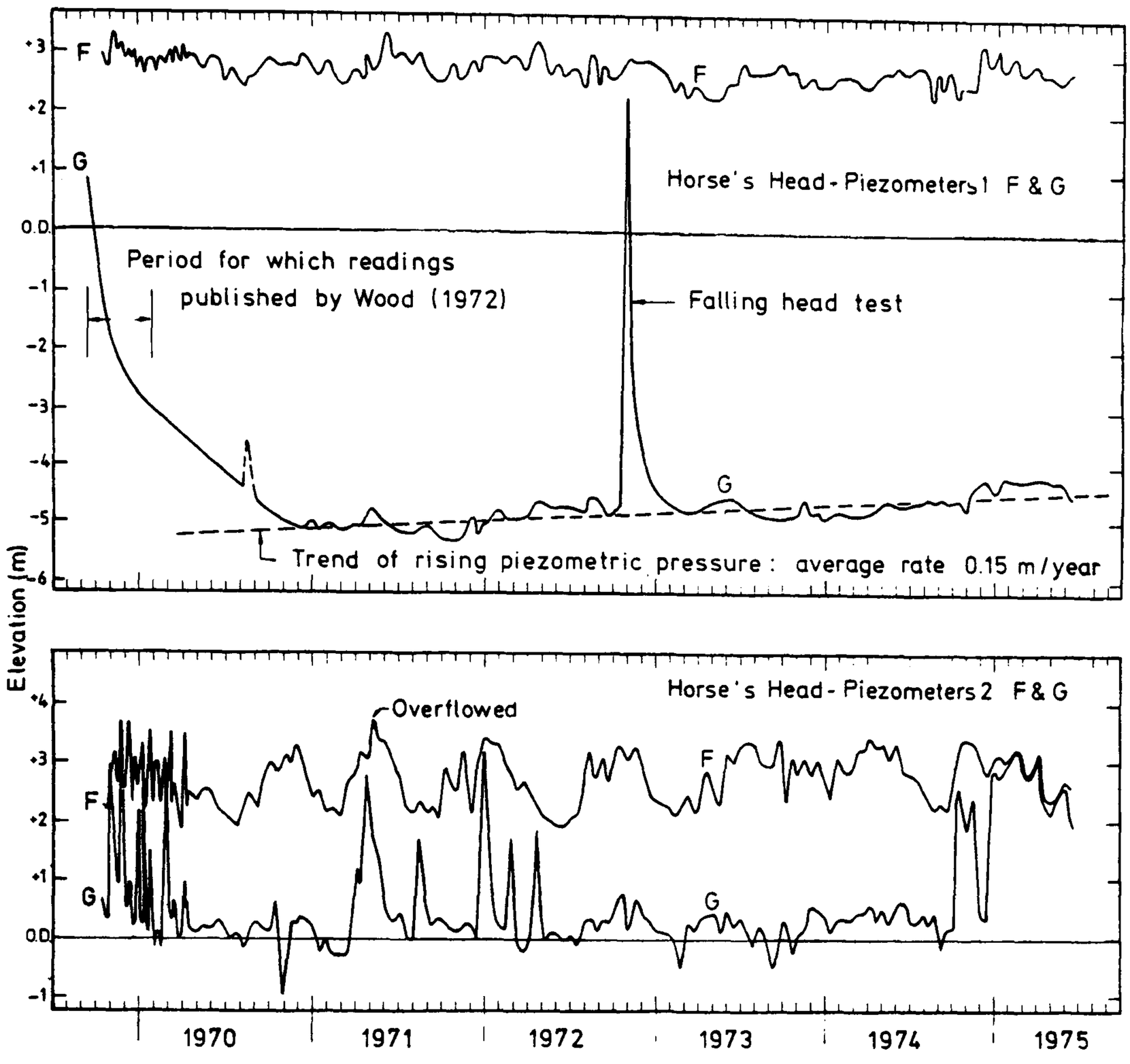


FIG. 14. Record of piezometric levels in boreholes 1 and 2 in the Horse's Head area, from installation in 1969 until readings were discontinued in 1975. The letters F and G refer, respectively, to piezometers with their tips in the Folkestone Beds and the slipped Gault. (Acknowledgments to Britsh Railways, Southern Region).

Of the three piezometers installed in the slip masses, 1G is of particular interest in that it records piezometric levels appreciably below sea level, as first noted by Wood (1971). Wood's (1972) plot of these, up to January 1970, indicated that the piezometric level in 1G was then about −3 m O.D. Subsequent measurements, summarized in Fig. 14, show that the piezometer had not then equalized and that the true minimum reading is even lower, at about −5 m O.D. Another point of interest which emerges from Fig. 16 is that since this piezometer equalized, at about the end of 1970, it has recorded a steady swelling, reflected in an average rise in piezometric level of about 0.15 m/yr, up to 1975. The falling head test carried out on this piezometer in the latter part of 1972 (Fig. 14) indicates an approximate k value of 7.3×10^{-11} m/sec for the slipped Gault surrounding the piezometer tip.

No oedometer tests on undisturbed Gault have been carried out in this investigation. Two such standard tests were carried out earlier at the Building Research Station, however, the results being described in Appendix I of Wood (1955). Over the stress range appropriate to the Gault Caly around and above piezometer 1G, these indicate an m_v value of approximately 2×10^{-5} m^2/kN, and hence, with the value of k given above, a c_s value of about 3.7 m^2/yr. Related values for remoulded Gault, derived from the consolidation stage (σ_n' increased from 439.8 to 790.7 kN/m^2) of the I.C. ring shear tests, are:

Sample	m_v (m^2/kN)	c_v (m^2/yr)
RSI (high L.L)	3.0×10^{-4}	0.14
RS2 (low L.L)	1.9×10^{-4}	1.9

From these data, the *in situ* value of c_s applicable to the Gault around piezometer 1G is estimated to lie in the range 1–10 m^2/year.

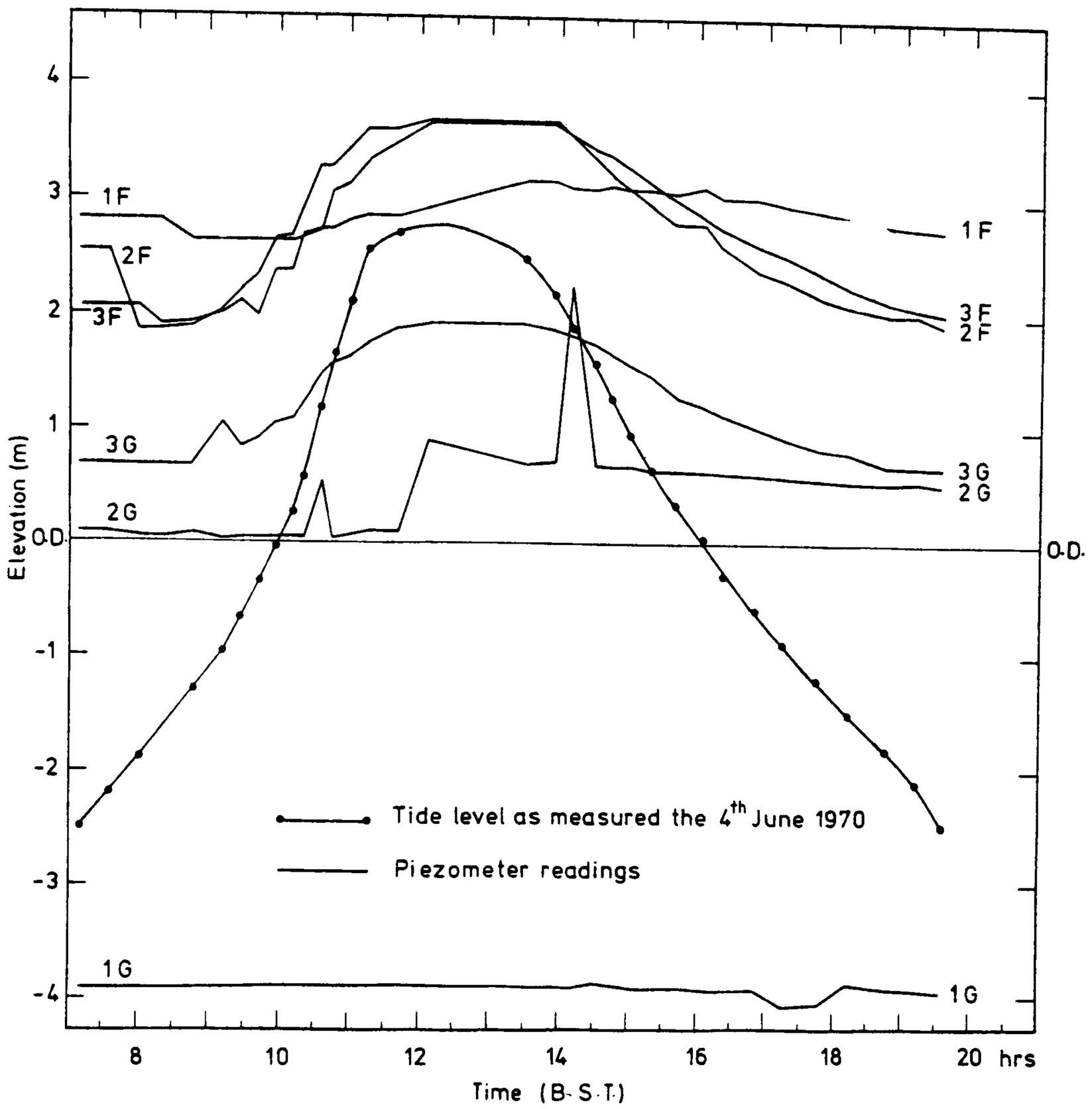


FIG. 15. Recorded of piezometric levels in the Horse's Head area throughout a part of the tidal cycle on the 4th of June 1970. (Acknowledgments to British Railways, Southern Region).

It is evident from a comparison of the stress levels in the undisturbed Gault behind the High Cliff with those in the slipped Gault in the Horse's Head area, that the latter has experienced a very large, progressive unloading (from more than 3000 to about 600 kN/m^2 in vertical effective stress) as a result of the backward rotation and forward and downward movements of the slip blocks, supplemented seaward of the sea cliff by marine erosion. The depressed levels recorded by piezometer 1G are considered to be associated predominantly with the latter stages of this complex and lengthy unloading process.

The other two piezometers, 2G and 3G, located in the slipped masses indicate piezometric levels slightly above O.D. and only about 2 m below those in the underlying Folkestone Beds, as shown for piezometer 2G in Fig. 16. The readings of piezometer 3G are closely similar. This is despite the fact that both these piezometers are situated seaward of the sea cliff, where the most recent increment of unloading of the slipped masses can be expected to have occurred. The reason for this is that both piezometers 2G and 3G are located within blocks of slipped Gault which have minimum drainage paths of only about 2 m to the surrounding Chalk rubble, whereas piezometer 1G has a minimum drainage path of about 13 m (Fig. 13). These drainage paths also influence the tidal response of piezometers 1G to 3G, as shown in Figs 14 and 15. Piezometers 2G and 3G respond fairly markedly to the tidal fluctuation, in fact much as do those in the Folkestone beds, while piezometer 1G is virtually unaffected. It follows that, with the order of c_s value suggested earlier, the swelling at piezometers 2G and 3G would be 95% complete within a few years, while

*The abrupt rise in the readings of piezometer 2G in late 1974, after which they are essentially the same as those in piezometer 2F, probably results from cracking of the grout seal by the continuing slip movement.

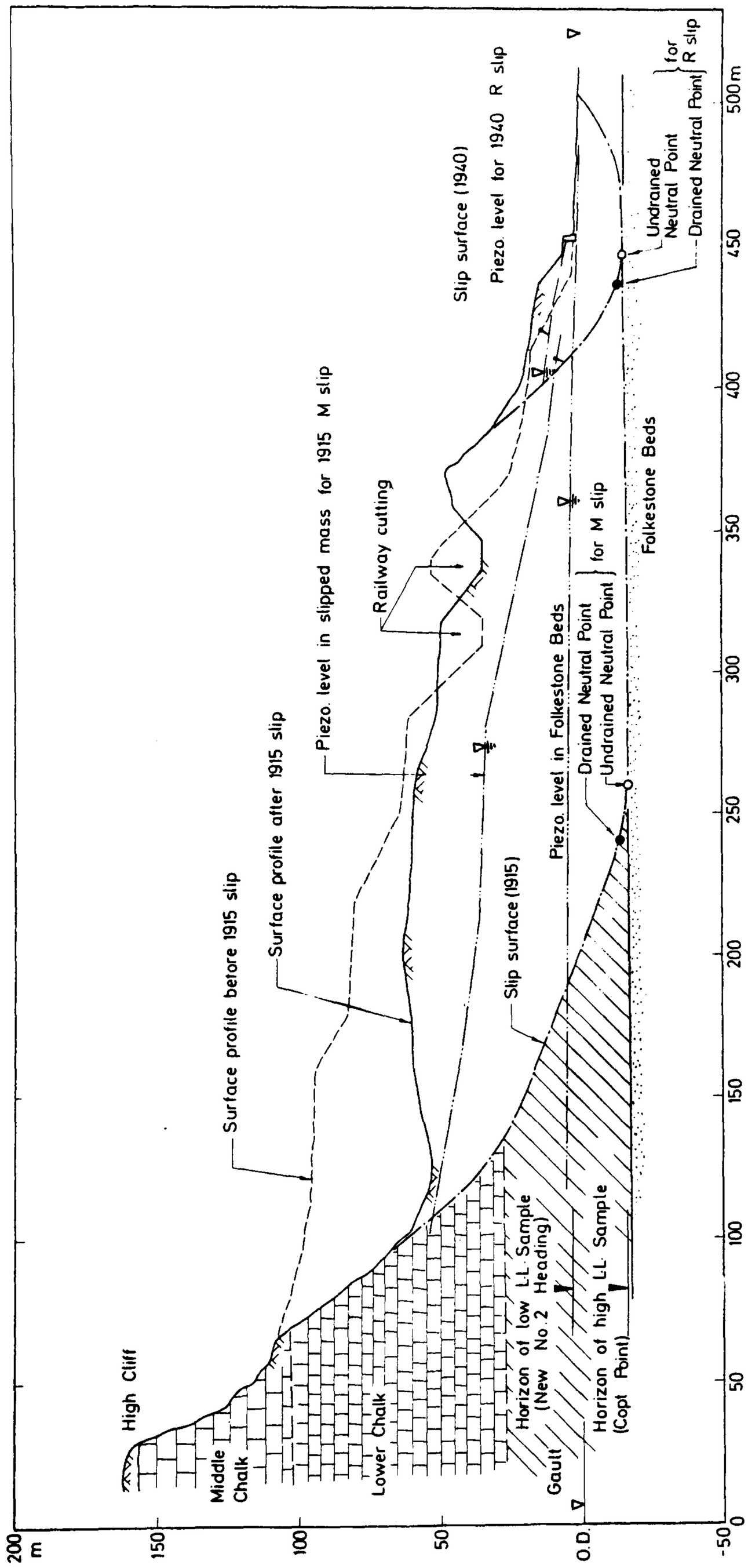


FIG. 16. Cross Sections W6 and W7, largely after Hutchinson (1969).

that at piezometer 1G would require several to many decades.

From these three piezometer holes it can be concluded that, at least in the vicinity of the seaward edge of the Warren and possibly elsewhere, the slipped masses consist of various sized blocks of Gault amongst Chalk blocks and debris which, in general, have become unloaded as the slips have developed. The piezometric pressures within the Chalk and the smaller masses of Gault have equalized with the long-term ground-water conditions, but negative excess pore-water pressures still exist within the larger blocks of slipped Gault. As these swell back to equilibrium the factor of safety on any slip surfaces traversing these blocks will, of course, steadily be reduced. From the geometry of the failure surfaces, it would seem that R type slips are more prone to be affected by this mechanism than those of M type. In the Gault block monitored by piezometer 1G, the pore-water pressures are currently increasing at an average rate of about 0.15 m/year and this is doubtless partly responsible for the continuing movements of the R type slip of the Horse's Head.

Back analyses

In the previous paper (Hutchinson 1969), back analyses were made of all the slips for which sufficient data were available. These were the slips of 1940 (Sections W5 and W7), 1937 (Sections W1 and W2) and 1915 (Sections W4, W6 and W8). In each case the analysis was carried out for the reconstructed situation just at failure, when $F = 1.0$, and a value of ϕ'_r inferred for the Gault, with $c'_r = 0$. Finally a weighted average ϕ'_r value was obtained for each of the three slips. These values were mutually consistent and indicated ϕ'_r values for the Gault ranging between 13.9 and 16.6°, depending on the pore-water pressure assumptions made (fig. 31 of that paper).

In the present paper the same general approach has been followed, again using the same maximum and minimum pore-water pressure assumptions (as set out in Fig. 21 of Hutchinson 1969) and the Morgenstern-Price method (1965) of stability analysis. This independent check confirmed all the previous analysis results. In the case of the 1915 slip, however, a critical re-appraisal has been made of the three cross-sections analysed, with the following results.

Section W6 (Fig. 16) is uncomplicated by falls from the rear scarp and appears to have reasonable surface and subsurface detail. Closer examination, however, reveals that a major imbalance exists between the pre- and post-failure volumes of the slip masses, and this casts doubt on the reliability of the pre-slip ground profile and, of course, any related back analyses.

Section W4 (fig. 28 of Hutchinson 1969) is interpolated between two of Osman's sections and, as a result, has upper and lower bounds of probable ground profile. The results of back analyses on both these profiles differ very little, however, and as there is negligible imbalance between pre- and post-slip volumes and no involvement of the Chalk, the back analysis results for this section may be accepted with some confidence.

Section W8 (Fig. 17) passes through the area involved in the Steady Hole fall. In the earlier treatment, following Osman, the overall failure surface was analysed assuming that an earlier 'set' had brought the shear strength on that part of the slip surface traversing the Chalk to its residual value. In the light of the development of the 1915 slip, detailed above, it is now considered that the rear scarp of the initial failure was located at the foot of the High Cliff (as noted in Fig. 17), and the section has been re-analysed on this basis.

The recent investigations in the vicinity of the Horse's Head permit one new section (H, Fig. 13) to be back-analysed. This is virtually identical with 'slip surface 1' of Wood (1972).* The results of all the immediately pre-failure analyses are summarized in Table 4.

While the pre-failure analyses have the advantage that $F = 1.0$, they have the weakness that no contemporaneous ground-water pressure measurements exist. In the case of the 1940 slip the movements were slight and the maximum ground-water pressures in the slipped masses measured post-failure can be taken to approximate those existing at failure. In the case of the 1937 slip, and even more the 1915 slip, the seaward movements and corresponding changes in ground profile were large and hence considerable uncertainty attaches to the ground-water conditions in the slipped masses prior to failure.†

In view of the above difficulties, back analyses have also been carried out, on the same sections, for the post-failure conditions. These analyses have the advantage of being based on accurately surveyed ground profiles and maximum measured ground-water pressures: their drawback is that the factor of safety is not known. However, as this is greater than unity, reliable mobilized residual strengths can be obtained from the back analyses which form a conservative lower bound to the actual residual strengths. The results of all the post-failure analyses are summarized in Table 5.

Discussion of the unusually large maximum displacement of the 1915 slip

In a discussion on the 1969 paper, Wood (1970) commented perceptively on the fact that the 1915 slip

*'Slip surface 2' of that paper appears to be largely conjectural and has not been analysed.

†The effect of this uncertainty on the back-calculated values of ϕ'_r is moderated by the considerable depths of the slips.

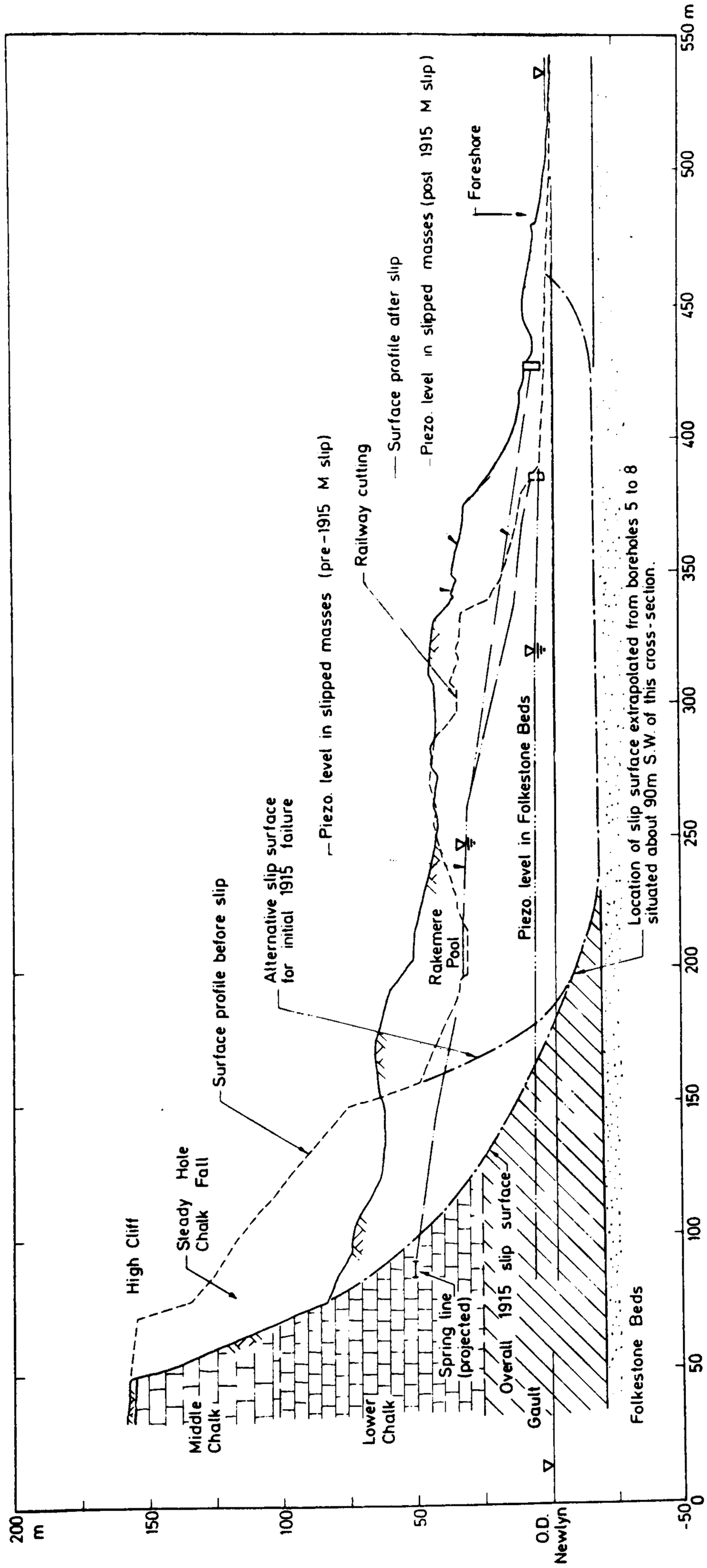


FIG. 17. Cross section W8, largely after Hutchinson (1969).

TABLE 4. *Results of back analyses of pre-slip cross sections*

Section (incldg date & type of slide)	Remarks on Section	Analysis using upper or maximum piezo. line: Average normal effective stress kN/m²	Average shear stress kN/m²	ϕ'_r mobilized	Analysis using lower or minimum piezo. line: Average normal effective stress kN/m²	Average shear stress kN/m²	ϕ'_r mobilized	General remarks
W4	1915(M)	Upper of interpolated profiles.	608	101	9.4°	749	101	7.7°	
			Railway cutting decreased FS by 4.2%			Railway cutting decreased FS by 5.1%			
		Lower of interpolated profiles	546	90	9.4°	688	90	7.4°	
			Railway cutting decreased FS by 4.0%			Railway cutting decreased FS by 5.8%			
W6	1915(M)		771	223	16.1°	918	221	13.6°	
			Railway cutting decreased FS by 2.9%			Railway cutting decreased FS by 2.9%			
W8	1915(M)	Taking residual of $\phi'_r = 20°$ through full thickness of Chalk.	547	221	22.0°	678	218	17.7°	The railway cutting is negligible on this section
		Alternative slip surface emerging *in front* of the High Cliff.	499	77	9.7°	575	76	7.5°	
W2	1937 (R)		402	118	16.3°	474	118	14.0°	
W5	1940 (R)		219	49	12.5°	237	49	11.6°	
W7	1940 (R)		212	67	17.6°	233	67	16.1°	
			Improvement in FS with toe load = 43.7%			Improvement in FS with toe load = 41.2%			
H	1968 (R)		323	80	14.0°	350	80	12.9°	Including effect of toe weighting

TABLE 5. *Results of back analyses of post-slip cross sections*

Section (incldg date & type of slide)		Analysis using upper or maximum piezo line: Average normal effective stress kN/m²	Average shear stress kN/m²	ϕ'_r mobilized	Analysis using lower or minimum piezo line: Average normal effective stress kN/m²	Average shear stress kN/m²	ϕ'_r mobilized	General remarks
W4	1915 (M)	429	67	8.9°	565	67	6.7°	No toe weighting
W6	1915 (M)	651	123	10.7°	795	121	8.7°	
		Improvement in FS with toe load = 4.7%			Improvement in FS with toe load = 5.1%			
W8	1915 (M)	691	137	11.2°	820	136	9.4°	*

*Net effect of toe weighting is modest, as much of it merely replaces the eroded-off toe heave

moved forward about 30 m, and asked how this could be reconciled with a renewal of movement on a pre-existing, residual slip surface.

It is certainly to be expected that, in general, failure on a pre-existing, residual and therefore non-brittle, slip surface will be quite gradual and of limited displacement. However, mechanisms which might explain a more energetic failure movement on such a surface do exist: nine of these are outlined below.

(a) In a strongly non-circular slip in brittle soil or rock, a sudden first-time failure on an internal shear surface could result in a sudden movement of the whole slip.

(b) In condition (a), where a rigid jointed cap-rock is also involved, the rearward failed block or blocks of this may force a shift in the slip surface, into hitherto unsheared material, in the process of moving round the rearward concavity of the basal shear surface, and thus give rise to some brittleness.

(c) Where a slope formed of clay dominated by calcium minerals—as at the Warren (Hutchinson 1969)—has sea-water at its foot, it may be possible for the seaward part of a pre-existing shear surface to develop a degree of brittleness by ion exchange from calcium to sodium.

(d) The production of a small peak when a slip surface is unloaded vertically with the shear force still acting has been observed in the laboratory by Bishop, *et al.* (1971). If this phenomenon occurs in the field, a degree of brittleness in a pre-existing shear surface could be developed by toe erosion, for instance.

(e) In cases where, as a result of past undrained unloading, negative excess pore water pressures exist in the clay of the slip, it is possible that, following a minor initial movement, cracks will open into the slip and allow surface of ground water to gain access to the low pore water pressure zones, rapidly neutralizing them. This mechanism, suggested by Wood (1971), would naturally tend to bring about an acceleration in the initial slow movement.

(f) In deep slips, heat may be generated on the basal slip surface by even a slow initial movement. This will tend to raise the pore water pressures locally which will in turn tend to accelerate the slip movements, further increasing the temperatures. Clearly, such a feed-back could lead to catastrophic movements even on a pre-existing, residual shear surface. the mechanism has been proposed by Patton (*pers. comm.* 1976) to explain the very rapid movement of the Vaiont slide.

(g) The sudden undrained loading (Hutchinson & Bhandari 1971) of the rear of a slide through rockfall, for example. This could occur either just before or just after the commencement of renewed movements of the slide itself.

(h) If fill is placed on the slide in such a way that further movement will extend the pre-existing slip surface through the fill (at head or toe), then the new part of the slip surface is 'first-time' and hence a degree of brittleness can be introduced.

(i) A sudden unloading at the toe of the slide. In the case of the Warren, this would demand an improbable degree of marine erosion, but in parts of the related Isle of Wight Undercliff landslides, particularly at Blackgang and Dunnose where the base of the Gault rises well above sea level, this may be an important factor.

All these mechanisms may be relevant to Folkestone Warren: (f) is considered the most doubtful and (d) too minor an effect to be significant. It is also questioned whether the cracking inherent in (e) would be as effective or deep-reaching as is inferred.

Most of the Warren slides, except that of 1915 and, to a lesser extent, those of 1936 and 1937, have been gradual and of modest displacement. Moreover in the 1915 M type slip, the displacement of 30 m occurred only opposite Warren Halt, the movement being generally very much smaller in the rest of the landslide. Wood's observation is thus particular to the Warren Halt area in the 1915 slip. It is concluded, therefore, that the unusually large displacement there is due to mechanism (g) above, i.e. the sudden undrained loading of the rear of the slide by the large, Steady Hole Chalk Fall, which occurred just after the slow initial type M movement immediately behind Warren Halt.

The comparatively large movements of the 1936 and 1937 slides, in contrast, are probably the result of mechanism (h), with new sections of slip surface being formed through the spoil heaps of chalk debris arising from the unloading of the Martello Tunnel some thirty years earlier.

Ring shear tests

It was emphasized in the earlier paper (Hutchinson 1969) that the Gault is highly variable, not only laterally but also with depth at any given locality. Unique values of the shear strength parameters do not therefore exist. The approach then adopted in the laboratory programme was to test samples from approximately the highest and lowest liquid limit horizons, in order to define the range of shear parameters obtaining. The same approach has been followed here. Block samples of high liquid limit material were taken, as before, from Copt Point, and similar samples of low liquid limit material were again obtained from the inner end of the New No. 2 Heading. On each of these samples drained ring shear tests were carried out in both the I.C/N.G.I (Geonor) apparatus and the recently developed Bromhead (Wykeham-Farrance) apparatus, at Imperial College and Kingston Polytechnic respectively, as described briefly below.

Tests at Imperial College

Two series of tests have been carried out: test RS1 on the high liquid limit Gault and test RS2 on the low liquid limit Gault.

The apparatus used has been described by Bishop *et al.* (1971). The samples were first thoroughly remoulded with distilled water and left for 48 hours. They were then kneaded into the confining ring assembly and consolidated initially to a normal effective stress of $\sigma'_n = 439.9\ kN/m^2$. This was then increased to $790.7\ kN/m^2$ and during this second stage of consolidation a c_v value, and hence an estimate of the maximum shearing rate for drained peak conditions, was obtained. The samples were then allowed to swell back to a normal effective stress of $439.9\ kN/m^2$ before shearing was started. Up to the (remoulded) peak the rates of shear were 7.6×10^{-4} mm/min for test RS1 and 5×10^{-3} mm/min for test RS2. Higher shear rates (up to 1.0 mm/min in both tests) were used post-peak to achieve large displacements. On reaching the required displacement, the slower rates were re-established and ample time for drainage allowed before any readings were taken. Details of the two tests carried out are given in Table 6 and Figs 18 and 19.

In the same test (stage 4, with $\sigma'_n = 88.9\ kN/m^2$), shearing was stopped for 28 days, with the torque released, at a displacement of 321.9 mm. On recommencing shearing no gain or loss of residual strength was observed over this short period. On dismantling the test, a thin section across the shear surface was prepared using the Carbowax impregnation technique. The results of the subsequent study of this thin section under a polarizing optical microscope are summarized in Fig. 22 and the Appendix.

Tests at Kingston Polytechnic

Two series of tests have again been carried out: test RS3 on the high liquid limit Gault and test RS4 on the low liquid limit Gault.

The apparatus used is described by Bromhead (1979). A 5 mm thick annular sample, of inner and outer diameters 100 and 70 mm respectively, is confined in a water bath and rotated about its axis by a motor driven, worm gear arrangement. Normal load is applied through a lever system and a top platten, the face of which is roughened so that shear occurs through the soil just below the platten. Drainage is through the platten faces which are of porous bronze. The torque transmitted through the sample is measured by proving rings bearing on a cross arm.

Tests were carried out both on samples at the natural moisture content and on samples which were air-dried, crushed, slaked with water and remoulded at a water content higher than that originally found in the specimen. No significant difference in residual strengths was measured. The test procedure was evolved as testing proceeded, since the high liquid limit sample was the first soil ever tested in this device. Among other procedures the following were explored:

(a) Fully drained shearing through the (remoulded) peak to residual at different normal stresses.

(b) Shearing on the shear surface so formed at different normal stresses, with both ascending and descending loading sequences.

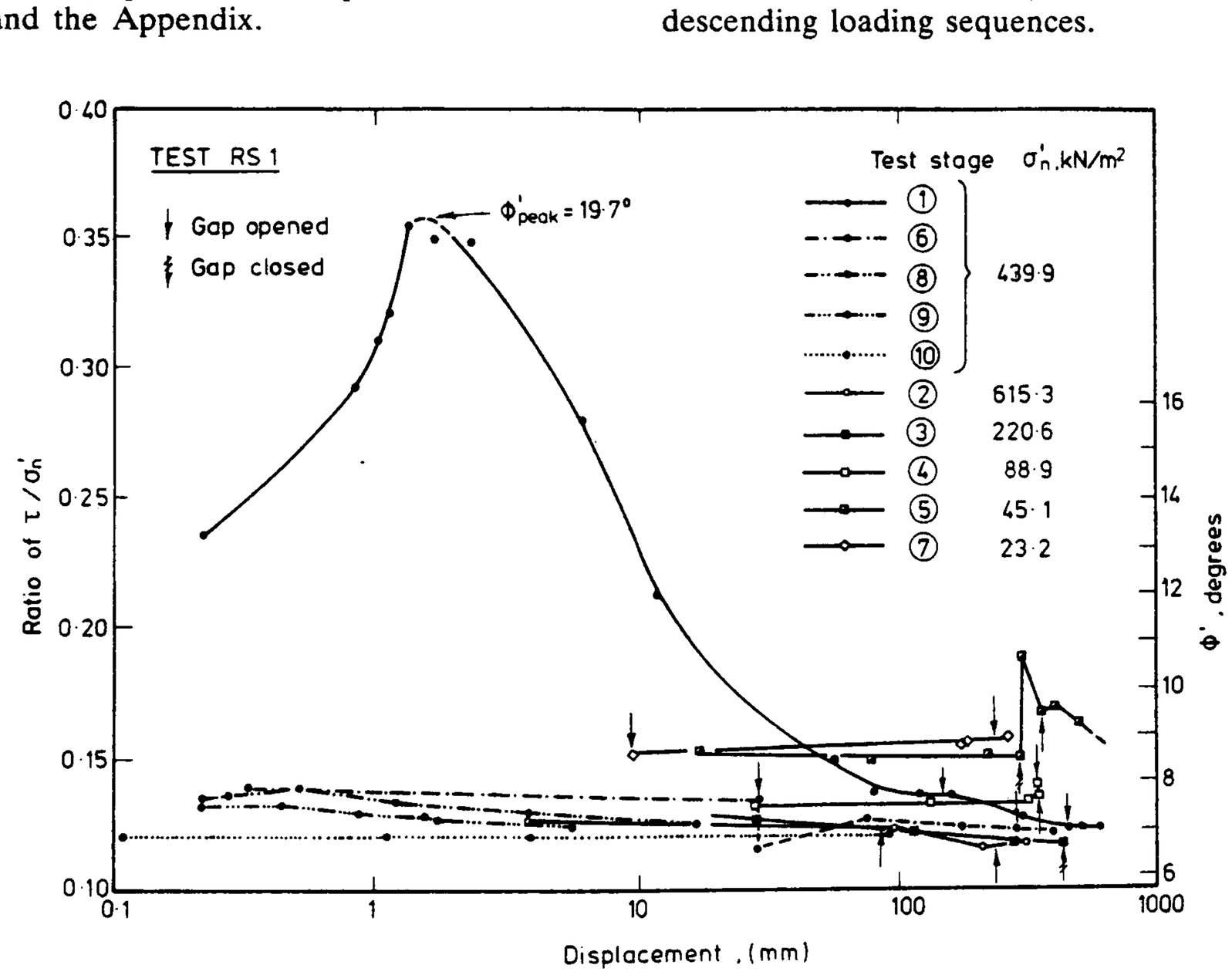


FIG. 18. Ring shear test RS1: ratio of shear stress to normal effective stress plotted against displacement.

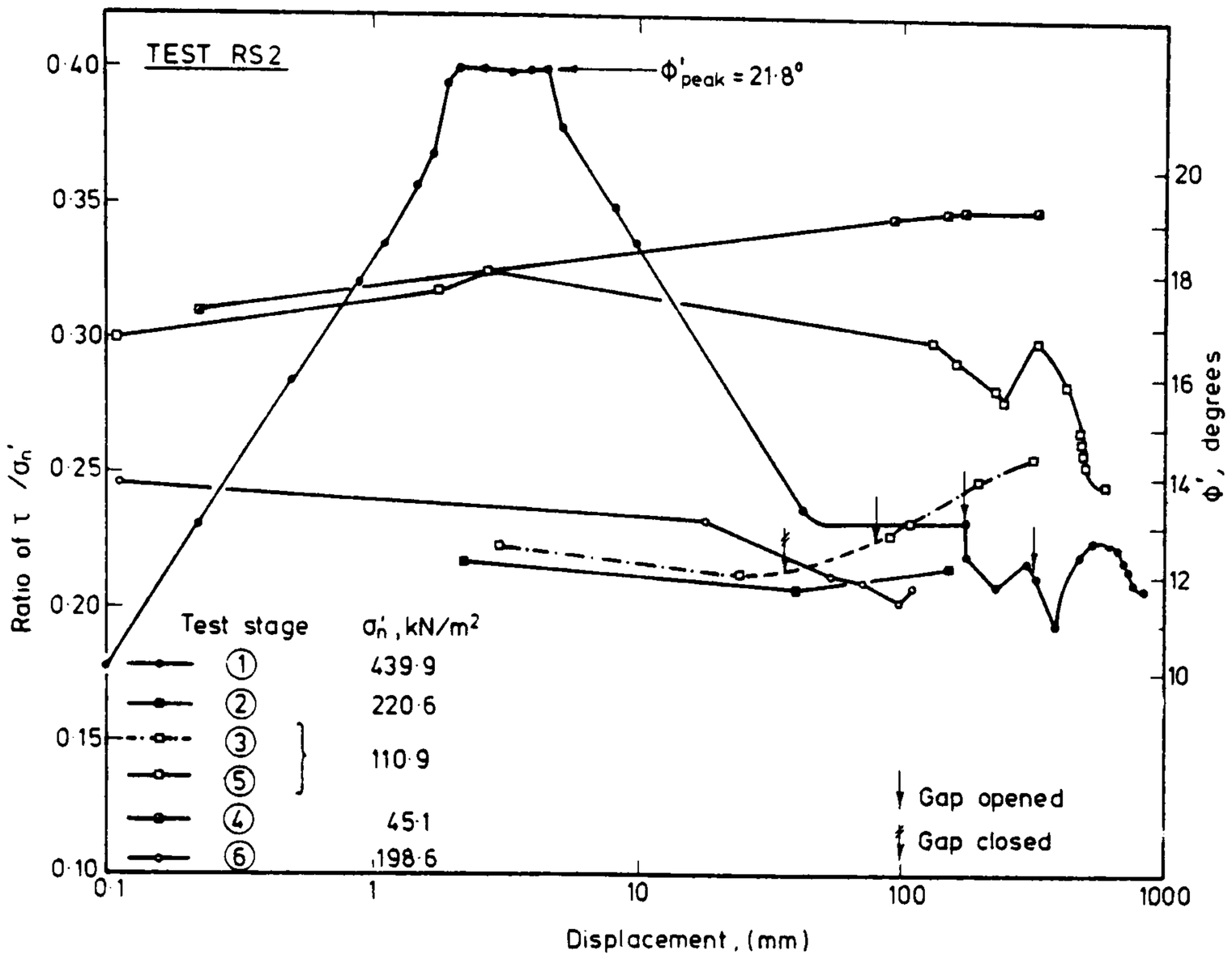


FIG. 19. Ring shear test RS2: ratio of shear stress to normal effective stress plotted against displacement.

(c) Shearing undrained to form a shear surface, then consolidating and shearing at a much slower rate for each of the different normal load stages.

Once again, no significant differences in behaviour were noted and method (c) with an ascending loading sequence is now generally used as being the quickest and most convenient.* In all, twenty-eight determinations of residual shear strength were made on six specimens of the low liquid limit clay and twenty-nine such determinations on four specimens of the high liquid limit clay. The results are tabulated in Table 7 and plotted for comparison with the Imperial College tests in Fig. 20.

*After completing a set of observations in an ascending loading sequence it is, however, advisable to measure again the residual strength at a low normal stress as the sample may have degraded during the course of the test.

Comparison of results

The results indicate that tests on virtually identical samples in the two different ring shear machines give

TABLE 6. *Results of ring shear tests RS1 and RS2 carried out at Imperial College*

Test series RS1 (high LL)		Test Series RS2 (low LL)	
Normal effective stress (kN/m²)	Ratio of shear to normal effective stress	Normal effective stress (kN/m²)	Ratio of shear to normal effective stress
439.9	0.122	439.9	0.206
615.3	0.116	220.6	0.215
220.6	0.119	110.9	0.255
88.9	0.134	45.1	0.349
45.1	0.150	110.9	0.245
439.9	0.119	198.6	0.210
23.2	0.158		
439.9	0.124		
439.9	0.122		
439.9	0.119		

TABLE 7. *Results of ring shear tests RS3 and RS4 carried out at Kingston Polytechnic*

Test Series RS3 (high LL)		Test Series RS4 (low LL)	
Normal effective stress (kN/m^2)	Ratio of shear to normal effective stress	Normal effective stress (kN/m^2)	Ratio of shear to normal effective stress
74.7	0.24*	79.0	0.245
148.2	0.135	127.0	0.225
221.6	0.133	227.0	0.205
295.1	0.130	327.0	0.220
368.6	0.124		
295.1	0.133	79.0	0.251
221.6	0.142	127.0	0.231
148.1	0.157	227.0	0.227
		327.0	0.229
74.7	0.151	427.0	0.222
148.2	0.133		
221.6	0.133	79.0	0.257
295.1	0.126	127.0	0.229
368.6	0.126	227.0	0.207
295.1	0.117	327.0	0.209
221.6	0.124	427.0	0.207
148.2	0.144		
74.7	0.144	79.0	0.231
		127.0	0.225
148.2	0.140	227.0	0.224
221.6	0.140	327.0	0.220
295.1	0.126	427.0	0.209
368.6	0.123		
442.0	0.118	38.0	0.234
515.5	0.114	79.0	0.244
588.9	0.105	127.0	0.222
664.7	0.107	227.0	0.216
765.1	0.116	327.0	0.216
		427.0	0.209
783.4	0.130†		
979.2	0.128†	490.0	0.208
		588.0	0.192
		783.4	0.195

*In retrospect, this test appears not to have been carried far enough: this was, however, the first test ever performed in the apparatus.

† These extra tests were carried out on a different lump of clay from the remainder of the tests in Series RS3.

similar results. The values of ϕ'_r measured agree to within about $\frac{1}{3}°$ for the low liquid limit samples at values of $\sigma'_n > 130\ kN/m^2$ and for the high liquid limit samples at values of $\sigma'_n > 190\ kN/m^2$. At lower normal effective stress levels differences equivalent to about 2° appear on the plot of τ/σ'_n against σ'_n (Fig. 20): the Mohr envelopes yielded by the two different machines are, however, almost indistinguishable. Linear regression for the test results on the high and the low L.L. clays are indicated in Fig. 21. and compared with the back-analyses.

Conclusions

The main conclusions are as follows:

1. The increased activity of the Warren slides in the second half of the nineteenth century and in the early twentieth century reflects to a considerable extent the progressive interruption of the littoral drift by the Folkestone Harbour works.

2. In the great M type slip of 1915 the renewal of movement on the pre-existing shear surfaces in the Gault commenced at the west end of the Warren and

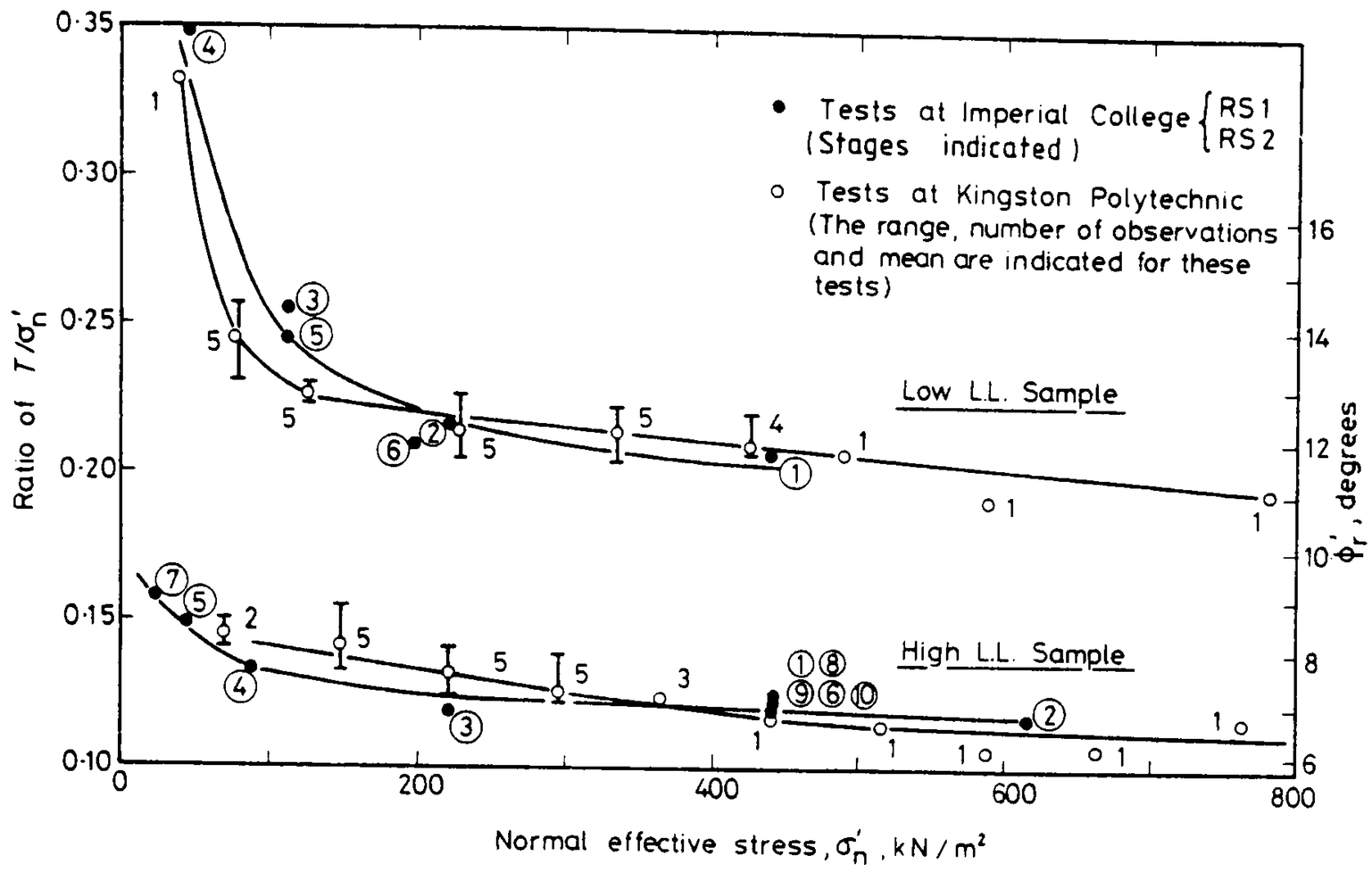


FIG. 20. Summary of ring shear test results, showing the comparison between the measurements at Imperial College and Kingston Polytechnic.

spread towards the east, triggering the various Chalk falls from the rear scarp in the process.

3. The Warren is a dynamic feature in which shifts of mass such as those produced by marine erosion, by falls of debris from the rear scarp, and even by the excavation of the railway cutting, have tended to reduce the stability of the M type slips by amounts of the same order as the corresponding improvement in stability resulting from the toe weighting. This improvement in stability is an order of magnitude greater for the R type slips than for the M type slips.

4. The broad morphology of the Warren reflects chiefly the interaction between the varying level of the Gault stratum and the local surface relief. The detailed morphology of the rear scarp is, in addition, influenced by the dominant joint trends in the Chalk and by the intervention of 'sets'.

5. The recent sub-surface investigations near Horse's Head indicate that the seaward part of the slipped masses consists of various sized blocks of Gault overlain by disturbed Chalk rubble. The pore water pressures in the chalky material and in the smaller Gault blocks are essentially in equilibrium with the ambient ground-water conditions: those in the larger Gault blocks are not, still being in appreciable negative excess (equivalent to a piezometric level of about 6 m below mean sea level) as a result of past unloading.

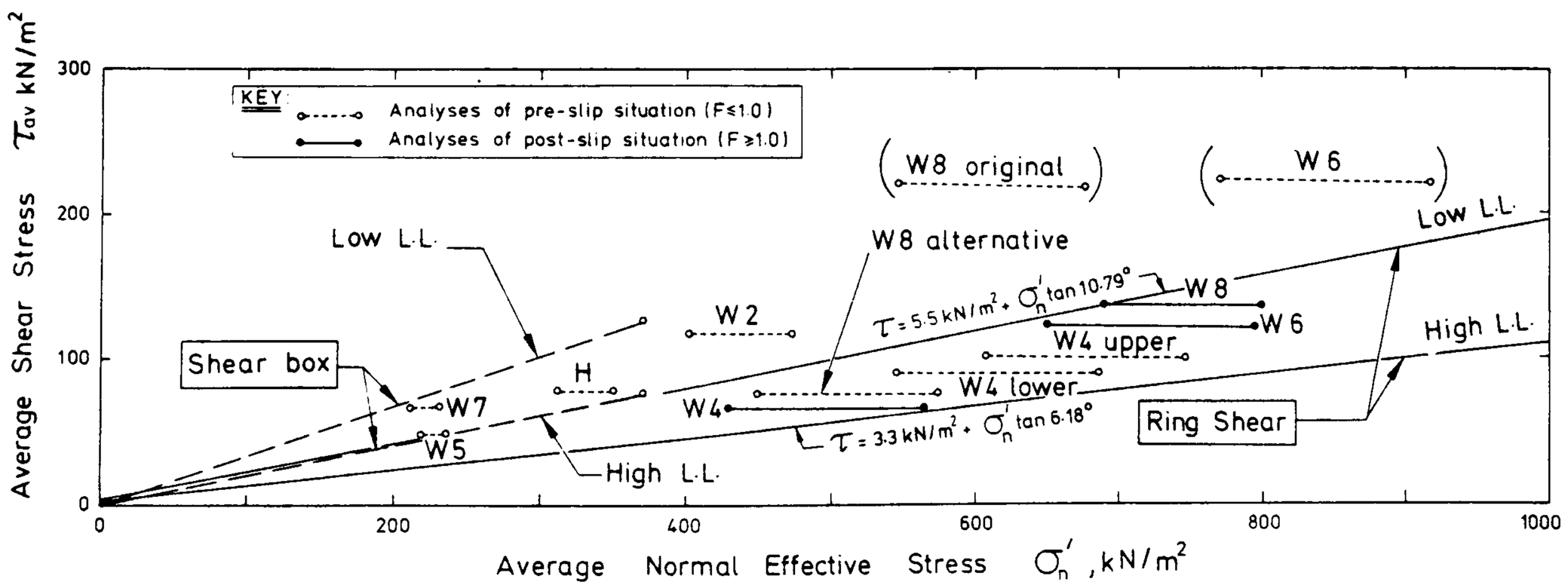


FIG. 21. Comparison of residual strengths in the Gault derived from back analyses with the corresponding envelopes obtained in the laboratory. Back analyses of doubtful reliability (see text) are shown in parenthesis.

6. The negative excess pore water pressures in the larger Gault blocks are continuing to dissipate; in the one case measured, at an average rate of 0.15 m head of water per year. This steady rise in piezometric levels in the toe area of the Warren is progressively reducing its stability, particularly against R type slips.

7. Critical re-examination of the pre-failure back-analyses of the 1915, M type, slip indicates that some doubt attaches to the reliability of the higher of the ϕ'_r values previously derived from cross sections W6 and W8. In view of this, the weighted averaging technique used in the 1969 paper, while in principle appropriate, has not been followed here.

8. The combined back-analyses of the various slips, both pre- and post-failure, indicate a considerable scatter of ϕ'_r. This reflects in part the differing reliability of the data used and in part the inherent variability of the Gault. In the range of average normal effective stress levels in the Warren, of from about 200 to 800 kN/m^2, the values of ϕ'_r indicated by the back-analyses range from about 7.5° to more than 17°. The higher values, however, all have to be qualified as noted in (7) above and a more realistic upper bound is probably about 15°.

9. The values of ϕ'_r for particular samples of Gault measured in both the Bishop and the Bromhead ring shear machines are closely similar. At the average normal effective stress levels in the Warren, these values of ϕ'_r are about 12° for the low liquid limit Gault and 7° for the high liquid limit Gault material. These values are as much as 7° lower than the corresponding values measured previously in cut-plane direct shear tests on similar material at lower normal effective stresses.

10. From (8) and (9) above, it is evident that while there is considerable overlap between the ranges of ϕ'_r for the Gault derived from back analyses and from ring shear tests, the latter tend to be the lower.

11. The main reason for the displacements of up to 30 m exhibited in the 1915 slip, surprisingly large for a renewal of movement on a pre-existing shear surface, is believed to be the considerable undrained loading applied to the rear of this slip, immediately following its failure, by the Steady Hole Fall.

ACKNOWLEDGMENTS. The authors are grateful to the Chief Civil Engineer, British Rail (Southern), and his colleagues for the generous provision of site investigation results and for the invaluable records of the 1915 landslip (Figs 4, 6, 7, 8, 9 & 10). They also wish to thank Mr A. M. M. Wood of Sir William Halcrow & Partners for his interest and useful comments, Dr S. D. Priest of Imperial College for his advice on the joint survey and its interpretation, and Dr M. B. Hart of Plymouth Polytechnic and Dr E. R. Shephard-Thorn of the Institute of Geological Sciences for their help with the French references. The authors are indebted to Professor J. K. S. St. Joseph, Director in Aerial Photography of the University of Cambridge, for Fig. 12, to the Building Research Station, Watford, for Fig. 11, and to Mr H. F. Andrews for bringing to light some early photographs of the 1915 slip (Figs 6–10 inclusive) taken by his father, who supervised the removal of the trapped train in 1916. Finally, thanks are given to Messrs. A. J. Harris, R. B. Higginson and N. J. Lambert, former students of Kingston Polytechnic, who ran most of the ring shear tests there; and to Mrs Ursula Schüler, Miss Joyce Gurr and Miss Dawn Goodhall of Imperial College for their work on the figures.

Mr J. F. Lupini was supported while at Imperial College by a grant from the Fundación Gran Mariscal de Ayacucho of Venezuela.

Appendix

Thin section of the ring shear test RS1 on the high liquid limit Gault

On completion of test RS1, a part of the sample was impregnated with Carbowax 6000 and a thin section made. Unfortunately some swelling is unavoidable, especially on unloading from a test, and the specimen split along the slip surface (even though the sample was wrapped in 'Sellotape' to minimize cracking). A photograph of this thin section is given in Fig. 22 together with a quasi-quantitative study of the shear-induced fabric.

Techniques for observing structural features and orientation in thin sections are based upon the properties of the clay minerals. When a clay crystal is viewed under polarized light it transmits a variable light intensity as the thin section is rotated with respect to the direction of polarization. In an aggregate of clay particles, the transmitted intensity also depends upon the spatial distribution of the particles. The ratio of the *minimum* to the *maximum* light intensity is called 'β', the birefringence ratio, and is a measure of the degree of orientation of the clay aggregate. Morgenstern & Tchalenko (1967) propose the following orientation scale:

β	Particle orientation
1.0	Random
0.9–1.0	Slight
0.5–0.9	Medium
0.0–0.5	Strong

It was noted that whereas there was comparatively little orientation of minerals throughout the specimen and that such orientation as there was could no doubt be attributed solely to the influence of consolidation stresses, the mineral particles immediately adjacent to the major shear surface showed extremely strong and very localized orientation in the direction of shear. On the basis of this and similar observations on other soils, it appears probable that if the residual strength in clay soils is achieved through a process of the

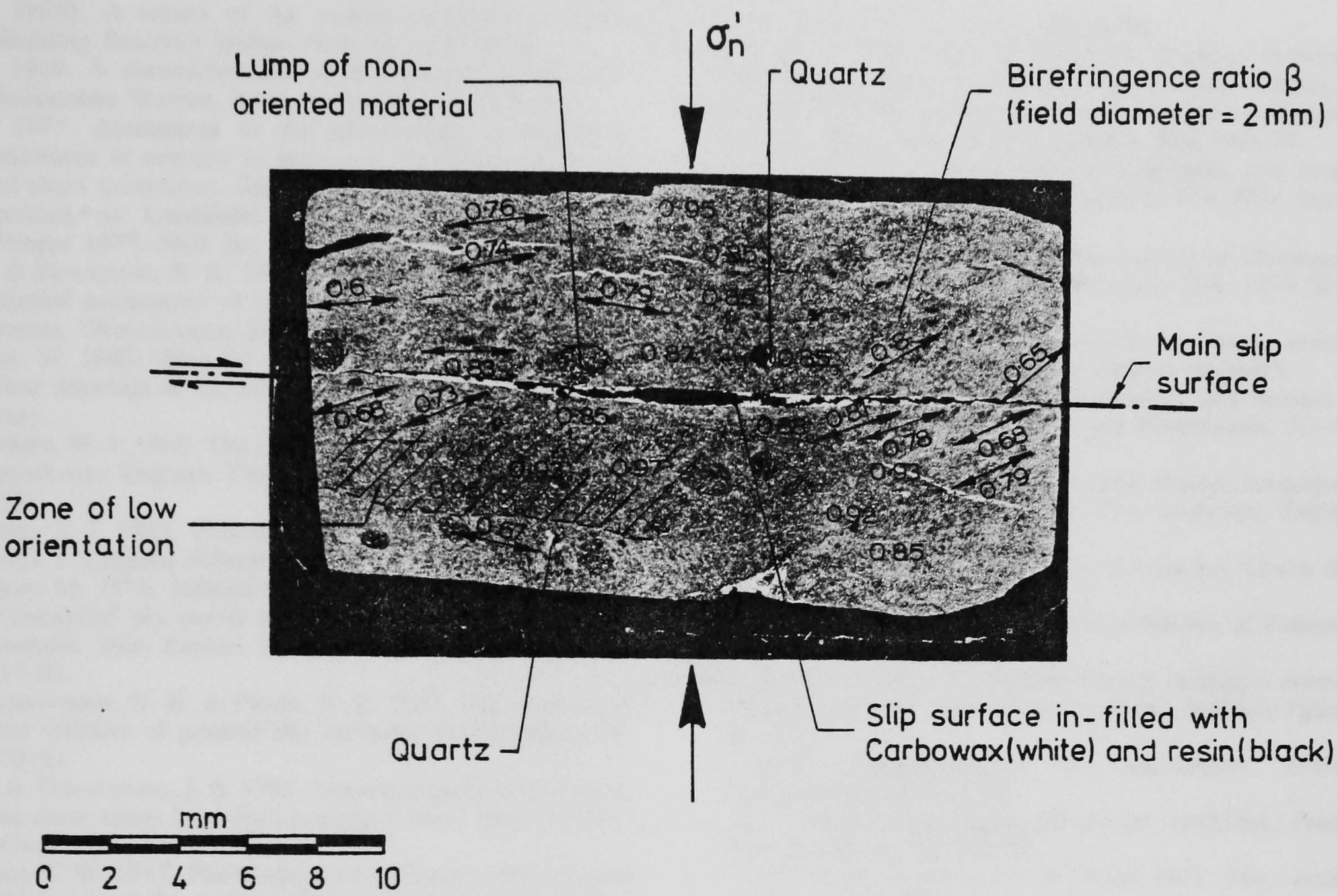


FIG. 22. (Photo). Thin section of ring shear specimen (Test RS1) showing particle orientation measurements in the vicinity of the slip surface.

complete alignment of platey mineral particles, then the ring shear test is satisfactorily reaching this condition. However, the zones in which this state is imposed on the soil are very thin, and this may have some bearing on certain of the mechanisms (particularly (b)) discussed above in the general context of the reasons for the unusually large displacements of, in particular, the 1915 slip.

References

ACLAND, C. L. 1869. The late landslip on the Warren. *Q. Jl Folkestone Nat. Hist. Soc.* **3,** 48–51.

ANON. 1865. *Folkestone Chronicle*, 11th February.

—— 1870. *The Boulogne Review and Visitors' Guide*, 15th January.

—— 1877. *Folkestone Chronicle*, 27th January.

—— 1915*a*. *Folkestone Express*, 25th December.

—— 1915*b*. *Folkestone Herald*, 25th December.

—— 1915*c*. Notes from unsigned report on 1915 slip (unpub.), British Railways (Southern Region).

—— 1916. *Folkestone Herald*, 1st January.

ARBER, M. A. 1940. The coastal landslips of south-east Devon. *Proc. Geol. Assoc. London.* **51,** 257–71

BERRYAT, J. 1956. *Collection Académique*, **6,** 605, F. Desventes, Dijon; F. Fournier, Auxerre.

BISHOP, A. W., GREEN, G. E., GARGA, V. K., ANDRESEN, A. & BROWN. J. D. 1971. A new ring shear apparatus and its application to the measurement of residual strength. *Géotechnique*, **21,** 273–328.

BISHOP, C. H. 1973. *Folkestone: The story of a town.* Headley Brothers Ltd., London & Ashford.

BROMHEAD, E. N. 1979. A simple ring shear apparatus. *Ground Eng.*, **12,** 40–4.

CHATWIN, C. P. 1961. East Anglia and adjoining areas. *Brit. Reg. Geol.* H.M.S.O., London.

CONYBEARE, W. D. & MRS BUCKLAND. 1840. *Ten Plates . . . . representing the changes produced . . . by the subsidence of the land . . . on the 26th December 1839, and 3rd February, 1840.* John Murray, London.

DAVIES, G. M. 1939. *Geology of London and south-east England.* Thomas Murby & Co., London.

DESTOMBES, J. P. & SHEPHARD-THORN, E. R. 1971. Geological Results of the Channel Tunnel site investigation 1964–65. *Institute of Geological Sciences*, Report 71/11. H.M.S.O., London.

DREW, F. 1864. The geology of the country between Folkestone and Rye, including the whole of Romney Marsh. *Mem. Geol. Surv.* H.M.S.O., London.

HALCROW, SIR W. 1970. Ground movements at Horsehead Point, Folkestone Warren, Kent. Report (unpubl.) to British Railways, Southern Region.

HOEK, E. & BRAY, J. 1977. *Rock Slope Engineering* (revised, 2nd ed.). The Institute of Mining & Metallurgy, London.

HUTCHINSON, J. N. 1965*a*. A reconnaissance of coastal landslides in the Isle of Wight. *Building Research Station.* Note No. EN 11/65.

—— 1965*b*. A survey of the coastal landslides of Kent. *Building Research Station*. Note No. EN 35/65.
—— 1969. A reconsideration of the coastal landslides at Folkestone Warren, Kent. *Géotechnique*, **19,** 6–38.
—— 1977. Assessment of the effectiveness of corrective measures in relation to geological conditions and types of slope movement. General report on Theme 3. Symposium on Landslides and other Mass Movements, Prague 1977. *Bull. Int. Assoc. Eng. Geol.*, **16,** 131–55.
—— & BHANDARI, R. K. 1971. Undrained loading, a fundamental mechanism of mudflows and other mass movements. *Géotechnique*, **21,** 353–8.
JESSOP, W. 1806. '*Plan for a harbour at Folkestone*'. One of four drawings in the same hand. Folkestone Public Library.
KENNEDY, W. J. 1969. The correlation of the Lower Chalk of south-east England. *Proc. Geol. Assoc. London*, **80,** 459–551.
MACKIE, S. J. 1883. *Folkestone and its neighbourhood* (2nd ed.). J. English, Folkestone.
MASSON, M. 1976. Influence des héritages périglaciaires sur l'instabilité des pentes naturelles. Application à la Normandie. *Bull. Liaison Labo. P. et Ch.*, No. Spécial **11,** 77–89.
MORGENSTERN, N. R. & PRICE, V. E. 1965. The analysis of the stability of general slip surfaces. *Géotechnique*, **15,** 79–93.
—— & TCHALENKO, J. S. 1967. Microstructural observations on shear zones from slips in natural clays. *Proc. Geotech. Conf., Oslo*, **1,** 147–52.
OSMAN, C. W. 1917. The landslips of Folkestone Warren and thickness of the Lower Chalk and Gault near Dover. *Proc. Geol. Assoc., London*, **28,** 59–84.
PALMER, H. R. 1826. Plan of Folkestone Harbour showing the Proposed Improvements. Folkestone Public Library.
PALMER, H. R. 1834. Observations on the motions of shingle beaches. *Phil. Trans. R. Soc. London*, **124,** 567–76.
REDMAN, J. B. 1852. On the alluvial formations, and local changes, of the south coast of England. *Min. Proc. Instn civ. Engrs*, **11,** 162–204.
ROBERTS, G. 1840. *An account of the landslip of Dowlands and Bindon near Lyme Regis. December 25th. 1839* (5th ed.). Daniel Dunster, Lyme.
TOMS, A. H. 1948. Coastal erosion—Kent and Sussex coastlines. British Railways, Southern Region (unpubl.).
—— 1966. Introduction to 'Chalk in cuttings and embankments'. In: *Chalk in Earthworks and Foundations*, 90–5. Instn. civ. Engrs, London.
VINER-BRADY, N. E. V. 1955. Folkestone Warren landslips: remedial measures, 1948–1954. *Proc. Instn civ. Engrs, Railway paper* **57,** 429–41.
WHEELER, W. H. 1902. *The sea coast.* Longmans, Green & Co., London.
WILLS, L. J. 1929. *The physiographical evolution of Britain.* Edward Arnold, London.
WOOD, A. M. M. 1955. Folkestone Warren landslips: investigations 1948–50. *Proc. Instn civ. Engrs, Railway Paper* **56,** 410–28.
—— 1970. Correspondence on Hutchinson 1969. *Géotechnique*, **20,** 110–13.
—— 1971. Engineering aspects of coastal landslides. *Proc. Instn civ. Engrs*, **50,** 257–76.
—— 1972. Reply to discussion on Wood 1971. *Proc. Instn civ. Engrs*, **53,** 401–16.

SOLUTIONS FOR SEEPAGE IN SOILS WITH AN EFFECTIVE STRESS DEPENDENT PERMEABILITY

E. N. BROMHEAD[/] and P. R. VAUGHAN[*]

ABSTRACT

Where soil permeability is dependent on the effective stress in the soil, the pore water pressure distributions may be considerably different to those predicted by a simple constant permeability theory. Closed form solutions have been obtained for certain simple, one-dimensional, cases with a specific nominated effective stress - permeability relationship and these are used as test cases for two iterative methods of analysis. One of these is applicable only to one-dimensional cases (but with any effective stress-permeability relationship), and the other, an iterative, finite element method is developed for two-dimensional work. The convergence of the numerical methods is discussed in the paper.

The effect of these non-linear permeability laws is investigated for a number of cases.

/ Senior Lecturer,
School of Civil Engineering,
Kingston Polytechnic.

* Reader in Soil Mechanics,
Department of Civil Engineering,
Imperial College of Science & Technology.

LIST OF SYMBOLS

A, B, C, D, E	Parameters used to simplify tabulated formulae.
b	Parameter relating effective stress to permeability.
e	Base of natural logarithms.
H, h_o	Limits of elevation.
k, k_o	Permeability, Permeability at zero effective stress
n	Number.
R_1, R_o	Limits of radius.
r	Radius.
x_1, x_o	Limits of horizontal distance.
x	Distance.
y	Elevation.
γ, γ'	Bulk and submerged unit weights.
γ_w	Unit weight of water.
ϕ_1, ϕ_0	Boundary potentials corresponding to positions R_1, R_o or x_1, x_o.
σ, σ'	Characteristic mean total and effective stresses.
$\int\phi$ dvol	Integral of potential over the whole volume of the seepage domain.

The assumption of constant permeability usually made in analysing seepage is demonstrably false, both by argument and by field observation. Not only do permeability coefficients vary with direction (anisotropy) but they vary from point to point in the seepage domain (non-homogeneity) due to such factors as lithological changes, bedding, anisotropic consolidation and so on. Furthermore, there are established correlations between effective stress and voids ratio, and between voids ratio and permeability, from which effective stress-permeability relationships can be deduced. It is therefore somewhat surprising to find that the modern trend, which is to consider the governing parameters in soil and rock mechanics to be non-linearly dependent on effective stress (particularly in problems of strength and deformation), has not been carried over into seepage analysis although it is recognised that with the advent of, for example, the finite element method, problems involving anisotropy and non-homogeneity are regularly analysed.

Ideally, it would be possible to define a basic or intrinsic permeability anisctropy on the basis of the stratigraphy, and to define not only the way that the magnitudes of the various permeabilities respond to changes in effective stress but also the way in which the permeability axes rotate from their inherent directions in response to stress rotations. At the present, these relationships are far from clear, and the best we can do is to assume that the initial anisotropy is maintained, and that the permeability magnitudes change from an initial value of k_o to k in response to a change in some average of the effective stresses from zero to σ'. Typically, if we postulate linear voids ratio - mean effective stress and voids ratio - log permeability relationships we obtain

$$\ell n \frac{k}{k_o} = -b\sigma' \qquad (1)$$

but with linear voids ratio - log effective stress and voids ratio - log permeability relationships we would have

$$\frac{k}{k_o} = \sigma'^{(-b)} \qquad (2)$$

Some idea of the form of these relationships can be judged from the fact that a five-fold reduction in permeability in the range 0-200 kN/m^2 effective stress results from b parameters of 0.01 (equation 1) and 0.3 (equation 2).

The former of these relationships ("logarithmic law") implies a relatively gradual change in permeability throughout the effective stress range whereas the latter ("power law") suggests a more rapid change in permeability for effective stress increments in the lower stress range.

Neither of these simple functions is entirely in accordance with field observations, and in particular they both fail to simulate the changes in behaviour which occurs at the pre-consolidation pressure in overconsolidated soils. However, they do provide a basis on which the more general numerical methods can be developed.

In particular, the logarithmic law (which is easily integrable) can be used to provide closed form solutions against which numerical models can be tested.

It should also be noted that there are two important factors that have a bearing on the use of an effective stress dependent permeability in seepage analysis. Firstly, when using anisotropic or non-homogenous permeability coefficients, the maximum departures from simple, constant permeability models arise when the permeability decreases in the direction of flow, and this is usually the case with a permeability subject to decrease with increasing effective stress. Secondly, the effect of a given effective stress-permeability relationship will be highly dependent on scale and thus become potentially more important in a physically large seepage domain than in a small one.

CLOSED FORM SOLUTIONS

It is possible to derive closed form solutions to one-dimensional cases with an effective stress-permeability relationship of the "log law" form (but not for the other proposed form of relationship) by invoking Darcy's law and integrating. Solutions for horizontal, axially symmetric and spherically symmetric seepage in a constant total stress field have been obtained and also downward seepage in an underdrained layer where the total stress increases linearly with depth. These indicate an exaggerated hydraulic gradient close to the lower potential boundary. A selection of these solutions are plotted in Fig. 1, and the analytical expressions are given in Tables 1 and 2.

In the three constant total stress solutions, the potentials are independent of the actual total stress applied. The implications of this are discussed below.

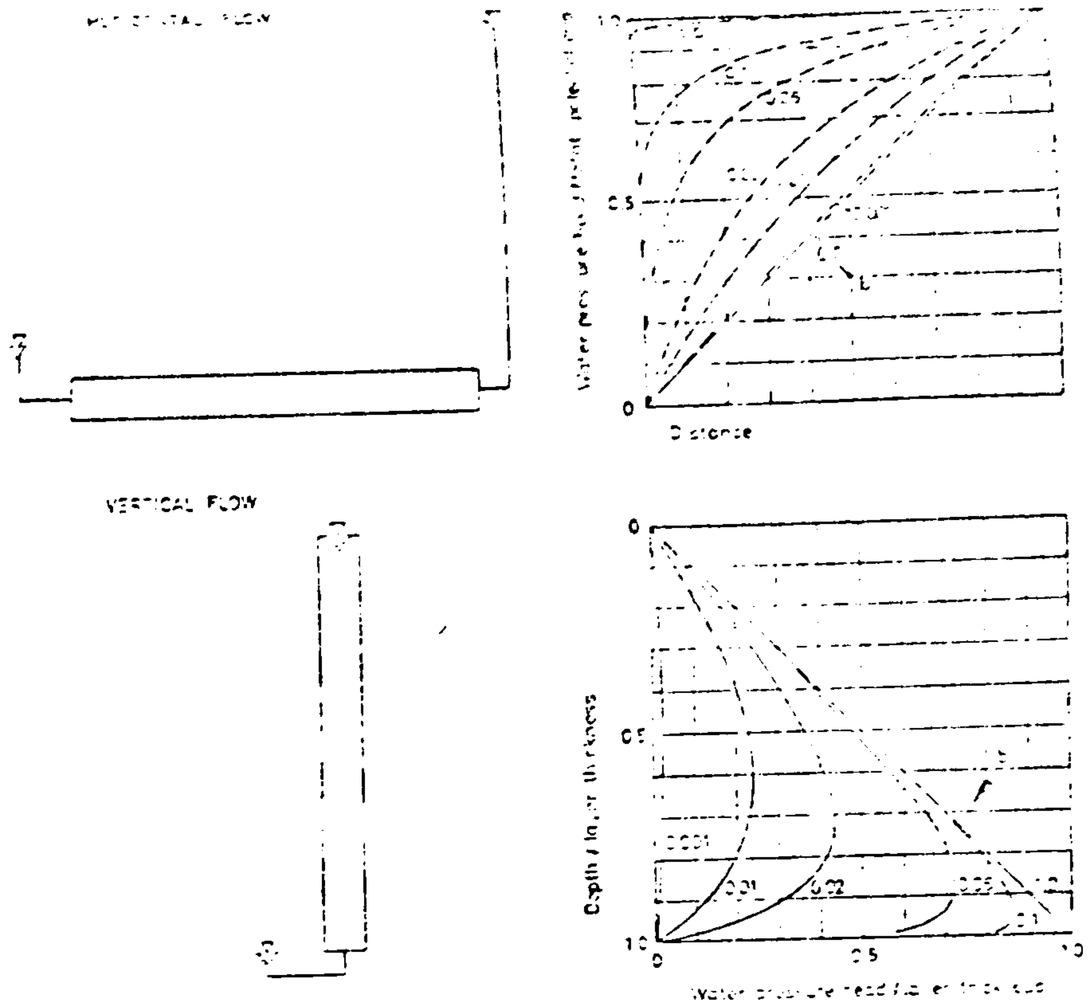


Figure 1. Solutions for vertical seepage in an underdrained soil layer and horizontal seepage. In both cases the length of the flow path is 10 m.

NUMERICAL METHODS

A simple technique for obtaining solutions to one-dimensional steady seepage with any relationship between permeability and effective stress is as follows.

The technique is simply to divide the domain into n intervals (these need not be equal but have been taken to be so here). An initial flow rate together with a simple, generally linear, initial distribution of potentials are assumed, on the basis of which it is possible to evaluate the total stress, potential, pore water pressure, effective stress and hence permeability at the centre of each interval. Making the further assumption that this permeability is constant over the interval, Darcy's Law can be invoked, and working through the intervals sequentially from one side of the domain to the other, a distribution of potentials at the interval contacts can be found, resulting in a misclosure in the potentials at the end. The potential distribution is scaled to eliminate the misclosure, and a new flow rate obtained by sampling the corrected potentials at one point within the domain. A number of repetitions of the process are necessary to reduce the final misclosure to acceptable limits.

Flow type	Potential at x or r	Flow rate
Horizontal	$\frac{1}{b\gamma_w}$ $\ell n\ (Ax/(x_1 - x_0) + B)$	C.A.
Axially-symmetric	$\frac{1}{b\gamma_w}$ $\ell n\ (A \frac{\ell n(r/R_o)}{\ell n(R_1/R_o)} + B)$	$2\pi R_o$.C.A.
Spherically symmetric	$\frac{1}{b\gamma_w}$ $\ell n\ (A\ R_o/r + B)$	$4\pi R_o$.C.A.

In the above $A = e^{b\phi_1\gamma_w} - B$

$B = e^{b\phi_0\gamma_w}$

$C = (k_o e^{-b\sigma})\frac{1}{b\gamma_w}$

$R_1 \geqslant r \geqslant R_o$ or $x_1 \geqslant x \geqslant x_o$

TABLE 1. Flow in a constant total stress field with a characteristic total stress σ.

It is probably more cost-effective to divide the region into non-equal intervals, with the finest subdivision where the potentials vary most rapidly, that is, close to the boundary where the lower of the two boundary potentials is applied, but this has not been explored in the present work. In view of this, the absolute limits of application of this technique have probably not been found. Failure to converge appears to be confined to the "strongest" effective stress permeability relationships, resulting mainly from the simple scaling process used. Furthermore, when using very strongly effective stress dependent permeability relationships, the number of intervals and iterations must be increased to conserve accuracy and to obtain a satisfactory solution. This technique is only of limited general applicability but has provided a range of solutions for the "power law" effective stress permeability case equivalent to those obtained analytically for the "logarithmic law" against which the finite element solution could be appraised and has enabled the two forms of the effective stress permeability relationship to be compared for simple cases at a comparatively low cost in computer resources. It gives results indistinguishable from the closed form solutions if more than 10 to 20 intervals are taken.

Surprisingly, there is little difference between the solutions obtained with the logarithmic and power laws, Fig. 2, the dominant factor appearing to be the total permeability change, rather than how this is distributed.

Potential at any elevation y	Flow rate
$\frac{1}{b\gamma_w}$ ℓn $(ABC/D + AE)$	$k_o\ \gamma'\ B/\gamma D$

In which $A = e^{b\gamma H}$

$B = e^{-b(\gamma H - \gamma_w h_o)} - E$

$C = e^{-b\gamma' y} - E$

$D = 1 - E$

$E = e^{-b\gamma' H}$

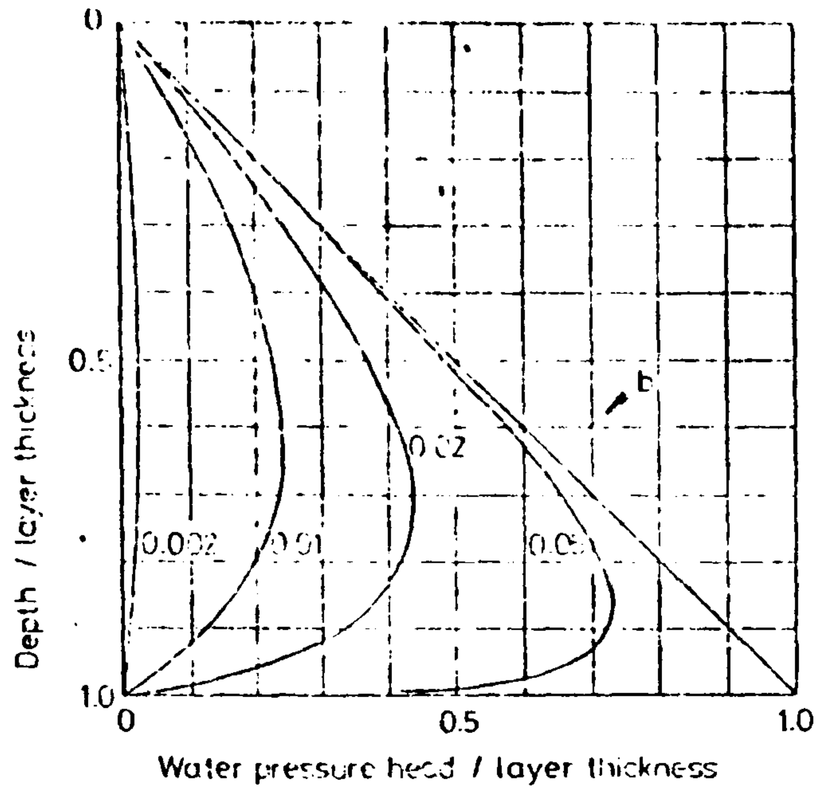
$H \geqslant y \geqslant h_o$

TABLE 2. Gravity underdrained seepage in a soil layer.

Two (and three) dimensional solutions can be obtained by a finite element method. An initial set of total stresses is obtained (at the Gauss points in the 8 noded, numerically integrated, serendipity, isoparametric elements used by the writers) together with an initial distribution of potentials. The selection of this initial potential field is of little importance as convergence has been obtained from potential fields which imply uniform initial pore water pressure as well as from potential fields predicted from a preliminary analysis with constant permeability. An ordinary finite element solution for the potentials is then produced with a "stiffness" matrix calculated using the appropriate effective stresses and effective stress permeability functions at each Gauss point. After solution, the integral $\int \phi$ dvol is computed for the whole seepage regime, and the above process repeated using the new potentials until changes in the integral $\int \phi$ dvol are negligible. This has been found to take of the order of four or five iterations. Since the rank of all the matrices involved in the calculations is small (due to the one degree of freedom per node nature of the problem) the computation penalties of a variable stiffness approach are not severe. In principle (although not examined by the writers) it may be possible to re-evaluate the total stresses at the start of each iteration.

The technique is extremely satisfactory, almost exactly replicating the closed form results, for mild effective stress permeability dependence. It is also adequate for the strongest relationships, in which cases the finite element solution indicates virtually all the potential changes in the element adjacent to the drainage boundary, Fig. 3. This is similar to the closed form result except that the closeness of the two solutions in this region is by and large dependent on the size of this last element. Close inspection of the potential distribution inside the edge element may reveal a reversal of the potential gradient direction at the Gauss points furthest from the drainage boundary, due to the enforced parabolic distribution of potentials in the element.

"Logarithmic law"



"Power law"

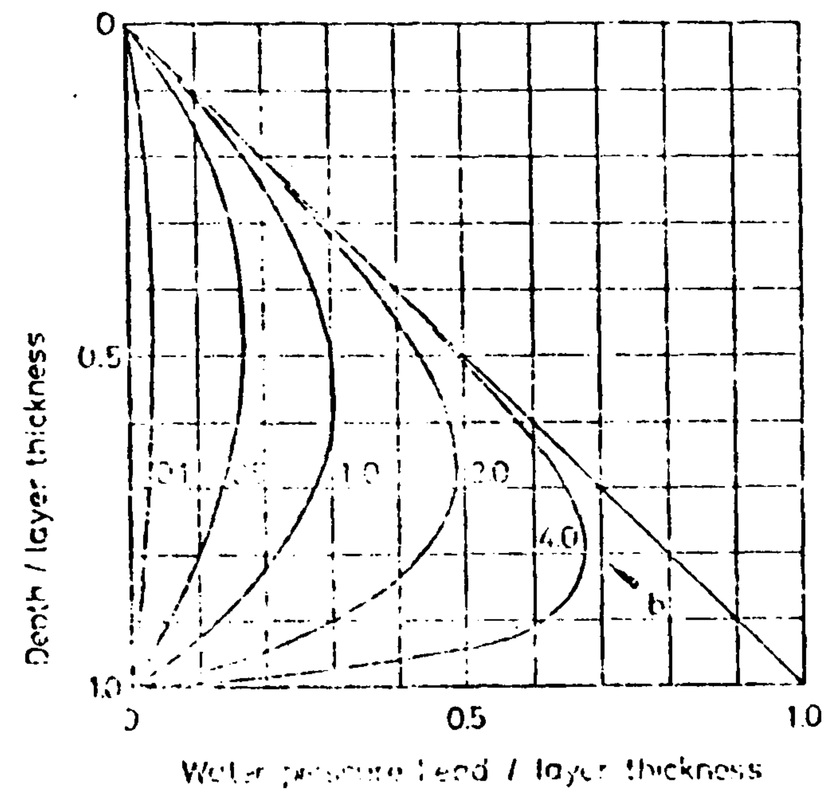
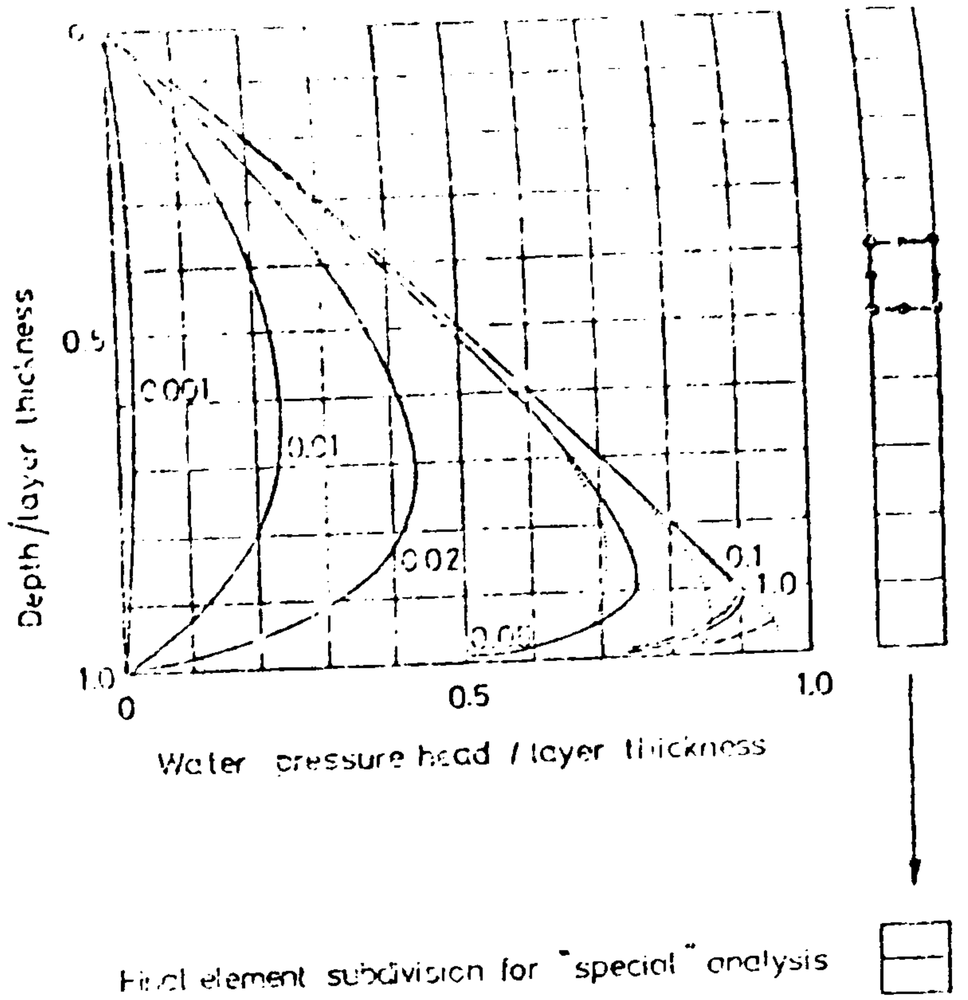


Figure 2. Comparison of pore water pressure depth curves for the logarithmic and power law permeability/effective stress relationships. The problem analysed is that of Fig. 1.



—— Finite element results

—— Analytical results (where not identical to above)

---- Finite element results – special analysis

Figure 3. Comparison of closed form and finite element solutions using the logarithmic permeability/effective stress relationship (cf Figs. 1 and 2.).

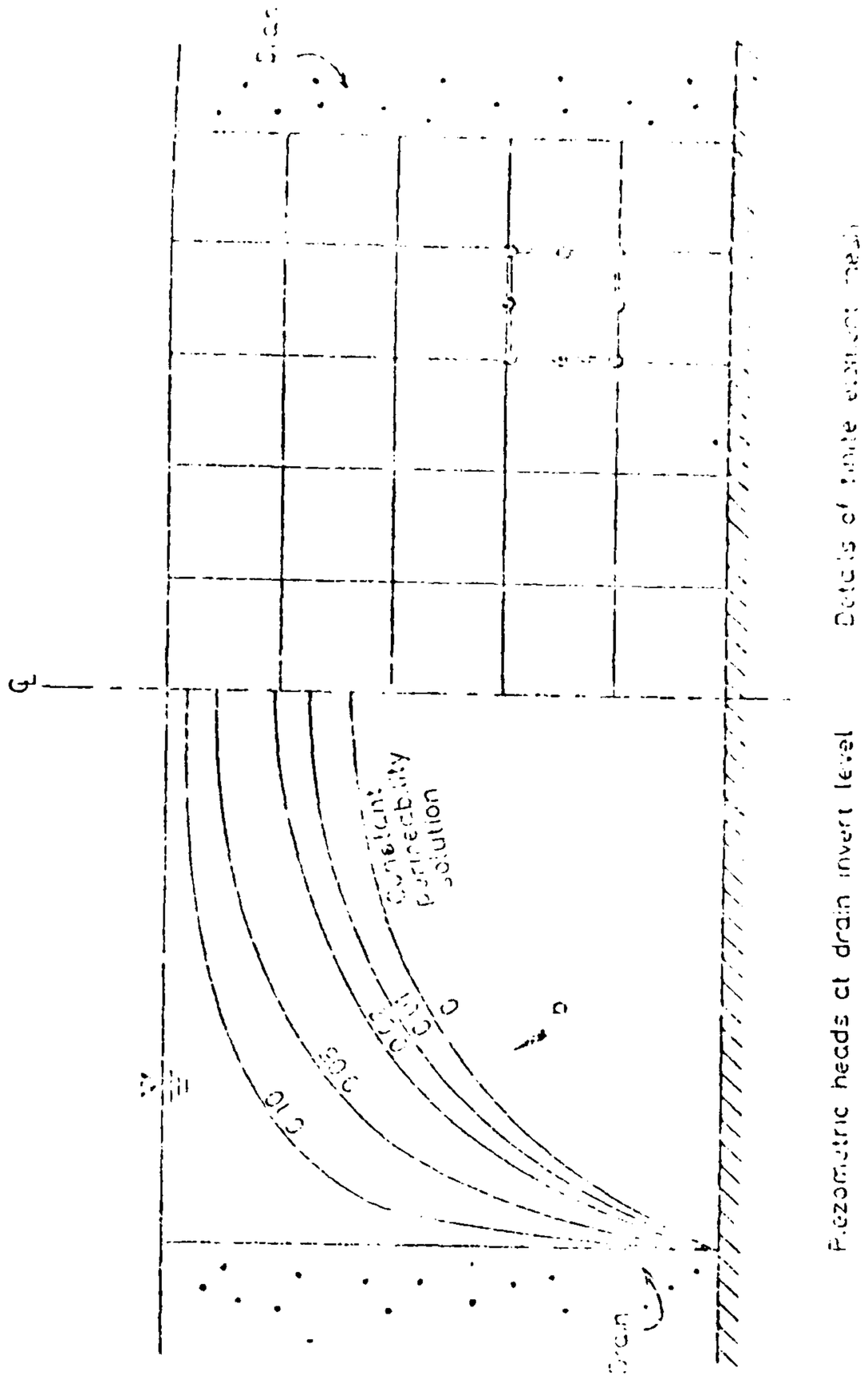


Figure 4. Pore water pressures at drain invert level in a soil layer with an effective stress dependent permeability (logarithmic relationship) between fully penetrating counterfort drains.

Some convergence problems have been found, and on investigation, these appear to arise largely from the nature of the elements used. The above effect is the clue to the oscillation (and sometimes non-convergency) where the effective stress dependence is intermediate in intensity since in these cases the direction of the potential gradient at certain Gauss points may reverse in consecutive iterations. A more satisfactory convergence behaviour may be obtained using a better element, for example the 9 noded Lagrangian element.

An example of the use of this finite element technique is given in Fig. 4. This represents a counterfort drain installation. The piezometric heads at drain invert level for various degrees of effective stress dependency are shown and are compared to the orthodox constant permeability solution. Where the permeability adjacent to the drains is reduced the pore water pressures throughout the seepage domain are increased.

CONCLUSIONS

Three important effects are predicted from this work. Firstly, the gradient of potential at the drained boundary is steeper where the permeability is effective stress dependent than when it is not. This partly offsets the decrease in permeability and thus the flow rate is much less dependent on the effective stress than is the permeability. Secondly, a correct effective stress-permeability relationship can only be defined if the differences in effective stresses are produced by varying the total stress. Varying the hydraulic conditions (e.g. using a different head in an in-situ permeability test) will not do this. Hence, field or laboratory testing using flow rate determinations alone will not yield the correct effective stress-permeability relationships unless correctly analysed.

Finally, the final steady seepage pore water pressure distributions may be radically different from those predicted by the simple, constant permeability approach. They usually indicate higher pore water pressures, with consequent strength and stiffness reductions, and in addition may well appear to be intermediate pore pressure conditions in a dissipation situation. In the latter case, the engineer may be misled into computing an excessive total settlement or assuming incorrectly that drainage measures are either ineffective or that they have become inoperative.

J.N. HUTCHINSON
Professor of Engineering Geomorphology, Imperial College, London, United Kingdom
M.P. CHANDLER
Research Student, Imperial College, London, United Kingdom
E.N. BROMHEAD
Senior Lecturer, Kingston Polytechnic, Kingston-upon-Thames, United Kingdom

Cliff Recession on the Isle of Wight SW Coast
Retraite des Falaises sur le Littoral S-O de L'Ile de Wight

SYNOPSIS The paper draws attention to the power of seepage erosion to cause instability in natural slopes. A 2 km length of actively retreating coastal cliffs, between 55 and 110 m high, in gently inclined Lower Cretaceous (Upper Aptian and Lower Albian) strata near Chale, Isle of Wight is examined. These cliffs exhibit a marked bench between a lower, sea cliff and an upper, rear scarp. The role of seepage erosion in forming this bench and the processes by which the resulting debris is moved across the bench into the sea are explored. The discussion centres around the lithological, structural and hydrogeological controls operating, the history of coast erosion and cliff recession, and the nature and mechanics of the mass movements taking place.

INTRODUCTION

The length of coast between Atherfield Point and Blackgang Chine (Fig.1) suffers a high rate of recession. This arises partly from the lithology and hydrogeology of these Lower Greensand cliffs and partly from their extreme exposure to Atlantic storms. When elucidating the stratigraphy, Fitton (1847) made some perceptive comments on the morphology and wastage of these cliffs but no subsequent work has been carried out. This paper reports the results of an exploratory engineering geological and geotechnical study of the SE half of the above length, from Walpen Chine to Blackgang Chine (Figs.2-4), which will be referred to as Chale cliffs.

GEOLOGICAL AND HYDROGEOLOGICAL SETTING

Chale cliffs trend approximately NW-SE and rise in height towards the SE from about 55 m at Walpen Chine to 110 m at Blackgang Chine (Fig.3). They constitute essentially a dip section through the SE end of the Brixton anticlinal dome, which is situated largely offshore (White 1921). The apparent dip of the strata in the cliffs of 2 to 2½° to the SE is therefore close to the true dip, and the component of dip normal to the coastline is inappreciable. Apart from a thin capping of Quaternary deposits, the cliffs are composed largely of the upper two-thirds of the Lower Greensand (Lower Cretaceous). The lithology of these sediments consists generally of alternations of rather weakly cemented sands with clayey sands and clays. This has led to the development of a number of perched water tables, probably sustained by infiltration into the outcrop of the Lower Greensand to landward, the presence of which is inferred from seepage lines in the cliff face. The more persistent of these are indicated in Fig.3. The existence of a reservoir of ground-water in the Lower Greensand here is indicated by a well in this formation at Pyle Farm, about 2 km N of the cliffs, which has a rest water level of + 43 m O.D.

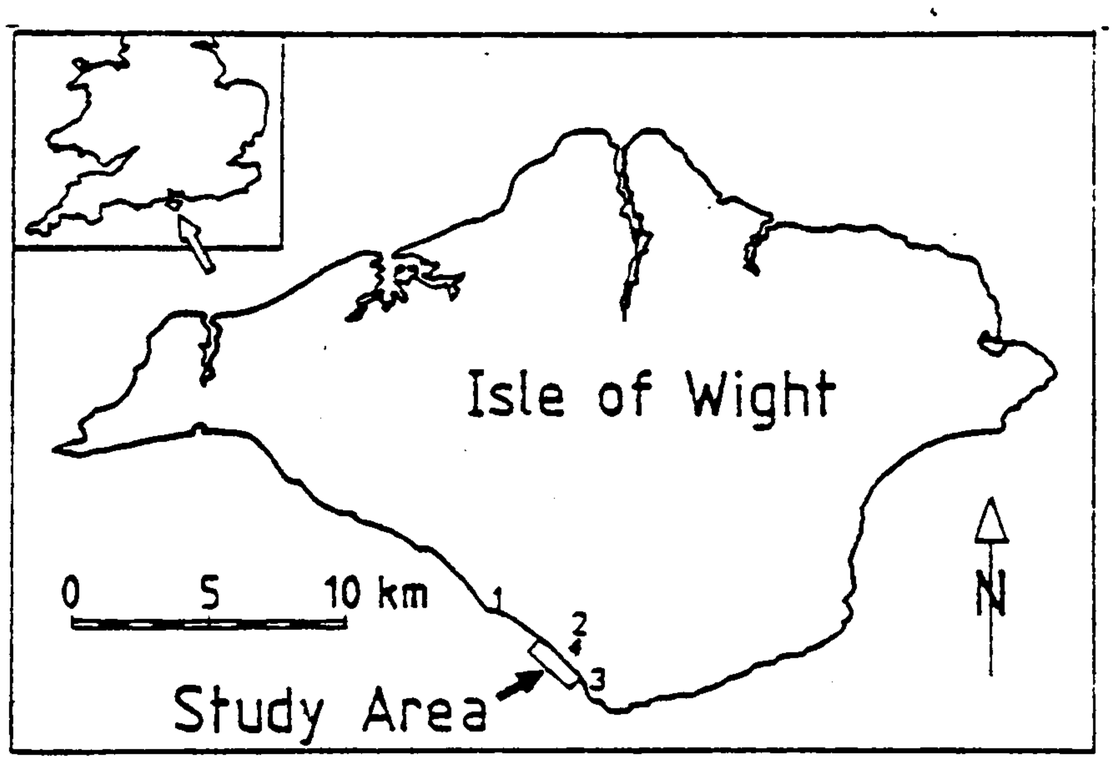
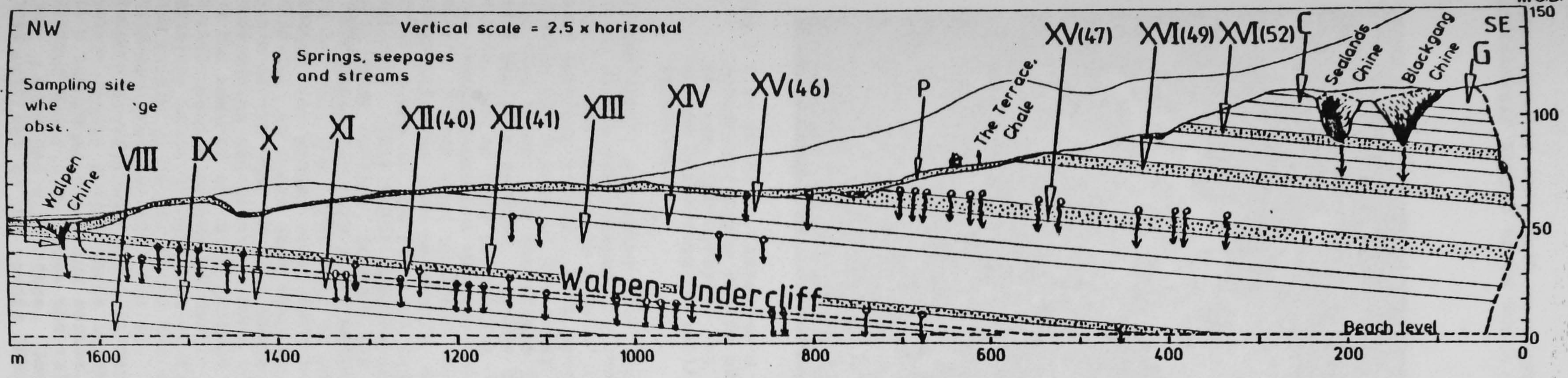


Fig.1 Key map: 1. Atherfield Point, 2. Chale village, 3. Blackgang Chine.

ORIGIN OF THE WALPEN UNDERCLIFF

The most striking feature of the Chale cliffs is the presence of a debris-covered bench (or "undercliff", to use the local term) which separates a precipitous rear scarp from a steep sea cliff (Fig.5). This bench, known as the "Walpen Undercliff", descends concordantly with the dip of the strata from near the cliff top just SE of Walpen Chine to about beach level below Blackgang Chine (Fig.3)*. Its width increases fairly steadily from a few metres at its NW end to about 100 m at its SE limit (Fig.4). Particularly in the SE third of this length, subsidiary benches tend to develop in the rear scarp. Currently the most important of these extends from just NW of CS3 to about CS4 (Fig.4): it is shown, partly developed, in CS3. During the 19th century and the early part of the 20th, this and other subsidiary

*The NW extension of the length of cliff considered here exhibits similar benches.



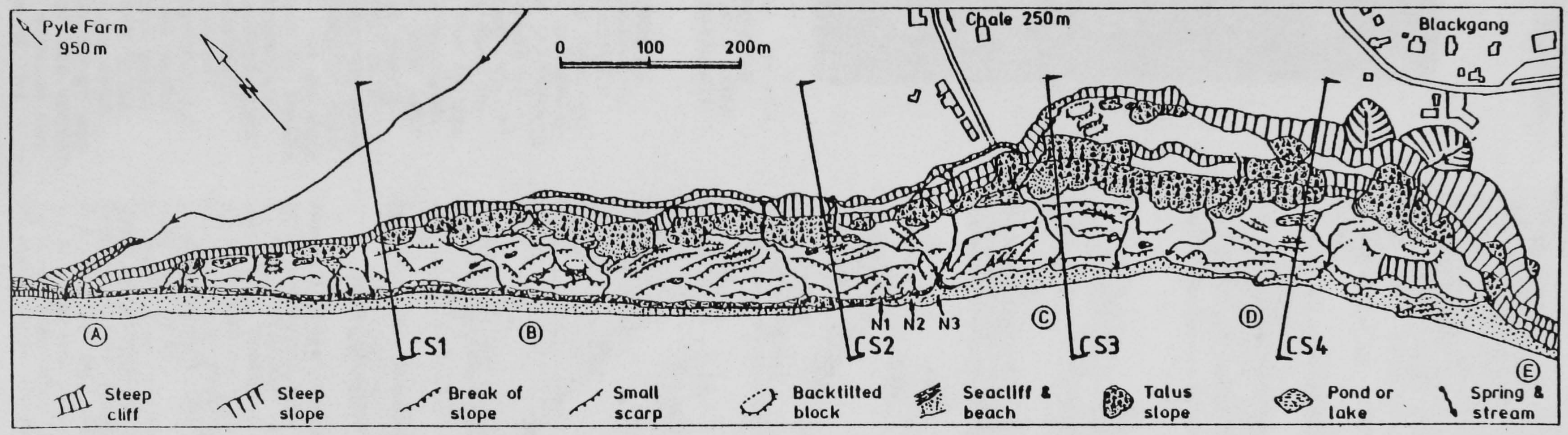


Fig.3 (upper). Geological elevation of the Lower Greensand in Chale cliffs. The scheme of Fitton (1847) is used, with later modifications by Casey (1961) and others:
Ferruginous Sands: VIII Upper Crioceras Group (14.0m), IX Walpen and Ladder Sand (12.8m), X Upper Gryphaea Group (4.9m), XI Cliff End Sand (8.5m), XII(40) Foliated Clay and Sand (7.6m), XII(41) "1st sandrock of Fitton" (3.0m), XIII Sands of Walpen Undercliff (24.1m), XIV Ferruginous Bands of Blackgang Chine (6.7m), XV(46) upper sandy clay (11.3m);
Sandrock Series: XV(47) "2nd sandrock of Fitton" (6.4m), XV(48) muddy sand and sandy mud (18.0m), XVI(49) "3rd sandrock of Fitton" (4.9m), XVI(50) fine yellow sands (8.5m), XVI(51) silty clay (6.7m), XVI(52) "4th sandrock of Fitton" (4.3m), XVI(53) yellow sands (5.5m), XVI(54) muddy sands (6.4m);
Carstone: C. ferruginous pebbly sands (3.7m);
Gault: G. P. indicates the Pleistocene capping.

Fig.4 (lower). Morphology of the Walpen Undercliff.

higher benches were much more extensive and sufficiently stable to be built upon (Fig.5,CS4).

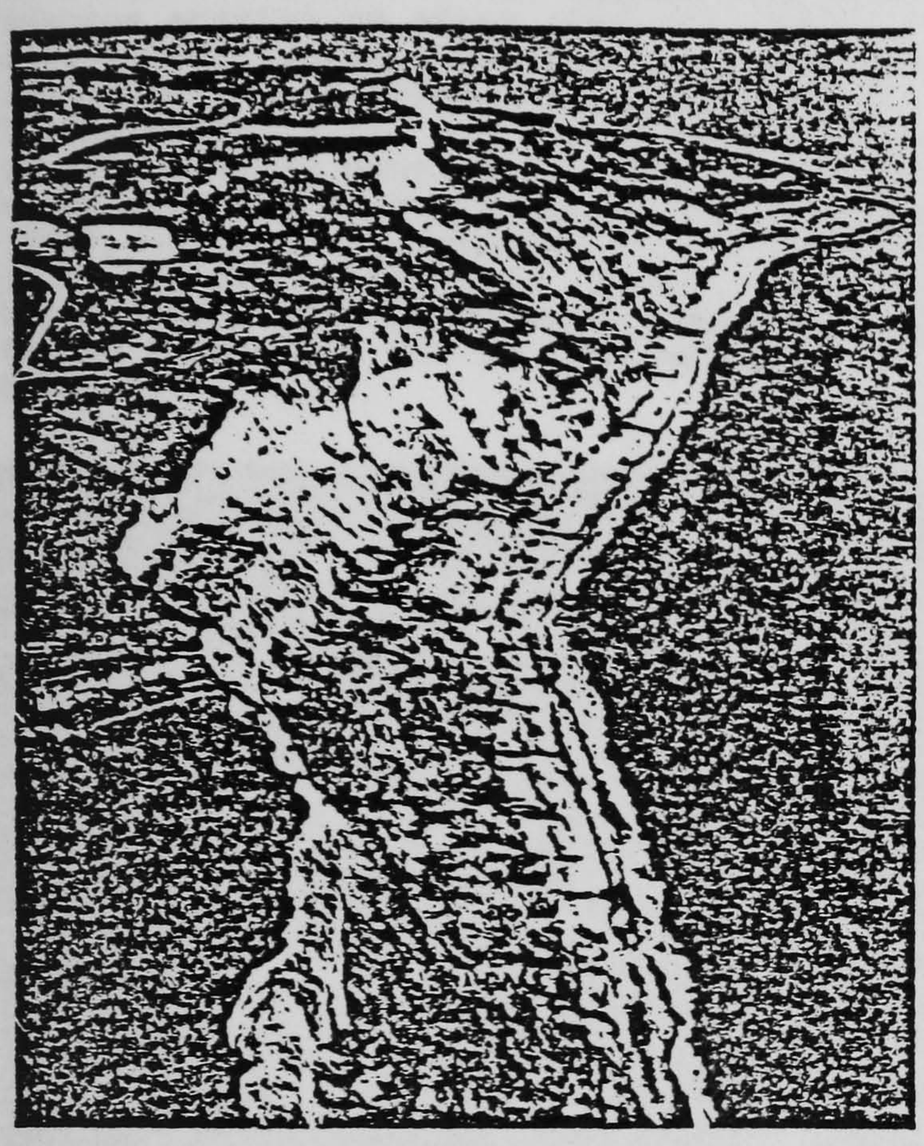


Fig.2 View SE to St Catherine's Point. In the foreground Chale cliffs and Blackgang village. Photographed 7th May 1978 (Cambridge University Collection: copyright reserved).

Fitton (1847) suggested that the benches in these cliffs are produced by the presence of certain less permeable beds within generally more pervious strata..."the water thus kept up carries off a part of the lower mass, undermining that above; and the result is the production of a shelf or terrace, between two ranges of cliffs, one of them supporting 'the Undercliff', the second forming a remoter vertical face behind". Fitton also observed that in the Walpen Undercliff the less permeable bed was provided by the clays of the Foliated Clay and Sand (Bed XII(40)). This still applies although the in situ bench surface, beneath the debris, is located generally only a few metres above the base of Bed XII, the upper half to two-thirds of this having been eroded away (Figs.3 & 5). It is more difficult to check that seepage erosion is taking place at the rear of this bench, back-sapping, undermining and bringing down the rearward cliff, as the seat of any such process is generally buried beneath metres of debris and located directly below an unstable cliff. Fortunately the stream in Walpen Chine has cut down about half-way into Bed XII (Fig.3). At this point seepage erosion was found in March 1980 to be active within a 60mm thick layer of fine sand in a laminated clay/sand series. This layer was located about 0.8m above the talweg of the stream, just in from the cliff face. Seepage erosion was then confined to the up-dip (NW) side of the chine. This is doubtless the reason for the asymmetry of the chine, its NW side being the less steep. The fine sand being transported away by the outflowing groundwater and the resultant undermining of the superincumbent strata are shown in Fig.6. The grading curve for the eroding sand, which is similar to the curves for other such sands reported in the literature (e.g. Ward 1948, Masannat 1980), is given in Fig.7.

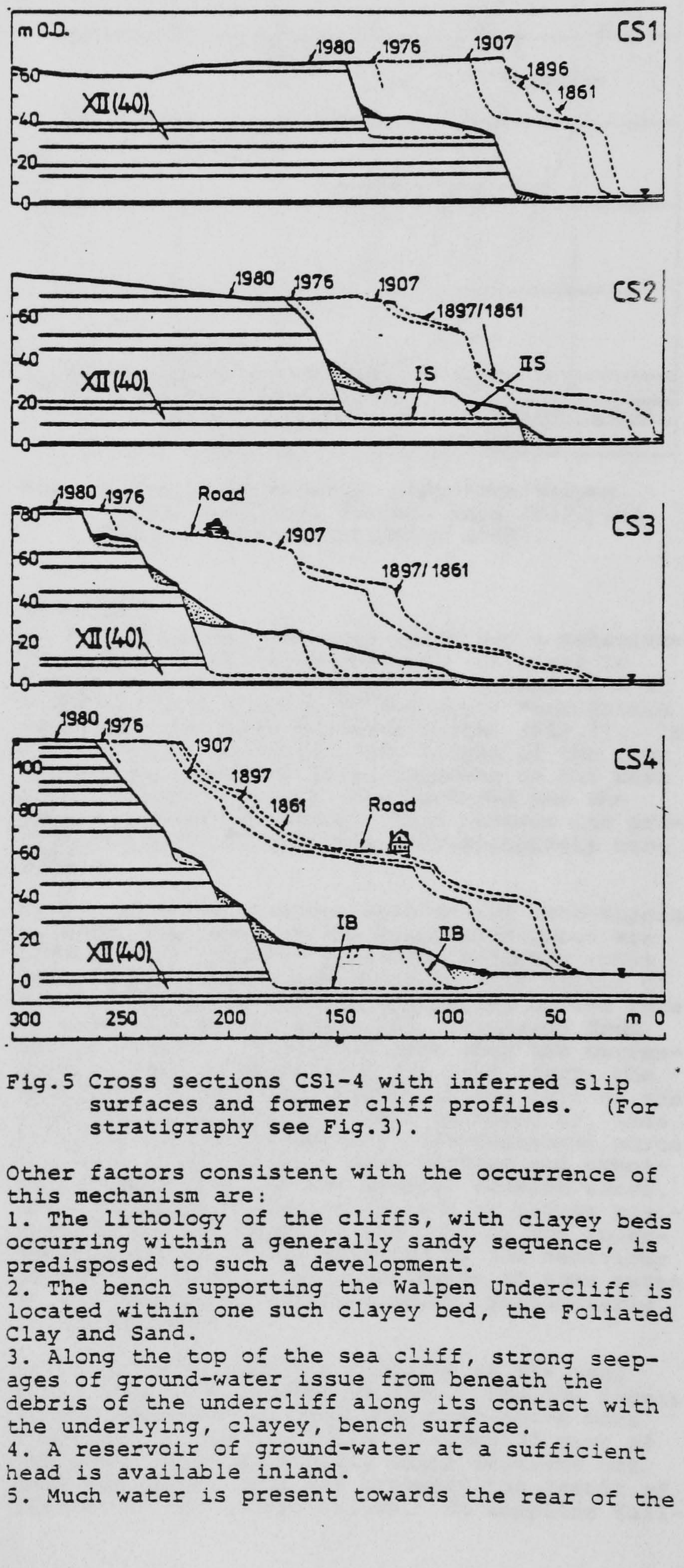


Fig.5 Cross sections CS1-4 with inferred slip surfaces and former cliff profiles. (For stratigraphy see Fig.3).

Other factors consistent with the occurrence of this mechanism are:

1. The lithology of the cliffs, with clayey beds occurring within a generally sandy sequence, is predisposed to such a development.
2. The bench supporting the Walpen Undercliff is located within one such clayey bed, the Foliated Clay and Sand.
3. Along the top of the sea cliff, strong seepages of ground-water issue from beneath the debris of the undercliff along its contact with the underlying, clayey, bench surface.
4. A reservoir of ground-water at a sufficient head is available inland.
5. Much water is present towards the rear of the

undercliff, particularly in its lower, SE parts.
6. Where the undercliffs are cut by deep chines, there is a tendency for a length of stable cliff to exist immediately down-dip from the chine, after which the undercliff reforms. This suggests that drainage to the chines suppresses the seepage erosion on their down-dip sides (Fitton 1847). Our own observations in Walpen Chine, described above, support this inference.
7. The alternative, and more general, mechanism of producing an undercliff, by deep-seated, usually multiple rotational slipping (Hutchinson 1968), requires the presence of a cap-rock and a thick substratum of clay. Except where noted below, the latter is generally absent in the Walpen Undercliff and so this mechanism is inhibited.



Fig.6 Erosion of fine sand in NW side of Walpen Chine. Undermining 0.18m, length of tool handle 0.46m.

PRESENT PROCESSES AFFECTING WALPEN UNDERCLIFF

It is convenient to discuss these processes under the following headings:

Sea Cliff

The in situ sea cliff declines from a height of around 35 m at A (Fig.3) to zero in the vicinity of C where the bench surface passes below beach level. It is formed by the middle part of the Ferruginous Sands. Further SE the sea cliff is composed of landslide debris which, as noted later, is considerably less resistant to marine erosion. This cliff is attacked by waves at most high tides. The available data on the positions and rates of recession of the sea cliff since the mid-19th century, derived from the 1:2500 Ordnance Survey maps, are shown in Fig.5.

The measurements for the in situ sea cliff (CS1 & 2) indicate an average retreat of about 51 m in the 119 years from 1861-1980 (0.43 m/yr). The contrast between the rates of recession in 1861-1907 and 1907-80 is marked, these being respectively 0.21 m/yr and 0.57 m/yr.

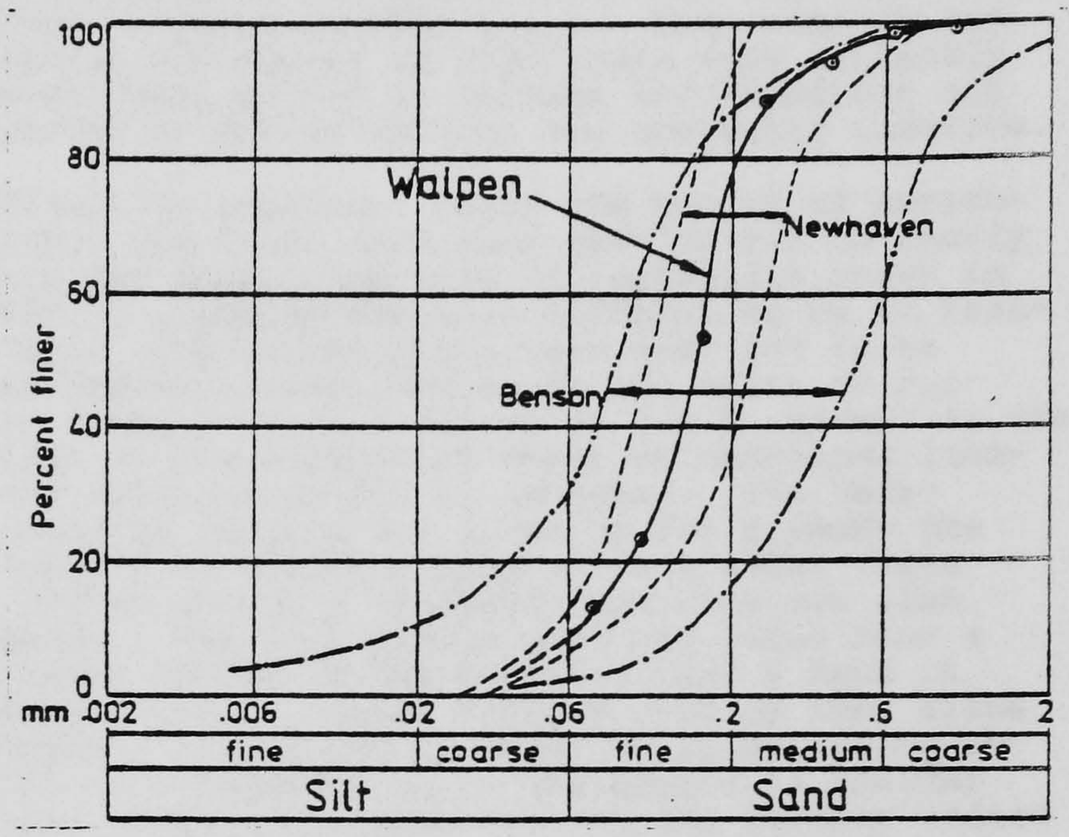


Fig.7 Gradings of eroding sands from Walpen Chine; Newhaven, Sussex (Ward 1948); and Benson, Arizona (Masannat 1980).

Rear Scarp

In its NW length, the rear scarp has a relatively simple, precipitous profile. It rises in height from about 15 m near A to around 55 m at C and consists chiefly of the upper Ferruginous Sands and the lower Sandrock Series (Fig.3). In the remaining SE length, the height of the rear scarp rises to about 90 m, bringing in the rest of the Sandrock Series, the Carstone and the lowest part of the Gault. This renders its profile and modes of collapse correspondingly more complex.

As argued above, seepage erosion and back-sapping at about the level of the undercliff bench are probably the dominant processes bringing about rear scarp collapse and retreat. The degree of activity of these will be influenced by the rate of recession of the sea cliff, resulting from marine attack. If this is less than the corresponding rate of retreat of the rear scarp, the thickness of saturated debris at the rear of the widening undercliff will tend to build up, thus reducing the out-of-balance pore-pressures across the face of the eroding sand stratum and eventually inhibiting further seepage erosion there, and vice versa. Seepage erosion at higher horizons, above the level of the rear of the undercliff and thus little affected by the behaviour of the sea cliff, also contributes to some extent to the retreat of the rear scarp, particularly in its SE parts.

It is unlikely that all failures of the rear scarp stem from seepage erosion. Shallow debris slides occurring in less competent above more competent strata and falls of slabs of rock of the order of a metre thick which separate off from the parent mass are probably the result of weathering and stress relief. No toppling fail-

ures have been seen in the Chale cliffs. Because of their generally weakly cemented nature the masses which fall from the rear scarp tend to disintegrate into a relatively fine scree. Thus, with the exception of a steep ridge of almost intact rock close to the SE end of the undercliff (Fig.4), there is a marked absence of slip blocks in the debris. The available data on the positions of the rear scarp are shown in Fig.5. These indicate that over the period 1861-1980, its recession averaged 48.4 m (0.41m/yr). Again, there is a marked difference between the rate of recession in the early part of this period, averaging 0.16 m/yr between 1861 and 1907, and that from 1907-80 which averaged 0.57 m/yr.

Undercliff

Evidence that the debris on the undercliff is moving seaward is provided by the patterns of scarps, fissures and side shears (Figs 2 & 4); the position of material, now halfway across the undercliff, that has fallen from the houses lost at the end of Chale Terrace; and the spillage of debris, particularly during the winter, over the sea cliff onto the beach. From the attitude of the bench, one would expect the direction of movement in the superincumbent debris to be inclined obliquely to the line of strike of the bench surface. That this is, indeed, the case is indicated by the scarp and fissure patterns in the undercliff debris and is reflected in the choice of section lines, particularly for CS1 and 2. Further evidence for this obliquity of movement is provided by the three notches (N1 to N3, Figs 2 & 4) which have been cut in the sea cliff by localised stream erosion. A metre or two of the bench surface on the down-dip side of the notches is exposed, probably by wave action, while their up-dip sides are completely buried by debris.

On the Walpen Undercliff two main types of mass movement can be distinguished (Fig.5):
I - Strongly non-circular, compound slides with a horizontal sole following the bench surface, and affecting the whole width of the undercliff.
II- Rotational slides, tangenting the bench surface, and affecting only the seaward margin of the undercliff.
These can be either slope or base failures (indicated by the suffixes S or B).

Slides of types IS and IIS are generally present from A to about C. The length from C to D is a transition zone, while between D and E worn down, back-tilted blocks of dark clay (probably part of stratum XII) may be seen in the beach (Figs 4 & 5), indicating that slides of types IB, and probably IIB, have taken place there. This SE end is thus distinct from the rest of the undercliff in having a strong component of deep-seated landslipping. This arises largely because the stress levels and pore-pressures are high enough there to induce such landslips in this predominantly clayey stratum, despite its being strong enough to resist such failures under the lower stresses which obtain to the NW. Shallow mudslides may develop in the SE part of the undercliff where there is both more water and stronger toe erosion.

The degree of stability of the undercliff tends generally to decrease from the vegetated length, A-B, towards the SE. This reflects the increase in height and instability of the rear scarp, the greater amount of ground and surface water and the stronger erosion of the slide toes especially between C and E, where the debris is no longer protected from marine attack by a resistant sea cliff. The resulting shallow bay cut in the slide debris there is well seen in Fig.4. Exceptions to the above trend are the deep-seated base failures between D & E. When seen in the spring and summer of 1980 these were evidently worn down, partly by streams and mudslides and partly by marine attack, and currently inactive.

Stability analyses, using the method of Morgenstern and Price, have been carried out on nearly all the type I and type II landslides shown in Fig.5, assuming the slip surfaces to be at residual. The calculations were made for three different assumptions as to the value of r_u; a) $r_u=0$, b) $r_u=0.5$ and c) as for b) except at the rear of the undercliff where an undrained loading (UDL), with $\bar{B}=1.0$, is taken. The back-analysis results are given in Fig.8 where the results of drained residual ring shear tests carried out in a Bromhead apparatus are also shown. The clay sample used was taken from a clayey facies of the Foliated Clay & Sand in Walpen Chine. These results confirm that slide types I and II can be expected to be active on CS1 to 3 whenever r_u in the debris is greater than about 0.25, even without the further effect of undrained loading. The results for CS4 are consistent with the field indications that the type IB & IIB slides there are currently inactive.

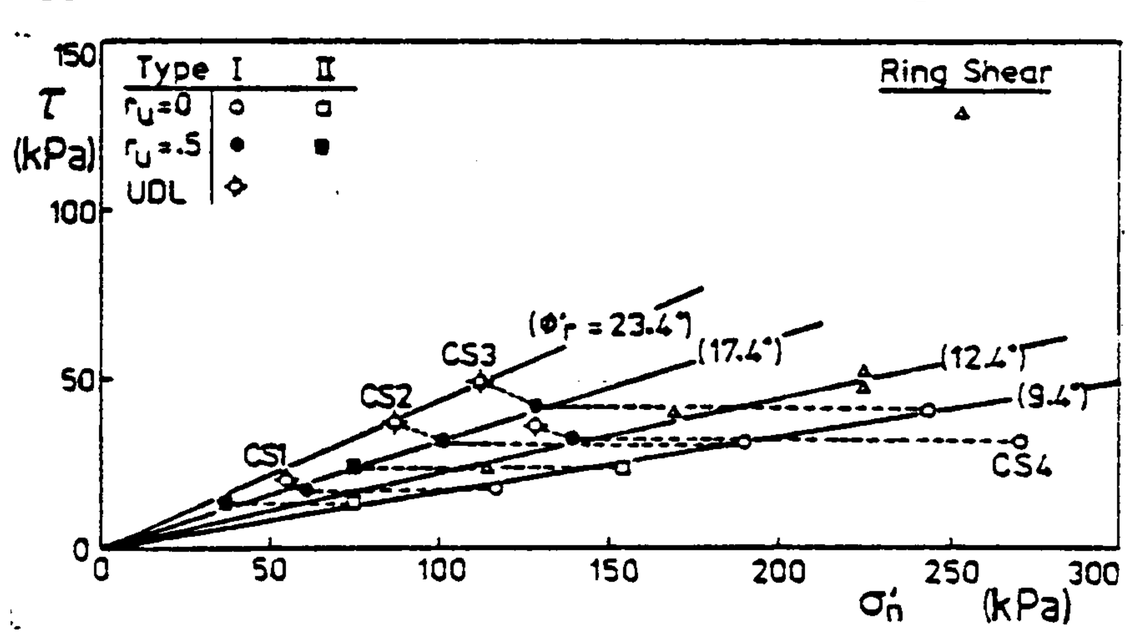


Fig.8 Stability analyses of sections CS1-4 with ring shear residual data (on clay of ω=25, ω_L=63, ω_p=31, fraction <2μm=31%)

An important feature of the rear of the undercliff is an irregular linear depression which runs along most of its length. This is occupied by several ponds, and is followed by some of the streams which traverse the undercliff (Figs 4 & 5, CS2). Counterscarps a few decimetres high run along much of its seaward margin. In view of the shape of the type I slides, the feature is probably a landslide graben. It has been modified however and possibly deepened in places by stream erosion. The counterscarps are probably connected with the graben, but in some cases they may reflect shallow slides moving in a landward direction into the associated streams. By this mechanism, by direct fluvial erosion and by irrigating the mudslides, the streams are probably responsible for moving a significant volume of debris across the bench into the sea.

The more intense erosion this century was accompanied by the destruction of several major inter-

mediate undercliffs. Thus, on CS3 (Fig.5), there were four undercliffs in 1907, the highest of which was built upon. The lowest of these undercliffs corresponded to the horizon of the present one. By 1980 the intermediate ones had been consumed by the development of the lowest one, apart from a small remnant of the uppermost. Similar trends can also be seen on CS2. Cliff development of this nature is probably characteristic of a situation where the dominant mass wasting process is seepage erosion associated with the lowest undercliff. Finally it is noted that the sea cliff and the rear scarp have generally been retreating at different rates, rather than in a steady state fashion. The present data do not allow firm conclusions to be drawn. There may be a tendency in the NW length, where the sea cliff is in situ and seepage erosion is the dominant process in the rear scarp, for the latter to have retreated faster than the former, while further SE, where the sea cliff is cut into slide debris and seepage erosion is accompanied by deep-seated base failures, the reverse seems to apply.

CONCLUSIONS

1. Seepage erosion in fine sand layers within the Foliated Clay and Sand stratum of the Ferruginous Sands is the main factor causing collapse of the superincumbent rear scarp and hence in the formation of the Walpen Undercliff.

2. The resultant debris moves, generally, obliquely, across the undercliff bench by compound slides embracing the whole width of the undercliff and by rotational slides in its seaward margin. Some debris is also transported across the undercliff by mudslides and by stream action.

3. The sole of the compound slides is inferred to follow a clayey layer of the Foliated Clay and Sands.

4. Analyses indicate that the inferred sliding of the debris will occur when the r_u value exceeds about 0.25. Undrained loading, although likely to be assisting the movements, is not a pre-requisite for these.

5. At the SE end of the length, where the cliffs are higher and the bench surface has dipped below sea level, the continuity of the bench is broken by deep-seated base failures.

6. Rates of recession have increased about threefold from the 19th to the 20th century and the sea cliff and the rear scarp generally retreat at different rates. Where seepage erosion is active in the rear scarp, this retreats the faster.

ACKNOWLEDGEMENTS

The Authors are grateful to the Natural Environment Research Council for supporting this work. Mr R.D. Curtis ran the ring shear tests.

REFERENCES

Casey, R. (1961). The stratigraphical palaeontology of the Lower Greensand. Palaeontology, (3), 487-621.

Fitton, W.H. (1847). A stratigraphical account of the section from Atherfield to Rocken End, on the south-west coast of the Isle of Wight. Q.J. geol. Soc. Lond., (3), 289-327.

Hutchinson, J.N. (1968). Mass Movement. In the Encyclopedia of Geomorphology (Ed. R.W. Fairbridge), pp.688-695. Reinhold Book Corpn: New York.

Masannat, Y.M. (1980). Development of piping erosion conditions in the Benson area, Arizona, U.S.A. Q.J. eng. Geol. Lond., (13), 53-61.

Ward, W.H. (1948). A coastal landslip. Proc. 2nd Int. Conf. Soil Mech. Found. Engg., (2), 33-38, Rotterdam.

White, J.H.O. (1921). A short account of the geology of the Isle of Wight. Mem. Geol. Surv. London: H.M.S.O.